Use of Stem Cell-derived macrophages and gene editing to investigate viral pathology and innate immunity



Alun Vaughan-Jackson

Sir William Dunn School of Pathology

Keble College

University of Oxford

A thesis submitted for the degree of Doctor of Philosophy

Hilary Term 2021

Acknowledgements

I would like to express my deepest gratitude to Prof. William James for his supervision of this thesis, and for giving me the opportunity to pursue a research question of my own from the very beginning. Also, his encouragement to get involved in teaching and scientific outreach has left me with invaluable experience that I will always appreciate. I would also like to particularly thank Dr Kenny Moore, who's supervision from afar was always extremely knowledgeable, inciteful, and without whom much of this thesis would not have been possible.

Thank you to my collaborators Prof. Greg Towers and Dr. Lucy Thorne of UCL for sharing resources and their guidance in all things TRIM5, Cyclophilin, and HIV related. Likewise, to Oxford colleagues, particularly Prof. Jan Rehwinkel for sharing resources, and Dr Kourosh Ebrahimi and Elisabete Pires, for their help with mass-spectrometry for the manuscript arising from Chapter 3. Also, thanks to Prof. Fiona Powrie and Prof. Ellie Barnes, for allowing me to undertake my first-year rotations in their labs, where I picked up valuable skills and perspectives that helped influence my own research. Of course, this could not have been possible without the Wellcome Trust Infection, Immunology, and Translational Medicine program, and in particular thanks to Prof. Christoph Tang, who provided a voice of calm when times became stressful.

I am ever grateful to everyone else in the James Lab, both past and present members, for their teaching, advice, and patience, but more importantly the fun and sense of family they brought to life in the lab and outside it. Thank you to Dunn School friends and colleagues for our nerdy chats and the inevitable rescue when I ran out of a reagent. To friends in Keble college, who have made my time in Oxford forever special, thank you for reminding me that there is more to life than just science.

Finally thank you to my patient and loving family, who put up with and encourage my love of science, and were always there when I was tired, burnt out, and in need of a holiday.

Abstract

Induced Pluripotent Stem Cell (iPSC)-derived macrophages are a rapidly emerging model of tissue resident macrophages for investigating human disease. As potentially infinitely replicating cells, iPSC lend themselves for genetic manipulation by CRISPR-Cas9 editing before terminal differentiation into a vast array of cell types. As such, long standing challenges in exploration of macrophage gene functions during inflammatory diseases and infections, such as HIV-1, caused by donor variability and immortalised cell line deficiencies can finally be overcome. With over 30 different protocols for macrophage differentiation from iPSC now described, culturing of these cells is gradually becoming more accessible to researchers, and essential processes for differentiation better understood. However, with this progress comes the ever-greater need for clear definition of culturing conditions of these cells, so that we can compare results between methodologies, and eliminate undesirable sources of variability.

This thesis sought to capitalise on this new system to explore the complicated and often contradictory role of TRIM5α in HIV-1 infection, and to explore with a precision only achievable through CRISPR-Cas9 genome editing the function of the cyclophilin family of peptidyl-prolyl isomerases. I demonstrate protection of HIV-1 from TRIM5α restriction by cyclophilin A, as well as regulation of the innate immune inflammatory response more generally by the cyclophilin family. However, prior to exploring this, this thesis sets out to address some of current issues in iPSC-derived macrophage culture and the ill-defined components of growth media and cellular environment. I describe a new macrophage differentiation medium using serum free, defined, and open-sourced components to bring needed transparency into the field. I also address the variability in macrophage phenotype and function brought about by the fundamental, but largely overlooked, impact of cell crowding in *ex vivo* culture. This revealed evidence for a potential plating density-dependent anti-inflammatory feedback loop relevant for human diseases like Alzheimer's disease.

Table of Contents

Acknowledgements **2**
Abstract **3**
Table of Contents **4**
Abbreviations **9**
Chapter 1:
Introduction **17**
1.1 Macrophages 18
1.2 Macrophage ontogeny 21
1.3 Macrophage activity 24
1.4 Regulating the macrophage cytokine response 29
1.5 Induced pluripotent Stem Cells: 33
1.6 Differentiation of macrophages from iPSC 36
1.7 Using iPSC-derived macrophages to study disease 38
1.8 CRISPR-Cas9 41
1.9 Gene editing in macrophages and iPSC 43
1.10 HIV, macrophages, and iPSC 46
1.11 Using iPSC-derived macrophages to study the cyclophilins 54
1.12 Scope of work 57
Chapter 2:
Materials and Methods **59**
2.1 Cell culture 60
2.1.1 Cell line culture 60
2.1.2 IPSC lines 60
2.1.3 iPSC culture 61
2.2 Genome engineering 62
2.2.1 CRISPR-Cas9 editing 62
2.2.2 Genomic DNA (gDNA) extraction from iPSC clones in a 96-well plate 64
2.2.3 Extraction using QIAGEN kit DNA 64
2.2.4 Screening iPSC clones by Polymerase Chain Reaction (PCR) 64
2.2.5 Sequencing 65
2.2.6 Single Nucleotide Polymorphism (SNP) analysis 66
2.3 Macrophages: phenotype and function 67
2.3.1 iPSC-derived macrophage differentiation 67
2.3.2 Cell measurements 69
2.3.3 Macrophage surface marker staining 69

2.3.4 Macrophage total marker staining 69
2.3.5 Zymossan-488 phagocytosis assay 70
2.3.6 Adhesion assay 71
2.4 RNA 72
2.4.1 RNA extraction 72
2.4.2 cDNA synthesis for Quantitative PCR (qPCR) 72
2.4.3 qPCR: Taqman 72
2.4.4 qPCR: SYBR green 73
2.4.5 Analysis of qPCR data 74
2.4.6 RNA-seq sample preparation, library construction, and data generation 75
2.4.7 RNA-Seq data analysis 76
2.5 Virus production and infection assays 78
2.5.1 Plasmid preparation 78
2.5.2 Production of lentivirus 79
2.5.3 Quantification of viral titres: VSV-G enveloped virus 79
2.5.4 Quantification of viral titres: BaL enveloped virus 80
2.5.5 HIV-1 GFP pseudo-virus single-cycle infectivity assay 80
2.5.6 Replication competent HIV-1 infectivity assay 81
2.5.7 Zika virus infectivity assay quantified by plaque assay 81
2.6 Cytokine analysis 83
2.6.1 Enzyme-linked immunosorbent assay (ELISA) 83
2.6.2 Proteome Profiler 83
2.7 General methods 84
2.7.1 Western blotting 84
2.7.2 Cell viability assay 85
2.7.3 Liquid Chromatography-Mass Spectrometry (LC-MS) 85
2.7.4 Quantification of glucose concentration 86
2.7.5 Lactate quantification 86
2.7.6 Software 87

Chapter 3:

Differentiation of human induced Pluripotent Stem Cells to authentic macrophages using fully defined, serum free, open-source medium 88

3.1 Introduction 89
3.2 Results 93
3.2.1 XVIVO medium, but not OXM medium, contains undisclosed molecules 93
3.2.2 Differentiation of iPSC to macrophages in novel fully defined, open-source medium, OXM 95
3.2.3 Macrophages cultured in OXM are phenotypically similar to, but distinct from, XVIVO-cultured cells 96

3.2.4 While transcriptionally very similar, OXM-cultured macrophages have a more homeostatic, and XVIVO-cultured macrophages a more immunologically active, signature 100

3.2.5 OXM and XVIVO cultured macrophages have different classical and alternative activation profiles 105

3.2.6 OXM-cultured macrophages are more susceptible to HIV-1 infection, but not to Zika virus 106

3.3 Discussion 109

3.4 Conclusion 111

3.5 Supplementary information 112

Chapter 4:

Density Dependent Regulation of Inflammation 118

4.1 Introduction 119

4.2 Results 122

4.2.1 Plating density of macrophages impacts their ability to respond to innate immune stimuli 122

4.2.2 Differential plating density primes macrophages for cell death post-LPS/IFNγ stimulation 125

4.2.3 DDRI regulates the cytokine response to LPS/IFNγ, with the possible exception of CXCL11 126

4.2.4 Density alters the phenotype of macrophages and drives formation of 2 morphologically and phenotypically distinct populations 128

4.2.5 Low and mid density plated cells share a transcriptional profile distinct from high density cells. 131

4.2.6 Density alters transcription of member genes of GO terms beyond regulation of cytokines and inflammation 137

4.2.7 The cause of DDRI may in part be secretory, with glucose metabolism products as candidates 152

4.3 Discussion 156

4.4 Conclusion 165

4.5 Supplementary figures 167

Chapter 5:

Cyclophilin A protects HIV-1 from TRIM5α mediated restriction and regulates viral reverse transcription 173

5.1 Introduction 174

5.2 Results 178

5.2.1 Cyclophilin A protects HIV-1 from TRIM5α 178

5.2.2 TRIM5α-mediated restriction is not envelope specific 179

5.2.3 TRIM5α blocks reverse transcription 182

5.2.4 Proteasome inhibition rescues TRIM5α-mediated inhibition of reverse transcription but not infectivity 184

5.2.5 TRIM5α restriction is independent of TAK1 or STING mediated signalling 185

5.2.6 TRIM5α restriction is independent of IFN and the immunoproteasome 190
5.2.7 Knock out of SAMHD1 and TREX1 partially rescues HIV-1 infection from TRIM5α-mediated restriction..... 193
5.2.8 CyPA has a secondary role in HIV-1 infection in addition to protection from TRIM5α 195
5.2.9 The second function of CyPA aids viral infection during reverse transcription ... 199
5.3 Discussion 201
5.4 Conclusion..... 208
5.5 Supplementary figures..... 209
Chapter 6:
Cyclophilins and Innate Immunity 214
6.1 Introduction..... 215
6.2 Results 222
6.2.1 Cyclophilins suppress the TLR-activated immune response independent of Calcineurin..... 222
6.2.2 Inhibition of cyclophilins alters mRNA levels of multiple cytokines early after LPS stimulation while Cn effects are delayed 223
6.2.3 Preliminary tests do not show clear changes in downstream signalling when cyclophilins or Cn are inhibited..... 228
6.2.4 Generation of cyclophilin knockouts: CyPA, CyPB, CyPD, and the cyclophilin receptor CD147..... 230
6.2.5 Knocking out CyPA does not influence iPSC-derived macrophage differentiation 233
6.2.6 Knocking out CyPA does not cause a compensatory upregulation of other cyclophilins 233
6.2.7 CyPA potentially regulates the response to TLRs but is not the only cyclophilin involved 238
6.2.8 Differences in the innate response between WT and CyPA KO cells vary greatly over macrophage differentiation culture age, and may occur later than 24 hours post-stimulation..... 240
6.2.9 Cyclophilins and TLR-signalling are influenced by cell plating density..... 241
6.2.10 CyPA does not regulate the cGAS-STING initiated antiviral response..... 241
6.2.11 CyPB regulates the TLR3 response but not through early transcriptional regulation 245
6.3 Discussion 250
6.4 Conclusion..... 256
6.5 Supplementary figures..... 257
Chapter 7:
General Discussion..... 264
7.1 Summary of Results 265
7.1.1 Chapter 3: Defined, serum free, open-sourced medium for macrophage culture265
7.1.2 Chapter 4: Density-dependent regulation of inflammation 266

7.1.3 Chapter 5: Cyclophilin A protects HIV-1 from TRIM5α 267
7.1.4 Chapter 6: Cyclophilin regulation of the innate immune response 267
7.2 Current limitations 268
7.2.1 iPSC-derived macrophage differentiation 268
7.2.2 Macrophage heterogeneity 269
7.2.3 CRISPR screening with iPSC-derived macrophages 270
7.3 Future directions 271
Appendix 273
Licences 273
References 275

Abbreviations

18S	18S ribosomal RNA
5Z-7	5Z-7-Oxozeaenol
ACTB	β-Actin
AD	Alzheimer's Disease
aDMEM	Advanced DMEM
ANOVA	Analysis Of Variance
AP-1	Activator Protein 1
APC	Allophycocyanin
ARE	AU-Rich Element
AUC	Area Under the Curve
B2M	β-2-Microglobin
BLAST	Basic Local Alignment Search Tool
BM	Bone Marrow
BMDM	Bone-Marrow Derived Macrophages
BMP4	Bone Morphogenic Protein 4
Bort	Bortozemib
BP	Biological Process
bp	base pair
BSG	Basigin
BSL3	Biosafety Level 3
C/EBP	CCAAT/Enhancer-Binding Protein beta
CA	Capsid
Cas	CRISPR associated protein
Cat No.	Catalogue number

CC	Cellular Component
CCL	C-C Motif Chemokine Ligand
CCR	C-C Chemokine Receptor
CD	Cluster of Differentiation
cDNA	complementary DNA
cGAMP	Cyclic Guanosine monophosphate–Adenosine Monophosphate
cGAS	cyclic GMP-AMP Synthase
CLR	C-type Lectin Receptor
Cn	Calcineurin
Conc	Concentration
CPSF6	Cleavage and Polyadenylation Specificity Factor 6
CRISPR	Clustered Regularly Interspaced Short Palindromic Repeats
CsA	Cyclosporine A
CSF-1	Colony Stimulating Factor 1
CXCL	C-X-C Motif Chemokine Ligand
CXCR	C-X-C chemokine receptor
CyP	Cyclophilin
DAMP	Danger Associated Molecular Patterns
DC	Dendritic Cell
DDRI	Density Dependent Regulation of Inflammation
DEG	Differentially Expressed Genes
DMEM	Dulbecco's Modified Eagle Medium
DMSO	Dimethyl Sulfoxide
dN	deoxynucleotide
DNA	Deoxyribonucleic Acid
dNTP	deoxynucleoside Triphosphate
EB	Embryoid Body

EC	Extracellular
ECM	Extracellular Matrix
EDTA	Ethylenediaminetetraacetic Acid
ELISA	Enzyme-linked Immunosorbent Assay
EMP	Erythromyeloid Progenitor
ER	Endoplasmic Reticulum
ERAD	ER Associated Degradation
ERK	Extracellular signal-Regulated Kinases
ESC	Embryonic Stem Cells
EtOH	Ethanol
FACS	Fluorescence-Activated Cell Sorting
FBS	Fetal Bovine Serum
FCS	Fetal Calf Serum
FGF	Fibroblast Growth Factor
FITC	Fluorescein Isothiocyanate
FKBP	FK506 Binding Proteins
FL	Fetal Liver
FSC-A	Forward Scatter Area
GAPDH	Glyceraldehyde 3-Phosphate Dehydrogenase
GFP	Green Fluorescent Protein
GM-CSF	Granulocyte-Macrophage Colony-Stimulating Factor
GO	Gene Ontology
gRNA	guide RNA
GTPase	Guanosine Triphosphate hydrolase
GWAS	Genome Wide Association Study
HAND	HIV-Associated Neurocognitive Decline
hES	human Embryonic Stem

hgDMEM	high glucose DMEM
HIV	Human Immuno-deficiency Virus
HKLM	Heat Killed Listeria Monocytogenes
HLA	Human Leukocyte Antigen
HPC	Haematopoietic Progenitor Cells
HSC	Haematopoietic Stem Cell
hTRIM5α	human TRIM5α
IFN	Interferon
IFNAR2	IFN Receptor 2
IL	Interleukin
iPSC	induced Pluripotent Stem Cells
IRF	Interferon Regulatory Factor
ISG	Interferon Stimulated Gene
IU	Infectious Units
JNK	c-Jun N-terminal Kinases
kb	kilobase
KD	Knock-Down
KO	Knock-Out
LB	Luria-Bertani
LC-MS	Liquid Chromatography-Mass Spectrometry
LDL	Low-Density Lipoprotein
LN	Liquid Nitrogen
LPS	Lipopolysaccharide
M1	Classically activated macrophages
M2	Alternatively activated macrophages
MAPK	Mitogen-Activated Protein Kinase
M-CSF	Macrophage Colony Stimulating Factor

MDA-5	Melanoma Differentiation-Associated protein 5
MDM	Monocyte Derived Macrophage
MEF	Mouse Embryonic Fibroblasts
MF	Molecular Function
MFI	Mean Fluorescence Intensity
MG	MG132
MHC	Major Histocompatibility Complex
min	minutes
MMP	Matrix Metallopeptidase
MOI	Multiplicity Of Infection
mRNA	messenger RNA
MyD88	Myeloid Differentiation primary response 88
NCBI	National Centre for Biotechnology Information
NEAA	Non-Essential Amino Acids
NFAT	Nuclear Factor of Activated T-cells
NF-kB	Nuclear Factor kappa-light-chain-enhancer of activated B cells
NK	Natural Killer
NLR	NOD-like Receptor
NMD	Nonsense Mediated Decay
NO	Nitric Oxide
NUP	Nucleoporin
ONX	ONX-0914
P/S	Penicillin-Streptomycin
p38	p38 mitogen-activated protein kinases
PAM	Protospacer Adjacent Motif
Pam3	Pam3CSK4
PAMP	Pathogen Associated Molecular Pattern

PBMC	Peripheral Blood Mononuclear Cell
PBS	Phosphate Buffered Saline
PCA	Principle Component Analysis
PCR	Polymerase Chain Reaction
PD	Parkinson's Disease
PE	Phycoerythrin
PF74	PF-3450074
PFA	Paraformaldehyde
Poly(I:C)	Polyinosinic:polycytidylic acid
PPI	Peptidylprolyl Isomerase
PPIase	Peptidylprolyl Isomerase
PPIL	Peptidylprolyl Isomerase-Like
PreMac	macrophage precursor cells
PRR	Pattern Recognition Receptor
PSC	Pluripotent Stem Cells
qPCR	quantitative PCR
rhTRIM5α	Rhesus TRIM5α
RIG-I	Retinoic acid-Inducible Gene I
RING	Really Interesting New Gene
RIPA	Radioimmunoprecipitation Assay
RLU	Relative Luminescence Units
RNA	Ribonucleic Acid
RNA-Seq	RNA Sequencing
RNP	Ribonucleoprotein
ROCKi	Rho-Kinase inhibitor
ROS	Reactive Oxygen Species
RT	Reverse Transcripts

s	seconds
SAMHD1	SAM Domain and HD domain-containing protein 1
SC	Stem Cells
SCF	Stem Cell Factor
SD	Standard Deviation
shRNA	short hairpin RNA
siRNA	short interfering RNA
SIV	Simian Immunodeficiency Virus
SNP	Single-Nucleotide Polymorphism
SSC-A	Side Scatter Area
ssRNA	single stranded RNA
STAT	Signal Transducer and Activator of Transcription protein
STING	Stimulator of Interferon Genes
TACE	Tumour necrosis factor-Alpha Converting Enzyme
TAK1	Transforming growth factor beta-Activated Kinase 1
TAM	Tyro3, Axl, and Mer
TBP	TATA-Binding Protein
TCR	T-cell Receptor
Temp	Temperature
TGF	Transforming Growth Factor
Th	T helper lymphocyte
TIC	Total Ion Chromatogram
TIDE	Tracking of Indels by Decomposition
TIM	T cell/transmembrane, Immunoglobulin, and Mucin
TLR	Toll-Like Receptor
T_m	melting temperature
TNFα	Tumor Necrosis Factor alpha

TPM	Transcripts Per Kilobase Million
TREX1	Three prime Repair Exonuclease 1
TRIM5α	Tripartite Motif-containing protein 5 alpha
tRNA	transfer RNA
VACV	Vaccinia Virus
VEGF	Vascular Endothelial Growth Factor
VSV-G	Vesicular Stomatitis Virus G
WT	Wild Type
XVIVO	XVIVO™-15
YS	Yolk-Sac
ZIKV	Zika Virus

Chapter 1:

Introduction

1.1 Macrophages

Famously first identified in 1882 by Elie Metchnikof in starfish larvae (1), macrophages are among the most evolutionarily ancient phagocytic cells found in all multicellular organisms and play an essential role in the immune response, tissue organisation, and homeostasis (2). The fundamental characteristic of a macrophage is the ability to phagocytose invading pathogens, dead cells, and other extracellular debris/foreign substances. In addition, they can produce reactive oxygen species (ROS) as part of their immune response to kill unicellular organisms like bacteria, and release large quantities of both pro- and anti-inflammatory cytokines and chemokines to recruit other cells of the innate and adaptive immune system (3, 4). These recruited cells include the adaptive immune T cells, with which macrophages can directly interact and activate through presentation of foreign peptides bound to MHC class I and class II molecules on the macrophage cell surface alongside costimulatory receptors like CD80 and CD86 (5–7). After the cause of injury/infection has been resolved, macrophages play an essential role in tissue repair through release of anti-inflammatory cytokines, growth factors, extracellular matrix remodelling, and clearance of dead cells (7–9).

Macrophages can be broadly classified into two types, tissue resident macrophages found in all organs of the body, and blood monocyte-derived macrophages (MDM), that emigrate out of the blood to the site of injury/infection during the immune response. Tissue resident macrophages are uniquely tailored to the niche they inhabit and have several names. For example, liver resident macrophages are known as Kupfer cells, bone as osteoclasts, brain as microglia, and lung as alveolar macrophages (3, 10). Within each organ they perform unique essential homeostatic tasks, like bone reabsorption, surfactant recycling, synaptic pruning, and clearance of extracellular misfolded proteins (11–14). Meanwhile, the monocytes from which MDM are derived are made up of three groups, classical $CD14^{high}$ $CD16^{-}$, intermediate $CD14^{high}$ $CD16^{low}$, and non-classical $CD14^{low}$ $CD16^{high}$ monocytes (15–17). Of these, classical monocytes make up 80-90% of all monocytes (17), which in turn make up approximately 10% of circulating leucocytes. Classical monocytes are typically inflammatory

and phagocytic, rapidly exiting the blood in response to inflammatory signals, while non-classical appear to patrol the vascular endothelium. Intermediate monocytes are not well understood, but can be inflammatory, sensing viruses and nucleic acids (18), and potentially serve as markers for diseases like cardiovascular disease (16). Tissue macrophages and monocytes are phenotypically distinct from each other, but upon infiltration into the tissues MDM take on many of the characteristics of tissue macrophages, sharing up 90% transcriptional identity (19). All macrophages express common surface proteins like CD11b, CD14, CD45, and CD64, and there are no definitive markers for tissue macrophages vs MDM. Nevertheless, some potential markers have been suggested, e.g. MARCO and Tim4 (20–22). On the other hand, different tissue macrophages can be separated by subtle changes in expression of these common markers (E.g. microglia are CX3CR1^{high} CD45^{low}), as well as having clear transcriptional differences, like expression of SALL1 in microglia, BACH2 in alveolar macrophages and ID3 in Kupffer cells (13, 14, 23) (Figure 1).

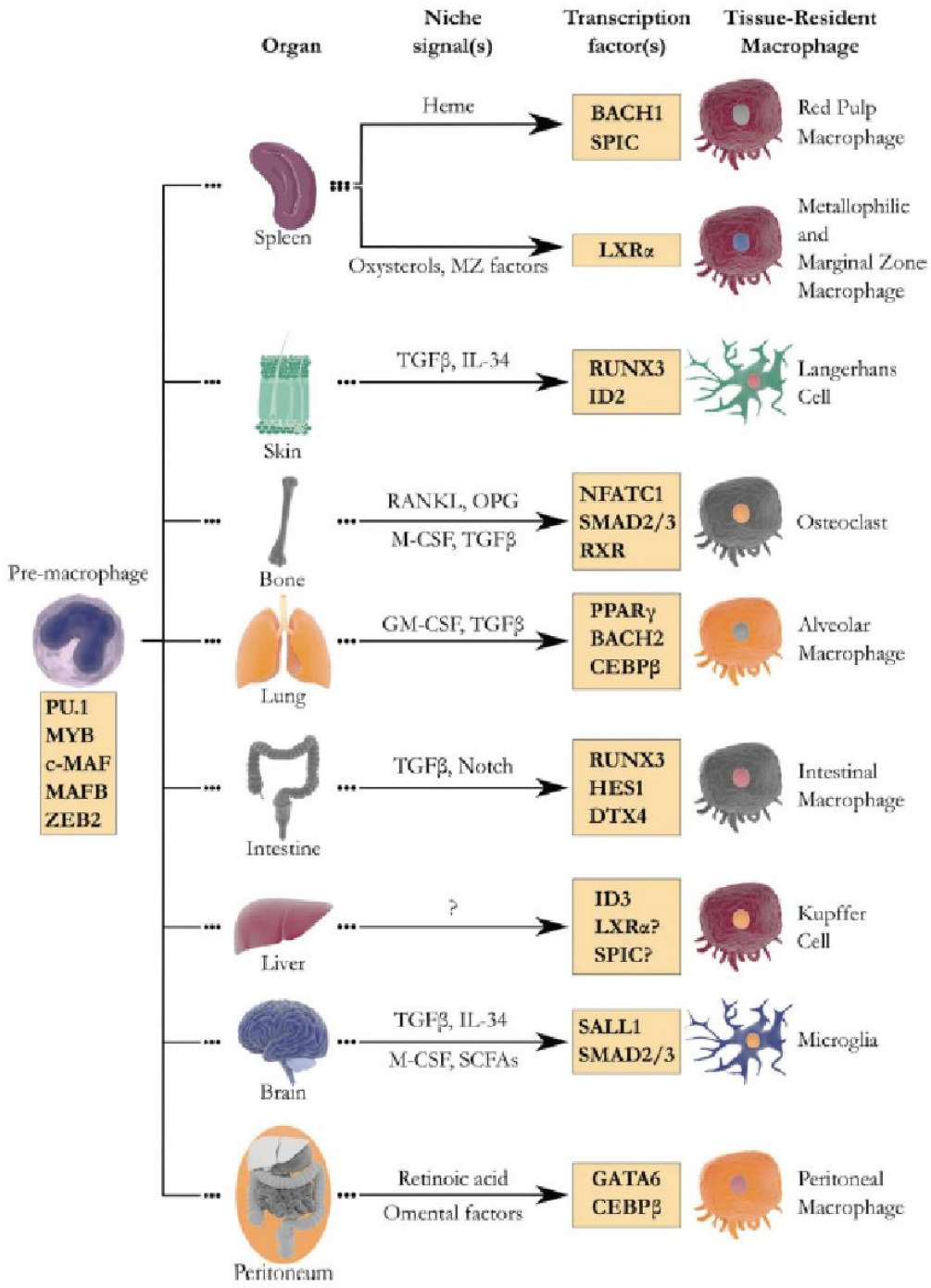


Figure 1: Macrophages of the different tissues. *Identity of macrophages in different tissues of the human body, and some of the known differentiation signals and transcription factors important for their development. Adapted from T'Jonck, Guilliams, & Bonnardel 2018* (14)**.**

1.2 Macrophage ontogeny

While the phenotype of tissue macrophages and MDM may be hard to distinguish, developmentally (their ontogeny) they are very different. Until recently, all macrophages were believed to be monocyte-derived (24, 25). However, several conclusive studies using donor monocytes and mouse parabiosis (surgical union to share blood circulation) have demonstrated this to be false, but rather many tissue macrophages are able to self-renew and develop independently of the bone marrow (BM) niche (26–29). It has now been shown that macrophages are produced in 3 waves (25). First, exiting the embryonic yolk-sac (YS) to populate the developing organs in the body. Second, erythromyeloid progenitors (EMPs) in the fetal liver (FL) produce macrophages to replace the macrophages produced in the first wave, excluding the brain microglia and epidermis. In some organs (E.g. the lung and liver) these will then become permanent, self-renewing populations of tissue macrophages. In others (the dermis, gut, and heart) they will be replaced over the lifespan of the animal by the third developmental wave, MDM from the BM (Figure 2A & B) (25, 30–32). The precise signals driving differentiation are complex and have been comprehensively reviewed elsewhere (25). One key determinant is the transcription factor c-Myb, which is required for development of FL- and BM- but not YS-derived macrophages. Deletion of c-Myb results in mice containing only tissue resident macrophages, both the microglia that form a permanent population, and in the other organs of the body that fail to be replaced by the FL-derived macrophages (25, 33). This will become especially important later when considering the use of iPSC-derived cells to model tissue macrophages (34, 35).

It is necessary to make these distinctions as developmental pathways can subtly alter the characteristics of cells, even in functionally plastic cells like macrophages. This is emphasized by the fact that MDM have been shown to be unable to become identical to tissue macrophages even when occupying the same niche (19, 21, 36, 37). Moreover, while transplantation of tissue resident macrophages from the peritoneum to the lungs will result in alveolar-like tissue macrophages, these cells will still retain epigenetic traits of peritoneal

macrophages (19). On the other hand, a recent single-cell RNA sequencing study engrafting macrophages from different developmental waves into neonatal mouse lungs resulted in relatively few transcriptional differences linked to ontogeny. Furthermore macrophages transplanted from other tissues were less efficient at transitioning to become alveolar macrophages (38). It can be argued, then, as Guilliams and Svedberg do (39), that the tissue niche and not the ontogeny is the principal restrictor of macrophage plasticity. However, in their study, Van de Laar et al. (38) also found that while all precursors could become alveolar macrophages, FL derived precursors had a greater capacity to expand and self-maintain their population (a fundamental feature of tissue-resident macrophages) than MDM. This supports earlier research demonstrating that tissue resident macrophages can self-maintain, whereas infiltrating MDM often do not and are lost during inflammatory resolution (39–42). Therefore, as location is a predominant restrictor of plasticity, while MDM may appear to be more plastic in nature, ontogeny still ought to be considered when studying tissue resident macrophages. This is likely to be even more relevant in niches such as the brain which are exclusively populated by YS derived macrophages and do not see monocyte infiltration throughout an individual's lifetime (Figure 2B) (25).

Overall, these observations are somewhat remarkable as they demonstrate just how flexible macrophages can be, and the importance of taking into consideration not only cell intrinsic signals but also external factors when studying them. Recently, Guilliams *et al.* explored the idea of establishing and maintaining the tissue macrophage niche, discussing the role of growth factors and cell-cell communication models, particularly in relation to the use of M-CSF (also known as CSF-1) to maintain the population and inducing proliferation (10). However, precisely what signals determine each tissue niche is still unknown and is the subject of ongoing investigation (10, 43–47).

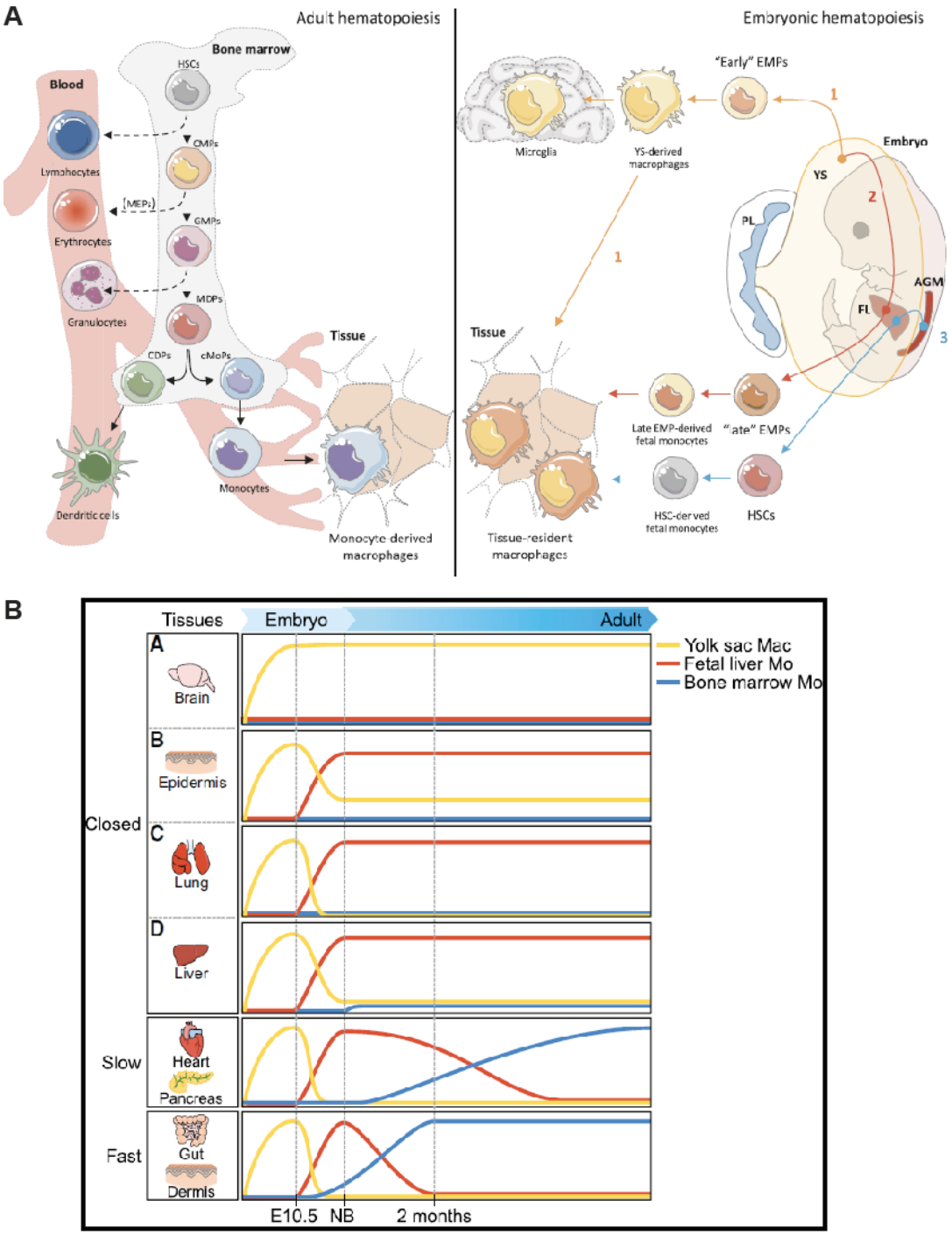


Figure 2: Ontogeny of different macrophages. *A) Schematic of haematopoiesis in adults in the bone marrow, and the 3 waves of macrophage development in the embryo. Adapted from Italiani & Boraschi 2017 (22). B) Relative proportion of macrophages derived from the 3 waves of embryonic hematopoiesis and how they change over time within mice. Adapted from Ginhoux & Guilliams 2016 (25)*

1.3 Macrophage activity

Activated macrophages are traditionally described to occupy one of two states, classically activated M1 or alternatively activated M2 macrophages. Well known inducers of these are LPS and IFNγ for M1, and IL-4, IL-10, TGFβ and M-CSF for M2 (2). The distinction was originally described in relation to the type of T helper (Th) cell they can induce; either proinflammatory Th1, or anti-inflammatory Th2 cells, and were identified by differences in arginine metabolism, an important component of nitric oxide production (48). Nowadays, these two macrophage states can typically be characterized by differences in surface marker expression (E.g. CD16, CD80 and CD86 expression for M1, CD163, CD200R and CD206 expression for M2 (5, 7, 49)), as well as the release of proinflammatory cytokines (TNFα, IL-1β, IL-12) and anti-inflammatory cytokines (TGF-β and IL-10), respectively (2, 5, 50). However, this assumes an extremely limited, bipolar, view of macrophages, and does not take into consideration that, just as how the Th1/Th2 paradigm misses other Th subsets like Th17 and Th22 cells, macrophages are highly plastic cells that continuously transition between states in response to cues within their local environment.

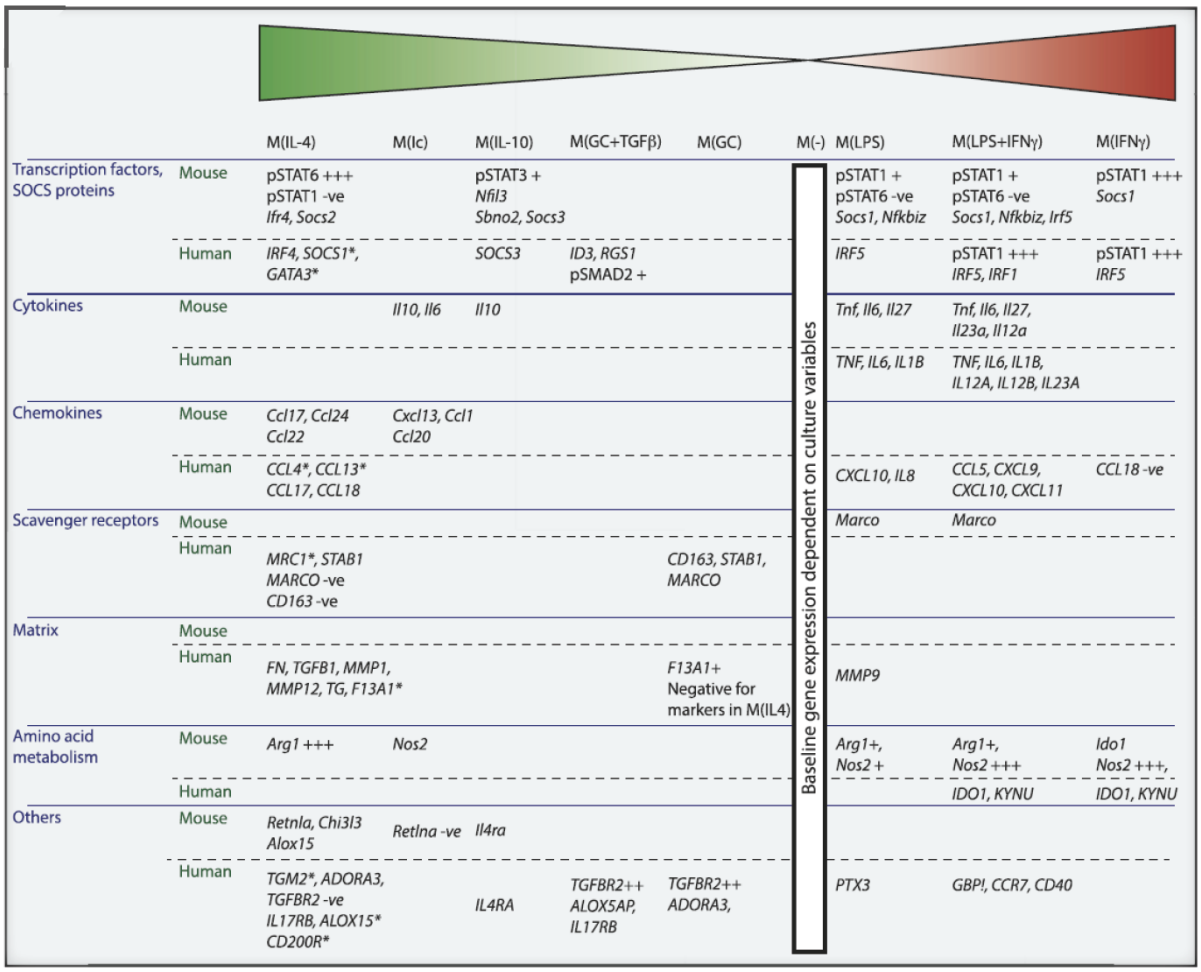
Pro- and anti-inflammatory signals come in many forms. As one of the first immune cells at the site of an infection, macrophages express a wide arsenal of pathogen recognition receptors (PRRs) and scavenger receptors for detection, uptake, processing and elimination of extracellular pathogens and debris (Summarised in Table 1) (47). Activation of PRRs will typically induce an inflammatory response by macrophages via transcription factors like NF-κB, AP-1, C/EBPβ, and the IRFs to produce cytokines and chemokines such as TNFα, IL-6, the CCL proteins, and interferons (IFNs) (51, 52). Which of these are produced will depend heavily on the original pathogen associated molecular pattern (PAMP) detected. For instance, activation of intracellular antiviral sensors, like cGAS, will drive a predominantly antiviral IFN production via IRF3, and other cytokines via NF-κB, but not AP-1 and C/EBPβ (53, 54). Likewise, these inflammatory pathways must also be carefully regulated to prevent an over-zealous and harmful response. Anti-inflammatory cytokines and growth factors like IL-10 and

TGFβ are produced both by macrophages themselves and neighbouring cells (55). Alternatively, inhibitory cell-cell receptor interactions, E.g. between CD200R on macrophages and CD200 on neurons, can act upon macrophages to suppress production of inflammatory mediators, redirecting them towards tissue repair and maintenance (56). In some situations, activation of an immune response by macrophages would both be unnecessary and detrimental, e.g. clearing away apoptotic cells. Under these situations, macrophages utilise a wide variety of scavenger receptors to clear away these dead cells (Table 1) (9, 57). Phagocytosis of apoptotic cells can actively suppress the production of inflammatory mediators by macrophages, inducing TGFβ production and amplifying the gene signatures typically associated with IL-4 and IL-13 stimulated anti-inflammatory macrophages (9, 57, 58). Alternatively, phagocytosis can prime macrophages for a secondary inflammatory response to release IL-1β, or induce the adaptive immune response by T cells after cross presentation of phagocytosed peptides on MHC molecules (6, 59). Post-phagocytic macrophage activity, therefore, is very much context/meal dependent.

The idea then of distinct M1 and M2 states is largely arbitrary as it may well be the case that macrophages will encounter signals for both at the same time. Therefore, macrophages should better be thought of on a continual spectrum of inflammatory states. Broadening of macrophage subsets has been proposed in the past, based on specific function or marker expression (5, 60, 61). For example, tolerance inducing CD169+ macrophages in the lymphoid tissues, tissue remodelling and growth promoting tumour associated macrophages, and inflammatory T cell receptor expressing macrophages have all been identified (5). Alternatively, moves were made to break up M1 and M2 based on the activator signal presented, such as distinguishing between IL-10 and IL-4 stimulation, or combinations of multiple factors (4, 50, 55). However, all of this led to a confusing array of subsets with no clear systematic nomenclature, especially because it was also shown that the macrophages could pass between states depending on the ordering of the stimuli encountered (62). Transcriptomic approaches have now shown that macrophages occupy at least 9 distinct

activation programs induced by 29 different agonists (63). Therefore, in 2014 Murray and colleagues sought to redefine the approach to macrophage nomenclature, focusing on a spectrum based model, incorporating the stimulus used, the origin and isolation method of the macrophage, and abandoning specific “markers” like arginine-1, in favour of a broader consensus of marker expression or lack of (Figure 3) (50). While definitely a more preferable approach, it could be considered too open ended given that there are almost infinite combinations of stimuli, and arguments have been made to define macrophages instead on their specific function within an environment (e.g. pruning neurons) (61). Nevertheless, old habits die hard, and new methods of identifying macrophages within an M1/M2 framework based on morphology, transcriptomics, and metabolomics are still being described to this day (64, 65).

If we combine the importance of the tissue environment, the stimuli applied, and the functional flexibility of macrophages, it is clear that if we are to understand how macrophages behave *in vivo*, 2 things are required: 1) Further studies on the macrophage niche *in vivo* utilising single cell informatic approaches, and 2) a greater understanding of all the variables associated with *in vitro* culturing of macrophage. For example, what influence does the medium in which we culture these cells have on their function? And is there a “right” way to culture them in monoculture? Given that they are heavily influenced by tissue specific cues, have we missed basic underlying regulatory systems in our rush to use these cells to study human disease? The first half of this thesis will seek to address some of these issues, particularly looking at how we culture macrophages and how this influences their ability to respond to external stimuli.



		M(IL-4)	M(Ic)	M(IL-10)	M(GC+TGFβ)	M(GC)	M(-)	M(LPS)	M(LPS+IFNγ)	M(IFNγ)
Transcription factors, SOCS proteins	Mouse	pSTAT6 +++ pSTAT1 -ve *Ifr4, Socs2*		pSTAT3 + *Nfil3* *Sbno2, Socs3*			Baseline gene expression dependent on culture variables	pSTAT1 + pSTAT6 -ve *Socs1, Nfkbiz*	pSTAT1 + pSTAT6 -ve *Socs1, Nfkbiz, Irf5*	pSTAT1 +++ *Socs1*
	Human	*IRF4, SOCS1*, GATA3**		*SOCS3*	*ID3, RGS1* pSMAD2 +			*IRF5*	pSTAT1 +++ *IRF5, IRF1*	pSTAT1 +++ *IRF5*
Cytokines	Mouse		*Il10, Il6*	*Il10*				*Tnf, Il6, Il27*	*Tnf, Il6, Il27, Il23a, Il12a*	
	Human							*TNF, IL6, IL1B*	*TNF, IL6, IL1B, IL12A, IL12B, IL23A*	
Chemokines	Mouse	*Ccl17, Ccl24* *Ccl22*	*Cxcl13, Ccl1* *Ccl20*							
	Human	*CCL4*, CCL13** *CCL17, CCL18*						*CXCL10, IL8*	*CCL5, CXCL9, CXCL10, CXCL11*	*CCL18 -ve*
Scavenger receptors	Mouse							*Marco*	*Marco*	
	Human	*MRC1*, STAB1* *MARCO -ve* *CD163 -ve*				*CD163, STAB1, MARCO*				
Matrix	Mouse									
	Human	*FN, TGFB1, MMP1, MMP12, TG, F13A1**				*F13A1+* Negative for markers in M(IL4)		*MMP9*		
Amino acid metabolism	Mouse	*Arg1 +++*	*Nos2*					*Arg1+, Nos2 +*	*Arg1+, Nos2 +++*	*Ido1* *Nos2 +++,*
	Human								*IDO1, KYNU*	*IDO1, KYNU*
Others	Mouse	*Retnla, Chi3l3* *Alox15*	*Retlna -ve*	*Il4ra*						
	Human	*TGM2*, ADORA3, TGFBR2 -ve* *IL17RB, ALOX15** *CD200R**		*IL4RA*	*TGFBR2++* *ALOX5AP, IL17RB*	*TGFBR2++* *ADORA3,*		*PTX3*	*GBP!, CCR7, CD40*	

Figure 3: Macrophage activation considered as a spectrum. *Summary of the changes seen in macrophages after various pro – and anti-inflammatory stimuli. Adapted from Murray et al. 2014* (50)

Signal Source	Stimulus	Sensor/Receptor	Reference
Bacteria	LPS, Flagellin, CpG DNA	TLRs	(51)
	β-glucan, mannose	CLRs	(66)
	Flagellin, pore-forming toxins	NLRs	(67)
Virus	dsRNA, ssRNA	TLR3, TLR7, RLRs	(51)
	DNA	AIM2, cGAS	(53, 68)
Fungus	β-glucan	TLRs	(51)
	β-glucan, mannose	CLRs	(66)
Dead Cell	Apoptotic cell	TAMs, TIMs	(69, 70)
	Necrotic cell	NLRP3, TLRs, $P2X_7$, $P2Y_2$	(51, 67, 71)
Tissue microenvironment	Hypoxia	HIF-1α	(72)
	pH	GPR65	(73)
	Heat	TRPV2, TRPM2	(74, 75)
	Osmolarity	NLRP3, NLRC4, TRPV2, NFAT5	(67, 74, 76, 77)
	Alum, asbestos, silica	NLRP3	(67)
Metabolite	Nucleotides and nucleosides	Purinergic receptors	(71)
	Heme	Bach1	(78)
	Vitamain A	Retinoic acid receptors	(79)
	Vitamin D	Vitamin D receptor	(80)
	Fatty acid	PPAR-γ, CD36, SR-A	(81–83)
	Omega-3	GPR120	(84)
	β-hydroxybutyrate	GPR109a	(85)
	Sphingosine-1-phosphate	Sphingosine 1-phosphate receptors	(86)
Extracellular matrix	Fibronectin	Integrin $\alpha_5\beta_1$	(87)
	Proteoglycans	SR-A	(88)
	Collagen	DDRs, LAIR1, mannose receptor	(89–91)
	Laminin	Integrin $\alpha_6\beta_1$	(92)
	Hyaluronic acid	CD44, Lyve-1, TLR2, TLR4	(93–95)

Table 1: The many stimuli of macrophages: *Examples of different stimuli from pathogens and the host that influence macrophage activation state and phenotype. Adapted from Okabe & Medzhitov 2016* (47)*.*

1.4 Regulating the macrophage cytokine response

One of the fundamental outcomes of macrophage activation is the secretion of cytokines and chemokines to initiate the immune response. In addition to integrating a variety of stimulatory signals to increase their gene transcription driven by a transcription factors like NF-kB and AP-1 (Figure 4A) (96, 97), cytokines are heavily post-transcriptionally regulated to finely tune the strength, timing, and duration of the inflammatory response. This regulation starts at the mRNA level, through regulated mRNA stability and alternative splicing (Figure 4B). Most mRNAs have control elements within their 3' UTR (untranslated region) that interact with trans-acting RNA binding proteins to either recruit mRNA degradation machinery, or stabilize mRNA (98). For example, TTP binds numerous cytokines including TNFα and IL-6 at AU rich elements (AREs) and recruits the deadenylation complex Ccr4/Caf1-Not1 and the decapping enzymes Dcp1/Dcp2, whereas Human antigen R (HuR) binds AREs and U-rich elements (UREs) to stabilize mRNA (98). Cytokines, and particularly their receptors, also undergo alternative splicing (42, 99). Generally, in the case of the cytokines, this will result in a loss of function, acting as a decoy to reduce the inflammatory response (E.g. IL-6 loss of exon 2 or 4 to act as an antagonist). When the receptors are alternatively spliced, this will often result in a soluble version of the receptor which will play an important role in suppressing and resolving the cytokine response (99).

Once the mRNA has been translated, cytokines are then trafficked out of the cell via one of two main routes – classical secretion, or non-classical secretion (Figure 4C-D) (41, 100–102). During classical secretion, cytokines first are synthesized into the ER and travel to the Golgi where they will frequently undergo modifications such as glycosylation. From the Golgi, specifically the trans-golgi network, cytokines will then be loaded into pleiomorphic vesicles and recycling endosomes for constitutive exocytosis, or secretory granules for receptor mediated regulated exocytosis. Secretory granules are preformed stores of cytokines, chemokines and enzymes for rapid release after stimulation found in innate immune cells like mast cells and eosinophils. However, macrophages do not have secretory granules, but rather

to a lesser extent contain lysosome-related organelles (LRO) which constitutively export their contents to the cell surface. Instead, macrophages typically rely on regulation of mRNA stability to alter cytokine release and use constitutive exocytosis via small vesicles and recycling endosomes to immediately secrete them (101). Finally, in some cases like TNFα, after fusion of the secretory vesicle to the cell surface, a membrane bound precursor must be cleaved (by TACE/ADAM17) to release the final soluble form of this cytokine (40, 101).

Alternatively, cytokines can be released by a non-classical pathway. Examples of these are the IL-1 family of cytokines (IL-1α, -1β, IL-18, and IL-23) and MIF (101). These are not translated into the ER but are instead produced in the cytosol. These cytokines exit the cell via poorly understood routes. Proposed mechanisms include release via secretory lysosomes, budding of microvesicles, fusion of multivesicular bodies with plasma membrane to release exosomes, membrane transporters, and cell lysis during pyroptosis (103–105). In the case of IL-1β and IL-18, these proteins, like TNFα, also have an additional regulatory step, requiring cleavage of a precursor protein before release. This precursor is cleaved by caspase 1, part of the NLRP3 inflammasome, which in turn is only activated after a second signal, e.g. extracellular ATP, is received by the cell in addition to the original PAMP/DAMP (106, 107).

Finally, secreted cytokines will interact with their cognate receptors on target cells to induce an immune response (Figure 4E). Typically monomeric cytokine will interact with a homodimer of their cognate receptor to initiate intracellular signalling, although in some cases multimeric receptor-cytokine complexes will form (e.g. IL-6 signalling via gp130) or multimereric cytokine is required for specific signalling functions (e.g. TNFα) (108, 109). However, to regulate this, extracellular cytokines can be neutralized by soluble receptors formed by alternative splicing, proteolytic cleavage, or distinct gene transcription (110). Similarly, decoy receptors or antagonistic receptors on the surface of target cells can lack signalling capabilities or induce anti-inflammatory responses to limit an excessive cytokine response (106, 111). For example, IL-1β receptor IL-1R1 induces signalling, while IL-1R2 lacks signalling capabilities due to a missing TIR domain (106). Alternatively, receptor

antagonists can also be released alongside a pro-inflammatory cytokine such as IL-1RA which competes against IL-1α and -1β (112). Lastly, once bound to a surface receptor, extracellular cytokines are typically taken up by receptor mediated endocytosis. This endocytosis can result in the breakdown and prevention of further immune activation, but also is an important step for additional cytokine signaling effects, e.g. TNFR1 induced apoptosis (113, 114).

In all, regulation of cytokine production is a complex and multifaceted process requiring RNA regulation, protein cleavage, targeted secretion, and rapid uptake. Throughout this thesis I will use cytokine secretion as a readout for macrophage activation. I will touch upon this regulation when looking at regulation of the macrophage innate immune response both under different culturing conditions, and specifically after knocking out individual proteins. While the preliminary findings in this thesis do not explore them in depth here, many of these post-transcriptional regulatory mechanisms should be considered during future work that will come after this thesis.

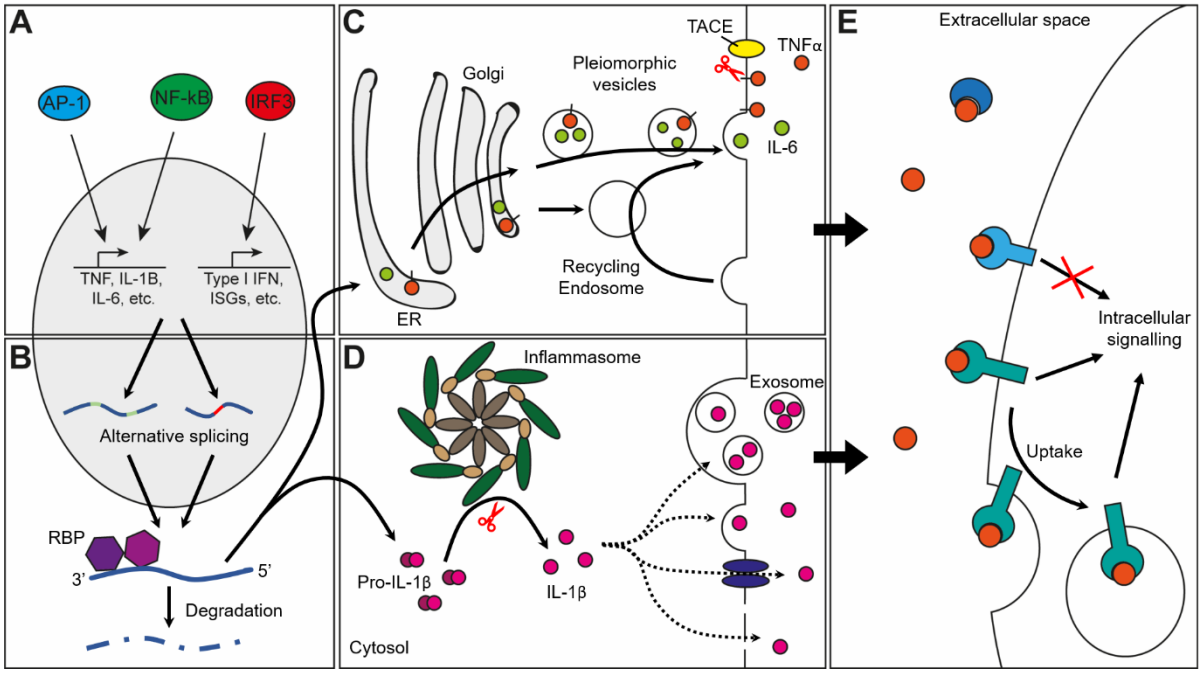


Figure 4: Regulation of cytokine secretion in macrophages: *A schematic of the cytokine production pathway and interaction with target cells. A) Transcriptional activation by pro-inflammatory transcription factors. B) mRNA regulation by alternative splicing and stability controlled by RNA-binding proteins (RBP). C) Secretion of cytokines via the classical secretory pathway. D) Secretion of cytokines via non-classical secretion pathways after cleavage of precursor protein by the inflammasome. E) Receptor interactions with secreted cytokines in the extracellular space or the cell surface by active (turquoise) or inactive (pale blue) receptors to induce intracellular signalling and receptor mediated uptake of cytokines.*

1.5 Induced pluripotent Stem Cells:

Pluripotent Stem Cells (PSC) are defined as cells that undergo self-renewal and can differentiate into all cell types of every tissue in the body. Unlike totipotent cells, they are incapable of additionally differentiating into extraembryonic cell types (e.g. the placenta). Their potential within biological research and medicine is almost immeasurable, offering up the ability to probe the precise mechanisms of any cell in the human body, find out what happens when specific disease relevant mutations occur, replace lost populations of cells in the body, and even possibly grow entire new organs, to name just a few applications. However, prior to 2006, PSC could only be sourced in one of two ways: somatic cell nuclear transfer (SCNT) into oocytes (115, 116), or isolation of embryonic stem cells (ESC) from blastocysts (117–119). Therefore, having been sourced from surplus cells used for *in vitro* fertilisation (IVF), use of human PSC from both methods obviously came with considerable ethical constraints, requiring either the destruction of an egg or pre-implantation embryo respectively. This all changed in 2006 and 2007 with the discovery by the lab of Prof. Shinya Yamanaka that just four factors are required to reprogram cells into PSC (120, 121). Retroviral vectors encoding for Oct3/4, Klf4, Sox2, and c-Myc introduced into fibroblasts were found to reprogram these cells into PSC highly similar to ESC. These induced pluripotent stem cells (iPSC) can differentiate into any cell of the three embryonic germ layers (endoderm, ectoderm, and mesoderm), can produce teratomas if transplanted into mice, and if inserted into a blastocyst, allow for development of a viable embryo. Soon after, the Thomson lab reported that c-MYC and KLF4 can be replaced by NANOG and LIN28 for reprogramming human somatic cells, and later on it was found that both c-Myc and Oct4 individually (but not together) can be removed from the cocktail without completely abrogating reprogramming (122–125). In the years following the initial discovery, an avalanche of research papers in this new field have described improved methodologies for introducing the reprogramming cocktail of factors into a variety of different somatic cells (from the skin, blood and even urine) and increase efficiency up to 100% of cells (126–136).

Using these new iPSC lines generated around the world, the exploration of human development and drive to reproduce every cell type in the human body has been unshackled and unleashed (Figure 5). Novel protocols are frequently being developed to differentiate iPSC into neuronal cells, cardiomyocytes, hepatocytes, gut epithelium, and even blood and platelets, to name a few (137–146). In turn, these models have brought new understanding to diseases ranging from inflammation driven Alzheimer's and Parkinson's disease, to muscular dystrophy and heart ischemia (147–151). Each advance brings us closer to new therapies as well as potentially using these iPSC themselves in cell therapy. However, there have been inevitably setbacks. From the outset of iPSC technology, it was noted that c-Myc was a powerful inducer of tumorigenesis, making these cells unsuitable for use in therapy (152). While overcome by removing c-Myc from the cocktail, the use of genome integrating vectors or plasmids (which can also integrate) again raised serious concerns regarding potential off target integrations driving cancer during potential therapies (153, 154). Sure enough, promising early findings of spinal injury repair using iPSC-derived neurospheres have been impaired by follow up studies showing increased formation of tumours depending on the iPSC clone use (155, 156). As each obstacle is overcome, new questions arise; are iPSC truly reprogrammed to a fully undifferentiated state? Precisely what cells are we differentiating them into? Are these differentiated cells embryonic-like, or adult-like? The answer to the first of these questions may in fact be no, as numerous papers have reported that iPSC tend to retain epigenetic features of their original somatic cell type, and this in turn appears to preferentially drive these iPSC to differentiate back into them if allowed (157–161). As for the other questions, each will depend explicitly upon the cell type of interest and the conditions used for differentiation; which developmental factors are used? At what time are they introduced? Are there other components of the differentiation media used that can influence development? For example, iPSC-derived β-cells have been found to be embryonic, not adult-like, potentially influencing their efficacy for cell therapy of diabetes (162). Similarly, proper modelling of Parkinson's disease, an age related condition, may require additional expression of Progerin

(an age related truncation of Laminin A) to better mimic an aging brain (150). Overall, there does not appear to be one correct method for any target cell type, but each will require close examination before reliable conclusions can be made using any chosen model.

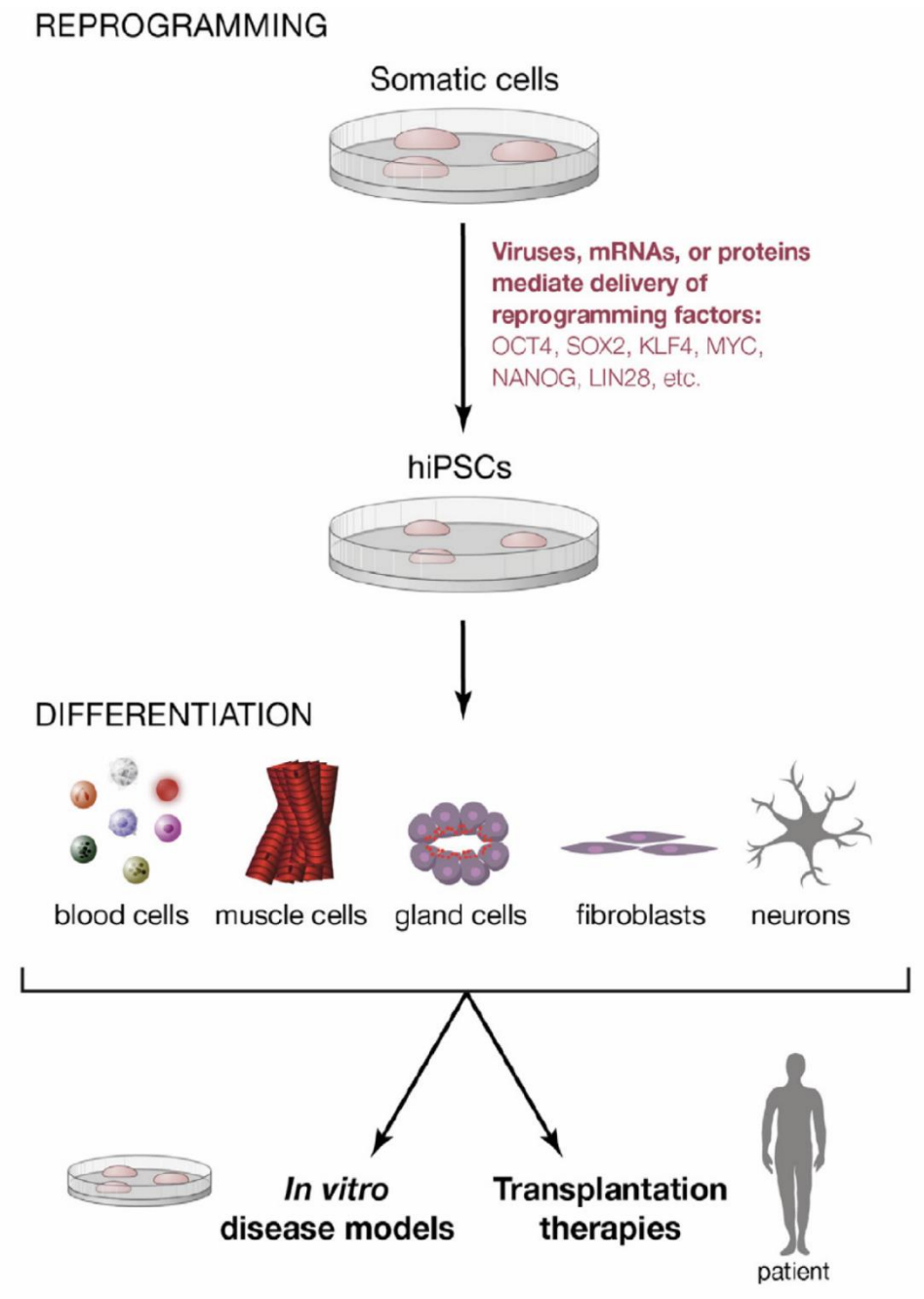


Figure 5: iPSC reprogramming and uses. *Overview of the factors used to reprogram cells into iPCS, and the cells they can then be differentiated into for disease studies and therapy. Adapted from Hockemeyer & Jaenisch* (153)

1.6 Differentiation of macrophages from iPSC

Soon after the derivation of ESC from blastocysts, protocols were developed for the differentiation of these cells towards the hematopoietic lineage, the end goal being to differentiate all types of blood cell. After nearly 4 decades of research in this field, a plethora of protocols now exist for the differentiation of T and B lymphocytes (163–165), macrophages (166) (for comprehensive list, see Chapter 3, Table 1), dendritic cells (167, 168), neutrophils (169–172), erythrocytes, and even platelets (173).

Initially, hematopoietic differentiation first required either the formation of an Embryoid Body (EB); a spherical culture of SC that have the potential to spontaneously differentiate into endoderm, ectoderm, and mesoderm (174, 175), or co-culturing with stromal cell lines such as OP9, S17, or C166 cells (176–178). Under these conditions, and in the presence of serum, SC can spontaneously differentiate into hematopoietic cells (174, 178). Extensive studies looking at the transcriptional profile of progenitor cell formation, overexpression of specific genes, and utilising targeted or trial and error approaches of media supplementation have since identified key genes, growth factors, and cytokines required for this haematopoiesis, extensively reviewed elsewhere (179–182). In summary, this differentiation can effectively be achieved by various combinations of the following growth factors and cytokines: SCF, BMP4, VEGF, Activin A, bFGF (also known as FGF-2), TPO, FLT3L, IL-3, IL-6, and G-CSF (183–191). Each of these factors have a particular purpose, such as supporting the proliferation of hematopoietic progenitors (VEGF)(189), or preventing their death (BMP4)(187). However, not all may be necessary, as Tian *et al.* showed that if hematopoietic cells are formed by coculture with OP9 cells, only SCF, FLT3L and TPO are necessary, while the feeder-free EB method additionally requires BMP4 and VEGF (188). Pearson *et al.* found that only BMP4, Activin A, bFGF, and VEGF are required for haematopoiesis (191), and more recently, Galat *et al.* even reported that none of them are required as long as WNT is activated using the drug CHIR99021 (185). Optimization of this process then is ongoing, with clear potential for better definition and simplification of the methods and media used.

Upon successful differentiation of hematopoietic cells, terminal differentiation into macrophages can be achieved through culturing cells in the presence of IL-3, GM-CSF and M-CSF (192). These factors have long been known to robustly drive macrophage differentiation, and M-CSF in particular is essential for macrophage survival (192). Alternatively IL-34, which also interacts with CSF-1R (the receptor for M-CSF), can be used in place of M-CSF and appears to be a key factor determining the microglia and Langerhans cell lineage versus a more general macrophage phenotype (192). As such, all terminal differentiation protocols have included some combination of these factors, while also occasionally including other cytokines such as IL-6, IL-1, and IL-11 (For comprehensive list see Chapter 3, Table 1) (166, 174, 178, 193–195). However, given that both IL-6 and IL-1β are pro-inflammatory, inclusion of these cytokines may be a questionable choice. Nevertheless, macrophages derived from SC have been shown to be fully functional, able to phagocytose, polarise in response to inflammatory signals, and be infected by known macrophage tropic pathogens (196, 197). Likewise, transcriptomics has shown that these cells closely resemble patient derived macrophages both pre- and post-stimulation, demonstrating them to be a suitable source of cells for studying macrophage biology (198).

1.7 Using iPSC-derived macrophages to study disease

MDM have been used for decades in biomedical research, and are a powerful tool for macrophage research, providing primary human tissue to probe for new scientific discoveries and confirm findings made in cell line and animal models. However, by the very nature of primary tissue culture, results generated from MDM are highly variable and require large numbers of independent donor samples to produce significant findings. Sources of variability in biological research are numerous. Some cannot easily be controlled for, such as stochastic differences in macromolecule availability or gene expression and can be viewed as mathematical probability functions (199). Others are routinely controlled for such as standardised culturing techniques and medium composition. However, with MDM, major sources of variation will come from the genetic background of the donor, their sex (200, 201), health, and even differences in sample isolation (202, 203). While monocytes/blood are typically taken from "healthy" individuals, we often have no knowledge of underlying genetic variations that may lead to development of late onset diseases like Alzheimer's disease. Furthermore, individuals' diets (e.g high in fat or protein (204, 205)), fitness (206), and daily routines (circadian rhythm (207, 208)) could all theoretically influence the number and phenotype of cells isolated due to differences in metabolite availability, hormone and cytokine levels, and cellular composition of the blood (e.g. more red blood cells in people who exercise more, or white blood cells soon after an un-symptomatic infection). It is in limiting these sources of variability that iPSC-derived macrophages show considerable promise. Having been reprogrammed, iPSC provide a more uniform baseline from which we can potentially generate reproducible, highly controlled, homogenous populations of macrophages for research with primary tissue cell-like physiology. While genetic variations remain a potential variable, as will be discussed shortly, this too can be controlled for by modern gene editing technology and whole genome sequencing to detect underlying risk factors.

Despite originally intended as a method to create blood monocytes in large quantities *in vitro*, analysis of macrophages differentiated from human SC (both ESC and iPSC) actually

more closely resembles the early embryonic YS stage of macrophage production, owing to their independence from c-Myb (34, 35). This means that SC-derived macrophages have emerged as a potentially powerful model of tissue resident macrophages. This has been advantageous for several reasons. Isolation of tissue macrophages is difficult in humans, requiring invasive and inflammatory procedures to isolate them. For example, alveolar macrophages are usually isolated from bronchoalveolar lavage fluid, and skin macrophages often drawn to a site of inflammation caused by administration of cantharidin, a secretion from blister beetles (209, 210). Tissue macrophages can also be isolated from autopsies and organ transplants, but at this point they are likely under stressed and/or diseased conditions, and extraction methods can alter function and phenotype (211, 212). Alternatively, tissue macrophages can be obtained from other animal species, most frequently mice, but yields are limited and frequently disease modelling in animals is not recapitulated in humans (213–216). Therefore, instead of using tissue macrophages, most macrophage studies have been carried out on MDM and BM-derived macrophages (BMDM). While acquiring these cells is easier, these cells would not normally be seen within a tissue until after initiation of an immune response and recruitment through cytokines and chemokines. They therefore may not accurately represent the patrolling and homeostatic functions of tissue resident macrophages prior to activation within their native environment.

In addition to increasing access to tissue specific macrophages, iPSC-derived macrophages also have the advantage of being able to be made from patients with hereditary diseases, and disease relevant genetic variations identified by genome wide association studies (GWAS) (216, 217). For example, iPSC-derived macrophages have been made from patients affected by Tangier Disease, a rare disease that can lead to neuropathy and cardiovascular disease. This study of the loss of function mutation in the cholesterol transporter ABCA1 showed that disease macrophages have a significantly increased inflammatory response to LPS compared to WT macrophages (198). Similarly, several labs have generated iPSC and then macrophages from patients suffering chronic granulomatous

disease (CGD), when granulomas form throughout the body due to impaired pathogen clearance through generation of ROS (197, 218). Macrophages derived from these patient lines likewise have an impaired ROS response, demonstrating the potential of these cells for modelling the disease *in vitro*, and screening candidate drugs and potential methods of genetic therapy (197). GWAS-identified variants of genes can also be studied in healthy cells, and in this regard the James lab has recently published works showing that mutations in LRRK2 (a Parkinson's disease risk factor) cause defects in macrophage phagocytic processes, and have begun to elucidate the impact of the R47H mutation in TREM2 (Alzheimer's related) on macrophage function, motility and adhesion (148, 149). In these reports on LRRK2 and TREM2, not only were patient specific cell lines made for comparison to wild type macrophages, but so too were iPSC genetically edited either for introducing the mutation, correcting it, or completely deleting the functional protein. With the discovery of new and powerful genetic editing methods, not only are iPSC-derived macrophages a good model for studying known disease relevant mutations, they can also be edited to study precise functions of proteins in previously difficult to alter cells.

1.8 CRISPR-Cas9

We currently live in an age of (relatively) easy methods for gene editing, especially since the discovery and application of the clustered regularly interspaced short palindromic repeats (CRISPR)-Cas9 bacterial endonuclease system (219–222). It is difficult to exaggerate the impact CRISPR-Cas9 genetic editing technology has had on biological research since its founding by Jennifer Doudna and Emmanuelle Charpentier in 2012, which has since earned them the 2020 Nobel Prize in Chemistry (220, 223). The ease and accessibility of the methodology has revolutionised genetic editing, fundamentally transforming our understanding of biological systems and opening up entire new fields of research and potential therapies. Very briefly, the CRISPR–Cas system is part of the prokaryotic antiviral immune system, causing targeted cutting of viral DNA and RNA sequences by the Cas protein after recognition by short CRISPR RNA (crRNA) sequences (224–227). crRNAs, also known as guide RNAs (gRNA), are approximately 20bp in length and will target nucleic acid sequences containing a PAM (protospacer-adjacent motif) specific to the Cas protein being utilised, the most famous of which being the 3-nucleotide NGG sequence corresponding to Cas9 cleavage (220, 227, 228). For a virus infecting a prokaryote, cleavage by the Cas protein will result in destruction of the viral genome, effectively terminating viral infection. However, by altering the sequence of the gRNA we can effectively redirect cleavage to almost any sequence within the genome as long as it contains the relevant PAM site (220, 229–231). This theoretically enables researchers to introduce changes into the human genome ranging from small insertions and deletions to the removal or replacement of entire genes. Genome editing is not new, as methods using site specific cutting by proteins called Zinc finger nucleases (ZFN) or transcription activator-like effectors (TALE) fused to an endonuclease Fox1, had already been invented (228, 232). However, it is the ease of use and flexibility of the CRISPR-Cas system that launched CRISPR-Cas editing to the preferred method of editing within the modern research lab, as demonstrated by an explosive growth of publications within the last decade referencing it (Figure 6).

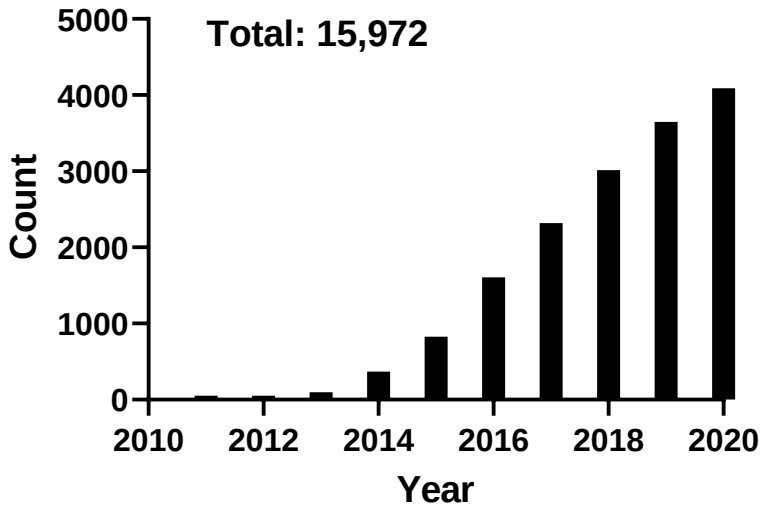


Figure 6: The explosion of CRISPR-Cas9 editing in biological research. *Number of manuscripts on the NCBI Pubmed database when queried for "CRISPR Cas9" between 2010-2020.*

1.9 Gene editing in macrophages and iPSC

Macrophages are considered difficult to genetically manipulate cells. This is primarily due to 2 reasons (233):

1) *They are almost entirely non-proliferating cells.*

   This decreases the likelihood of nucleic acids reaching the nucleus during mitotic breakdown of the nuclear envelope, thus reducing editing e.g., with repair templates to introduce specific mutations. It also means that producing a culture of 100% edited cells requires selective markers and large numbers of cells to compensate for the loss/death of unedited cells. Finally, this means making a pure, clonal, population of edited cells is impossible, as clones cannot be selected and expanded.

2) *Macrophages are programmed to recognise and neutralise foreign nucleic acids*.

   As shown in Table 1, macrophages express a large number and quantity of nucleic acid sensors as part of their antiviral function. In turn, this means introduction of plasmids, short hairpin RNA (shRNA), short interfering RNA (siRNA) and other common tools of genetic manipulation will be ineffective and result in activation of an inflammatory macrophage response.

Therefore, gene manipulation in macrophages has, until recently, relied on two primary approaches: 1) using immortalised/cancer macrophage cell lines like mouse peritoneal RAW264.7 cells and human monocytic THP-1 cells, or 2) using genetically edited mice as a source of macrophages. Naturally, use of cancerous lines is less than ideal, as these cells frequently have mutations/defects in principle immune signalling networks and cell death pathways that have developed as the tumour evolved to escape detection and death (234–236). Mice on the other hand are a more favourable model. Within mice, specific gene editing can be achieved using the loxP-Cre inducible system (237), and can be targeted to specific cells by co-expression of the Cre protein with lineage specific markers. However, this has

been found to not always be 100% cell-type specific, particularly in myeloid cells. Abram *et al.* demonstrated that co-expression of Cre with supposed macrophage specific *Csfr1* and *Cx3cr1* not only resulted in sometimes incomplete gene editing in these cells, but also collateral editing in a variety of other immune cells including mast cells, NK cells, T and B cells (238). Attempts then to make "good" macrophage specific deletions is ongoing, frequently beset by these off target limitations (239, 240).

Overall, studies in mice must always inevitably be recapitulated in humans somehow. A current popular methodology for ablating gene expression in macrophages is using shRNA introduced by lentiviral vector under puromycin selection (241, 242). However, this only provides a knock-down (KD), not a knock-out (KO) of genes targeted. Recently, great progress has been made in CRISPR editing of primary macrophages. Efficiency of lentiviral transduction methods has improved by overcoming cytoplasmic nucleotide depletion by SAMHD1 using virions containing the HIV-2 accessory protein Vpx (241, 243–245), enabling up to 100% transduction efficiency in primary monocytes and macrophages (244). Alternatively, gRNA and Cas9 protein can be introduced as ribonucleoprotein complexes (RNPs) to overcome detection by nucleic acid sensors and endogenous nucleases (246–251). If introduced by electroporation, >90% editing efficiency can be attained, although precise optimisation of voltage and buffer used is needed (246). Alternatively, RNPs can be introduced by nanoparticles with around 8-20% editing efficiency (247, 250, 251). While this is low, it has been demonstrated as a potential method for *in vivo* editing and is therefore of interest therapeutically. One of the main problems though with all these advances is that they result in pools of edited cells, not clonal populations. This introduces variability and in effect potentially only achieves similar results to use of KD methods. Making inducible immortalised macrophages that express Hoxb8 has been proposed, which would allow for clonal selection and infinite production of edited macrophages (252). However, these would be unviable as a therapeutic method and questions could be asked as to whether they still accurately represent macrophages.

We therefore must find some sort of alternative to editing primary macrophages. One approach would be to edit macrophage progenitors, providing a replicative/infinite source of specifically modified macrophages. Editing of Haematopoietic Stem Cells (HSC) has been shown to be a feasible method for altering gene expression, e.g. glucocerebrosidase induction for treating Gaucher disease, prior to differentiating into macrophages (253). However, HSC produce monocytes and thus only works for MDM, not tissue macrophages. Therefore, it may be better to go yet further back in terms of macrophage development, by targeting pluripotent stem cells. Editing in iPSC overcomes all the limitations of editing macrophages. Their infinite proliferation potential and their lack of expression of nucleic acid sensors makes for easy editing, and successfully edited cells can be made into clonal populations simply through expansion of single cell colonies. These can then be stored indefinitely in liquid nitrogen and be used to make large numbers of clonally edited macrophages. Better still, we can now create co-culture systems of edited and unedited cells of different lineages (e.g. macrophages, astrocytes, and neurons) and can explore gene functions in models of specific organs and diseases more closely reflecting *in vivo* conditions than ever before (254).

By combining CRISPR-Cas9 technology with advances in iPSC differentiation into tissue macrophages, we now find ourselves at the dawn of a new era in research into innate immune cell function and regulation. In this thesis, I will be utilising these new opportunities to interrogate gene functions in specific disease scenarios, specifically HIV-1, and more broadly looking at the regulation of the innate immune response.

1.10 HIV, macrophages, and iPSC

Due to their distribution throughout the body, tissue resident macrophages play an essential role in the early detection and response to invading pathogens. However, being at the front line also makes subversion of macrophages an evolutionarily successful strategy for pathogens, and several have evolved to target macrophages as one of their primary host cells. This includes bacterial infections like *M. tuberculosis* in the lungs, Zika and Dengue viruses (ZIKV and DENV) in the skin, and Human immunodeficiency virus (HIV)-1 in the mucosa. In addition, as these diseases disseminate throughout the body, they can also infect macrophages in remote and difficult to access compartments, such as the brain and heart. This makes them difficult to clear with therapeutics and can in-turn lead to chronic diseases such as cardiac disease and HIV-associated neurocognitive decline (HAND) (255–258). Given then the importance of tissue macrophages in pathogenic disease progression, iPSC-derived macrophages offer themselves as an ideal model to better understand host-pathogen interactions, as well as trial novel approaches to therapy. For example, use of iPSC-derived macrophages has shown that ZIKV, unlike DENV, is able to suppress the induction of inflammatory cytokines and chemokines through disruption of the NF-kB-MIF positive feedback loop, potentially explaining why a cytokine storm and haemorrhagic fever is only seen after DENV infection and not ZIKV (259).

In this thesis, I will apply our iPSC-macrophage system to interrogate early events during HIV-1 infection. HIV-1 is a retrovirus of the lentivirus family that primarily infects CD4+ T cells through interaction with the receptors CD4, CCR5, and CXCR4 (260). An overview of the viral life cycle is shown in Figure 7. Monocytes and macrophages also express these receptors and are therefore also susceptible to infection (261). Monocytic cells only account for approximately 4% of all HIV DNA within the body, but because they populate all the tissues of the body, and particularly the mucosal regions, they play an important role in disease establishment and progression (262). Macrophages in the mucosa (e.g. the rectum), despite being resistant to infection by the very first founder viruses of infection (263), are infected

within the first few days of infection (258), likely through transfer of virus across a virological synapse between macrophages and T-cells or though engulfment of infected T-cells (261, 264, 265). Within 14 days of initial infection, tissue macrophages throughout the body, including the brain, become infected (258, 260, 266, 267). It is believed that these tissue resident cells can then become a reservoir for the virus (258, 267–270). Unlike T-cells, macrophages are resistant to the cytopathic effects of HIV-1 infection, and their ability to self-maintaining their population while inhabiting difficult to access *loci* provides a barrier to viral clearance by anti-retroviral therapy (ART) (271–273). For example, the blood brain barrier (BBB) blocks entry of many drugs, and it is still unclear whether current therapeutics reach microglia at a sufficient concentration to effectively inhibit/eradicate the virus (270). Further more, different tissue macrophages have different susceptibilities to HIV-1. For example, alveolar macrophages are more susceptible to infection than gut macrophages (261). If we are to effectively eliminate this virus, a better understanding of its lifecycle in tissue macrophages is therefore clearly needed.

Infecting cells of the immune system has its difficulties. Macrophages express high levels of antiviral sensors and interferon stimulated genes (ISGs) to prevent and eradicate viral infections (271–273). These include surface proteins like tetherin (CD317) which retains budding viral particles at the plasma membrane (like a tether) (274), cytoplasmic inhibitors of reverse transcription like the cytidine deaminase APOBEC3G and the deoxynucleoside triphosphate phosphohydrolase (dNTPase) SAMHD1 (275, 276), DNA sensors like cGAS and IFI16 (277, 278), capsid binding proteins like TRIM5α and MX2 (279, 280), and stimulators of the adaptive immune response like MHC class I and II molecules. To parry these defences of the host, the virus has evolved accessory proteins; Vpr, Vpu, Vif, and Nef, to impair and degrade these factors (260). These accessory proteins are highly promiscuous in their effects on the host intracellular environment, inducing cell cycle arrest (281, 282), both inhibition and activation of innate immune signalling via NF-kB and IFN (260, 283–285), inhibition of apoptosis (267, 283), and targeting over 38 different proteins for ubiquitin mediated

degradation (283). However, the viral genome is only so big (around 9 kb) and can only fit a few of these proteins. It therefore is not provided the luxury afforded to larger DNA viruses that can have over 200 accessory proteins to specifically target every important pathway in the host cell (e.g. vaccinia virus and cytomegalovirus) (286, 287). Instead, in some cases it has evolved to be less susceptible to the effect of host proteins, like increasing reverse transcriptase efficiency in low dNTP environments caused by SAMHD1 or mutating its capsid to reduce affinity for TRIM5α (288, 289). In others, it uses host proteins to act as immunological invisibility cloaks. For example, the endonuclease TREX1 protects the virus from detection by cGAS by removing excess reverse transcribed genome (289). Similarly, Cyclophilin A (CyPA) and CPSF6 both protect from innate sensing within macrophages, interacting with the viral capsid proteins to regulate reverse transcription, viral trafficking within the cell, and nuclear entry (289–293).

A key component of HIV-1 for regulating post-viral entry events is the viral capsid. The capsid forms the cone shaped (fullerene) core made up of ~250 hexamers and 12 pentamers (Figure 8A) (294). The capsid protein interacts with a range of host proteins to regulate trafficking to the nucleus, nuclear entry, reverse transcription, and integration (for good reviews on the capsid see (294–298)). Studying precise mechanisms regulating capsid stability and eventual uncoating are intrinsically difficult due to cell-type variability and distinction between successful viral infection and abortive viral particles (only ~1:50 particles within a cell result in successful infection (299, 300)). For a long time, capsid uncoating was thought to occur immediately post-viral entry (295, 301, 302). However, this would seem a highly risky method of entry, exposing the genome to cytoplasmic nucleic acid sensors. Moreover, it left unexplained how the viral genome could enter the nucleus of non-dividing cells (303, 304). Instead, more recent research indicates that it remains intact up to and possibly after entry into the nucleus, thus protecting the genome and possibly explaining roles of the capsid in nuclear entry (299, 305–308).

The capsid protein monomers are arranged as hexamers with a central pore in the middle, and each vertex interacts with 3 other hexameric complexes (Figure 8A)(294). Latest reports suggest the pore acts as a regulator of reverse transcription by allowing entry of nucleotides while excluding restriction factors (309, 310). At each tri-hexameric interface is an exposed proline loop between helices 4 and 5 in the N-terminal domain, ~13 amino acids in length, also known as the CyPA loop (Figure 8B & C) (298). The precise role of this CyPA interaction here is still being elucidated, but in addition to protecting against an interferon response (290), CyPA is described to regulate capsid stability and reverse transcription (311–315). Furthermore, mutations within the CyPA loop alter viral nuclear entry and integration, suggesting a potential for CyPA regulating these functions also (291, 316). CyPA binds glycine-89 (G89) and proline-90 (P90) via its catalytic cyclophilin domain but it is unclear whether it catalyses the transformation of this proline between a *cis* or *trans* conformation (for more information on cyclophilin activity see Chapter 6.1 Introduction) (317, 318). In addition, CyPA was recently described to interact with this loop via 2 more non-canonical interaction sites, which may be important for capsid stabilization (Figure 8D) (311). Including P90, neighbouring amino acids are also important for CyPA interactions. Notable of these are A92 and G94 which can be mutated to make the virus resistant to the effects of the CyPA inhibitor cyclosporine A (CsA) (319).

As well as CyPA, other host proteins can interact with this exposed loop. Some benefit infection, such as the nucleoporin Nup358 (291, 320–322), while others restrict it, like Mx2 and TRIM5α (Figure 8E) (279, 323–327). For this thesis, a particular interest is taken in TRIM5α. Within human cells, TRIM5α is a curiosity. Its interaction with HIV-1 CA had long been believed to be species dependent, with human TRIM5a unable to directly recognize the capsid (see Chapter 5.1 Introduction for more information) (328). However, recent work including that contained within this thesis would dispute this, and instead point to a connection between CyPA-CA interactions and TRIM5α function (242, 329). Several hypotheses of how TRIM5α restricts HIV-1 have been proposed and yet no clear answer has been discovered.

Current consensus would appear to be that TRIM5α primarily triggers early uncoating of the viral core and dysregulation of reverse transcription (330, 331). Ultimately this leads to activation of the innate immune response via cytoplasmic sensors, such as cGAS and IFI16 (332–334). It has long been known that uncoating may involve targeting of the viral CA to the proteasome via the E3 ubiquitin ligase activity of TRIM5α, or more recently a specific form of proteasome called the immunoproteasome after interferon induced increased TRIM5α turnover (335–341). However, inhibition of the proteasome has only been reported to rescue reverse transcription and not viral infectivity (341). Lastly, there have been reports of TRIM5α displaying regulatory activity of NF-κB and AP-1 signalling via TAK1. As well as aiding the induction of an antiviral state via type I interferon (IFN) production, this may directly inhibit viral infection (342–344).

It is clear then that there is much to be unravelled about the precise roles and mechanisms of both CyPA and TRIM5α during HIV-1 infections. To do so though will require knocking out both proteins in primary, disease relevant, cells to provide the most accurate and precise picture of these. iPSC-derived cells have already been applied for HIV-1 research to demonstrate the feasibility of editing macrophages for gene therapy by targeting the viral promotor, CDK2, or CCR5 (345–347). More recently they have also been used to study the viral life cycle, using CRISPR-Cas9 editing to interrogate the finetuning of HIV-1 replication by USP18 (348), and are being evaluated as models for HIV-1 infection in the brain (349, 350). In this thesis, I too will apply iPSC-derived macrophages to unravel the mysteries of HIV-1 infection. Using CRISPR-Cas9 editing, I will explore the finer details of how CyPA regulates and protects the virus during entry into the cell, and in turn reveal how this influences restriction by TRIM5α, SAMHD1, and TREX1.

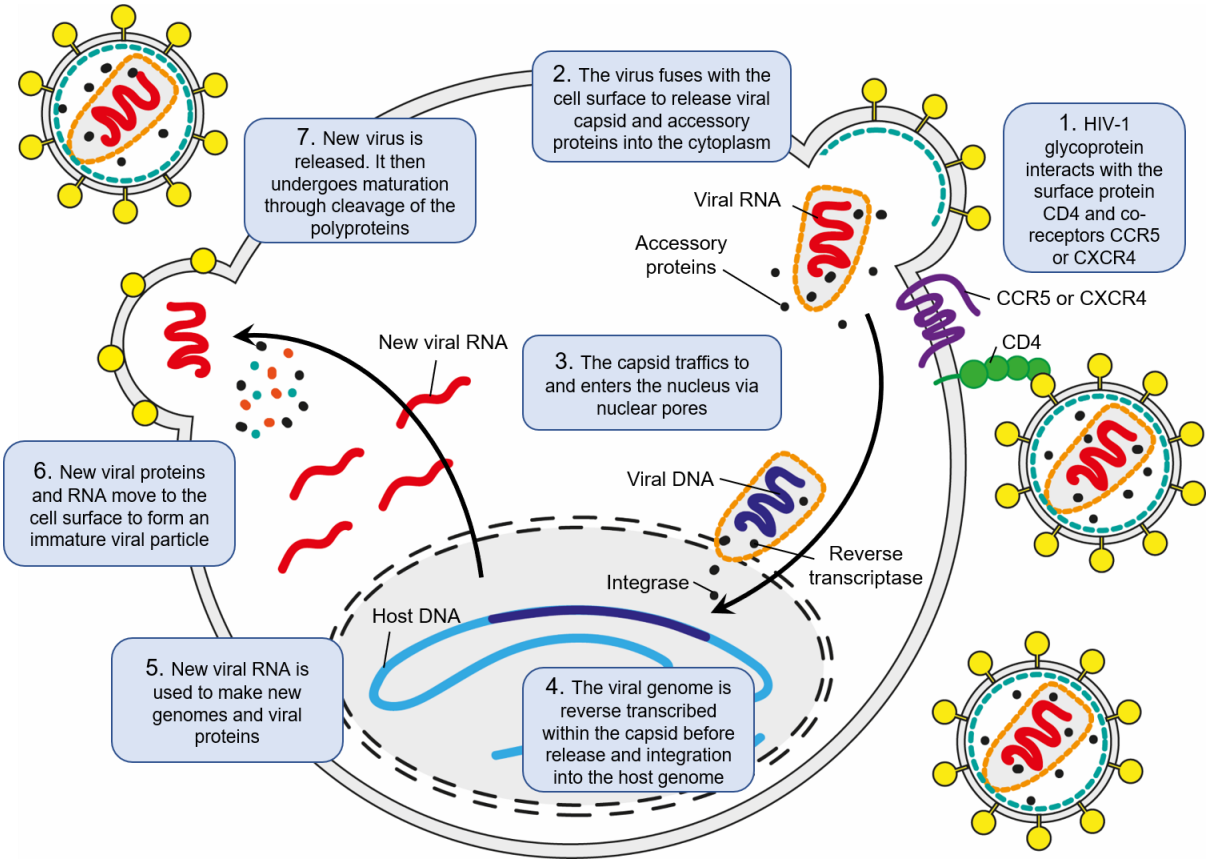


Figure 7: The HIV-1 replication cycle. *A simplified schematic of the HIV lifecycle within a cell. Precise timing and location of viral genome reverse transcription and capsid uncoating is still a matter of some debate. Previous models proposed this took place within the cytoplasm soon after viral entry, but latest research would suggest reverse transcription may actually occur within the capsid, and not until after entry of the complete capsid into the nucleus (299, 351). This schematic has been based on the schematic from the NIH and updated to reflect recent advances. (https://www.niaid.nih.gov/diseases-conditions/hiv-replication-cycle - accessed 20/02/2021)*

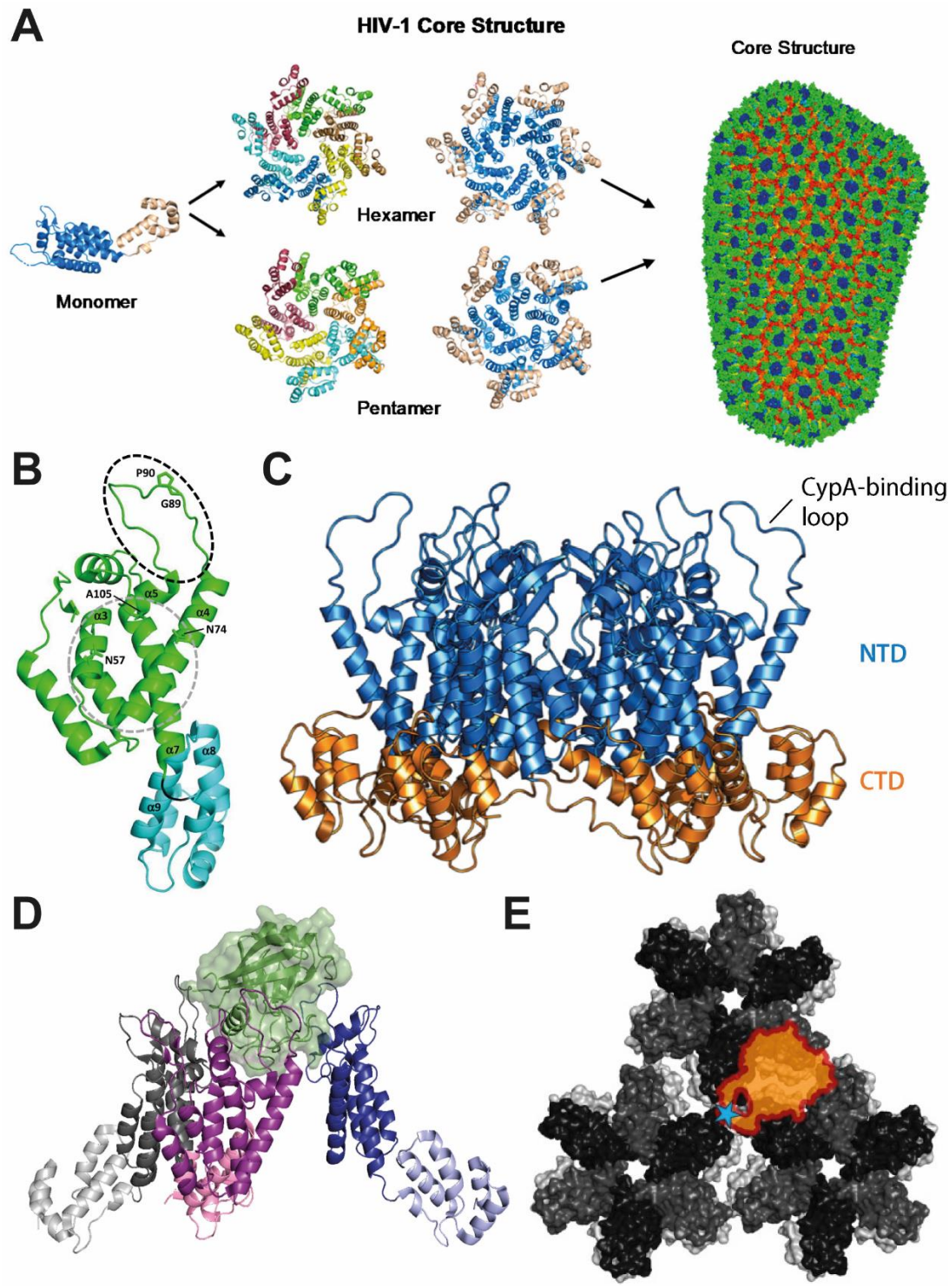


Figure 8: HIV-1 Capsid structure and interaction with CyPA and TRIM5α *A) Structure of the HIV-1 fullerene core, assembled out of capsid monomers arranged as hexamers and pentamers, as depicted by Rossi et al. 2021 (294). B & C) The capsid CyPA loop. B) From Yamashita and Engelman 2017 (352) where CyPA/Nup358 interaction site has been highlighted by a dashed black oval, and the CPSF6/Nup153 interaction site in a grey dashed*

circle. Green is the N-terminal domain (NTD) and cyan is the C-terminal domain (CTD) C) From James and Jacques 2018 (298) showing a side view of a hexamer and the relative positioning of the CyPA loop within it. D) Schematic of CyPA (green) interaction with 3 adjacent monomers of capsid from 3 independent hexamers (grey, purple, and dark blue), enabled due to the intrinsic curvature of the capsid (REF) taken from Rossi et al. 2021 (294) E) Overlay of TRIM5α binding region (orange) between adjacent hexamers. Blue star indicates the location of a proline residue in Rhesus Macaque TRIM5α that determines species specificity of HIV-1 restriction by TRIM5α. Adapted from Morger et al. 2018 (326).

1.11 Using iPSC-derived macrophages to study the cyclophilins

So far, I have discussed how iPSC-derived macrophages offer an ideal model for unstimulated tissue macrophages, which can readily be genetically altered using CRISPR-Cas9 at the iPSC stage. In turn this enables us to ask specific questions about genes identified by largescale GWAS screens and their role in macrophage functionality. With both iPSC culture and CRISPR editing becoming cheaper and easier to manage, the time seems right to push the use of edited iPSC-derived macrophages into more exploratory waters, looking at genes not simply identified due to known disease phenotypes.

As stated earlier, CyPA is a host protein utilized by HIV-1 to protect itself from the immune response. However, CyPA is just one member of a very large family of proteins found in all kingdoms of life (353). Numerous homologues are found in multicellular organisms, with as many as 29 members in plants (*Arabidopsis)* and 17 in humans (354). In single cellular organisms their numbers are fewer, with 8 in yeast (*Saccharomyces*), 1-4 in the *Streptomyces* bacteria (355), and 2 in *M. Tuberculosis* (356). One has even recently been reported in the *Mimivirus* species of giant viruses (357). The shared structural homology of these proteins can impede investigations into specific cyclophilin functions, as pharmacological inhibition (primarily by Cyclosporine A (CsA)) of one will result in the impairment of others. Therefore, proper investigations into the functionality of cyclophilins absolutely requires genetic editing to isolate each individual member of the family.

Viruses are masters of using our own proteins against us, repurposing them to completely alter the structure and function of cells and directly protect themselves. There is considerable data on viruses interacting with cyclophilins, with a majority being protective for the virus, but in some cases (e.g. influenza and rotavirus) these can be inhibitory for viral replication (358–362). Why viruses routinely interact with cyclophilins is unclear, as cyclophilins can interact with all stages of the viral life cycle and do not have a single common effect on infectivity (Figure 9). Therefore, one hypothesis can be that viruses interact with cyclophilins to sequester them away from the innate immune response. In support of this,

CyPB is reported to influence IRF3, a major component of antiviral sensor signaling (363). CyPA has been described as a key regulator of signaling by the RNA sensor RIG-I by both stabilizing the effector MAVS while simultaneously increasing RIG-I interaction with TRIM25 to aid RIG-I recruitment to MAVS (364). More recently, my collaborators Prof. Greg Towers and Dr Lucy Thorne from University College London have evidence to suggest that CyPA may influence IRF3 and NF-κB signaling downstream of the DNA sensor cGAS in immortalized macrophage cell lines. Even within the duration of this thesis investigation, Cyclophilin J (*PPIL3*) was reported to modulate TLR intracellular signaling, indicating clear precedent for cyclophilins regulating the broader immune response (365).

Therefore, removal of these genes in iPSC-derived macrophages is of interest to determine if other cyclophilins can influence the innate response. Not only is this important to broaden our understanding of innate immune regulation, but also because 12 of the 17 human cyclophilins are inhibited by the drug CsA (366). This drug is a powerful immunosuppressant routinely prescribed for organ transplants and autoimmune conditions (367). In fact, the number of diseases being treated with this drug is increasing, being used in over 200 clinical trials between 2014 and 2016 (368). However, it can also cause paradoxical and severe side effects, particularly renal damage, and the causes of these are unclear (369). Off-target deregulation of the innate immune response by cyclophilins could therefore be partially or totally responsible. To help solve this, in this thesis I set out to interrogate the function of not just 1, but 8 members of the cyclophilin family within macrophages, looking at how they influence the response to bacteria, fungi, and viruses.

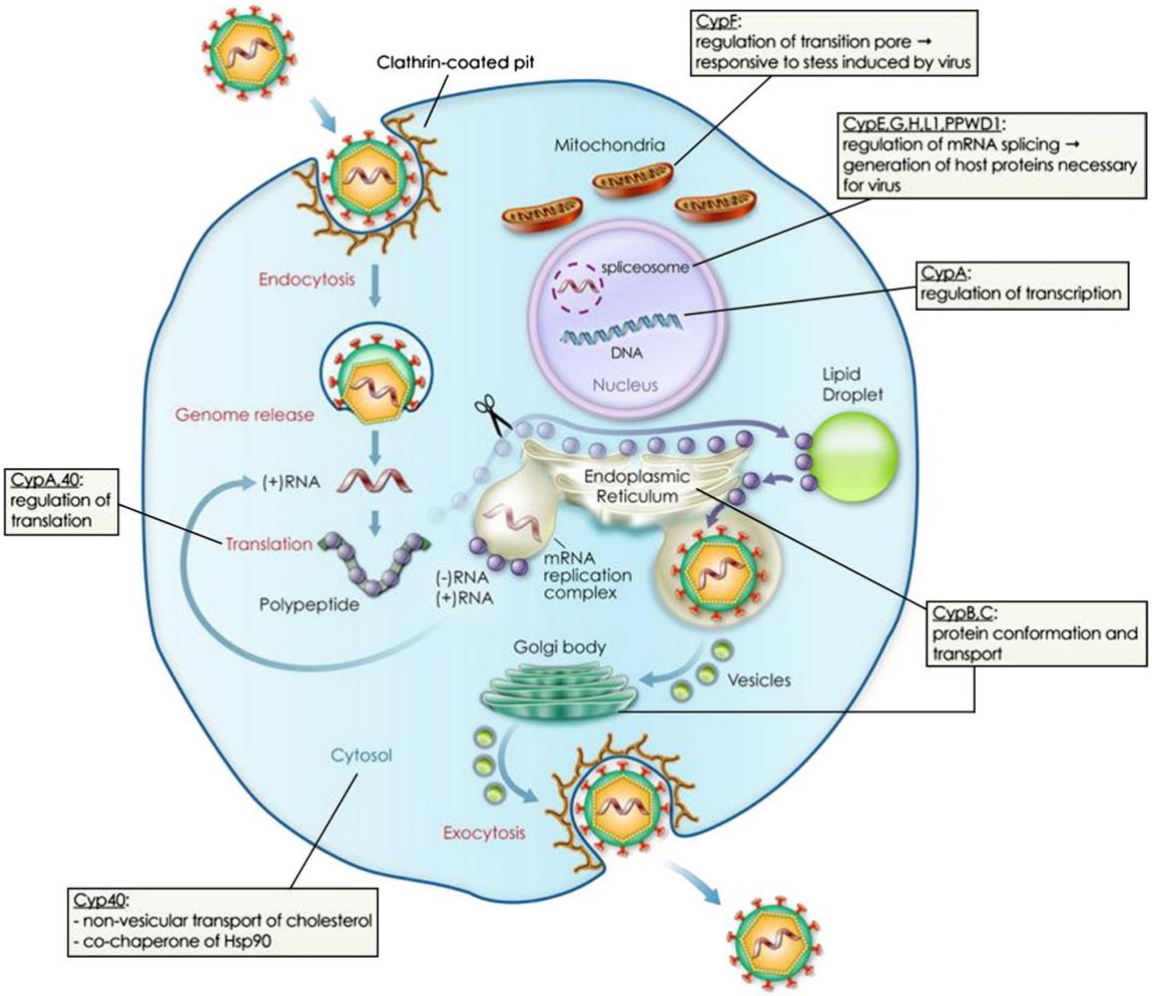


Figure 9: Localization and potential interactions with cyclophilins in the viral life cycle.

Schematic of cyclophilin-mediated pathways that play a role in maintaining viruses, particularly HCV, adapted from Gaither et al. 2009 (360)

1.12 Scope of work

Given the variety of macrophage types within the body, and the importance of environmental cues, stimuli, and culturing conditions in influencing macrophage phenotype and function, new and clearly defined models of macrophages are needed if we are to improve our understanding of these cells. In this regard, iPSC-derived macrophages offer themselves as an ideal system to work with. Their potentially infinite abundance of genetically identical cells and tissue macrophage ontology opens new frontiers in macrophage research. In addition, this system is now well enough established and accepted in the macrophage research field that we can apply them to investigate specific diseases and start to use them more routinely for exploratory studies.

As such, this thesis is set out to broadly achieve two main aims.

1) Improve our culturing of iPSC-derived macrophages, better defining the conditions within which they are grown, and what impact this has on their morphology, phenotype, and function.

2) Using CRISPR-Cas9 genome editing, investigate the role of a specific proteins, in particular CyPA, in macrophages during HIV-1 infection and the innate immune response.

Part 1 can be further divided into two parts. In chapter 3, I will describe a new medium in which to culture cells. This medium is relatively simple, defined, serum free, and open-sourced. I will compare this to our prior culture medium which, while fully defined, is not open-sourced. In chapter 4, I will then look in more depth at the environment in which macrophages are cultured, looking specifically at the impact cell crowding has on macrophage phenotype and function.

Likewise, part 2 can also be divided into two parts. In chapter 5, I will characterise in depth how CyPA protects HIV-1 from restriction by the host proteins TRIM5α, SAMHD1, and TREX1, while also introduce evidence for an alternative function of CyPA in regulating viral

reverse transcription. Finally, chapter 6 will explore more broadly the role CyPA plays in regulating the macrophage immune response. This will be alongside other members of the cyclophilin family, with the hypothesis being that multiple members of the family are able to regulate the inflammatory response.

Chapter 2:

Materials and Methods

2.1 Cell culture

2.1.1 Cell line culture

HEK-293T, HeLa based TZM-Bl luciferase reporter, and Vero 76 cell lines were all maintained in DMEM high glucose (hgDMEM) (Sigma, D6429-500ML) supplemented to 10% v/v FBS (Sigma, F9665-500ML) and 1% v/v Penicillin-Streptomycin (P/S) (Gibco, 15140122). During plaque assays and infectivity assays, Vero cells were maintained in hgDMEM supplemented with 1% v/v FBS and 1% v/v P/S. All cells were cultured at 37°C 5% CO_2. HEK-293T cells were lifted with TrypLE™ Express Enzyme (Gibco, 12604013) for 2 minutes at 37°C. Vero cells were lifted with TrypLE™ for 5 minutes at 37°C. TZM-bl reporter cells were lifted with 10mM EDTA for 1 hour at room temperature (RT). All cells were pelleted by centrifugation at 400g for 5 minutes at 4°C prior to resuspension.

2.1.2 IPSC lines

The derivation and characterisation of the iPSC lines used for this work is described elsewhere: SFC840-03-03 (370), SFC841-03-01 (371), SFC856-03-04 (372). All lines were derived from dermal fibroblasts from disease-free donors recruited through StemBANCC (373) and the Oxford Parkinson's Disease Centre: participants were recruited to this study having given signed informed consent, which included derivation of hiPSC lines from skin biopsies (Ethics Committee: National Health Service, Health Research Authority, NRES Committee South Central, Berkshire, UK, who specifically approved this part of the study (REC 10/H0505/71)). The iPSC lines were all derived using non-integrating Sendai reprogramming vectors (Cytotune, Life Technologies), cultured in mTeSR™1 (StemCell Technologies), on hESC-qualified Matrigel-coated plates (BD), passaging as clumps using 0.5 mM EDTA in PBS (374). Large-scale, low-passage frozen SNP-QCed batches were used for experiments to ensure consistency.

2.1.3 iPSC culture

iPSC were provided by the James Martin Stem Cell facility. Cells were stored long term in liquid nitrogen (LN). Cells were thawed into 10ml Advanced-DMEM/F12 (Gibco, 12634028) and centrifuged at 400g for 5 minutes at 15°C before resuspension in either mTeSR™1 (StemCell Technologies, 85850), Essential 8™ (Gibco, A1517001), or OXE8 (Table 1) supplemented with 10µM Y-27632 (ROCKi) (Abcam, ab120129) for the first 24 hours of growth after plating. Cells were plated on Geltrex™ (Gibco, A1413302) -coated plates. Cells were cultured at 37°C, 5% CO_2 with 100% media changes every 24 hours. When cells were 80-90% confluent they were passaged by lifting either with TrypLE™ for 3-5 minutes at 37°C to achieve a single cell suspension, or as clumps by 2-4 minutes with 0.5mM EDTA in phosphate buffered saline (PBS) at 37°C. Cells in single cell suspension were supplemented with 10 µM ROCKi for 24 hours after re-plating.

Media	Component	End Concentration	Supplier	Catalogue number
OXE8	Advanced DMEM/F12	97.4%	Gibco Thermo Fisher	12634010
	GlutaMAX (100x)	2 mM	Gibco ThermoFisher	35050-038
	Herparin solution 0.2%	100 ng/mL	STEMCELL™	07980
	Ascorbic Acid-2-phosphate magnesium salt	0.22 mM	Sigma Aldrich	A8960
	HEPES 1M pH 7.4	15 mM	Gibco ThermoFisher	15630080
	FGF-2 basic 145aa	100 ng/mL	Bio-Techne (R&D Systems)	4114-TC-01M
	TGF-beta	2 ng/mL	Peprotech	AF-100-21C
	30% human serum albumen (HSA) in water, filter-sterilized (used as buffer for FGF-2)	0.001%	Sigma	A9080-10ML

Table 1: composition of iPSC culture medium

2.2 Genome engineering

2.2.1 CRISPR-Cas9 editing

CRISPR-Cas9 was used to generate homozygous knock out (KO) clone iPSC lines. Guide RNAs (gRNA) are listed in Table 2.

TRIM5α KO: To KO TRIM5 and create the 639 wild-type (WT) control line, a lentiviral CRIPSR vector was used. gRNA Oligos used targeted exon 2 of TRIM5. Lentiviral vector plasmid was prepared as previously described (375). Briefly described; The lentivector plasmid pLentiCRISPRv2.0 (gift from Feng Zhang, Addgene plasmid #52961) was digested and dephosphorylated by incubation with *BsmB*I for 30 minutes at 37ºC followed by gel purification and extraction with the QIAquick Gel Extraction Kit (QIAGEN, 28704). Meanwhile gRNA oligos were phosphorylated and annealed by incubation in T4 ligation buffer (NEB, M0202S) and T4 PNK enzyme (NEB, M0201S) for 30 minutes at 37ºC, then 95ºC for 5 minutes followed by ramp down at 5ºC/minute to 25ºC. Oligos were diluted 1:40 with H_2O before ligating into the plasmid backbone using the Quick Ligation™ Kit (NEB, M2200S). The resulting lentivector plasmid was transformed into Stbl3 bacteria for amplification and used to make VSV-G enveloped lentiviral pseudovirus as described in 2.5.2 Production of Lentiviruses. SFC840-03-03 iPSC were transduced, and 24 hours later subsequently selected with 1µg/mL puromycin (Sigma, P8833-25MG) for 7 days before single cell cloning on mouse embryonic fibroblasts (MEFs) as described below.

Cyclophilin KO: To KO members of the cyclophilin family and their surface receptor CD147/*BSG*, a ribonucleoprotein (RNP) CRISPR-Cas9 system from IDT™ was used. Design of gRNA and rationale behind the methodology used is described in Chapter 6. iPSC were transfected with the CRISPR-Cas9-RNP complex according to manufacturer's instructions (376) adapted for stem cells. These adaptations are; adding 10 µM ROCKi to the cells 1 hour before lifting, Lifting by incubation for 3 minutes at 37ºC with 0.5 mM EDTA followed by a further 4 minutes at 37ºC without EDTA for gentle lifting as a single cell suspension, centrifugation steps at 400g for 5 minutes, $2.2x10^5$ cells/electroporation, electroporation by

1400v for 20ms 1 pulse, and plating cells into 1 well of a 24-well plate coated with Geltrex™ in 500 µL mTeSR™1 supplemented with 10 µM ROCKi for 24 hours. Once confluent, cells were passaged onto MEFs for single cell cloning.

To select clones, single iPSC were plated onto CF1 MEFs. MEFs were plated 24 hours prior on gelatin-coated 6-well cell-culture plates at $3.0x10^5$ cells/well in hES medium (KO DMEM (Gibco, 10829), 20% v/v KO Serum replacement (Gibco, 10828), 1% v/v NEAA (Gibco, 11140), 1% v/v GlutaMAX, 1:1000 2-ME, 1% v/v P/S and 5 ng/mL bFGF (R&D, 234-FSE/CF). iPSC and MEFs were first pre-treated for 1 hour with 10 µM ROCKi in before lifting the iPSC with TrypLE™ and plating on top of the MEFs at $2x10^3$, $4x10^3$, and $8x10^3$ cells/well in hES media supplemented with 10 µM ROCKi. Cells were then cultured for ~6-8 days with daily 50% media changes. Once colonies of clones were visible and large enough for picking, hES media was exchanged for mTeSR™1 media for 1 hour before individual colonies were scraped off using a 200 µL pipette and plated in mTeSR™1 into a 96-well plate precoated with Geltrex™. Clones were then cultured a further ~6-7 days until nearly confluent before passaging 1:2, lifting with 0.5 mM EDTA for 5 minutes at 37^{o}C, into 2x96-well plates for further culturing for another ~3-4 days before a second 1:2 passage. This gave 2 plates of clones to be used to extract DNA for KO screening by PCR/sequencing, and 2 plates for freezing in 60% FBS (ES cell qualified, Sigma, ES-009-B), 20% mTeSR™1, 20% Dimethyl sulfoxide (DMSO) and storage in LN. Once desired clones were identified, cells were thawed from the 96-well plate into a 96-well v-bottom plate and washed with PBS before resuspension in mTeSR™1 supplemented with ROCKi and plated onto a Geltrex™-coated plate. Cells were expanded in number over 2-3 passages to create a master stock to be frozen and stored in LN.

Gene	gRNA 1	gRNA 2	Method
TRIM5α	CACCGTTGATCATTGTGCAC-GCCA	AAACTGGCGTGCACAATGAT-CAAC	Lenti
PPIA	CTTAGTACCCATGTCTTTAG	ATGGACCAACCTGCTGTCTT	RNP
PPIB	GTGCTACTAAGTGAGCGGGC	TCTTCAAAGAAGGGTGCCGC	RNP
PPIF	GTCCAGTTACATAGCGAGTT	GAGAAGGGCTTCGGCTACAA	RNP
BSG	CAACAACTTCTCCCGACAGT	GTCGTCAGAACACATCAACG	RNP

Table 2: CRISPR guide RNAs

2.2.2 Genomic DNA (gDNA) extraction from iPSC clones in a 96-well plate

Cells were washed with PBS before addition of 50 µL lysis buffer (10 mM Tris pH 7.5, 10 mM EDTA, 10 mM NaCl, 0.25% Triton-X100, 1 mg/mL Proteinase K) and incubation at 55^{o}C overnight under humidified conditions. gDNA was then precipitated by addition of ice-cold precipitation solution (75 µM NaCl in 100% Ethanol (EtOH)) and incubating for 2 hours at room temperature. Precipitation solution was then removed by inversion of the plate, and precipitate washed twice with 70% EtOH, aspirating by inverting the plate. DNA was resuspended in 50-100 µL H_2O and incubated at 4^{o}C overnight.

2.2.3 Extraction using QIAGEN kit DNA

In all other instances of DNA extraction, the DNeasy Blood and Tissue Kit was used (QIAGEN, 69506) using as least 2.5x10^5 cells. When extracting from iPSC, cells were lifted with TrypLE™ for 3-5 minutes at 37^{o}C and resuspended in PBS. Macrophages were lifted by scraping into PBS. Both cell types were spun at 400g for 5 minutes and washed in PBS and spun a second time. Cells were then resuspended in 200 µL PBS and DNA then extracted as per manufacturer's instructions, resuspending in 35-50 µL H_2O. DNA concentration was determined by Nanodrop 2000c (Thermo Scientific).

2.2.4 Screening iPSC clones by Polymerase Chain Reaction (PCR)

gDNA sequences spanning target cas9 cut sites were amplified by PCR for homozygous KO clone screening by visualisation on a 1% w/v agarose gel or sequencing. Q5® Hot Start

High-Fidelity DNA Polymerase (NEB, M0493S) was used in 25 µL reactions, adding 1-2 µL of DNA. Primers with their cycling conditions are shown in Table 3.

Gene	Forward Primer	Reverse Primer	Annealing temp (°C)	Annealing time (s)	Elongation time (s)	Sequencing
TRIM5α	GTGAAAGCCCTGAGGCATAA	CCTGCTGAAAGGGGTAATCA	65.2	15	20	Forward
TREX1	CTTAACACTGGGCACTCACA	AGTGATGCTATCCACACAGAAG	67. 5	5	20	Forward
PPIA	CCTTATGGCTGTCAGGAGCAGT	CTTGCCACCAGTGCCATTATGG	63	20	30	Forward
PPIB	CTTTCCATTGAGCCAGCAGGTG	AGTGCTGGGATCACAGAGTCAC	67	20	45	Forward
PPIF	AAGGCAGATGTCGTCCCAAAGA	CTTCCATGTGCAGTGAAGCCTG	69	20	45	Reverse
BSG	GGGACCCCAGGAGTTCTTTTGA	TGGCTTCTCACCTTGTCCTCAG	64.3	30	45	Forward

Table 3: PCR Primers and cycling conditions

2.2.5 Sequencing

PCR products sent for sequencing were first cleaned using either the Monarch® PCR & DNA Clean-up Kit (NEB, T1030L) (cyclophilin family and *BSG* clones), or by Exonuclease I – Shrimp Alkaline Phosphatase (Exo-SAP) clean-up of PCR products (TRIM5α and TREX1 clones). Exo-SAP protocol is as follows: for every 25 µL of PCR product, 10 µL of Exo-SAP master mix is added (0.025 µL Exonuclease I (NEB, M0293S), 0.25 µL Shrimp Alkaline Phosphatase (Sigma, 4898133001), 9.725 µL MilliQ water). The mix is then incubated 30 minutes at 37°C followed by 5 minutes at 95°C. Samples were stored at 4°C. Sequencing was done by Source BioScience using their SpeedREAD service. Results were visualised on SnapGene Viewer version 5.0.2. Analysis of the KO status was done manually, by alignment to a control on https://benchling.com/ using MAFFT version 7 (377), or by TIDE (Tracking of

Indels by Decomposition) analysis through https://tide.nki.nl/ (378). TIDE parameters are shown in Table 4.

Gene	TRIM5α	TREX1
Alignment window	1-201	1-100
Decomposition window	201-685	115-400
Indel size range	1-50	1-50
P value threshold	0.001	0.001

Table 4: TIDE parameters

2.2.6 Single Nucleotide Polymorphism (SNP) analysis

gDNA from iPSC clones was sent to the Wellcome Trust Centre for Human Genetics to assess genome integrity post-editing of iPSC lines using the Illumina Human CytoSNP-12v2.1 beadchip array or OmniExpress24 SNP array and resulting data analysed using KaryoStudio software (Illumina).

2.3 Macrophages: phenotype and function

2.3.1 iPSC-derived macrophage differentiation

iPSCs were differentiated into macrophages using a protocol based on that previously described by van Wilgenberg *et al.* 2013 (196). The updated method is as follows. 4x10^6 iPSC previously grown in OXE8 media on Geltrex™ were plated in AggreWell™ 800 plates (Stemcell technologies, 34815) to encourage Embryoid body (EB) formation. AggreWells were prepared before plating by addition of 0.5 mL Anti-Adherence Rinsing solution (Stemcell technologies, 07010) and centrifugation at 3000g for 3 minutes at 15^{o}C to remove bubbles from the microwells. Rinse solution was then aspirated and replaced with 1 mL of 2X concentrated EB medium (OXE8 media supplemented with 50 ng/mL BMP4 (Peprotech, PHC9534), 50 ng/mL VEGF (Peprotech, PHC9394), and 20 ng/mL SCF (Miltenyi Biotec, 130-096-695) supplemented with 10 µM ROCKi. iPSC were resuspended by washing with TrypLE™ and incubating for 3-5 minutes at 37^{o}C, 5% CO_2, lifting in advanced-DMEM/F12 to achieve single-cell suspension. Cells were counted and pelleted by centrifugation at 400g for 5 minutes. Cells were then resuspended at 4x10^{6} cells/mL in OXE8 supplemented with 10 µM ROCKi and added to the AggreWell™. The plate was then spun at 100g for 3 minutes at 4^{o}C with no braking to encourage even distribution of cells across microwells. Cells were then incubated for 4 days at 37^{o}C, 5% CO_2 with daily feeding by 75% media change with EB medium, by aspiration of 1 mL by pipette and gentle addition of 1 mL fresh media, repeated twice, to avoid disturbing to the EBs. After 4 days, EBs were gently lifted using a Pasteur pipette and passed over a 40 µm cell strainer to remove dead cells, before washing into a 50 mL tube with differentiation media (Table 5). EBs were divided evenly into 2xT175 flasks and topped up to 20 mL with differentiation medium. These differentiation cultures were incubated at 37^{o}C, 5% CO_2, with weekly feeding of an additional 10 mL until macrophage precursors (PreMacs) started to be produced. After this point, PreMac cells were collected weekly and a minimum of equal volumes of media to the volume removed were replaced into the differentiation cultures. Each harvest of cells involved a 25-50% media change. Harvested

PreMac cells were either used directly or centrifuged at 400g for 5 minutes and resuspended in XVIVO or OXM Macrophage medium (Table 5) for plating in appropriately sized tissue culture plates at stated densities of cells/well. Plated cells were cultured 7 days, with a 50% media change on day 4, to terminally differentiate into macrophages.

Media	Component	End Conc.	Supplier	Catalogue number
XVIVO differentiation medium	X-VIVO-15™	97.8%	SLS (Lonza)	BE02-060F
	GlutaMAX (100x)	2mM	Gibco ThermoFisher	35050-038
	2-Mercaptoethanol (2ME)(1000x)		Gibco ThermoFisher	31350-010
	IL-3	25ng/mL	Invitrogen	PHC0033
	M-CSF	50ng/mL	Invitrogen	PHC9501
	Penicillin-Streptomycin (P/S 100x)	1%	Gibco ThermoFisher	15140-122
XVIVO Macrophage medium	X-VIVO 15	97.9%	SLS (Lonza)	BE02-060F
	GlutaMAX (100x)	2mM	Gibco ThermoFisher	35050-038
	M-CSF	50ng/mL	Invitrogen	PHC9501
	Penicillin-Streptomycin (P/S 100x)	1%	Gibco Thermo Fisher	15140-122
OXM differentiation medium	Advanced DMEM/F12	96.3%	Gibco Thermo Fisher	12634010
	GlutaMAX (100x)	2mM	Gibco ThermoFisher	35050-038
	HEPES 1M pH 7.4	15mM	Gibco ThermoFisher	15630080
	Human recombinant Insulin solution	5µg/mL	Sigma	I9278-5ML
	Tropolone	15µM	Sigma	T89702-1G
	IL-3	25ng/mL	Invitrogen	PHC0033
	M-CSF	50ng/mL	Invitrogen	PHC9501
	Penicillin-Streptomycin (P/S 100x)	1%	Gibco Thermo Fisher	15140-122
OXM Macrophage medium	Advanced DMEM/F12	96.5%	Gibco Thermo Fisher	12634010
	GlutaMAX (100x)	2mM	Gibco ThermoFisher	35050-038
	HEPES 1M pH 7.4	15mM	Gibco ThermoFisher	15630080
	M-CSF	50ng/mL	Invitrogen	PHC9501
	Penicillin-Streptomycin (P/S 100x)	1%	Gibco Thermo Fisher	15140-122

Table 5: iPSC-derived macrophage culturing media

2.3.2 Cell measurements

To quantify cell number, size, and viability before plating or before antibody staining for flow cytometry, cells were stained with Solution 13 AO-DAPI (Chemometec, 910-3013) at a ratio 1 µL dye: 19 µL cell suspension. Measurements were made using the NucleoCounter® NC-3000™ (Chemometec).

2.3.3 Macrophage surface marker staining

Macrophages were lifted by incubation for 5 minutes at 37ºC with StemPro™ Accutase™ (Gibco, A1110501). No difference in surface marker levels using this method are observed compared to use of 5mM EDTA/12mM Lidocaine (372, 379). Cells in suspension were kept at 4ºC or on ice throughout staining. Cells were washed with PBS and resuspended in FACS buffer (PBS supplemented to 1% FBS, 10 µg/ml human-IgG (Sigma, I8640-100MG), and 0.01% Sodium azide) and incubated for 10 minutes to block non-specific Fc-receptor interactions. 0.5-1x10^5 macrophages/antibody were stained directly without fixation in FACS buffer using antibodies as listed in Table 6, incubating for 0.5-1 hour at 4ºC in the dark. Isotype controls with the same fluorophores from the same company were used at the same concentration. To reduce the number of cells required, antibodies from 3 different colours were used on the same samples (APC, PE, and FITC). After staining, cells were washed twice with FACS buffer and then fixed by resuspension in FACS buffer supplemented to 4% PFA. Fluorescence was measured using the BD LSRFortessa™ X-20 (BD Biosciences).

2.3.4 Macrophage total marker staining

To quantify total expression of macrophage specific markers, cells were lifted and washed with PBS as described above. Cells were then fixed with 2% PFA in PBS for 10 minutes at room temperature. After a wash in FACS buffer, cells were permeabilized with 0.1% saponin in FACS buffer for 30 minutes at room temperature with shaking. 0.5-1x10^5 macrophages/antibody were then stained for 1 hour at room temperature in the dark, with

shaking, using antibodies as listed in Table 6. After, cell were washed twice with FACS buffer and resuspended in FACS buffer in preparation for acquisition using the BD LSRFortessa™ X-20 (BD Biosciences).

Target	Clone	Fluorochrome	Isotype	Dilution	Company	Cat No.
CD4	11830	APC	IgG2a	1:25	R&D systems	FAB3791A
CD11b	ICRF44	APC	IgG1k	1:50	Bio-legend	301310
CD206	15-2	APC	IgG1k	1:50	Bio-legend	321109
IgG1k	MOPC-21	APC	-	1:50	Bio-legend	400120
IgG2a	20102	APC	-	1:25	R&D systems	IC003A
CCR5	45531	PE	IgG2b	1:25	R&D	FAB182P
CD14	18D11	PE	IgG1	1:50	Immunotools	21620144
CD16	LNK16	PE	IgG1	1:50	Immunotools	21279164
CD86	IT2.2	PE	IgG2bk	1:50	Bio-legend	305405
CD163	215927	PE	IgG1	1:50	R&D	FAB1607P
CXCR4	44717	PE	IgG2b	1:25	R&D	FAB173P
IgG1	PPV-06	PE	-	1:50	Immunotools	21275514
IgG2bk	MPC-11	PE	-	1:50	Bio-legend	400311
IgG1	11711	PE	-	1:50	R&D	IC002P
IgG2b	133303	PE	-	1:25	R&D	IC0041P
CD14	MEM-18	FITC	IgG1	1:50	Immunotools	21270143
CD45	MEM-28	FITC	IgG1	1:50	Immunotools	21270453X2
CD68	Ki-M7	FITC	IgG1	1:50	BIO-RAD	MCA2375F
CD86	BU63	FITC	IgG1	1:25	Immunotools	21480863
HLA-DR	MEM-12	FITC	IgG1	1:25	Immunotools	21388993
IgG1	PPV-06	FITC	-	1:25	Immunotools	21335013

Table 6: Macrophage markers

2.3.5 Zymossan-488 phagocytosis assay

$2x10^5$ macrophages plated in a 24-well plate (~$1x10^5/cm^2$) were used to measure phagocytic uptake of Zymosan A (S. cerevisiae) BioParticles™, Alexa Fluor™-488 conjugate (Invitrogen, Z23373). 1 hour prior to addition of BioParticles™, a control well was treated with 10 µM of cytochalasin D (Cambridge bioscience, 11330-1 mg-CAY) in macrophage medium, 250 µL per well. The other well was given 250µl macrophage media. Before addition of 50 µg/mL BioParticles™ in macrophage medium, BioParticles™ were first sonicated for 30 seconds at medium power. 250 µL was then added direct to the well (end concentration 25 µg/mL) and cells incubated for 30 minutes at 37^{o}C, 5% CO_2. After incubation, extracellular BioParticle™ fluorescence was quenched by washing with 0.025% Trypan Blue diluted in PBS

(Sigma, T8154). Cells were then lifted with Accutase™ for 10 minutes at 37°C. Cells were resuspended directly in Accutase™ and fixed by addition of 4% PFA in PBS (end concentration of 2% PFA). Intracellular fluorescence was acquired using the BD LSRFortessa™ X-20.

2.3.6 Adhesion assay

$5x10^4$ PreMacs were plate in triplicate in a 96-well plate in differentiation or macrophage medium for terminal differentiation. To assess adhesion, differentiated cells were incubated with StemPro™ Accutase™ for the indicated period of time before washing once with PBS followed by nuclear staining with NucBlue™ (Life Technologies, R37605) in live cell imaging solution (Life technologies, A14291DJ) for 15 minutes at room temperature. NucBlue™ solution was then reomoved and cells fixed in 2% PFA in PBS. Adherent cells were then counted by fluorescent imaging on the EVOS Fl auto and analysed on ImageJ. Percentage adherent cells was calculated by normalisation against an Accutase™ untreated and unwashed, stained and fixed only control.

2.4 RNA

2.4.1 RNA extraction

$2x10^5$–$1x10^6$ cells were lysed over ice in RLT buffer from RNeasy Mini Kit (QIAGEN, 74104) supplemented with 10 µL/mL β-mercapotoethanol. Lysates were homogenised using the QIAshredder kit (QIAGEN, 79656) and stored at -80^{o}C until extraction. All RNA extractions were done using the RNeasy Mini Kit (QIAGEN, 74104) including the optional DNase treatment step (RNAse-Free DNase Set, QIAGEN, 79254) and eluted in 35-50 µL RNAse-free water. RNA concentration was quantified with the Nanodrop 2000c.

2.4.2 cDNA synthesis for Quantitative PCR (qPCR)

RNA needed to be reverse transcribed into complementary DNA (cDNA) to quantify RNA transcripts by qPCR. cDNA was made using the High-Capacity RNA-to-cDNA™ Kit (Applied Biosystems™, 10704217). For each experiment, equal quantity of RNA was added across samples, using up to 9µL RNA.

2.4.3 qPCR: Taqman

Inflammatory mediator expression was determined by Taqman primer-probe based qPCR (Table 7). cDNA was first diluted 1:40-1:100 in nuclease free water before adding 1 volume of cDNA to 2 volumes of mastermix (mixture of primer-probe, TaqMan™ Gene Expression Master Mix (Applied Biosystems, 4369016), and nuclease-free water at a ratio of 1 µL : 10 µL : 2.33 µL respectively). Reactions were carried out in triplicate either in a 96-well format (MicroAmp™ Optical 96-well Reaction Plate, Applied Biosystems, N8010560) in 20µL reactions, or 384-well format (MicroAmp™ Optical 384-Well Reaction Plate, AB, 4309849) in 6µL reactions using in the StepOnePlus (Applied Biosystems) or QuantStudio 5 (Applied Biosystems). Cycling conditions are shown in Table 8. All ramp rates were 1.6^{o}C/s.

Formation of HIV-1 late reverse transcripts was measured by quantification of GFP viral gDNA extracted by QIAGEN kit, normalised against human gDNA. Primers and probes for

GFP were ordered from IDT (Fwd: CAACAGCCACAACGTCTATATCAT, Rev: TGTTGTGGCGGATCTTGAAG, Probe: 5′-FAM-CCGACAAGCAGAAGAACGGCATCAA-3′TAMRA) and were compared against genomic β-actin (ACTB) (eurogentec, RT-CKYD-ACTB). Equal volumes of DNA across all samples for each experiment were used, in 10 µL reactions; 5 µL Taqman™ Gene Expression Master Mix, 0.15 µL 10mµM probe, 0.3 µL of each 10 µM primer, 1.25 µL nuclease-free water, and 3 µL DNA diluted in nuclease-free water. Reactions were run in the 384-well format on the QuantStudio 5.

Gene	ID	Fluorophore	Quencher
IL6	Hs00174131_m1	FAM	TAMRA
IFIT1	Hs00356631_g1	FAM	TAMRA
IFNB1	Hs01077958_s1	FAM	TAMRA
CXCL10	Hs00171042_m1	FAM	TAMRA
IFNG	Hs00989291_m1	FAM	TAMRA
IL1B	Hs01555410_m1	FAM	TAMRA
TNF	Hs00174128_m1	FAM	TAMRA
IL10	Hs00961622_m1	FAM	TAMRA
GAPDH	Hs04420632_g1	FAM	TAMRA
HMBS	Hs00609297_m1	FAM	TAMRA
B2M	Hs99999907_m1	FAM	TAMRA
TBP	Hs00427620_m1	FAM	TAMRA
18S	Hs99999901_s1	FAM	TAMRA

Table 7: Taqman qPCR primers and probes

Stage	Temperature (ºC)	Time (min:sec)	Cycles
Hold	50	02:00	1
	95	10:00	
PCR	95	00:15	40
	60	01:00	

Table 8: Taqman cycling conditions

2.4.4 qPCR: SYBR green

Expression of TRIM5α or members of the Cyclophilin family was determined using the double-stranded DNA intercalating dye, SYBR™ Green. Optimised primers for TRIM5α with required concentrations and annealing temperatures are listed in Table 9. Cyclophilin family primers are listed in Chapter 6, Table 2. Primers were first assessed by PCR using 2x PCRBIO Taq Mix Red (PCR Biosystems, PB10.13) across multiple annealing temperatures and different primer concentrations, visualised by 1-2% w/v agarose gel. Efficiency was

determined by SYBR™ green qPCR as described below across 5x3-fold dilutions of cDNA and calculated in Microsoft Excel as $Efficiency = (10\text{^}(-1/Slope) - 1) * 100$ where slope is calculated for the plot of average Ct against Log(sample quantity). Primers with efficiency between 90-105% are deemed efficient and used for qPCR. qPCR reactions comprised of 1 volume sample cDNA to 3 volumes mastermix (Power SYBR™Green PCR Master Mix (Applied Biosystems, 4367659), forward and reverse primer mix, and nuclease-free water at a ratio of 5 µL : 1 µL : 2 µL respectively). Reactions were in run in triplicate in either 96-well format, 16 µL/sample, or 384-well format, 8 µL/sample. Cycling conditions are shown in table 10.

Gene	Forward Primer	Reverse Primer	Annealing Temp (ºC)	Primer conc. (nM)	Efficiency (%)
TRIM5α exon junction 2	CCCGGGAGTACCAAG-TGAAG	GCTCATTGCTCTCC-TCCCAG	64	100	96.97
TRIM5α exon junction 7	CGACGCTACTGGGTT-GATGT	ACTTTGAGAGCCC-AGGATGC	64	200	102.91

Table 9: SYBR green primers

Stage	Temperature (ºC)	Time (min:sec)	Ramp rate (ºC/s)	Cycles
Hold	50	02:00	1.6	1
	95	10:00	1.6	
PCR	95	00:15	1.6	40
	variable	01:00	1.6	
Melt Curve	95	00:15	1.6	1
	variable to match PCR	01:00	1.6	
	95	00:01	0.15	

Table 10: SYBR green cycling conditions

2.4.5 Analysis of qPCR data

Analysis of gene expression was performed by normalisation of Ct values to the average Ct value of two housekeeper genes, B2M and TBP, and displayed as fold difference as calculated by $2^{-\Delta Ct}$. Further normalisation against a control sample was sometimes calculated

and displayed as fold difference calculated by $2^{-\Delta\Delta Ct}$. Likewise, HIV-1 late reverse transcripts were analysed by normalisation of GFP Ct against ACTB and further normalised against untreated controls, displaying results as $2^{-\Delta Ct}$ and $2^{-\Delta\Delta Ct}$.

2.4.6 RNA-seq sample preparation, library construction, and data generation

RNA-Seq data was generated by Novogene. RNA was extracted from $1x10^6$ macrophages using the RNeasy Mini Kit, including optional DNase treatment step. Samples were sent to Novogene on dry ice. RNA degradation and contamination was monitored on 1% agarose gels. RNA purity was checked using the NanoPhotometer® spectrophotometer (IMPLEN, CA, USA). RNA integrity and quantitation were assessed using the RNA Nano 6000 Assay Kit of the Bioanalyzer 2100 system (Agilent Technologies, CA, USA). A total amount of 1 µg RNA per sample was used as input material for the RNA sample preparations. Sequencing libraries were generated using NEBNext® Ultra TM RNA Library Prep Kit for Illumina® (NEB, USA) following manufacturer's recommendations and index codes were added to attribute sequences to each sample. Briefly, mRNA was purified from total RNA using poly-T oligo-attached magnetic beads. Fragmentation was carried out using divalent cations under elevated temperature in NEBNext First Strand Synthesis Reaction Buffer (5X). First strand cDNA was synthesized using random hexamer primer and M-MuLV Reverse Transcriptase (RNase H-). Second strand cDNA synthesis was subsequently performed using DNA Polymerase I and RNase H. Remaining overhangs were converted into blunt ends via exonuclease/polymerase activities. After adenylation of 3' ends of DNA fragments, NEBNext Adaptor with hairpin loop structure were ligated to prepare for hybridization. In order to select cDNA fragments of preferentially 150~200 bp in length, the library fragments were purified with AMPure XP system (Beckman Coulter, Beverly, USA). Then 3 µl USER Enzyme (NEB, USA) was used with size-selected, adaptorligated cDNA at 37 °C for 15 min followed by 5 min at 95 °C before PCR. Then PCR was performed with Phusion High-Fidelity DNA polymerase, Universal PCR primers and Index (X) Primer. At last, PCR products were purified (AMPure

XP system) and library quality was assessed on the Agilent Bioanalyzer 2100 system. The clustering of the index-coded samples was performed on a cBot Cluster Generation System using PE Cluster Kit cBot-HS (Illumina) according to the manufacturer's instructions. After cluster generation, the library preparations were sequenced on an Illumina platform and paired-end reads were generated.

2.4.7 RNA-Seq data analysis

Raw reads were pre-processed using fastp (v.0.20.1) software (380). In addition to the default filtering parameters, polyN sequences in read tails and adapter sequences were trimmed, and mismatched base pairs were corrected by overlap analysis. Filtered and trimmed reads were mapped to a full decoy-aware transcriptome using the Gencode version 34 reference human transcriptome and GRCh38 primary assembly genome. Salmon (v.1.3.0) selective alignment was used for transcript quantification with optional flags correcting for GC and random hexamer priming biases (381). All downstream analyses were done using the R (v.4.0) programming language (R Core Team 2020). Raw counts were imported, scaled to the average transcript length over samples and the library size ('LengthScaledTPM'), and summarised to the gene level using the tximport package (v.1.16.0) (382). Lowly expressed genes with length-scaled abundance estimates less than 10-in-3 samples were filtered out. Differential expression was tested using limma-voom (383). GO enrichment analysis was conducted using the EGSEA package (384). GO terms with less than 10 genes were excluded from the enrichment analysis. The background gene set used for the analysis was the total number of the unique genes observed in the experiment. A publicly available dataset of human *ex vivo* and iPSC-derived microglia was processed as above and used as a reference (385). Principal component analysis was performed with the prcomp package to represent the level of transcriptomic similarity amongst the samples from both studies. To visualise expression of genes from a particular GO term, the length-scaled gene abundance estimates from both

studies were transformed to counts per million (TMM-adjusted), Z-score standardise and presented on a heatmap using the pheatmap package.

2.5 Virus production and infection assays

2.5.1 Plasmid preparation

Plasmids are summarised in table 11. For production, plasmids were transformed into Stbl3 chemically competent *E. coli.* 100 ng plasmid was added to 20 µL of cells and incubated on ice for 30 minutes. Bacteria were then heat shocked at 42°C for 30 seconds followed by 5 minutes on ice. Cells were then added to 450 µL SOC medium and incubated at 37°C with 250rpm shaking for 30 minutes. Cells were spread on agar plates containing 100 µg/mL ampicillin and incubated overnight at 37°C. Clones were selected and added to the required volume of LB broth supplemented with 100 µg/mL ampicillin (Sigma, A9518-25G) and cultured overnight at 37°C with 250rpm shaking, for plasmid isolation using QIAfilter Plasmid Midi/Maxi Kits (QIAGEN, 12243/12262).

Plasmid	Size (kb)	Lentiviral component	2/3-plasmid system	Purpose	Source
pCMV-VSVg	6.5	envelope	Both	Infectivity assays, Lenti-CRISPR	M.D.Moore, Addgene
pCMV-BaL	8.7	envelope	2	Infectivity assays	NIH-AIDS
pNL4.3-e-r-GFPT2ANef	15.6	gagpol, genome	2	Infectivity assays	M.D.Moore, G.Towers
pNL4.3-e-r-GFPT2ANef-P90A	15.6	gagpol, genome	2	Infectivity assays	M.D.Moore, G.Towers
pCMV-dR9.91	12.1	gagpol	3	Lenti-CRISPR	M.D.Moore, Addgene
pCMV-dR8.2	13.5	gagpol	3	Infectivity assays	G.Towers
pCMV-dR8.2-A92E	13.5	gagpol	3	Infectivity assays	G.Towers
pCMV-dR8.2-G94D	13.5	gagpol	3	Infectivity assays	G.Towers
pCMV-dR8.2-N74D	13.5	gagpol	3	Infectivity assays	G.Towers
pGIP	6.0	genome	3	Infectivity assays, Lenti-CRISPR control	M.D.Moore
pPGK-GFP-IRES-puro-WPRE-SIN	10.8	genome	3	Infectivity assays	M.D.Moore
pLentiCRISPRv2.0	14.9	genome	3	Lenti-CRISPR	M.D.Moore, F. Zhang

Table 11: Plasmids

2.5.2 Production of lentivirus

$6x10^6$ per 10cm dish HEK293T cells were plated 24 hours prior to transfection in 10 mL hgDMEM supplemented to 10% v/v FBS and 1% v/v P/S, achieving 70-80% confluency at the time of transfection. To transfect in plasmid components of the lentivirus (both 2-plasmid or 3-plasmid systems, identified in Table 11), per 10cm dish, 2.5 mL hgDMEM (without FBS or P/S) supplemented with 164 µL 10 µM polyethylenimine (PEI, Sigma, 9002-98-6) was mixed by dropwise addition with 2.5 mL hgDMEM containing 20-25 µg DNA. This is an approximate ratio of 2 parts PEI : 1 part DNA. The DNA/PEI/hgDMEM solution was incubated for 20 minutes at room temperature before gentle addition to HEK293T cells, replacing culture medium. Cells were incubated for 4 hours at 37°C, 5% CO_2 before the DNA/PEI/hgDMEM mix was removed and replaced with fresh hgDMEM supplemented with FBS and P/S for a further 48-hours. After 48 hours, successful transfection of GFP genome could be confirmed by visualisation by fluorescent microscopy. Virus containing supernatant was collected and passed through a 0.45 µm filter. Virus was then concentrated using either Lenti-X™ concentrator (Clontech, PT4421-2) according to manufacture's instructions, or polyethylene glycol-6000 (PEG-6000) based concentration reagent (50 % polyethylene glycol 6000 (VWR, 443912S) w/v in H2O, 4 M NaCl (Sigma) w/v in H2O, and PBS) at a ratio 2 parts filtrate : 1 part concentration reagent, incubating for 1.5 hours at 4°C with the occasional shake and spun at 4500g for 45 minutes at 4°C. Virus was concentrated to 100x its original concentration, resuspending in macrophage medium and stored at -80°C.

2.5.3 Quantification of viral titres: VSV-G enveloped virus

VSV-G enveloped, GFP encoding lentivirus, was titrated on HEK293T cells. 24 hours prior to infection, $1.6x10^5$ cells per well of a 24-well plate were plated to achieve 70-80% confluency at the time of infection. Cells were infected with a 2-fold serial dilution of virus (top viral volume 20-100 µL) in culture medium, 11 dilutions, and incubated 48 hours at 37°C, 5% CO_2. Cells were then lifted by incubating 1 minute at 37°C with TrypLE™ and resuspended in

4% PFA in PBS. GFP expression was assessed by fluorescence acquisition using the BD LSRFortessa™ X-20. Infectious units per mL (IU/mL) were calculated in Microsoft Excel by plotting percentage infection (GFP^+) against volume of virus and applying the following equation to the linear portion of the graph: $IU = (320000 * (\%\, infected/100)) / (volume\ of\ virus\ in\ \mu L/1000)$ where 320000 is the approximated number of cells at the time of infection.

2.5.4 Quantification of viral titres: BaL enveloped virus

BaL enveloped virus was quantified using the TZM-bl luciferase reporter cell line. TZM-bl cells were resuspended by 1 hour incubation at room temperature in 10 mM EDTA to preserve CD4 surface expression. $1x10^4$ cells in 100 µL were plated per well of a 96-well plate. While cells were still in suspension, a 3-fold serial dilution of virus was added, starting at 50 µL of undiluted, or prediluted virus, with a total of 11 dilutions. Cells were then incubated for 48 hours at 37°C, 5% CO_2. After 48 hours, supernatant was removed, cells washed with PBS, and then lysed in 100 µL 1X Reporter Lysis buffer (Promega, E3971), incubating for 5 minutes at room temperature. Lysate was moved to -80°C for ≥1 hour to ensure complete lysis. To quantify luciferase expression, lysate was thawed in the dark and mixed 50 µL lysate to 50 µL Luciferase Assay reagent (Promega, E1500). After 2-minute incubation at room temperature in the dark, luminescence was quantified using the Spectramax M5 Plate reader, 1000ms integration. To quantify virus, luminescence values were analysed in Microsoft Excel, subtracting background luminescence (defined as 2x average luminescence of uninfected control) before calculation of 50% infectious dose (ID_{50}) using the National Institutes of Health ID-50 program (386).

2.5.5 HIV-1 GFP pseudo-virus single-cycle infectivity assay

Infectivity of single-cycle pseudo-virus was determined by measuring GFP in infected cells by flow cytometry. Viral dose and pharmacological agents are stated in the main text.

$5x10^4$ PreMacs were plated per well of a 96-well plate (~$1.5x10^5/cm^2$) and differentiated for 7 days as described earlier. After 7 days, only 50% of the medium was removed to prevent macrophage lifting, and replaced with medium containing virus/pharmacological agents. Cells were incubated for 48-72 hours at 37°C, 5% CO_2. Supernatant was then transferred to a 96-well v-bottom plate and spun at 400g for 5 minutes at 4°C to collect floating cells. Adherent cells were resuspended by incubation in 5mM EDTA for 30-60 minutes at 4°C. Cells were transferred to the v-bottom 96-well plate and spun at 400g for 5 minutes at 4°C and resuspended in 1% PFA in PBS. Fluorescence was then acquired on the BD LSRFortessa™ X-20 using the 488-laser compared against the 647 laser to distinguish macrophage autofluorescence.

2.5.6 Replication competent HIV-1 infectivity assay

Macrophages were plated as described above for single-cycle infectivity assay. Cells were infected at an MOI of 0.02 with Bal-Luc (ID: 2613) (387) and treated with/without 1 µM cyclosporine A (Abcam, ab120114-25mg). At each time point, virus containing supernatant was collected and virus inactivated by addition of 15 µL 5% Empigen BB™ (Sigma, 45165) to 135µL of supernatant, incubating for 1 hour at 56°C. Inactivated supernatant could be removed from BSL3 containment and stored at -80°C. Remaining cells were lysed using Glo Lysis buffer (Promega, E2661), incubating 5 minutes at room temperature before moving to -80°C for ≥1 hour. To quantify luciferase expression, lysate was thawed in the dark and mixed 50 µL lysate : 50 µL Renilla-Glo™ Luciferase Assay reagent (Promega, E2710). The lysate/substrate mixture was then incubated 10 minutes at room temperature in the dark before quantification of luminescence using the Spectramax M5 Plate reader, 1000ms integration.

2.5.7 Zika virus infectivity assay quantified by plaque assay

$2.5x10^5$ PreMacs were plated per well of a 24-well plate (~$1.32x10^5$ cell/cm^2) and differentiated into macrophages as described earlier. Cells were infected with African MR1766

Zika virus, MOI=1. Viral titre at each time point was determined by plaque assay as follows. Zika virus was titrated on Vero cells. Virus containing supernatant was serially diluted in 10-fold dilutions, 6 dilutions, in Vero maintenance medium. 100 µL of viral dilution was added to each well of a 24-well plate and $2.5x10^5$ Vero cells added on top in 500 µL. Cells were then incubated for 3 hours at 37°C, 5% CO_2 before addition of 500 µL semi-solid overlay made of 1.5% Carboxymethyl cellulose (CMC, Sigma, C5678) in Vero maintenance medium. Cells were incubated a further 48-72 hours at 37°C, 5% CO_2. To visualise plaques, overlay was aspirated, and cells washed with PBS before adding 500 µL Amido Black stain (1g Naphthol Black (Sigma, 195243), 60 mL glacial acetic acid, 13.6 g sodium acetate, made to 1 L with water) and incubating ≥30 minutes at room temperature. Stain was then removed, and excess washed off with water to reveal the plaques. Plaque forming units (P.f.u.) were calculated as follows: $P.f.u. = (n/0.1)/D$ where *n* = average number of plaques, 0.1 is the volume of virus added in mL, and *D* = dilution factor.

2.6 Cytokine analysis

2.6.1 Enzyme-linked immunosorbent assay (ELISA)

Production of TNFα, IL-6, and IL-8 by resting or stimulated macrophages was quantified using Human Uncoated ELISA Kits (Invitrogen, 88-7346-88, 88-7066-88, 88-8086-88). Supernatants were spun at 400g for 5 minutes to remove floating cells/debris and stored at -80^{o}C until required. After thawing, supernatants were diluted 1:10 and 1:100 for quantification of TNFα, 1:20 and 1:200 for IL-6, or 1:1000 for IL-8. Absorbance was measured on the Spectramax M5 Plate reader, analysing in Microsoft Excel and by Interpolating a standard curve using the Linear or Hyperbola (X is concentration) calculator on Graphpad Prism version 8.2.1. Values above and below the range of the standards were excluded, and values averaged between the two dilutions of each sample.

2.6.2 Proteome Profiler

The Proteome Profiler Human Cytokine Array Kit (R&D Systems, ARY005B) measured a panel of 36 cytokines, chemokines, and acute phase proteins. Supernatants were prepared as per ELISA, storing at -80^{o}C until required. 1 mL of undiluted supernatant was used. The assay was run according to manufacturer's instructions as instructed for use of Proteome Profiler Arrays with LI-COR Detection, as can be accessed at https://www.rndsystems.com/resources/technical/use-proteome-profiler-arrays-li-cor-detection. Arrays were visualised on the LI-COR Odyssey 9260 and quantified using Image Studio Lite version 5.2.

2.7 General methods

2.7.1 Western blotting

$2.5x10^5$ – $1x10^6$ cells were lysed over ice in Radioimmunoprecipitation (RIPA) buffer supplemented with cOmplete™ ULTRA Tablets, Mini, EDTA-free, EASYpack Protease Inhibitor Cocktail (Roche, 5892791001). Lysate was homogenized by sonication for 30 seconds at medium power and centrifuged for 3 minutes at full speed (>20,000g) before use. Protein concentrations were quantified by Quick Start™ Bradford Protein Assay kit (BIO-RAD, 5000201). Samples were prepared as follows; 6.8 µL NuPAGE™ LDS sample buffer (4X) (Invitrogen, NP0007), 2.7 µL NuPAGE™ Sample Reducing Agent (10X) (Invitrogen, NP0009), 18 µL lysate in RIPA buffer, diluted with water as required to normalise protein concentration. Samples were heated at 70ºC for 10 minutes before running ≤25µL on a Novex™ WedgeWell™ 8-16%, Tris-Glycine gel (Invitrogen, XP08165BOX) in Novex™ Tris-Glycine SDS Running Buffer (Invitrogen, LC2675). After electrophoresis, gels were rinsed in Pierce™ 1-Step Transfer Buffer (Thermo Scientific, 15175204) before semi-dry transfer of protein to a Low-Fluorescence PVDF transfer membrane (Thermo Scientific, 10501664) using the Mixed Protein Size setting on the Pierce™ Power Blotter (Thermo Scientific). After transfer, membranes were blocked for 1 hour in either 5% milk in Tris-buffered saline (TBS)-Tween v/v 0.1% or with iBind™ Flex solution (Invitrogen, SLF2020). Membranes were stained using the antibodies listed in Table 12. Cyclophilin A and B were stained using the iBind Flex Western System with α-Tubulin as a loading control, all other primary antibody staining was overnight in 5% milk or flex solution at 4ºC with shaking, with secondary antibody staining, after washing with TBS-T, for 1 hour in the dark at room temperature with shaking. Blots stained with LI-COR fluorophore conjugated secondary antibodies were visualised using the LI-COR Odyssey 9260. HRP conjugated secondary antibody staining was revealed using Western Lightning® ECL Pro (PerkinElmer, NEL120E001EA) and visualised with the Amersham Imager 600 (General Electrics).

Protein target	Species	Manufacturer	Cat No.	Dilution
Cyclophilin A	Rabbit	Abcam	ab41684	1:1000
Cyclophilin B (PA1-027A)	Rabbit	Invitrogen	PA1027A	1:2000
BSG/CD147 (E1S1V)	Rabbit	Cell Signalling	13287S	1:500
IRF3 (EP2419Y)	Rabbit	Abcam	ab76409	1:500
p38 MAPK (D13E1)	Rabbit	Cell Signalling	9926T	1:1000
SAPK/JNK (9252)	Rabbit	Cell Signalling	9926T	1:500
ERK1/2 (137F5)	Rabbit	Cell Signalling	9926T	1:2000
Phospho-p38 (D3F9)	Rabbit	Cell Signalling	9910T	1:500
Phospho-ERK1/2 (D13.14.4E)	Rabbit	Cell Signalling	9910T	1:2000
Phospho-JNK (81E11)	Rabbit	Cell Signalling	9910T	1:500
IKKβ (D30C6)	Rabbit	Cell Signalling	9936T	1:500
Phospho-IKKα/β (16A6)	Rabbit	Cell Signalling	9936T	1:250
NF-κB p65 (D14E12)	Rabbit	Cell Signalling	9936T	1:500
Phospho-NF-κB p65 (93H1)	Rabbit	Cell Signalling	9936T	1:500
IκBα (L35A5)	Mouse	Cell Signalling	9936T	1:1000
Phospho-IκBα (14D4)	Rabbit	Cell Signalling	9936T	1:500
GAPDH (6C5)	Mouse	Abcam	ab8245	1:2000
α-Tubulin (B.1.5.2)	Mouse	Sigma	T5168	1:500-1:2000
IRDye® 800CW anti-mouse	Goat	LI-COR	926-32210	1:3000
IRDye® 800CW anti-rabbit	Goat	LI-COR	926-32211	1:3000
IRDye® 680RD anti-mouse	Donkey	LI-COR	925-68072	1:3000
IRDye® 680RD anti-rabbit	Donkey	LI-COR	925-68073	1:3000
Anti-rabbit IgG, HRP Linked (7074)	Goat	Cell Signalling	9936T	1:2000
Anti-mouse IgG, HRP linked (7076)	Horse	Cell Signalling	9936T	1:2000

Table 12: Antibodies for western blotting

2.7.2 Cell viability assay

To assess toxicity of pharmacological agents, viability was assessed by the uptake of Gly-Phe-AFCoumarin dye, which is cleaved by proteases in viable cells to release a fluorophore. Dye was provided as part of the CellTiter-Fluor Cell Viability Assay (Promega, G6080) using manufacturer's instructions. Fluorescence was measured on the Spectramax M5 plate reader using SoftmaxPro software version 5.

2.7.3 Liquid Chromatography-Mass Spectrometry (LC-MS)

Samples of the media were prepared for LC-MS analysis as described before (388). Briefly, 500 µL of each media was filtered using Amicon Ultracentrifugal filters (3-10 kDa cut

off). The flow through was used for analysis of metabolites using high-resolution negative ion LC-MS (accuracy better than 5 ppm). The setting and methods were as described previously (388, 389). The total ion chromatograms were analysed using MesReNova software. The MS peaks were putatively assigned using the human metabolome database (HMDB).

2.7.4 Quantification of glucose concentration

A modification of the protocol for the detection of glucose using the Glucose (HK) Assay Kit (Supelco, # GAHK20-1KT) was as follows: 100 µL of culture media were diluted 1:10 and 1:20 in dH2O. 20 µL of each dilution was added into a well of a 96-well flat-bottom cell culture treated plate. Glucose solution was freshly made up by resuspending the vial in 20 mL dH2O. 100 µL of glucose solution was added per well. Plates were incubated at 35^{o}C for 15 minutes before measuring absorbance at 340 nm using the Spectramax M5 plate reader. Values were compared to known values from a standard curve. The standard curve was made using seven serial dilutions (top 2.5 mM) of media culture with known composition (DMEM – 25 mM).

2.7.5 Lactate quantification

Supernatant from cells was spun 400g for 5 minutes to remove floating cells and stored at 4^{o}C until quantification. 5 µL sample was mixed with 100 µL freshly made running buffer and incubated at 37^{o}C before measuring absorbance at 340 nm on the SpectraMax M5 plate reader. Readings were compared against a standard curve of lactate (starting concentration 4 mM). 10 mL Running buffer is made of 3.5 mL glycine buffer, 6.5 mL dH_2O, 165 µL lactate dehydrogenase (LDH) (1000 units) and 10 mg nicotinamide adenine dinucleotide (NAD+). 100 mL glycine buffer is made of 4.5 g glycine (0.6M), 1.3 mL 50-50% pure hydrazine hydrate, 600 µL 10 M potassium hydroxide, and 95 mL dH_2O.

2.7.6 Software

At the time of writing, the versions of each software used were as follows. Microsoft Office 365 (2019), Graphpad Prism version 8.2.1, FlowJo version 10.4, Image Studio Lite version 5.2. QuantStudio™ Design and Analysis software version 1.4.3. Snapgene Viewer version 5.0.2. ImageJ version 1.52a.

Chapter 3:

Differentiation of human induced Pluripotent Stem Cells to authentic macrophages using fully defined, serum free, open-source medium[1]

[1] This chapter is made from the publication “Differentiation of Human induced Pluripotent Stem Cells to Authentic Macrophages using Fully Defined, Serum Free, Open Source Media”, currently under submission for publication and found on the BioRxiv preprint server (421). It was contributed towards by Szymon Stodolak, Kourosh H. Ebrahimi, Cathy Browne, Paul K. Reardon, Elisabete Pires, Javier Gilbert-Jaramillo, Sally A. Cowley and William S. James. Text has been written by myself and contributions to analysis and design of figures by individuals have been stated where relevant.

3.1 Introduction

Ultimately, it is envisaged that SC-derived (preferably iPSC-derived) hematopoietic cells and/or their derivatives will be introduced into patients as a supplementary therapy, to correct genetic defects, or replace lost cells. To achieve this, though, clearly characterised cells cultured in fully defined media at sufficient yields must be produced. The essential signal processes involved in haematopoiesis and macrophage terminal differentiation have been explored in depth (179–181, 390). Based on this, numerous methods for the differentiation of macrophages from stem cells have been developed over the years. These can be broadly categorised into three types: monolayer cultures, co-cultures with xeno cells, and via embryoid body (EB) intermediates. Each vary in number of growth factors applied, timing, complexity, yield, and cost. A summary of these methodologies can be found in Table 1. Overall, protocols continue to need refining and improvement to overcome current limitations, particularly yield and the use of undefined and/or xeno components.

In order to investigate the molecular pathways involved in the pathogenesis of both infectious diseases, such as those caused by HIV-1 (196) and *Mycobacterium tuberculosis* (391), and degenerative diseases, especially Parkinson's disease (148, 392) and Alzheimer's disease (393, 394), the James lab previously developed a pathophysiologically authentic, yet genetically tractable model of human tissue macrophages derived from pluripotent stem cells. The first method involved spontaneous differentiation of mesoderm from embryonic stem cells via EBs, followed by myeloid differentiation using M-CSF (CSF-1) and IL-3 in a serum-supplemented medium (395). Since this was not effective for all pluripotent stem cell lines, and in order to remove the undefined serum component, a subsequently serum-free method was developed, using BMP4, VEGF and SCF to promote mesodermal lineage and prime haemogenic endothelium differentiation during EB formation, and the serum-free X-VIVO™ 15 (XVIVO) medium (Lonza) during the M-CSF/IL-3-directed myeloid differentiation stage (196).

With a greater focus than ever on ensuring research integrity in the life sciences through the adoption of open practices in data curation, publication and the sharing of materials (396–398), it is desirable to replace proprietary media used for culturing and differentiating human pluripotent stem cells with ones that are both defined and fully open-source. While great improvements have been made to move away from xeno-material containing co-culture and serum-based methodologies towards well defined monolayer and EB protocols, of the methods described in Table 1, only one has been described to utilise fully defined and open-sourced media throughout differentiation (Cao *et al.*, 2019). The remainder either supplement cultures with serum, or rely on commercial, serum-free alternatives of undisclosed composition. The suppliers of both the commercial induced pluripotent stem cell (iPSC) culture medium Essential 8, used previously for early EB differentiation, and X-VIVO (StemCell Technologies and Life Technologies) decline to publish the composition of these materials on commercial grounds. Consequently, the scientific community does not know whether components that may have a material effect on macrophage physiology are present, nor their concentration. Examples could include, but are not limited to, anti-infectives, anti-inflammatories, cell-permeable iron-chelators cryoprotectants, and excessive concentrations of glucose. Accordingly, our lab has sought to base replacement media on widely available and open-source materials, enabling others to reproduce our experiments conveniently and without undue dependence on particular suppliers.

In this chapter, I describe OXM, an open-source alternative macrophage differentiation medium based on Advanced DMEM/F12. I show that OXM generates homogeneous macrophage precursors very comparable to those produced by our earlier methods, both phenotypically and transcriptionally. These cells show signatures consistent with more complete terminal differentiation, including improved morphology and cell cycle arrest, and have lower basal expression levels of interferon-inducible genes while being more responsive to inflammatory stimulation. This method, therefore, generates cells that are even closer models of the “surveilling” state of homeostatic tissue macrophages.

Author and Date	Species	Stem Cell	Co-culture, EB, or monolayer?	# steps	Duration	Defined?	# supplemented growth factors	Serum?	Proprietary component?	Approx. Yield	Notes	References
Wiles and Keller, 1991	Mouse	ESC	EB	2	2-8 weeks	No	IL-3, M-CSF	10-15%	No	N/A	Primarily a haematopoiesis protocol with details on driving Macrophage differentiation	(174)
Nakano *et al.*, 1994	Mouse	ESC	Co-culture with OP9 cells	2	10 days	No	M-CSF	20%	No	700/ stem cell	Primarily a haematopoiesis protocol with details on driving Macrophage differentiation	(178)
Moore *et al.*, 1998	Mouse	ESC	EB	3	15-17 days	No	IL-3, M-CSF	10-15%	No	1-4/stem cell	media based on Wiles and Keller 1991	(174, 400)
Lindmark *et al.*, 2004	Mouse	ESC	EB	3	15-17 days	No	IL-3, M-CSF, IL-1B	10%	Yes	N/A	Based on Moore *et al.* 1998	(195, 400)
Anderson *et al.*, 2006	Human	ESC	Co-culture with S17 cells	3	30-37 days	No	GM-CSF, M-CSF	10-15%	No	N/A		(176)
Odegaard *et al.*, 2007	Mouse	ESC	EB	5	Infinite	No	SCF, B-estradiol, IL-3	10-15%	Yes	Infinite	Myeloid progenitors immortalised using retrovirus expressing Hox9a	(401)
Karlsson *et al.*, 2008	Human	ESC	EB	3	2 weeks - 4 months	No	IL-3, M-CSF	10%	No	3-5x10^6/EB	Macrophages produced long term	(395)
Senju *et al.*, 2009	Mouse	iPSC	Co-culture with OP9 cells	3	22-25 days	No	GM-CSF, M-CSF	20% & 5%	No	400-600/ stem cell	Yield for dendritic cells, not macrophages	(402)
Choi *et al.*, 2009	Human	ESC and iPSC	Co-culture with OP9 cells	3	15-24 days	No	GM-CSF, M-CSF, IL-1B	10%	No	15 per stem cell		(403)
Subramanian *et al.*, 2011	Human	ESC	EB	4	21-22 days	No	SCF, IL-3, IL-6, M-CSF, BMP-4, FLT3L, G-CSF, GM-CSF, M-CSF	20%	No	0.45/ CD34+ progenitor		(404)
Choi *et al.*, 2011	Human	ESC and iPSC	Co-culture with OP9 cells	3	16-19 days	No	GM-CSF, M-CSF, IL-1B	10%	No	1 per stem cell	optimized protocol of Choi *et al.* 2009	(403, 405)
Senju *et al.*, 2011	Human	iPSC	Co-culture with OP9 cells	3	31-44 days	No	GM-CSF, M-CSF	10-20%	No	N/A		(406)
	Human	iPSC	Monolayer	3	>36 days	Yes	GM-CSF, M-CSF	No	Yes	N/A		
Salvagiotto *et al.*, 2011	Human	ESC and iPSC	Monolayer	5	18-22 days	Yes	BMP4, FGF, TPO, SCF, FLT3L, IL-6, IL-3, GM-CSF, M-CSF, IL-1B	No	Yes	3 per CD34+ progenitor		(407)
Klimchenko *et al.*, 2011	Human	ESC	EB	3	15-40 days	No	BMP4, VEGF, SCF, FLT3L, TPO, IL-3, GM-CSF, M-CSF	15%	No	300,000		(408)
Kambal *et al.*, 2011	Human	iPSC	Co-culture with OP9 cells	3	>9 days	No	GM-CSF, M-CSF	10%	Yes	N/A	method based on Vodyanik *et al.*, 2005	(409, 410)
Zhuang *et al.*, 2012	Mouse	ESC	EB	3	10-30 days	No	IL-3, M-CSF	10%	No	20-40/stem cell		(411)

Author and Date	Species	Stem Cell	Co-culture, EB, or monolayer?	# steps	Duration	Defined?	# supplemented growth factors	Serum?	Proprietary component?	Approx. Yield	Notes	References
Yanagimachi *et al.*, 2013	Human	iPSC	Monolayer	5	22-38 days	No	BMP4, VEGF, SCF, FGF, IL-3, TPO, FLT3L, GM-CSF, M-CSF	10%	Yes	6x10^6/30 stem cell colonies		(412)
van Wilgenburg *et al.*, 2013	Human	iPSC	EB	3	2 weeks - 12 months	Yes	VEGF, BMP4, SCF, FGF, IL-3, M-CSF	No	Yes	50/ stem cell	Based on Karlsson *et al.* 2008 method.	(196, 395)
Brault *et al.*, 2014	Human	iPSC	Co-culture with OP9 cells	4	25-31 days	No	GM-CSF, M-CSF	10%	No	3/ stem cell		(218)
Schwartz *et al.*, 2015	Human	iPSC	Monolayer	6	17-25 days	No*	BMP4, Activin A, FGF, VEGF, TPO, SCF, GM-CSF, M-CSF, IL-1B	10%	No	N/A	*Haematopoietic progenitor differentiation in fully defined medium from Uenishi *et al.*, 2014	(194, 413)
Lachmann *et al.*, 2015	Human	iPSC	EB	3	17 days - 5 months	No	FGF, IL-3, M-CSF	10%	No	1x10^6/week		(414)
Zhang *et al.*, 2015	Human	iPSC	EB	5	22 days	No	BMP4, VEGF, SCF, TPO, FLT3L, FGF, M-CSF	20%	Yes	2x10^6/6-well plate		(198)
Mucci *et al.*, 2016	Mouse	iPSC	EB	3	18-28 days	No	IL-3, SCF	10-15%	No	10/ stem cell	similar protocol to Lachmann *et al.* 2015	(414, 415)
Takata *et al.*, 2017	Mouse	iPSC	Monolayer	4	11-13 days	Yes	FGF, BMP4, Activin A, VEGF, SCF, IL-3, M-CSF	No	Yes	N/A		(416)
	Human	iPSC	Monolayer	6	23 days	Yes	BMP4, VEGF, CHIR99021*, FGF, SCF, DKK1, IL-3, IL-6, M-CSF	No	Yes	10-20/stem cell	*CHIR99021 is a WNT agonist	
Hansen *et al.*, 2018	Human	iPSC	Monolayer	5	27-28 days	Yes	VEGF, BMP4, IL-3, IL-6, TPO, SCF, FLT-3, G-CSF, GM-CSF	No	Yes	2000/ stem cell	to make myeloid cells - not just macrophages	(417)
Ackermann *et al.*, 2018	Human	iPSC	EB	4	10 days - 7 weeks	No	IL-3, M-CSF	10%	Yes	1-3x10^7/week	Similar method to Lachmann et al 2015	(414, 418)
Mukherjee *et al.*, 2018	Human	iPSC	EB	3	4 weeks – 8 months	No	IL-3, M-CSF	10%	Yes	N/A	Based on van Wilgenburg *et al.* 2013	(196, 419)
Cao *et al.*, 2019	Human	iPSC	Monolayer	5	19 days	Yes	BMP4, Activin A, CHIR99021*, VEGF, FGF, SCF, SB431542**, IL-6, TPO, IL-3, M-CSF	No	No	30-40/ stem cell	Media based on Uenishi *et al.* 2014. * CHIR99021 - WNT agonist. †SB431542 - TGFb inhibitor	(399, 413)
Monkley *et al.*, 2020	Human	iPSC	EB	5	13-39 days	No	BMP4, VEGF, SCF, FGF, IL-3, TPO, FLT3L, GM-CSF, M-CSF	10%	Yes	~40/stem cell	Based on Yanagimachi et al 2013	(412, 420)
Vaughan-Jackson et al.	*Human*	*iPSC*	*EB*	*3*	*2 weeks - 4 months*	*Yes*	VEGF, BMP4, SCF, FGF, IL-3, M-CSF	*No*	*No*	*20-30/ stem cell*	*Method based on van Wilgenburg et al. 2013*	(196, 395, 421)

***Table 1: Protocols for differentiation of macrophages from stem cells**. Not including specific macrophage subsets e.g. microglia.*

3.2 Results

3.2.1 XVIVO medium, but not OXM medium, contains undisclosed molecules

Based on preliminary optimization by Prof. William James, I first characterised a serum-free, defined, open-source medium, named OXM, for differentiation of iPSC to macrophages. Previously the James lab described methodologies for differentiation to macrophages (196, 395) using Advanced DMEM (aDMEM) or RPMI supplemented with 10% fetal calf serum (FCS), or a serum free alternative, X-VIVO-15™ (XVIVO). However, because the composition of XVIVO is proprietary, we could not know whether the medium contained additives that may affect the phenotype of cells differentiated in this medium. We therefore decided to use aDMEM/F-12 buffered with HEPES as the base of OXM, as used for iPSC culture in OXE8, above. To replace FCS, additional insulin and Tropolone, a cell-permeable iron chelator previously shown to be a suitable substitute for transferrin in cell culture (Field, R.P., Lonza Group, 2003. Animal cell culture. U.S. Patent 6,593,140), were included. M-CSF and IL-3 were supplemented independently (Composition in Material and Methods: 2.3.1, Table 5).

To identify the cause of any potential differences between XVIVO and OXM-cultured macrophages, a limited investigation into the chemical composition of each was medium was carried out using high-resolution negative ion liquid chromatography-mass spectrometry (LC-MS), specifically screening for metabolites and polar molecules, but not proteins or non-polar molecules. This was run and analysed by Dr Kourosh Ebrahimi and Elisabete Pires from the McCullagh lab, Oxford Chemistry department. A comparison of the total ion chromatograms (TIC) showed that there are differences in the chemical composition between OXM and XVIVO (Figure 1A) as indicated by the intensity of individual peaks. A list of predicted metabolites is given in the supplementary information (Supplementary Table 1). Specifically, we noted a two-fold difference in C6 sugar concentration between XVIVO and OXM. With the help of Javier Gilbert in the James lab, I subsequently independently confirmed this by enzymatic assay, finding 34.3 mM glucose in XVIVO and 16.7 mM in aDMEM/F-12 (Figure 1B). LC-MS also predicted that the level of amino acids were at higher concentration in OXM than in XVIVO

except for Tryptophan (predicted concentration: 44 nM in OXM, 6.3 µM in XVIVO) (Supplementary table 1). Additionally, we noted that three peaks in the TIC of the XVIVO media were absent in that of the OXM media (Figure 1A). The best predicted molecules for these peaks are Isolariciresinol 9'-O-alpha-L-arabinofuranoside, (CID: 131751348, Figure 1C), Methyl glucosinolate (CID: 9573942, Figure 1D) and Dithinous acid (CID: 24490, Figure 1E) These molecules were either absent from the OXM media or below detection limit.

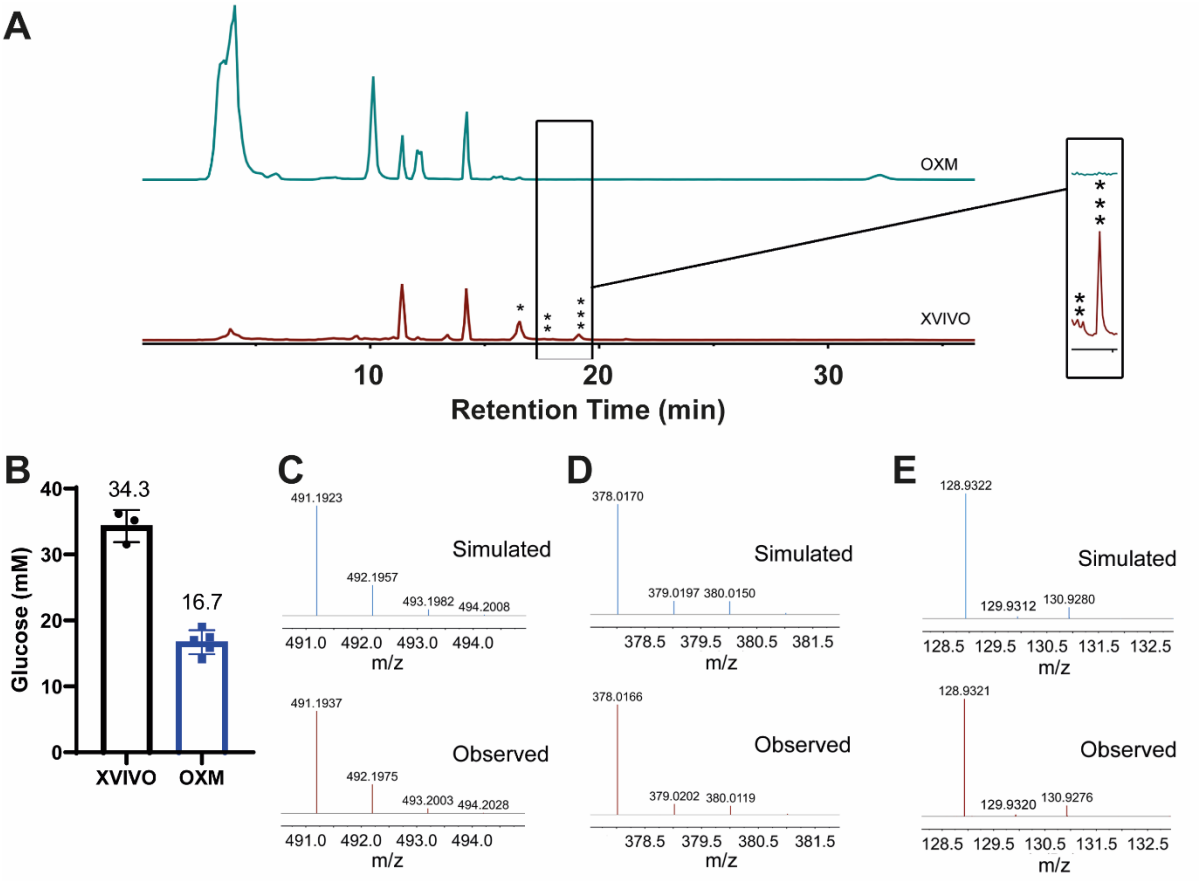


Figure 1: XVIVO medium, but not OXM medium, contains undisclosed molecules. *Negative ion high-resolution LC-MS spectroscopy was used to analyse different compounds in the media. A) TIC of the molecules in the XVIVO medium is compared to that of molecules in the OXM medium. B) Concentration of glucose in XVIVO and OXM media. n=3 (XVIVO) and 5 (OXM) independent experiments. Error bars represent ± SD. C) Comparison of the observed MS spectrum of the main peaks absent in OXM with the simulated spectrum of [M-H]$^-$ adduct of Isolariciresinol 9'-O-alpha-L-arabinofuranoside (*), D) that of [M+FA-H]$^-$ adduct of Methyl glucosinolate (**), and E) that of [M-H]$^-$ adduct of Dithionous acid (***).*

3.2.2 Differentiation of iPSC to macrophages in novel fully defined, open-source medium, OXM

I next sought to compare the maturation states of OXM-differentiated and cultured macrophages against those differentiated and cultured in XVIVO. Embryoid bodies (EBs) were formed and cultured for 4 days according to our prior publication (196). Minor modifications to methodology were made, including culturing in an in-house, defined, open-source Essential 8 alternative medium we call OXE8. OXE8 contains FGF-2 and TGF-β and further supplements of VEGF, BMP4, and SCF. For composition see Materials and Methods: 2.1.3, Table 1). After EB formation, as in our earlier methods, differentiation medium was supplemented with IL-3 and M-CSF while, in terminal macrophage differentiation media, IL-3 and tropolone were omitted (Figure 2A, Material and Methods: 2.3.1, Table 5). Morphological differences between differentiation cultures were immediately apparent. Embryoid bodies (EBs) produced larger cyst-like structures and greater adherent stromal growth in OXM medium (Figure 2A). By week 3 of differentiation, monocyte-like macrophage precursors cells (PreMacs) had started to be released into the supernatant. This continued for >16 weeks (Figure 2B, 2C). Interestingly, OXM differentiation cultures produced a large number of PreMacs in the first 3 weeks of production before their yield reduced to between 7-8x10^4 cells/mL/week. XVIVO differentiation cultures were slower to yield PreMacs but by week 6 produced approximately 2-fold more cells, an average of 1.4x10^5 cells/mL/week (Figure 2B). After 16 weeks the average total yield was (4.48 ± 1.26)x10^7 cells in OXM, and (7.99 ± 2.61)x10^7 cells in XVIVO (Figure 2C). PreMacs produced in OXM were significantly smaller than in XVIVO (range 15.8 - 19.5 µm, mean 17.9 µm, vs 13.8 - ≥20 µm, mean 19.5 µm respectively (Figure 2D)). Note that owing to limitations of the Nucleocounter® NC-3000, 20 µm is the upper limit of cell size, so XVIVO-produced cells may have been larger.

For terminal differentiation of PreMacs into macrophages, cells were cultured a further 7 days in macrophage differentiation medium. After 7 days, as previously observed, XVIVO-cultured cells remain rounded or acquire a bipolar morphology, with large vesicle-like structures visible. OXM-cultured cells were more adherent and morphologically heterogeneous with rounded cells, large, flattened cells, and cells with multiple projections (Figure 2A, expanded view in 2E). The size of adherent macrophages was measured after resuspension. OXM-cultured macrophages were significantly smaller than those in XVIVO: mean 17.51 µm (range 16.28 - 18.53 µm) vs mean 19.85 µm (range 19.35 - ≥20 µm), (Figure 2F). Differences in time taken to resuspend OXM vs XVIVO cells showed that OXM cells were more adherent, both when cultured in macrophage medium or in fresh differentiation medium (Figure 2G-H). In summary, OXM supports the production of more adherent, smaller macrophages than XVIVO, albeit with a lower cumulative yield.

3.2.3 Macrophages cultured in OXM are phenotypically similar to, but distinct from, XVIVO-cultured cells

To determine macrophage phenotype, surface marker abundance was determined by flow cytometry. Key markers of macrophage lineage, the LPS co-receptor CD14 (Figure 3A), and the pan-leukocyte marker CD45 (Figure 3B), were highly expressed in macrophages derived using both media, with no significant differences. Nor was a difference observed with the expression of scavenger receptor CD163 (Figure 3C). Levels of the Fcγ IgG receptor, CD16, were significantly higher in OXM-cultured cells (Figure 3D). Conversely, both the β_2-integrin receptor, CD11b, and the costimulatory receptor, CD86, were more highly expressed in XVIVO cultured cells, suggesting a more M1-like phenotype (49) (Figure 3E, 3F). Consistent with our previous reports (196, 372, 395), MHC class II (HLA-DR) expression is low in these unstimulated cells in either condition (Figure 3G). Expression of the tissue-resident macrophage marker CD68 was observed intracellularly but not on the cell surface, consistent with prior literature (3) and was significantly higher in OXM-cultured cells (Figure 3H, S1H).

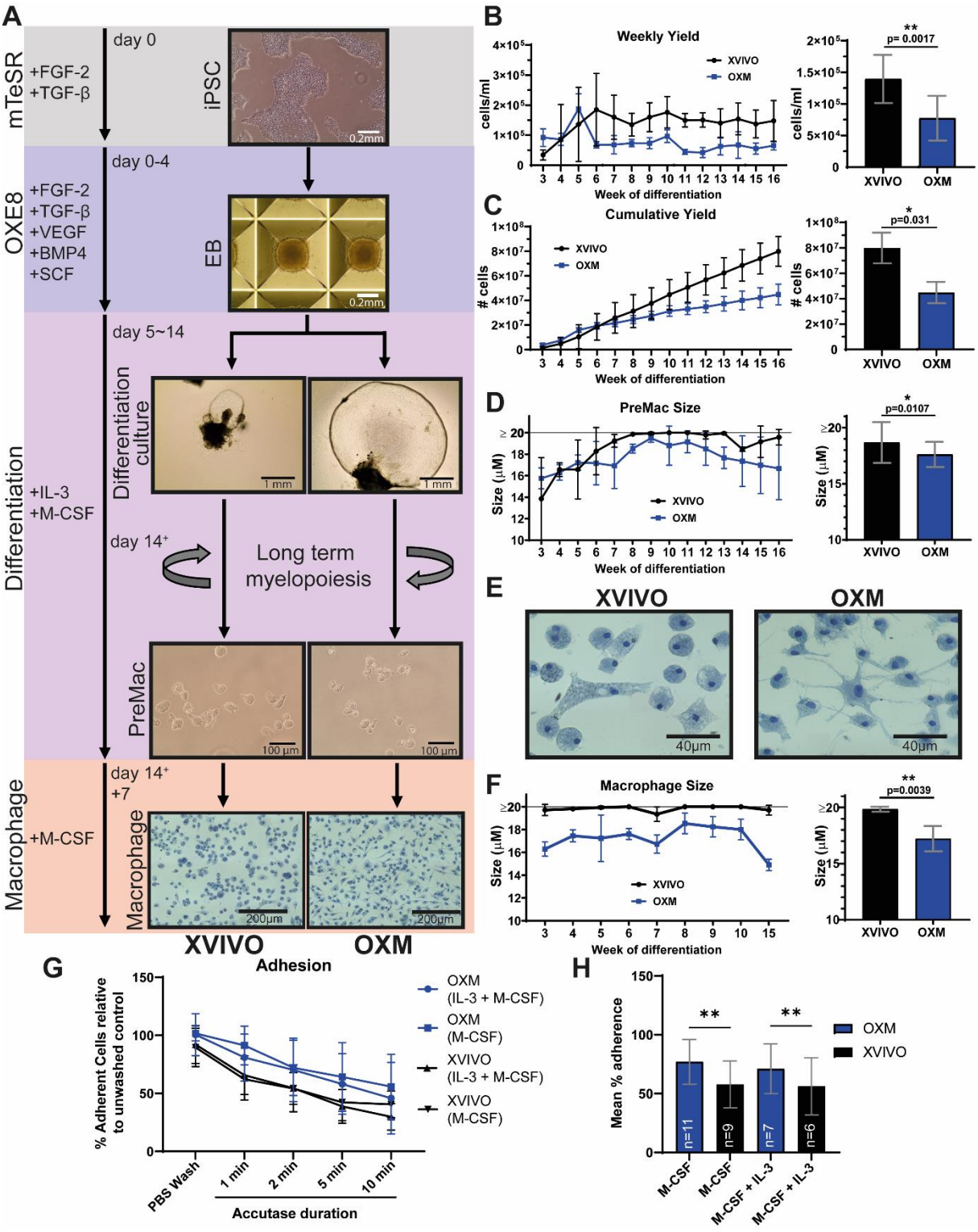

A
mTeSR
+FGF-2
+TGF-β
day 0
iPSC
0.2mm
OXE8
+FGF-2
+TGF-β
+VEGF
+BMP4
+SCF
day 0-4
EB
0.2mm
Differentiation
+IL-3
+M-CSF
day 5~14
Differentiation culture
1 mm
day 14+
Long term myelopoiesis
PreMac
100 µm
Macrophage
+M-CSF
day 14+ +7
Macrophage
200µm
XVIVO
OXM
B
Weekly Yield
cells/ml
Week of differentiation
XVIVO
OXM
** p= 0.0017
C
Cumulative Yield
cells
Week of differentiation
* p=0.031
D
PreMac Size
Size (µM)
Week of differentiation
* p=0.0107
E
XVIVO
OXM
40µm
F
Macrophage Size
Size (µM)
Week of differentiation
** p=0.0039
G
Adhesion
% Adherent Cells relative to unwashed control
OXM (IL-3 + M-CSF)
OXM (M-CSF)
XVIVO (IL-3 + M-CSF)
XVIVO (M-CSF)
PBS Wash
1 min
2 min
5 min
10 min
Accutase duration
H
Mean % adherence
**
**
OXM
XVIVO
n=11
n=9
n=7
n=6
M-CSF
M-CSF
M-CSF + IL-3
M-CSF + IL-3

Figure 2: Morphology throughout macrophage differentiation. *A) Schematic of iPSC-derived macrophage differentiation. Base media is displayed on the left with main growth factor supplements adjacent. B) Average weekly yield (left) and overall average weekly yield (right) of PreMac cells per mL of media removed from differentiation cultures. C) Cumulative yield of PreMac cells over 16 weeks of differentiation (left), final total yield (right). D) PreMac size over the lifespan of the differentiation culture (left), overall average PreMac size (right). E) Methylene blue (1% w/v) staining to show macrophage morphology. F) Macrophage size over multiple weeks of differentiation (left), overall average macrophage size (right). G) Percentage adherent cells cultured in fresh differentiation medium (M-CSF + IL-3) or macrophage medium (M-CSF) after incubation with Accutase™ normalised to untreated control. H) Average of adherent cells over time-course shown in (G). B-F) XVIVO-cultured cells represented in black vs OXM-cultured cells in blue, mean ± SD. B-C) n=2 experiments in each of 3 independent donors' cell lines. D, F) n=1 experiment in each of 3 independent donors' cell lines. G-H) n is displayed within the bars of (H) and made up from 2 independent donors' cell lines. B-F) Significance was calculated by Wilcoxon matched-pairs signed rank t-test. H) Significance was calculated by 2way ANOVA, Tukey's multiple comparison test. Significance is shown when p<0.05 (*), <0.01 (**), <0.001 (***).*

PreMac cells gave broadly similar results to those of fully differentiated macrophages although with differences in CD14 and CD16 expression from full differentiated macrophages (Figure S2). Overall, the PreMacs and macrophages produced using both OXM and XVIVO media display a macrophage phenotype but show small and consistent differences that may reflect differences in polarization.

Finally, to test the phagocytic capacity of macrophages produced under the two conditions, I measured phagocytic uptake of Alexa-488 conjugated zymosan, a yeast-derived particulate glycan. Phagocytic uptake of zymosan after 30 minutes was not significantly different between conditions across 3 genetic backgrounds (Figure S3), indicating that macrophages cultured in OXM are phagocytically competent.

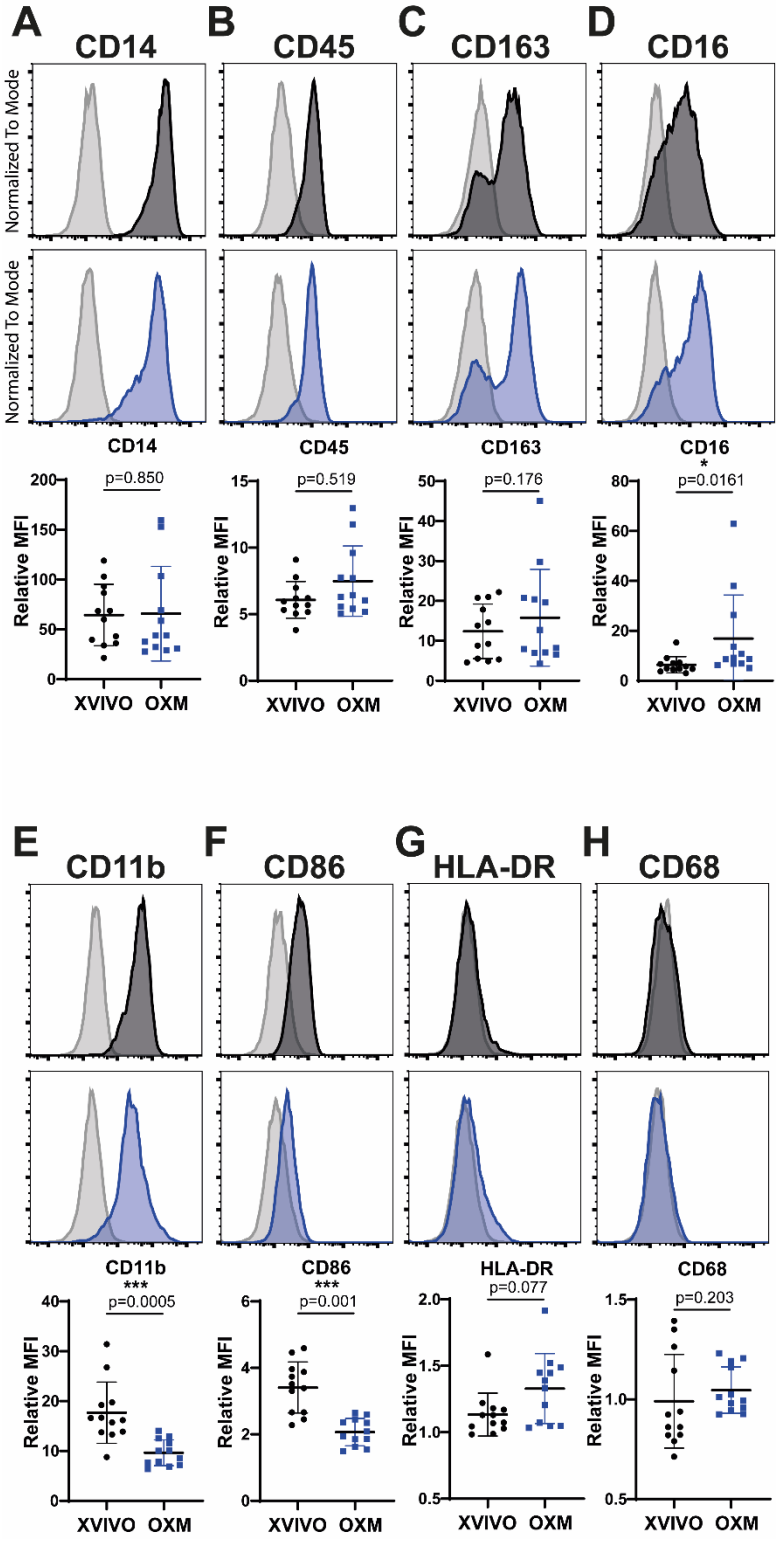


Figure 3: Macrophage surface marker phenotype.

Surface expression of A) CD14, B) CD45, C) CD163, D) CD16, E) CD11b, F) CD86, G) HLA-DR, and H) CD68 as measured by flow cytometry on macrophages. Histograms show fluorescence intensity (x-axis) normalised to the mode (y-axis) for macrophages cultured in XVIVO (black) or OXM (Blue), relative to the isotype control (grey). Dot plots show ratio of the geometric MFI compared to the isotype control. Bars display mean ± SD. n=4 experiments in each of 3 independent donors' cell lines. Significance was calculated by Wilcoxon matched-pairs signed rank t-test. Significance is shown when p<0.05 (*), <0.01 (**), <0.001 (***).

3.2.4 While transcriptionally very similar, OXM-cultured macrophages have a more homeostatic, and XVIVO-cultured macrophages a more immunologically active, signature

With Szymon Stodolak and Dr. Paul Reardon who together carried out the bioinformatical analysis, I used RNA-Seq to investigate the expression profile of the iPSC-derived macrophages. Taking a similar approach to previously published work by our group (149), I first compared the macrophages cultured in XVIVO or OXM to a published dataset of iPSC-derived human microglia (tissue resident macrophages of the brain) in order to ascertain as to what kind of macrophage our cells displayed most similarity. These had been differentiated via Hematopoietic Progenitor Cells (iHPCs), derived using modified protocols from prior reports, (183, 385, 422). This dataset was selected owing to its use of both MDM and iPSC-derived tissue macrophages (microglia) and the transcriptomics was run on bulk RNA-Seq data rather than single cell derived data. To limit variation introduced due to differences in sample preparation and transcriptomic data acquisition using different equipment (I.e. technical batch effects) both datasets were run through the same analytical pipeline, outputting gene expression as transcripts per kilobase million (TPM) (for more information see Chapter 2: Materials and Methods, 2.4 RNA). Naturally, without a common control cell line cultured equivalently between both datasets, some variation introduced through technical batch variation cannot be compensated for (e.g. using methods such as *ComBat* and *exploBatch* (423, 424)). However, considering experimental variation will influence cells of different type, genetic background, and culture method differently, even a control line would have limited efficacy in controlling for experimental batch variation. We therefore used routinely applied PCA as an unbiased test for overall trends in differences in gene expression to best control for variation as well as cell-type differences. Nevertheless, precise comparisons of gene expression between ours and the Abud dataset (385) would be inappropriate, but rather should only be used as a general guide for trends in expression to determine overall phenotype.

PCA analysis, in which PC1 explained 27% of the variance, and PC2 explained 18%, showed tight clustering of OXM- and XVIVO-cultured cells together. The iPSC-derived macrophages showed closest similarity to microglia rather than iHPCs or monocyte-derived macrophages (MDM), and least similarity to pluripotent cells and definitive hematopoietic lineages such as dendritic cells (Figure 4A). This was expected because iPSC-macrophages have a primitive tissue macrophage ontogeny, similar to that of microglia which develop from primitive, yolk sac/embryonic fetal macrophages, and unlike adult definitive MDM that develop from hematopoietic progenitors in the bone marrow (25, 34, 35). Further differential expression analysis found 15,951 genes shared in both OXM and XVIVO populations, and 2335 genes unique to either OXM (1331) or XVIVO (1004) (Figure 4B). Analysis of the sources of this variation showed that the media used explained approximately 30% of the variation between samples, while the age of the differentiation culture (as indicated by the week of PreMac harvesting)) accounted for approximately 15%, and the remainder was due to residual, undefined sources (Figure 4C).

The three genes most significantly upregulated in OXM versus XVIVO were the carbohydrate binding lectin, *CHI3L1*, the tetraspanin, *CD37*, and the protease, *HTRA4* (p=0.0028, 0.0049 and 0.006, respectively). In XVIVO the most upregulated genes were the interferon-inducible protein *IFIT3*, the endonuclease *RNASE1*, and the epoxidase *SQLE* (p=0.0028, 0.006 and 0.006 respectively). The most enriched GO term in XVIVO compared to OXM-cultured cells, was “Response to virus” (Figure 4D-E). Multiple interferon inducible genes, e.g. *MX2*, *RSAD2*, and the *IFIT* family of proteins, were more highly expressed in XVIVO-cultured cells. However, some antiviral receptors like *TLR8* are more highly expressed in OXM-cultured cells. We also found enrichment of metabolism-related processes. In OXM-cultured cells, the most highly enriched GO term was “triglyceride homeostasis” (Figure S4A), and in XVIVO-cultured cells the “cholesterol biosynthetic process” was highly enriched with 23/33 genes in this term upregulated in these cells (Figure 4D, 4F). The term “DNA replication initiation” was enriched in XVIVO-cultured cells (Figure S4B). To test whether XVIVO cells may therefore be in cell cycle, I measured total KI67, which transcriptionally has 2.66-fold

higher expression in XVIVO-cultured cells (Figure S4C), by immuno-staining and flow cytometry. This confirmed expression is higher but note that only a small proportion of cells (XVIVO; 1.15% +/- 0.90%, OXM; 0.54% +/- 0.55%) are in cell cycle (Figure S4D). In OXM, the inflammation related term “complement activation, classical pathway”, cell adhesion, and several developmental terms are enriched (Figure 4E, S4E). The enrichment of the cell adhesion term supports observations that OXM cultured cells were more adherent than XVIVO cultured cells (Figure 2G-H). Overall, when compared against adult microglia, both OXM and XVIVO-cultured cells show similar but distinct expression profiles of genes within the GO terms mentioned above (Figure S5). However, OXM macrophages, particularly, display more similar patterns of expression of genes regulating the cell cycle and cholesterol metabolism compared to microglia (Figure S5C-D). Transcriptomic analysis has shown that although cells cultured in these different media are highly similar, XVIVO-cultured macrophages display a greater tendency towards proliferation and an activated antiviral response, and OXM-cultured macrophages towards homeostasis, adhesion, and inflammation.

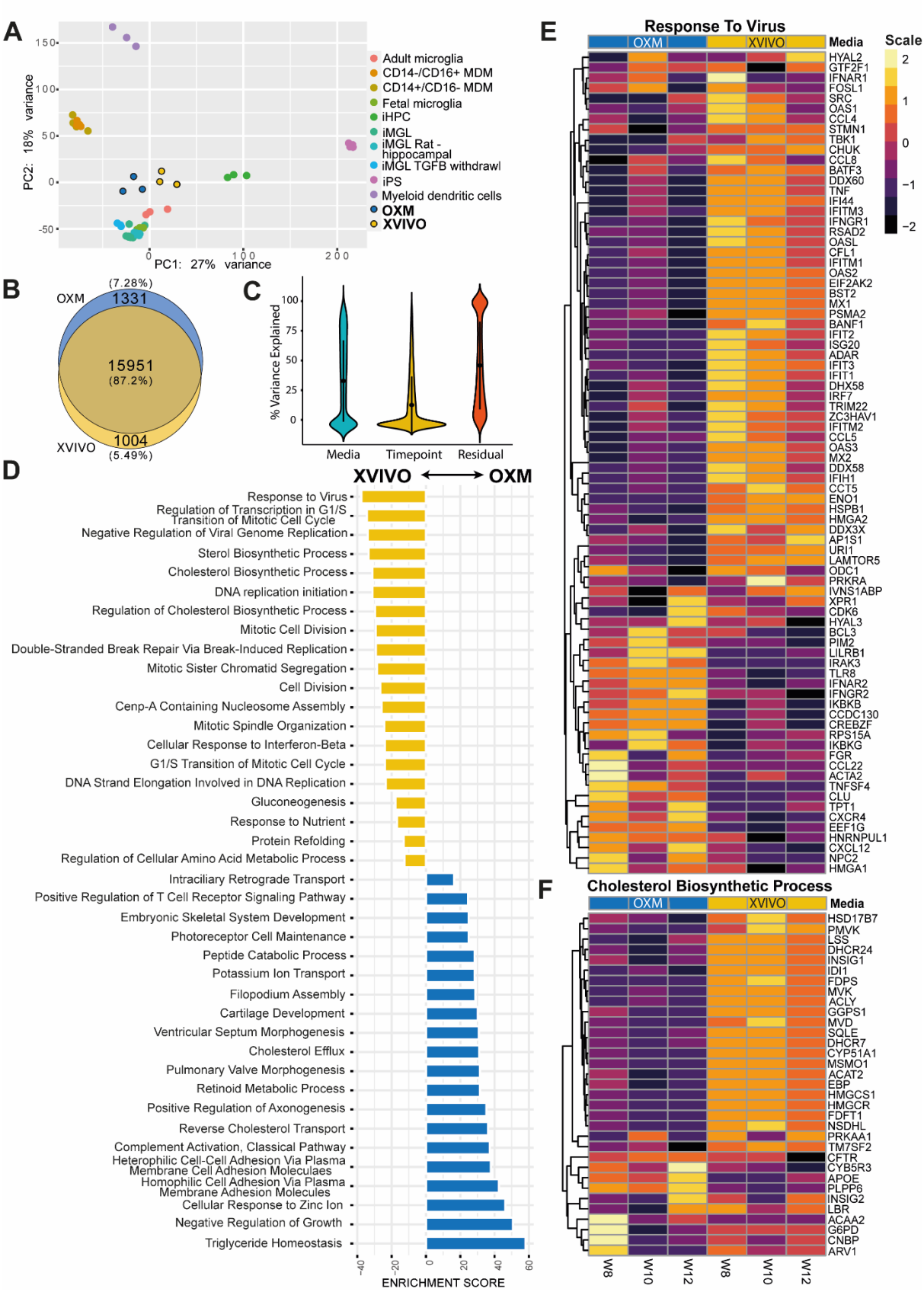

A
PC2: 18% variance
PC1: 27% variance
Adult microglia
CD14-/CD16+ MDM
CD14+/CD16- MDM
Fetal microglia
iHPC
iMGL
iMGL Rat - hippocampal
iMGL TGFB withdrawl
iPS
Myeloid dendritic cells
OXM
XVIVO
B
OXM
1331
(7.28%)
15951
(87.2%)
XVIVO
1004
(5.49%)
C
% Variance Explained
Media
Timepoint
Residual
D
XVIVO ⟷ OXM
Response to Virus
Regulation of Transcription in G1/S Transition of Mitotic Cell Cycle
Negative Regulation of Viral Genome Replication
Sterol Biosynthetic Process
Cholesterol Biosynthetic Process
DNA replication initiation
Regulation of Cholesterol Biosynthetic Process
Mitotic Cell Division
Double-Stranded Break Repair Via Break-Induced Replication
Mitotic Sister Chromatid Segregation
Cell Division
Cenp-A Containing Nucleosome Assembly
Mitotic Spindle Organization
Cellular Response to Interferon-Beta
G1/S Transition of Mitotic Cell Cycle
DNA Strand Elongation Involved in DNA Replication
Gluconeogenesis
Response to Nutrient
Protein Refolding
Regulation of Cellular Amino Acid Metabolic Process
Intraciliary Retrograde Transport
Positive Regulation of T Cell Receptor Signaling Pathway
Embryonic Skeletal System Development
Photoreceptor Cell Maintenance
Peptide Catabolic Process
Potassium Ion Transport
Filopodium Assembly
Cartilage Development
Ventricular Septum Morphogenesis
Cholesterol Efflux
Pulmonary Valve Morphogenesis
Retinoid Metabolic Process
Positive Regulation of Axonogenesis
Reverse Cholesterol Transport
Complement Activation, Classical Pathway
Heterophilic Cell-Cell Adhesion Via Plasma Membrane Cell Adhesion Moleculaes
Homophilic Cell Adhesion Via Plasma Membrane Adhesion Molecules
Cellular Response to Zinc Ion
Negative Regulation of Growth
Triglyceride Homeostasis
ENRICHMENT SCORE
E
Response To Virus
OXM
XVIVO
Media
Scale
HYAL2
GTF2F1
IFNAR1
FOSL1
SRC
OAS1
CCL4
STMN1
TBK1
CHUK
CCL8
BATF3
DDX60
TNF
IFI44
IFITM3
IFNGR1
RSAD2
OASL
CFL1
IFITM1
OAS2
EIF2AK2
BST2
MX1
PSMA2
BANF1
IFIT2
ISG20
ADAR
IFIT3
IFIT1
DHX58
IRF7
TRIM22
ZC3HAV1
IFITM2
CCL5
OAS3
MX2
DDX58
IFIH1
CCT5
ENO1
HSPB1
HMGA2
DDX3X
AP1S1
URI1
LAMTOR5
ODC1
PRKRA
IVNS1ABP
XPR1
CDK6
HYAL3
BCL3
PIM2
LILRB1
IRAK3
TLR8
IFNAR2
IFNGR2
IKBKB
CCDC130
CREBZF
RPS15A
IKBKG
FGR
CCL22
ACTA2
TNFSF4
CLU
TPT1
CXCR4
EEF1G
HNRNPUL1
CXCL12
NPC2
HMGA1
F
Cholesterol Biosynthetic Process
OXM
XVIVO
Media
HSD17B7
PMVK
LSS
DHCR24
INSIG1
IDI1
FDPS
MVK
ACLY
GGPS1
MVD
SQLE
DHCR7
CYP51A1
MSMO1
ACAT2
EBP
HMGCS1
HMGCR
FDFT1
NSDHL
PRKAA1
TM7SF2
CFTR
CYB5R3
APOE
PLPP6
INSIG2
LBR
ACAA2
G6PD
CNBP
ARV1
W8
W10
W12
W8
W10
W12

Figure 4: Transcriptome of iPSC-derived macrophages*. Transcriptome of macrophages as measured by RNA-Seq of 3 biological replicates per media condition from one genetic background (SFC840-03-03). A) PCA plot of transcriptional profile for iPSC-derived macrophages cultured in XVIVO or OXM compared to iPSC, induced haematopoietic progenitor cells (iHPC), microglia (MGL) (adult, fetal, iPSC-derived, and iPSC-derived with TFGB withdrawal), monocytes (MDM), and dendritic cells previously reported (Abud et al., 2017). B) Venn diagram representing total number of genes expressed by iPSC-derived macrophages in either media composition. C) Violin plot of the percentage variance attributed to each variable (media, timepoint, and residual). D) GO term enrichment between media compositions. Top 15 most enriched results in each medium are shown. Yellow represents terms enriched in XVIVO-cultured cells, and blue in OXM-cultured cells. E-F) Heatmaps of GO terms for; "Response to Virus" and "Cholesterol Biosynthetic Process". Results across 3 repeat measurements are shown. XVIVO in yellow, OXM in blue. The colour in each row represents the z-score of the log2 fold difference from the mean TPM value for that gene.*

3.2.5 OXM and XVIVO cultured macrophages have different classical and alternative activation profiles

To test whether the subtle transcriptomic differences between the cells differentiated in the two media resulted in functional detectable differences, I measured cytokine secretion and polarisation after stimulation. Cytokine secretion was measured at resting state and after classical (LPS and INFγ) or alternative (IL-4) activation, as previously described (196, 197). Cytokine profiles under both conditions were consistent with the previous reports (Figure 5A). OXM-cultured cells produced noticeably more GROα, ICAM-1, IL-1ra, and IL-8 in the resting state, while XVIVO-cultured cells produced more IP-10 (CXCL10). After classical activation, XVIVO-cultured cells produced more TNFα, as well as low levels of IL-12p70, while OXM-cultured cells produced more RANTES (CCL5) and small quantities of IL-1β. Alternative activation suppressed secretion of resting state cytokines in both media. Consistent with the results above, LPS-induced TNFα secretion from OXM-cultured cells quantified by enzyme-linked immunosorbent assay (ELISA) was lower than from XVIVO cells (Figure 5B).

Considering the differences in cytokine production, I next assessed macrophage surface marker polarisation towards classically defined M1 and M2 states after activation. This was measured by immuno-staining for CD86 and CD206, respectively (49, 425) (Figure 5C-D). Although activation had no effect on CD45 expression in both conditions, CD86 expression significantly increased in OXM-cultured cells compared to XVIVO-cultured cells after classical activation (4.75-fold vs. 0.81-fold). CD206 expression increased in both conditions after alternative activation and was not significantly different between conditions (1.86-fold vs 2.16-fold) (Figure 5C-D). In conclusion, although cells cultured under either condition can respond well to stimuli, they differ in their cytokine profile, and cells cultured in OXM display greater changes in typical macrophage polarization surface markers than those in XVIVO.

3.2.6 OXM-cultured macrophages are more susceptible to HIV-1 infection, but not to Zika virus

Due to their positioning as sentinel cells throughout the body, tissue resident macrophages are often the first members of the immune system to respond to infection. Consequently, several pathogens have evolved to use these cells as a host during early infection, including viruses like human immunodeficiency virus-1 (HIV-1) and Zika virus (ZIKV). In the case of HIV-1, macrophages are hypothesised to act as a potential reservoir for chronic infection due to the long lived, non-replicating state of these cells (426, 427). To determine whether iPSC-macrophages would be a suitable model for modelling this disease, macrophages were infected with a macrophage-tropic (CCR5-tropic Ba-L envelope), GFP expressing, HIV-1 pseudotype virus. Infectivity was measured by expression of GFP after 72 hours by flow cytometry. A significantly higher proportion of macrophages cultured in OXM than in XVIVO were infected (6.76 ± 3.69% compared to 1.77 ± 1.23%; Figure 6A). Expression of the HIV-1 entry receptors CD4 and CXCR4 was not-significantly different between conditions, and CCR5 was higher in XVIVO-cultured macrophages (MFI relative to isotype: 6.16 ± 3.18 XVIVO vs 2.67 ± 1.52 OXM; Figure 6B). This difference in viral entry may be explained by the higher expression of known HIV-1 restriction factors in XVIVO-cultured cells including the *IFITM* and the *APOBEC* families of proteins, and *TRIM5α* (Figure 4F). To test whether differences in susceptibility are restricted to lentiviruses, I also assessed replication of ZIKV strain MR-766 (Uganda, 1947) in these cells. Cells produced in both media released virus after an eclipse phase of ~6 hours post infection with no difference in output titre ((3.36 ± 1.83)x10^7 pfu/mL XVIVO, (2.26 ± 1.14)x10^7 pfu/mL OXM at 48hpi; Figure 6C). Therefore, OXM-cultured macrophages are a good model for HIV-1 infection, and differences in viral susceptibility between culturing conditions are not pan-viral.

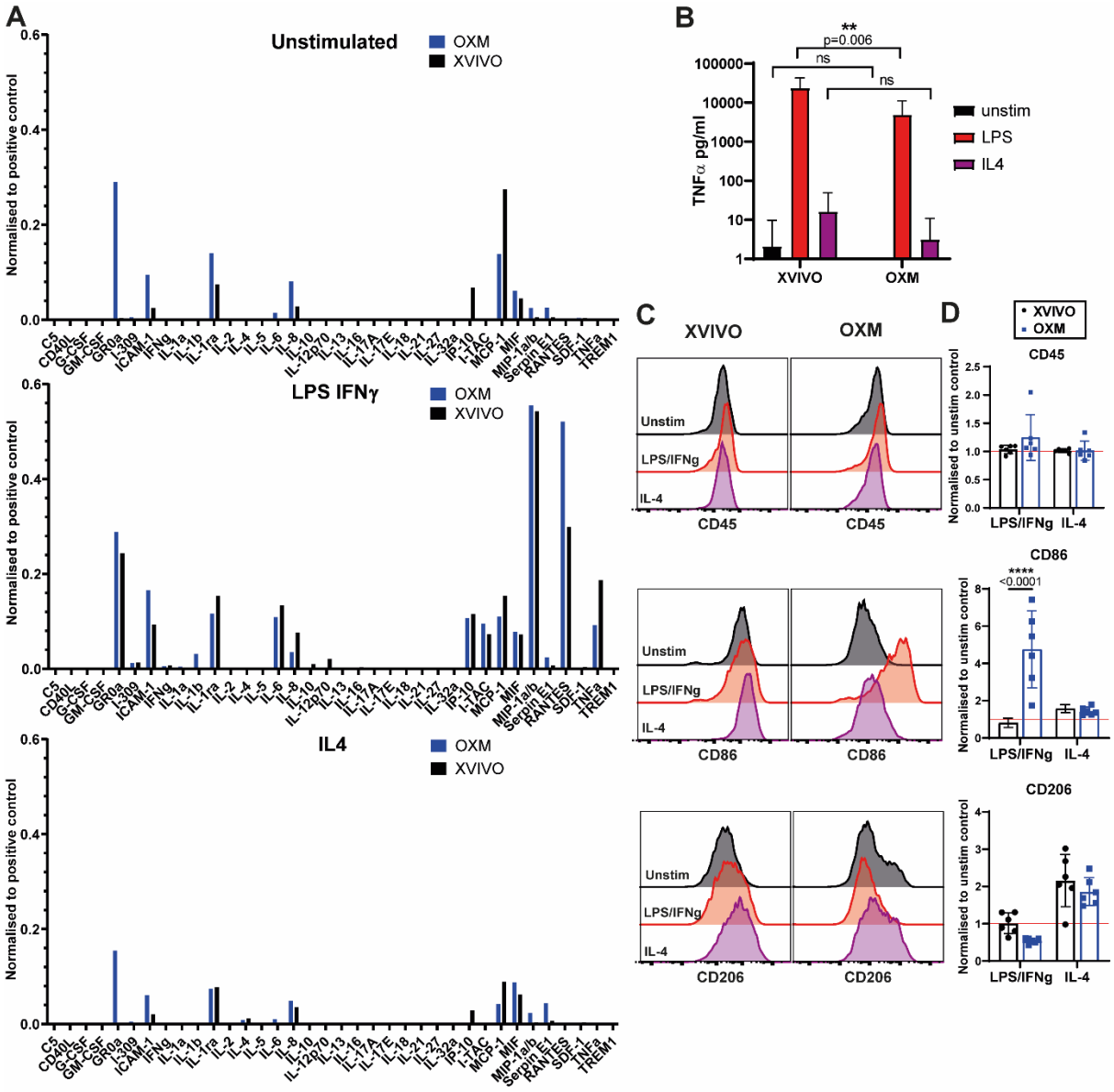


Figure 5: Macrophage activation states between culture media. *A) Cytokine secretion into the supernatant under unstimulated resting conditions (top), stimulated with 100 ng/mL LPS + 20 ng/mL IFNγ (middle), or 50 ng/mL IL-4 (bottom) normalised to a positive control. n=1 experiment. B) TNFα secretion from unstimulated (black), 100 ng/mL LPS (red), or 50 ng/mL IL-4 (purple) stimulated cells. Mean ± SD, n=5 experiments in each of 3 independent donors' cell lines. C) Surface expression of CD45, CD86, or CD206 measured by flow cytometry after stimulation, coloured according to (B). Histograms show fluorescence intensity (x-axis) normalised to the mode (y-axis). D) Geometric MFI relative to unstimulated control. Mean ± SD, n=3 experiments in each of 2 independent donors' cell lines. B-E) Significance was*

calculated by 2-way ANOVA, Sidak's multiple comparison test. Significance is shown when p<0.05 (*), <0.01 (**), <0.001 (***), <0.0001 (****).

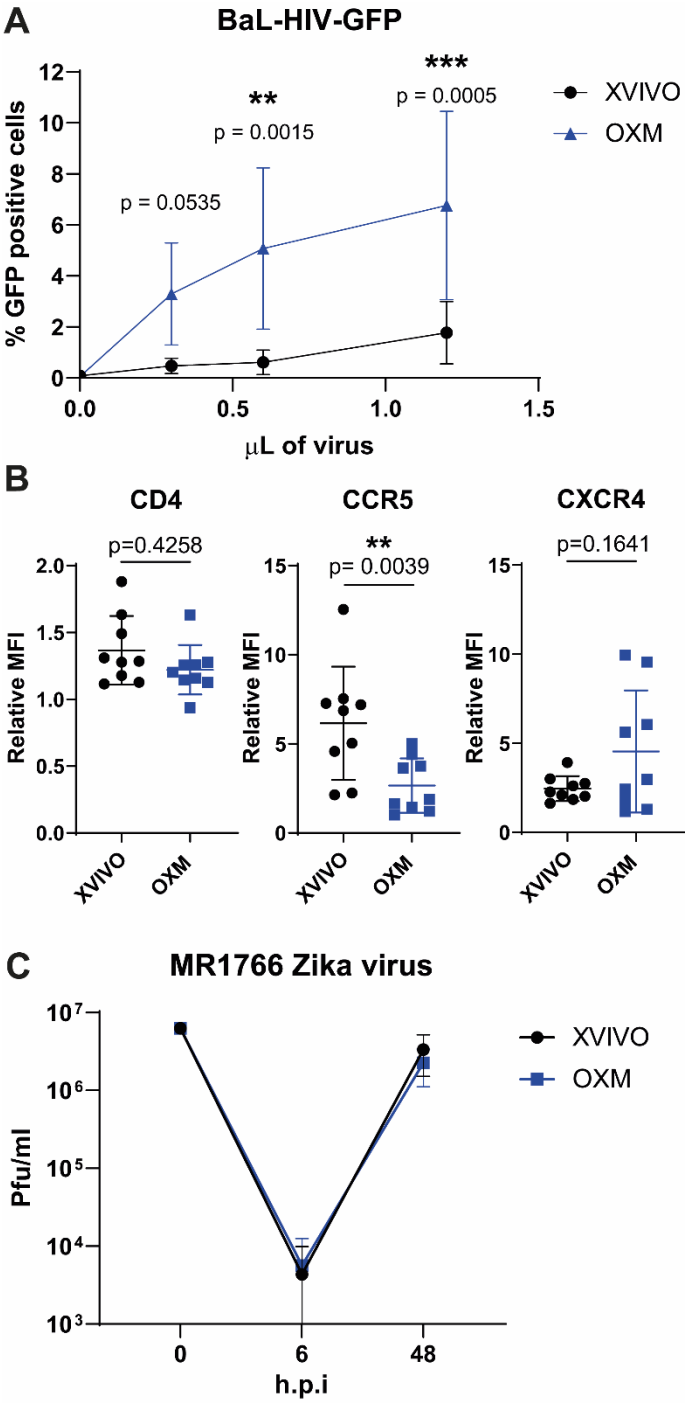


Figure 6: Macrophage infection by HIV-1 or Zika virus in different culture conditions.

A) Percentage of macrophages infected with a GFP-encoding, single-round HIV-1 pseudotyped virus measured by flow cytometry. B) CD4, CCR5, and CXCR4 surface expression measured by flow cytometry shown as ratio of geometric MFI to the isotype control. C) MR1766 Zika virus titre from infected macrophages shown in plaque forming units (pfu)/ml. Significance was calculated by A) 2-way ANOVA, Sidak's multiple comparison test, B) Wilcoxon matched-pairs signed rank t-test. A-C) Mean ± SD n=4 experiments in each of 2 independent donors' cell lines. Significance is shown when p<0.05 (*), <0.01 (**), <0.001 (***).

3.3 Discussion

The need to define an open-source medium for differentiating macrophages from iPSC was driven by two requirements. Firstly, to understand the finer changes in macrophage response to stimuli we must have a clear understanding of the resting conditions of these cells. Secondly, LC-MS analysis indicated the potential presence of several undisclosed molecules in the commercial serum-free alternative media, XVIVO™ 15, some of which could inhibit, or polarize the macrophage response if present. Our analysis putatively identified isolariciresinol 9'-O-alpha-L-arabinofuranoside, a lignan glycoside, which is known to have anti-inflammatory effects (428), as well as methyl glucosinolate and dithionous acid. While the precise functions of these molecules are unknown, it is worth noting that indole glucosinolates have been reported to have potent anti-inflammatory effects (429). In its ionised form (dithionite), dithionous acid is a strong reducing agent capable of affecting the redox state of haem-containing enzymes, such as cytochrome b, which may affect cell physiology (430).

I found that basing our new media, OXM, on aDMEM/F-12, did not prevent differentiation of macrophages from iPSC. However, I did see considerable differences in both yield and morphology. OXM-cultured cells were significantly more adherent, with the increased expression of adherence-related genes. This appeared to limit the harvestability of the cells cultured in OXM to once per week, most probably due to inducing cell adherence to plastic seen when cultured in fresh differentiation medium, but does not explain the observed reduced yield of macrophages cultured in this medium. The James lab has previously shown that XVIVO-cultured iPSC-macrophages are significantly larger than blood monocyte-derived macrophages (196), which are closer in size to OXM-cultured cells. Considering the very high levels of glucose in XVIVO medium, I suspected that there could be major differences in cell metabolism. I was therefore unsurprised to see that metabolism-related GO terms were among the most abundant terms differentially enriched between the media types. Whereas OXM-cultured cells were enriched for triglyceride homeostasis, reverse cholesterol transport and peptide catabolic process, XVIVO-cultured cells upregulated many genes involved in lipid

metabolism and cholesterol biosynthesis such as fatty acid synthase (*FASN*), 7-Dehydrocholesterol Reductase (*DHCR7*), and Acetyl-CoA Acetyltransferase 2 (*ACAT2*).

Macrophage metabolism differs substantially between activated states (M1 vs M2), with fatty acid synthesis upregulated in M1 cells and fatty acid oxidation upregulated in M2 cells (431). Unsurprisingly then, I observed that XVIVO-cultured cells had higher expression of markers of classical M1 (pro-inflammatory) polarization (17, 49). It is possible that this activated state in XVIVO is responsible for their relative insensitivity to LPS and IFNγ–induced changes in CD86 expression, unlike OXM-cultured cells, which displayed significant changes in this marker, although this does not appear to impact the cytokine response by these cells. Conversely, OXM-cultured cells showed similarities to non-classical or inflammatory monocytes, with increased expression of CD16. This potential pro-inflammatory phenotype may therefore be linked to the constitutive secretion of some inflammatory cytokines such as IL-6 and GROα, but its importance in cellular function is unclear. Nevertheless, this cytokine profile observed is consistent with previous work from the James lab (372) in which iPSC-derived microglia released similar cytokines in monoculture that were reduced when co-cultured with neurons. This suggests that my tissue resident macrophages likely receive anti-inflammatory signals from neighboring stromal cells as part of a regulatory feedback system. Overall, neither resting OXM or XVIVO-cultured macrophages clearly fell into conventional phenotypes, such as “classical”, “non-classical”, “M1-activated” or “M2-activated”. However, iPSC-derived macrophages have been shown to more closely resemble tissue macrophages, and therefore such categories, which are largely derived from work with adult blood MDM cultured in serum-containing medium, are an imperfect system for the phenotypic characterization of these cells (50, 61). Instead, tissue macrophages such as my iPSC-derived macrophages (35) ought to be considered more along a spectrum of activation states, subtly influenced by nutrient availability and extracellular matrix and cell-cell interactions in the various tissue environments they may occupy (10, 50, 55).

One surprising observation was that XVIVO-cultured cells appear to be transcriptionally primed for an antiviral response. I found higher expression of many interferon inducible genes

and constitutive secretion of the interferon inducible cytokine IP-10 (CXCL10). This clearly translated into a reduced infectivity of HIV-1 pseudotype virus in these cells compared to OXM-cultured cells despite the cells having higher expression of the surface receptor CCR5. However, it did not result in a difference in ZIKV infection of these cells. This is supported by the fact that OXM-cultured cells had higher expression of the interferon receptors *IFNAR2* and *IFNGR2*, and therefore are likely capable of mounting a strong antiviral response. It is worth noting that although expression of interferon genes was lower in OXM-cultured cells, it was not absent. These cells may therefore be a better model of pre-viral exposure macrophages.

3.4 Conclusion

To conclude, I describe the successful development of a defined and open-source medium for culturing human iPSC-derived macrophages. The hope is that the open-source nature of this medium will enable it to be used as a foundation for future improved differentiation protocols not only for macrophages, but also other iPSC-derived cell types. Cells cultured in OXM retain a majority of features to those cultured in XVIVO, but it is important to note that there are clear differences between them. This highlights the necessity of open composition of media if we are to compare between different methodologies, as well as the clear impact small changes in culture environment can have on macrophage morphology, phenotype, and function.

3.5 Supplementary information

Most likely molecule	OXM		XVIVO			Measured	Theoretical
	Intensity	Conc. (mol/L)	Intensity	calculated conc. (mol/L)	Ion	m/z	m/z
Tropolone	8.10E+05	1.50E-05	1.00E+06	1.85E-05	[M-H]	121.0293	121.0295
Pyruvic acid	8.00E+08	1.00E-03	6.70E+06	8.38E-06	[M-H]	87.009	87.0087
Leucine/isoleucine	3.00E+06	4.50E-04	nd	0.00E+00	[M-H]	130.0524	130.0509
L-Aspartic acid	4.70E+07	5.00E-05	nd	0.00E+00	[M-H]	132.0301	132.0302
Glutamic acid	1.80E+09	5.00E-05	2.00E+07	5.56E-07	[M-H]	146.0458	146.0458
Thymidine	7.00E+05	1.50E-06	1.40E+07	3.00E-05	[M-H]	241.083	241.083
Phenylalanine	1.80E+05	2.15E-04	3.00E+04	3.58E-05	[M-H]	164.0716	164.0717
C6 sugars (1)	2.60E+08	---	5.40E+08	---	[M-H]	179.0559	179.05611
C6 sugars (2)	4.90E+09	---	1.00E+07	---	[M-2H]	89.0243	89.024
Tryptophan	1.10E+05	4.40E+05	1.60E+07	6.40E+07	[M-H]	203.0827	203.0826

Supplementary Table 1: List of metabolites present in both media. Related to Figure 1.

Note: the C6 sugars (1) and (2) are different because the intensity ratio (C6 (1)/C6 (2)) is different between OXM and XVIVO.

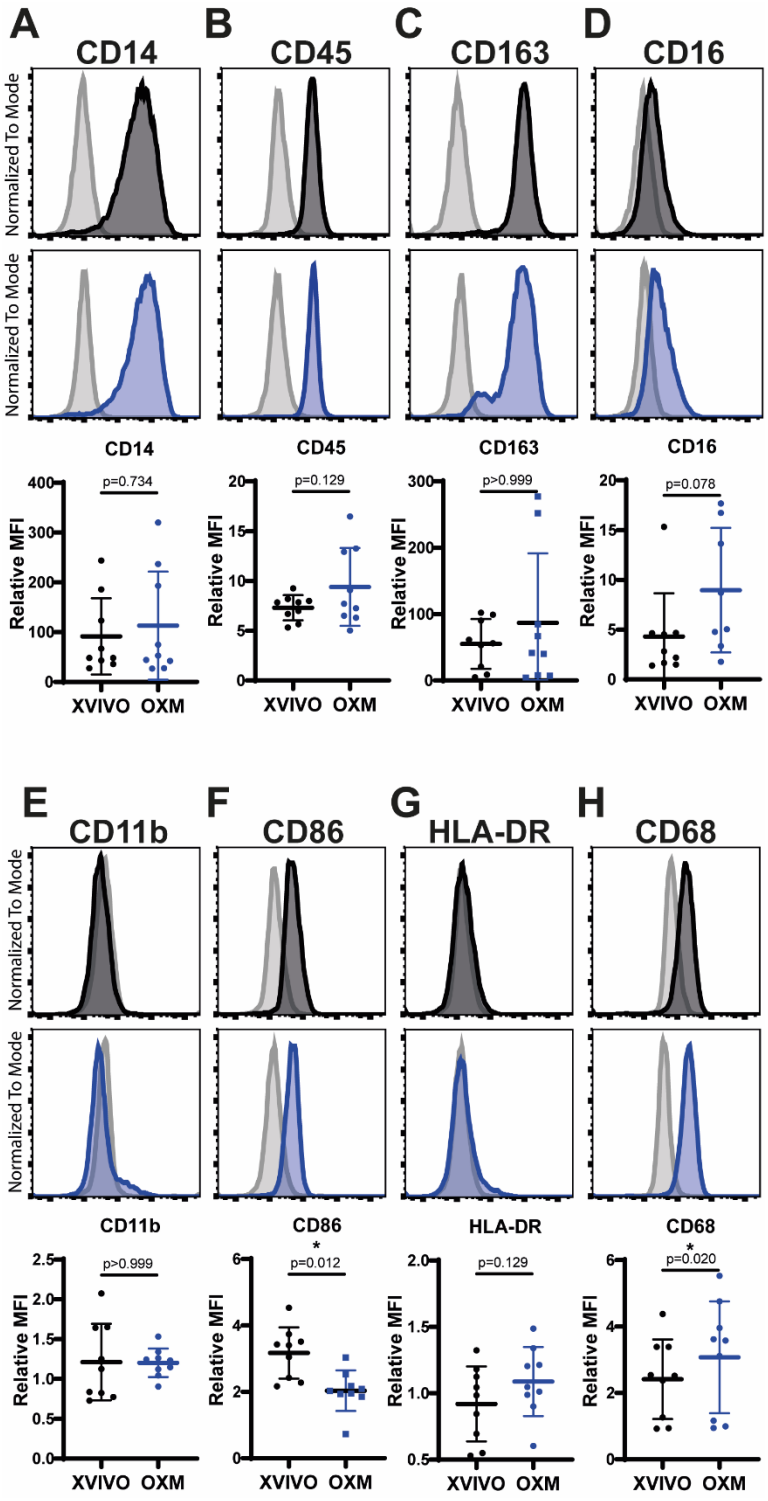


Figure S1: Macrophage total marker phenotype. Related to Figure 3. *Total expression of A) CD14, B) CD45, C) CD163, D) CD-16, E) CD11b, F) CD86, G) HLA-DR, and H) CD68 as measured by flow cytometry in macrophages. Histograms show fluorescence intensity (x-axis) normalised to the mode (y-axis) for macrophages cultured in XVIVO (black) or OXM (Blue), relative to the isotype control (grey). Dot plots show ratio of the geometric MFI compared to the isotype control. Bars display mean ± SD. n=12 across 3 independent cell lines. Significance was calculated by Wilcoxon matched-pairs signed rank t-test. Significance is shown when p<0.05 (*), <0.01 (**), <0.001 (***).*

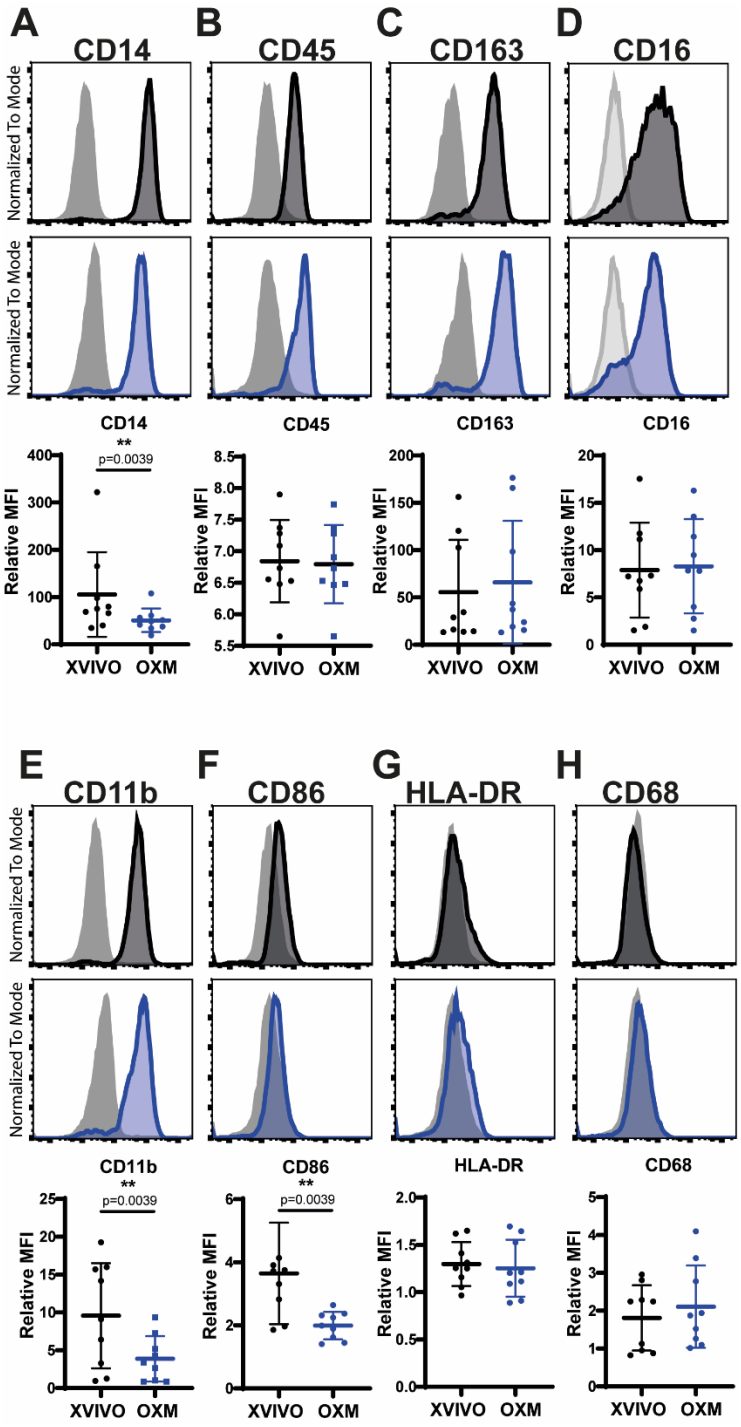


Figure S2: PreMac surface marker phenotype. Related to Figure 3. *Surface expression of A) CD14, B) CD45, C) CD163, D) CD-16, E) CD11b, F) CD86, G) HLA-DR, and H) CD68 as measured by flow cytometry on PreMac cells. Histograms show fluorescence intensity (x-axis) normalised to the mode (y-axis) for macrophages cultured in XVIVO (black) or OXM (Blue), relative to the isotype control (grey). Dot plots show ratio of the geometric MFI compared to the isotype control. Bars display mean ± SD. n=12 across 3 independent cell lines. Significance was calculated by Wilcoxon matched-pairs signed rank t-test. Significance is shown when p<0.05 (*), <0.01 (**), <0.001 (***).*

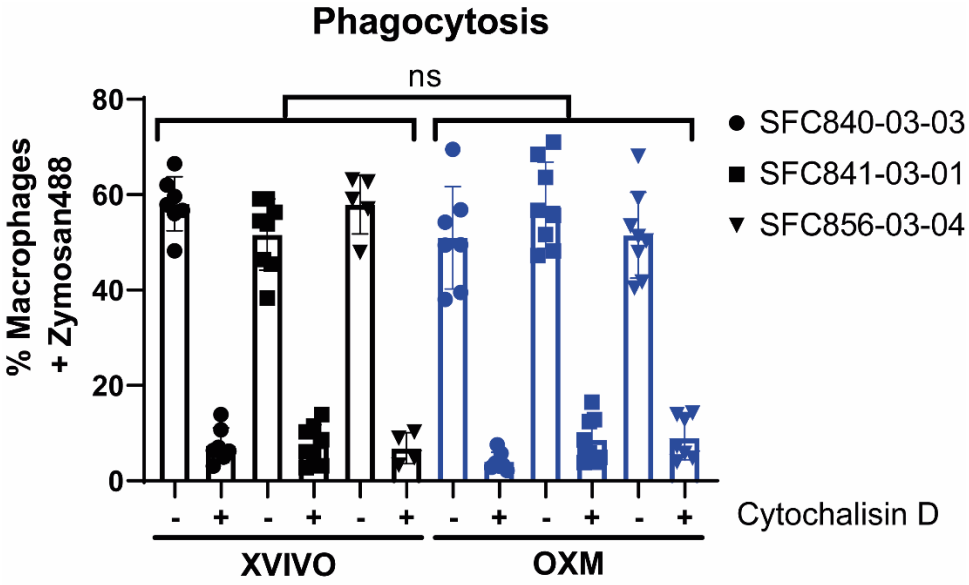


Figure S3: Phagocytosis in different culture conditions. Related to Figure 3. *Number of macrophages that are positive for Alexa-488 conjugated zymosan coated beads after 30-minute incubation, as measured by flow cytometry. Control cells were pre-treated with 10µM Cytochalasin D for 1 hour to inhibit phagocytosis. n=8 across 3 independent cell lines. Significance was calculated by 2-way ANOVA, Sidak's multiple comparison test. Significance is shown when p<0.05 (*), <0.01 (**), <0.001 (***).*

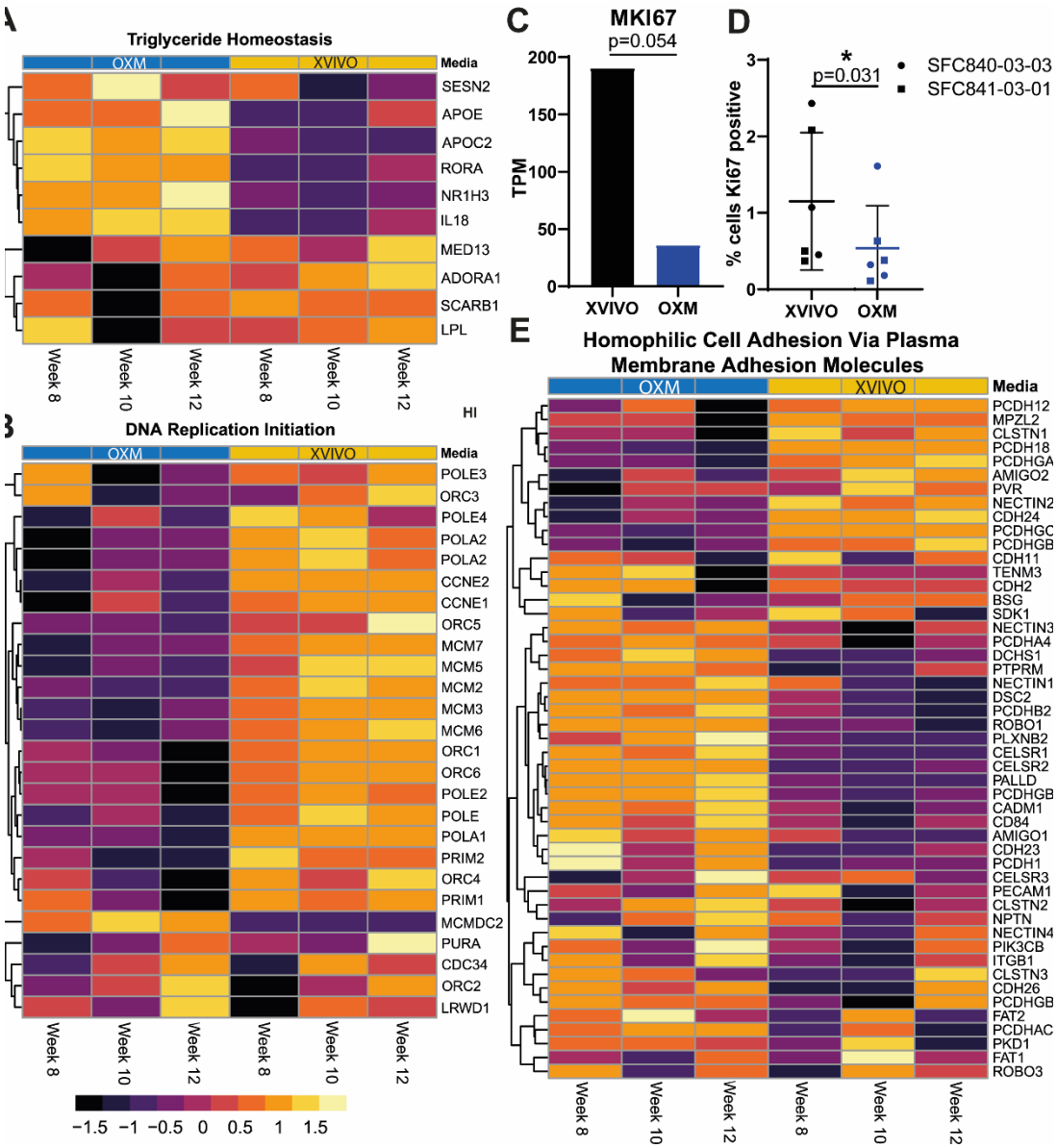


Figure S4: Macrophage cell cycle state. Related to Figure 4. *A-B, E) Heatmaps of GO terms for; A) Triglyceride Homeostasis, B) DNA Replication Initiation, and E) Homophilic Cell Adhesion Via Plasma Membrane Adhesion Molecules. Results across 3 repeat measurements are shown. XVIVO in yellow, OXM in blue. The colour in each row represents the z-score of the* log_2 *fold difference from the mean TPM value for that gene. C) Mean TPM values for MKI67 (KI67) expression in XVIVO vs OXM-cultured cells. D) Percentage of KI67 positive cells measured by immune-staining and flow cytometry. XVIVO in black, OXM in blue. n=6 in 2 independent cell lines. Mean and standard deviation shown. Significance was calculated by Wilcoxon matched-pairs signed rank t-test. Significance is shown when p<0.05 (*), <0.01 (**), <0.001 (***), <0.0001 (****).*

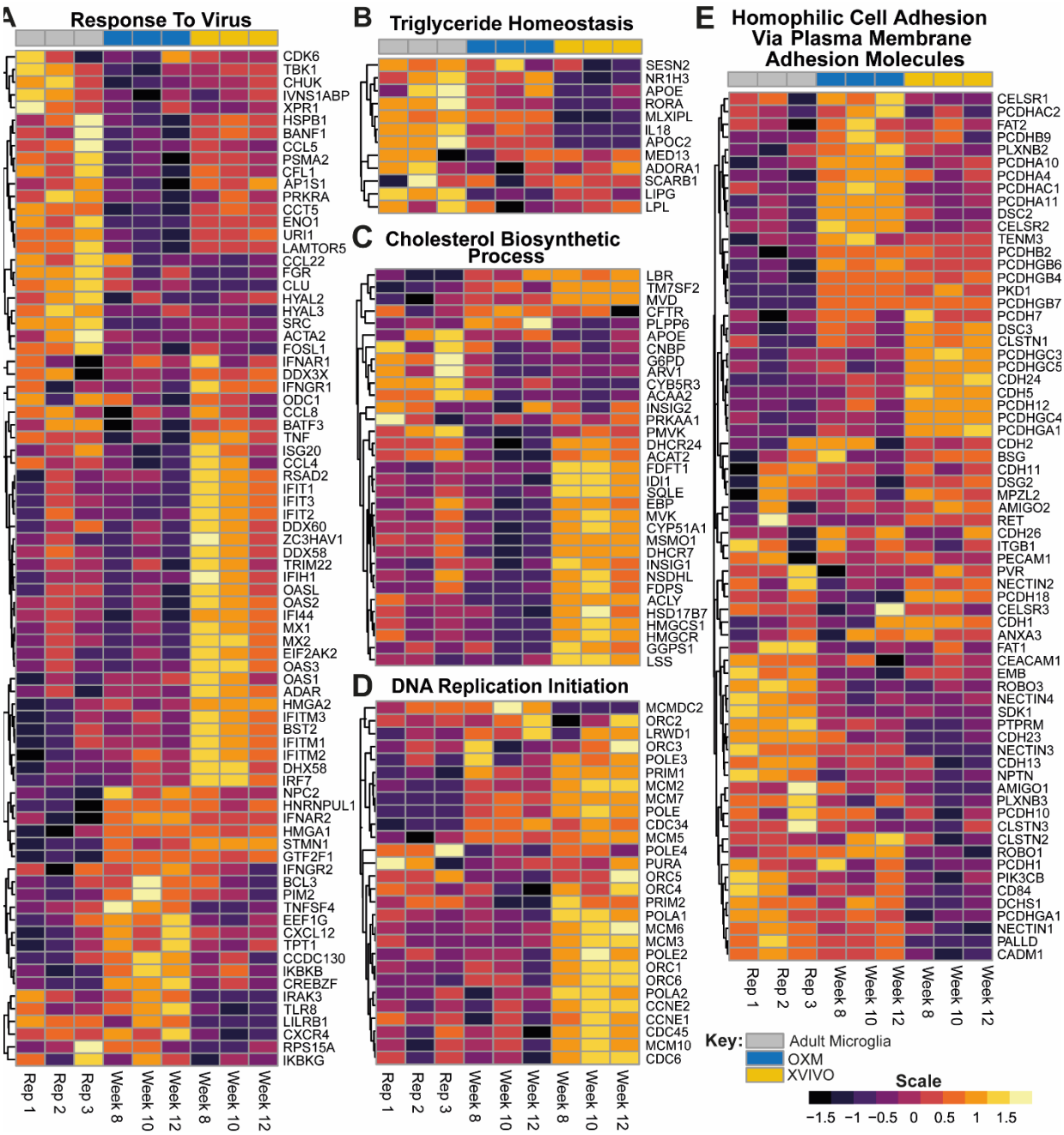


Figure S5: OXM and XVIVO cultured macrophage GO terms compared to adult microglia. Related to Figure 4. *A-E) Heat maps from figures 4 and S4 here comparing gene expression data from Abud et al. 2017 Adult Microglia (grey - left), OXM (blue - middle) and XVIVO (yellow - right) for the GO terms; A) Response to Virus, B) Triglyceride Homeostasis, C) Cholesterol Biosynthetic Process, D) DNA Replication Initiation, and E) Homophilic Cell Adhesion Via Plasma Membrane Adhesion Molecules. The colour in each row represents the z-score of the* log_2 *fold difference from the mean TPM value for that gene.*

Chapter 4:

Density Dependent Regulation of Inflammation

4.1 Introduction

It is tempting to classify macrophages in tidy categories such as “classical”, “non-classical”, “M1-polarized” or “M2-polarized”. However, there is clear evidence that this would be a mistake (50, 61). Macrophages form a highly plastic population of cells not only in their resting phenotype, but also in response to varying stimuli. For instance, Xue *et al.* (2014) (63) investigated 28 different stimulatory conditions and identified at least 9 different clear phenotypic responses by human macrophages. There is no single precise cause of variation in macrophage populations, but rather they are influenced by a broad spectrum of intrinsic and extrinsic factors. While some factors are non-specific, such as the impact of age on the immune system (reviewed by Weiskopf *et al.*, 2009 and Simon *et al.*, 2015) and the broad circadian regulation of the immune system (reviewed by Haspel *et al.*, 2020), here I am referring to local factors.

As discussed in Chapter 1, the term “tissue macrophage” is a term used to broadly classify a variety of highly adapted mono-nuclear innate immune cells found throughout the body (3). These cells are uniquely differentiated for their individual niches, and their developmental origin varies between organ, with many seeded early during embryogenesis (10, 25). However, it has been found that MDM recruited to tissues to replace lost macrophages can differentiate into macrophages almost indistinguishable from the original tissue resident cells (10, 435, 436). Therefore, each niche must provide specific cues as part of its environment to specialize these cells in their homeostatic roles. These cues can come in many forms, from specific growth factors and hormones, to non-specific changes in environmental nutrient availability and tissue structure.

A good example of this is seen in the brain. IL-34 expressed by neurons combined with astrocyte derived GM-CSF is known to be sufficient to differentiate iPSC-derived macrophages into microglia (372, 437). In addition, our lab has shown that co-culturing these microglia with neurons completely changes their cytokine and chemokine response profile to LPS and IFNγ stimulation, while also significantly altering the transcriptional profile of these

cells (372). Ultimately, these changes enable to the microglial cells to carry out their homeostatic functions in the brain, including synaptic pruning and removal of toxic extracellular proteins (438). Another example would be macrophages in the placenta, termed Hoffbauer cells, which are exposed to the hormone-like chemical prostaglandin-E2, as well as a nutrient and oxygen rich environment due to their proximity to maternal blood vessels (439). These cells typically occupy an M2-like phenotype, especially when co-cultured with mesenchymal cells (440). This could be in part due to the high nutrient availability allowing for oxidative phosphorylation (431, 441). When in hypoxic, high glucose, or high succinate conditions, most macrophages will transition to an M1-like phenotype after stimulation (431, 441–444). In this state, they produce much of their energy through glycolysis, while also secreting large amounts of RO, nitric oxide (NO), and lactate. In turn, these can feed back on to the macrophage response, either enhancing or suppressing it, depending on the local concentration (431, 445–448).

It is clear, then, that macrophages, both tissue-derived and monocyte-derived, are highly sensitive to, and strongly influenced by, local environmental cues around them. Until recently, one such potential cue that has been largely understudied is the importance of cell density. Cell density has long been known, if perhaps also ignored, as an important regulator of growth, motility, gene expression, and survival for a variety of cells types (449–458). Its role in regulation of immune cells though is mostly unknown. In the 1990's, regulation of neutrophil expression of 5-Lipoxygenase (5-LO), Five-Lipoxygenase-Activating Protein (FLAP) and Interleukin-1β (IL-1β), and a delay of neutrophil apoptosis, were described to be dependent on cell density (459, 460). In monocytes, expression of chondroitin sulfate proteoglycan was shown to be density dependent back in 1988 (461). Since then, there has been a dearth of research in the field, with the occasional description of density-dependent phenomena, e.g. regulation of IL-1β expression by microglia in response to LPS (462). However, recently there has been considerable interest in the idea of quorum sensing systems in MDM, a term usually attributed to bacterial behavior. Several papers in the last two years have described negative feedback loops on macrophages inflammation and proliferation involving NO and colony

stimulating factor-1 (CSF-1/M-CSF) in what have been described as a quorum sensing models of response (445, 463–468). Also, Muldoon *et al.* (2020) (469) coined the term “Quorum licensing” to describe a density-dependent positive regulation of TNFα production by RAW 264.7 and mouse BMDM.

Here, I seek to bring cell density back into the limelight, showing how density-dependent regulation of inflammation controls the ability of iPSC-derived macrophages to respond to both TLR-dependent and independent stimuli. Moreover, I provide evidence for a model in which low density macrophages may initiate an inflammatory response through secretion of large quantities of cytokines and chemokines. This is then followed by high density macrophages executing the immune response, clearing away potential infections and cellular debris, while also activating an adaptive immune response. The cause of this DDRI is still unclear, but I here provide evidence of both soluble and insoluble factors, emphasizing the complexity of macrophage regulation by cell density.

4.2 Results

4.2.1 Plating density of macrophages impacts their ability to respond to innate immune stimuli

While plating macrophages for various experiments, I observed differences in macrophage morphology depending on the density at which they were plated (i.e. the number of cells per cm^2). Low density plated cells (~$4.4x10^4/cm^2$) were flattened and had longer and more numerous extensions from the main cell body, while increasing the density (~8.8 and ~$17.6x10^4/cm^2$) resulted in the increased frequency of rounded smaller cells (Figure 1A).

While quantifying TNFα production after Toll like receptor (TLR) stimulation in macrophages of different genetic backgrounds, discussed later in Chapter 6, I also observed variation in the quantity of TNFα secreted that appeared dependent on plating density. With the exception of TLR3 stimulation, lower cell density, ($5x10^4$ cells/well in a 96 well plate, ~$1.5x10^5$ cells/cm^2), produced between 1.5-fold (TLR6) to 45.8-fold (TLR5) less TNFα than higher density plated cells ($1x10^5$ cells/well, ~$3x10^5$ cells/cm^2) (Figure S1A). This difference was even more apparent when TNFα production was normalised to cell number (Figure S1B). To ensure that this was not due to experimental variability, and to test if this was TLR dependent, I directly compared TNFα production by macrophages plated at two different densities after stimulation with Pam3, Flagellin, and TNFα. All three induced a greater than 10-fold higher response per cell from low density cells (Figure 1B). At this point, I decided to investigate what I will call here “Density Dependent Regulation of Inflammation” (DDRI) stimulating cells with either LPS, the most commonly used TLR agonist, or Pam3 due to its reliable induction of a TNFα response.

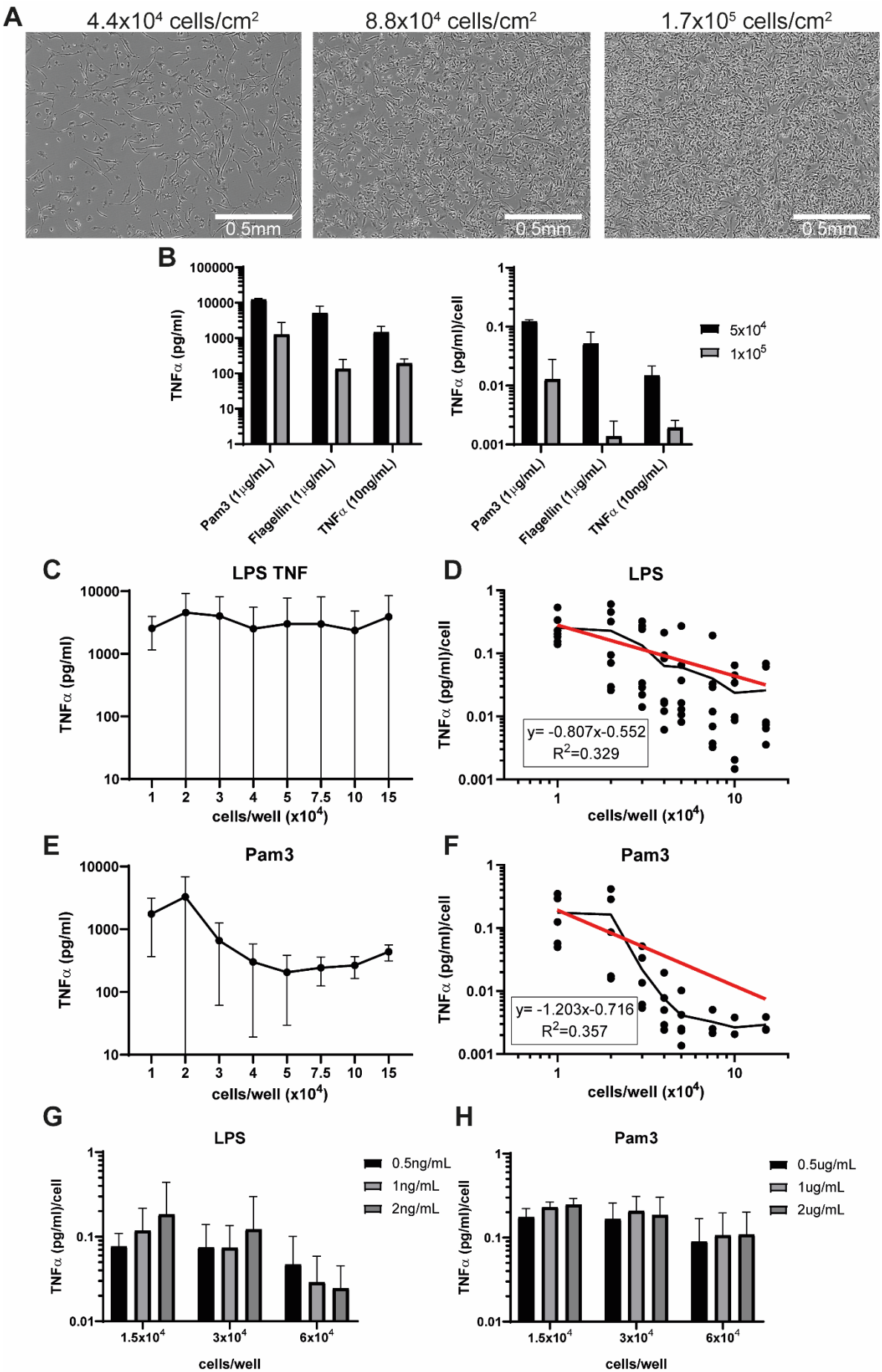

A
4.4x10⁴ cells/cm²
8.8x10⁴ cells/cm²
1.7x10⁵ cells/cm²
0.5mm
0.5mm
0.5mm
B
TNFα (pg/ml)
TNFα (pg/ml)/cell
5x10⁴
1x10⁵
Pam3 (1μg/mL)
Flagellin (1μg/mL)
TNFα (10ng/mL)
C
LPS TNF
TNFα (pg/ml)
cells/well (x10⁴)
D
LPS
TNFα (pg/ml)/cell
y= -0.807x-0.552
R²=0.329
cells/well (x10⁴)
E
Pam3
TNFα (pg/ml)
cells/well (x10⁴)
F
Pam3
TNFα (pg/ml)/cell
y= -1.203x-0.716
R²=0.357
cells/well (x10⁴)
G
LPS
TNFα (pg/ml)/cell
0.5ng/mL
1ng/mL
2ng/mL
1.5x10⁴
3x10⁴
6x10⁴
cells/well
H
Pam3
TNFα (pg/ml)/cell
0.5ug/mL
1ug/mL
2ug/mL
1.5x10⁴
3x10⁴
6x10⁴
cells/well

Figure 1: Plating density of macrophages alters their response to innate immune stimuli. *A) Image of macrophages plated at 4.41x10^4, 8.81x10^4, and 1.76x10^5 cells/cm^2 after 7-day differentiation. B) TNFα secretion measured 24 hours after stimulation with 1 µg/mL Pam3CSK4 (TLR2 agonist), 1 µg/mL S. typhimureum flagellin (TLR5 agonist) and 10 ng/mL TNFα by cells plated at 5x10^4/well and 1x10^5/well in a 90-well plate. n=2 (2 cell line clones, 1 experiment). C-F) Secretion of TNFα by cells plated at different densities in response to C-D) 1 ng/mL LPS or E-F) 1 µg/mL Pam3CSK4. C&E) display total quantities of TNFα per condition, D&F) display this total normalised to cell number. Linear regression was calculated using the GraphPad Prism Nonlinear fit Log-log line method. C-D) n=7 (2 clones, 4 experiments) E-F) n=5 (2 clones, 3 experiments). G-I) TNFα secretion after 24 hours stimulation with 3 different doses of G) LPS or H) Pam3CSK4. TNFα is displayed as a normalised value to cell number. n=5 (2 clones, 3 experiments).*

I first induced an inflammatory response to LPS or Pam3 over a range of cell plating densities, starting at 1x10^4 macrophages/well of a 96-well plate (2.95x10^4 cells/cm^2), up to 1.5x10^5 cells/well (5x10^5 cells/cm^2), and measured secretion of TNFα and IL-6 after 24 hours. Across all densities, the total quantity of TNFα secreted in response to LPS was approximately the same, 3240 ± 810 pg/mL (Figure 1C). However, if normalised to the number of cells plated, there was a clear inverse relationship between cell number and TNFα secretion (Figure 1D). Total response to Pam3, on the other hand, was not consistent across densities. First it declined as cell number increased up to 5x10^4 cells/well, before then increasing again (Figure 1E). Plotted as TNFα (pg/mL)/cell, there is approximately a 100-fold change between the lowest and highest plating densities (Figure1F). A similar trend was observed in IL-6 secretion after LPS (Figure S1C) and Pam3 stimulation (Figure S1D). Considering how DDRI has not been reported by previous investigations using iPSC-derived macrophages, and that prior work has used alternative media composition, I briefly evaluated if DDRI was a particular

feature of OXM-cultured cells. However, DDRI was still observed in macrophages cultured in XVIVO (Figure S1E-F).

One potential explanation is that as cell number increases, the relative ratio of agonist concentration to cell number decreases, theoretically resulting in a reduced response. To investigate this, I plated cells at $1x10^4$, $3x10^4$, and $6x10^4$ cells/well of a 96-well plate ($4.41x10^4$, $8.81x10^4$, and $1.76x10^5$ cells/cm^2). From here onwards, these three plating densities will be referred to as "Low", "Mid", and "High" plating densities. I stimulated these cells with 0.5, 1, and 2 ng/mL LPS, or 0.5, 1, and 2 µg/mL Pam3. A theoretical TNFα response per cell is shown in Figure S1G. In response to LPS, the low and mid density response was similar to the prediction. However, the response in high density cells reverses, with TNFα (pg/mL)/cell showing a trend to decrease as concentration increases (Figure 1G). The response to Pam3, on the other hand, displayed only marginal, non-significant, increases in response as concentration increases. This was far from the theoretical 2-fold increase as concentration increases 2-fold (Figure 1H). These results were unsurprising as previous titrations at higher doses of LPS and Pam3 on cells plated at ~$1.5x10^5$ cells/cm^2 had shown an increase in the response to LPS as concentration decreased, while response to Pam3 decreased as concentration did (Figure S1H-I). In summary, I have found that the quantity of the inflammatory cytokines TNFα and IL-6 produced after TLR stimulation decreases as the plating density of cells increases, independently of the concentration of agonist used.

4.2.2 Differential plating density primes macrophages for cell death post-LPS/IFNγ stimulation

Having discovered that density influences the TNFα and IL-6 response by iPSC-derived macrophages, I next sought to investigate how many other cytokines were similarly regulated. I have previously shown in Chapter 3, Figure 5, the profile of cytokines produced by macrophages cultured in OXM-media, plated at ~$1.1x10^5$ cells/cm^2 (between mid and high density). I therefore replicated this experiment at low, mid, and high densities, stimulating the cells for 16 hours with 100 ng/mL LPS and 20 ng/mL IFNγ. Morphologically, I observed a

density-dependent response to the stimuli across densities. High density cells clustered together while substantial cell death was visible at low density, and mid displayed a response somewhere in between the two (Figure 2A-B). Quantification of cell viability at time 0 showed similar viability across densities, with a small, but not significant, reduction at low density relative to high (Figure 2C). After 16 hours, viability of high density cells remained at 94.4 ± 3.28%, but decreased to 83.1 ± 12.9% and 64.9 ± 9.70% at mid and low densities respectively (Figure 2C). Overall, low density cells displayed a significant relative decrease in viability compared to time 0 (Figure 2D).

4.2.3 DDRI regulates the cytokine response to LPS/IFNγ, with the possible exception of CXCL11

Consistent with Chapter 3, unstimulated macrophages secreted CCL2 (MCP1), CCL3/CCL4 (MIP1α/MIP1β), CXCL1 (GROα), ICAM1, IL-1RA, IL-6, IL-8, MIF, and SERPINE1 (Figure 3A). In addition, CCL5 (RANTES) could clearly be detected in supernatants from low density cells, as well as low levels of CCL1, CXCL12, IL-16 and TNFα (Figure S2A). Of these, more CCL2, CXCL12, and IL-8 was secreted from high density cells, but normalising to plating density (Fig. S2B), and further normalisation to the low density condition (Figure 3B), showed this was less per cell than low density. Most strikingly, total MIP1α/β secreted was substantially higher from low and mid densities compared to high density cells. Similarly, CCL1, CCL5, IL-6, CXCL1, SERPINE1 and TNFα concentrations all increased as cell density decreased. Only IL-1RA, IL-8, and MIF concentrations were consistent across all three densities, yet all cytokines secreted at resting state appeared to be affected by DDRI (Figure 3B).

After stimulation with LPS and IFNγ, I observed increases in secretion of CCL1, CCL3/CCL4, CCL5, CXCL10, CXCL11, ICAM1, IL-1β, IL-6, MIF, SERPINE1, and TNFα (Figure 3C). Smaller increases in G-CSF, GM-CSF, IL-1α, IL-10 and IL-12 were also observed (Figure S2C). On the other hand, expression of IL-1RA, and IL-8 decreased after stimulation.

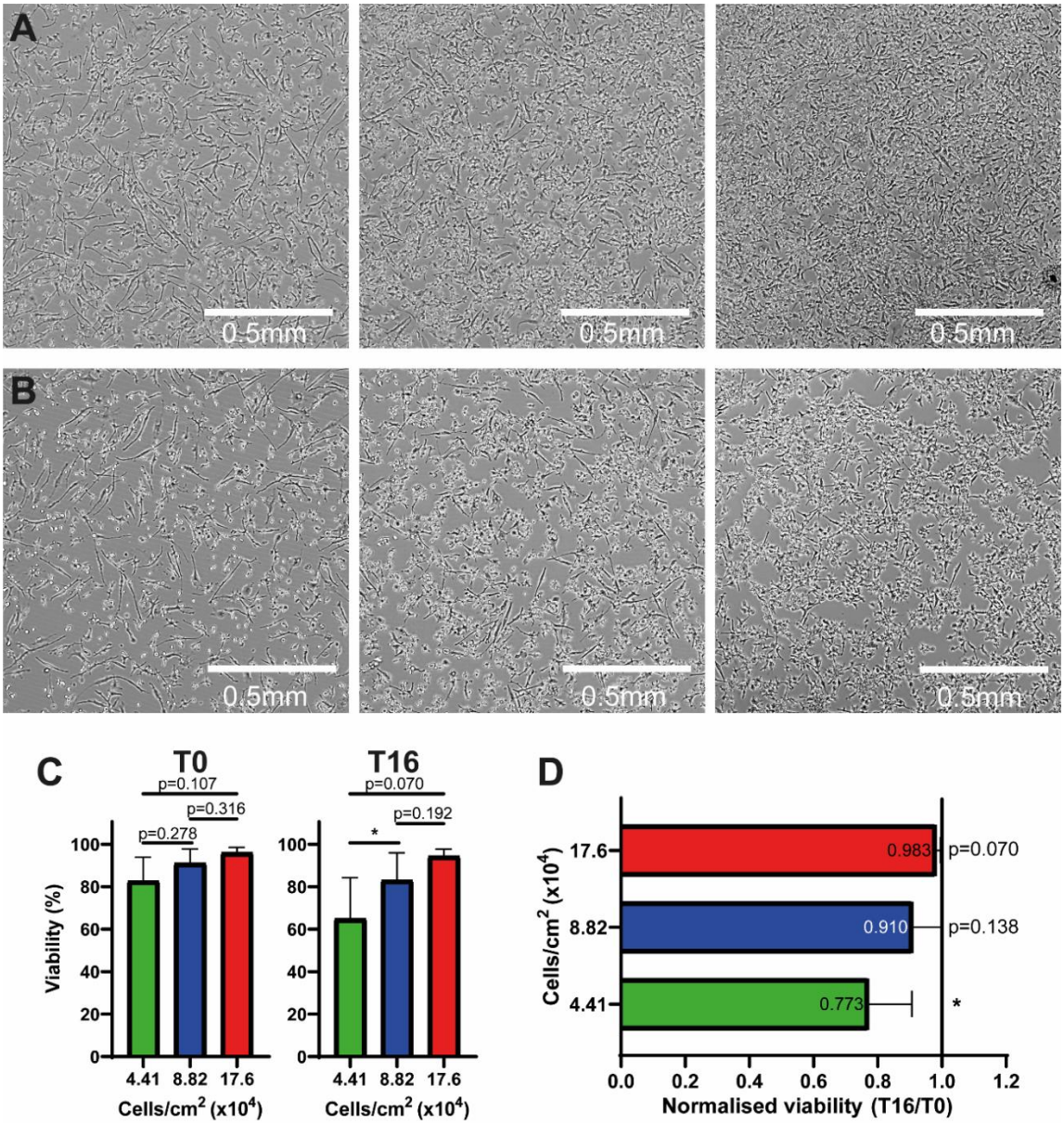


Figure 2: High density macrophages are more resistant to LPS and IFNγ induced cell death. *A) Images of 4.41x10^4, 8.81x10^4, and 1.76x10^5 cells/cm^2 after 7-day differentiation. B) Images of these 3 densities 16 hours post-stimulation with 100 ng/mL LPS and 20 ng/mL IFNγ. C) Quantification of macrophage viability before stimulation (T0) and after stimulation (T16). High density is displayed in red, mid in blue, and low in green. n=4 (2 different cell lines, 4 experiments). D) Normalised viability calculated by dividing T16 by T0. C) significance was calculated by RM one-way ANOVA, Tukey's multiple comparisons test. D) significance was calculated by one sample t-test comparing to a hypothetical value of 1. Significance is defined as * <0.05, ** <0.01, ***<0.001, ****<0.0001.*

Interestingly, changes in secretion were not uniform, with often the high or mid density cells showing the greatest fold change in secretion. Low density showed a reduced fold change compared to high density, and in the cases of CCL3/CCL4, actually displayed a reduction in secretion after stimulation (Figure 3E, S2E). Again, when normalised to cell number, almost all cytokines display DDRI (Figure S2D). However, when we normalise further against the low density control, one gene, CXCL11, does not follow the trend of DDRI. CXCL11 secretion per cell was >2-fold higher at high density than low, and mid density was almost 3-fold higher. In addition, 2 other genes can be observed to have similar secretion per cell across densities; CXCL12 and IL-10, although total secretion of these 2 proteins is low (Figure 3D). Overall, these results show that a majority of cytokines secreted from iPSC-derived macrophages tested are regulated by DDRI before and after stimulation with the exception of CXCL11.

4.2.4 Density alters the phenotype of macrophages and drives formation of 2 morphologically and phenotypically distinct populations

So far, I have shown differences in morphology and cytokine response by iPSC-derived macrophages during DDRI. Considering the clear differences even before stimulation, I next determined the surface marker phenotype of these cells by immuno-staining followed by flow cytometry, using the same samples from Figure 3. Unstimulated cells formed distinct populations measured by FSC-A and SSC-A (Figure 4A). High density cells had a greater proportion of cells in the smaller (lower FSC-A value) population 1, while mid and low densities were not significantly differentially distributed between the two populations (high: 73.4% population 1 vs 25.8% population 2, mid: 53.4% vs 39.3%, low: 48.9% vs 39.5%). After stimulation with LPS and IFNγ these two distinct populations were lost, and cells became more uniformly similar to population 1 (Figure 4B).

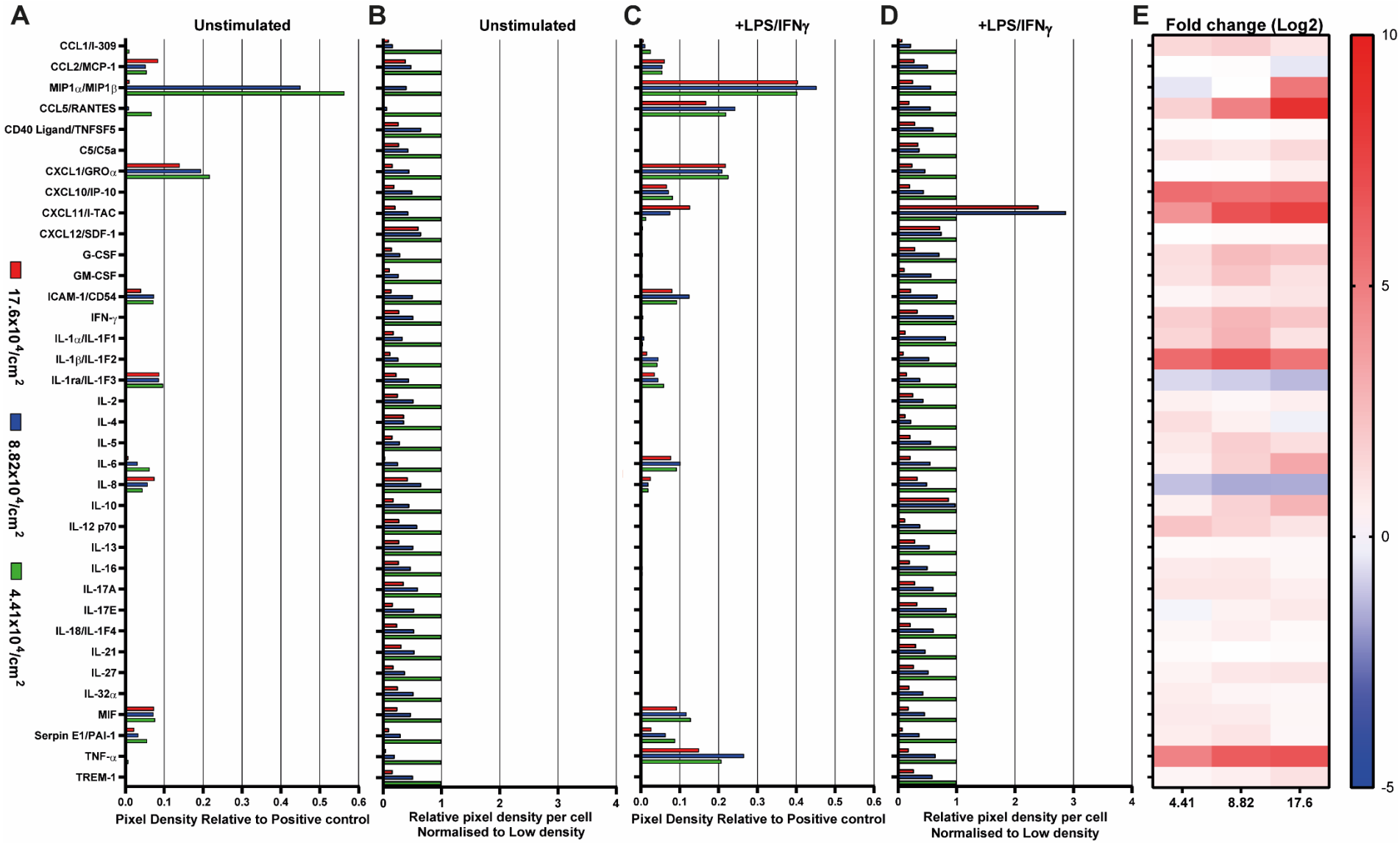

A
Unstimulated
B
Unstimulated
C
+LPS/IFNγ
D
+LPS/IFNγ
E
Fold change (Log2)
CCL1/I-309
CCL2/MCP-1
MIP1α/MIP1β
CCL5/RANTES
CD40 Ligand/TNFSF5
C5/C5a
CXCL1/GROα
CXCL10/IP-10
CXCL11/I-TAC
CXCL12/SDF-1
G-CSF
GM-CSF
ICAM-1/CD54
IFN-γ
IL-1α/IL-1F1
IL-1β/IL-1F2
IL-1ra/IL-1F3
IL-2
IL-4
IL-5
IL-6
IL-8
IL-10
IL-12 p70
IL-13
IL-16
IL-17A
IL-17E
IL-18/IL-1F4
IL-21
IL-27
IL-32α
MIF
Serpin E1/PAI-1
TNF-α
TREM-1
17.6x10^4/cm^2
8.82x10^4/cm^2
4.41x10^4/cm^2
0.0 0.1 0.2 0.3 0.4 0.5 0.6
Pixel Density Relative to Positive control
0 1 2 3 4
Relative pixel density per cell
Normalised to Low density
0.0 0.1 0.2 0.3 0.4 0.5 0.6
Pixel Density Relative to Positive control
0 1 2 3 4
Relative pixel density per cell
Normalised to Low density
4.41 8.82 17.6
10
5
0
-5

Figure 3: DDRI regulates the broad cytokine and chemokine response of macrophages with the possible exception of CXCL11. *Proteome profile of A-B) unstimulated macrophages and C-D) macrophages stimulated for 16 hours with 100 ng/mL LPS and 20 ng/mL IFNγ. A&C) relative secretion of cytokines and chemokines relative to the kit reference control. B&D) relative secretion normalised to secretion by low density cells (green). E) Fold change of cytokines and chemokines show in Log_2 scale displayed where red indicates increased secretion and blow indicates a reduction. n=1*

Just as in Chapter 3 Figures 3 and 5, total unstimulated and stimulated cells were stained for CD11b, CD14, CD16, CD45, CD86, and CD206 to determine possible macrophage classification in relation to M1 and M2 activation state phenotypes. Representative plots of total cell mean fluorescence intensity (MFI) are shown in Figure 4A-B, and individual unstimulated populations in Figure S3A-B. No differences in CD16 and CD86 expression were observed between densities (Figure 4D). Normalisation of expression relative to the high density condition showed a trend towards increased CD11b and CD45 expression in low and mid density cells (Figure 4E). By interrogating each population independently, this difference in expression appears dependent on cells occupying population 2, as population 1 cells show uniform expression of CD11b and CD45 (Figure S3C-F). On the other hand, CD14 and CD206 were significantly downregulated in low and mid density cells (Figure 4D-E). This difference was independent of population group, indicating a universal change in expression in unstimulated cells (Figure S3C-F).

After stimulation, a complex pattern of changing surface marker expression was observed (Figure 4B). Only CD86 was upregulated in all three densities, and this increase was greatest in mid density cells, which was significantly higher than low density, but not high density cells (Figure 4F-H). Differences were highly variable between repeats. CD11b expression was reduced to an even expression across all three densities (Figure 4F-G), therefore showing a greater fold change in mid and low densities than at high density (Figure

4H). Intriguingly, now, not only were CD14 and CD206 significantly more highly expressed at high density, but so too were CD16 and CD45 (Figure 4G). Comparison of fold change shows that CD45 was downregulated in low and mid densities but increased in high density cells. CD16 was downregulated approximately 2-fold at all densities after stimulation (Figure 4H). Similar to CD45, CD14 expression appeared unaffected by LPS/IFNγ stimulation of high density cells but was downregulated in low and mid densities. This amplified the previous difference in expression observed in unstimulated cells. CD206, on the other hand, was more substantially down regulated in high density cells, but this was still insufficient to reduce expression to the same levels as low and mid densities. Low and mid densities now displayed almost no observable expression of CD206 above isotype staining levels (Figure 4B). To summarise, unstimulated iPSC-derived macrophages show differences in CD11b and CD45 expression depending on cell size, and CD14 and CD206 expression independent of cell size. After stimulation, surface markers are broadly downregulated, except for CD86, with low and mid densities displaying the greatest potential for changes in expression.

4.2.5 Low and mid density plated cells share a transcriptional profile distinct from high density cells.

It is now clear that DDRI not only regulates cytokine secretion but also the resting phenotype of iPSC-derived macrophages. I therefore determined the broad transcriptional profiles of these cells by RNA-Seq, again using samples from the same experiments in Figures 3 and 4. All bioinformatical analysis of transcriptomic data was carried out by Szymon Stodolak from the James Lab, under supervision by myself and Dr Kirk Reardon, University of Columbia. Initial comparisons to the Abud *et al.*, 2017 data set used in Chapter 3, Figure 4, showed similar clustering of all 3 densities close to microglia and distant from dendritic cells, MDM ($CD14^{+}CD16^{-}$ and $CD14^{-}CD16^{+}$) and progenitors, consistent with these cells still being tissue resident macrophages (Figure 5A).

Differential expression analysis showed that 10549/15148 of all genes expressed in these macrophages are not significantly differentially expressed between densities, with 318 uniquely upregulated in low density, 2090 upregulated in both mid and low, 623 upregulated in mid and high, and 1495 upregulated in high density plated cells (Figure 5B). 47 genes and 26 genes were up regulated in mid density or both low and high density respectively, but a low $-\text{Log}_{10}$ adjusted P-value and Log_2-fold change of these genes would suggest these are due to factors independent of cell density (Figure 5B-C). The top 20 most significantly differentially expressed genes (DEG) between high and low, high and mid, and mid and high densities are shown in Table 1, and all significantly DEG are shown in Figure 5D. It is clear that mid and low density cells largely share a transcriptional profile as indicated by the limited number of DEG between them. However, sufficient genes are differentially expressed that are common with high density cells to start to identify trends in gene expression as density changes (Figure 5B, 5D). Within the top 20 DEG, expression of the low affinity Fc-receptor, Fc Fragment of IgG Receptor IIb (FCGR2B), consistently increases as density increases. On the other hand, the matrix metallopeptidase 9 (MMP9) and the complement receptor 1 (CR1) both decrease in expression as density increases (Figure 5D, Table 1). In addition to regulators of the immune response, genes not typically understood primarily as regulators of inflammation, such as regulators of metabolism, e.g. Glutamate-Ammonia Ligase (GLUL), and Solute Carrier Family 18 Member B1 (SLC18B1), are also differentially expressed across densities. In conclusion, iPSC-derived macrophages retain their tissue macrophage-like transcriptional phenotype, even at different densities. However, they are clearly transcriptionally different, with numerous inflammatory mediators beyond those identified so far differentially expressed.

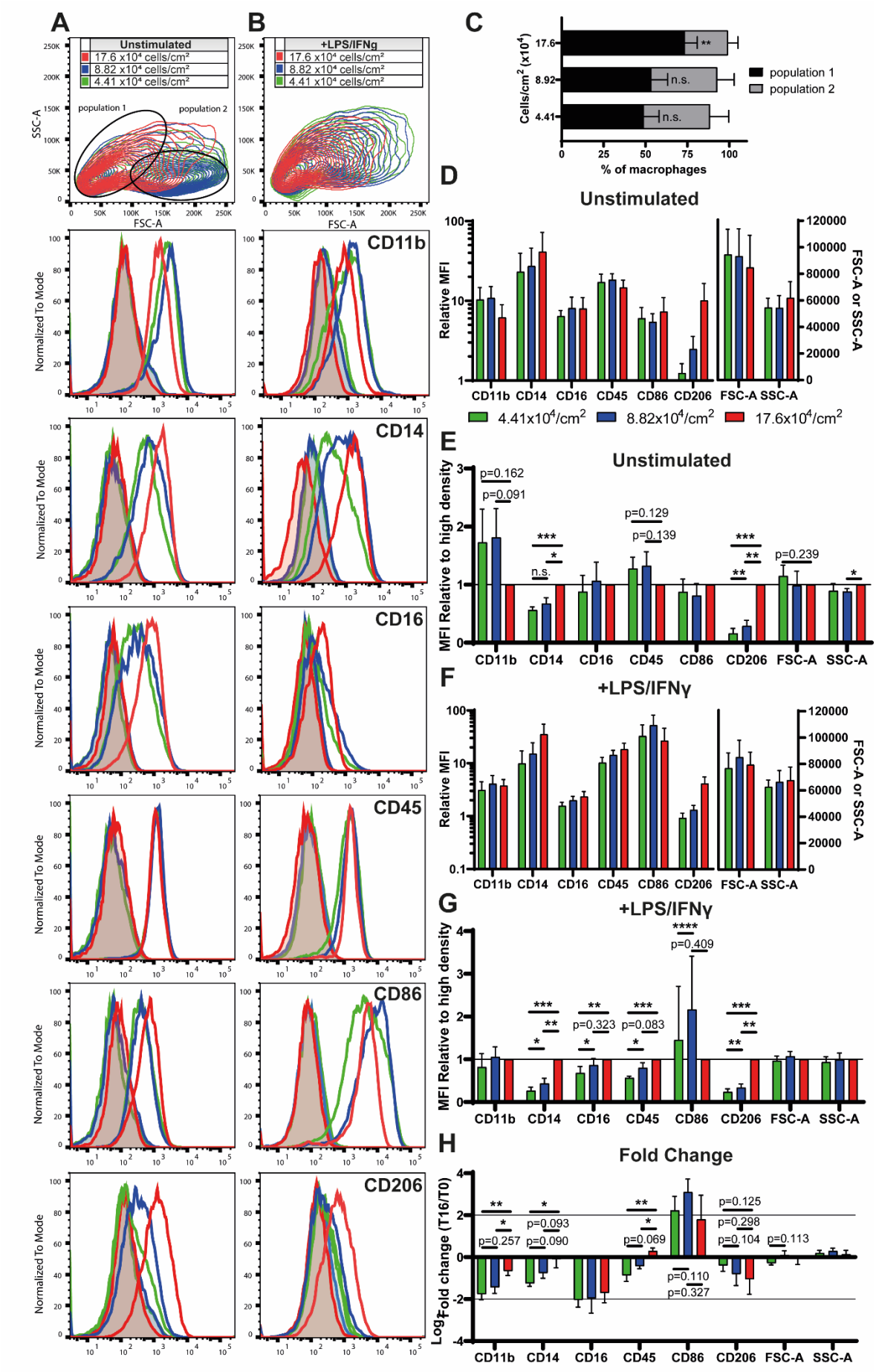

A
B
C
D
E
F
G
H
Unstimulated
+LPS/IFNg
17.6 x10⁴ cells/cm²
8.82 x10⁴ cells/cm²
4.41 x10⁴ cells/cm²
population 1
population 2
SSC-A
FSC-A
CD11b
CD14
CD16
CD45
CD86
CD206
Normalized To Mode
Cells/cm² (x10⁴)
17.6
8.92
4.41
n.s.
**
% of macrophages
Relative MFI
FSC-A or SSC-A
CD11b CD14 CD16 CD45 CD86 CD206 FSC-A SSC-A
4.41x10⁴/cm²
8.82x10⁴/cm²
17.6x10⁴/cm²
MFI Relative to high density
p=0.162
p=0.091
p=0.129
p=0.139
p=0.239
+LPS/IFNγ
p=0.409
p=0.323
p=0.083
Fold Change
Log₂Fold change (T16/T0)
p=0.257
p=0.093
p=0.090
p=0.069
p=0.125
p=0.298
p=0.104
p=0.113
p=0.110
p=0.327

Figure 4: Density alters the phenotype of macrophages and drives formation of 2 morphologically and phenotypically distinct populations. *A-B) Top: Density plots of low (green), mid (blue), and high (red) density plated macrophages measuring SSC-A and FSC-A by flow cytometry. Other 6 panels: Histograms of macrophage surface marker staining where x = intensity and y = frequency normalised to mode. From top to bottom, histograms show expression of; CD11b, CD14, CD16, CD45, CD86, and CD206. A) unstimulated cells, B) cells after 16-hour stimulation with 100 ng/mL LPS and 20 ng/mL IFNγ. Graphs are representative of 4 repeats across 2 different cell lines. C) Percentage of cells that occupy either population 1 or 2 shown in the top panel of A). D&F) Left segment; Geometric mean fluorescence intensity (MFI) of total cells relative to the isotype control for each surface marker. Right segment; mean FSC-A and SSC-A values of total cells. D) displays unstimulated cells, F) shows cells stimulated with LPS and IFNγ. E&G) MFI relative to the MFI of high density cells of E) unstimulated, and G) LPS and IFNγ stimulated cells. H) Fold change in MFI between stimulated and unstimulated cells shown in Log_2 value. C) significance was calculated by 2-way ANOVA, Sidak's multiple comparisons test. E, G&H) significance was calculated by 2-way ANOVA, Tukey's multiple comparisons test. C-H) n=4 (2 different cell lines across 4 experiments). Significance is defined as * <0.05, ** <0.01, ***<0.001, ****<0.0001.*

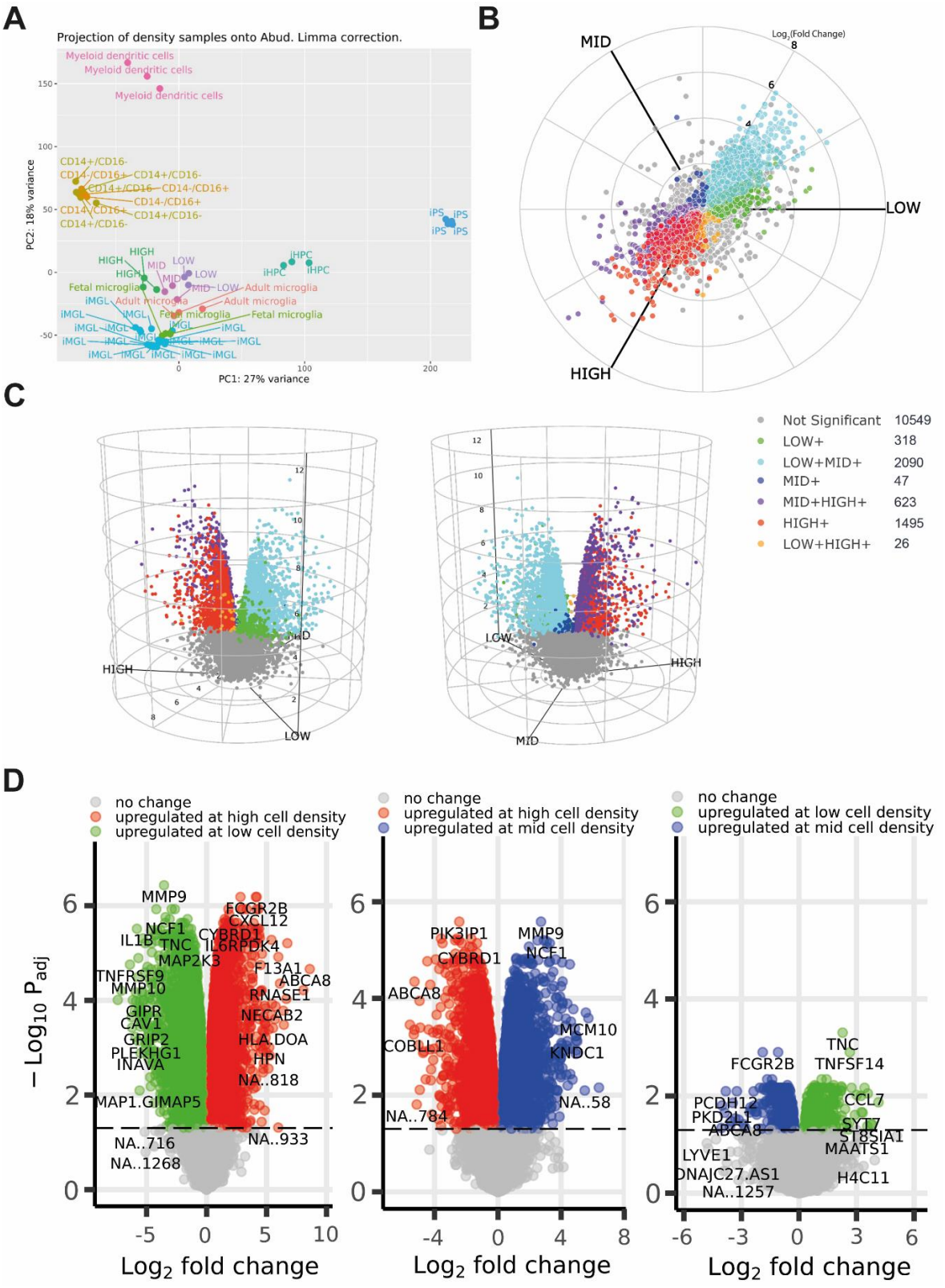


Figure 5: Different density cells are macrophages with distinct transcriptional profiles.

A) PCA plot of transcriptional profile for iPSC-derived macrophages cultured at low (dark purple) mid (light purple) or high density (Dark green) compared to iPSC (dark blue), induced

haematopoietic progenitor cells (iHPC, turquoise), microglia (adult (salmon), fetal (light green),and iPSC-derived (iMGL, light blue)), monocytes (CD14 high/CD16 low (gold) and CD14 low/CD16 high (orange)), and dendritic cells (pink). B) Radial plot of differentially expressed genes where Log_2 fold change is shown increasing as distance from the centre increases. C) 3D representation of the radial plot, where the y-axis also displays $-Log_{10}$ P-value. Values >0.05 were considered significant. D) 2D volcano plot of comparing $-Log_{10}$ P-value and Log_2 fold change of genes differentially expressed between densities. Left: Low density vs High density, Middle: High density vs Mid density, Right: Mid density vs Low density.

High vs Low	log2FC	adj.P.Val		High vs Mid	log2FC	adj.P.Val		Mid vs Low	log2FC	adj.P.Val
MMP9	-3.545	3.72E-07		*MMP9*	-2.726	2.59E-06		TNC	-2.273	4.96E-04
PIK3IP1	2.822	6.57E-07		*PIK3IP1*	2.439	2.59E-06		*FCGR2B*	1.894	1.26E-03
CR1	4.102	6.57E-07		*SLC18B1*	2.587	5.78E-06		PYGL	1.092	1.26E-03
FCGR2B	4.180	6.57E-07		*ABCC5*	1.687	5.78E-06		TNFSF14	-2.648	1.26E-03
SLC18B1	3.007	1.19E-06		*CXCL12*	3.593	5.78E-06		*CR1*	1.403	4.54E-03
CXCL8	-4.195	1.19E-06		*CR1*	2.699	6.30E-06		LILRB5	1.657	4.54E-03
C15orf48	-2.642	1.19E-06		*GPNMB*	2.456	6.30E-06		MCOLN3	-1.177	4.54E-03
GPNMB	2.891	1.19E-06		*NCF1C*	-2.914	6.30E-06		MARCKSL1	-1.437	4.54E-03
MS4A4A	3.339	1.19E-06		*NCF1*	-3.093	6.56E-06		NA	1.372	5.98E-03
HLA-DMB	4.174	1.19E-06		SLC2A6	-2.509	6.30E-06		*MMP9*	-0.819	5.98E-03
ABCC5	1.817	1.19E-06		*FCGR2B*	2.286	7.20E-06		MYO7A	1.467	5.98E-03
SLC2A6	-2.916	1.19E-06		*GLUL*	1.315	7.20E-06		NINJ1	0.604	5.98E-03
ASAH1	1.885	1.54E-06		CYBRD1	1.789	8.51E-06		LFNG	-0.890	6.37E-03
CXCL12	4.330	1.19E-06		*C15orf48*	-1.970	8.51E-06		NA	1.375	6.37E-03
NCF1	-3.423	1.76E-06		NCF1B	-3.281	7.20E-06		STX1A	-1.811	5.98E-03
GLUL	1.511	1.93E-06		*CXCL8*	-3.115	8.76E-06		*HLA-DMB*	1.485	6.37E-03
NIBAN2	-1.589	1.93E-06		EPAS1	1.630	8.76E-06		OCSTAMP	-2.205	6.37E-03
NCF1C	-3.075	1.93E-06		DPEP2	3.501	7.20E-06		GLIS3	-1.394	6.80E-03
ADA2	1.628	2.10E-06		EPHX1	2.083	1.11E-05		*MS4A4A*	1.146	6.80E-03
CREG1	1.862	2.31E-06		*ADA2*	1.320	1.15E-05		LPAR6	1.145	6.80E-03

Table 1: Top 20 most significantly differentially expressed genes (DEG) between high, mid, and low densities. *Genes listed in italics are significantly different across 2 comparison of the top 20 DEG. Genes in red are different in all 3. NA denotes genes unassigned a name in the Ensembl database.*

4.2.6 Density alters transcription of member genes of GO terms beyond regulation of cytokines and inflammation

I next performed further analysis of gene ontology (GO) enrichment to identify whether any other biological processes (BP) (Figure 6), cellular components (CC) (Figure 7), and molecular functions (MF) (Figure 8) were affected by DDRI.

As expected, BP GO terms related to the secretion of cytokines and chemokines which recruit other leukocytes were the most highly enriched terms in low density cells when compared to high (Figure 6A) and mid densities (Figure 6C), as well as mid density compared to high (Figure 6B). Closer examination of cytokine and chemokine profiles across densities (Figure 9) shows upregulation of genes such as the CCL family of cytokines, matrix metallopeptidases, and interleukins (IL), at low and mid densities. However, receptors and intracellular signalling mediators in response to these cytokines appear upregulated in high density, for example IL6R, IFNAR2, JAK1, STAT3. This indicates that DDRI is not just pro-inflammatory at low densities and anti-inflammatory at high. In agreement with this, some pro-inflammatory elements of BP terms such as “Complement activation, classical pathway” (Figure 6A) and “positive regulation of Interferon-gamma production” (Figure 6B) were enriched in high density cells when compared to mid density. These terms include genes for members of the complement family, C1Q and C2, and signalling components TLR4 and IRF8 (Figure 10A-B). Both low and high densities appear to enrich for terms regulating gene transcription and translation, For example, “Positive regulation of Telomerase RNA localisation to Cajal body” (Figure 6A) and “tRNA aminoacylation for protein translation” (Figure 6B), are enriched at low densities, while “Histone H3-K9 demethylation” (Figure 6A) and “Translation” (Figure 6C), were enriched at high density. Some homeostatic and metabolic terms were enriched, including “Cellular Zinc Ion homeostasis” in low density cells (Figure 6A), and “Insulin receptor signalling pathway” in high density cells, within which metabolic regulatory genes (e.g. PDK2, FOXO1) are upregulated (Figure 6A, Figure 11). Finally, there is some evidence that low and mid density cells may have entered the cell replication cycle

through upregulation of genes, such as MCM3, MCM10, and ORC1, which are part of the GO term “DNA replication initiation” (Fig. 6B, Fig. 12).

Analysis of CC GO terms continue the observation of translational regulation in different densities, with terms for preribosome complex regulation, and “RNA polymerase III complex”, enriched in low and mid density cells (Figure 7A-B). Interestingly though, mid density enriches for ribosomal terms when compared to low (Figure 7C), and closer analysis of high densities found that ribosomal, in contrast to preribosomal, terms are enriched when compared against low density (e.g. small ribosomal subunit, adjusted p value $1.28e^{-6}$, Log_2 fold change 0.478). However, of the top ranked GO terms enriched in high density cells, the most highly enriched term by a considerable margin was “MHC class II protein complex” (Figure 7A-B). All members of the HLA-D family expressed in these macrophages were significantly upregulated at high densities, and closer analysis of MHC related genes also found that HLA-A, -B, -C, -E, B2M, and CD74 are all upregulated in these cells (Figure 13). However, the peptide transporter proteins TAP1 and TAP2 are upregulated in low and mid densities compared to high. Due to this significant upregulation of MHC class II genes, other GO terms including these genes, such as “Clathrin coated-endocytic vesicle membrane”, “transport vesicle membrane” and “Integral component of luminal side of endoplasmic reticulum membrane” are all enriched in high density cells (Figure 7A-B). However, terms for the late endosome and lysosome were nonetheless enriched in high density cells, potentially indicating a higher turnover of surface and extracellular proteins in these cells (Figure 14). On the other hand, mid and low densities may preferentially recycle and secrete proteins as indicated by the enrichment for “secretory granule membrane” when comparing mid and high densities, which includes genes like RAB10 and RAB18 (Figure 7B, 15). Lastly, and as expected through my observation of morphological differences between the cells, cellular structure related GO terms such as “Stress fibre”, “Ruffle membrane”, and “Integrin complex” are all enriched in low density and mid density plated cells (Figure 7A-C).

MF GO term comparisons between densities are largely in agreement with the enrichment of terms so far described by BP and CC GO term analysis. “Chemokine activity”

and “Peptide antigen binding” are enriched MF GO terms in low and high densities respectively (Figure 8A-B). GO terms for “DNA replication origin binding” and “DNA polymerase binding” reinforce the potential increased proportion of cells in the cell cycle at low and mid densities (Figure 8A-B). “Insulin receptor binding” and “mannose binding” terms enriched in high density cells support a possible change in metabolism between densities (Figure 8A). One of the most intriguing terms that was most highly enriched in high density cells compared to low during BP GO term analysis, and confirmed again with MF analysis, was “Cellular response to amyloid beta” (BP) and “Amyloid beta binding” (MF) (Figure 6A, Figure 8A-C, Figure 15). Amyloid beta is one of the principle causes of Alzheimer’s disease (AD) (470), a disease characterised by neuronal cell death, formation of toxic tangles of extracellular protein, and activation of inflammation by microglia cells. I, therefore, further analysed differences in expression of genes identified by genome wide association study (GWAS) in humans and in mouse models to confer risk to develop AD. While not all genes are differentially expressed, several of those related to the immune response are (e.g. TREM2, CR1, CD33, PLD3). In addition, genes related to endocytosis (e.g. SORL1, PTK2B, and BIN1), and cholesterol and lipid processing (e.g. APOE, CLU, and SLC27A4), are differentially expressed. Overall, 14/25 (56%), 27/39 (69%), 62/134 (50%), and 96/119 (81%) of the genes identified in the Lane *et al.* (471), Jones *et al.* (472), Jansen *et al.*(473), and Salih *et al.*(474) datasets, respectively, are differentially expressed between high and low densities (Lane & Jones gene sets not shown, Jansen & Salih Figure 16A-B). To conclude, GO term analysis of the transcriptional profile of these cells plated at different densities confirmed previous findings of altered cytokine and chemokine inflammatory response, as well as identified several new and unexpected pathways, processes, and cellular components that are differentially regulated.

A

LOW vs HIGH DENSITY					
Top 10 Ranked in Low density macrophages	**Rank (/2042)**	**Enrichment score (/100)**	**Top 10 Ranked in High density macrophages**	**Rank (/2042)**	**Enrichment score (/100)**
Lymphocyte Chemotaxis	1	95.39	Regulation Of Complement Activation	9	27.63
Eosinophil Chemotaxis	2	61.74	Complement Activation, Classical Pathway	26	26.87
Monocyte Chemotaxis	3	69.42	Negative Regulation Of Interferon-Gamma Production	29	20.89
Chemokine-Mediated Signaling Pathway	4	100.00	Inner Ear Development	33	27.53
Cellular Zinc Ion Homeostasis	5	53.70	Cytoplasmic Translation	35	13.08
Cellular Response To Interleukin-1	6	65.22	Cellular Response To Amyloid-Beta	36	28.71
Neutrophil Chemotaxis	7	87.68	Insulin-Like Growth Factor Receptor Signaling Pathway	42	24.13
Detoxification Of Copper Ion	8	52.76	Viral Transcription	45	17.65
Positive Regulation Of Telomerase Rna Localization To Cajal Body	10	14.19	Histone H3-K9 Demethylation	47	18.20
Cellular Response To Interferon-Gamma	11	29.54	Srp-Dependent Cotranslational Protein Targeting To Membrane	50	16.16

B

MID vs HIGH DENSITY					
Top 10 Ranked in Low density macrophages	**Rank**	**Enrichment score (/100)**	**Top 10 Ranked in High density macrophages**	**Rank**	**Enrichment score (/100)**
Positive Regulation Of Telomerase Rna Localization To Cajal Body	1	19.17	Histone H3-K9 Demethylation	37	23.27
Neutrophil Chemotaxis	2	91.45	Regulation Of Complement Activation	52	23.61
Cellular Response To Interleukin-1	3	57.61	Complement Activation, Classical Pathway	78	24.90
Lymphocyte Chemotaxis	4	90.64	Insulin Receptor Signaling Pathway	85	20.29
Positive Regulation Of Cytokine Secretion	5	32.70	Positive Regulation Of Interferon-Gamma Production	108	33.07
Trna Aminoacylation For Protein Translation	6	28.82	Microtubule Anchoring	111	12.46
Positive Regulation Of Transcription Of Nucleolar Large Rrna By Rna Polymerase I	7	13.19	Insulin-Like Growth Factor Receptor Signaling Pathway	119	21.05
Monocyte Chemotaxis	8	72.67	Hormone-Mediated Signaling Pathway	129	24.06
Positive Regulation Of Establishment Of Protein Localization To Telomere	9	16.99	Adrenal Gland Development	130	31.43
Dna Replication Initiation	10	53.53	Regulation Of Glucose Metabolic Process	131	26.17

C

LOW vs MID DENSITY					
Top 10 Ranked in Low density macrophages	**Rank (/2009)**	**Enrichment score (/100)**	**Top 10 Ranked in High density macrophages**	**Rank (/2009)**	**Enrichment score (/100)**
Eosinophil Chemotaxis	1	56.27	Nuclear-Transcribed Mrna Catabolic Process, Nonsense-Mediated Decay	3	37.86
Chemokine-Mediated Signaling Pathway	2	69.97	Srp-Dependent Cotranslational Protein Targeting To Membrane	4	59.68
Extracellular Matrix Disassembly	5	26.89	Negative Regulation Of Phagocytosis	6	19.49
Cellular Response To Interleukin-1	8	52.55	Cytoplasmic Translation	7	20.97
Lymphocyte Chemotaxis	9	100.00	Viral Transcription	10	40.81
Neutrophil Chemotaxis	11	62.55	Translation	13	23.27
Protein Hexamerization	12	12.96	Translational Initiation	15	40.71
Cell-Cell Signaling	14	40.61	Myd88-Dependent Toll-Like Receptor Signaling Pathway	17	13.11
Camera-Type Eye Morphogenesis	16	19.18	Phospholipase C-Activating G Protein-Coupled Receptor Signaling Pathway	20	23.70
Positive Regulation Of Cellular Protein Metabolic Process	18	19.94	Ribosomal Large Subunit Assembly	24	4.64

Figure 6: Biological Process GO term enrichment. *Top 10 ranked Biological Process GO terms significantly enriched per density condition when comparing A) Low vs High density, B) Mid vs High density, and C) Low vs Mid density. Rank is determined by ordering terms in order of lowest to highest median score assigned when analysed across the 12 different GO analysis tools. Total number of GO terms that are significantly enriched for each comparison is shown in the brackets under Rank. Enrichment score is calculated using both fold change and p-value and the term with the highest score assigned the value of 100.*

A

LOW vs HIGH DENSITY					
Top 10 Ranked in Low density macrophages	**Rank (/483)**	**Enrichment score (/100)**	**Top 10 Ranked in High density macrophages**	**Rank (/483)**	**Enrichment score (/100)**
Preribosome, Large Subunit Precursor	2	5.89	Mhc Class Ii Protein Complex	1	100.00
Preribosome, Small Subunit Precursor	4	5.11	Clathrin-Coated Endocytic Vesicle Membrane	3	20.01
Aminoacyl-Trna Synthetase Multienzyme Complex	7	5.58	Cytosolic Large Ribosomal Subunit	5	4.50
Small-Subunit Processome	10	4.94	Endocytic Vesicle Membrane	6	16.24
Mitochondrial Small Ribosomal Subunit	15	4.02	Cytosolic Small Ribosomal Subunit	8	4.13
Ruffle Membrane	16	8.48	Lysosome	9	8.40
Rna Polymerase Iii Complex	23	6.58	Lysosomal Lumen	11	9.17
Lamellipodium Membrane	24	10.51	Integral Component Of Lumenal Side Of Endoplasmic Reticulum Membrane	12	16.78
Mitochondrial Nucleoid	25	4.86	Azurophil Granule Membrane	13	7.94
Stress Fiber	27	10.16	Late Endosome Membrane	14	7.84

B

MID vs HIGH DENSITY					
Top 10 Ranked in Low density macrophages	**Rank (/483)**	**Enrichment score (/100)**	**Top 10 Ranked in High density macrophages**	**Rank (/483)**	**Enrichment score (/100)**
Mitochondrial Nucleoid	1	7.64	Mhc Class Ii Protein Complex	2	100.00
Proteasome Complex	3	7.05	Clathrin-Coated Endocytic Vesicle Membrane	4	25.79
Mitochondrial Large Ribosomal Subunit	6	7.80	Endocytic Vesicle Membrane	5	24.07
Small-Subunit Processome	7	7.37	Integral Component Of Lumenal Side Of Endoplasmic Reticulum Membrane	15	21.37
Proteasome Accessory Complex	8	6.49	Er To Golgi Transport Vesicle Membrane	25	16.18
Secretory Granule Lumen	9	9.80	Lysosomal Lumen	33	10.83
Preribosome, Large Subunit Precursor	10	9.01	Lysosome	36	11.66
Aminoacyl-Trna Synthetase Multienzyme Complex	11	9.00	Transport Vesicle Membrane	44	31.52
Stress Fiber	13	13.38	Ciliary Transition Zone	63	7.86
Mitochondrion	14	11.83	M Band	73	15.29

C

LOW vs MID DENSITY					
Top 10 Ranked in Low density macrophages	**Rank (/461)**	**Enrichment score (/100)**	**Top 10 Ranked in High density macrophages**	**Rank (/461)**	**Enrichment score (/100)**
Lamellipodium Membrane	10	10.30	Cytosolic Large Ribosomal Subunit	1	27.40
Desmosome	13	10.08	Cytosolic Small Ribosomal Subunit	2	24.69
Postsynaptic Density Membrane	15	13.64	Polysomal Ribosome	3	15.47
Basement Membrane	19	11.71	Small Ribosomal Subunit	4	7.86
Glutamatergic Synapse	20	7.25	Azurophil Granule Membrane	5	13.22
Integrin Complex	21	11.21	Early Phagosome	6	28.75
Postsynaptic Density, Intracellular Component	23	9.05	Ficolin-1-Rich Granule Membrane	7	8.56
Presynaptic Active Zone	27	4.26	Ribosome	8	3.99
Presynaptic Active Zone Membrane	29	10.95	Bloc-1 Complex	9	3.81
Cytoskeleton	30	7.63	Eukaryotic Translation Initiation Factor 3 Complex	11	3.95

Figure 7: Cellular component GO term enrichment. *Top 10 ranked Cellular component GO terms significantly enriched per density condition when comparing A) Low vs High density, B) Mid vs High density, and C) Low vs Mid density*

A

LOW vs HIGH DENSITY					
Top 10 Ranked in Low density macrophages	**Rank (/570)**	**Enrichment score (/100)**	**Top 10 Ranked in High density macrophages**	**Rank (/570)**	**Enrichment score (/100)**
Ccr Chemokine Receptor Binding	1	81.34	Carboxypeptidase Activity	4	19.24
Chemokine Activity	2	100.00	Peptide Antigen Binding	5	30.66
Methyl-Cpg Binding	3	12.27	Amyloid-Beta Binding	12	18.64
Cytokine Activity	6	46.84	Phosphatidylinositol-3,4-Bisphosphate Binding	15	17.49
Structural Constituent Of Cytoskeleton	7	17.25	Insulin Receptor Binding	17	17.20
Map Kinase Tyrosine/Serine/Threonine Phosphatase Activity	8	24.34	Mannose Binding	19	11.79
Rna Cap Binding	9	7.13	Gaba Receptor Binding	22	6.66
Dna Replication Origin Binding	10	25.95	Translation Regulator Activity	29	6.51
Dna Polymerase Binding	11	14.15	Structural Constituent Of Ribosome	34	7.96
Rna Polymerase Iii Activity	13	9.68	Transmembrane Signaling Receptor Activity	36	22.00

B

MID vs HIGH DENSITY					
Top 10 Ranked in Low density macrophages	**Rank (/569)**	**Enrichment score (/100)**	**Top 10 Ranked in High density macrophages**	**Rank (/569)**	**Enrichment score (/100)**
Ccr Chemokine Receptor Binding	1	80.47	Carboxypeptidase Activity	2	23.02
Dna Polymerase Binding	3	21.93	Peptide Antigen Binding	6	34.23
Chemokine Activity	4	100.00	Dna-Binding Transcription Factor Activity, Rna Polymerase Ii-Specific	17	41.08
3'-5' Dna Helicase Activity	5	30.60	Insulin Receptor Binding	19	17.51
Dna Replication Origin Binding	7	34.35	Proteoglycan Binding	25	15.88
Rna Polymerase Iii Activity	8	12.59	Insulin Receptor Substrate Binding	31	22.04
Cytokine Activity	9	37.48	Mhc Class Ii Protein Complex Binding	39	32.08
Single-Stranded Dna Helicase Activity	10	23.23	Cytokine Binding	47	18.53
Protein Disulfide Isomerase Activity	11	11.16	Amyloid-Beta Binding	53	20.59
Rna Cap Binding	12	9.99	Scavenger Receptor Activity	57	17.41

C

LOW vs MID DENSITY					
Top 10 Ranked in Low density macrophages	**Rank (/540)**	**Enrichment score (/100)**	**Top 10 Ranked in High density macrophages**	**Rank (/540)**	**Enrichment score (/100)**
Chemokine Activity	1	76.00	Structural Constituent Of Ribosome	3	29.90
Ccr Chemokine Receptor Binding	2	100.00	5s Rrna Binding	5	4.71
Cytokine Activity	4	84.69	Rrna Binding	8	5.08
Serine-Type Endopeptidase Activity	6	34.54	Mrna 5'-Utr Binding	11	6.05
Map Kinase Tyrosine/Serine/Threonine Phosphatase Activity	7	19.71	Phospholipase Activity	14	9.33
Calcium Channel Regulator Activity	9	23.08	Aspartic-Type Endopeptidase Activity	15	18.07
Nad+ Kinase Activity	10	12.79	Translation Regulator Activity	16	4.68
Signaling Receptor Complex Adaptor Activity	12	11.27	Manganese Ion Binding	20	8.00
Tumor Necrosis Factor Receptor Binding	13	18.96	Amyloid-Beta Binding	21	13.98
Metalloendopeptidase Activity	17	23.00	Drug Binding	24	13.34

Figure 8: Molecular function GO term enrichment. *Top 10 ranked Molecular function GO terms significantly enriched per density condition when comparing A) Low vs High density, B) Mid vs High density, and C) Low vs Mid density.*

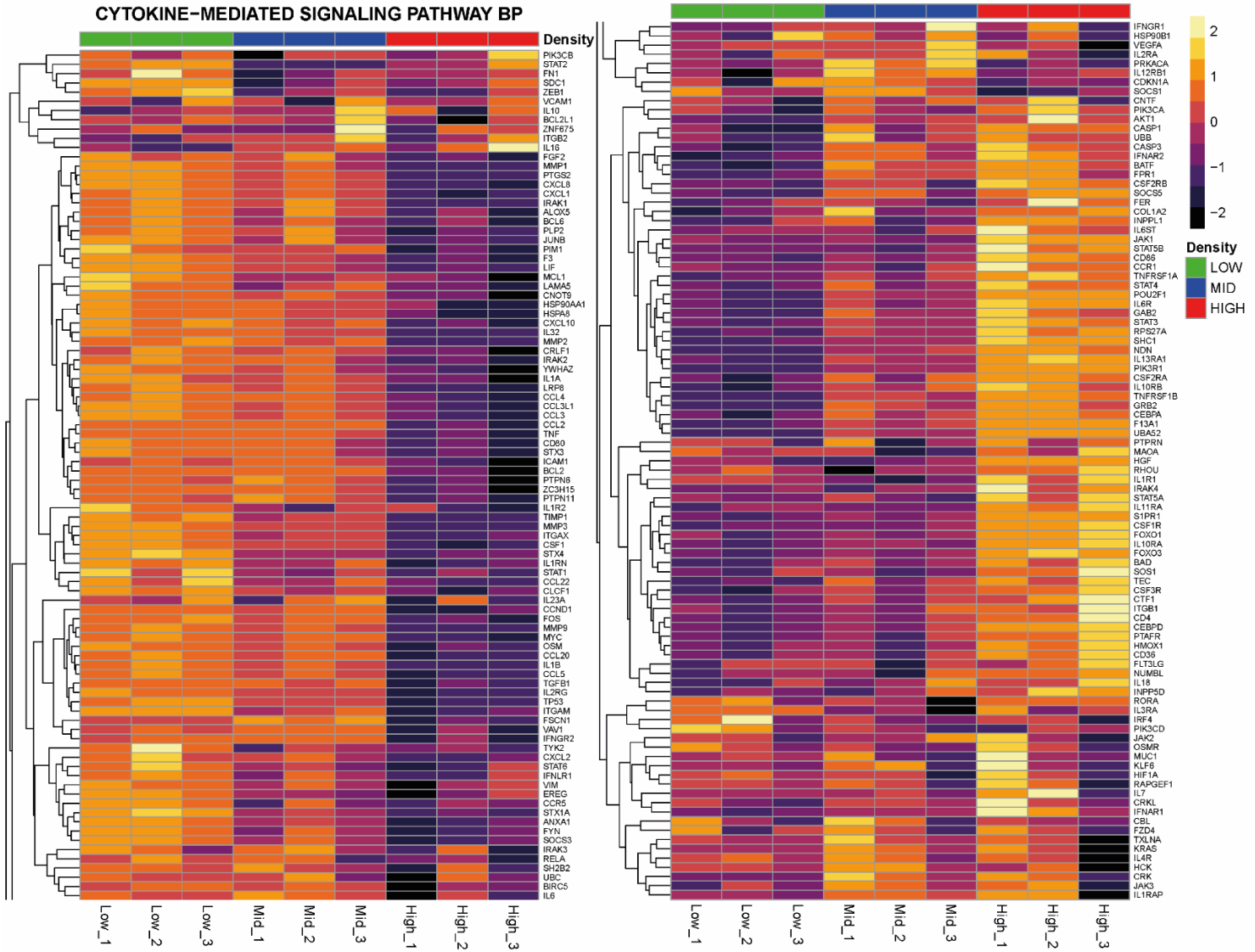


Figure 9: Biological process GO term "Cytokine-mediated signalling pathway".

Heatmap of gene expression relative to the median fragments per kilobase million (TPM) value of each gene at low, mid, and high densities. Temperature displays Log_2-fold difference from the median, where yellow > median, and purple < median. Each column is one experimental repeat and repeats are matched over 3 different dates.

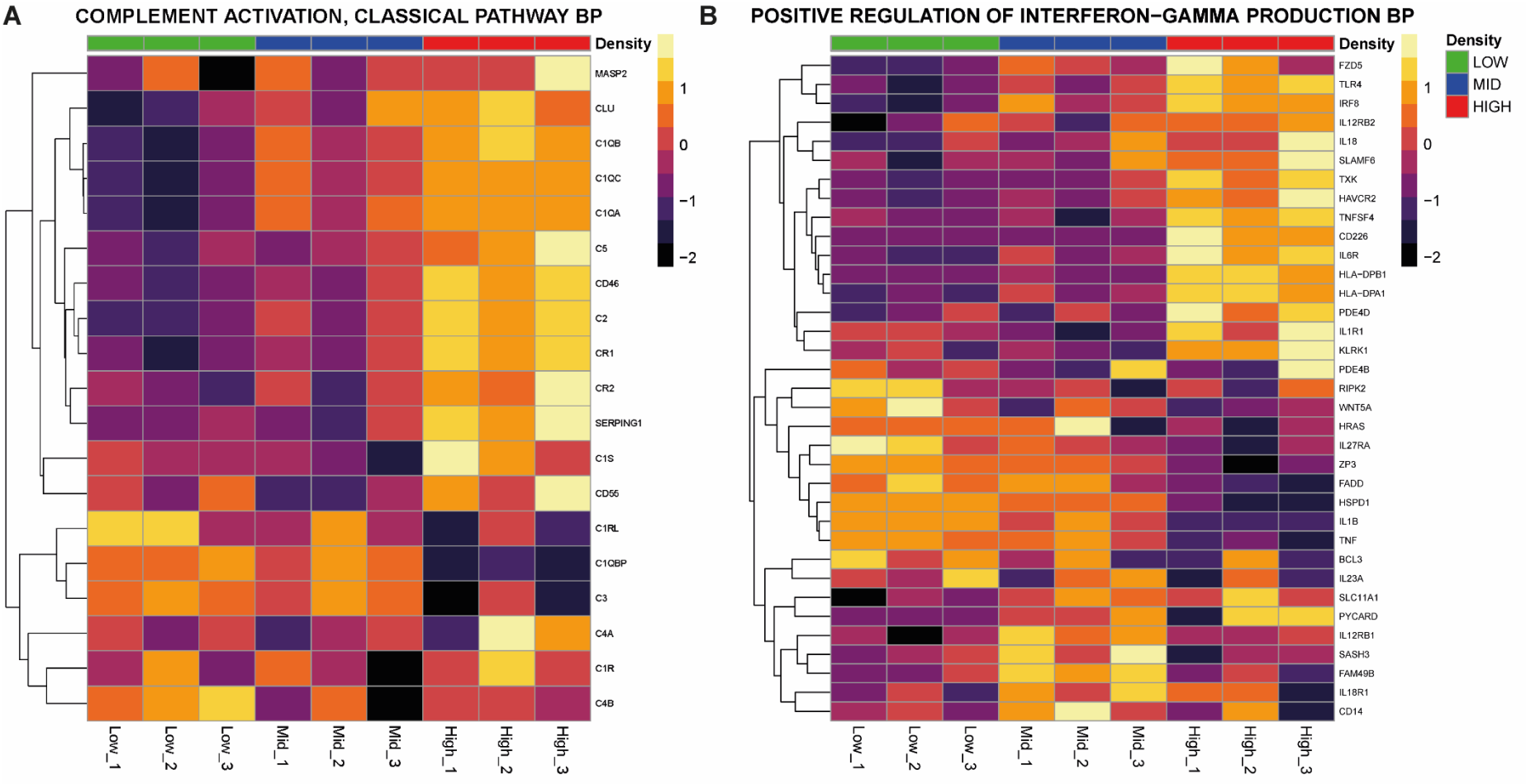


Figure 10: Inflammation related terms enriched in high density macrophages. *Heat maps of biological process GO terms for A) "Complement activation, classical pathway" and B) "Positive regulation of interferon-gamma production". Temperature displays Log_2-fold difference from the median TPM, where yellow > median, and purple < median.*

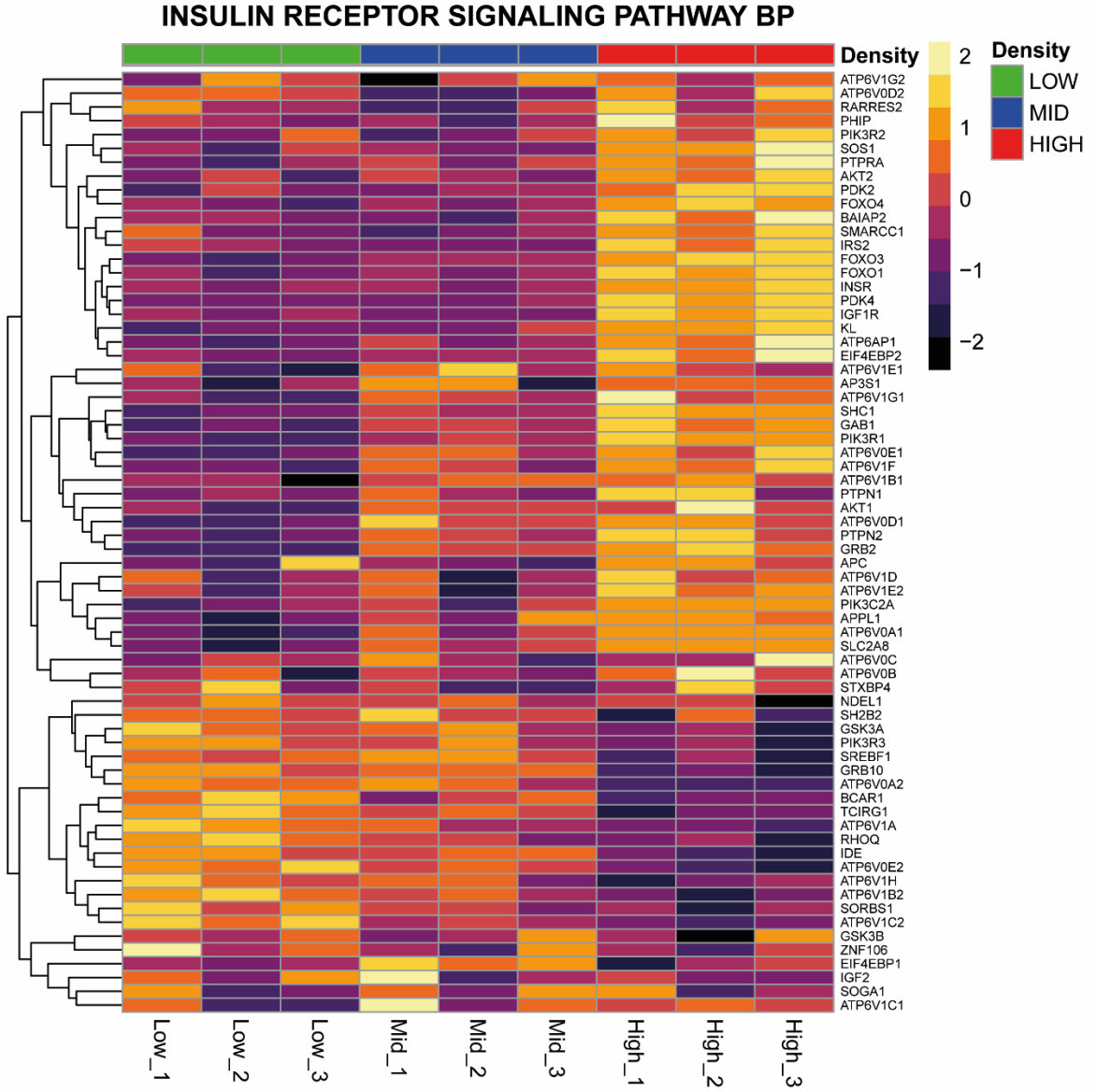


Figure 11: Biological process GO term "Insulin receptor signalling pathway". *Temperature displays Log_2-fold difference from the median TPM, where yellow > median, and purple < median.*

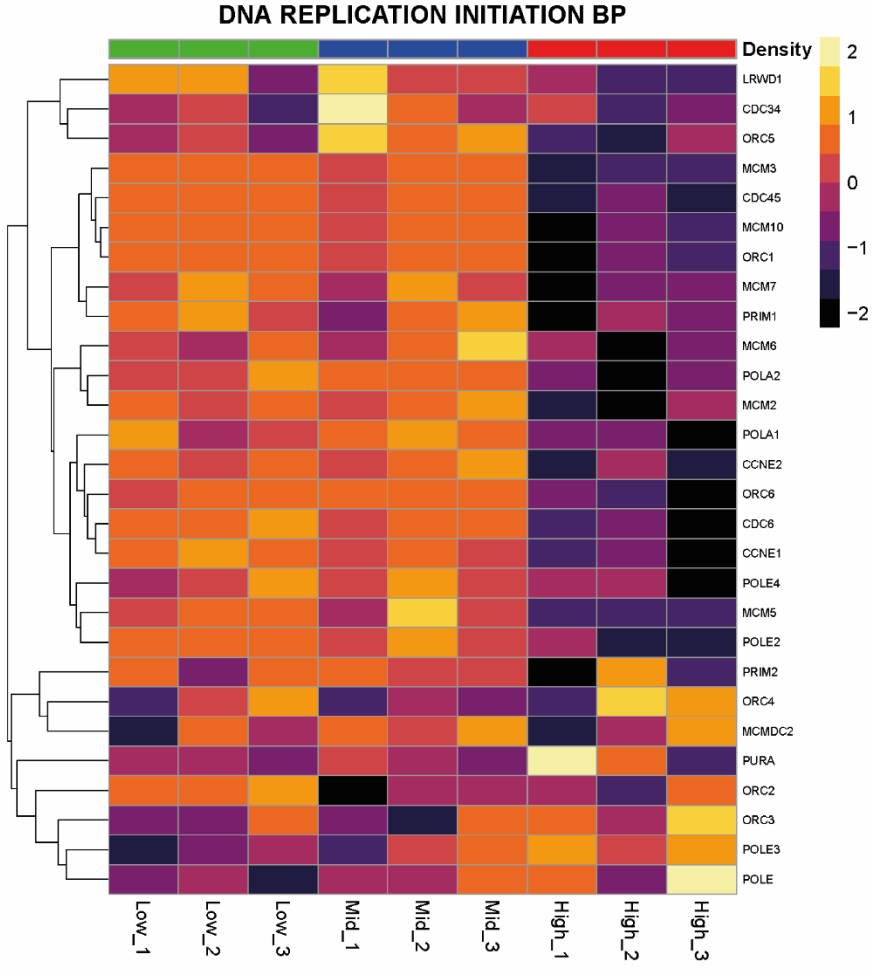


Figure 12: Biological process GO term "DNA replication initiation". *Temperature displays Log_2-fold difference from the median TPM, where yellow > median, and purple < median.*

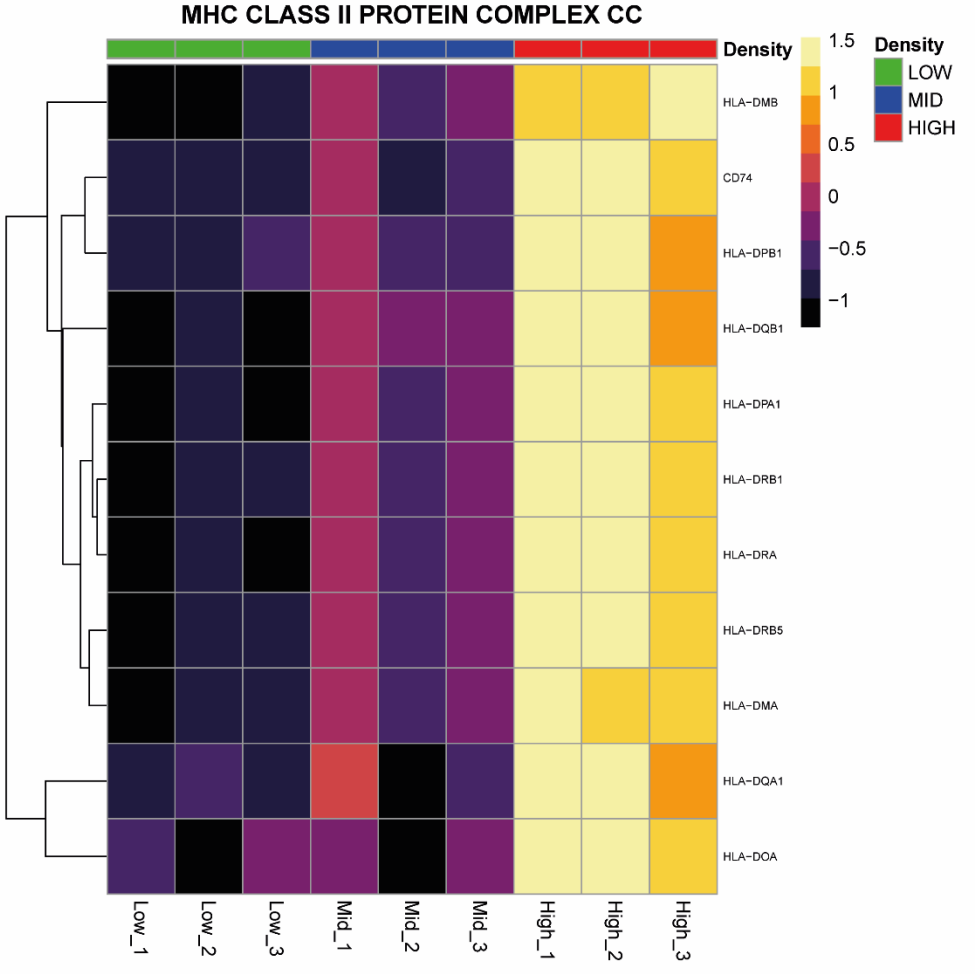


Figure 13: Cellular component GO term "MHC class II protein complex". *Temperature displays Log_2-fold difference from the median TPM, where yellow > median, and purple < median.*

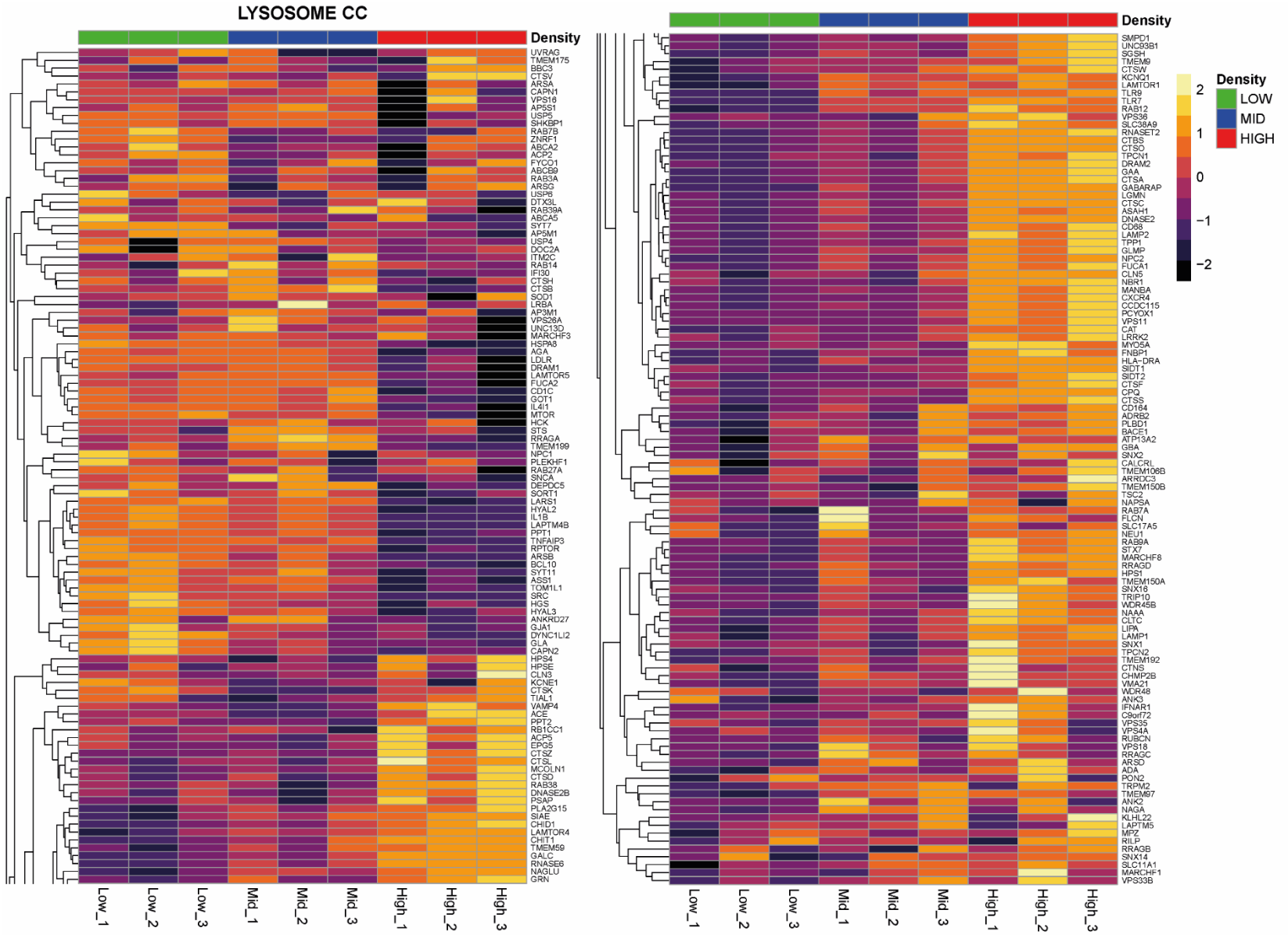


Figure 14: Cellular component GO term "Lysosome". *Temperature displays Log_2-fold difference from the median TPM, where yellow > median, and purple <median.*

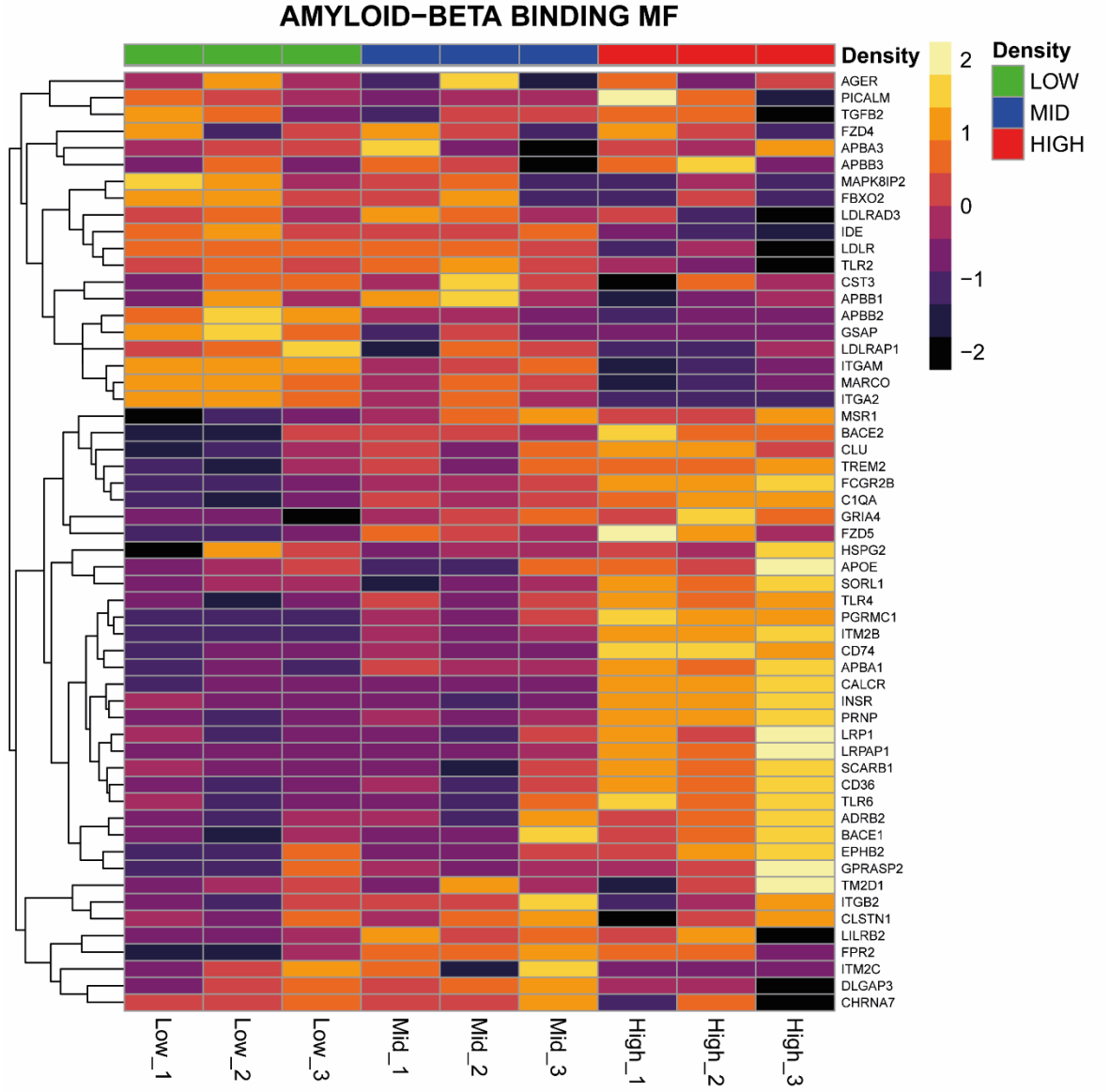
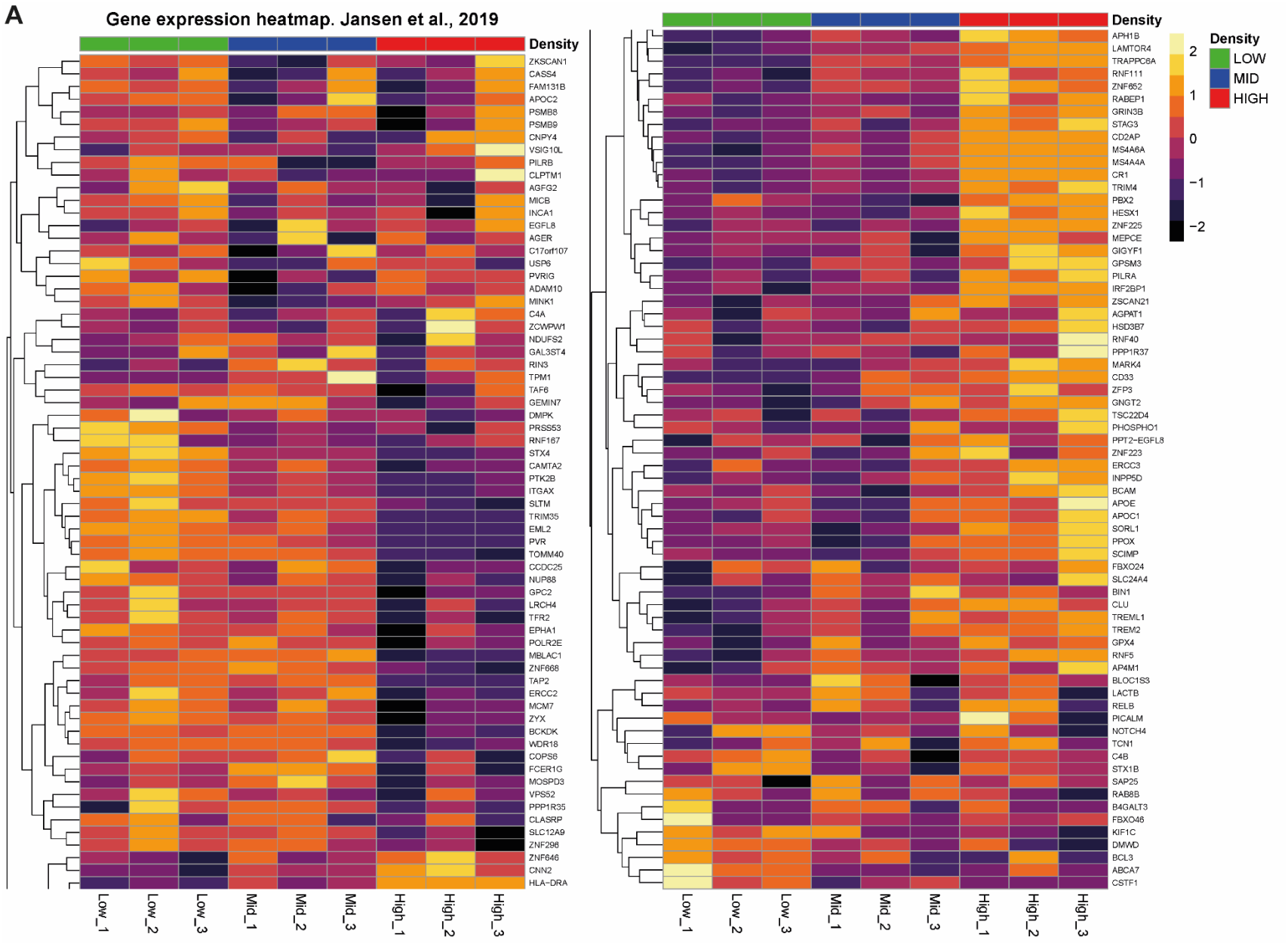
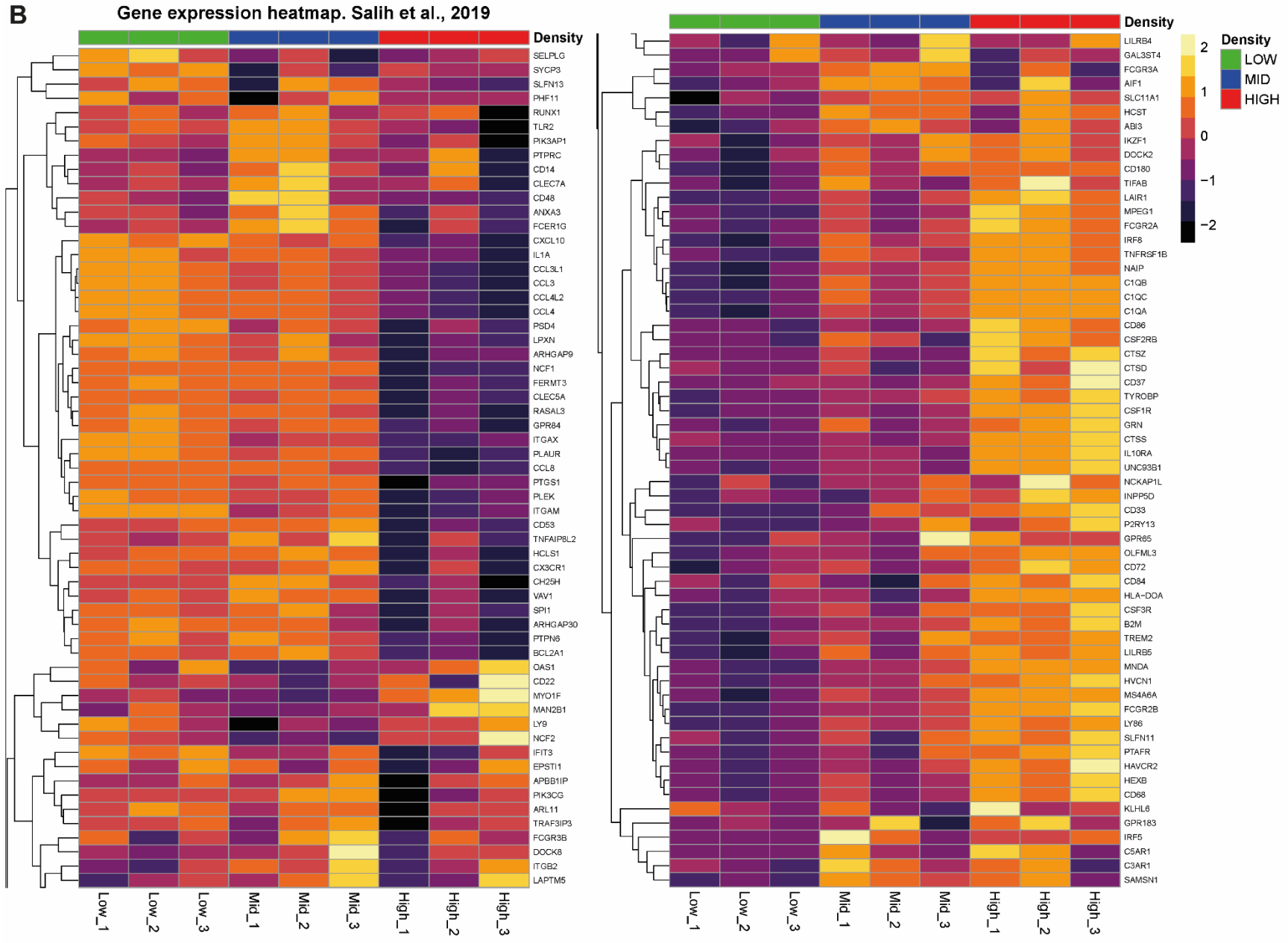


Figure 15: Molecular function GO term "Amyloid-beta binding". *Temperature displays Log$_2$-fold difference from the median TPM, where yellow > median, and purple < median.*

Figure 16: DDRI regulates over half of known AD-associated genes. *Heat maps for all genes expressed in iPSC-derived macrophages identified in A) Jansen et al. (2019)* (473) *and B) Salih et al. (2019)* (474)*. Temperature displays Log$_2$-fold difference from the median TPM, where yellow > median, and purple < median.*


A
Gene expression heatmap. Jansen et al., 2019
Density
ZKSCAN1
CASS4
FAM131B
APOC2
PSMB8
PSMB9
CNPY4
VSIG10L
PILRB
CLPTM1
AGFG2
MICB
INCA1
EGFL8
AGER
C17orf107
USP6
PVRIG
ADAM10
MINK1
C4A
ZCWPW1
NDUFS2
GAL3ST4
RIN3
TPM1
TAF6
GEMIN7
DMPK
PRSS53
RNF167
STX4
CAMTA2
PTK2B
ITGAX
SLTM
TRIM35
EML2
PVR
TOMM40
CCDC25
NUP88
GPC2
LRCH4
TFR2
EPHA1
POLR2E
MBLAC1
ZNF668
TAP2
ERCC2
MCM7
ZYX
BCKDK
WDR18
COPS6
FCER1G
MOSPD3
VPS52
PPP1R35
CLASRP
SLC12A9
ZNF296
ZNF646
CNN2
HLA-DRA
Low_1
Low_2
Low_3
Mid_1
Mid_2
Mid_3
High_1
High_2
High_3
Density
APH1B
LAMTOR4
TRAPPC6A
RNF111
ZNF652
RABEP1
GRIN3B
STAG3
CD2AP
MS4A6A
MS4A4A
CR1
TRIM4
PBX2
HESX1
ZNF225
MEPCE
GIGYF1
GPSM3
PILRA
IRF2BP1
ZSCAN21
AGPAT1
HSD3B7
RNF40
PPP1R37
MARK4
CD33
ZFP3
GNGT2
TSC22D4
PHOSPHO1
PPT2-EGFL8
ZNF223
ERCC3
INPP5D
BCAM
APOE
APOC1
SORL1
PPOX
SCIMP
FBXO24
SLC24A4
BIN1
CLU
TREML1
TREM2
GPX4
RNF5
AP4M1
BLOC1S3
LACTB
RELB
PICALM
NOTCH4
TCN1
C4B
STX1B
SAP25
RAB8B
B4GALT3
FBXO46
KIF1C
DMWD
BCL3
ABCA7
CSTF1
Low_1
Low_2
Low_3
Mid_1
Mid_2
Mid_3
High_1
High_2
High_3
Density
LOW
MID
HIGH
2
1
0
−1
−2


B
Gene expression heatmap. Salih et al., 2019
Density
SELPLG
SYCP3
SLFN13
PHF11
RUNX1
TLR2
PIK3AP1
PTPRC
CD14
CLEC7A
CD48
ANXA3
FCER1G
CXCL10
IL1A
CCL3L1
CCL3
CCL4L2
CCL4
PSD4
LPXN
ARHGAP9
NCF1
FERMT3
CLEC5A
RASAL3
GPR84
ITGAX
PLAUR
CCL8
PTGS1
PLEK
ITGAM
CD53
TNFAIP8L2
HCLS1
CX3CR1
CH25H
VAV1
SPI1
ARHGAP30
PTPN6
BCL2A1
OAS1
CD22
MYO1F
MAN2B1
LY9
NCF2
IFIT3
EPSTI1
APBB1IP
PIK3CG
ARL11
TRAF3IP3
FCGR3B
DOCK8
ITGB2
LAPTM5
Low_1
Low_2
Low_3
Mid_1
Mid_2
Mid_3
High_1
High_2
High_3
Density
LILRB4
GAL3ST4
FCGR3A
AIF1
SLC11A1
HCST
ABI3
IKZF1
DOCK2
CD180
TIFAB
LAIR1
MPEG1
FCGR2A
IRF8
TNFRSF1B
NAIP
C1QB
C1QC
C1QA
CD86
CSF2RB
CTSZ
CTSD
CD37
TYROBP
CSF1R
GRN
CTSS
IL10RA
UNC93B1
NCKAP1L
INPP5D
CD33
P2RY13
GPR65
OLFML3
CD72
CD84
HLA-DOA
CSF3R
B2M
TREM2
LILRB5
MNDA
HVCN1
MS4A6A
FCGR2B
LY86
SLFN11
PTAFR
HAVCR2
HEXB
CD68
KLHL6
GPR183
IRF5
C5AR1
C3AR1
SAMSN1
Low_1
Low_2
Low_3
Mid_1
Mid_2
Mid_3
High_1
High_2
High_3
Density
LOW
MID
HIGH
2
1
0
−1
−2

4.2.7 The cause of DDRI may in part be secretory, with glucose metabolism products as candidates

Having demonstrated clear differences in the morphology, phenotype, transcriptional profile, and response of iPSC-derived macrophages during DDRI, I now needed to identify potential causative agents. Considering low density cells have elongated morphology and appear to be more adherent to the tissue-culture plastic (data not shown), and expression of cellular adhesion molecules (e.g. the integrin family) are upregulated in low density cells, one hypothesis could be that providing an extracellular matrix (ECM) to which cells can interact will supress the inflammatory phenotype of low density plated cells. To investigate this, I plated PreMacs on tissue culture plastic, the integrin substrate, Fibronectin, or Geltex™ (a basement membrane used for culturing of iPSC containing laminin, collagen IV, entactin, and heparin sulfate proteoglycans). Macrophages were then stimulated for 24 hours with 1 ng/mL LPS or 1 μg/mL Pam3. Consistent with earlier work, TNFα secretion post stimulation, and IL-6 secretion prior to stimulation (time 0), was higher, per cell, at low and mid density than high density, but the presences of either ECM did not reverse this effect (Figure 17A-B). Culturing on Geltrex™ did slightly reduce the inflammatory response, but macrophages did not adhere strongly to this matrix and were morphologically unhealthy (data not shown). I therefore did not pursue this hypothesis further.

I next tested to see whether DDRI was caused by a soluble factor in the supernatant of the cells. 48 hours or 24 hours prior to stimulation of cells with LPS, media was either exchanged between cells plated at contrasting plating densities, replaced with fresh medium, or left unchanged. After stimulation, DDRI was measured by secretion of TNFα after 24 hours stimulation, or IL-6 at time 0. Again, cells cultured in unchanged medium displayed DDRI (Figure 17C-D). In contrast, cells in which the medium was replaced with fresh medium 24 hours before stimulation showed supressed TNFα secretion, and IL-6 secretion to levels comparable to those observed with high density cells in unchanged media. Exchange of media between densities 24 hours prior to LPS stimulation was sufficient to induce a stronger TNFα response from mid and high density cells when cultured in low density conditioned medium,

while high density conditioned medium suppressed the response by low and mid density cells (Figure 17C). This would, therefore, suggest that regulation of cytokine release between densities is mediated by a soluble compound. However, after 48 hours of culture in exchanged media (i.e low cells in high cell supernatant etc.) DDRI was observed, indicating that this soluble compound may be replaced or removed by cells. Interestingly, IL-6 secretion from unstimulated cells did not change after exchange of supernatants either 24 or 48 hours prior to stimulation (Figure 17D). Therefore, possible regulation of inflammation by any soluble factor may be a product, not a cause, of DDRI.

Although a suppression of TNFα and IL-6 was observed if medium was replaced with fresh medium 24 hours prior to stimulation, the absence of a change to IL-6 secretion after media exchange would suggest that the effect of fresh medium is actually independent of the soluble factor responsible for changes in the TNFα response. Therefore, the soluble compound that regulates the TNFα response may be produced by high density cells, not low. I observed visually that media on high density cells was more acidic (yellow colouring due to the presence of phenol red) than lower densities (data not shown), indicating the production of lactic acid. I therefore measured changes in glucose and lactate levels over the course of the 7-day differentiation period, and for 72 hours after refreshing the medium, to investigate whether metabolic changes and products could be the causative soluble component of DDRI. Although results are only preliminary (from a single experimental repeat), there is evidence that glucose is metabolised by high and mid density cells at different rates, and that low density cells, after initially metabolising glucose, may even transition to gluconeogenesis (Figure 17E). Lactate could also be detected, with concentrations increasing as density increases (Figure 17F). In conclusion, I have found that DDRI is likely regulated by both a soluble component, and an insoluble process. A potential candidate for this soluble component may be lactate.

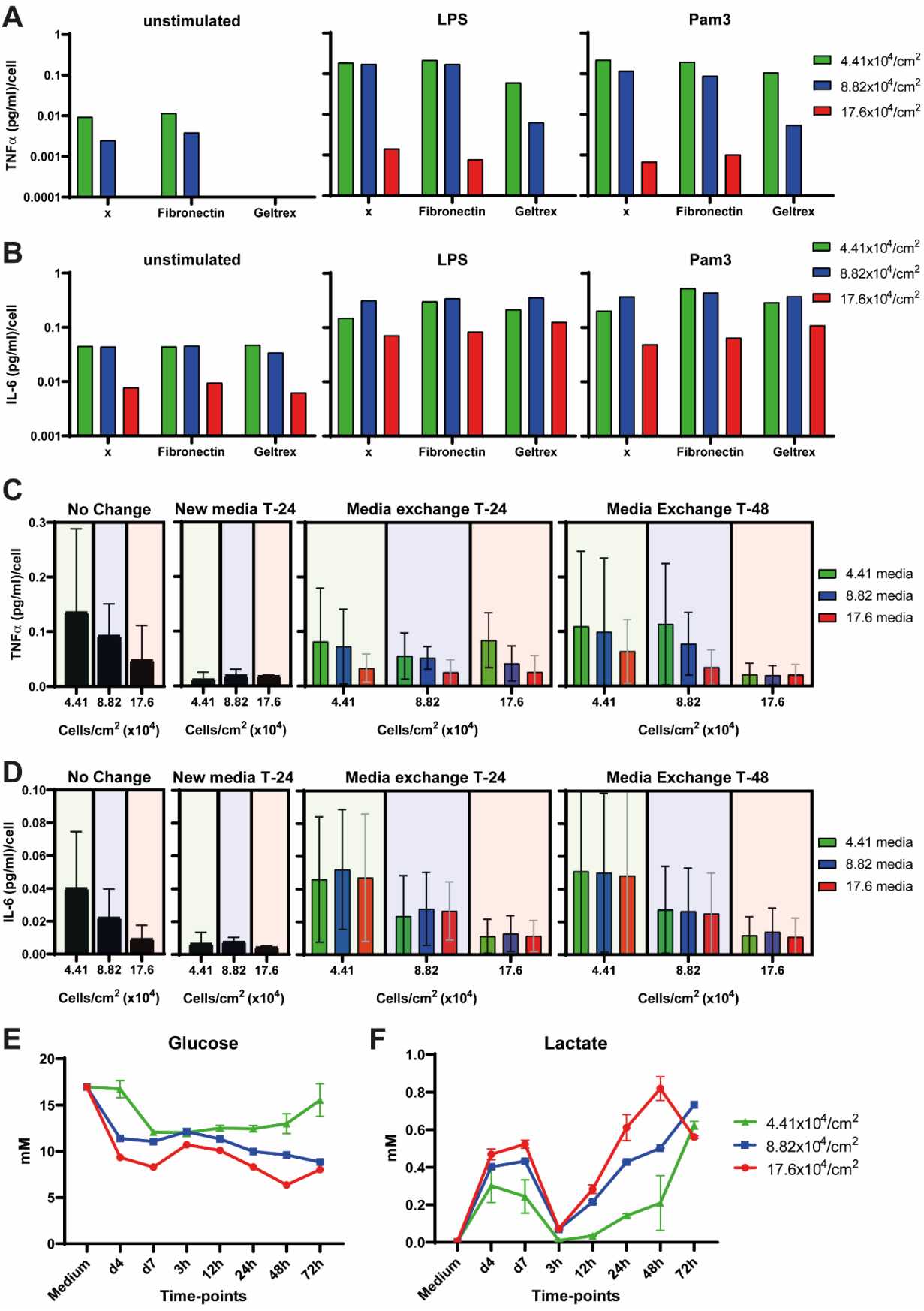

A
unstimulated
LPS
Pam3
TNFα (pg/ml)/cell
1
0.1
0.01
0.001
0.0001
x
Fibronectin
Geltrex
4.41x10^4/cm^2
8.82x10^4/cm^2
17.6x10^4/cm^2
B
IL-6 (pg/ml)/cell
0.001
C
No Change
New media T-24
Media exchange T-24
Media Exchange T-48
0.3
0.2
0.0
4.41 8.82 17.6
Cells/cm^2 (x10^4)
4.41 media
8.82 media
17.6 media
D
0.10
0.08
0.06
0.04
0.02
0.00
E
Glucose
mM
20
15
10
5
0
Medium
d4
d7
3h
12h
24h
48h
72h
Time-points
F
Lactate
1.0
0.8
0.6
0.4
0.2

Figure 17: DDRI may be regulated by a secretory and non-secretory signal. *A) Total TNFα secretion per cell and B) Total IL-6 secreted per cell from macrophages plated at different densities stimulated for 24 hours with 1 ng/mL LPS, or 1 µg/mL Pam3CSK4. Cells were plated on tissue-culture plastic, 5 µg/cm^2 fibronectin, or 100 µL/cm^2 Geltrex™ and differentiated for 7-days as usual before stimulation. n=1. C) Total TNFα secreted per cell from different density macrophages cultured in: left; unchanged media, centre left; media changed 24 hours prior to stimulation, centre right; media exchanged between each density 24 hours prior to stimulation, or right; media exchanged between each density 48 hours prior to stimulation. Cells were stimulated for 24 hours with 1 ng/mL LPS. n=3 (2 different cell lines, 3 experiments) D) Total IL-6 secreted per cell from the same cells as part C) before stimulation. n=2 (2 different cell lines, 2 experiments). E) Glucose concentration and F) lactate concentration in the supernatant of macrophages plated at different densities. Samples were taken at day 4 of differentiation when cells were fed 50% fresh media, and day 7 of differentiation, at which time media was completely changed to fresh media and cells incubated a further 72 hours with samples taken periodically over this time. E) high and mid density n=1, low density n=2 (2 cell lines, 1 experiment). F) n=2 (2 cell lines, 1 experiment).*

4.3 Discussion

In this chapter, I have shown that cell plating density is a major regulator of iPSC-derived macrophages, altering their phenotype, transcriptome, and response to stimuli. I first demonstrated how density regulates the macrophage response to both TLR agonists (LPS and Pam3CSK4) as well as non-TLR stimulating agonists (TNFα) (Figure 1B-D). Distinction between these is important, not only because it shows a broad impact on immune signaling, but also because it identifies possible shared downstream signaling mediators that are regulated in response to cell density. TLR2 and TLR4 signal intracellularly via an MyD88-dependent pathway which drives an NF-κB-mediated response through TAK1 and PI3K activation, and an AP-1 (c-Jun and c-Fos)-mediated response through MAPK activity (52). On the other hand, TNFα also induces NF-κB and AP-1 activity through TAK1, PI3K and MAPK pathways, but recruits different mediators to its receptors to initiate this response, using RIPK1, TRAF1, -2, -3, and -5, and TRADD (475). Regulation of intracellular components and not the receptors themselves may, then, explain why transcriptionally I observe higher expression of both TLR4 and the TNF receptors TNFR1 and TNFR2 (TNFRSF1A and TNFRSF1B, Figure 9) at high densities, but do not observe higher TNFα and IL-6 responses from these cells after stimulation. Interestingly though, TLR2 is more highly expressed at low and mid densities than high density, which may explain the clearer difference in response to Pam3 than to LPS observed as cell numbers increase. The macrophage response to external stimuli is finely tuned yet can be highly variable. For example, macrophages integrate LPS shape (rough or smooth) and concentration, with co-receptor usage and binding to LPS by accessory proteins (476–481). Therefore, it was important to rule out the possibility that DDRI was simply due to depletion of agonist by increasing cell density. While my data suggest that DDRI is independent of the agonist concentration, it is interesting to note that the response to LPS declined as dose increased in high density cells, but not in low or mid density cells (Figure 1G-H, Figure S1H-I). This trend has been reported before by Meng and Lowell (1997) (482),

who reported a similar trend in BMDM plated at a high density (10^5 cells/well of a 96-well plate) while investigating the role of Src-family kinases in the LPS response.

After stimulation with LPS and IFNγ, I found that low density macrophages are more likely to die (Figure 2). Whether this is through apoptosis or necroptosis was not tested here and will be essential future research. However, having found that low density cells appear inflamed at steady state, this is reminiscent of apoptosis mediated through the inflammasome. After a "priming" signal, which increases expression of pro-IL-1β, a subsequent "activation" signal will result in cleavage of pro-IL-1β and caspases to trigger cell death (483). Alternatively, this could be due to an absence of a survival signal under these culturing conditions. The primary survival signal utilized by macrophages is M-CSF, which is supplemented into the media in which iPSC-derived macrophages are cultured (484). We would therefore expect low density cells to have internalized and degraded less of the available M-CSF and be more likely to survive (485). What is more, low density cells transcriptionally produce close to 20 times more M-CSF mRNA than high density cells (Figure 9). However, expression of the surface receptor, CSFR1 is more than twice as high in high density cells than low density. This could prime the cells for survival despite a potentially smaller pool of M-CSF. Additional evidence of an increased M-CSF-cell interaction at high density is seen in the down regulation of TLR2 and upregulation of CD14, as reported by Sweet *et al.* (2004) and Ji *et al.* (2002) respectively (484, 486–488). However, expression of TLR1, 6, and 9 do not follow the expected patterns reported, demonstrating either inconsistencies between the experimental models used, or a secondary influence during DDRI.

Stimulation with LPS and IFNγ induced a broad range of cytokines and chemokines from the iPSC-derived macrophages (Figure 3, S2). A majority of these were regulated by DDRI, i.e., more protein was produced per cell at low density than at mid or high densities. One clear exception to this rule though was CXCL11 (Figure 3D). CXCL12 and IL-10, too, appeared only modestly influenced by DDRI, however actual secretion of both was low (Figure S2D). Nevertheless, IL-10 is an anti-inflammatory cytokine and therefore may play part of a feedback loop to suppress inflammation in DDRI. IL-10 (along with IL-6) has been reported to be

secreted under high density conditions but not single cell conditions (489), which Antonioli *et al.* (2018) (466) proposed as evidence of a possible quorum sensing mechanism during the immune response. CXCL12 on the other hand interacts with CXCR4 and CXCR7 to recruit leukocytes to the site of inflammation, so the rationale for not regulating its secretion during DDRI is not apparent (490, 491).

CXCL11, also known as interferon-inducible T-cell alpha attractant (I-TAC), as its name suggests, is induced by interferon signaling through STAT3 and recruits T-cells, natural killer (NK) cells, macrophages, and plasmacytoid dendritic cells (pDC) to the site of infection. Its receptors are CXCR3 and CXCR7 (491–494). CXCR3 is also bound by CXCL9 and CXCL10 and there is some evidence of competitive binding between these 3 chemokines, with CXCL11 having the highest affinity (493). Competitive inhibition also exists between CXCL11 and CCL3/CCL4, both of which are highly secreted by low and mid density cells, and CCL5. CXCL11 has been reported to bind both CCL receptors CCR3 and CCR5 as an antagonist (493, 495). Considering it is uniquely un-regulated by DDRI after LPS and IFNγ stimulation, one possible avenue for future research could be to investigate whether gene transcription is being driven by a different transcription factor or set of transcription factors. To identify possible targets for investigation, I have compared transcription factor usage between CXCL11 and the other cytokines and chemokines measured (with the exception of CXCL12 and IL-10). By comparing the shared transcription factors used by all cytokines and chemokines using the TRRUST version 2 database, with the reported transcription factors for CXCL11 using the TF2DNA database, I identified transcription factors unique to CXCL11. After comparing their expression in the 3 different densities (Table 2) possible future targets of investigation more highly expressed in high density cells could be BATF and IKZF1. BAFT is a member of the AP-1 family of transcription factors that is related to IL-4 signaling, is up regulated by STAT3, and interacts with IRF4. IKZF1 is a zinc-finger DNA-binding protein family member which is involved in lymphocyte differentiation and hematopoietic stem cell differentiation (496).

Transcription factor	Expression pattern
ARNT2	Undetected
BATF	High = Mid > Low
EHF	Undetected
ESRRG	Undetected
HOXD12	Undetected
HOXD4	Undetected
IKZF1	High > Mid = Low
MAFA	Undetected
MYF6	Undetected
NFAT5	High < Mid < Low
NR2C1	High = Mid = Low
RARG	High = Mid = Low
RORA	High = Mid = Low
SOX15	Undetected
SOX2 (QSOX2)	High < Mid = Low
SOX4	High < Mid = Low
TP63	Undetected
ZNF75A	High = Mid = Low

Table 2. Potential transcription factors not regulated by DDRI.

I have found that density not only dramatically alters the response by iPSC-derived macrophages to inflammatory stimuli, but also completely alters the cell phenotype (Figure 4, S3). High density cells have higher expression of CD14 and CD206, but potentially lower CD11b and CD45 than low and mid density cells (Figure 4E). This means that different densities do not fit into clear phenotypes according to established descriptions made of monocyte-derived macrophages. For example, CD14 is typically a marker of classical inflammatory macrophages (15), while CD206 is more typically considered a marker of M2 polarization (425, 497). As already stated, this difference in CD14 expression appears inconsistent with the response of these cells to LPS but could be explained by dose and presence of M-CSF (488). CD206 on the other hand is unsurprising, as high density cells appear to be less inflammatory. It is consistent with expression of scavenger receptors (of which CD206 is one) and lysosomal genes being upregulated in high density cells. As for CD11b, the link between cell size (FSC-A) and expression (Figure S3) can potentially be explained. CD11b, also known as Integrin alpha M (ITGAM) or complement receptor 3 (CR3),

is a member of the β2 Integrin family that regulate inflammation through adhesion and migration (498). Considering the clear morphological differences between densities, and increased expression of numerous adhesion molecules in low and mid densities, one would likely expect an increased expression of CD11b in these cells. Furthermore, when all cells were stimulated with LPS and IFNγ they became more uniform in shape, and CD11b expression changed to reflect this (Figure 4B, 4F). On the other hand, the difference in CD45 depending on cell morphology in unstimulated low and mid density cells (Figure S3), and the change in expression after stimulation cannot easily be explained. Further immune phenotyping using techniques like mass cytometry would be needed to generate a more complete map of surface marker expression of these cells to broadly classify them. For instance, expression of CD34 would be of interest to test whether these cells may be similar to another monocyte-derived cell called a fibrocyte, a highly plastic cell which morphologically shares similarities with low density cells, and shares many of its functions with both macrophages and fibroblasts (499–501).

Using RNA-Seq, I have shown here that, although different densities display considerable differences in their response profile and resting phenotype, they are still transcriptionally similar to the microglial cells reported by Abud *et al.* (2017) (385). We should therefore still considered them as tissue resident macrophages (Figure 5A). Between the densities, mid density cells are transcriptionally most similar to low density cells sharing 2090 upregulated genes when compared against high density, while mid only shares 623 upregulated genes with high density compared to low density (Figure 5B-D). Comparing the three densities, it was unsurprising to see that GO terms for proinflammatory cytokine and chemokine signaling were upregulated in low and mid density cells (Figure 6, 9-10), along with cytoskeletal and surface adhesion complexes (Figure 7). Perhaps more unexpected was the upregulation of terms related to cell proliferation (Figure 6, 12). This would suggest, much like as was shown with cancerous cells back in the 1960s, that density regulates proliferation of macrophages. Density dependent regulation of cancer cells is termed contact inhibition of proliferation (CIP), and although known for 60 years (449, 452), the mechanism has only

recently been discovered. The Hippo family of kinases, MST1/-2 and LATS1/-2 regulate activity of the transcription factors YAP and TAZ (502–504). Importantly, the kinases themselves are regulated through a variety of signals including through adherence proteins like E-cadherin, structural changes in F-actin and stress fibers, and G-protein coupled receptor signaling through Rho-GTPases (450, 504–506). Therefore, the signal to start proliferating can come directly from interactions with cells, or through differences in the structure of the environment around them. Similarly, cell adhesion molecules like ICAM-1 (upregulated in low density cells) are known to regulate the inflammatory response of astrocytes (507) and simply changing the elasticity of the surface on which macrophages are grown, mimicking a high density environment of interacting with cell membranes instead of rigid surfaces, can alter their response to LPS and IFNγ through actin polymerization and Rho-GTPase activity (508–510). Therefore, it will be interesting to test if the proliferative activity, and the pro-inflammatory state, of low density cells can be reversed by inhibition of the Rho signaling pathway and actin polymerization using inhibitors like Y-27632 (ROCKi) and cytochalasin D respectively, or by changing the elasticity of the culture surface to that more akin to that of the cell membrane.

Overall, high density cells appear to upregulate genes related to effector functioning in response to an inflammatory signal. Receptors for various cytokines and chemokines are upregulated, but not the cytokines and chemokines themselves (Figure 9-10). This actually raises the possibility that this could explain differences in cytokine secretion measured here between densities. As discussed in Chapter 1.4: Regulation of the macrophage cytokine response, cytokine uptake or binding by decoy receptors is a major mechanism by which their stimulatory activity is regulated and resolved. It is, therefore, somewhat unsurprising that the cytokine response is lower from high density cells. To thoroughly test, then, if this is responsible for the cytokine effect seen, a proper time course experiment measuring release over time is needed to determine if uptake drives cytokine suppression or if it is just another contributing factor towards DDRI. Nevertheless, this still leaves unanswered questions as to what is driving the increased cytokine receptor expression in high density cells.

In addition to cytokine receptor upregulation, processes required for uptake of extracellular material, processing of it, and cross presentation to the adaptive immune system appear to be enriched in high density cells (Figure 13-14). To exemplify this, the GO term “Scavenger receptor activity” is enriched in these cells (Figure 8B) and including macrophage scavenger receptors 1 (MSR1) and CD163. Intracellularly I observe increased expression of endosome and lysosome associated proteins like RAB7A and LAMP1. Lastly all isoforms of MHC class II and MHC class I are upregulated in high density cells (Figure 13). I therefore propose that DDRI at low densities is driving the initial response to danger and damage to recruit other immune cells to the site of insult. Once there, rather than escalate the recruitment of cells leading to a hyper response and tissue damage, high density macrophages switch to an effector phenotype to carry out the required immune response either resolving the issue, or in the case of true infections, activate the adaptive immune response through MHC interactions. This model could then potentially explain why clearance of some infections, e.g. *M. tuberculosis,* is density dependent (511), but its general role in infectious disease needs further exploration.

Now one of the key questions left unanswered is: what is the cause of DDRI? By exchanging conditioned media, I have shown that it is likely to be two separate signals, one soluble, and one not (Figure 17C-D). I earlier discussed the potential importance of cytoskeletal differences and cell surface interactions as a possible insoluble signal, and I have preliminary data showing that this is not dependent on the ECM (Figure 17A-B). As for a soluble signal, one recent theory that has gained popularity is quorum sensing by macrophages. Quorum sensing typically refers to regulation of bacteria by the relative abundance of an “autoinducer” signal. Once a critical threshold is reached through sufficient numbers of the bacteria being present, quorum sensing drives a change in bacterial virulence, metabolism, and biofilm formation (465). Models for quorum sensing in macrophages have been proposed in homeostatic repair after plucking of hair follicles via CCL2 (464), regulation of macrophage proliferation by M-CSF (468), and as part of the regulation of the TNFα response (469). One study that appears consistent with my results is the production of NO as

a negative feedback quorum signal to drive the resolution of inflammation at high cell density (445). Future work will therefore need to investigate whether NO is secreted from my iPSC-derived macrophages at different densities, and whether it is the soluble factor responsible for DDRI. The increased concentration of lactate in the supernatant of high density cells would support a metabolic shift in these cells that can result in increased NO production (431) (Figure 17F). However, iNOS, the protein responsible for production of NO, is not differentially expressed between conditions nor clearly expressed at all in these cells at resting state.

Finally, one of the most surprising findings of this investigation was the impact density had on expression of a significant number of genes implicated in Alzheimer's disease (AD). Of the genes included in the GO term "Amyloid-beta binding" 40/56 (71%) genes appear to be differentially expressed between high and low conditions (Figure 8, 15). Moreover, comparisons of genes expressed in these cells that are identified as part of large scale genomic screens reported by Lane *et al.* (2018) (471), Jones *et al.* (2010) (472), Jansen *et al.* (2019) (473), and Salih *et al.* (2019) (474), shows that greater than half of all AD-related genes are differentially expressed in high density and low density cells (Figure 16). These genes tend to be involved in, but are not exclusive to, the regulation of amyloid precursor protein (APP) processing, amyloid deposition, endocytosis, lipid and cholesterol metabolism, and the immune response. Differences in expression of these genes may not necessarily be observed in AD patients nor the actual cause of the disease. Importantly, while they identify that these genes are in some way important for developing AD, these GWAS studies primarily look at SNPs that correlate to disease, and not whether these cause changes in transcription of these genes, nor which cell type is responsible for their function in disease. For example, TREM2 is a well-known disease risk related gene, but its correlated mutation for disease, R47H, does not result in changes in expression of this gene (at least in microglia) (149). Salih et al. (474) did compare GWAS data against RNA-Seq from microglia, however this transcriptomic data was produced from a mouse model of AD which introduces its own limitations in comparability to human disease. Therefore, more work is needed to investigate the relative importance of these genes and their expression levels in macrophages/microglia before true correlations

between the results shown here and to disease can be made. Nonetheless, the non-stochastic nature of this enrichment profile for AD related genes does at least highlight a potential for a critical role of DDRI in preventing AD, and one can hypothesise that a breakdown in this regulatory system may be a principal cause of the disease. For instance, a hypothetical scenario may be that microglia in the brain, local triggering of a low density inflammatory response due to an infection or ischemia may produce a strong inflammatory response. Failure to then transition to the high density phenotype would result in increased damage to the ECM, neuronal death through inflammatory mediators like TNFα, and failure to remove deposits of amyloid-β through endocytosis and lysosomal degradation. A curious observation of the AD genes differentially expressed between these conditions is that some, e.g. S100B, CD46, CD55 (DAF) and CD59, which are more commonly associated with astrocytes and not microglia, are upregulated in low density cells, either indicating a potential shift of microglia into an astrocyte-like phenotype, or the potential for DDRI in astrocytes as well as macrophages (512).

4.4 Conclusion

In this chapter, I have built upon the importance of culturing conditions emphasized in Chapter 3 to include the importance of plating density. Through analysis of cytokine and chemokine profiles, immuno-staining and flow cytometry, and transcriptomics, I have shown how DDRI is a major regulator of iPSC-derived macrophage phenotype and functionality. The model I propose is that when macrophages are exposed to a low cell density environment, either through death of surrounding cells e.g., through injury, or breakdown of barriers, like during bacterial infections of the gut, they are induced into a proinflammatory state that recruits more macrophages to the site of inflammation through cytokine and chemokine secretion, and by increasing proliferation. Once macrophage density reaches a certain threshold, cells then transition to an effector phenotype to prevent an over-exuberant recruitment of immune cells and therefore tissue damage. Instead, high density macrophages carry out receptor mediated functions to clear the extracellular environment of cell debris, pathogens, and inflammatory mediators. These are then processed intracellularly by the phagosome and lysosome and at the same time cross presented on cell surface MHC molecules to activate an adaptive immune response when necessary (Summarized in Figure 18). By linking antigen presentation to high density cell phenotype, this may prevent premature triggering of an adaptive response by low density cells in the early stages of an inflammatory response, while also optimizing the adaptive functional response due to the already high abundance of immune cells at the site of infection. Moreover, I have demonstrated clear potential for its importance in autoimmune inflammatory diseases through a possible link to Alzheimer's disease. Further investigations into possible DDRI of macrophages in models for Alzheimer's and by macrophages containing known disease relevant polymorphisms is therefore essential. Finally, whether it is also important in other pro-inflammatory macrophage mediated diseases, for example rheumatoid arthritis, or inflammatory suppression of macrophages, like during tumor infiltration in cancer, has yet to be explored. This will be of considerable interest to future investigations of DDRI as a fundamental regulatory system in disease. Ultimately, these findings highlight the

importance of consistency across experimental design in macrophage research. Not only could this prevent important disease relevant discoveries but also make it difficult for other researchers to reproduce findings if not properly reported. This is not to say that there should be one standardized plating density for macrophage research though, as functional differences seen in cells plated at one density may not always be reproduced at another.

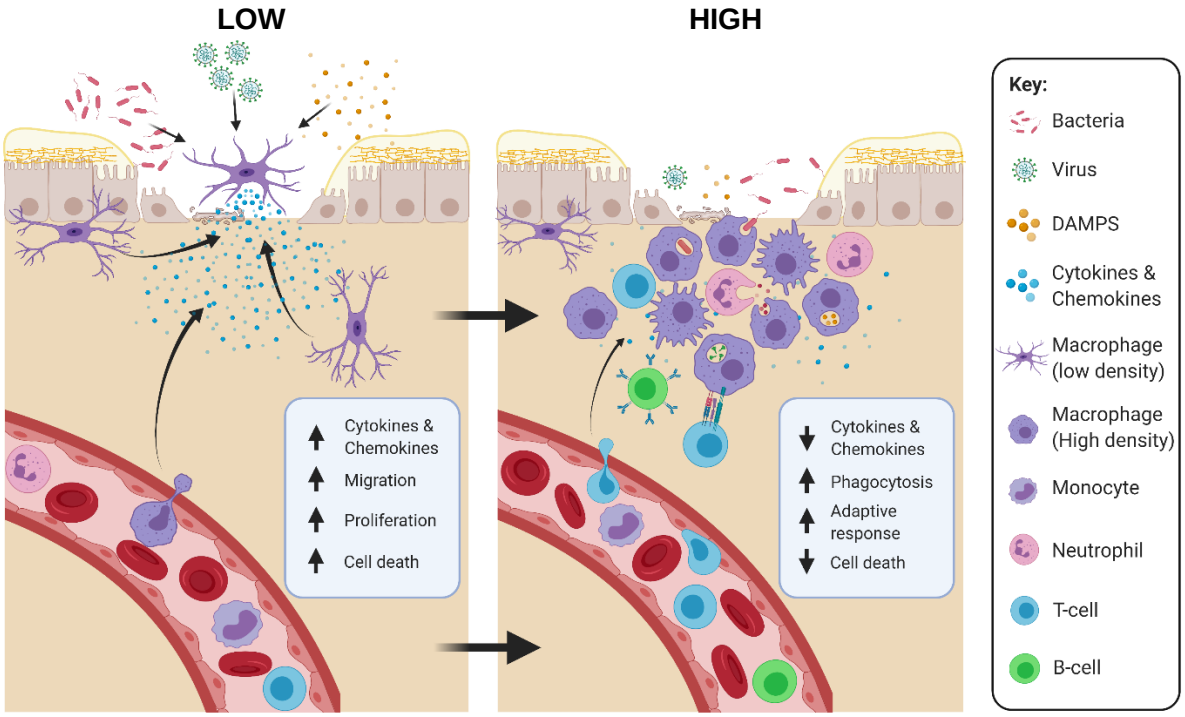


Figure 18: Schematic of proposed DDRI model during an inflammatory response. *Created with BioRender.com*

4.5 Supplementary figures

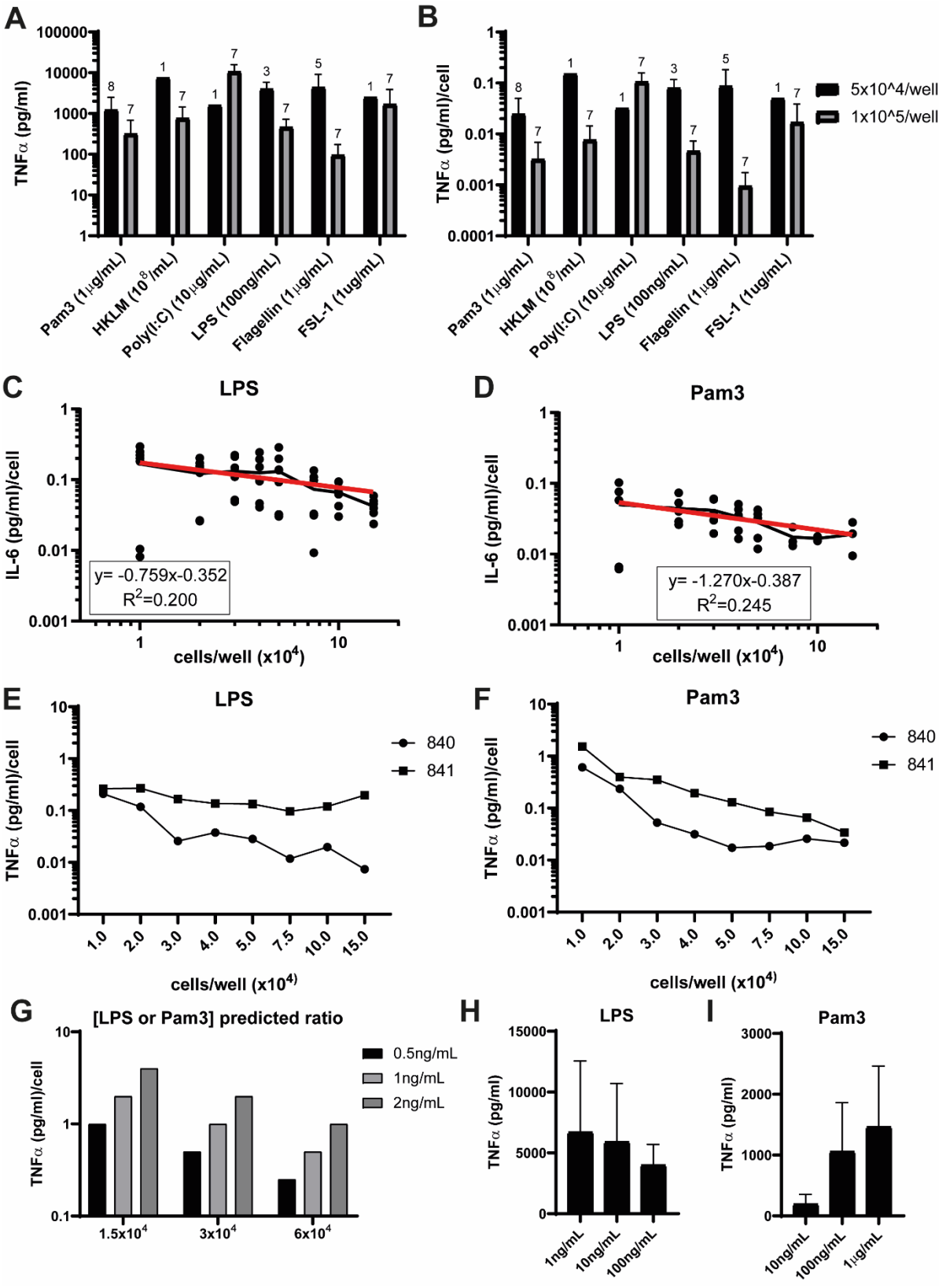


Figure S1: Plating density of macrophages impacts their response to innate immune stimuli. Related to Figure 1. *A-B) Total secretion of TNFα after 24-hour of TLR stimulation. TLRs were stimulated as follows; TLR2 by Pam3CSK4 (Pam3), TLR3 by Polyinosinic:polycytidylic acid (Poly(I:C), TLR4 by lipopolysaccharide (LPS), TLR5 by S. typhimureum flagellin, and TLR6 by Pam2CGDPKHPKSF (FSL-1). A) displays total TNFα, B) displays this normalised to cell number. number of repeats per condition is displayed above each bar, using 3 clones across 3 experiments. C-D) total secretion of IL-6 normalised to cell number after 24 hours of stimulation with C) 1 ng/mL LPS or D) 1 µg/mL Pam3CSK4. Linear regression was calculated using the GraphPad Prism Nonlinear fit Log-log line method. C) n=7 (2 clones, 4 experiments), D) n=5 (2 clones, 3 experiments). E-F) Total secretion of TNFα normalised to cell number by 2 cell lines cultured in XVIVO-based macrophage medium in response to E) 1 ng/mL LPS or F) 1 µg/mL Pam3CSK4, n=1. G) prediction of the LPS or Pam3 response where total TNFα secretion doubles as concentration doubles, and halves as number of cells doubles. H-I) Total TNFα secreted by $5x10^4$ cells/well of a 96-well plate after stimulation with a titration of LPS or Pam3CSK4. n=5 (2 clones, 3 experiments)*

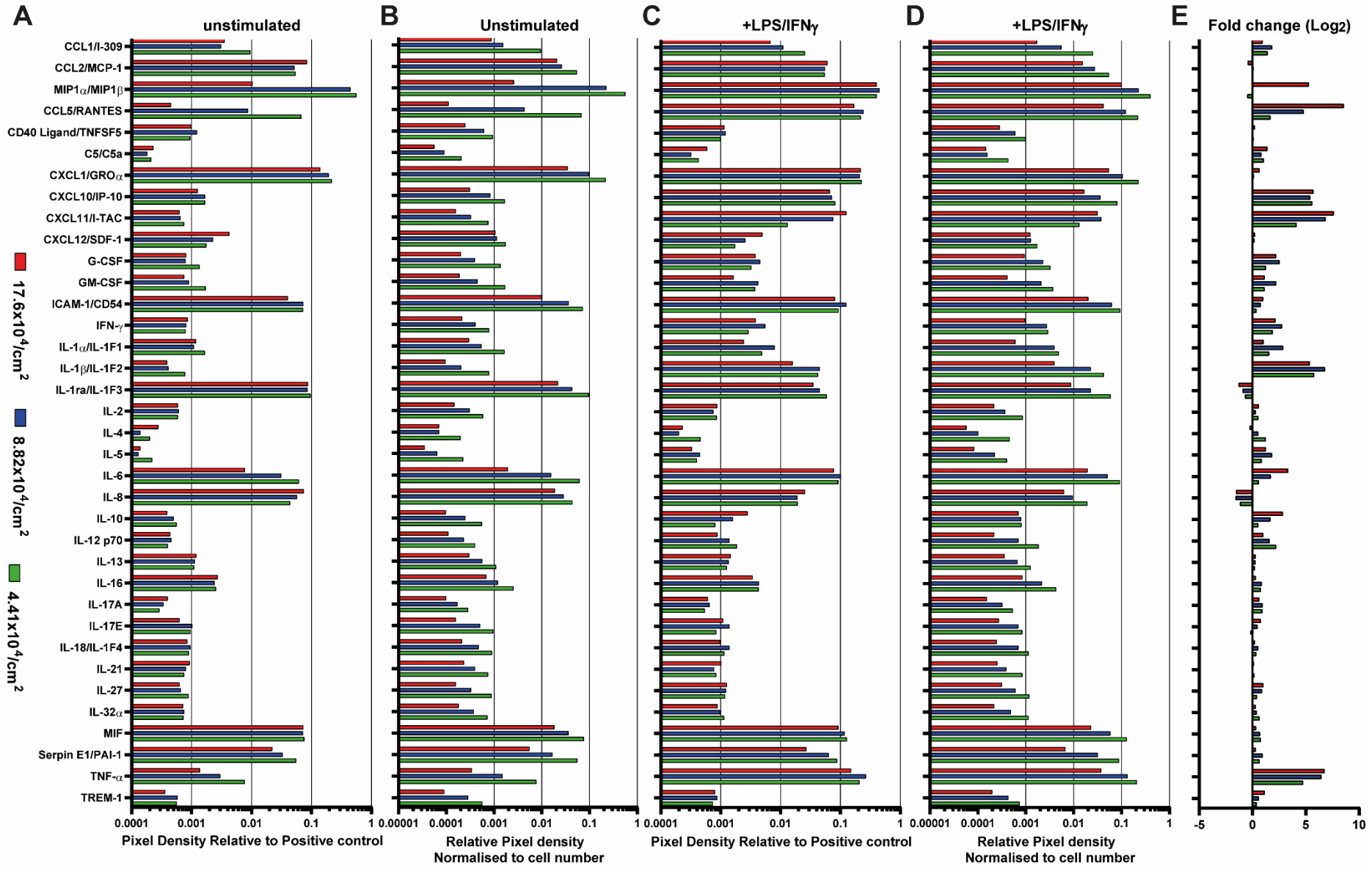

A
unstimulated
B
Unstimulated
C
+LPS/IFNγ
D
+LPS/IFNγ
E
Fold change (Log2)
CCL1/I-309
CCL2/MCP-1
MIP1α/MIP1β
CCL5/RANTES
CD40 Ligand/TNFSF5
C5/C5a
CXCL1/GROα
CXCL10/IP-10
CXCL11/I-TAC
CXCL12/SDF-1
G-CSF
GM-CSF
ICAM-1/CD54
IFN-γ
IL-1α/IL-1F1
IL-1β/IL-1F2
IL-1ra/IL-1F3
IL-2
IL-4
IL-5
IL-6
IL-8
IL-10
IL-12 p70
IL-13
IL-16
IL-17A
IL-17E
IL-18/IL-1F4
IL-21
IL-27
IL-32α
MIF
Serpin E1/PAI-1
TNF-α
TREM-1
17.6x10^4/cm^2
8.82x10^4/cm^2
4.41x10^4/cm^2
0.0001 0.001 0.01 0.1 1
Pixel Density Relative to Positive control
0.00001 0.0001 0.001 0.01 0.1 1
Relative Pixel density
Normalised to cell number
0.0001 0.001 0.01 0.1 1
Pixel Density Relative to Positive control
0.00001 0.0001 0.001 0.01 0.1 1
Relative Pixel density
Normalised to cell number
-5 0 5 10

Figure S2: DDRI regulates the broad cytokine and chemokine response of macrophages with the possible exception of CXCL11. Related to figure 3. *Proteome profile of A-B) unstimulated macrophages and C-D) macrophages stimulated with 100 ng/mL LPS and 20 ng/mL IFNγ. A&C) relative secretion of cytokines and chemokines relative to the kit reference control displayed on a logarithmic scale. B&D) relative secretion normalised to cell number, where low = 1, mid =2, and high = 4. E) Fold change of cytokines and chemokines show in* Log_2 *scale. n=1*

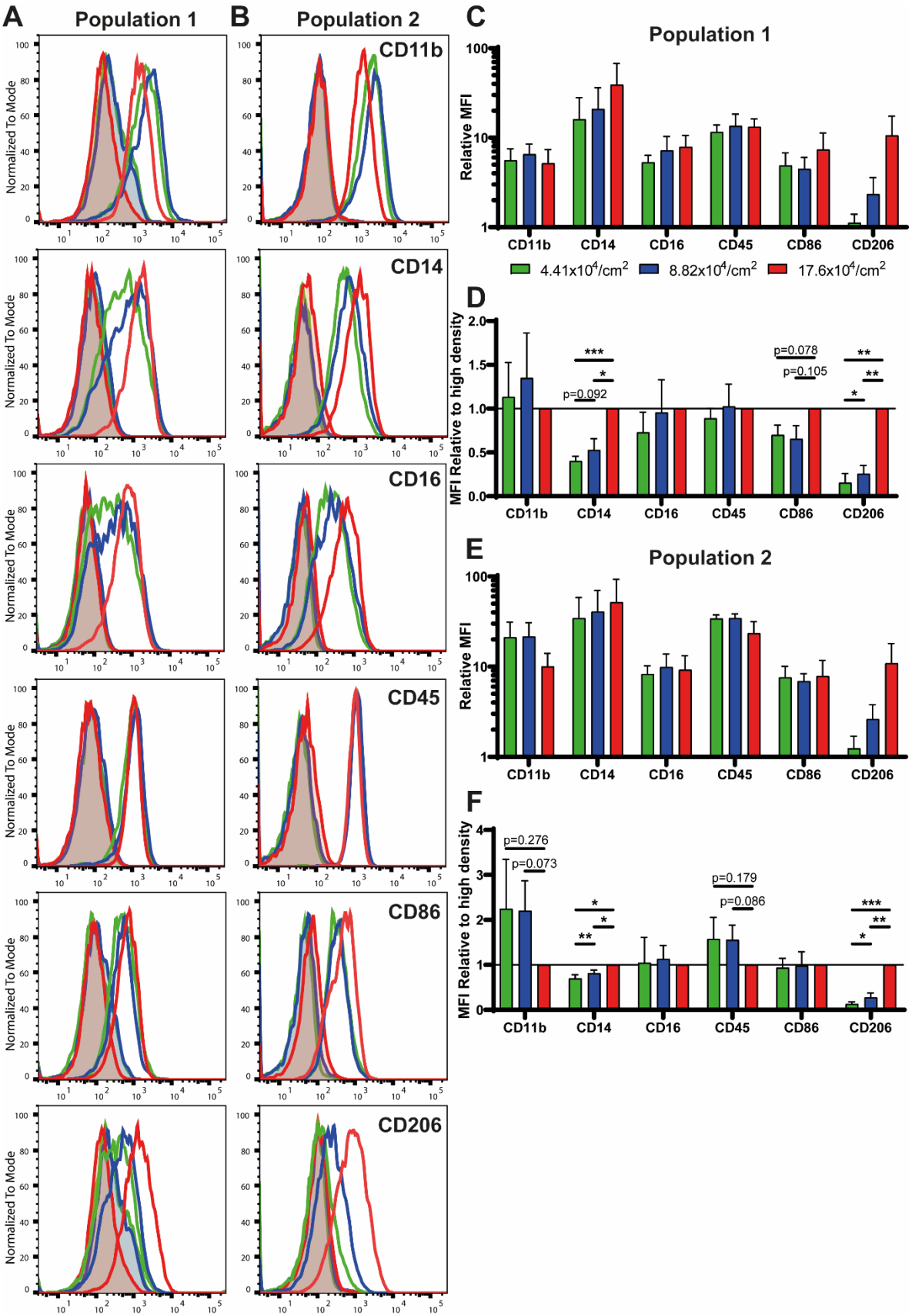

A
Population 1
B
Population 2
CD11b
CD14
CD16
CD45
CD86
CD206
Normalized To Mode
C
Population 1
Relative MFI
CD11b
CD14
CD16
CD45
CD86
CD206
4.41x10^4/cm^2
8.82x10^4/cm^2
17.6x10^4/cm^2
D
MFI Relative to high density
p=0.092
p=0.078
p=0.105
E
Population 2
Relative MFI
F
MFI Relative to high density
p=0.276
p=0.073
p=0.179
p=0.086

Figure S3: Phenotype of two distinct populations of unstimulated macrophages at different densities. Related to Figure 4. *A-B) Histograms of low (green), mid (blue), and high (red) density plated macrophages measuring surface marker staining where x = intensity and y = frequency normalised to mode. From top to bottom, histograms show expression of; CD11b, CD14, CD16, CD45, CD86, and CD206. A) unstimulated cells, B) cells after 16-hour stimulation with 100 ng/mL LPS and 20 ng/mL IFNγ. Graphs are representative of 4 repeats across 2 different cell lines. C&E) Geometric mean fluorescence intensity (MFI) of cells relative to the isotype control for each surface marker. C) displays population 1 identified in Fig. 4A, F) shows population 2. D&F) MFI relative to the MFI of high density cells of D) population 1, and G) population 2 cells. D&F) significance was calculated by 2-way ANOVA, Tukey's multiple comparisons test. n=4 (2 different cell lines across 4 experiments). Significance is defined as * <0.05, ** <0.01, ***<0.001, ****<0.0001.*

Chapter 5:

Cyclophilin A protects HIV-1 from TRIM5α mediated restriction and regulates viral reverse transcription

5.1 Introduction

In previous chapters, I have established an updated methodology for culturing iPSC-derived macrophages in fully defined, open-source medium, and then identified one of the major variability factors that can occur during culturing of these macrophages. Now it is time to apply this cellular system to a specific question for which this model is uniquely suited to answer. As discussed in Chapter 1, macrophages are host cells for HIV-1 infection and could play essential roles in viral reservoir formation and chronic disease. Therefore, a better understanding of tissue macrophage infection by HIV-1 is needed if we are to create more targeted therapies.

Consistent with their role as a first line of defence during the immune response, macrophages are not as easily infected by HIV-1 as T-cells. This is due to a relatively low CD4 expression and high expression of restriction factors, including, but not limited to, the dNTPase SAMHD1, the amine transferase APOBEC3G, the GTPase Mx2, and the E3 ubiquitin ligase TRIM5α (280, 513–517). In addition, macrophages have multiple antiviral pathogen recognition receptors (PRRs) such as ZAP, TLR7/8, RIG-I, cGAS, and IFI16 (332, 333, 518–521). Viral evolution within this hostile intracellular environment has allowed HIV-1 to developed several strategies for evasion, invading specific subsets of macrophages (522), depleting restriction factors with viral accessory proteins, and recruitment of host factors by the viral capsid (CA). Reviews of these evasion methods can be found here (352, 523). A diagram of the numerous host factors utilised by HIV-1 is shown in Figure 1A, but for this chapter I will focus on the role of Cyclophilin A (CyPA), and the restriction factor TRIM5α (tripartite motif containing protein 5 alpha). CyPA is a small, 20kDa, peptidyl-proly isomerase highly abundant throughout the cell and made of a single cyclophilin domain. TRIM5α on the other hand is a large multi-domain protein comprising of a B30.2 domain (also known as the PRYSPRY, or SPRY domain) for CA recognition, coiled-coil and B-Box domains for multimerization, and a RING domain, which has E3-ubiquitin ligase activity (Figure 1B-C).

When bound to the HIV-1 CA, TRIM5α forms a trimeric lattice that coats the entire viral particle (Figure 1D).

Interactions between viral CA and CyPA or TRIM5α have been known about since 1993 and 2004, respectively (524–526). Yet still their precise interactions and functionality remain somewhat of an enigma. Despite restricting HIV-1 in other primate species including Rhesus macaques and African green monkeys, TRIM5α is apparently unable to recognise and restrict HIV-1 in humans (279, 328). However, as little as replacing a single amino acid in human TRIM5α (hTRIM5α) with that from Rhesus macaques (rhTRIM5α) is sufficient to rescue the ability of hTRIM5α to recognise HIV-1 CA (526, 527). Meanwhile, it is clear that HIV-1 recruits CyPA in human cells to protect itself from a block to reverse transcription that induces an antiviral response (290, 315, 528–531). However, in African green monkeys, CyPA is required to restrict HIV-1 by TRIM5α (316, 532). This interplay between CyPA and TRIM5α applies not only to HIV-1, but also to simian immunodeficiency virus (SIV), where inhibiting CyPA-CA interactions in human cells makes them susceptible to infection, and *vice-versa* in macaque cells (533). To add to the confusion, in human non-dividing cells, the effect of CyPA-virus interactions appear to reverse when mutations are made in the viral CA, no longer protecting HIV-1, but instead exposing it to the host response (319, 534, 535). Both CyPA and TRIM5α interact with the lentivirus at an exposed proline loop at position 90 of the CA. The requirement for a shared site has resulted in an evolutionary arms race between lentiviruses and the host resulting in the emergence of a TRIM5α-CyPA fusion protein named TRIMCyp in some monkey species (E.g. Owl monkeys) and even shrews (536–539). By replacing the B30.2 domain with CyPA, TRIMCyp overcomes any inhibitory or activator role of CyPA for TRIM5α-mediated restriction by relying on CyPA's ability to bind to the CA (Figure 1B-C). In all, the viral dependence on CyPA and resistance to TRIM5α is very much species dependent (Table 1), but can easily be altered by small mutations in either the CA or TRIM5α. Why this is the case though is still a matter of some debate.

While investigating the potential application of CRISPR-Cas9 editing of iPSC to produce stable TRIMCyp expressing macrophages, Dr Kenny Moore observed differences in HIV-1

infectivity between WT cells treated with the cyclophilin inhibitor Cyclosporine A (CsA) and cells in which TRIM5α has been replaced with TRIMCyp treated with CsA (data not shown). These observations have led us to formulate the hypothesis that, contrary to previous assumptions, hTRIM5α is capable of binding to HIV-1 CA. However, through its prolyl isomerase activity, CyPA alters the conformation of HIV-1 CA to inhibit TRIM5α binding, restriction, and ultimately the antiviral response that follows.

Owing to the complex nature of this question, and the clear variability observed previously when manipulating either protein, my iPSC-derived macrophages offer themselves as an ideal model to genetically ablate these molecules and investigate the resulting impact on HIV-1 infection in primary, disease relevant, cells. Moreover, thanks to the unimpaired homeostatic and immune signalling capabilities of these cells, I am here able to interrogate the existing hypotheses for how TRIM5α restricts HIV-1. I here show how TRIM5α works alongside two other factors, SAMHD1 and TREX1, to restrict HIV-1, while also providing clear evidence of multiple functions of CyPA during HIV-1 infection.

Species	TRIM5 isoform	Blocks HIV-1?	Blocks SIV?	CyPA effect	Reference
Human	TRIM5α	No*	Yes	Protects HIV-1 but restrictive in non-dividing cells if CA is mutated. Restricts new HIV-1 production in Dendritic cells. Required to restrict SIV	(290, 319, 533, 540)
Rhesus monkey (OWM)	TRIM5α	Yes	No	Required for HIV-1 restriction. Protects SIV	(533, 541)
African Green Monkey (OWM)	TRIM5α	Yes	No	Required for HIV-1 restriction.	(541)
Owl Monkey (NWM)	TRIMCyp	Yes	Yes	None	(539)

Table 1: Restriction of lentivirus by TRIM5 is species dependent. *OWM = old world monkey, NWM = new world monkey. * here I demonstrate it can when CyPA is removed*

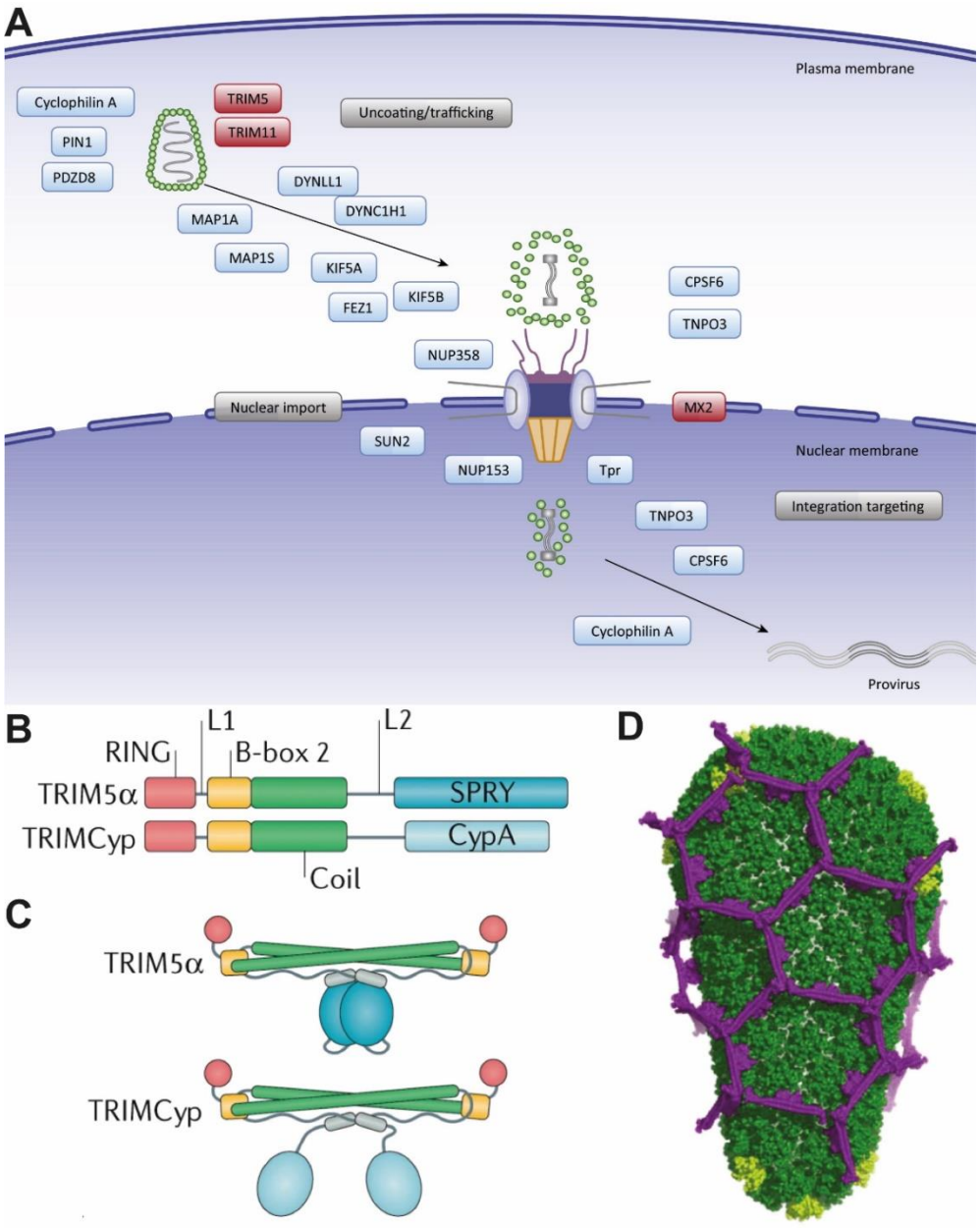


Figure 1: Schematics of HIV-1 co-factor usage and TRIM5α structure. *A) Schematic modified from Yamashita and Engelman (2017)* (352) *displaying host proteins known to interact with incoming HIV-1 CA to aid trafficking along microtubules, uncoating, nuclear import and integration. Those that aid viral infection are shown in blue, while inhibitors are shown in red. Position does not strictly correspond to location and timing of the interaction. B) Domain structure of TRIM5α and the fusion protein TRIMCyp. L = linker. C) Multimeric organization of TRIM5 when assembled for CA recognition. D) Lattice structure of TRIM5α bound to the HIV-1 core. B-C have been adapted from Ganser-Pornillos & Pornillos 2019* (279)

5.2 Results

5.2.1 Cyclophilin A protects HIV-1 from TRIM5α

My working hypothesis was that under normal, WT infection conditions, HIV-1 CA is bound by CyPA following its entry into the cytoplasm, protecting HIV-1 from being bound by TRIM5α, which would otherwise result in inhibition of viral infectivity. If this CyPA-CA interaction was disrupted pharmacologically with CsA, or by mutation of the binding interface by mutation of the Proline-90 residue to an Alanine (P90A), then TRIM5α would be capable of restricting viral infection (Figure 2A). To test this, I made homozygous KO for TRIM5α and CyPA (gene name *PPIA*) using CRISPR-Cas9 in iPSC, as described in Chapter 2 and Chapter 6 respectively. I identified two KO clones for TRIM5α with a single base pair (bp) deletion and heterozygous 4bp deletions, respectively (Figure S1A), that displayed no karyotypic abnormalities (Figure S1B). After differentiation of these iPSC into macrophages, I demonstrated robust non-sense mediated decay (NMD), and therefore the KO status, of TRIM5α specific RNA transcripts by qPCR, with a greater than 10-fold reduction in transcripts (Figure S2A-B). Furthermore, these clones displayed no defects in expression of the macrophage surface markers CD14, CD16, and CD45, nor the HIV-1 receptor and co-receptors CD4, CCR5, and CXCR4 (Figure S2B). A third potential TRIM5α KO clone was originally identified, but ultimately rejected for the purpose of this study as it displayed reduced NMD and altered HIV-1 receptor expression. Characterisation of the CyPA KO clones can be found in Chapter 6.

Having generated KO clones for TRIM5α and CyPA, I infected macrophages plated at ~$1.5x10^5$ cells/cm^2 with a VSV-G enveloped, singe round infection competent, HIV-1 pseudotype virus made using a single plasmid NL4.3 construct or a 2-plasmid R8.91 construct. The single plasmid system contains a complete viral genome, except for the accessory protein Vpr or a functional viral envelope. Using a T2A peptide, GFP expression is driven alongside HIV-1 Nef expression. The 2-plasmid system lacks any viral accessory proteins and GFP is encoded on a separate plasmid under a PGK promoter. In the absence of CsA, WT and

TRIM5α KO cells were readily infected by the virus, while CyPA KO were resistant to infection consistent with previous reports (290, 531). Similarly, treatment of cells with 1 μM CsA at the time of infection reduced infectivity in WT cells to the same level of CyPA KO cells, demonstrating that CyPA is entirely responsible for the CsA effect in these cells. However, KO of TRIM5α rescued viral infectivity in CsA treated cells (Figure 2B, 2C). Likewise, using the P90A CA mutant, I also observed complete rescue of viral infectivity in TRIM5α KO cells, with CyPA KO and WT cells displaying equal capacity for infection (Figure 2D). Infection with the G94D CsA escape mutant, which should be resistant to TRIM5α restriction based on these results, showed no clear difference in infection of WT, TRIM5α KO, or CyPA KO cells, with or without CsA present (Figure 2E). In conclusion, CyPA protects VSV-G pseudotyped HIV-1 from restriction by TRIM5α.

5.2.2 TRIM5α-mediated restriction is not envelope specific

HIV-1 entry into cells is known to require interaction with the cell surface receptor CD4 and interactions with co-receptors CCR5 or CXCR4. Interaction between the virus envelope protein and these receptors results in virus-cell membrane fusion and release of the viral core into the cytoplasm (542). VSV-G enveloped viruses on the other hand interact with LDL receptor, triggering endocytosis and eventual viral membrane fusion upon acidification of the endosomal compartment (542). Therefore, to confirm that my observed rescue to viral infectivity by VSV-G-enveloped HIV-1 pseudotype virus in TRIM5α KO cells is not dependent on this alternative entry mechanism, I replaced the VSV-G envelope with the macrophage tropic BaL HIV-1 envelope. Infection with this virus shows TRIM5α KO still clearly rescues viral infectivity in the presence of CsA (Figure 3A).

So far, all infectivity assays have been performed using single round infection competent viruses only. To ensure that CyPA protects HIV-1 from TRIM5α also in fully replication competent, spreading viral infection, WT, TRIM5α KO, or CyPA KO macrophages were

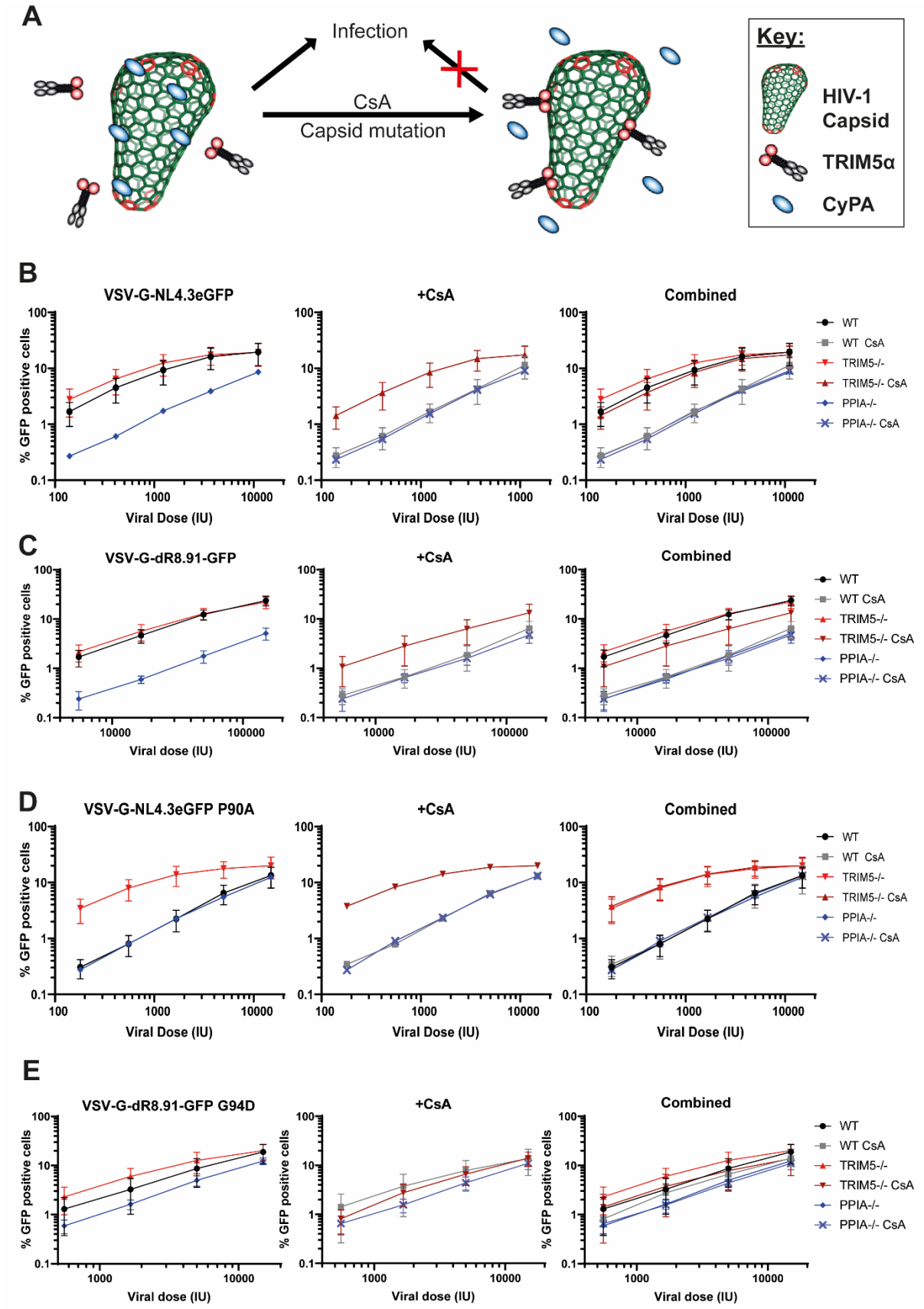

A
Infection
CsA
Capsid mutation
Key:
HIV-1 Capsid
TRIM5α
CyPA
B
VSV-G-NL4.3eGFP
+CsA
Combined
% GFP positive cells
Viral Dose (IU)
WT
WT CsA
TRIM5-/-
TRIM5-/- CsA
PPIA-/-
PPIA-/- CsA
C
VSV-G-dR8.91-GFP
+CsA
Combined
% GFP positive cells
Viral dose (IU)
WT
WT CsA
TRIM5-/-
TRIM5-/- CsA
PPIA-/-
PPIA-/- CsA
D
VSV-G-NL4.3eGFP P90A
+CsA
Combined
% GFP positive cells
Viral Dose (IU)
WT
WT CsA
TRIM5-/-
TRIM5-/- CsA
PPIA-/-
PPIA-/- CsA
E
VSV-G-dR8.91-GFP G94D
+CsA
Combined
% GFP positive cells
Viral dose (IU)
WT
WT CsA
TRIM5-/-
TRIM5-/- CsA
PPIA-/-
PPIA-/- CsA

Figure 2: Cyclophilin A protects HIV-1 from TRIM5α. *A) Schematic of my hypothesis. TRIM5α, here shown in a dimer form (red), is unable to interact with viral CA (green) due to CyPA interactions (blue), resulting in uninhibited infection. Inhibition of CyPA interactions by addition of Cyclosporine (CsA) or mutation of the viral CA prevents CyPA interactions, exposes CA to TRIM5α which blocks viral infection. B) Titration of WT NL4.3 based, C) WT dR8.91 based, D) P90A CA mutant NL4.3 based, or E) G94D CA mutant dR8.91 based VSV-G enveloped GFP encoding HIV-1 pseudovirus in macrophages. B-E) 5x10^4 macrophages were infected with the stated number of Infectious units (IU, x-axis) of virus and the percentage GFP expressing cells after 72 hours was determined by flow cytometry (y-axis). Cells were either untreated (left) or treated with 1μM CsA (centre) at time the time of infection and remained throughout the experiment. WT macrophages are shown in black/grey, TRIM5α KO in red/burgundy, and CyPA KO (PPIA-/-) in blue/grey-blue. n=8, 2 clones per cell line across 4 experiments.*

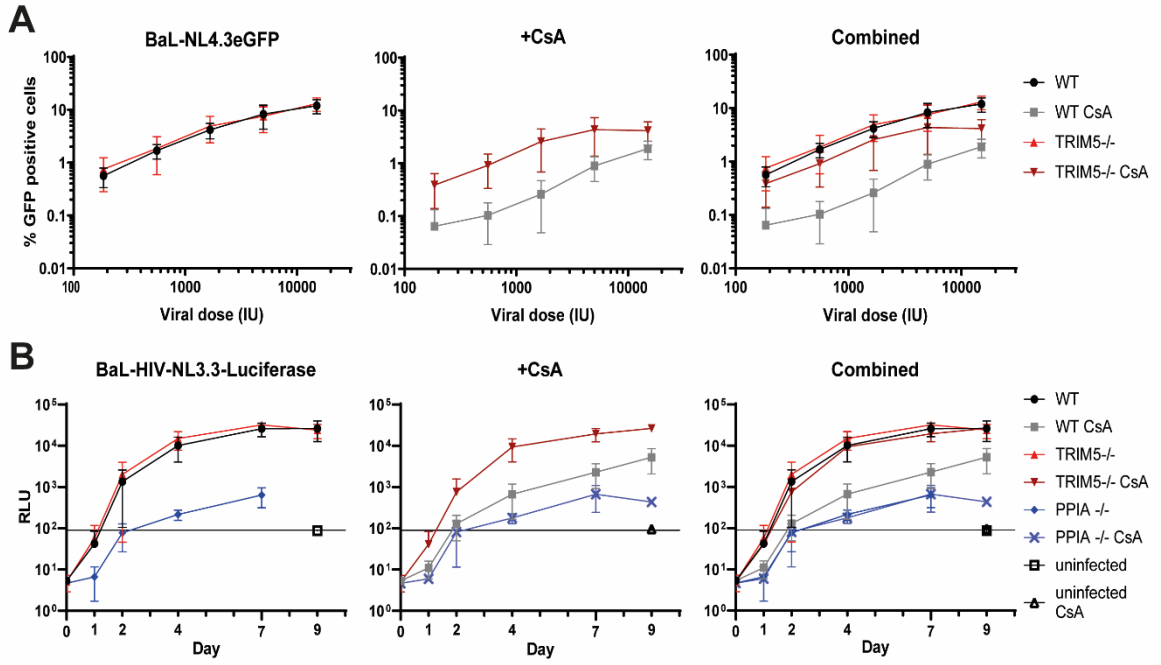


Figure 3: TRIM5α-mediated restriction is not envelope specific. *A) Titration of WT NL4.3 based BaL enveloped GFP encoding HIV-1 pseudovirus on macrophages. Macrophages were infected as described in Figure 2. WT n=5, TRIM5α KO n=10 (2 clones over 5 experiments).*

B) Time course of BaL-Luc fully replication competent HIV-1 infection in WT, TRIM5α KO, or CyPA KO cells over 9 days with samples taken at day 1, 2, 4, 7 and 9 (x-axis). 5x10^4 macrophages were infected at an MOI = 0.02 and production of new virus was determined by determination of luciferase activity from cell lysates as relative luminescence units (RLU, y-axis). Background luciferase activity of uninfected macrophages after 9 days of culture is shown (hollow symbols and line). Cells were either untreated (left) or treated with 1μM CsA (centre) at time the time of infection and remained throughout the experiment. WT and TRIM5α KO n=6 (2 clones each, 3 experiments). CyPA KO n=3. A and B) Again WT macrophages are shown in black/grey, TRIM5α KO in red/burgundy, and CyPA KO (PPIA-/-) in blue/grey-blue.

---

infected with the BaL enveloped luciferase reporter virus at an MOI of 0.02 and then incubated for 9 days. This was carried out by Dr Rebecca (Russell) Moore within a BSL3 facility. By measuring changes in production of luciferase over this period, I observed TRIM5α KO completely rescued viral infectivity when 1 μM CsA was present (Figure 3B). Intriguingly, CsA treatment did not lower the luciferase output to the same level observed in CyPA KO cells. However, this could simply be due to instability of the compound over this period of time. Therefore, the data indicates that both VSV-G and BaL enveloped HIV-1 are protected from TRIM5α restriction by CyPA.

5.2.3 TRIM5α blocks reverse transcription

Previous reports have found that TRIM5α mediated restriction occurs prior to reverse transcription (340, 543, 544). In macrophages, reverse transcription and nuclear entry of the viral genome occurs over a longer time frame than reported in T-cells (545, 546), with late reverse transcription requiring ~24 hours as compared to ~6 hours seen in T-cells (Figure S3A). I therefore measured late reverse transcripts (RT) by qPCR at 24 hours in my WT or KO cells (Figure 4A, 4B) after infection with virus stock pre-treated with DNAase to remove

any contaminating viral genomic DNA or plasmid carried over from the viral production in HEK293T cells. Again, consistent with prior reports, CyPA KO, inhibition, or disruption to CA interaction, potently inhibited reverse transcription (315). This was rescued in TRIM5α KO cells. Viral infectivity with this DNase treated virus was consistent with infectivity shown in Figure 1 (Figure 4C, 4D). In addition, I observed that TRIM5α KO displayed a small, but significant (1.8-fold, p=0.0015), increase in late RT when infected with WT virus, but not the P90A mutant, in the absence of CsA. Although possibly explained by the small, but not significant, increase in the percentage of infected cells under these conditions (Figure 4C), this may indicate a low capacity for TRIM5α mediated restriction of HIV-1 even in the presence of CyPA. Overall, I demonstrated here that CyPA prevents HIV-1 restriction at or before the reverse transcription stage of its life cycle by TRIM5α in macrophages.

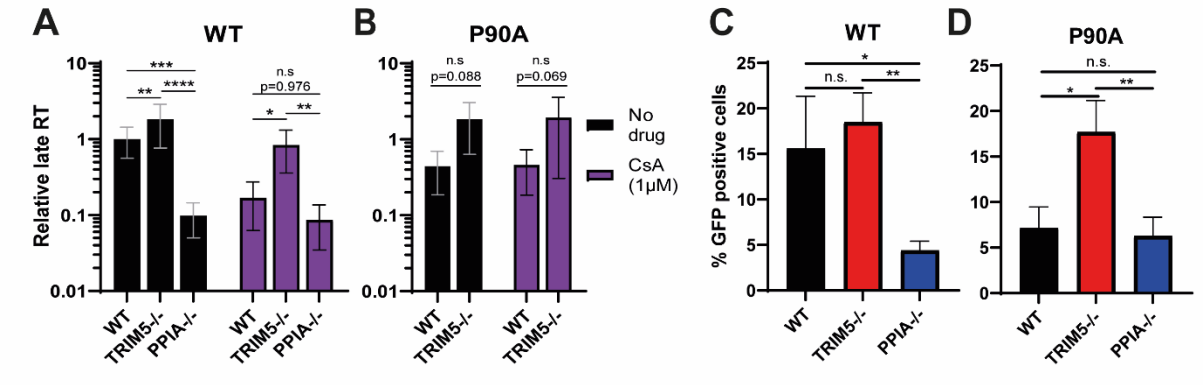


Figure 4: TRIM5α blocks reverse transcription. *A-B) Relative copy number of late reverse transcripts (RT) in WT, TRIM5α KO, or CyPA (PPIA) KO cells 24 hours post infection with A) WT or B) P90A mutant GFP virus as calculated by normalising all values to the average fold difference in Ct value ($2^{-\delta Ct}$) between viral GFP genome and cellular β-actin (ACTB) in WT cells. C-D) Percentage of GFP expressing cells (infected) 72 hours post-infection with C) WT, or D) P90A mutant GFP virus. A-B) 5x10^5 macrophages were infected with 9000IU of virus. C-D) 5x10^4 macrophages infected with 900IU. A-D) Significance was calculated by 2-way ANOVA Sidak's multiple comparison test. WT n=12 (3 clones, 4 experiments), TRIM5α KO and PPIA KO n=8 (2 clones each, 4 experiments). Significance is defined as * <0.05, ** <0.01, ***<0.001, ****<0.0001.*

5.2.4 Proteasome inhibition rescues TRIM5α-mediated inhibition of reverse transcription but not infectivity

Several mechanisms by which TRIM5α restricts HIV-1 have been proposed but no clear answer has been found As discussed in the Chapter 1.10, potential mechanisms include proteasome dependent degradation or innate immune signalling triggered directly by TRIM5α via TAK1, or indirectly by cGAS and STING signalling. In addition, I would propose that as well as revealing the virus to these sensors, it also likely exposes the virus to other cellular factors such as the inhibitor of reverse transcription, SAMHD1, or the nuclease TREX1. Therefore, using my iPSC derived macrophage model, I sought to elucidate further which of these mechanisms (Figure 5A) is responsible for my observations so far.

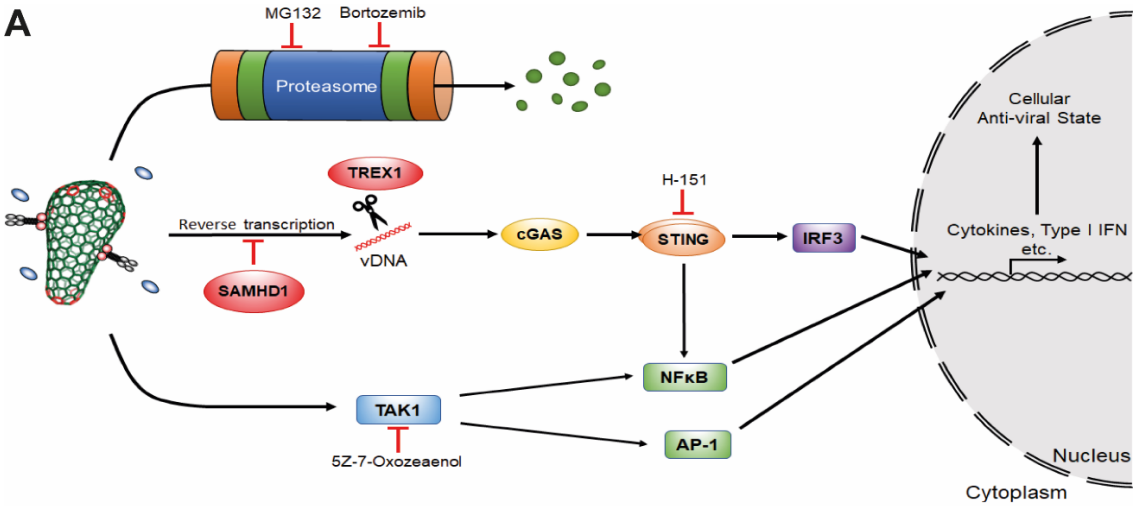
To investigate the role of the proteasome, I first measured infection of macrophages infected with WT or P90A VSV-G-pseudotyped virus in the presence of 2 proteasome inhibitors, MG132 (MG), or Bortozemib (Bort) for the first 24 hours of the 72-hour assay. To confirm functional activity of MG132 at 1 μM, and Bortozemib at 1 μM and 100 nM concentrations, I measured the increased accumulation of phosphorylated IκB, and accumulation of non-specific protein 1 hour after the stimulation of macrophages with 1 ng/mL LPS (Figure S3B). At these concentrations, neither drug rescued viral infectivity in CyPA KO cells infected with WT virus (Figure 5B, 5C), nor WT or CyPA KO cells infected with the P90A mutant (Figure 5D, 5E). TRIM5α KO had no impact on the relative changes in viral infectivity across drug concentrations. On the contrary, high concentrations of these drugs clearly reduced the percentage of GFP^+ cells. However, this may be due to additive toxicity of HIV-1 infection with high drug dosages, which I observed under the microscope (data not shown). In accordance with this observation, MG132 concentrations above 2.5 μM without virus present clearly reduced cell viability (Figure S3C).

Despite no increase in HIV-1 infection in cells treated with MG132 or Bortozemib, I did observe a clear trend towards an increase in late RT products in WT and CyPA KO cells

infected with WT or P90A CA variant HIV-1 VSV-G-pseudovirus but not in TRIM5α KO cells (Figure 5F, 5G). This increase was significant in CyPA KO cells treated with 1 μM MG132 and infected with P90A virus. Therefore, these trends show that while inhibiting the proteasome fails to rescue viral infectivity, it none-the-less plays some role in TRIM5α interactions with the virus.

5.2.5 TRIM5α restriction is independent of TAK1 or STING mediated signalling

Having demonstrated that inhibition of the proteasome is not sufficient to rescue HIV-1 from TRIM5α-mediated restriction, I next sought to investigate the relative importance of innate immune signalling after detection of the virus either directly by TRIM5α (343, 344), or secondarily by the DNA sensor cGAS after reverse transcription as reported when CyPA-CA interactions are inhibited (290). I first inhibited TRIM5α initiated signalling by inhibition of TAK1 using 5Z-7-Oxozeaenol (5Z-7). Like my observations with the proteasomal inhibitors, increasing the dose of 5Z-7 when infecting cells with WT or P90A virus not only did not rescue infection in a TRIM5α dependent manner, but actually reduced viral infection in all macrophages (Figure 6A, 6B). However, unlike the proteasomal inhibitor MG132, higher doses of 5Z-7 were non-toxic to macrophages, implying an alternative mechanism for inhibition of HIV-1 by this inhibitor (Figure S3C). To investigate if this inhibition also occurs at reverse transcription like TRIM5α, I measured late RT products after 24 hours of infection with WT or P90A virus in the presence of 5Z-7 (Figure 6C, 6D). Unlike the proteasomal inhibitors, 5Z-7 did not affect reverse transcription, and therefore must inhibit HIV-1 infection at a later stage of the viral life cycle.


A
MG132
Bortozemib
Proteasome
TREX1
Reverse transcription
SAMHD1
vDNA
cGAS
H-151
STING
IRF3
Cellular
Anti-viral State
Cytokines, Type I IFN
etc.
NFκB
TAK1
5Z-7-Oxozeaenol
AP-1
Nucleus
Cytoplasm

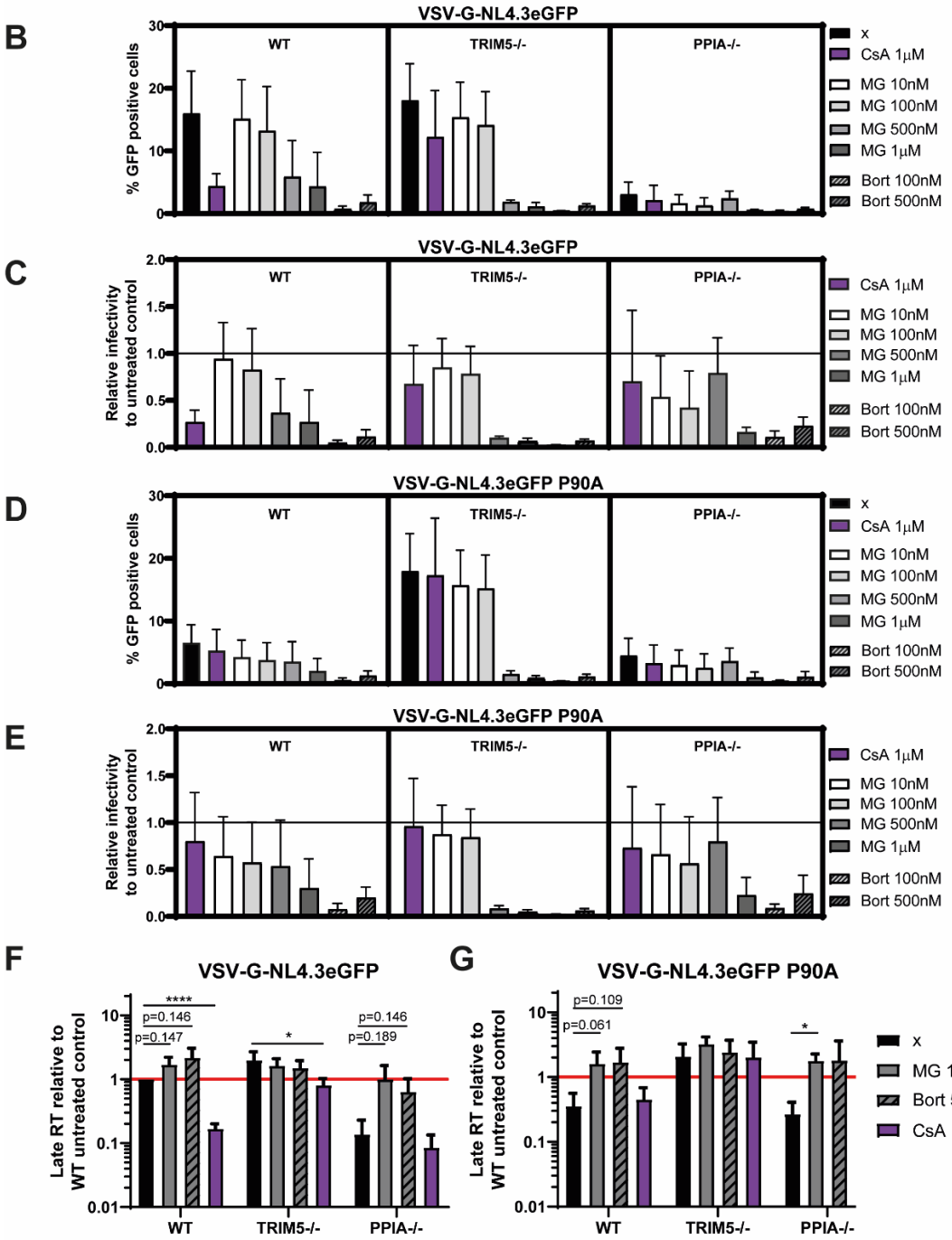

B
VSV-G-NL4.3eGFP
WT
TRIM5-/-
PPIA-/-
% GFP positive cells
x
CsA 1μM
MG 10nM
MG 100nM
MG 500nM
MG 1μM
Bort 100nM
Bort 500nM
C
VSV-G-NL4.3eGFP
Relative infectivity
to untreated control
D
VSV-G-NL4.3eGFP P90A
E
VSV-G-NL4.3eGFP P90A
F
VSV-G-NL4.3eGFP
Late RT relative to
WT untreated control
p=0.146
p=0.147
p=0.146
p=0.189
G
VSV-G-NL4.3eGFP P90A
p=0.109
p=0.061

Figure 5: Proteasome inhibition rescues TRIM5α-mediated inhibition of reverse transcription but not infectivity. *A) Schematic of the 3 major hypotheses of how TRIM5α restricts HIV-1. For more information, see Chapter 1.10. B-E) Titration of proteasome inhibitors MG132 (MG) or Bortozemib (Bort) on WT, TRIM5α KO, or CyPA (PPIA) KO macrophages infected with 900IU of B-C) WT GFP virus, or D-E) P90A mutant GFP virus. B and D) Percentage of GFP expressing cells (infected) or C and E) relative infectivity calculated by normalising the percentage GFP positive cells to the untreated control, 72 hours post infection of $5x10^4$ macrophages with 900IU of virus. Cells were treated with MG or Bort for the first 24 hours of infection before replacing with fresh macrophage media. For all 3 genetic lines n=5 (2 clones over 3 experiments). F-G) Relative copy number of late reverse transcripts (RT) in WT, TRIM5α KO, or CyPA (PPIA) KO cells treated with CsA, MG, or Bort, 24 hours post infection with F) WT or G) P90A mutant GFP virus as calculated by normalising all values to the average fold difference in Ct value ($2^{-\delta Ct}$) between viral GFP genome and cellular β-actin (ACTB) in untreated WT cells. $5x10^5$ macrophages were infected with 9000IU of virus. Untreated n=8, CsA, MG132, or Bortozemib treated n=4. Significance was calculated by 2-way ANOVA Sidak's multiple comparison test. Significance is defined as * <0.05, ** <0.01, ***<0.001, ****<0.0001.*

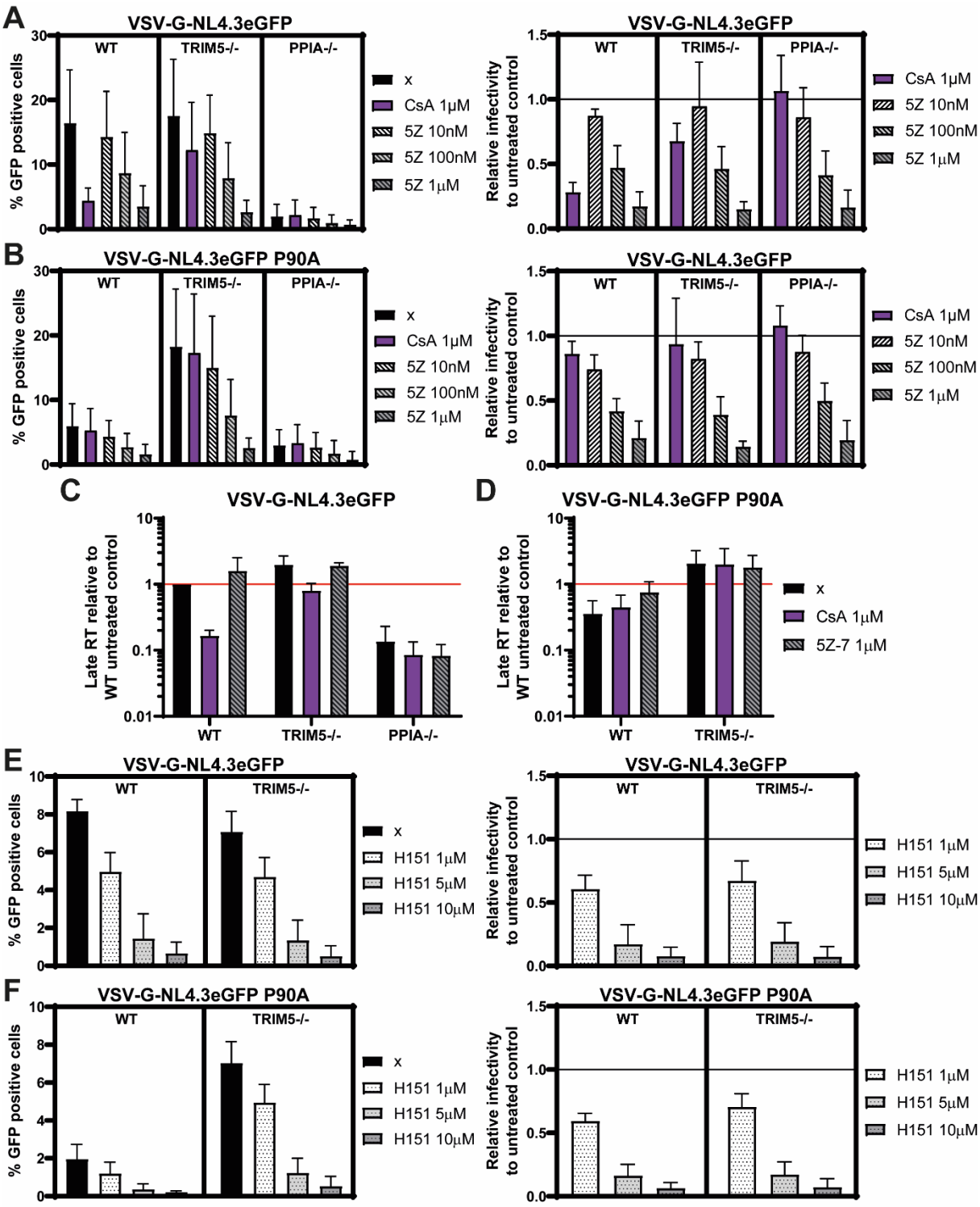

A
VSV-G-NL4.3eGFP
% GFP positive cells
WT
TRIM5-/-
PPIA-/-
x
CsA 1μM
5Z 10nM
5Z 100nM
5Z 1μM
VSV-G-NL4.3eGFP
Relative infectivity to untreated control
B
VSV-G-NL4.3eGFP P90A
C
VSV-G-NL4.3eGFP
Late RT relative to WT untreated control
D
VSV-G-NL4.3eGFP P90A
5Z-7 1μM
E
VSV-G-NL4.3eGFP
H151 1μM
H151 5μM
H151 10μM
F
VSV-G-NL4.3eGFP P90A

Figure 6: TRIM5α restriction is independent of TAK1 or STING mediated signalling. *A-B) Titration of TAK1 inhibitor 5Z-7-Oxozaeanol (5Z), or E-F) titration of STING inhibitor H-151, on TRIM5α KO, or CyPA (PPIA) KO macrophages infected with 900IU of A and E) WT GFP virus, B and F) P90A mutant GFP virus for 72 hours. Left; Percentage of GFP expressing cells (infected). Right; relative infectivity calculated by normalising the percentage GFP positive cells to the untreated control. Cells were treated with 5Z or H-151 for the first 24 hours of infection before replacing with fresh macrophage media. C-D) Relative copy number of late reverse transcripts (RT) in WT, TRIM5α KO, or CyPA (PPIA) KO cells treated with CsA, or 5Z, 24 hours post infection with C) WT or D) P90A mutant GFP virus as calculated by normalising all values to the average fold difference in Ct value ($2^{-\delta Ct}$) between viral GFP genome and cellular β-actin (ACTB) in untreated WT cells. $5x10^5$ macrophages were infected with 9000IU of virus. A-B) WT and CyPA KO lines n=5, TRIM5α KO n=4 (2 clones each, 3 experiments). C-D) Untreated n=8, CsA or 5Z treated n=4. E-F) WT n=4, TRIM5α KO n=8 (2 clones, 4 experiments).*

Having ruled out TAK1 signalling as critical for TRIM5α-mediated restriction, I next used H-151, an inhibitor of the downstream effector of cGAS, STING, to interrogate the relative importance of this pathway for viral restriction (547). As with TAK1 inhibition, HIV-1 infectivity decreased as H-151 concentration increased under both WT and TRIM5α sensitive (P90A mutant virus) infectious conditions, and this inhibition was TRIM5α independent (Figure 6E, 6F). To ensure that this decreased infectivity occurred at functional concentrations of either compound, 5Z-7 or H-151, I measured changes in transcription of the NF-κB regulated cytokine IL-6, and the IRF3 regulated cytokines IFNB1 and IFIT1 4 hours after stimulation of macrophages with either LPS, or cGAMP. TAK1 inhibition, which is upstream of NF-κB and AP-1 but not IRF3, by doses greater than or equal to 100nM reduced IL-6 transcription but increased transcription of IFNB1 and IFIT1 (Figure S3D). Inhibition of STING on the other hand, which is upstream of NF-κB and IRF3, by 10 nM or higher concentrations of H-151 decreased transcription of all three genes (Figure S3E). Therefore, having shown functionality of these compounds, I can conclude that neither TAK1 nor STING signalling pathways are essential for the TRIM5α restriction, but conversely both may be necessary for HIV-1 infectivity.

5.2.6 TRIM5α restriction is independent of IFN and the immunoproteasome

By inhibiting TAK1 and STING I have shown that immune signalling is likely not responsible for TRIM5α mediated restriction of single round viral infections. However, pharmacological inhibition of these pathways results in multifaceted changes that enhance both pro-inflammatory cytokine and type 1 IFN responses, as shown in Figures S2D-E. TRIM5α has been recently shown to be one of several IFN inducible factors after IFN stimulation (548, 549). Jimenez-Guardeño *et al.* have reported that IFN stimulation increased turn-over of TRIM5α by a subtype of the proteasome called the immunoproteasome, and in turn this increased turn-over resulted in increased restriction of HIV-1 (338). Therefore, I next investigated the relative impact of IFN as a potential mechanism for TRIM5α-mediated viral restriction.

Firstly, I assessed the relative importance of IFN produced post viral infection by broadly inhibiting the secondary signalling of IFN using knock out iPSC-macrophages for the IFN receptor subunit IFNAR2 (a kind gift from Dr Chris Duncan, Newcastle University). Titrating both WT and P90A mutant VSV-G-pseudotyped virus on these cells displayed no differences in infectivity, in the presence or absence of CsA (Figure 7A, 7B).

I next investigated the role of the immunoproteasome. I have already observed that broad inhibition of the proteasome by MG132 or Bortozemib rescues reverse transcription but not infectivity (Figure 5B-G). However, high doses of either drug reduced infectivity, likely due to toxicity of broad proteasome inhibition. Therefore, it was still necessary to test specific inhibition of the immunoproteasome. As seen with broad inhibition though, increased doses of the immunoproteasome inhibitor ONX-0914 (ONX) also resulted in decreased infectivity of WT or P90A mutant virus, was independent of TRIM5α, and is likely to also be due to additive toxicity (Figure 7C, 7D, S3C).

Finally, Jimenez-Guardeño *et al.* (338) reported that the immunoproteasome activity was only vital post IFN pre-treatment of cells. Therefore, to confirm their findings, I also pre-treated macrophages for 24 hours with 500 units of IFN-α before infecting cells with WT or P90A mutant virus, in the presence or absence of ONX. Again, I witnessed decreased infectivity in cells treated with ONX independent of TRIM5α (Figure 7E). However, I did not observe any significant change in infectivity between WT and TRIM5α or CyPA KO cells when pre-treated with IFN, inconsistent with prior reports, as demonstrated when I normalise infectivity as fold-inhibition (IFN treated/IFN untreated) (Figure 7E, 7F). IFNα treated CyPA KO did significantly reduce inhibition compared to WT cells. However, with the total number of infected cells never greater than 1.5% of all macrophages, this could be explained by experimental inaccuracy and variability. In summary, I can comprehensively conclude that IFN signalling is not required for TRIM5α-mediated restriction of infection and is not dependent on IFN or the immunoproteasome.

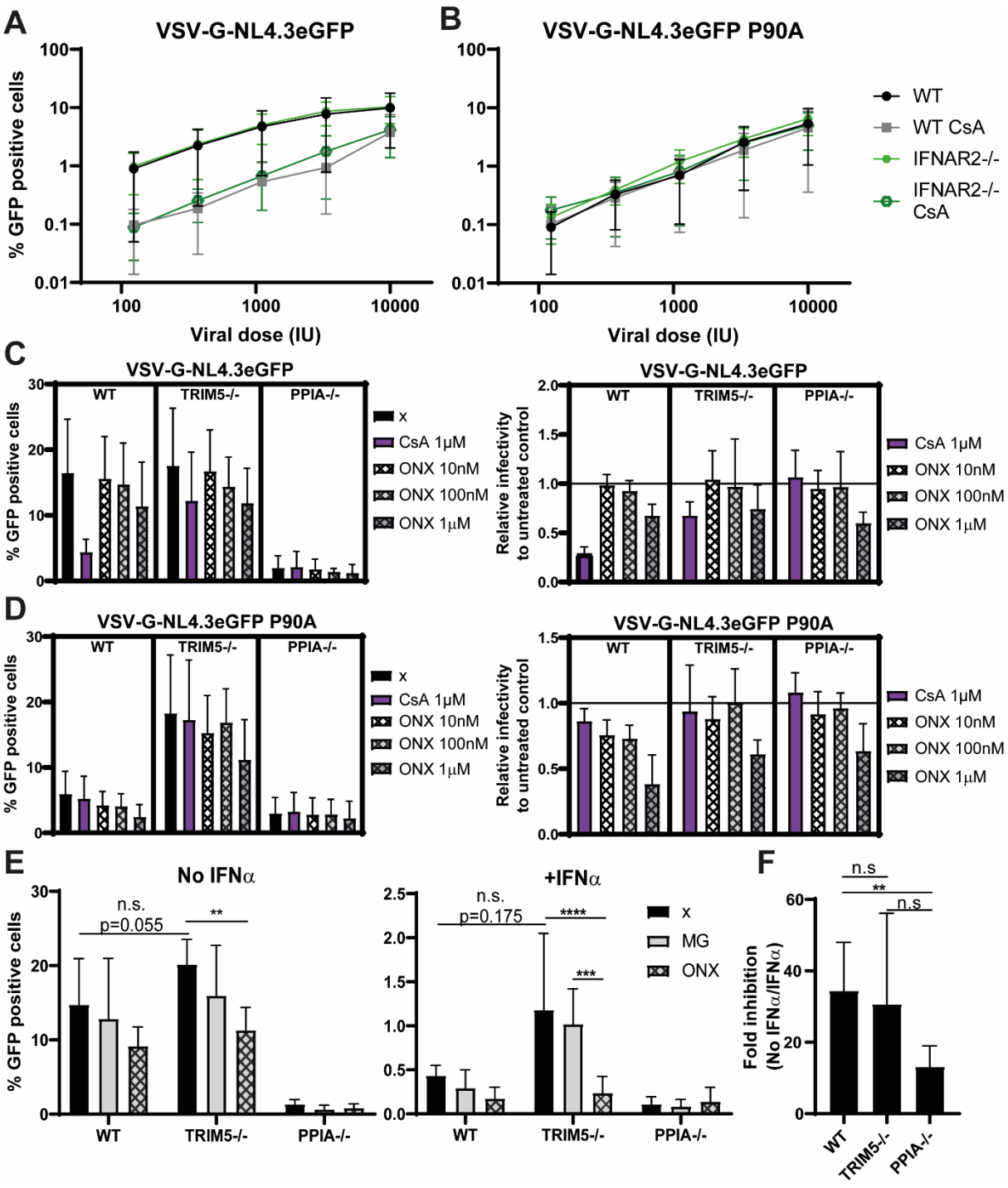


Figure 7: TRIM5α restriction is independent of IFN and the immunoproteasome. *A-B) Titration of A) WT or B) P90A mutant NL4.3 based VSV-G enveloped GFP virus on WT (black/grey) and IFNAR2 KO (green/dark-green) macrophages. Macrophages were infected as described in figure 1 with and without 1μM CsA. n=4 (1 clone, 4 experiments). C-D) Titration of immunoproteasome inhibitor ONX-0914 (ONX) on WT, TRIM5α KO, or CyPA (PPIA) KO macrophages infected with 900IU of C) WT GFP virus, or D) P90A mutant GFP virus for 72*

*hours. Left; Percentage of GFP expressing cells (infected). Right; relative infectivity calculated by normalising the percentage GFP positive cells to the untreated control. Cells were treated with ONX for the first 24 hours of infection before replacing with fresh macrophage media. WT n=5, TRIM5α KO n=4, CyPA KO n=6 (2 clones each,3 experiments). E) Percentage GFP positive (infected) macrophages, untreated (left) or pre-treated with 500 units IFNα for 24 hours before infection (right), 72 hours post infection with WT GFP virus. F) Fold inhibition of infection caused by IFNα pre-treatment on macrophages calculated by dividing IFN untreated infectivity over IFN treated infectivity in WT, TRIM5α KO, or CyPA KO cells. E-F) WT and TRIM5α KO n=6, CyPA KO n=5 (2 clones each, 3 experiments). E-F) statistical comparisons within genotypes were calculated by 2-way ANOVA Sidak's multiple comparison test. Comparisons between genotypes were calculated by mixed-effects analysis Tukey's multiple comparisons test. Significance is defined as * <0.05, ** <0.01, ***<0.001, ****<0.0001.*

5.2.7 Knock out of SAMHD1 and TREX1 partially rescues HIV-1 infection from TRIM5α-mediated restriction

I have now investigated the roles of the proteasome, immune signalling downstream of TAK1 and STING, and the impact of IFN in WT, TRIM5α KO and CyPA KO cells. In collaboration with Dr Kenny Moore, I finally assessed the relative role of specific secondary restriction factors during TRIM5α restriction. I aided in identification of TREX1 KO cells in WT and SAMHD1 KO parent lines, Dr Moore designed, edited, and established the TREX1 KO lines. The SAMHD1 KO line was originally made by Damien Warner. Dr Moore also carried out infectivity assays with these lines using macrophages cultured in XVIVO medium, rather than OXM medium.

Despite the use of different culture media, we still observed the reduction of HIV-1 infection when CsA (5μM) was present. Knock out of TREX1 alone did not significantly increase susceptibility to HIV-1 infection, nor rescue infection when CsA is present, although

a trend towards rescue was observed. SAMHD1 KO did increase basal infectivity, consistent with previous reports (550, 551) and partially rescued infectivity when CsA is present. Additional knock out of TREX1 in SAMHD1 KO cells reduced basal infection back to SAMHD1+/+ levels, as well as increasing infection in CsA treated cells above that of SAMHD1 or TREX1 KO alone. However, this increased infection was still significantly lower than the untreated control (Figure 8A, 8B). Therefore, KO of both SAMHD1 and TREX1 is not sufficient to fully rescue TRIM5α-mediated restriction of HIV-1.

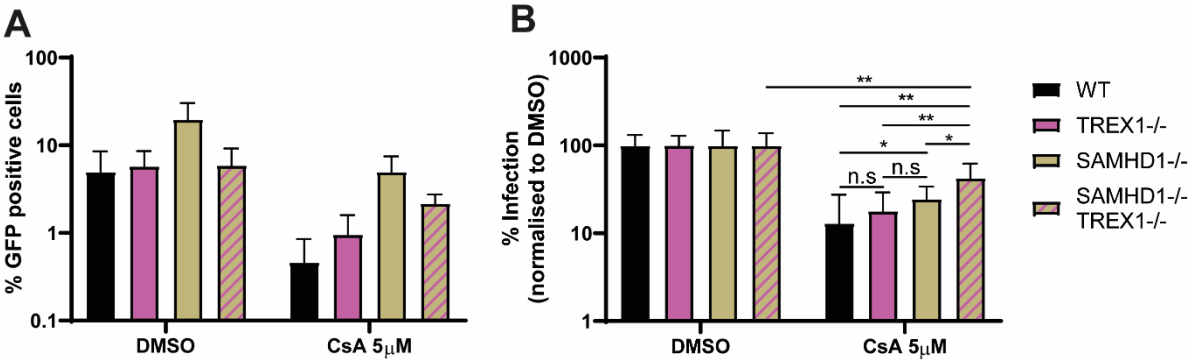


Figure 8: Combined knock out of SAMHD1 and TREX1 partially rescues HIV-1 infection from TRIM5α-mediated restriction. *A) Infection of 5x10^4 WT (black), SAMHD1 KO (pink), TREX1 KO (gold), or SAMHD1 and TREX1 double KO (pink and gold stripes) with 0.3μL of concentrated untitrated WT VSV-G enveloped GFP pseudovirus in the presence of 5μM CsA or DMSO. B) Normalised infectivity from part A) to the average DMSO control for each cell line. A-B) n=9, statistical comparisons within genotypes were calculated by 2-way ANOVA Sidak's multiple comparison test. Comparisons between genotypes were calculated by mixed-effects analysis Tukey's multiple comparisons test. Significance is defined as * <0.05, ** <0.01, ***<0.001, ****<0.0001.*

5.2.8 CyPA has a secondary role in HIV-1 infection in addition to protection from TRIM5α

Although TRIM5α KO rescues HIV-1 infection in the presence of CsA, I consistently observed that this rescue is incomplete. When titrating WT virus, both NL4.3. and R8.91, VSV-G or BaL enveloped, a small reduction in viral infection was seen in CsA treated cells (Figure 2B, 2C, 3A). One possible reason could be that the TRIM5α KO cells are actually incomplete KO cells. However, infection of these cells with P90A mutant virus displayed a complete rescue of infectivity to levels observed with WT virus in WT cells untreated with CsA (Figure S4A). In addition, the lack of difference between infection of P90A virus in the presence or absence of CsA demonstrates that this phenotype is not due to non-CyP-CA interactions of the drug, such as its known anti-inflammatory interaction with NFAT (552) (Figure 2D).

Considering I was observing a second function of CyPA in cells infected with WT but not P90A mutant virus, I sought to interrogate whether other CA mutants known to be important for HIV-1-CyPA interactions also showed differences in their infection profile in my macrophages. The G94D CsA escape mutant shown in Figure 2E displayed a potential decline in infectivity when CsA is present or if CyPA is knocked-out, but the results are unclear looking at just the titration curve. Using a second CsA escape mutant, A92E, I found that CyPA KO cells were less infectable than WT or TRIM5α KO cells despite this virus being mostly resistant to the impact of CsA as shown by its minimal effect on WT and TRIM5α KO cells (Figure 9A). Infection with the N74D mutant, which disrupts CA interactions with CPSF6, a host factor that protects against immune activation and is important for nuclear entry (290, 293, 553, 554), showed rescue of infection in TRIM5α KO cells but not WT or CyPA KO cells, similar to that observed during P90A virus infection (Figure 9B, 2D). However, unlike P90A, treatment of TRIM5α KO cells with CsA substantially reduced N74D viral infection, but not to the same level as observed in CyPA KO cells. Because the N74D mutant cannot bind CPSF6, I tested to see if CPSF6 interactions with WT or P90A mutant VSV-G-pseudotyped virus may also be protecting HIV-1 from TRIM5α using the CPSF6-CA interaction inhibitor PF74. PF74 treatment of macrophages during infection potently inhibited HIV-1 infection, but I did not observe any

significant differences between WT and TRIM5α KO cells (Figure S4B). Therefore, this N74D phenotype must be CPSF6 independent.

Having now titrated WT and P90A CA variants viruses in the NL4.3 expression plasmid, and WT, G94D, A92E and N74D CA variants from the R8.91 backbone, I calculated the area under the curve (AUC) of all plasmids across the linear portion of the titration curve (NL4.3: WT 0 - 1230IU, P90A 0 – 1660IU, R8.91: WT, G94D, A92E and N74D 0 – 150,000IU) in order to reduce the variation between CsA untreated and treated cells to a single dimension (Figure 9C, 9D). AUC analysis showed that across all virus variants except P90A, addition of 1μM CsA reduces viral infectivity in WT or TRIM5α KO. These differences are statistically significant when AUC is normalised between CsA treated and untreated samples and a one-sample t-test against the hypothetical mean of 1 is calculated. WT cells infected with G94D was not significant but showed a similar trend, having a normalised value of 0.768, p=0.06 (Figure 9E). Interestingly, CsA treatment of cells infected with G94D or A92E does not reduce viral infectivity in WT to the same level as in CyPA knock out cells, yet normalised infection in these cells is significantly higher than in TRIM5α KO cells with A92E (WT=0.896 vs TRIM5=0.723, p=0.0006) and a possible similar trend with G94D (WT=0.768 vs TRIM5=0.652, p=0.178) (figure 9E, 9F). However, N74D normalised values are not significantly different between WT and TRIM5α KO cells (WT=0.535 vs TRIM5=0.431, p=0.414). Again, I did not observe CsA treatment to reduce infection in TRIM5α KO cells to CyPA KO levels (Figure 9E, 9F). Across all viral CA variants, CyPA KO cells treated with or without CsA displayed no difference in infection, clearly demonstrating that this secondary Cyclophilin effect is CyPA dependent. Therefore, to conclude, I have shown here that as well as protecting the virus from TRIM5α, CyPA plays a secondary critical role in viral infectivity that is important for reverse transcription. This appears to be dependent on the P90 CA residue, but not N74, and only partially dependent on A92 and G94.

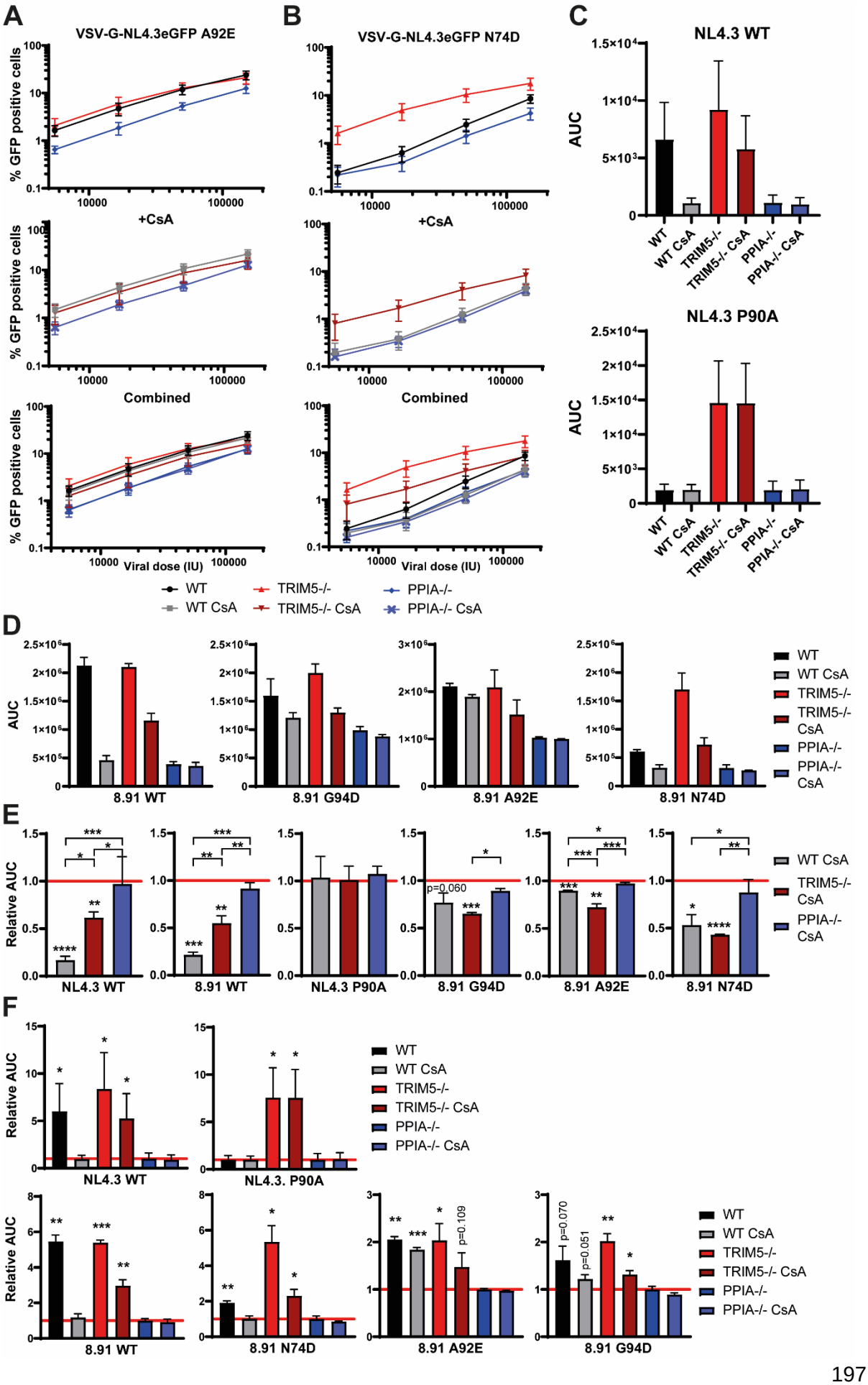

A
VSV-G-NL4.3eGFP A92E
% GFP positive cells
+CsA
Combined
Viral dose (IU)
B
VSV-G-NL4.3eGFP N74D
C
NL4.3 WT
NL4.3 P90A
AUC
WT
WT CsA
TRIM5-/-
TRIM5-/- CsA
PPIA-/-
PPIA-/- CsA
D
8.91 WT
8.91 G94D
8.91 A92E
8.91 N74D
E
Relative AUC
NL4.3 WT
8.91 WT
NL4.3 P90A
8.91 G94D
8.91 A92E
8.91 N74D
p=0.060
F
NL4.3 WT
NL4.3. P90A
8.91 WT
8.91 N74D
8.91 A92E
8.91 G94D
p=0.070
p=0.051
p=0.109

Figure 9: CyPA has a secondary role in HIV-1 infection in addition to protection from TRIM5α. *A-B) Titration of A) A92E CA mutant or B) N74D mutant dR8.91 based VSV-G enveloped GFP virus. Infection was as described in Figure 1. WT macrophages are shown in black/grey, TRIM5α KO in red/burgundy, and CyPA KO (PPIA-/-) in blue/grey-blue. n=8, 2 clones per cell line across 4 experiments. C-D) Area under the curve (AUC) analysis of viral titrations depicted in figures 2B-E, 9B-C. Area was calculated using the trapezoid rule, calculating the area beneath the average curve of each genotype (2 clones each) across 4 experiments. E) Relative AUC as calculated by normalisation of CsA treated to CsA untreated AUC independently for each genotype. F) Relative AUC as calculated by normalisation of all conditions to CyPA untreated AUC. E-F) One sample t-tests against a hypothetical mean of 1 were used to show deviation by the normalised value from the control. E) comparisons between genotypes were calculated using Ordinary one-way ANOVA, Tukey's multiple comparisons test. NL4.3 based virus all genotypes n=4 (average used of 2 clones each, 4 experiments). dR8.91 based virus WT and TRIM5α KO n=3, CyPA KO n=2 (average used of 2 clones each, 3 experiments). Significance is defined as * <0.05, ** <0.01, ***<0.001, ****<0.0001.*

5.2.9 The second function of CyPA aids viral infection during reverse transcription

In figures 4F, 4G, 5C, and 5D, I could observe that this difference in infectivity between untreated and CsA treated TRIM5α KO cells was accompanied by a block to reverse transcription when infected with WT virus, but not P90A virus. If I normalise the late RT products in CsA treated WT, TRIM5α KO or CyPA KO cells to the untreated control, I can clearly see a significant decrease in late RT products in both WT and TRIM5α KO cells, but not CyPA KO cells. There is a significant increase when comparing TRIM5α KO to WT cells. There is no difference between WT or TRIM5α KO late RT products normalised to the untreated control when infected cells are infected with the P90A mutant (Figure 8A). Therefore, the second CyPA function during HIV-1 infection occurs at reverse transcription or earlier.

As a preliminary test whether the second function of CyPA directly impacts reverse transcription of WT or P90A virus, I compared viral infection when the concentration of deoxyribonucleotides (dN) was increased to 2 mM (baseline concentrations are normally around 100-200 nM (555)). As increasing nucleotide concentration also helps overcome the restriction imposed by SAMHD1 in macrophages, I was unsurprised to observe an increase in basal infectivity of both viruses (Fig. 10B&D). However, when normalised to the CsA untreated control +/- dN, I observed an increase in infection in CsA + dN treated cells compared to the CsA only condition (Fig. 10C). This was seen in both WT and TRIM5α KO macrophages but was not observed when macrophages were infected with the P90A mutant virus (Fig. 10E). Therefore, I conclude that CyPA has a second function in directly regulating reverse transcription of HIV-1 in addition to protecting the virus from TRIM5α.

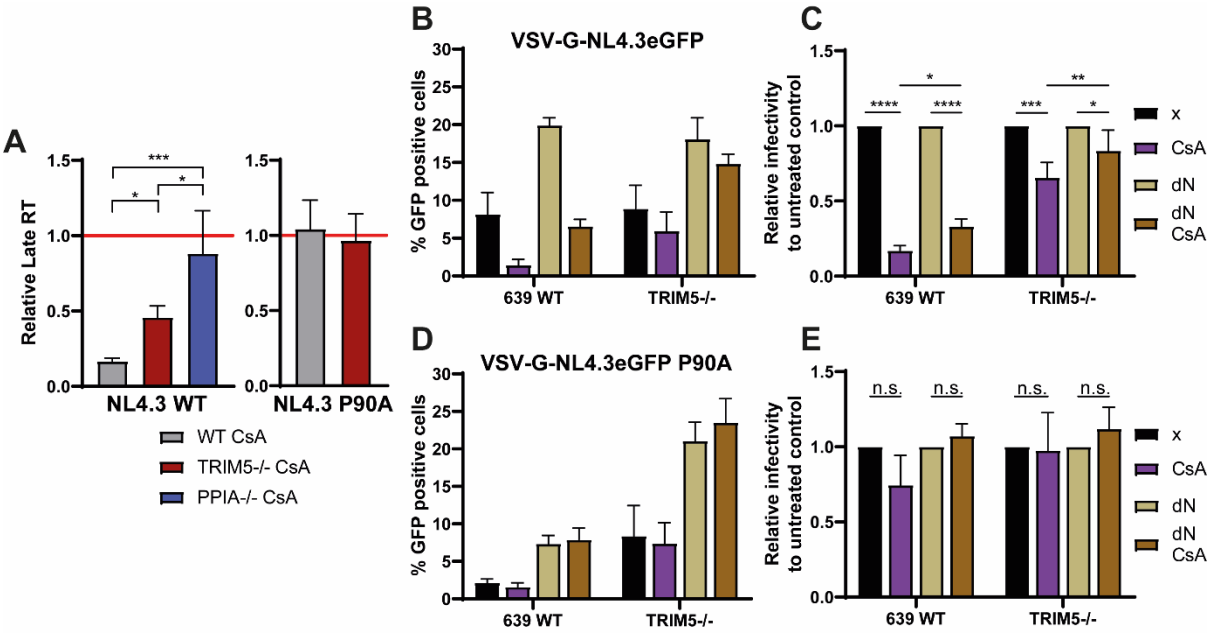


Figure 10: The second function of CyPA aids viral infection during reverse transcription. *A) Relative late reverse transcripts (RT) calculated by normalising CsA treated values to the average fold difference in Ct value ($2^{-\delta Ct}$) between viral GFP genome and cellular β-actin (ACTB) in CsA untreated cells for each genetic background. WT. TRIM5α KO, or CyPA (PPIA) KO cells were infected with 9000IU WT (left) or P90A mutants (right) VSV-G enveloped GFP pseudovirus for 24 hours. B-E) Infection of $5x10^4$ WT or TRIM5α KO cells with 900IU of B & C) WT, or D & E) P90A mutant GFP virus with 1μM CsA (purple), 2mM dN (gold), or 2mM dN and 1μM CsA (brown). B & D) percentage of GFP positive (infected cells). C & E) relative infectivity calculated by normalisation to the CsA untreated controls. A) significance was calculated by Ordinary one-way ANOVA Holm-Sidak's multiple comparisons test, n=4, (average of 2 clones each, 4 experiments). B-E) Significance was calculated by mixed-effects analysis Tukey's multiple comparisons test. WT n=5, TRIM5α KO n=8 (2 clones, 4 experiments). Significance is defined as * <0.05, ** <0.01, ***<0.001, ****<0.0001.*

5.3 Discussion

Human TRIM5α (hTRIM5α) has long been "known" to be unable to recognise HIV-1 CA, previously believed to be due to structural differences between different species isoforms of TRIM5α (527). Here, I have shown that this is not true, but instead, CyPA is actively protecting HIV-1 from hTRIM5α. Using iPSC derived macrophages genetically engineered to remove TRIM5α or CyPA, I have shown that when CyPA interactions with HIV-1 are inhibited, HIV-1 is restricted, consistent with prior reports (Figure 1). However, this restriction is TRIM5α dependent and occurs prior to reverse transcription (Figure 3). Importantly, I have shown that this restriction is not due to the mode of entry of VSV-G pseudotyped virus by also infecting cells with the CCR5 tropic HIV-1 BaL envelope. It is important to clarify this as HIV-1 has been shown to not only enter cells through CD4 mediated membrane fusion (542, 556, 557). A recent report using dendritic cells has shown that entry via the C-type lectin receptor Langerin, but not DC-SIGN, in dendritic cells targets HIV-1 for autophagy mediated degradation dependent on TRIM5α (Figure 2), highlighting the potential impact of entry pathways regarding TRIM5α-mediated restriction (558).

My findings support several recent reports; Firstly, Morger *et al.* (2017) (326), showed that that rhTRIM5 and hTRIM5 are both equally capable of interacting with viral CA in both monomeric and multimeric complexes. This called into question the hypothesis that hTRIM5α is unable to recognise HIV-1 CA due to structural differences. Secondly, as long ago as 2001, there had been reports of CyPA potentially protecting HIV-1 in human T-cells from Lv1 and Ref-1 prior to these being identified as TRIM5α (531, 559). However, these were later rejected by research describing CyPA protection and TRIM5α restriction to be independent activities from the Luban group. Now, though, the Luban group appears to be correcting this statement, with Kim *et al.* (2019) (242), showing that CyPA protects HIV-1 from TRIM5α in both primary human T-cells and monocyte derived macrophages using a lentiviral shRNA knockdown system. This even further supported by Selyutina *et al.* 2020 (329) who likewise show protection by CyPA against TRIM5α in lymphocytes. Combined with my robust complete KO

system in iPSC-derived macrophages, we have disproven the old theory that hTRIM5α is unable to recognise HIV-1 CA. What is still unclear though is how exactly this CA-CyPA interaction protects the virus from TRIM5α. Does CyPA sterically inhibit TRIM5α interactions, or does CyPA alter the CA structure through its prolyl isomerase activity? I would propose that it is the latter, because CA mutants that are grown in the presence of CsA (and therefore should not interact strongly with CyPA) appear equally as infectious as WT virus in TRIM5α KO cells (319). These mutants have altered structure proximal to the CyPA-binding proline loop and, therefore, likely alter the structure of this domain, perhaps into a structure unrecognisable by hTRIM5α. Meanwhile mutating the proline residue likely to be sterically altered by CyPA, P90, to alanine could lock the CA structure into a TRIM5α sensitive conformation.

Having demonstrated the importance for CyPA for TRIM5α-mediated restriction by taking advantage of genetic manipulation of macrophages, I next sought to bring clarity to our understanding of the mechanism by which TRIM5α restricts HIV-1. Consecutive studies of each component of TRIM5α, the B30.2 (SPRY), the coiled-coil, the linker, and the E3 Ubiquitin ligase RING domains have shown that while the coiled-coil and the linker domains are required for multimerization of TRIM5α to form hexagonal nets (560–564), and the B30.2 domain is required for CA interactions (328, 527, 544, 565, 566) , it is the RING domain that is necessary for current known effector functions (335–337, 549, 566, 567). Several ubiquitin-mediated modes of activity have been ascribed to the TRIM5α RING domain but can ultimately be defined by two alternative systems. 1; increased turnover of TRIM5α and CA by the proteasome (335), and 2; activation of innate signalling through NF-kB and AP-1 via TAK1 activation (336, 342, 344). RING domain functionality involves self-ubiquitination at the E2 ubiquitin binding domain and this self-ubiquitination drives both the proteasomal turn over and activation of innate immune signalling (336). However, abrogation of either was still insufficient to rescue viral infectivity. Here, I too show that inhibition of either pathway is insufficient to rescue viral infectivity (Figures 4B-G and 5A-D).

Not only did inhibiting these pathways fail to rescue infection from TRIM5α-mediated restriction, but on the contrary, inhibition of innate immune signalling actually reduced the proportion of GFP producing cells. I found this inhibition occurs post reverse transcription, but further work is needed to investigate nuclear entry, integration, and viral gene transcription to identify the exact point of inhibition. It has been reported that HIV-1 LTR transcription is driven by C/EBP, AP-1 and NF-kB which would be consistent with my results of TAK1 inhibition (568–570). Furthermore, inhibition of an alternative innate signalling pathway involving cGAS also reduced the number of GFP producing cells. Considering how NF-kB is a shared mediator of both these pathways, this lends further support to this being the potential mechanism. Overall though, this suggests that it is beneficial for HIV-1 to stimulate some level of immune signalling early during infection. How this is beneficial to the virus is unclear, as it will result over prolonged viral replication cycles in an anti-viral state detrimental to the spread of infection. Furthermore, these results go against the accumulating body of evidence that HIV-1 very actively suppresses an innate immune response triggered by cGAS and NF-κB activation. The accessory proteins Vpu, Vif and Vpr have all been reported to inhibit NF-κB activation and recently Vpr in particular has been shown to inhibit nuclear translocation of both NF-κB and IRF3 in order to facilitate viral replication, especially in macrophages (571–574). However, this was not seen to have an effect on single round infectious virus systems (572). Furthermore, several other papers have also reported Vpr induces an inflammatory state depending on the experimental assay utilised to measure Vpr activity and on the cell type used, including CD4+ T cells, Jurkat, THP1, or 293T and HeLa cells reconstituted for innate signalling via transfection of plasmids (284, 575–577). Therefore, further investigation is needed to determine if the suppression observed here is unique to this iPSC-macrophage model used and/or single round viral infections within them. Here, I have ruled out both the proteasome and innate signalling as the principal methods by which TRIM5α restricts single round infections of HIV-1, but I have not tested whether inhibition of both simultaneously rescues infectivity or investigated their impact over prolonged spreading viral infection, which would

require follow up experimentation. However, I did investigate the role of IFN on TRIM5α mediated restriction (Figure 7). Unsurprisingly, I did not find TRIM5α-induced IFN severely impacted single round viral infection, however nor did pre-treating cells with IFN protect my macrophages from HIV-1 through increased turnover of TRIM5α, as reported by Jimenez-Guardeño *et al.* (2019) (338). Therefore, any prolonged restriction driven by IFN induced by TAK1 or STING signalling would not appear to be TRIM5α dependent. I also did not investigate another known ubiquitin regulated process described for TRIM5α-mediated restriction, autophagy (558, 578–581). Further work is required to conclusively demonstrate if RING domain mediated autophagy is important, especially as a recent manuscript by Saha *et al.* (2020) reports that TRIM5α induced autophagy relies on TAK1 activity, which I have here shown is non-essential for TRIM5α-mediated restriction (581).

As direct RING-domain mediated activity of TRIM5 alone is insufficient to block HIV-1 infection, I here evaluated the potential role of other restriction factors working cooperatively with TRIM5 to restrict HIV-1. Using KO iPSC-derived macrophages for SAMHD1 and TREX1, I have shown that TRIM5α required both to inhibit HIV-1. Both factors have been described to have nuclease activity during HIV-1 infection, although that of SAMHD1 is contentious, and this activity or the dNTPase activity could reduce the quantity of HIV-1 late reverse transcripts (517, 550, 582–585) .

However, rescue of viral infectivity in SAMHD1/TREX1 double KO cells is incomplete. Most likely, this is due to the presence of other restriction factors, such as the APOBEC3 family of proteins which block HIV-1 reverse transcription through its deamination activity, and the GTPase Mx2 (also known as MxB), which blocks viral nuclear accumulation and integration (280, 513–515, 523). Interestingly, Mx2 also interacts with HIV-1 CA at the CyPA binding site, but the role of CyPA in its activity seems unclear (324). Knock out of CyPA appears to block Mx2-mediated restriction, but CA mutations A88T and G89V, which cannot bind CyPA, aids Mx2. However, these differences may be cell type specific because the authors of this paper did not observe a block of viral RT in CyPA KO cells (SupT1) which I saw in my macrophages. In addition, Mx2 potency is increased in non-dividing cells, another cell-type variability that

also will apply to my non-dividing macrophages (323). It is possible then that Mx2 is the factor responsible for the secondary role of CyPA protection of HIV-1, although I also show that the second role of CyPA, at least in part, protects from restriction at a stage prior to viral reverse transcription. Therefore, Mx2 alone will likely not be the sole contributing factor. Future work is required involving production of further HIV-1 restriction factor KO in combination with TRIM5α, and identifying their relative rescue to infectivity and reverse transcription would be of great interest.

Finally, as just stated, I provide clear evidence here of a second role for CyPA in protecting HIV-1 inside macrophages during single round infections that appears to occur prior to reverse transcription. It is important to note though that this second role is not clear when we investigate spreading viral infection over 9 days. This implies that TRIM5α-mediated restriction is dominant enough to mask any limited protection still offered by CyPA, likely due to the innate immune signalling triggered via cGAS/STING and TAK1. The visibility, or lack of, this second cyclophilin effect during infection with different viral CA mutants is highly intriguing. As expected, due to its inability to bind CyPA, the P90A mutant does not display a second role for CyPA protection. Moreover, this informs us that this second effect is not due to CyPA packaged into the virus during preparation in non-CyPA KO HEK-293T cells (530). However, surprisingly, P90A mutant virus infects TRIM5α KO cells equally to WT virus when CsA is not present, not to the level of WT infection when CsA is present (figure S4A). This implies that the P90A CA is structured such that whatever the second effector of viral restriction is, it is unable to recognise the P90A virus. The CsA escape mutants G94D and A92E on the other hand, which are resistant to TRIM5α, are not resistant to this second effector. However, in neither case do we observe infectivity reduced to CyPA KO levels in WT or TRIM5s KO cells treated with CsA. This may even go so far as to imply that there are not only one, but two or more effectors in addition to TRIM5α that HIV-1 is protected from by CyPA, one of which may be insensitive to CsA. While this seems contradictory because CsA inhibits CyPA function, it has been reported that CyPA can interact with multiple *loci* on the viral CA via a non-canonical binding domain (311, 586). Therefore, the secondary function of CyPA may, in part, depend

on this second interface. Lastly, the N74D CA mutant showed sensitivity to TRIM5α restriction but is also highly susceptible to the second effector inhibited by CyPA. What is more, even in the presence of CsA, infectivity of N74D virus in TRIM5α KO cells never dropped below that of WT cells without CsA. In turn viral infectivity in WT cells only dropped to the level as in CyPA KO cells in the presence of CsA. These results tell us that N74D is capable of being restricted by TRIM5α like the P90A mutant, despite not being described as a CyPA or TRIM5α binding location. Unlike P90A virus, though, it is susceptible to CsA induced restriction of infection.

Why N74D is susceptible to TRIM5α will require further investigation. At the very least, by inhibiting CPSF6 interactions with WT viral CA using the drug PF74 (587), I have shown that this susceptibility is not due to CPSF6 protecting the viral core as CyPA does, nor that it may stabilise CyPA protection. A very recent publication by Ohainle *et al.* (2020) (549) perhaps answers this conundrum. They show how TRIM34, a closely related TRIM family member encoded at the same gene locus as TRIM5α, is capable of restricting the N74D CA variant prior to reverse transcription, but only when TRIM5α is present. TRIM34 does not restrict the P90A mutant virus but the authors did not investigate what role it may play during WT viral infection when CsA is present and so it is possible that TRIM34 may also contribute in some way as a second effector that CyPA protects against.

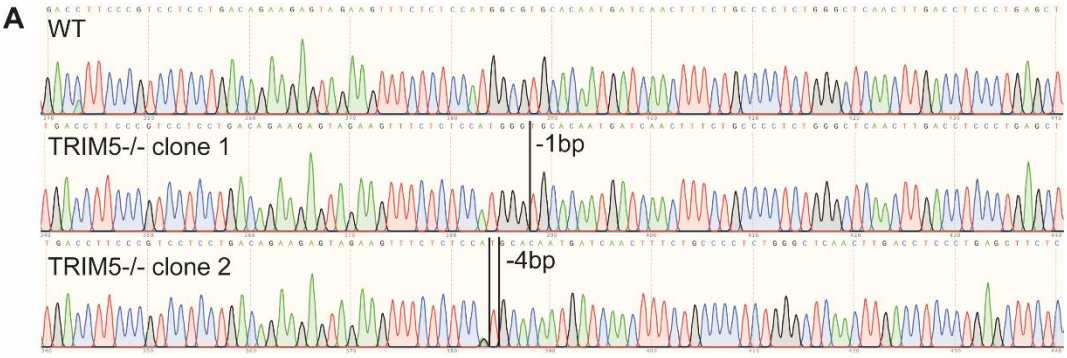
Given that Mx2 blocks post reverse transcription and is therefore unlikely to be the cause of the second cyclophilin sensitive block to infection, or at least the reverse transcription dependent element of it, a final alternative possibility is the disruption of nuclear pore interactions. It has been shown that CyPA regulates trafficking of viral particles to the nuclear pore (291, 352), that nuclear pore interactions regulate viral core stability (588), and that core uncoating regulates reverse transcription. CyPA interactions dictate targeting of the virus towards specific nuclear pores, and CA mutants P90A and N74D can alter this, particularly nuclear entry via the nucleoporins (NUPs) 153, 155, and 358 (291, 553, 588). It is still unknown where and when exactly reverse transcription occurs, although there is evidence that it can occur within the CA due to the existence of pores that allow entry of dNTPs into the CA (295,

589). Therefore, there is some debate as to whether it can occur during interaction with the nuclear pore, and if so, this would be supported by my data that the second protective role of CyPA also involves reverse transcription. In the future, it will be important to investigate changes in nuclear entry and the integration capability and location of HIV-1 in TRIM5α KO cells using these various CA mutants and perhaps to attempt to create inducible KO iPSC derived macrophage lines for these NUPs, considering non-inducible knockouts are lethal.

5.4 Conclusion

In this chapter, I have shown how genetic editing in iPSC can be applied to investigate a question involving fully functional macrophages to induce immune signalling and identify the specific role of individual genes during viral infections. I have here explained the rationale behind inconsistent patterns of HIV-1 restriction by the host factor TRIM5α, and partially solved how co-option of CyPA results in protection of the virus. Owing to the ability of iPSC-derived macrophages to carry out fully functional immune responses via cytoplasmic sensors, unimpaired protein turnover by the proteasome, and unaltered expression of cellular nucleases and restriction factors, I have been able to decipher some of the precise elements by which TRIM5α interactions with HIV-1 result in viral restriction. I have found that SAMHD1 and TREX1 are required and shown possible evidence for the involvement of other restriction factors such as APOBEC3, Mx2, and TRIM34. This demonstrates the importance of co-operation between multiple antiviral factors to effectively inhibit HIV-1. Because genetic manipulation of iPSC is more reliable than manipulation of primary immune cells, I have clear evidence for additional roles for CyPA in HIV-1 infection. I believe it will therefore be possible to use these cells, and future genetic manipulations of them, to completely solve the roles of TRIM5α and CyPA during the HIV-1 entry stages of its life cycle and beyond.

5.5 Supplementary figures



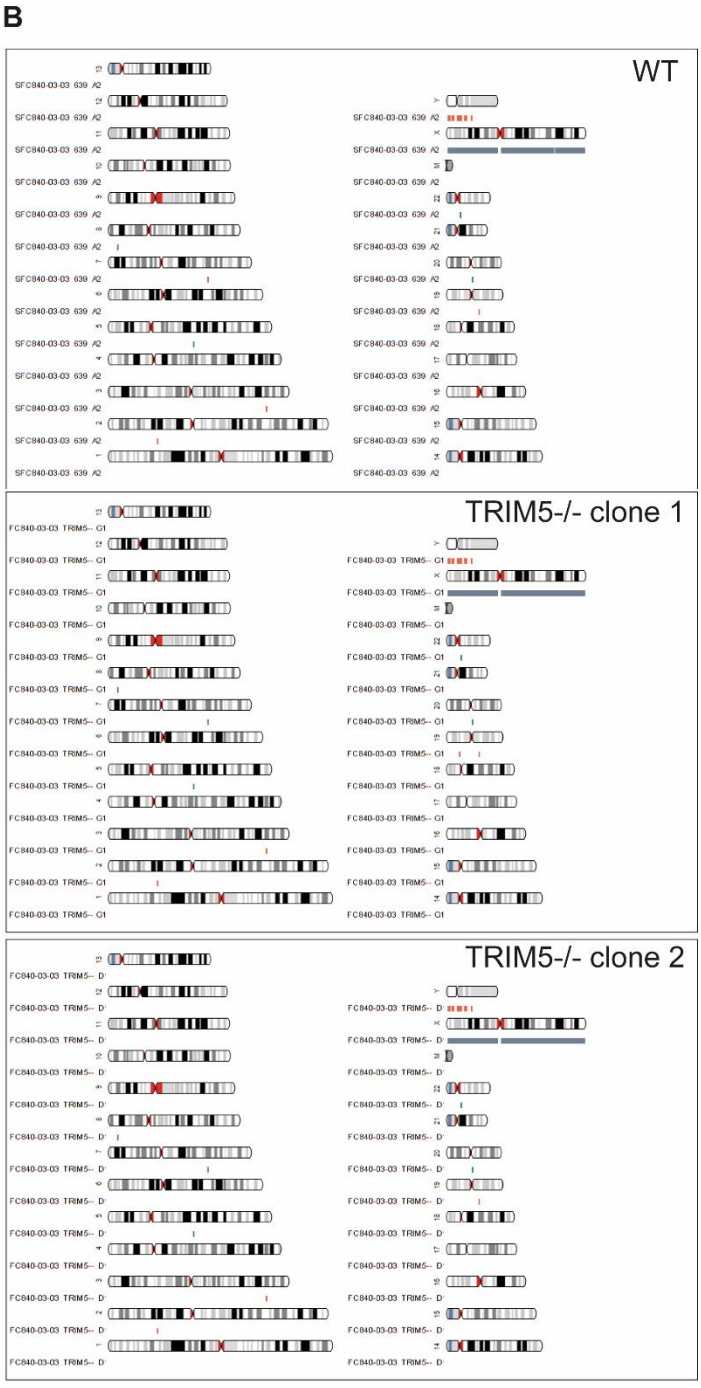
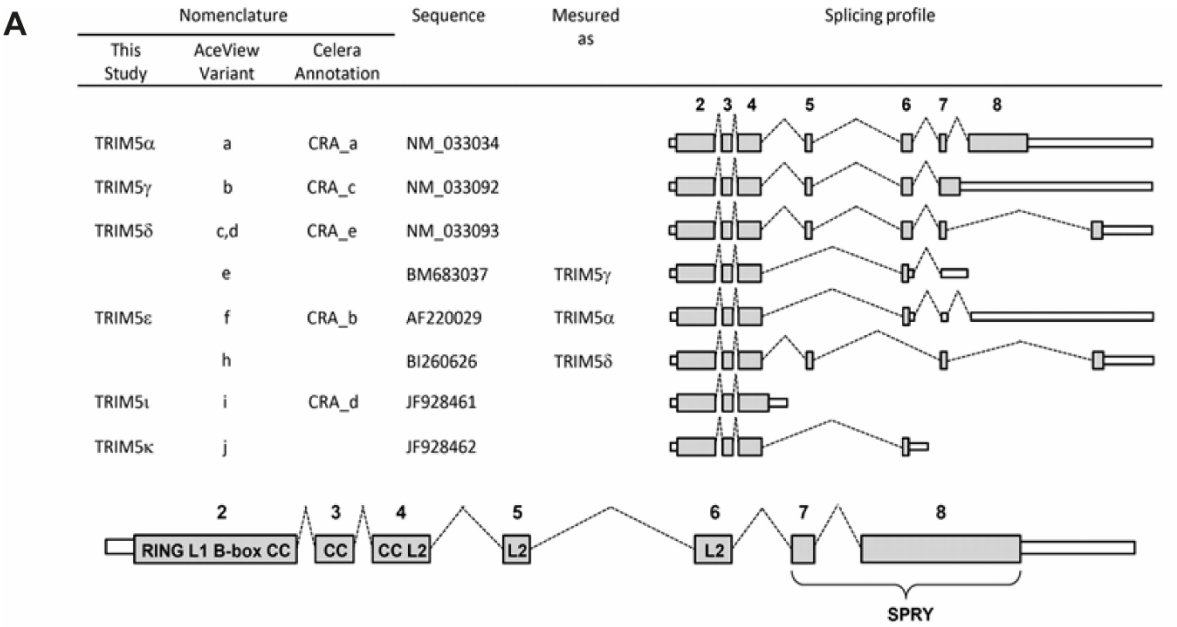
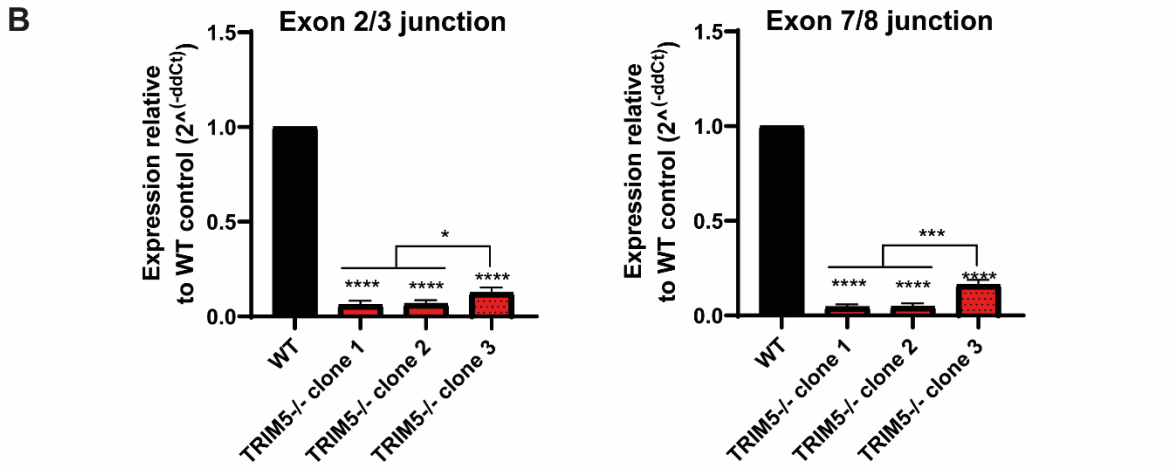


Figure S1: iPSC TRIM5α KO clone identification. Related to Figure 1. *A) Sequence traces of WT (639, clone A2), and 2 TRIM5α KO clones (clone 1 = D11, clone 2 = G10). B) Karyograms for these clones following single nucleotide polymorphism (SNP) analysis showing no clear chromosomal abnormalities in these genetic clones.*


A
Nomenclature
This Study
AceView Variant
Celera Annotation
Sequence
Mesured as
Splicing profile
TRIM5α a CRA_a NM_033034
TRIM5γ b CRA_c NM_033092
TRIM5δ c,d CRA_e NM_033093
e BM683037 TRIM5γ
TRIM5ε f CRA_b AF220029 TRIM5α
h BI260626 TRIM5δ
TRIM5ι i CRA_d JF928461
TRIM5κ j JF928462
2 3 4 5 6 7 8
RING L1 B-box CC
CC
CC L2
L2
L2
SPRY


B
Exon 2/3 junction
Exon 7/8 junction
Expression relative to WT control (2^(-ddCt))
1.5
1.0
0.5
0.0
*
***
****
WT
TRIM5-/- clone 1
TRIM5-/- clone 2
TRIM5-/- clone 3

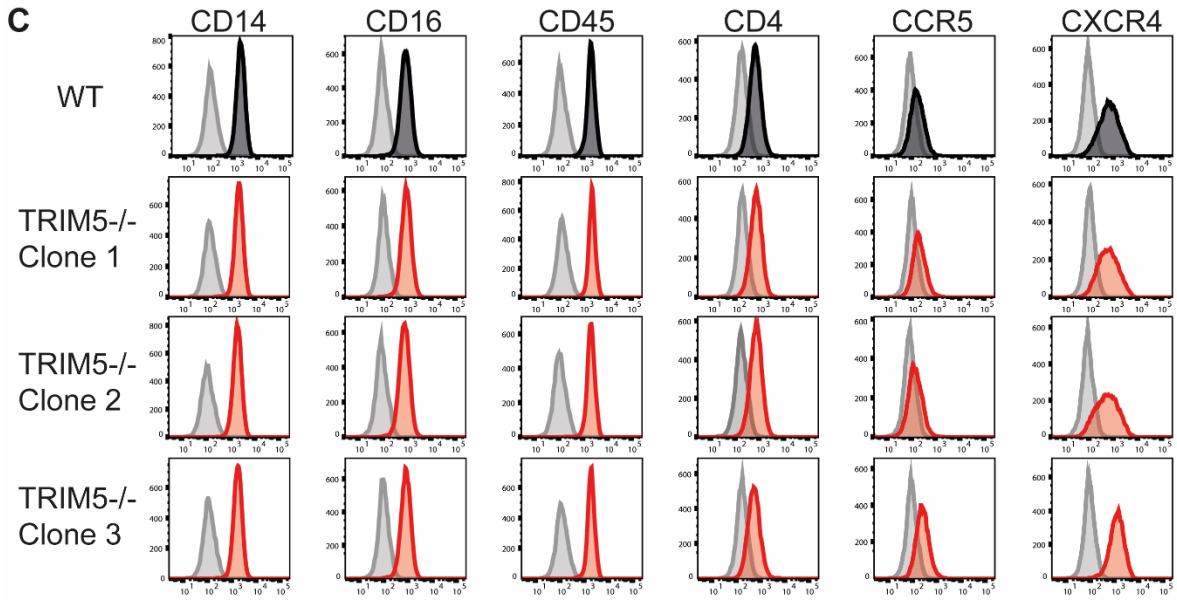

C
CD14
CD16
CD45
CD4
CCR5
CXCR4
WT
TRIM5-/- Clone 1
TRIM5-/- Clone 2
TRIM5-/- Clone 3

Figure S2: Validation of TRIM5α KO macrophages. Related to Figure 1. *A) Table taken from Battiveli et al. (2011)* (590) *showing 8 different splice variants of TRIM5α. B) Expression of TRIM5α in macrophages normalised to WT cells in 3 TRIM5α KO clones (clone 3 = C8) as determined by qPCR using primers spanning either the exon 2/3 junction (pan-isoform specific) or Exon 7/8 junction (TRIM5α and ε specific). Significance was calculated by ordinary one-way ANOVA Tukey's multiple comparisons test. n=3. C) Surface expression of typical macrophage markers CD14, CD16, CD45, and HIV-1 receptors CD4, CCR5, and CXCR4 in WT (black) or TRIM5α KO (red) iPSC-derived macrophages. Y-axis displays event count, vs fluorescence intensity on the x-axis. Isotype staining is shown in grey. n=1.*

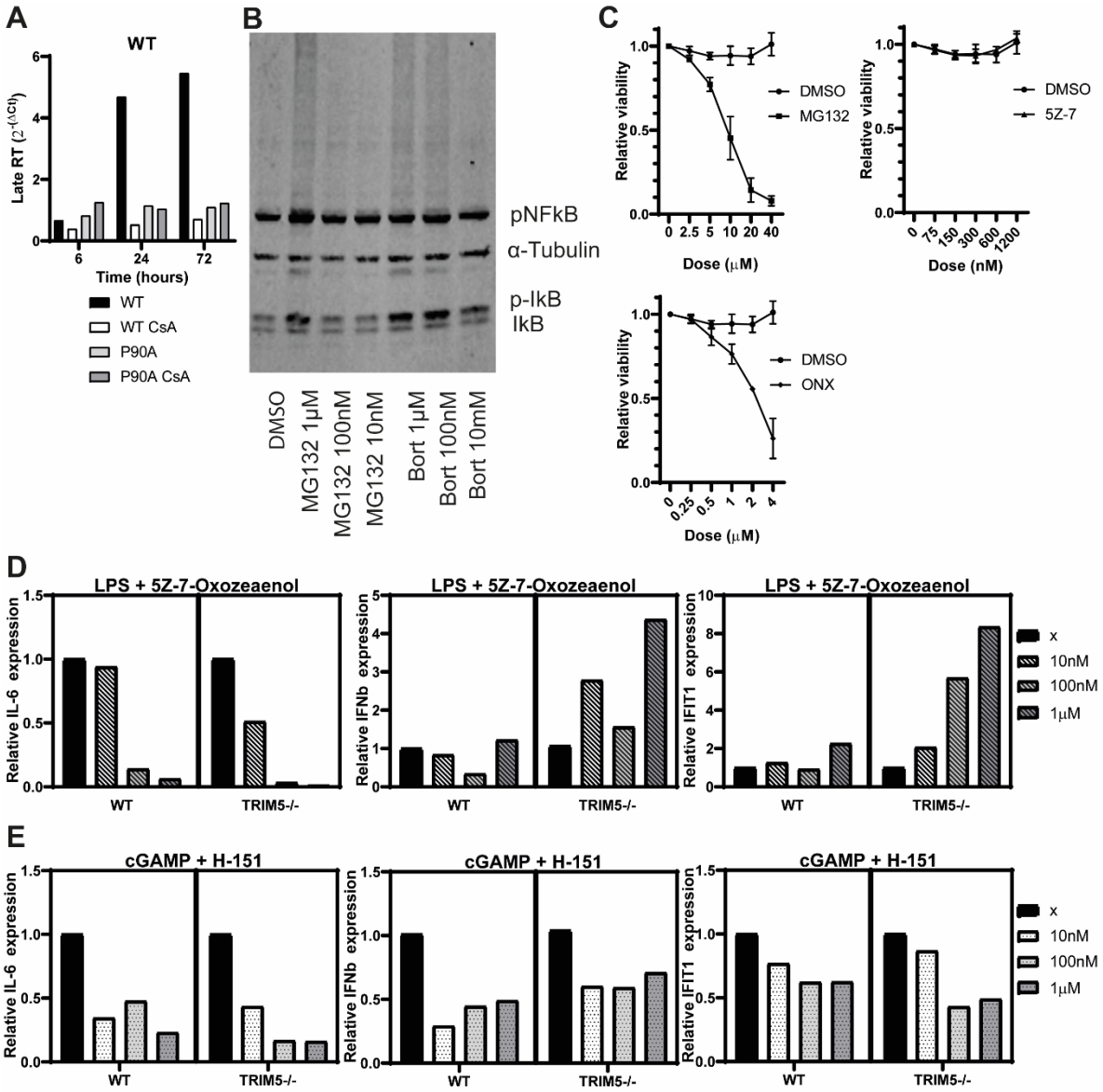


Figure S3: Optimization of conditions for late RT investigation and validation of drug functionality. Related to Figures 4-7. *A) Time-course of production of late reverse transcripts (RT) in WT cells infected with WT and P90A mutant VSV-G enveloped GFP pseudovirus. n=1. B) Western blot for phosphorylated NF-kB, α-tubulin, phosphorylated IκB, and IκB during titration of proteasome inhibitors in WT macrophages stimulated with 1ng/mL LPS for 1 hour. C) Viability relative to the untreated control of macrophages after 72 hours treatment with a titration of MG132 (top left), ONX-0914 (ONX) (bottom left), or 5Z-7-Oxozaeanol (5Z-7) (right). n=3. D-E) Relative expression of IL6 (left) IFN-β (middle), and IFIT1 (right) as calculated as $2^{-\delta\delta Ct}$ where Ct has first been normalied to the housekeeper control,*

and then is normalised to the untreated control within each genotype. WT or TRIM5α KO macrophages have been stimulated for 4 hours with D) 1ng/mL LPS, or E) 500ng/mL cGAMP in the presence of titrated D) 5Z-7, or E) H-151. n=1

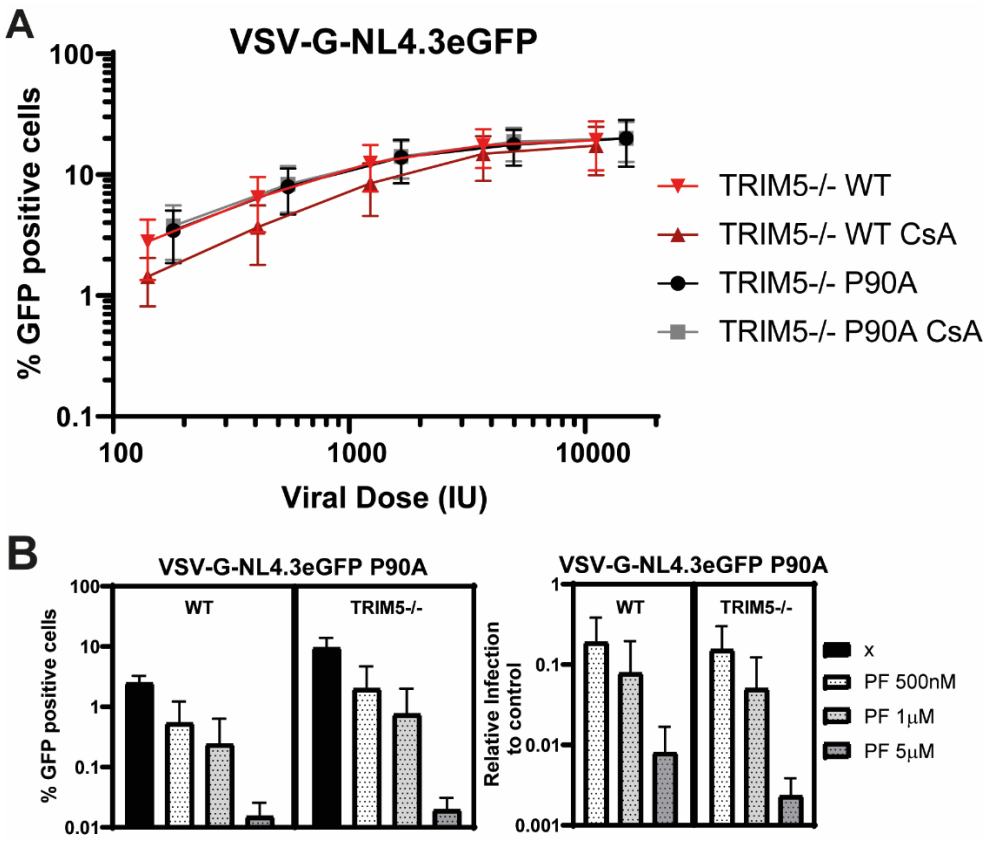


Figure S4: CyPA has a secondary role in HIV-1 infection independent of CPSF6. Related to Figure 9. *A) Overlapping of figures 1B and 1D, showing percentage GFP positive (infected) TRIM5α KO macrophages infected with either WT GFP virus (red/burgundy) or P90A mutant virus (black/grey) in the presence of absence of 1μM CsA. B) Titration of CA binding inhibitor of CPSF6, PF-74 on WT or TRIM5α KO macrophages infected with 900IU of P90A mutant GFP virus for 72 hours. Left; Percentage of GFP expressing cells (infected). Right; relative infectivity calculated by normalising the percentage GFP positive cells to the untreated control. Cells were treated with PF-74 at time the time of infection and remained throughout the experiment. WT n=4, TRIM5α KO n=8 (2 clones, 4 experiments).*

Chapter 6:

Cyclophilins and Innate Immunity

6.1 Introduction

In the previous chapter, I introduced Cyclophilin A (CyPA) as an essential host co-factor for HIV-1 infectivity. In this chapter, I sought to further investigate this protein and its fellow family members in their broader role in macrophage function, specifically as part of the innate immune response. Before we consider this though, it is important to first understand the history of the cyclophilin inhibitory drug Cyclosporine A (CsA) and the current known functions of this extensive protein family. The prototypical member of this family, CyPA, was first discovered in bovine thymocytes as the binding target of the immunosuppressive drug CsA, hence the name cyclophilin (591). Binding of CsA to CyPA results in a 3D complex capable of interacting with, and inhibiting the kinase activity of, calcineurin (Cn) after T-cell receptor (TCR) activation (552, 592–594). This prevents phosphorylation and nuclear translocation of nuclear factor of activated T-cells (NFAT), suppressing T-cell activation and proliferation. Owing to this immunosuppressive activity, CsA, as well as another Cn inhibitor FK506, have long been used to prevent organ transplant rejection and treat a variety of immune pathologies including arthritis, Lupus erythematosus, dermatitis, and potentially sclerosis and Sjögren's syndrome (367, 368, 595–598). In fact, the number of diseases treated with CsA appears to be increasing, being used in over 200 clinical trials between 2014 and 2016 (368).

While this immunosuppression is primarily of the adaptive immune response, more recently studies have investigated what effects CsA may have on the innate immune system (599). Results have often been conflicting, with CsA treatment being anti- or pro-inflammatory depending on cell type and conditions. For example, CsA is anti-inflammatory in murine macrophages, peripheral blood mononuclear cells, and dendritic cells, through induction of the unfolded protein response, suppression of inflammatory cytokines, or increased anti-inflammatory cytokine production (599–604). Also, CsA can reduce oxidative stress in rat mesangial cells by inhibiting IL-1β production, in JEG-3 cells through p53 and JNK inhibition, and in neutrophils (599, 605–607). Conversely, simply treating rat hepatocytes and endothelial cells with CsA is reported to induce ROS production (608, 609), and numerous papers have

shown that CsA alone induces a pro-inflammatory response, particularly in renal and endothelial cells (610–616). While some of these occur after treatment with both CsA and FK506, and are therefore believed to be Cn dependent, others are CsA dependent. CsA is known to cause severe side effects of nephrotoxicity, and the precise mechanism of this is poorly understood (369).

Cn inhibition by the CsA-CyPA complex is due to a gain-of-function activity of CyPA. The primary function of CyPA is as a peptidyl-prolyl isomerase (PPIase, also referred to as a Rotamase) (Figure 1A) and was originally believed to play an important role in protein folding (353, 617). More recently, PPIases have been proposed to act as potential signalling switches or timers and interactions outside of the PPIase catalytic site can influence protein interaction dynamics (618–622). In addition to CyPA, 16 other PPIase domain containing proteins have been identified (Figure 1, Table 1). Of these, 12 retain CsA binding potential, but only 7 have been actively shown to have PPIase activity. Several members (PPIL2, PPIL4, PPIL6, and CWC27) have explicitly lost catalytic activity due to the substitution of essential residues within the active site (366). The functions of the various cyclophilins have been extensively reviewed over the last 3 decades (353, 354, 362, 617, 623–626) and I will, therefore, not cover them all here, but instead will focus primarily on potential functions within inflammation and macrophages. However, it is worth noting that while CyPA has been extensively studied, the functions of the other cyclophilins remain largely unknown, especially the nuclear cyclophilins and the peptidyl-prolyl isomerase-like (PPIL) proteins (Table 1).

Given the number of CsA binding cyclophilins, it is reasonable to hypothesize that some, if not most, of the regulatory effects of CsA on the innate immune response are cyclophilin, not Cn, dependent as is often believed (366). In fact, numerous cyclophilins have been shown to interact with innate immune regulators, especially CyPA. In T-cells, CyPA interacts with the SH2 and SH3 domains of Itk or Crk, preventing downstream signalling via PLCγ and integrin dependent motility, respectively (619, 621, 627, 628). In neurons, CyPA can regulate apoptosis through interactions with apoptosis inducing factor (AIF) and cytochrome C (629–631). In cancer cell lines (e.g. breast cancer and multiple myeloma), both CyPA and CyPB

promote growth, motility, and tumour invasion by altering the conformation and nuclear translocation of JAK/STAT proteins down-stream of immune receptors e.g. TCR (632–634). In HEK293 and HeLa cells, CyPA can regulate ASK1 phosphorylation, preventing JNK and p38 MAPKs activation (635), and in MEFs, CyPA can interact with NF-κB, aiding its nuclear translocation (636). Finally, even in macrophages, CyPA, and more so PPIL3 (CyPJ), has very recently been found to regulate the TLR mediated innate immune response, altering cytokine transcription (365).

Beyond CyPA and PPIL3, the other cytoplasm resident cyclophilin, CyP-40 plays an important role in the stress response, interacting with the heat shock proteins (hsp) hsp70 and hsp90, and regulating hypoxia induced factor (HIF)-1α expression (637, 638). In the ER, CyPB and CyPC regulate ER redox homeostasis and the ER associated degradation (ERAD) pathway in a CsA sensitive manner, which can in turn impact protein folding and secretion (639–641). Additionally, the CyPC associated protein (CyCAP), and its homologues Mac-2 and 90K, can induce T-cell activation and MMP expression, and bind integrins, collagens, and fibronectin, all of which are important components for immune cell motility (642–647). As a key regulator of the mitochondrial permeability transition pore (MPTP), CyPD may have a broad influence on apoptosis and necroptosis (648), and regulate mitochondrial DNA release, a potent inducer of the inflammasome and ROS production (649–651). Finally, there are numerous nuclear resident cyclophilins, many of which are components of the spliceosome (354), which have the potential to regulate gene transcription and mRNA trafficking and stability (354, 652, 653).

In addition to their intracellular functions CyPA, CyPB, and CyPC have been shown to be secreted from cells in response to LPS, hypoxia, and CsA (654–658). Here, they are well understood to act as cytokines/danger associated molecular patterns (DAMPS) to induce pro-inflammatory responses through the surface molecule CD147 (659–664). CyP-CD147 interactions trigger intracellular signalling via ERK1/2 to alter cytokine and ROS production (662, 665–673). However, CyPB released from the extracellular matrix can also be anti-inflammatory through inducing BCL3 expression in human macrophages (674).

Overall, there is a wealth of literature indicating that the cyclophilin family is either already known to influence inflammation, or has the clear potential to do so, as summarized in Figure 2. Therefore, backed by preliminary findings of the Towers Lab (UCL), in this chapter I sought to deconvolute the role cyclophilins play in the macrophage innate immune response. I found a clear cyclophilin-dependent conflict in the function of Cn inhibitors on the macrophage innate immune response, and went on to show that both CyPA and CyPB can both regulate the innate response, although the precise mechanisms remain unknown.

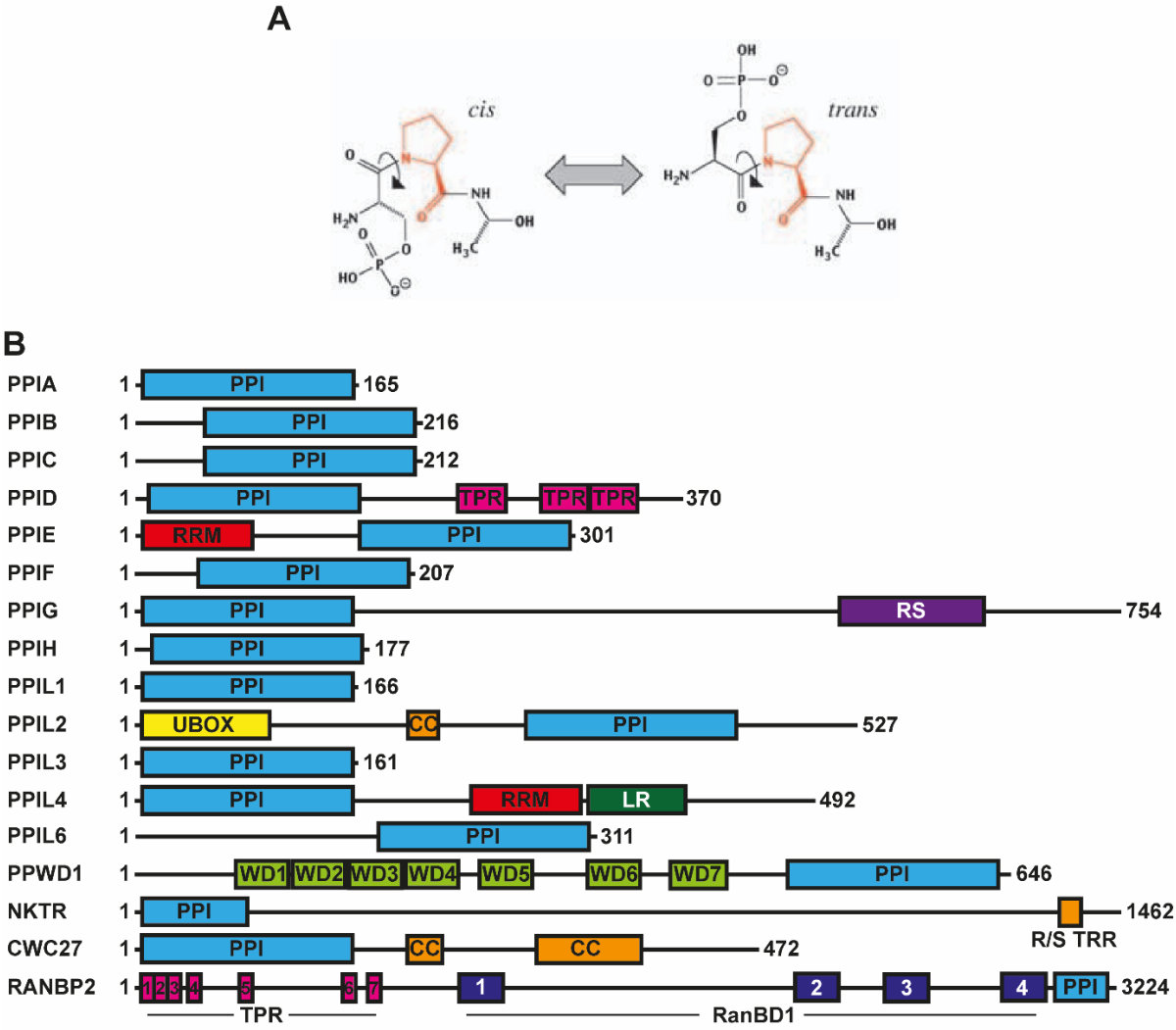


Figure 1: Function and domain structures of the cyclophilins. *A) Schematic of the transition between a cis and trans of proline that is catalysed by peptidyl-prolyl isomerases. Adapted from Shaw 2002. B) Schematic of the 17 members of the cyclophilin family. Abbreviations: PPI = Peptidyl-prolyl isomerase, TPR = tetratricopeptide repeat, RRM = RNA recognition motif, RS = arginine serine, WD = WD40 repeat, CC = coiled-coil, TRR = tandem repeat rich.*

Protein name(s)	Gene name	Size (kDa)	CsA binding	PPIase activity	Location(s)	Function(s)	Reference(s)
CyPA	PPIA	18	Yes	Yes	Cytoplasm, nucleus, EC	Protein folding, growth, apoptosis, differentiation, inflammation, chemotaxis, RNA binding, intracellular trafficking, stress response	(362, 364, 627, 631, 634, 662, 666, 676–683)
CyPB	PPIB	23.7	Yes	Yes	ER, EC	Protein folding, inflammation, protein degradation, hormone receptor signalling	(363, 639, 673, 684–686)
CyPC	PPIC	22.7	Yes	Yes	ER, EC	Protein binding, protein degradation	(640, 687)
CyP40	PPID	40.7	Yes	Yes	Cytoplasm	Protein folding, stress response, inactive steroid receptor, intracellular trafficking,	(637, 688–690)
CyPE	PPIE	22.4	Yes	Yes	Nucleus	RNA binding, spliceosome, gene expression	(691–693)
CyPD / CyPF	PPIF	22	Yes	Yes	Mitochondria	Regulation of mitochondrial permeability transition pore, stress response	(648, 649)
CyPG / SR-CyP	PPIG	88.6	Yes	Yes	Nucleus	Spliceosome, differentiation	(694, 695)
CyPH	PPIH	19.2	Yes	Yes	Nucleus	Spliceosome, scaffold protein	(696, 697)
PPIL1	PPIL1	18.2	Yes	Yes	Nucleus	Spliceosome, growth, morphology	(698, 699)
PPIL2	PPIL2	59.5	No	No	Nucleus	Ubiquitin ligase, gene expression	(653, 700–702)
PPIL3 / CyPJ	PPIL3	18.2	Yes	Yes	Cytoplasm, nucleus	Inflammation, growth, apoptosis, cell-cycle	(365, 703, 704)
PPIL4	PPIL4	57.2	N/A	N/A	Nucleus	RNA-binding, angiogenesis	(705, 706)
PPIL6	PPIL6	35.2	No	No	Nucleus	N/A	(366)
PPWD1	PPWD1	73.6	Yes	Yes	Nucleus	Spliceosome, RNA binding, differentiation, growth	(707, 708)
NKTR	NKTR	165.7	Yes	N/A	Plasma membrane	Tumor recognition receptor	(709)
CWC27 / SDCCAG-10	CWC27	53.8	No	No	Nucleus	Spliceosome, gene expression	(652, 710)
RANBP2 / Nup358	RANBP2	358.2	No	No	Nuclear envelope	Nuclear pore protein	(711)

Table 1: The Cyclophilin family of proteins; size, location, and function*. ER = Endoplasmic Reticulum, EC = Extra-cellular, PPIase = peptidyl-prolyl isomerase. CsA binding and PPIase activity based on Davis et al. 2010, with updated results included.*

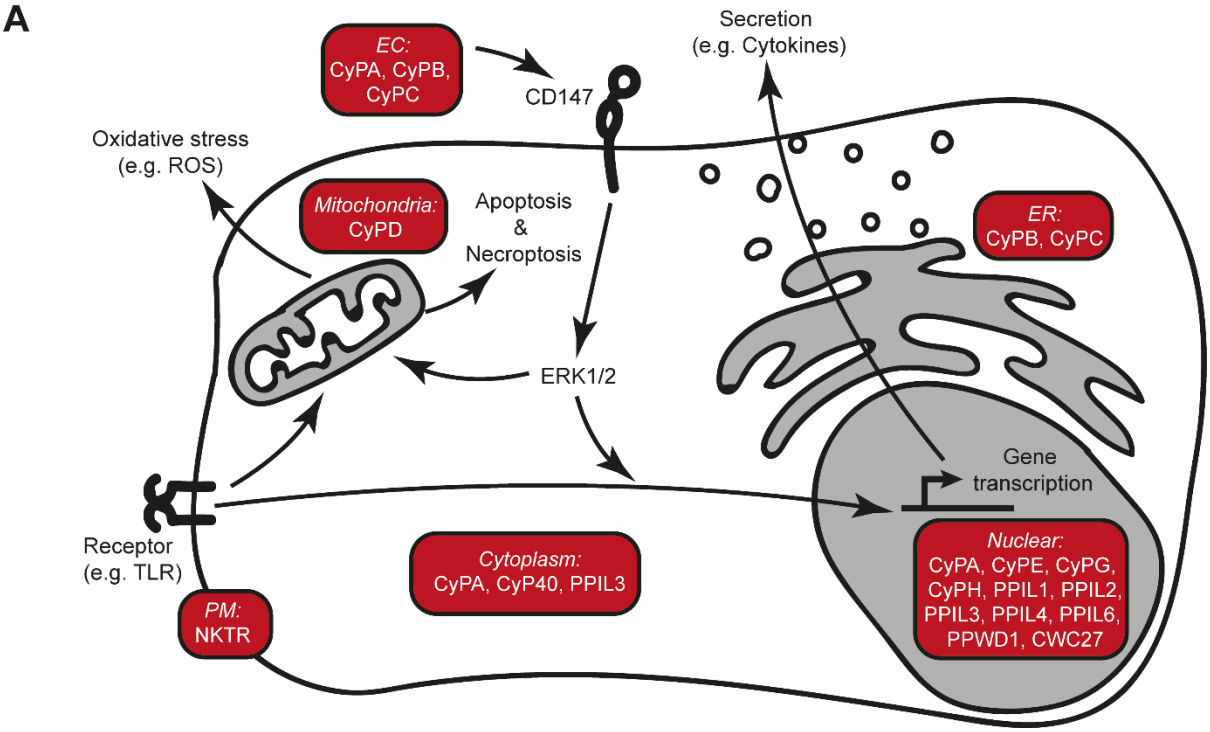


Figure 2: Localization and potential interactions with cyclophilins in immunity. *Schematic of a typical innate immune receptor mediated response and the cyclophilin induced CD147 signalling pathway. Locations of cyclophilins are shown in red boxes (PM = plasma membrane, EC = extracellular, ER = Endoplasmic Reticulum) next to the steps of a response they could interact with.*

6.2 Results

6.2.1 Cyclophilins suppress the TLR-activated immune response independent of Calcineurin

My hypothesis was that one or more of the cyclophilins are regulators of the innate immune response. From the current literature it is unclear if they will be pro-inflammatory, or anti-inflammatory. Therefore, I initially screened the response of iPSC-derived macrophages to a panel of TLR agonists or TNFα and measured the secretion of TNFα 24 hours after stimulation. To determine if any cyclophilin was regulating the response, I treated the macrophages with 1 µM cyclosporine A (CsA) simultaneous to stimulation (Figure 3A). In cells plated at $1x10^5$/well of a 96-well plate, TNFα secretion significantly increased 5.34-fold after stimulation of TLR1/TLR2 (Pam3CSK4 stimulation), and 5.17-fold after TLR2/TLR6 (FSL-1) stimulation. A small but significant 1.32-fold increase in TNFα secretion was observed after stimulation of the intracellular TLR, TLR3 (Polyinosinic:polycytidylic acid, Poly(I:C)). A trend towards significance was also observed after LPS (TLR4) stimulation. However, results from this stimulation assay were highly variable. In Chapter 4, I showed how a major cause of variability in the TLR response by iPSC-derived macrophages is the density at which they are plated. This observation was originally made while investigating the role of cyclophilins in innate immunity shown here. I found that reducing the density of plated cells to $5x10^4$/well of a 96-well plate reduced the fold-change in TNFα secretion by macrophages treated with 1 µM CsA to ≤2 (Figure 3B). Excluding post TNFα stimulation, CsA treated macrophages remained more responsive to stimulation, with LPS and Flagellin (TLR5) now significantly more responsive, although the response to TLR3 was no-longer significant. While CsA inhibits binding and PPIase activity, it also causes a gain-of-function interaction with calcineurin (Cn), preventing it from phosphorylating NFAT (617). To ensure that the increased TNFα secretion by CsA treated cells is cyclophilin and not Cn-dependent, I stimulated macrophages with LPS in the presence of CsA, the non-Cn-interacting (non-immunosuppressive) analogue, NIM811 (712), or the alternative Cn inhibitor FK506 over a range of drug concentrations (Figure 3C).

When compared to untreated-cell TNFα secretion, CsA appeared to have a bimodal influence on the innate response. At low concentrations (0.25 and 0.5 μM), CsA significantly suppressed TNFα secretion. At higher concentrations (2.5 and 5μM), however, secretion was enhanced. If treated with NIM811 on the other hand, TNFα was significantly enhanced by doses between 0.25 and 5 μM. For both CsA and NIM811, very high doses (10-20 μM) did not significantly increase TNFα secretion, but this was due to drug toxicity (Figure 3D). Inhibition of Cn by FK506 resulted in TNFα suppression at all doses without any toxicity (Figure 3C-D). Overall, inhibiting at least 1 cyclophilin enhances the macrophage response to TLR stimulation, and this is independent of Cn.

6.2.2 Inhibition of cyclophilins alters mRNA levels of multiple cytokines early after LPS stimulation while Cn effects are delayed

Having shown that cyclophilin inhibition causes an increase in TNFα secretion after TLR stimulation, I next sought to determine how they regulate inflammation. I first measured mRNA levels of several cytokines after LPS stimulation. However, before I could analyse any potential changes in mRNA levels, it was important to first select appropriate housekeeper genes to compare against. To do this I measured changes in mRNA levels of five candidate genes, GAPDH, HMBS, B2M, 18S, and TBP, in unstimulated and LPS stimulated cells, at either 4 or 6 hours post stimulation, and at 24 hours post stimulation. I found that the commonly used housekeeper GAPDH showed a clear increase in mRNA (decreased qPCR Ct value) for 24 hours (Figure S1A-B). Likewise, HMBS mRNA levels changed not only after LPS stimulation, but also over time in unstimulated cells (Figure S1C-D). Therefore, neither GAPDH nor HMBS are appropriate housekeepers for my study. B2M, 18S, and TBP on the other hand did not appear to consistently change over time in unstimulated and LPS-stimulated cells (Figure S1E, G, and I). However, B2M mRNA did significantly differ between unstimulated and stimulated cells while TBP and 18S did not (Figure S1F, H, and J). Therefore, I proceeded to analyse all future mRNA quantification against an average of these two genes.

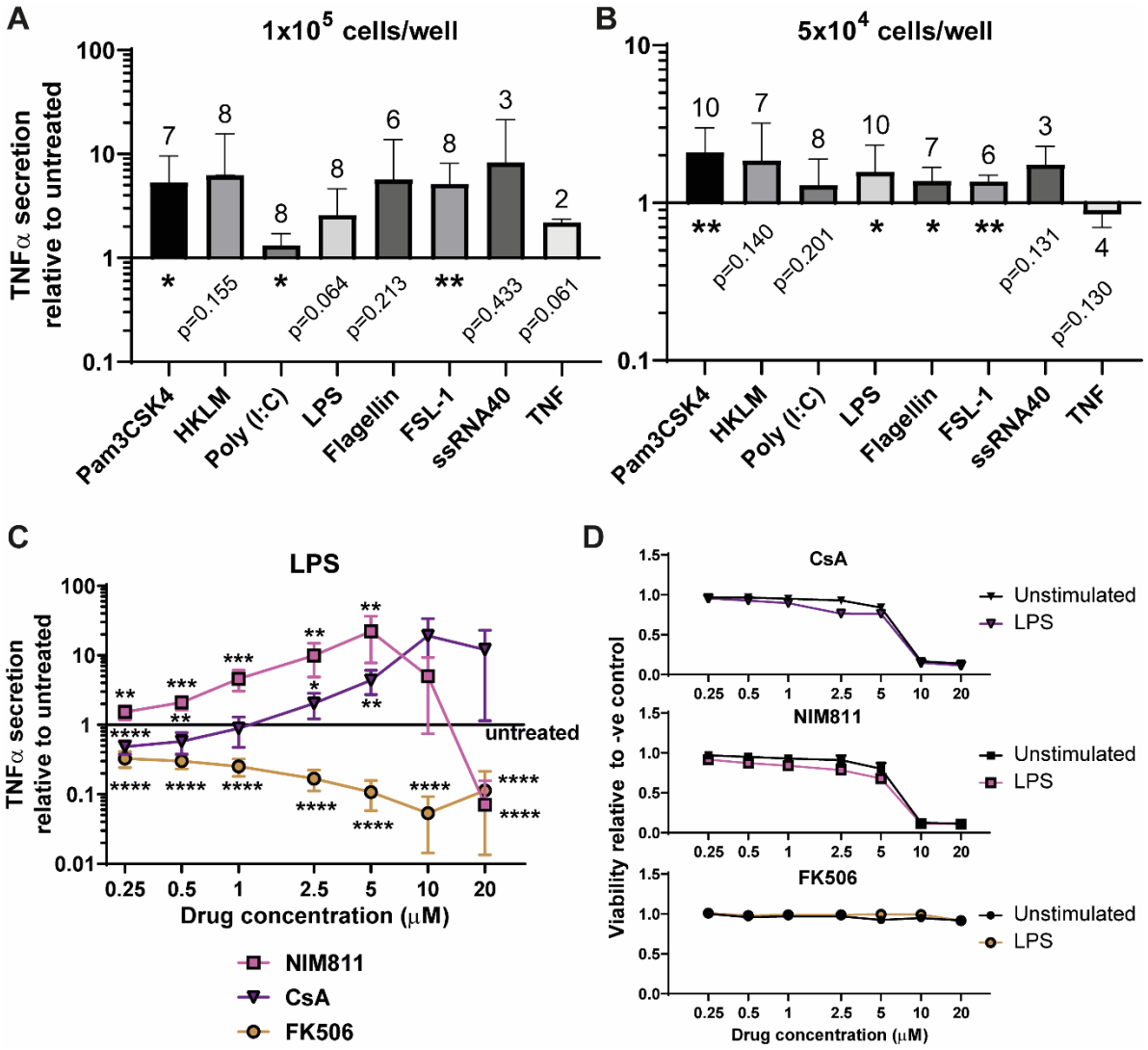


Figure 3: Cyclophilins suppress the TLR response in macrophages. *Secretion of TNFα 24 hours after innate immune stimulation (TLR1-2; 1 µg/mL Pam3CSK4, TLR2; 108 cells/mL HKLM, TLR3; 10 µg/mL Poly(I:C), TLR4; 100 ng/mL LPS, TLR5; 1 µg/mL Flagellin, TLR2-6; 1 µg/mL FSL-1, TLR9; 10 µg/mL ssRNA40, TNFR; 10 ng/mL TNFα) by 1 µM CsA treated macrophages plated at A) 1x105 cells/well of a 96-well plate or B) 5x104 cells/well, normalised to untreated controls. Number of repeats for each agonist is displayed above each bar. C) TNFα secretion by macrophages 24-hours post stimulation with LPS, treated at the time of stimulation with CsA (purple), NIM811 (pink), or FK506 (gold). n=3. D) Viability of cells from part C after the 24 hour stimulation, n=1. Mean ± SD is displayed. A-C) Significance was calculated by one-sample t-test, theoretical mean = 1. Significance is shown when p<0.05 (*), <0.01 (**), <0.001 (***), <0.0001 (****).*

I first measured expression of the pro-inflammatory cytokines TNFα, IL-6, and IL-1β, the anti-inflammatory cytokine IL-10, the IFN-γ induced cytokine CXCL10, and the antiviral cytokine IFN-β, 4 hours after LPS stimulation in the presence of NIM811 or FK506. Stimulation with LPS clearly induced expression of all these genes above that of unstimulated cells, with observable differences in TNFα, IL-1β, and CXCL10 between drug treated and untreated cells (Figure 4A-F). When normalised to the LPS-stimulated untreated control I found a significant increase in total TNFα (ratio of 2.42 ± 0.692) and IL-1β (1.42 ± 0.209), and decrease in CXCL10 (0.408 ± 0.099) in NIM811 treated cells (Figure 4G-H, K). IL-10 also displayed a trend towards a significant reduction with a ratio of 0.814 ± 0.148 p=0.087 (Figure 4J). On the other hand, FK506 treatment had no effect on mRNA levels for any of the genes measured at this time point.

By 24 hours, expression of all genes had clearly declined (Figure 5A-E), and IFN-β was not able to be detected in either unstimulated or LPS stimulated cells. TNFα and CXCL10 levels were comparable between unstimulated and LPS-stimulated cells (Figure 5A, E) while IL-1β and IL-6 remained ≥10-fold higher in stimulated cells (Figure 5B-C). Now, when normalised against the LPS-stimulated untreated control, only IL-1β was significantly higher in NIM811 treated cells (ratio 1.23 ± 0.113) (Figure 5H). IL-6, IL-10 and CXCL10 all showed a trend towards increased mRNA (p=0.170, 0.176 and 0.072, respectively) (Figure 5I-K). In FK506 treated cells, TNFα, IL-1β, and IL-10 all remained insignificantly different from the untreated control (Figure 5G-H, J). However, IL-6 and CXCL10 were both significantly suppressed, with ratios of 0.716 ± 0.084 and 0.264 ± 0.072, respectively, compared to the untreated control (Figure 5I, K). Furthermore, CXCL10 mRNA levels were lower even than unstimulated cells (Figure 5E). In conclusion, inhibition of cyclophilins exerts a clear regulatory effect on mRNA expression of inflammatory cytokines over a 24-hour period, while inhibition of Cn suppresses inflammatory cytokine mRNA levels later than 4 hours post stimulation.

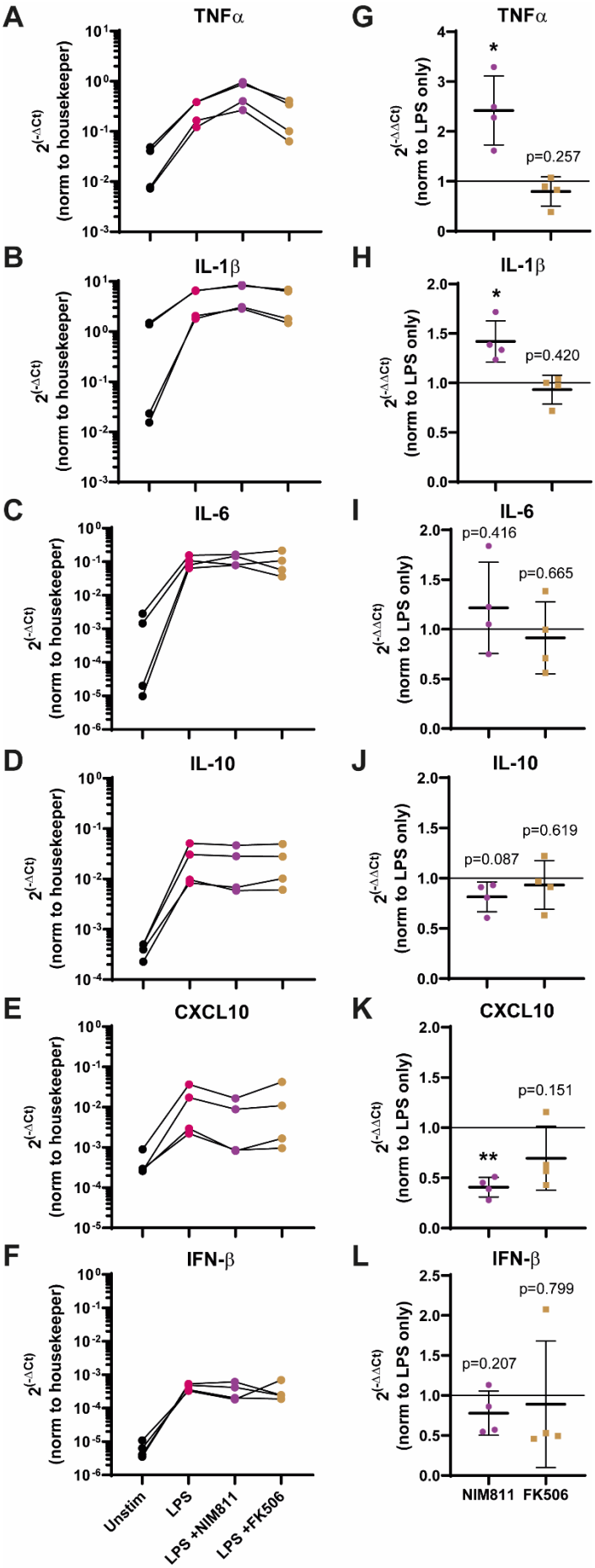


Figure 4: Inhibition of cyclophilins, but not calcineurin, alters inflammatory cytokines expression 4 hours after LPS stimulation.

A-F) Quantification of A) TNFα, B) IL-1β, C) IL-6, D) IL-10, E) CXCL10, F) IFN-β mRNA 4 hours post LPS (1 ng/mL) stimulation relative to the average of 2 housekeepers (TBP and 18S) expressed as fold difference in Ct value. n=4 where 2 independent WT clones were used across 2 independent experiments. J-L) Normalisation of mRNA expression in NIM811 and FK506 treated macrophages stimulated with LPS to the untreated, LPS stimulated control. Mean ± SD is displayed. Significance was calculated by one-sample t-test, theoretical mean = 1. Significance is shown when p<0.05 (*), <0.01 (**), <0.001 (***), <0.0001 (****).

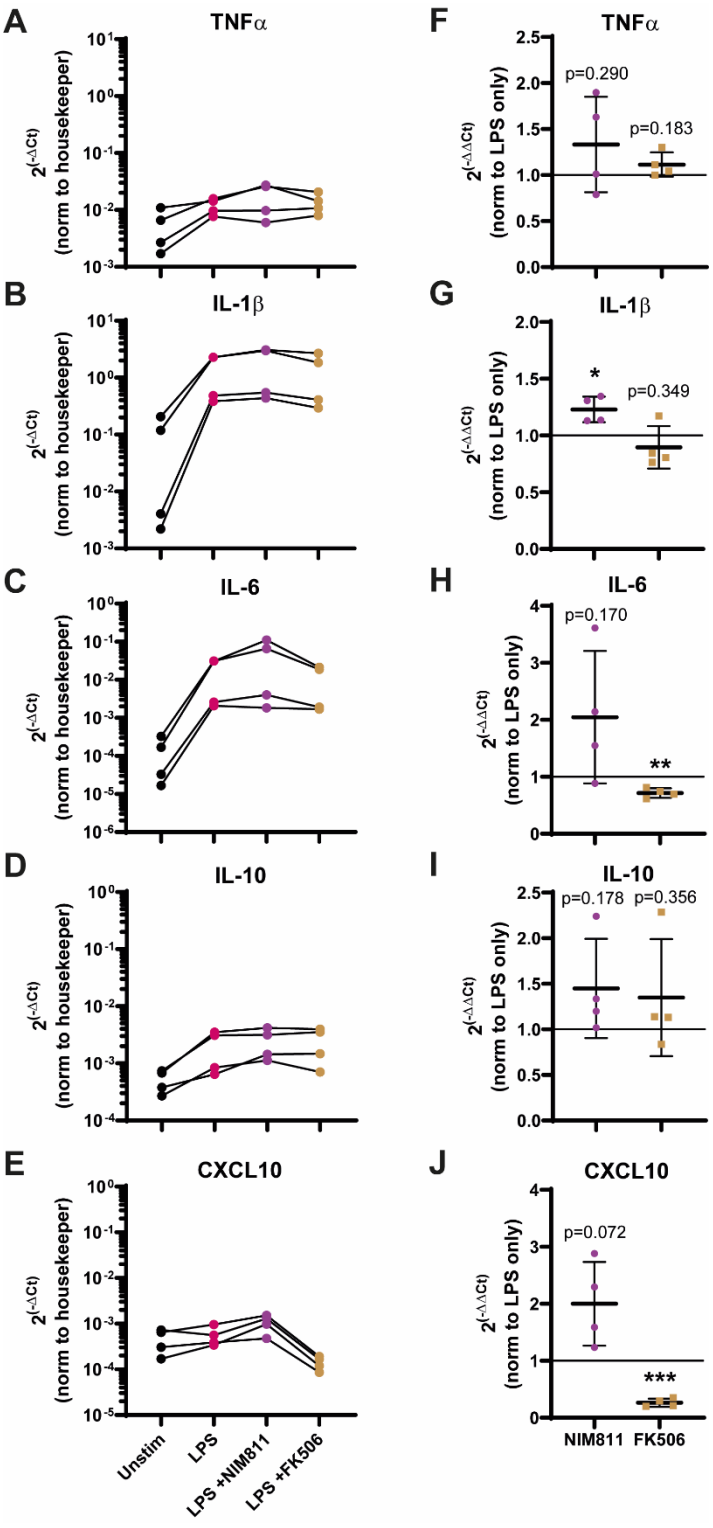


Figure 5: Inhibition of cyclophilins prolongs increased expression of cytokines, while calcineurin inhibition induces tolerance-like state.

A-F) Quantification of A) TNFα, B) IL-1β, C) IL-6, D) IL-10, E) CXCL10 mRNA 24 hours post LPS (1 ng/mL) stimulation relative to the average of 2 housekeepers (TBP and 18S) expressed as fold difference in Ct value. n=4 where 2 independent WT clones were used across 2 independent experiments. F-J) Normalisation of mRNA expression in NIM811 and FK506 treated macrophages stimulated with LPS to the untreated, LPS stimulated control. Mean ± SD is displayed. Significance was calculated by one-sample t-test, theoretical mean = 1. Significance is shown when p<0.05 (*), <0.01 (**), <0.001 (***), <0.0001 (****).

6.2.3 Preliminary tests do not show clear changes in downstream signalling when cyclophilins or Cn are inhibited

Cyclophilins have been reported to interact with multiple components of the TLR signalling pathway. These include the TAB proteins (TAB2 and TAB3) (365), NF-κB (713), and the MAPKs; ERK1/2, p38, and JNK (635, 714). Cn, on the other hand, influences the inflammatory response via NFAT regulation, or through direct interactions with TLR2, TLR4, TRIF, and MyD88 (616). A diagram of these signalling pathways from British Society for Immunology, 2019, is shown in Figure 6A.

I therefore ran a preliminary experiment to measure by western blotting the activation state of these mediators as indicated by phosphorylation. Macrophages were stimulated for 30 minutes, 1 hour, or 4 hours with 1 ng/mL LPS in the presence of either 2.5 μM NIM811 or 5 μM FK506. Phosphatase inhibitors were not included though and will be needed in future repeats. I first measured phosphorylation of components of the NF-κB activation pathway starting at IKK, which in turn phosphorylates IκB, targeting it for degradation after ubiquitination, releasing NF-κB. NF-κB can also be transactivated by TBK1 and IKKε by phosphorylation of Ser536 which I measured here (716). As expected, I observed transient phosphorylation of the IKKα/β complex (Figure 6B) accompanied with a loss of IκB after 1 hour (Figure 6C). Phosphorylation of NF-κB was detected as early as 30 minutes post stimulation and was maintained beyond 4 hours (Figure 6D). Unfortunately, problems with protein transfer during blotting made it impossible to interpret the 30-minute timepoint of IKKβ and p-NF-κB, but there was no clear indication that phosphorylation of any signalling component significantly changed in the presence of NIM811 or FK506. Similarly, activation of the MAPKs p38 (Figure 6E), ERK1/2 (Figure 6F), and JNK (Figure 6G) did not appear to be influenced by the addition of these drugs. There may be a possible subjective difference in p38 phosphorylation at 30 minutes in FK506 treated cells, and 4 hours with NIM811 but further repeats are needed to test if these are artefacts from the protein transfer (Figure 6E Top). Overall, I did not find any clear evidence for changes in phosphorylation of intracellular signalling proteins after TLR4 activation, but repeats are needed.

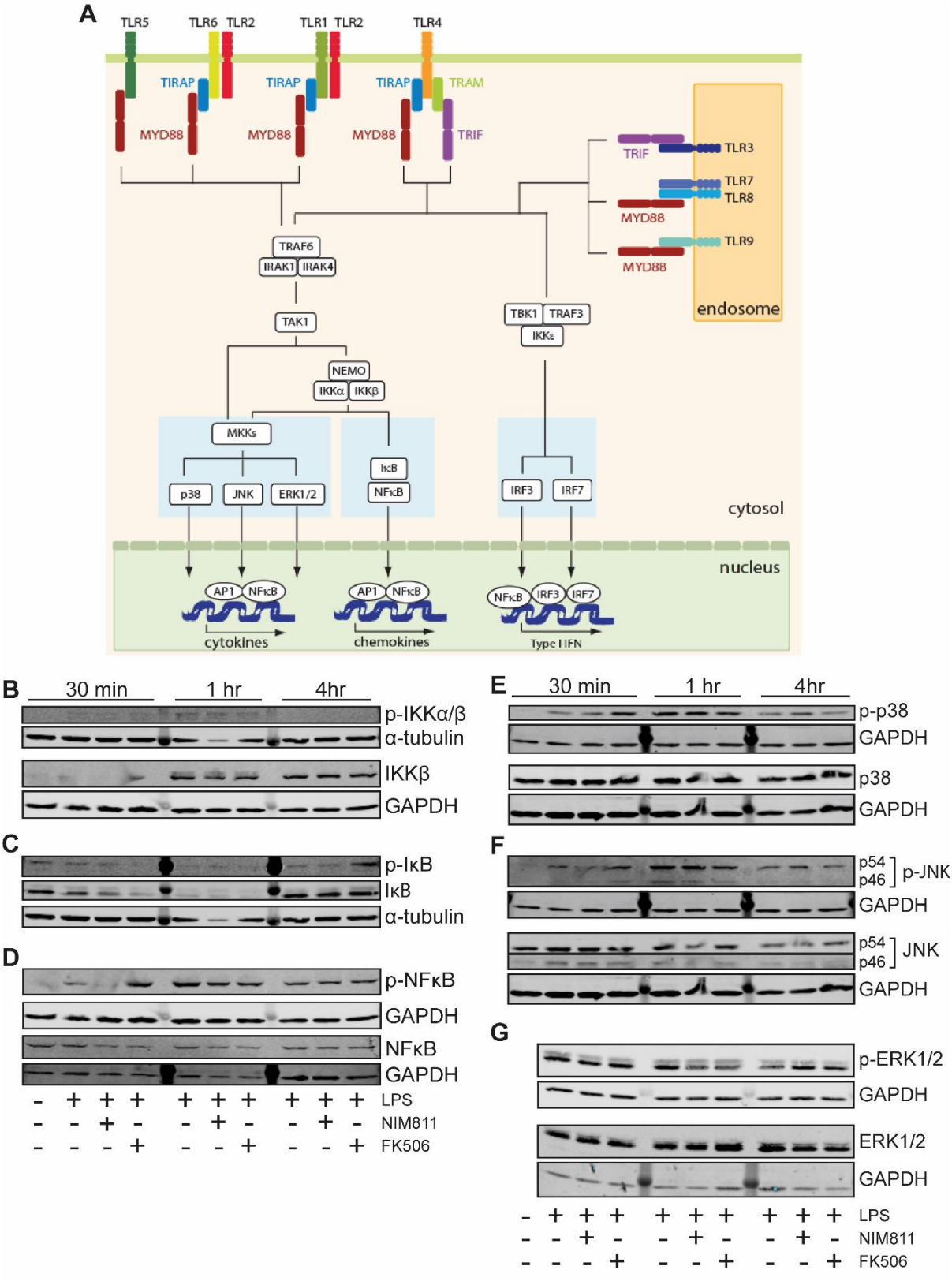

A
TLR5
TLR6 TLR2
TLR1 TLR2
TLR4
TIRAP
TIRAP
TIRAP
TRAM
MYD88
MYD88
MYD88
TRIF
TRIF
TLR3
TLR7
TLR8
MYD88
TLR9
MYD88
endosome
TRAF6
IRAK1 IRAK4
TAK1
TBK1 TRAF3
IKKε
NEMO
IKKα IKKβ
MKKs
IκB
NFκB
p38
JNK
ERK1/2
IRF3
IRF7
cytosol
nucleus
AP1 NFκB
AP1 NFκB
NFκB IRF3 IRF7
cytokines
chemokines
Type I IFN
B
30 min
1 hr
4hr
p-IKKα/β
α-tubulin
IKKβ
GAPDH
C
p-IκB
IκB
α-tubulin
D
p-NFκB
GAPDH
NFκB
GAPDH
LPS
NIM811
FK506
E
30 min
1 hr
4hr
p-p38
GAPDH
p38
GAPDH
F
p54
p46
p-JNK
GAPDH
p54
p46
JNK
GAPDH
G
p-ERK1/2
GAPDH
ERK1/2
GAPDH
LPS
NIM811
FK506

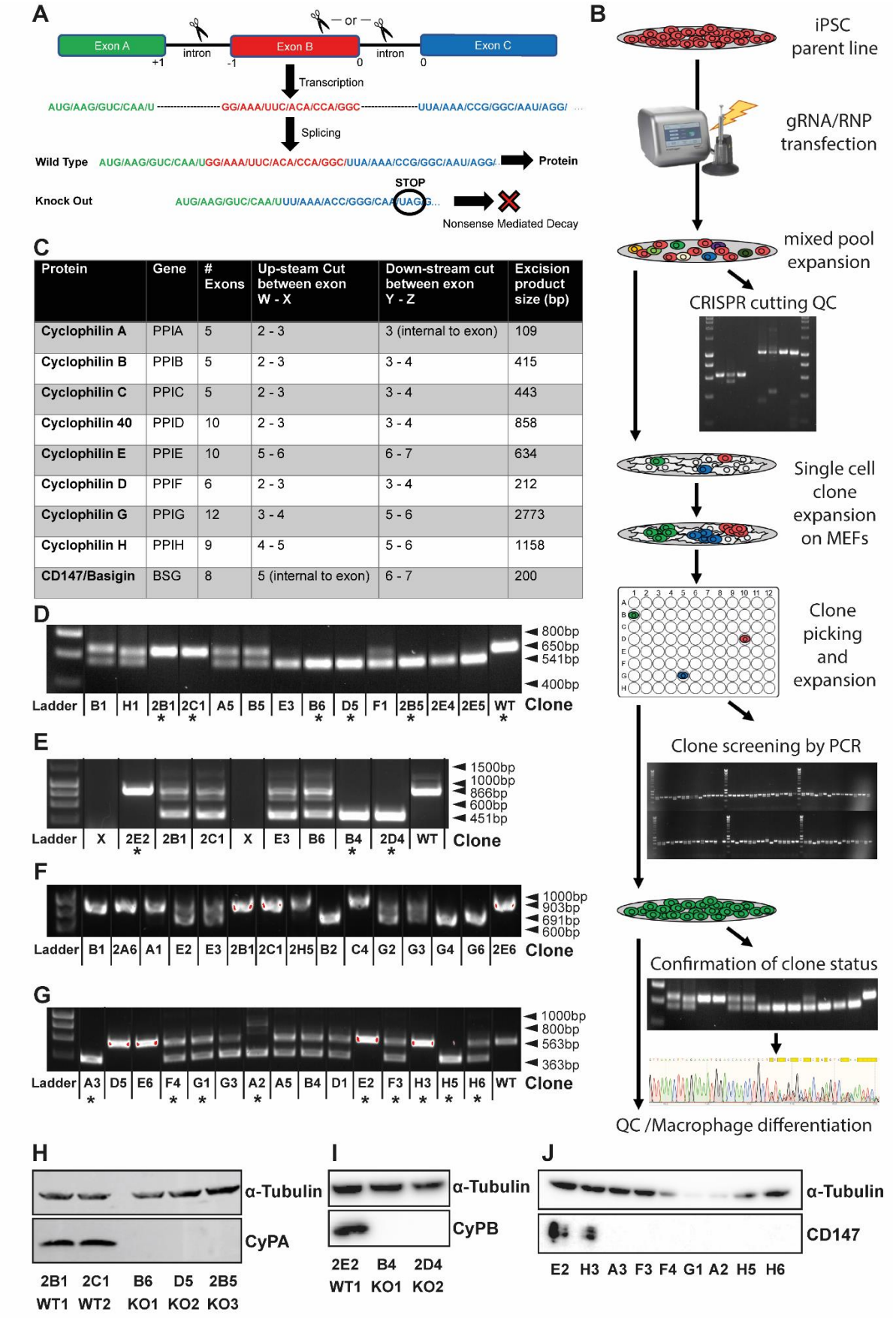
Figure 6: Preliminary investigation into activation of TLR intracellular signalling components *A) Schematic of the TLR signalling pathway adapted from The British Society for Immunology 2019. B-G) Western blotting for phosphorylated and total protein content in macrophages stimulated ±LPS (1 ng/mL) in the presence of NIM811 (2.5 μM) or FK506 (5μM) for 30 minutes, 1 hour or 4 hours. B) IKKα/β compared to GAPDH as a housekeeper, C) IκB compared to α-tubulin, D) NF-κB relative to GAPDH, E) p38 compared to GAPDH, F) JNK compared to GAPDH, and G) ERK1/2 compared to GAPDH. For G) blotting was done on PPIA-/- macrophages.*

6.2.4 Generation of cyclophilin knockouts: CyPA, CyPB, CyPD, and the cyclophilin receptor CD147

Having established that cyclophilins are involved in regulation of the innate immune response, I continued my plan to KO multiple members of the family using CRISPR-Cas9. To make screening for edited clones easier, I utilised a double guide RNA (gRNA) approach to remove entire exons/exon-intron junctions, first described by the Zhang group (717). Criteria for the selection of suitable exons to remove were: 1. They are shared by all splice variants, 2. Exons to either side of the chosen exon are out of frame with each other, and 3. The targeted exon preferably contains essential residues for protein function. By removing an exon flanked by out of frame neighbouring exons, after splicing of transcribed RNA has occurred, the combination of two out of frame exons will cause a frame shift mutation that results in an early stop codon being introduced into the mRNA. This will then trigger NMD and the suppression of this gene. A schematic of this methodology is shown in Figure 7A. A complete methodology is reported in Chapter 2: Materials and Methods section and a summary diagram is shown in Figure 7B. Importantly, successful editing was determined by the appearance of a second, smaller, band in an agarose gel after PCR across the edited location, indicating removal of the targeted exon. This streamlined the cost and speed of KO efficiency evaluation compared to small indel forming approaches that require sequencing or high-resolution melting (HRM)

qPCR analysis. PCR analysis was done 3 times during the editing process. First on the pooled edited iPSC before single cell cloning to ensure gRNA cutting efficiency. Second on individual clones, and finally on the expanded clonal population master stock. This master stock was then ready for sequencing, quality control, and differentiation into macrophages.

My initial plan was to KO half of the known cyclophilins, all of which are reported to bind CsA (366), and the known cell surface receptor for cyclophilins CD147. The selected cyclophilins are listed in Figure 7C with their gene names, exons targeted for excision, and the size of the resulting excised product. However, I was unable to efficiently identify any KO clones for *PPIC*, *PPID*, and *PPIG*, and although there was clear evidence of cutting occurring within *PPIE* and *PPIH*, no double allele KO of either gene were identified (data not shown). However, I was successful in identifying multiple single allele and double allele KO for CyPA (*PPIA*), CyPB (*PPIB*), CyPD (*PPIF*), and CD147 (*BSG*) as shown by the PCR of individual clones in Figures 7D-G, respectively. By PCR I identified 6 *PPIA*-/- clones (Figure 7D), 2 *PPIB*-/- clones (Figure 7E), 3 *PPIF*-/- clones (Figure 7F), and 2 *BSG*-/- clones (Figure 7G). These clones were confirmed as KO by sequencing (*PPIA* Figure S2A, *PPIB* S2B, *PPIF* S2C, and *BSG* S2D). Interestingly, sequencing of both the single allele and double allele KO for BSG found that many of the single allele KO identified by PCR were actually double allele KO. Finally, I confirmed that removal of an exon prevented protein expression by measuring total CyPA (Figure 7H), CyPB (Figure 7I), and CD147 (Figure 7J) in the clones identified in Figures 7D, E, and G with asterisks (*). Of these, the CyPA and CyPB clones were then used for differentiation into macrophages for assaying their role in innate immunity but there was insufficient time to investigate CD147.



Protein	Gene	# Exons	Up-steam Cut between exon W - X	Down-stream cut between exon Y - Z	Excision product size (bp)
Cyclophilin A	PPIA	5	2 - 3	3 (internal to exon)	109
Cyclophilin B	PPIB	5	2 - 3	3 - 4	415
Cyclophilin C	PPIC	5	2 - 3	3 - 4	443
Cyclophilin 40	PPID	10	2 - 3	3 - 4	858
Cyclophilin E	PPIE	10	5 - 6	6 - 7	634
Cyclophilin D	PPIF	6	2 - 3	3 - 4	212
Cyclophilin G	PPIG	12	3 - 4	5 - 6	2773
Cyclophilin H	PPIH	9	4 - 5	5 - 6	1158
CD147/Basigin	BSG	8	5 (internal to exon)	6 - 7	200

Figure 7: Making cyclophilin knock-out iPSC lines*. A) Schematic of duplex CRISPR-Cas9 to knock out a gene by inducing nonsense mediated decay. +1, 0, -1 represent number of bases since the last codon. B) Schematic of the protocol for making knock-out iPSC lines. C) Table of the cyclophilins targeted for CRISPR-cas9 editing. D-G) PCR products of iPSC edited for D) PPIA, E) PPIB, F) PPIF, G) BSG. H-J) Western blotting of iPSC wild type and knock-out clones for H) PPIA, I) PPIB, J) BSG.*

6.2.5 Knocking out CyPA does not influence iPSC-derived macrophage differentiation

There have been reports that CyPA is potentially essential for or enhances M-CSF dependent macrophage differentiation (676, 718). Therefore, I first had to establish that there was no difference in the differentiation state of mu *PPIA*-/- cells. I found that surface staining for the macrophage markers CD14, CD16, CD45, CD68, CD86, and CD163 on parental WT macrophages (840, Figure 8A) a clonal WT line that has been through the editing process (2C1, Figure 8B) and three *PPIA*-/- clones (B6, D5, 2B5, Figure 8C-K) showed no significant difference in expression between WT and KO lines. To test if basic functions of the macrophages may be affected, I also measured the phagocytic uptake of Alexa-488 conjugated zymosan. Again, no difference was observed between clonal lines (Figure 8L). Therefore, CyPA KO has no obvious impact on macrophage phenotype and phagocytic functionality, and is therefore not essential for iPSC-derived macrophage differentiation.

6.2.6 Knocking out CyPA does not cause a compensatory upregulation of other cyclophilins

Given that the cyclophilin family is a large, highly conserved family, there are concerns of redundancy between members exists and that knocking out one member may result in a compensatory upregulation of another member (719). I therefore designed a panel of qPCR primers for 16 members of the family (excluding PPIL6 due to personal oversight) to measuring gene expression. Primers were either selected from previous literature or designed

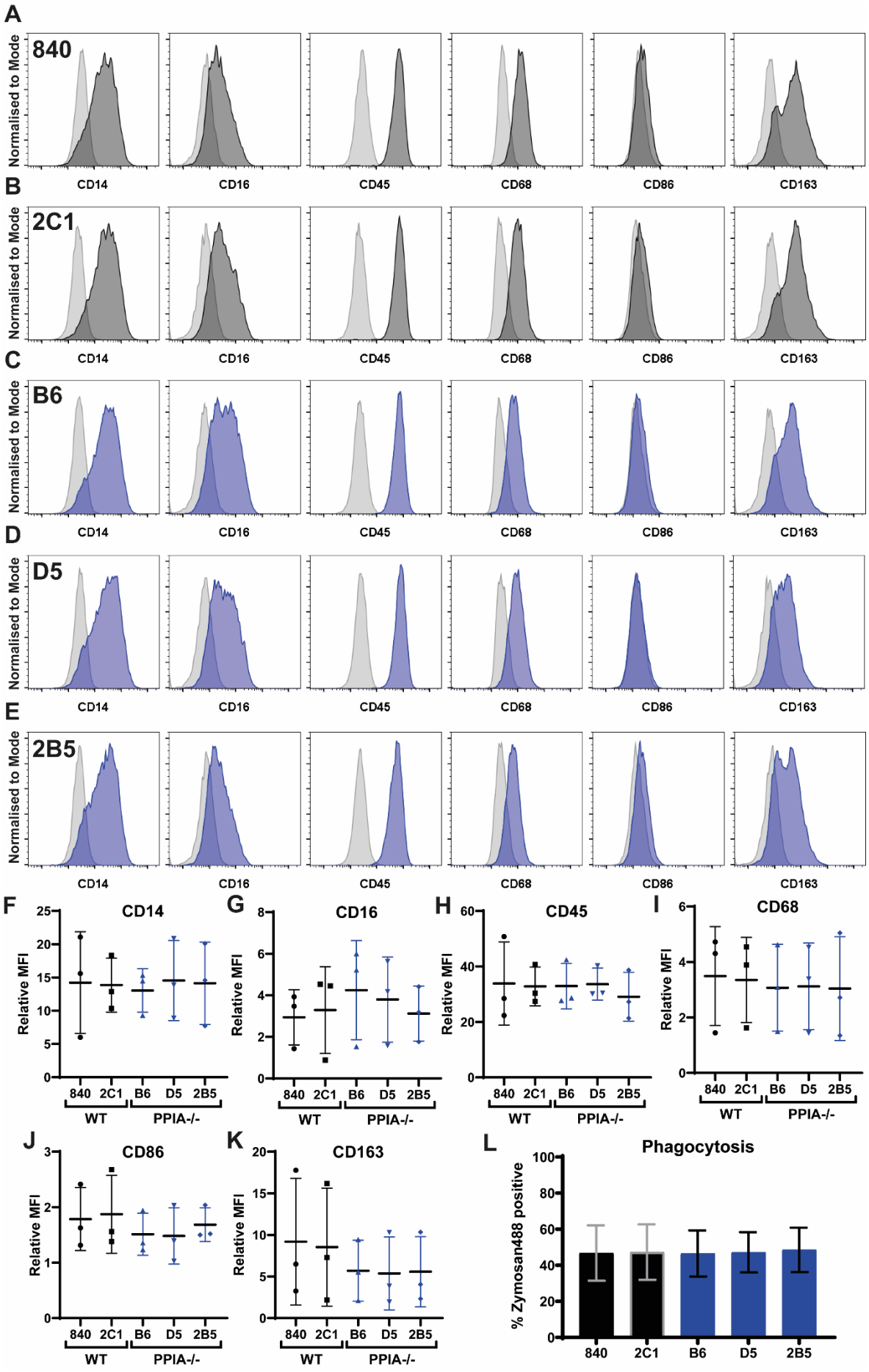

A
840
Normalised to Mode
CD14
CD16
CD45
CD68
CD86
CD163
B
2C1
C
B6
D
D5
E
2B5
F
CD14
Relative MFI
840 2C1 B6 D5 2B5
WT
PPIA-/-
G
CD16
H
CD45
I
CD68
J
CD86
K
CD163
L
Phagocytosis
% Zymosan488 positive

Figure 8: Knocking out PPIA expression does not affect iPSC-derived macrophage differentiation. *A-E) Flow cytometry histograms for surface expression of CD14, CD16, CD45, CD68, CD86, and CD163. Expression is shown in A-B) black (WT clones) and C-E) blue (PPIA-/- clones) compared to isotype staining controls in grey. 840 is the parental SFC840-03-03 cell line. F-K) Quantification of surface protein expression relative to the isotype control for WT and PPIA-/- for F) CD14, G) CD16, H) CD45, I) CD68, J) CD86 and K) CD163. n=3 independent expreiments. L) Percentage of macrophages that have taken up Alexa-488 conjugated zymosan coated beads by phagocytosis. WT clones are shown in black and PPIA-/- clone in blue. n=8 independent experiments.*

---

using the NCBI Primer BLAST tool. As an extra precaution, I used OligoEvaluator (Sigma) to predict secondary structure and primer dimer formation. Having selected desired primers, I optimised the necessary temperature and primer concentration by standard PCR of complementary DNA (cDNA) and genomic DNA (gDNA). With the exception of *PPIA*, all my primers either did not amplify gDNA, or amplified gDNA with a clear difference in size that could be distinguished either by electrophoresis (Figure S3A) or by melting temperature (T_m) (Figure S3C). Surprisingly, all 10 pairs of *PPIA* primers used, published (365, 720–723) and unpublished, amplified gDNA with the same size and comparable melting T_m as cDNA making them unsuitable for qPCR using intercalating dyes such as SYBR-green. Final primer sequences and optimised PCR cycling conditions for the cyclophilins and 2 housekeeper genes are listed in Table 2.

I quantified expression of the cyclophilins compared to the average housekeeper expression in unstimulated macrophages from 2 WT and 2 *PPIA*-/- clonal lines (Figure 9A). The most highly expressed cyclophilins were *PPIA*, *PPIB*, and *PPIF*, and the lowest were *PPIC*, *PPIL3* and *NKTR*. Despite the potential for amplification of gDNA, a clear reduction in *PPIA* expression was detected in *PPIA*-/- cells as expected. When normalised against the parental line (840), this reduction in *PPIA*-/- cells was to ~35% of the level in WT cells (Figure

9B). *PPIA* KO had no effect on expression of any other cyclophilin relative to the parental line indicating transcriptional compensation does not occur in unstimulated *PPIA-/-* macrophages.

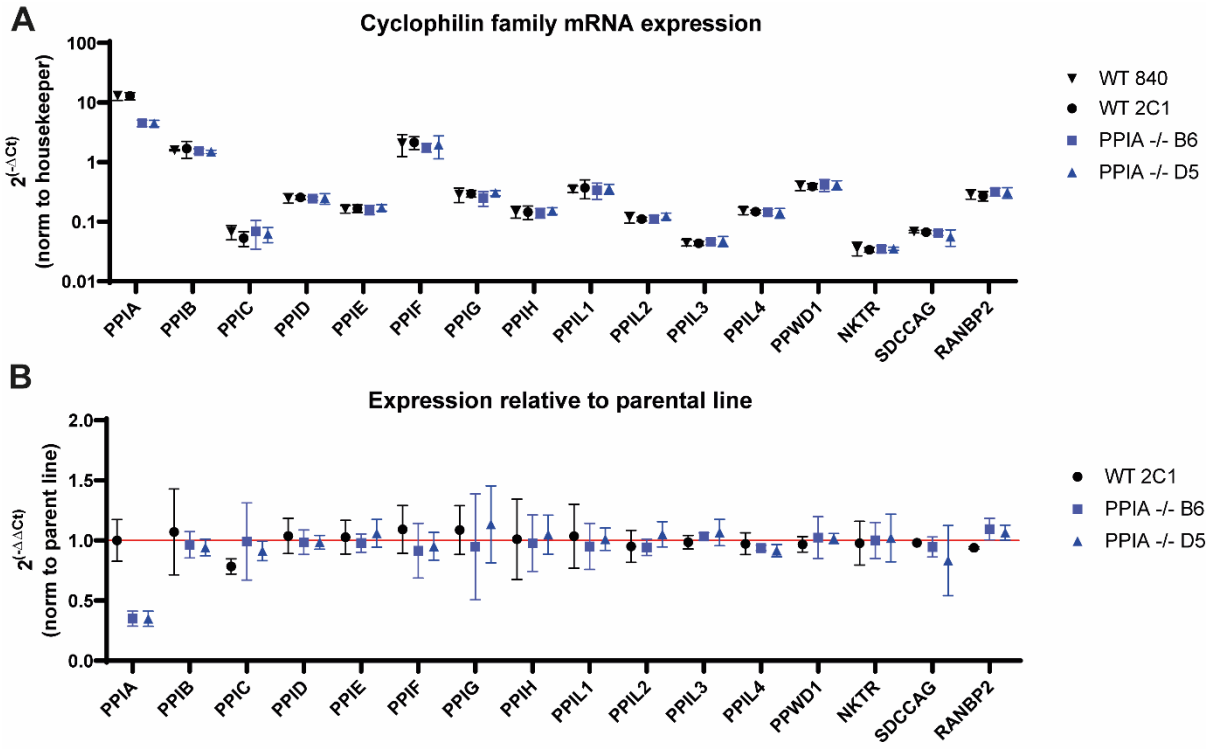


Figure 9: Knocking out PPIA does not result in a compensatory increase in expression of another cyclophilin. *Expression of the cyclophilin family members in unstimulated WT and PPIA-/- macrophages quantified by qPCR and displayed as A) fold difference in Ct (ΔCt) compared to the average of 2 housekeepers (B2M and TBP) and B) ΔΔCt comparing against expression in the parental SFC840-03-03 line.*

Gene	Forward primer	Reverse Primer	Anneal Tm (°C)	Primer conc. (nM)	Primer Efficiency (%)	cDNA melt curve Tm (°C)	cDNA melt curve intensity	gDNA melt curve T_m (°C)	gDNA melt curve Intensity	Reference
PPIA *	AACTTCATCCTAAAGCATACGG	TTGCCATCCAACCACTCAG	60	400	90.68	80.50 ± 0.07	$7.67 \times 10^4 \pm 1.19 \times 10^3$	77.45 ± 10.39	$2.35 \times 10^4 \pm 1.63 \times 10^3$	(365)
PPIB	TTCCATCGTGTAATCAAGGACT-TC	GCTCACCGTAGATGCTCTTTC	60	400	98.36	79.64 ± 0.07	$8.02 \times 10^4 \pm 2.46 \times 10^3$	83.05 ± 5.09	$8.74 \times 10^3 \pm 6.76 \times 10^3$	(724)
PPIC	AGCAAGTTTCATCGTGTCATCA	TGGAAATGTCTCACCATAGA-TGC	60	400	102.3	78.59 ± 0.07	$1.07 \times 10^5 \pm 4.89 \times 10^3$	84.57 ± 4.42	$9.85 \times 10^3 \pm 1.20 \times 10^4$	(725)
PPID	AGGCATTGGACACACGACTGG	AACCCTCCCGATCATGCTTGT	60	400	105.26	76.55 ± 0.07	$1.25 \times 10^5 \pm 5.74 \times 10^3$	80.09 ± 9.60	$2.01 \times 10^4 \pm 1.57 \times 10^4$	(726)
PPIE	CTTGTACGTGGGTGGACTGG	GCTCAGATTCATTCATGTTGT-CG	64	400	100.25	79.68 ± 0.07	$1.07 \times 10^5 \pm 1.31 \times 10^3$	81.69 ± 2.38	$1.93 \times 10^4 \pm 1.97 \times 10^3$	N/A
PPIF	TTACACTGAAGCACGTGGGG	TGCCATCCAACCAGTCTGTC	60	400	98.29	81.27 ± 0.11	$5.44 \times 10^4 \pm 6.51 \times 10^2$	74.81 ± 7.92	$1.03 \times 10^4 \pm 3.75 \times 10^3$	N/A
PPIG	TCTACCGGTGCAGGAGCA	GTTCTCGCATGTTTTGGGGC	66	100	95.95	77.66 ± 0.00	$7.46 \times 10^4 \pm 3.89 \times 10^3$	81.66 ± 0.13	$1.31 \times 10^4 \pm 4.28 \times 10^3$	N/A
PPIH	ATGGCGGTGGCAAATTCAAG	GGCACAACGTCTGCAAAGAG	64	200	103.53	80.81 ± 0.07	$8.59 \times 10^4 \pm 5.27 \times 10^3$	86.62 ± 0.06	$4.90 \times 10^4 \pm 1.44 \times 10^3$	(727)
PPIL1	ACTTGAAATTCACGGGGGCT	CTATGCCCTGACACACTCGG	64	100	105.06	83.94 ± 0.07	$3.96 \times 10^4 \pm 5.78 \times 10^2$	79.60 ± 7.38	$1.43 \times 10^4 \pm 8.89 \times 10^3$	N/A
PPIL2	AAGAAGCCAGATCTCCCACAA	GGAGTGCAGACTGGGTAGAC	64	100	98.77	78.89 ± 0.00	$5.85 \times 10^4 \pm 9.76 \times 10^2$	91.71 ± 0.11	$1.76 \times 10^3 \pm 1.09 \times 10^2$	N/A
PPIL3	AACAGACCTCTGCTGGCATC	GCGAGCTCAAAAATAAGTCT-TTGG	64	400	103.68	78.73 ± 0.11	$1.18 \times 10^5 \pm 7.43 \times 10^3$	80.54 ± 2.93	$2.72 \times 10^4 \pm 7.60 \times 10^3$	N/A
PPIL4 †	CCGCGTGCCTGCTTGAATTT	GCCAGTCCCTGTAGGATCGC-CA	60	400	99.22	75.63 ± 0.00	$1.61 \times 10^5 \pm 2.75 \times 10^3$	75.52 ± 0.00	$1.91 \times 10^5 \pm 1.34 \times 10^4$	N/A
PPWD1	TTCGTAGTCACCTGGGAGTT	TTGCATCCCCTGGGCAATAG	64	100	98.27	78.96 ± 0.00	$4.16 \times 10^4 \pm 2.49 \times 10^3$	71.22 ± 14.59	$1.30 \times 10^3 \pm 1.68 \times 10^2$	N/A
NKTR	TCGGAGCAGAGGATGGTACA	TGTAGGACCTGGATCGACTGT	64	100	96.20	82.96 ± 0.00	$6.40 \times 10^4 \pm 1.43 \times 10^3$	75.27 ± 13.22	$8.17 \times 10^3 \pm 9.88 \times 10^3$	N/A
SDCCAG	GATGGTGCTGTTGCCGAATAC	AGTGCAAGGGTCTGATCTTCC	66	100	105.95	77.96 ± 0.07	$8.02 \times 10^4 \pm 2.46 \times 10^3$	78.45 ± 0.00	$8.74 \times 10^3 \pm 6.76 \times 10^3$	N/A
RANBP2	TCAGGAAGCTCAAAAATCTCA-GAC	CATCACTTCAGTCCCACCTGT	64	100	106.34	75.05 ± 0.00	$9.31 \times 10^4 \pm 1.38 \times 10^3$	60.01 ± 0.00	$1.67 \times 10^3 \pm 3.17 \times 10^2$	N/A
TBP	GAACCACGGCACTGATTTTC	CCCCACCATGTTCTGAATCT	60	400	103.41	79.57 ± 0.11	$1.14 \times 10^5 \pm 5.68 \times 10^3$	81.41 ± 7.94	$3.43 \times 10^4 \pm 2.26 \times 10^4$	N/A
B2M	ACTGAATTCACCCCCACTGA	CCTCCATGATGCTGCTTACA	60	400	105.01	78.97 ± 0.07	$1.15 \times 10^5 \pm 3.03 \times 10^3$	78.27 ± 9.07	$9.11 \times 10^3 \pm 1.48 \times 10^4$	N/A

Table 2: Optimised cycling conditions for qPCR of the cyclophilin family. ** amplifies gDNA with same size and T_m as cDNA. † amplifies gDNA with different size but same T_m as cDNA (See Figure S3)*

6.2.7 CyPA potentially regulates the response to TLRs but is not the only cyclophilin involved

Having shown that CyPA KO does not affect macrophage differentiation and is not compensated for by upregulation of other CyPs, I could now analyse its role in the TLR response. I first measured the response to TLR1/2, -2, -3, -4, -5, and -2/6 stimulation compared to WT cells (Figure 10A). When the *PPIA*-/- results were compared against the WT cell TNFα secretion, it appeared that WT + CsA cells and *PPIA*-/- untreated cells secreted similar amounts of TNFα, while treating *PPIA*-/- cells with CsA increased this further (Figure 10A). However, if this is normalised against the WT untreated cells, only Poly(I:C) stimulated *PPIA*-/- + CsA cells showed a significant increase in TNFα secretion. Clonal variation across experimental repeats meant that WT + CsA results were not significantly different from the untreated control, only showing a trend towards significance in FSL-1 stimulated cells (p=0.082). Likewise, only *PPIA*-/- untreated cells stimulated with LPS or FSL-1 showed a trend towards increased TNFα secretion (p=0.082 and 0.099 respectively), along with LPS stimulated *PPIA*-/- + CsA cells (p=0.066). Given that treating *PPIA*-/- cells with CsA appeared to further increase TNFα secretion, it is likely that CyPA is not the only cyclophilin regulating the TLR response. To confirm this, I titrated CsA, NIM811 and FK506 on *PPIA*-/- cells stimulated with 1 ng/mL LPS. Like Figure 1C, NIM811 treatment at doses 0.25 – 10 μM significantly increased TNFα secretion from these cells, as did high doses of CsA (2.5 – 20 μM) (Figure 10C), and toxicity was observed at the top concentrations (Figure 10D, 3D). FK506 on the other hand reduced TNFα secretion across all doses. However, in *PPIA*-/- cells, the bimodal activity of CsA, specifically the reduction in TNFα secretion at low doses, was no longer observed, with 0.25 – 1 μM CsA not significantly changing TNFα secretion relative to the untreated control (Figure 10C, 3C). In conclusion, CyPA potentially regulates the response to TLR stimulation in macrophages, but the additive impact of pharmacological cyclophilin inhibition on this response indicates another cyclophilin is at play.

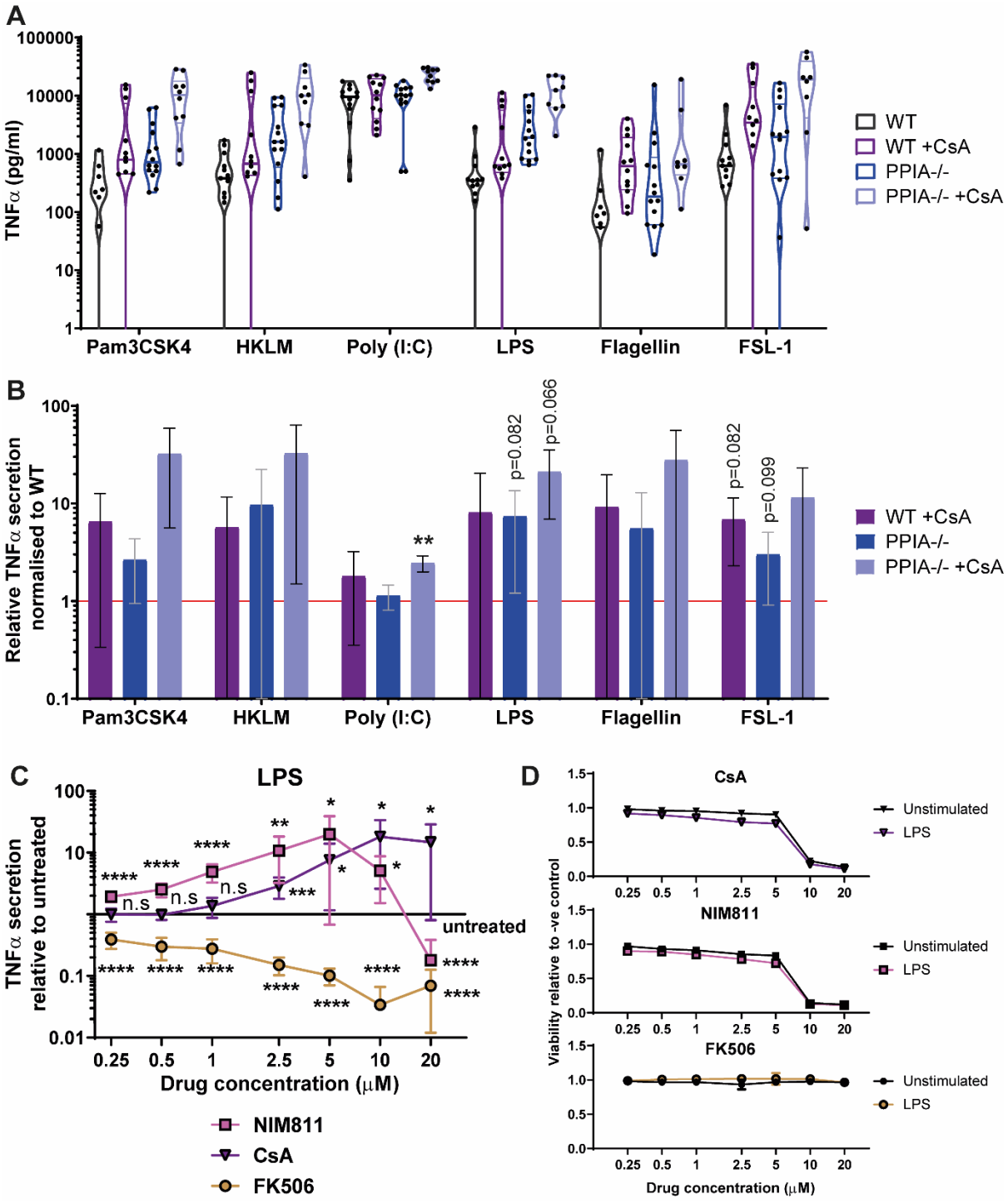


Figure 10: Cyclophilin A is not responsible for increased TNFα secretion after broad cyclophilin inhibition by CsA or NIM811. *A) TNFα secretion 24 hours post stimulation from WT and PPIA-/- macrophages treated ± 1 μM CsA at the time of stimulation with a panel of TLR agonists (TLR1-2; 1 μg/mL Pam3CSK4, TLR2; 10^8 cells/mL HKLM, TLR3; 10 μg/mL Poly(I:C), TLR4; 100 ng/mL LPS, TLR5; 1 μg/mL Flagellin, TLR2-6; 1 μg/mL FSL-1). WT n=13*

across 3 independent clones and 5 experiments. KO n=14 across 3 independent clones and 5 experiments B) Combined clone average TNFα secretion normalised to the average WT - CsA control. n=5 independent experiments. Mean ± SD. C) TNFα secretion by PPIA-/- macrophages 24-hours post stimulation with LPS, treated at the time of stimulation with CsA (purple), NIM811 (Pink), or FK506 (gold). n=3. D) Viability of cells from part C after the 24-hour stimulation, n=1. Mean ± SD is displayed. B-C) Significance was calculated by one-sample t-test, theoretical mean = 1. Significance is shown when p<0.05 (*), <0.01 (**), <0.001 (***), <0.0001 (****).

6.2.8 Differences in the innate response between WT and CyPA KO cells vary greatly over macrophage differentiation culture age, and may occur later than 24 hours post-stimulation

Considering the variability in response to stimuli between clones and experiments, I next sought to understand the causes to minimise these variables in the future. First, I tracked the TNFα response of macrophages differentiated from harvests of PreMac cells over the 14-week productive lifespan of one differentiation culture to evaluate the importance of culture age. I found that the TNFα response to 1 ng/mL LPS varied dramatically between weeks, ranging 136 ng/mL - 20.7 µg/mL (Figure 11A). Nevertheless, the response by *PPIA*-/- macrophages was overall significantly greater than WT macrophages. (Figure 11B). The TNFα response to 1 µg/mL Pam3CSK4 stimulation was also highly variable (range 45 ng/mL – 11.7 µg/mL), but showed the same weekly variation pattern as LPS (Figure 11C). Again, *PPIA*-/- macrophages overall produced more TNFα than WT cells (Figure 11D). Next, I ran a preliminary time course experiment over 24 hours stimulation with LPS to better understand the kinetics of the TNFα response by these macrophages (Figure 11E). Between 0 and 12 hours, the response by WT and KO macrophages was indistinguishable. By 24 hours, TNFα quantities declined compared to 12 hours post-stimulation, but an approximate 2-fold difference in TNFα secretion between WT and *PPIA*-/- cells was now observable. From the

same cell samples RNA was collected and expression of TNFα, IL-6, CXCL10, and IL-10 quantified (Figure 11F-I). No difference was observed between WT and KO samples for TNFα and IL-6 (Figure 11F-G). While there appeared to be a potential difference in CXCL10 and IL-10 expression at the 24-hour timepoint, this difference was not replicated in later independent experiments (Figure 11J-K). In summary, although highly variable between weeks of culture, *PPIA*-/- macrophages secrete significantly more TNFα in response to TLR stimulation, and this difference is potentially greatest ≥24 hours post-stimulation.

6.2.9 Cyclophilins and TLR-signalling are influenced by cell plating density

As part of my investigation into the source of variation in these experiments, I also evaluated the effect of plating the cells at $5x10^4$/well in a 96-well plate, and $1x10^5$/well. It was these observations that led to the description of DDRI examined in depth in Chapter 4. By applying the transcriptomic data from Chapter 4 to the cyclophilins and TLR signalling, I observed that 7/15 cyclophilins (PPIL6 and SDCCAG10 were not detected) were differentially expressed between densities (Figure 12A). Within the TLR signalling pathway GO term, most TLRs, except for TLR1, TLR2 and TLR10, are upregulated in high density cells (Figure 12B). However, the intracellular signalling components display a mixed expression profile, with the key mediator MYD88 upregulated at low and mid densities along with the downstream component IRAK1, but the partner of IRAK1, IRAK4, is upregulated in high density cells (Figure 6A, 12B). Therefore, both the TLR response, and the cyclophilins, may be regulated by cell density.

6.2.10 CyPA does not regulate the cGAS-STING initiated antiviral response

So far, I only investigated the innate immune response after TLR activation. Preliminary data generated in immortalised cell lines by Dr Lucy Thorne in the Tower's lab at University College London gave evidence that CyPA regulates the macrophage response to cyclic guanosine monophosphate–adenosine monophosphate (cGAMP), a key component of the

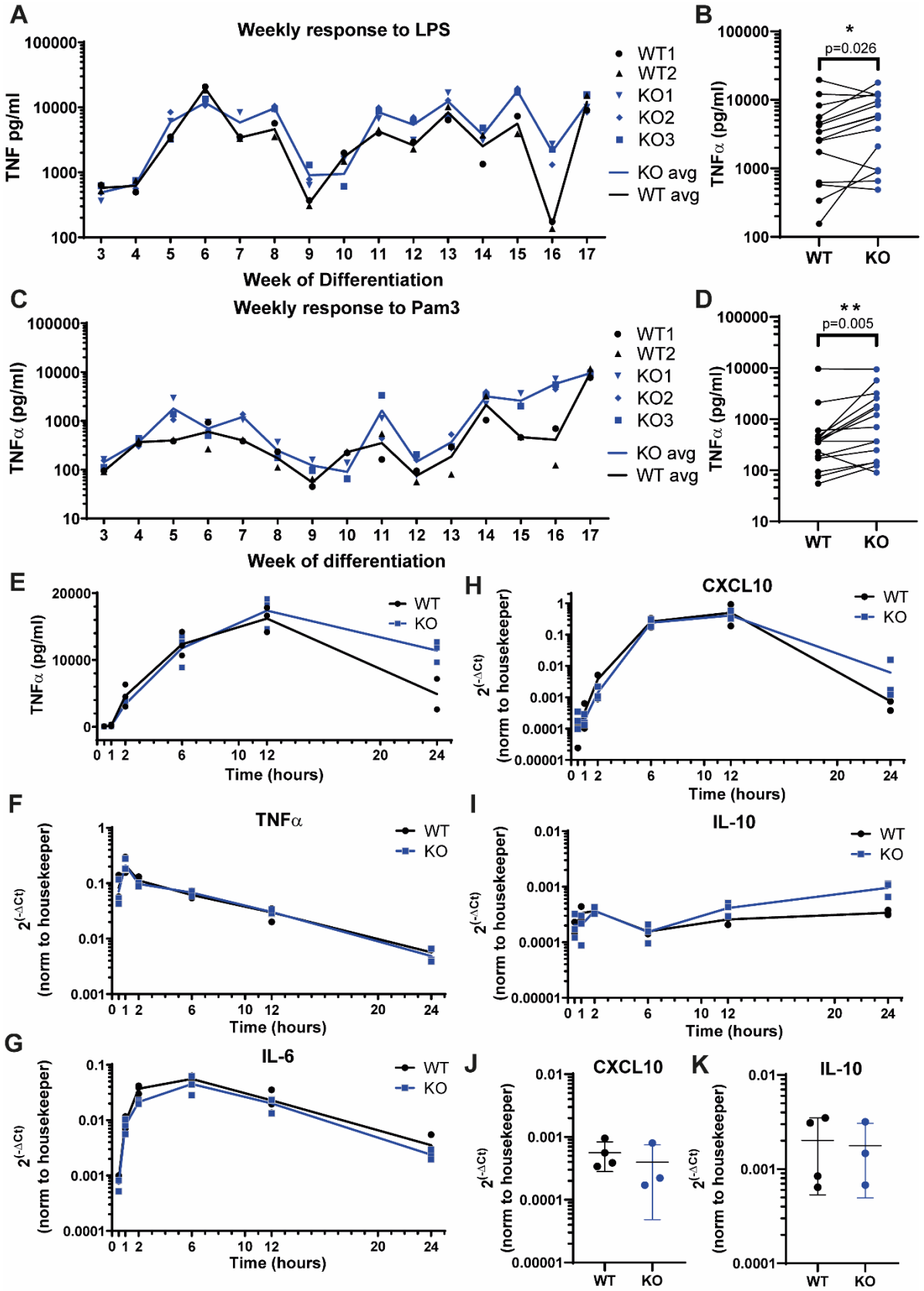
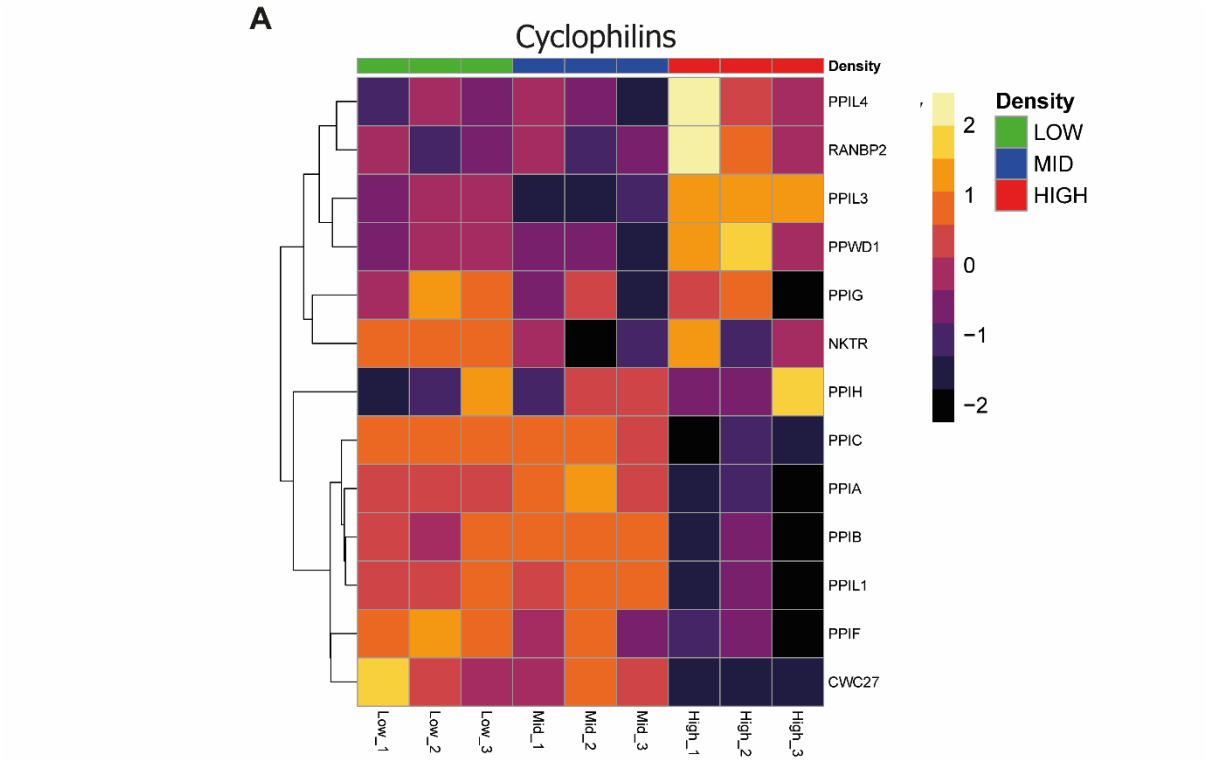
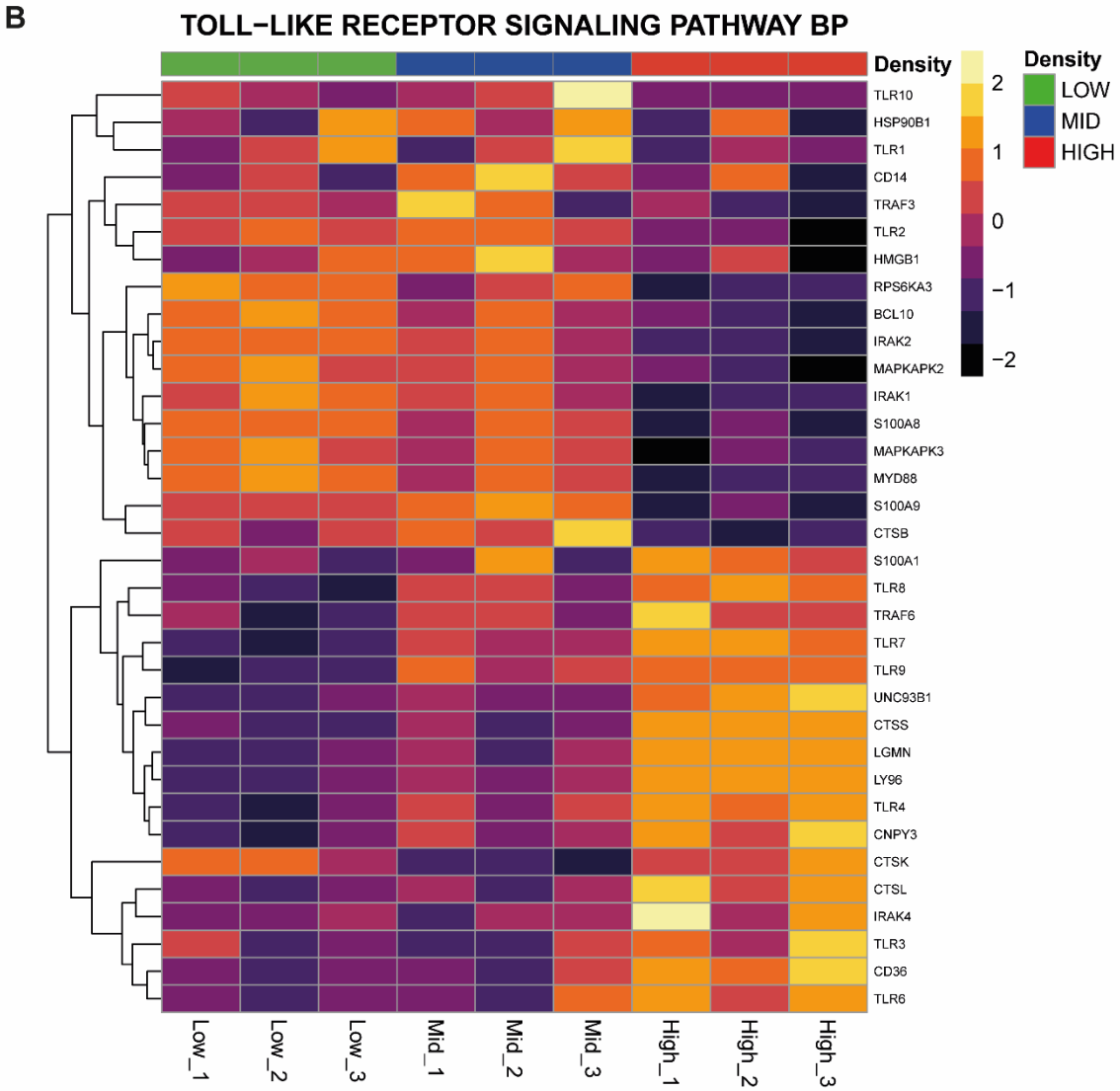

A
Weekly response to LPS
TNF pg/ml
Week of Differentiation
WT1
WT2
KO1
KO2
KO3
KO avg
WT avg
B
*
p=0.026
TNFα (pg/ml)
WT
KO
C
Weekly response to Pam3
TNFα (pg/ml)
Week of differentiation
D
**
p=0.005
E
TNFα (pg/ml)
Time (hours)
H
CXCL10
2^(-ΔCt) (norm to housekeeper)
F
TNFα
I
IL-10
G
IL-6
J
CXCL10
K
IL-10

Figure 11: Cyclophilin A supresses TNFα secretion after surface TLR activation but does not alter cytokine mRNA levels. *Secretion of TNFα across weekly harvests of macrophages from 2 WT and 3 PPIA-/- clonal cell lines after stimulations with A-B) LPS 1 ng/mL or C-D) Pam3CSK4 1 µg/mL for 24 hours. A&C) displays total TNFα levels each week. n=1 per clone. B&D) compares WT vs PPIA-/- across all weeks. n=14. E) Secretion of TNFα over 24 hours of stimulation with 1 ng/mL LPS in WT and PPIA-/- macrophages. F-I) mRNA expression over 24 hours of LPS stimulation in the same cells from part E. mRNA levels are displayed as fold difference in Ct compared to the average Ct of 2 housekeepers (TBP and 18S). E-I) n=2 clones each of WT and PPIA-/- macrophages in 1 experiment. J-K) mRNA expression of CXCL10 and IL-10 in WT and PPIA-/- macrophages 24 hours post stimulation with 1 ng/mL LPS n=4 (WT) and 3 (PPIA-/-) independent experiments. B&D) Significance was calculated by two-tailed ratio paired t-test. Significance is shown when p<0.05 (*), <0.01 (**), <0.001 (***), <0.0001 (****).*

Figure 12: Cyclophilins and TLR signalling are both regulated by cell density. *Heat maps of A) the cyclophilin family members detected by RNA-Seq and B) biological process GO terms for "Toll-like receptor signalling pathway" in macrophages plated at low ($4.41x10^4/cm^2$), mid ($8.82x10^4/cm^2$), or high density ($1.76x10^5/cm^2$) (see Chapter 4). Temperature displays Log_2-fold difference from the median TPM, where yellow > median, and purple < median.*


A
Cyclophilins
Density
PPIL4
RANBP2
PPIL3
PPWD1
PPIG
NKTR
PPIH
PPIC
PPIA
PPIB
PPIL1
PPIF
CWC27
Low_1
Low_2
Low_3
Mid_1
Mid_2
Mid_3
High_1
High_2
High_3
2
1
0
−1
−2
Density
LOW
MID
HIGH


B
TOLL−LIKE RECEPTOR SIGNALING PATHWAY BP
Density
TLR10
HSP90B1
TLR1
CD14
TRAF3
TLR2
HMGB1
RPS6KA3
BCL10
IRAK2
MAPKAPK2
IRAK1
S100A8
MAPKAPK3
MYD88
S100A9
CTSB
S100A1
TLR8
TRAF6
TLR7
TLR9
UNC93B1
CTSS
LGMN
LY96
TLR4
CNPY3
CTSK
CTSL
IRAK4
TLR3
CD36
TLR6
Low_1
Low_2
Low_3
Mid_1
Mid_2
Mid_3
High_1
High_2
High_3
2
1
0
−1
−2
Density
LOW
MID
HIGH

cGAMP-synthase (cGAS)/STING antiviral pathway (confidential data not shown). To investigate whether this was the case in my primary cell model of iPSC-derived macrophages, I stimulated WT and *PPIA*-/- macrophages with cGAMP, an alternative cGAS/STING activator, 70 base pair Vaccinia virus genome DNA (VACV 70mer) transfected into cells with lipofectamine, or LPS as a positive control. I then measured changes in inflammatory mediator and antiviral gene expression 6 hours post stimulation in replication of the work by Dr Thorne (Figure 13A-D). While lipofectamine had no effect on expression of IFN-β, IFIT1, IL6, or IL10, VACV 70mer robustly induced IFN-β, IFIT1, and IL-6 expression, but did not induce IL-10. IFN-β induction in response to cGAMP was >100-fold lower than VACV-70mer, but a clear increase in IFIT1 and IL-6 indicated that it had activated STING. As expected, LPS strongly induced IL-6 and IL-10, but only partially induced IFIT1 and did not affect IFN-β transcription. Importantly though, *PPIA*-/- showed no significant difference in response to any stimuli, contradicting the results of Dr Thorne. In case this inconsistency was due to different sensitivities to the dose of agonist used, I titrated cGAMP and LPS, increasing the dose of cGAMP, and reducing the dose of LPS (Figure 13E-H). As expected, expression of IFN-β, IFIT1 and IL-6 all marginally increased as dose of cGAMP increased, but IL-10 remained unchanged, and IFIT1 and IL-10 decreased as LPS concentration declined. Surprisingly, IFN-β and IL-6 expression increased as LPS dose decreased (Figure 13E, G). This supports my earlier observation in Chapter 4 Supplementary Figure 1 that lower doses of LPS are stronger inducers of the innate response than high dose LPS. Once again though, presence of CyPA had no significant effect on the response, and I therefore conclude that CyPA does not regulate the cGAS/STING mediated antiviral response.

6.2.11 CyPB regulates the TLR3 response but not through early transcriptional regulation

Having shown a role of CyPA in regulation of the innate immune response by macrophages, I also sought to characterise any role of other cyclophilins. Due to limitations

on time, I was only able to run preliminary experiments on *PPIB*-/- macrophages. I first stimulated WT and *PPIB*-/- macrophages with my panel of TLR agonists with or without 1 μM CsA (Figure 14A). Like Figure 8A, the TNFα secretion response by both WT and *PPIB*-/- cells was highly variable across experimental repeats and no clear difference was initially visible. When normalised, the response to Poly(I:C), however, was significantly different between WT and *PPIB*-/- macrophages untreated with CsA (ratio 0.609 ± 0.134, p=0.037) (Figure 14B-C). Both WT and *PPIB*-/- cells treated with CsA were not significantly different from the WT untreated control, although the response by *PPIB*-/- + CsA cells was highly variable (ratio 0.669 ± 0.497). Given this influence on the TLR3 response, and because prior literature has reported CyPB regulates IRF3 signalling (363), I next tested if CyPB regulates inflammatory mediator and antiviral gene expression post stimulation of the viral sensors TLR3, RIG-I, MDA-5, and STING. To stimulate RIG-I and MDA-5, I transfected my macrophages with low molecular weight (0.2-1kb) or high molecular weight (1.5-8kb) Poly(I:C), respectively (728). Extracellular and intracellular Poly(I:C) induced both a strong NF-κB/MAPK mediated cytokine gene expression response of TNFα, IL-6 and IL-1β (Figure 14D-F), and robust expression of the interferon inducible genes IFIT1, IFN-β and CXCL10 (Figure 14G-I). The clear difference in IFN-β response between extracellular and intracellular Poly(I:C) suggests successful stimulation of RIG-1 and/or MDA-5 and not only TLR3 (Figure 14H). Unfortunately, here cGAMP only reliably induced IFIT1 and CXCL10 expression, limiting potential conclusions on the role of CyPB in this antiviral sensory pathway (Figure 14G and I). Nevertheless, no clear difference in gene expression was observed for any genes under all stimulatory conditions between WT and *PPIB*-/- macrophages. Therefore, while CyPB regulates TNFα secretion after TLR3 activation, observed 24 hours post stimulation, this is not due to early changes in mRNA levels observed 6 hours post stimulation.

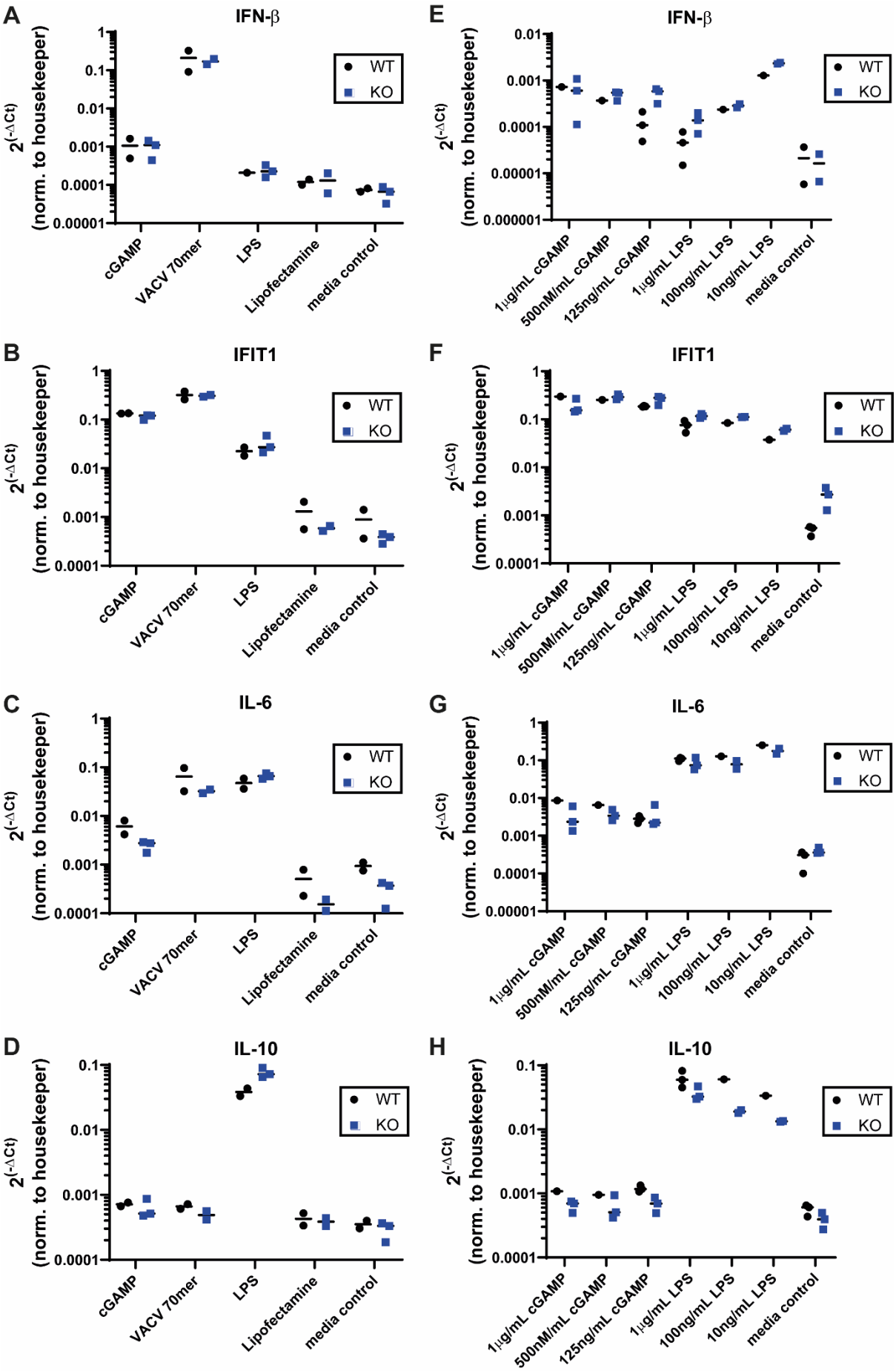
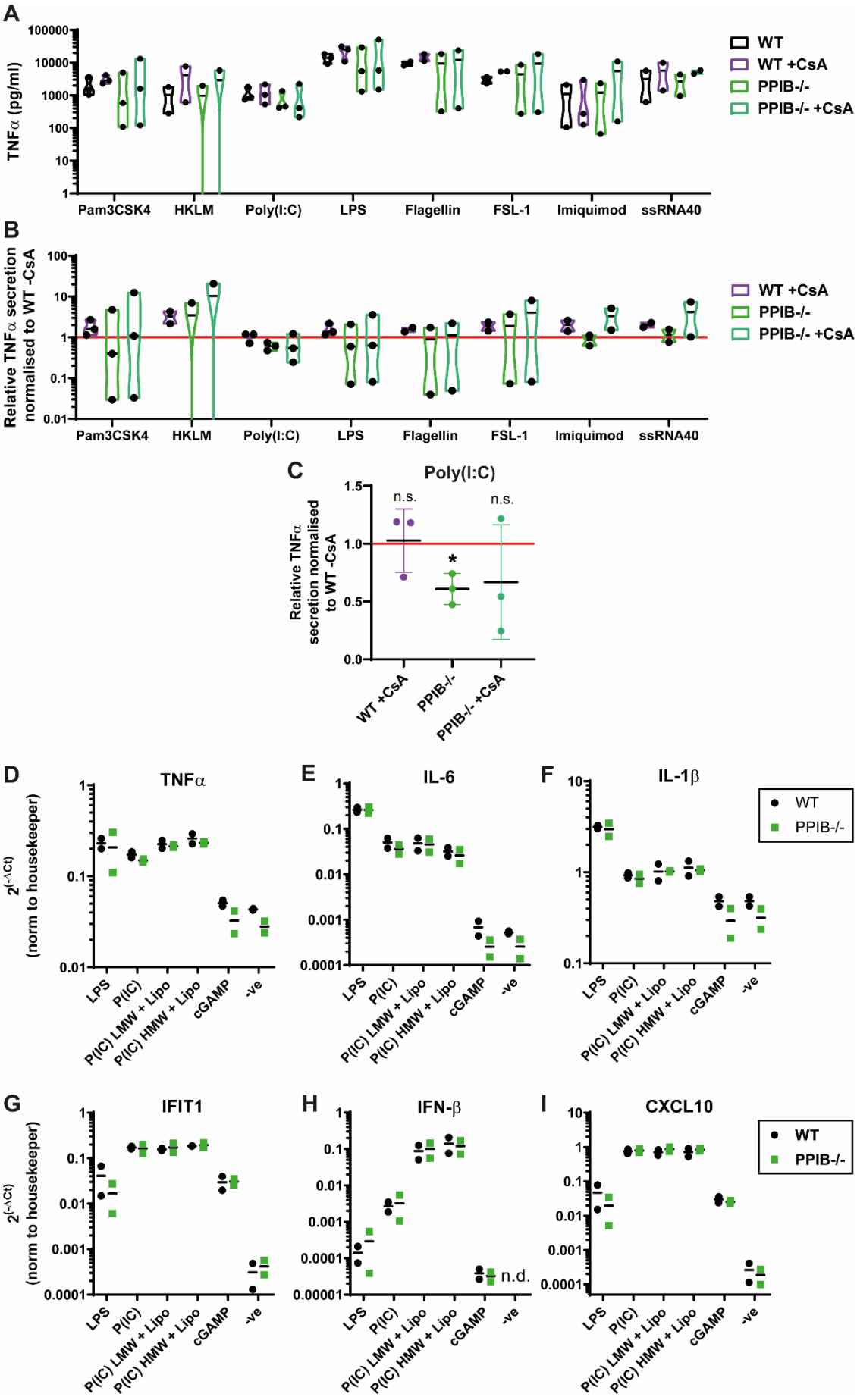

A
IFN-β
2^(-ΔCt) (norm. to housekeeper)
WT
KO
cGAMP
VACV 70mer
LPS
Lipofectamine
media control
E
IFN-β
1μg/mL cGAMP
500nM/mL cGAMP
125ng/mL cGAMP
1μg/mL LPS
100ng/mL LPS
10ng/mL LPS
media control
B
IFIT1
F
IFIT1
C
IL-6
G
IL-6
D
IL-10
H
IL-10

Figure 13: Cyclophilin A does not regulate cGAS-induced cytokine transcription. *A-D) Changes in A) IFN-β, B) IFIT1, C) IL-6, and D) IL-10 expression 6 hours after stimulation of DNA sensing pathways by 125 ng/mL 2'-3' cGAMP, 1 ug/mL VACV70mer DNA or TLR signalling with 100 ng/mL LPS, compared to a lipofectamine and media control, in WT and PPIA-/- macrophages. n=2 independent WT clones and 3 independent PPIA-/- clones in 1 experiment. E-H) Changes in E) IFN-β, F) IFIT1, G) IL-6, and H) IL-10 expression 6 hours in macrophages after stimulation with a titration of 2'-3' cGAMP or LPS. n=1-3 independent WT clones and 2-3 independent PPIA-/- clones in 1 experiment.*

Figure 14: Cyclophilin B suppresses TNFα secretion after TLR3 activation but does not alter cytokine mRNA expression. *A) TNFα secretion 24 hours post stimulation from WT and PPIB-/- macrophages treated ± 1 μM CsA at the time of stimulation with a panel of TLR agonists (TLR1-2; 1 μg/mL Pam3CSK4, TLR2; 10^8 cells/mL HKLM, TLR3; 10 μg/mL Poly(I:C), TLR4; 100 ng/mL LPS, TLR5; 1 μg/mL Flagellin, TLR2-6; 1 μg/mL FSL-1, TLR7; Imiquimod 10 μg/mL, TLR9; ssRNA40 10 μg/mL). WT n=2-3 independent experiments. B) TNFα secretion normalised to the WT -CsA control. n=2-3 independent experiments. C) Focus on TNFα secretion by PPIB-/- macrophages 24-hours post stimulation with Poly(I:C). Mean ± SD, n=3. D-I) Changes in D) TNFα, E) IL-6, F) IL-1β, and G) IFIT1, H) IFN-β or I) CXCL10 expression 6 hours after stimulation of TLR3, RIG-I or MDA-5 RNA sensing pathways by 1 μg/mL Poly(I:C) ± lipofectamine, TLR4 signalling by 1 ng/mL LPS, and cGAS signalling by 250ng/mL 2'-3' cGAMP compared to a media control, in WT and PPIB-/- macrophages. n=2 independent WT clones and 2 independent PPIB-/- clones in 1 experiment. C) Significance was calculated by one-sample t-test, theoretical mean = 1. Significance is shown when p<0.05 (*), <0.01 (**), <0.001 (***), <0.0001 (****).*


A
TNFα (pg/ml)
100000
10000
1000
100
10
1
Pam3CSK4
HKLM
Poly(I:C)
LPS
Flagellin
FSL-1
Imiquimod
ssRNA40
WT
WT +CsA
PPIB-/-
PPIB-/- +CsA
B
Relative TNFα secretion normalised to WT -CsA
100
10
1
0.1
0.01
Pam3CSK4
HKLM
Poly(I:C)
LPS
Flagellin
FSL-1
Imiquimod
ssRNA40
WT +CsA
PPIB-/-
PPIB-/- +CsA
C
Poly(I:C)
Relative TNFα secretion normalised to WT -CsA
1.5
1.0
0.5
0.0
n.s.
*
n.s.
WT +CsA
PPIB-/-
PPIB-/- +CsA
D
TNFα
E
IL-6
F
IL-1β
2(-ΔCt) (norm to housekeeper)
LPS
P(IC)
P(IC) LMW + Lipo
P(IC) HMW + Lipo
cGAMP
-ve
WT
PPIB-/-
G
IFIT1
H
IFN-β
n.d.
I
CXCL10

6.3 Discussion

In this chapter, I sought to elucidate further the role cyclophilins play in macrophages. I have shown that multiple cyclophilins including, but not limited to CyPA and CyPB, may be capable of regulating different members of the TLR family. Broad inhibition of cyclophilins results in changes in cytokine/chemokine transcription, although the precise upstream regulation by the cyclophilins is unclear. These changes in transcription are not seen though when CyPA or CyPB are knocked out. Therefore, the major immunosuppressive activity of cyclophilins seen through pharmacological inhibition by CsA and NIM811 suggests additional alternative regulatory roles of these proteins.

Both immunosuppressive and non-immunosuppressive cyclophilin inhibitors augmented the TLR response, while the FKBP binding alternative Cn inhibitor, FK506, suppressed it (Figure 3A-C). Furthermore, low (but not high) doses of CsA inhibited TNFα secretion in a CyPA-dependent manner (Figure 10C). This is consistent with previous literature on the importance of the NFAT pathway during the macrophage response (368), which will have been inhibited by CsA-CyPA or FKBP-FK506 complexes interacting with Cn (552). On the other hand, NIM811 treatment did not suppress TNFα secretion, even at low doses. NIM811 is an analogue of CsA with an additional methyl group at position 8 on the peptide ring. This sterically blocks the interaction of the NIM811-CyPA complex with Cn, preventing immunosuppression of the NFAT pathway (712). Overall, this is compelling evidence that Cn aids the inflammatory response and that cyclophilins suppress it. However, specific inhibition of Cn is still required. The FK506-FKBP complex inhibition of Cn is a gain of function activity, just like CsA and CyPA. The FKBPs are their own distinct family of peptidyl-prolyl isomerases with important roles in the innate and adaptive immune response, developmental biology, and progression of cancer (729). Therefore, for a conclusive demonstration that Cn is required for the TLR response, I will need to target it specifically in the future with the inhibitor VIVIT (730).

To better understand how the immune response is changed by cyclophilin or Cn inhibition by NIM811 or FK506, respectively, I measured changes in transcription of

inflammatory mediators, 4 and 24 hours post LPS stimulation. While some effectors were upregulated at 4 hours in NIM811 treated cells (TNFα and IL-1β), others were not (IL-6 and IL-10) and CXCL10 was even down regulated (Figure 4A-E, G-K). Macrophages treated with FK506 on the other hand showed no difference in expression of any gene measured 4 hours post-stimulation. As discussed in Chapter 1, The Introduction, it is interesting to note that TNFα and IL-1β are heavily regulated proteins post-transcriptionally and post-translationally. Both require protein cleavage to release mature signalling protein (731, 732), and both proteins' mRNA quantity is regulated by differential mRNA decay (733). In other words, both genes can be relatively highly transcribed in unstimulated cells, as I observed here, but the mRNA transcripts are rapidly degraded unless told otherwise during an inflammatory response. On the other hand, IL-6 and IL-10, which are also regulated by mRNA decay (733), do not appear to be highly expressed under resting conditions in my macrophages. Therefore, a hypothesis that will need testing in the future is that the cyclophilins in iPSC-derived macrophages regulate mRNA turnover of TNFα and IL-1β, especially given that many cyclophilins are known RNA interacting proteins (Table 1).

The unusual regulation of CXCL10 seen in both NIM811 and FK506 treated macrophages may offer some insight into the mechanisms of these drugs influence on inflammation. Firstly, while the CXCL10 gene promotor region contain NF-κB, AP1, C/EBP-β and IRF binding sites (734), both AP-1 and C/EBP-β can actually negatively regulate transcription. Given the literature on cyclophilin interactions with p38, ERK1/2, and JNK (which function upstream of AP-1) (362, 606, 635, 654, 714), one can hypothesize that AP-1 is again regulated by cyclophilins during TLR4 signalling. However, preliminary attempts to investigate whether activation of these kinases changes in the presence of NIM811 or FK506 were inconclusive (Figure 6) and will need further repeating to evaluate this hypothesis. Secondly, the potentially increased expression of CXCL10 relative to the LPS-only control at 24 hours may be indicative of a secondary signal in NIM811 treated cells. CXCL10 expression is induced/enhanced by IL-1β and TNFα (735), which may be acting back in an autocrine/paracrine manner after earlier release. Therefore, a more regular and prolonged

time course experiment is needed to better map the innate immune response of these macrophages. Lastly, the reduction of CXCL10 expression (and to some degree IL-6) 24 hours post-stimulation in FK506 treated macrophages to levels below unstimulated cells suggests FK506 may be inducing some form of LPS tolerance-like state. This is a reported function of Cn in macrophages (601, 602), and therefore future research into a secondary stimulation response in these cells may be of interest.

Overall, I have shown here clear evidence of a contradictory response in macrophages treated with different Cn inhibitors. This is extremely important as CsA and FK506 are routinely used as immunosuppressants in organ transplant patients (368). Furthermore, both drugs, particularly CsA, are known to have serious side effects of nephrotoxicity (369). Both TNFα and IL-1β are capable of inducing cell death, and as such small changes in expression of these proteins, as seen in my iPSC-macrophages, could explain nephrotoxicity seen in patients treated with CsA. Therefore, future *in vivo* investigations of nephrotoxicity in healthy and macrophage deficient, WT, and *Ppia*-/- mice treated with CsA and NIM811 would be of considerable interest.

As a majority of cyclophilins bind to and are inhibited by CsA (366), in this chapter I sought to decipher the roles of specific members by making KO cell lines for 8 of the cyclophilins, and the known receptor for secreted cyclophilin, CD147. I completed making KO clones for CyPA (*PPIA*), CyPB (*PPIB*), CyPD (*PPIF*), and CD147 (*BSG*). Due to limitations of time imposed by the SARS-CoV-2 pandemic, I ultimately only investigated the role of CyPA in macrophage functionality, with a smaller investigation into CyPB. However, before studying the impact of CyPA on macrophage function, it was first important to establish whether knocking it out had any impact on both macrophage differentiation and expression of other cyclophilin family members. There have been several papers reporting CyPA as essential for macrophage proliferation, and that it enhances differentiation in high glucose conditions (which OXM media, with 16mM glucose, would be) (676, 718). However, expression of macrophage markers and assaying for phagocytic potential in both WT and *PPIA*-/- macrophages showed no significant difference between clones. Therefore, this is an example

of how specific conclusions on cyclophilin function based on pharmacological inhibition data is inappropriate (676). Alternatively, CyPG is also reported to regulate macrophage differentiation, and this may be an example of misidentification of cyclophilins involved (695). Nevertheless, mice lacking CyPA have bone defects which includes increased osteoclast number (736, 737). Osteoclasts are bone tissue macrophages (738), and it is therefore possible that defects in macrophage differentiation may only be observed in specific tissue niches not recapitulated in this model.

CyPA KO did not induce compensatory changes in expression of other cyclophilin family members. However, I was surprised to find that all primer sets used for amplification of *PPIA* also amplified genomic DNA of the same size, despite the amplicon being designed to span exon-exon junctions. On closer analysis by BLAST (NCBI BLAST tool) of the amplicon, I found that these primers also amplified as many as 116 pseudogenes distributed across all chromosomes. Whether any of these pseudogenes are transcribed is unclear and understanding how they have come to be so widespread in the genome would likely be an evolutionary genetics project within itself. Nevertheless, researchers should be aware of their existence when studying CyPA, and I recommend that only the use of probe-based qPCR would be appropriate for accurate quantification of *PPIA* expression in the future.

Utilising the same approach taken to demonstrate CsA inhibition of cyclophilin results in an increased macrophage inflammatory response, I here show that removing CyPA results in a small but significant increase in TNFα secretion post TLR1/2 and TLR4 stimulation. However, treating *PPIA*-/- cells with CsA or NIM811 increased this inflammatory response further, demonstrating that not only may CyPA play a role in suppressing the TNFα response, but so too is another cyclophilin. As the difference in response between WT and *PPIA*-/- macrophages was not apparent until ≥24 hours post-stimulation, this would indicate either a failure to shut down the innate immune response, or the presence of a secondary signal induced by the initial stimulation. One hypothesis of the latter may be that removing CyPA results in increased expression and/or secretion of other cyclophilins after LPS/Pam3 stimulation. Numerous studies have reported extracellular cyclophilins inducing an

inflammatory response through binding to CD147 and inducing ERK1/2 signalling (654). Therefore, by quantifying cyclophilin expression by qPCR after stimulation, and using the *BSG*-/- cell lines I made, I could deduce if other cyclophilins like CyPB and CyPC are secreted within my experimental model to induce a pro-inflammatory response. Alternatively, by introducing recombinant proteins like TNFα, IL-6, and IFN, or their inhibitors (E.g. anti-TNFα antibodies infliximab/Remicade) after the primary stimulation, I could identify secondary signal pathways regulated by CyPA. For example, CyPA has been reported to be secreted in response to ROS (671), and directly interacts with members of the JAK/STAT families which are important mediators of IL-6 and IFN induced responses (632–634).

I also investigated the antiviral response in both *PPIA*-/- and *PPIB*-/- macrophages given recent evidence for a role in CyPA regulation of RIG-I signalling (364), and extensive literature of cyclophilin-virus interactions (358, 739). By measuring changes in effector expression by qPCR, I was unfortunately unable to reproduce preliminary findings of the Towers lab who had investigated CyPA function during cGAS mediated signalling. This again highlighted the importance of the model used, as the original observations were made in HEK293 and THP-1 cells using CRISPR-Cas9 and plasmid-based overexpression systems. However, a time course experiment is needed to definitively conclude whether the timescale of a CyPA regulated cGAS response varies between cell models used. On the other hand, I have preliminary evidence that CyPB does regulate the antiviral response induced by TLR3 signalling. TNFα secretion from *PPIB*-/- macrophages stimulated with 1 µg/mL Poly(I:C) was approximately 3/5th that of WT macrophages. Initial investigations would, again, suggest this difference is not due to transcriptional regulation. However, a more comprehensive time-course experiment of cytokine secretion and effector transcription is needed to evaluate if this is a rapid TNFα release response, or a slower, secondary signal induced response. Overall, this may be consistent with reported CyPB-IRF3 interactions that aid virus-induced IRF3 phosphorylation (363), especially given that CyPB localizes to the ER and vesicular compartments similar to TLR3.

Finally, as CyPA and CyPB are not alone in regulating the TLR response, as indicated by the increased TNFα response post TLR stimulation in these KO macrophages, future investigations will be needed targeting other members of cyclophilin family. Given its high expression in macrophages, and its well-known importance in regulating the MPTP (648), repeating these studies in my CyPD (*PPIF*) cell lines should be a future priority. Additionally, CyPJ (*PPIL3*) has recently been reported to suppress the TLR response through TAB2 and TAB3 interactions in macrophages (365). Although I observed CyPJ expression to be low in iPSC-macrophages (Figure 9), adding this cyclophilin to the panel of KO iPSCs will be necessary to decipher the cyclophilin regulation of the innate immune response.

6.4 Conclusion

In conclusion, I have provided here clear evidence for cyclophilin regulation of the innate immune response by macrophages. The implications of these findings are potentially far reaching, as CsA is routinely used as an immunosuppressant for organ transplants and a variety of immune pathologies including rheumatoid arthritis and psoriasis. However, the precise member, or members, of the cyclophilin family responsible for this regulation are still unknown. As too are the inflammatory mediator pathways involved. I have provided evidence that CyPA and CyPB, while not the principal regulators of inflammation inhibited by CsA and NIM811, nevertheless likely play some role in regulating the TLR-mediated response. Overall, I found that timing, culture age, and plating density are all key elements that can differ between experiments, resulting in substantial experimental variation. This demonstrates that the iPSC-derived macrophage system is still in need of further optimisation and is currently limited in its capacity to measure ~2-fold differences in inflammatory cytokine secretions such as those reported in this chapter.

6.5 Supplementary figures

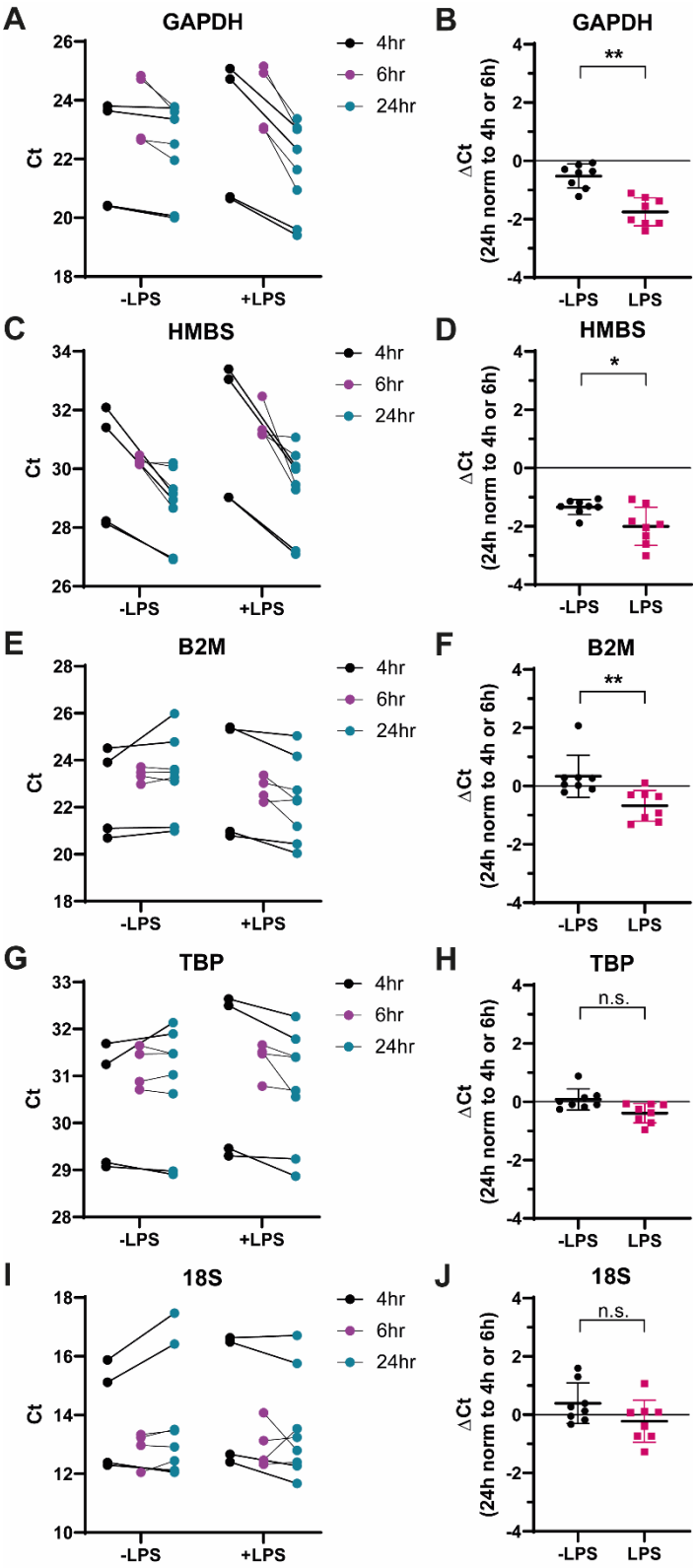


Figure S1: TBP and 18S, but not GAPDH, B2M and HMBS, are suitable housekeepers for qPCR of the LPS response. Related to Figure 4-5.

A, C, E, G, I) Quantification of A) GAPDH, C) HMBS, E) B2M, G) TBP, I) 18S mRNA 4, 6 and 24 hours ±LPS (1 ng/mL) stimulation displayed as raw Ct value. n=2 independent experiments for 4 and 6 hours, and 4 for 24 hours. B, D, F, H and J) Normalisation of mRNA expression to the 4 or 6 hour time point displayed as difference in Ct value. Mean ± SD is displayed. Significance was calculated by one-sample t-test, theoretical mean = 0. Significance is shown when p<0.05 (*), <0.01 (**), <0.001 (***), <0.0001 (****).

A



Figure S2: Sequences of iPSC knock-out clones. Related to Figure 7. *Illumina Sequences of PCR amplification products shown in figure 5D-G for knock out clones for A) PPIA, B) PPIB, C) PPIF, D) BSG.*

B

```
        2625                                                                2706
Genbank aactttccattgagccagcaggtgacctttcttctcagttttcttgtatctgttcttatgattggaagaaatgaggggaaaa
WT      NNNTTNNCCCNTTTNCAGCAGGTGACCTTTCTTCTCAGTTTTCTTGTATCTGTTCTTATGATTGGAAGAAATGAGGGGAAAA
B4      NTCTTTCCNNTTTACCAGCAGGTGACCTTTCTTCTCAGTTTTCTTGTATCTGTTCTTATGATTGGAAGAAATGAGGGGAAAA
2D4     -CTTTCCCATTNTNCCAGCAGGTGACCTTTCTTCTCAGTTTTCTTGTATCTGTTCTTATGATTGGAAGAAATGAGGGGAAAA

..................................................................................................

        2707                                                                2788
Genbank gcattatgtgatgtagaattgtataaagcttgggaattgtatggaggcagagggatttccacatctgtgtgtaccatgcctg
WT      GCATTATGTGATGTAGAATTGTATAAAGCTTGGGAATTGTATGGAGGCAGAGGGATTTCCACATCTGTGTGTACCATGCCTG
B4      GCATTATGTGATGTAGAATTGTATAAAGCTTGGGAATTGTATGGAGGCAGAGGGATTTCCACATCTGTGTGTACCATGCCTG
2D4     GCATTATGTGATGTAGAATTGTATAAAGCTTGGGAATTGTATGGAGGCAGAGGGATTTCCACATCTGTGTGTACCATGCCTG

..................................................................................................

        2789                                                                2870
Genbank tcctgtggcgcctgcccgctcacttagtagcacactgaacagtgaaagtggtcagcagtggtgtctcttctgcgagcaggag
WT      TCCTGTGGCGCCTGCCCGCTCACTTAGTAGCACACTGAACAGTGAAAGTGGTCAGCAGTGGTGTCTCTTCTGCGAGCAGGAG
B4      TCCTGTGGCGCCTGCC----------------------------------------------------------------
2D4     TCCTGTGGCGCCTGCC----------------------------------------------------------------

..................................................................................................

        2871                                                                2952
Genbank ttgtggacttgttcctgtgaggcctatttaatgtaatgtcttcctgctgccccataccacctccttaccttctcttccctttt
WT      TTGTGGACTTGTTCCTGTGAGGCCTATTTAATGTAATGTCTTCCTGCTGCCCCATACCACCTCCTTACCTTCTCTTCCCTTT
B4      --------------------------------------------------------------------------------
2D4     --------------------------------------------------------------------------------

..................................................................................................

        2953                                                                3034
Genbank ttctagaaaggatttggctacaaaaacagcaaattccatcgtgtaatcaaggacttcatgatccagggcggagacttcacca
WT      TTCTAGAAAGGATTTGGCTACAAAAACAGCAAATTCCATCGTGTAATCAAGGACTTCATGATCCAGGGCGGAGACTTCACCA
B4      --------------------------------------------------------------------------------
2D4     --------------------------------------------------------------------------------

..................................................................................................

        3035                                                                3116
Genbank ggggagatggcacaggaggtaaccacaggtcctctgggccaaggagtatgtcagtgtagcctccacagtgggagggccaggt
WT      GGGGAGATGGCACAGGAGGTAACCACAGGTCCTCTGGGCCAAGGAGTATGTCAGTGTAGCCTCCACAGTGGGAGGGCCAGGT
B4      --------------------------------------------------------------------------------
2D4     --------------------------------------------------------------------------------

..................................................................................................

        3117                                                                3198
Genbank tctgctggggagaccaggcctctttcttccccagctctagaggcaggcctacttattacttacctactttgagaccagcggc
WT      TCTGCTGGGGAGACCAGGCCTCTTTCTTCCCCAGCTCTAGAGGCAGGCCTACTTATTACTTACCTACTTTGAGACCAGCGGC
B4      ----------------------------------------------------------------------------GC
2D4     ----------------------------------------------------------------------------GC

..................................................................................................

        3199                                                                3280
Genbank acccttctttgaagagggaacccagtacaaaggagagagaataatggggtggacctgatggtagatctaagagaatctctcc
WT      ACCCTTCTTTGAAGAGGGAACCCAGTACAAAGGAGAGAGAATAATGGGGTGGACCTGATGGTAGATCTAAGAGAATCTCTCC
B4      ACCCTTCTTTGAAGAGGGAACCCAGTACAAAGGAGAGAGAATAATGGGGTGGACCTGATGGTAGATCTAAGAGAATCTCTCC
2D4     ACCCTTCTTTGAAGAGGGAACCCAGTACAAAGGAGAGAGAATAATGGGGTGGACCTGATGGTAGATCTAAGAGAATCTCTCC

..................................................................................................
```

C

```
        1723                                                                1804
Genbank agaagagtcggggctcagagacccctgacagatgggagctccatgtgtggctcagccattgggtgctctggggcagccctgc
WT      AGAAGAGTCGGGGCTCAGAGACCCCTGACAGATGGGAGCTCCATGTGTGGCTCAGCCATTGGGTGCTCTGGGGCAGCCCTGC
B2      AGAAGAGTCGGGGCTCGGAGACCCCTGACAGATGGGAGCTCCATGTGTGGCTCAGCCATTGGGTGCTCTGGGGCAGCCCTGC
G4      AGAAGAGTCGGGGCTCGGAGACCCCTGACAGATGGGAGCTCCATGTGTGGCTCAGCCATTGGGTGCTCTGGGGCAGCCCTGC
G6      AGAAGAGTCGGGGCTCGGAGACCCCTGACAGATGGGAGCTCCATGTGTGGCTCAGCCATTGGGTGCTCTGGGGCAGCCCTGC

.....................................................................................

        1805                                                                1886
Genbank catccctctctgggcctcaacgttggctctgccctcctctctcatagtagctgggagcctcagagccagtggaaggcacatg
WT      CATCCCTCTCTGGGCCTCAACGTTGGCTCTGCCCTCCTCTCTCATAGTAGCTGGGAGCCTCAGAGCCAGTGGAAGGCACATG
B2      CATCCCTCTCTGGGCCTCAACGTTGGCTCTGCCCTCCTCTCTCATAGTAGCTGGGAGCCTCAGAGCCAGTGGAAGGCACATG
G4      CATCCCTCTCTGGGCCTCAACGTTGGCTCTGCCCTCCTCTCTCATAGTAGCTGGGAGCCTCAGAGCCAGTGGAAGGCACATG
G6      CATCCCTCTCTGGGCCTCAACGTTGGCTCTGCCCTCCTCTCTCATAGTAGCTGGGAGCCTCAGAGCCAGTGGAAGGCACATG

.....................................................................................

        1887                                                                1968
Genbank taaatttcccggagacttccccactcctggtgcccagtgaggcagggtgatgggcacacagcccttgagtccgtgccctgct
WT      TAAATTTCCCGGAGACTTCCCCACTCCTGGTGCCCAGTGAGGCAGGGTGATGGGCACACAGCCCTTGAGTCCGTGCCCTGCT
B2      TAAATTTCCCGGAGACTTCCCCACTCCTGGTGCCCAGTGAGGCAGGGTGATGGGCACACAGCCCTTGAGTCCGTGCCCTGCT
G4      TAAATTTCCCGGAGACTTCCCCACTCCTGGTGCCCAGTGAGGCAGGGTGATGGGCACACAGCCCTTGAGTCCGTGCCCTGCT
G6      TAAATTTCCCGGAGACTTCCCCACTCCTGGTGCCCAGTGAGGCAGGGTGATGGGCACACAGCCCTTGAGTCCGTGCCCTGCT

.....................................................................................

        1969                                                                2050
Genbank ggccagcacagccatgagcctgtactcttgtcacagtgctcaggtactgaggacagggaaggggagtgacttgtccagttac
WT      GGCCAGCACAGCCATGAGCCTGTACTCTTGTCACAGTGCTCAGGTACTGAGGACAGGGAAGGGGAGTGACTTGTCCAGTTAC
B2      GGCCAGCACAGCCATGAGCCTGTACTCTTGTCACAGTGCTCAGGTACTGAGGACAGGGAAGGGGAGTGACTTGTCCAGTTAC
G4      GGCCAGCACAGCCATGAGCCTGTACTCTTGTCACAGTGCTCAGGTACTGAGGACAGGGAAGGGGAGTGACTTGTCCAGTTAC
G6      GGCCAGCACAGCCATGAGCCTGTACTCTTGTCACAGTGCTCAGGTACTGAGGACAGGGAAGGGGAGTGACTTGTCCAGTTAC

.....................................................................................

        2051                                                                2132
Genbank atagcgagttgggcagagcagacccaagaggtgggccagagtctttatccccctgttcactgctggggatgtagcagggatt
WT      ATAGCGAGTTGGGCAGAGCAGACCCAAGAGGTGGGCCAGAGTCTTTATCCCCCTGTTCACTGCTGGGGATGTAGCAGGGATT
B2      ATAGCGA-------------------------------------------------------------------------
G4      ATAGCG--------------------------------------------------------------------------
G6      ATAGCG--------------------------------------------------------------------------

.....................................................................................

        2133                                                                2214
Genbank ttggctggaacgggtatgaccctggaattggggcctggccctgttgacctgtgtttctcttcgaccctcagagaacttcaga
WT      TTGGCTGGAACGGGTATGACCCTGGAATTGGGGCCTGGCCCTGTTGACCTGTGTTTCTCTTCGACCCTCAGAGAACTTCAGA
B2      -------------------------------------------------------------------------------
G4      -------------------------------------------------------------------------------
G6      -------------------------------------------------------------------------------

.....................................................................................

        2215                                                                2296
Genbank gccctgtgcactggtgagaagggcttcggctacaaaggctccaccttccacagggtgatcccttccttcatgtgccaggtaa
WT      GCCCTGTGCACTGGTGAGAAGGGCTTCGGCTACAAAGGCTCCACCTTCCACAGGGTGATCCCTTCCTTCATGTGCCAGGTAA
B2      ------------------------------ACAAAGGCTCCACCTTCCACAGGGTGATCCCTTCCTTCATGTGCCAGGTAA
G4      ------------------------------ACAAAGGCTCCACCTTCCACAGGGTGATCCCTTCCTTCATGTGCCAGGTAA
G6      ------------------------------ACAAAGGCTCCACCTTCCACAGGGTGATCCCTTCCTTCATGTGCCAGGTAA

.....................................................................................
```

D

```
        9021                                                                    9102
Genbank tcactgtgccgtggttgggcccctggagaaccctgggtccttggaggcgtcctgcagagctggtacgcggctcacctgcctg
E2      TNNNNNNGCNNNGGTNGGGCCCNNGNNNAACCTNGGNNCNTNGGNGGNNNCTNNNNNNGNNNGNNNNNGGNTNNCNTNCNNN
H3      TCACTGTGCCGTGGTTGGGCCCCTGGAGAACCCTGGGTCCTTGGAGGCATCCTGCAGAGCTGGTACGCGGCTCACCTGCCTG
A2      TCACTGTGCCGTGGTTGGGCCCCNGGAGAACCCTGGGTCCNNGGAGGCGTCCTGCAGAGNNGGTACGCGGCTCACNNGCCTG
F3      TCACTGTGCCGTGGTTGGGCCCCTGGAGAACCCTGGGTCCTTGGAGGCATCCTGCAGAGCTGGTACGCGGCTCACCTGCCTG
F4      TCACTGTGCCGTGGTTGGGCCCCTGGAGAACCGTGAGTCCTTGGAGGCGTCGCGCAGAGCTGGTACGAGGCTCACGTCCCCG
G1      TCACTGTGCCGTGGTTGGGCCCCTGGAGAACCGTGGGTCCTTGGAGGCATCGCGCAGAGCTGGTACGCGGCTCACGTGCCCG
A3      TCACTGTGCCGTGGTTGGGCCCCTGGAGAACCCTGGGTCCTTGGAGGCNTCCTGCAGAGCTGGTACGCGGCTCACCTGCCTG
H5      TCACTGTGCCGTGGTTGGGCCCCTGGAGAACCCTGGGTCCTTGGAGGCNTCCTGCAGAGCTGGTACGCGGCTCACCTGCCTG
H6      TCACTGTGCCGTGGTTGGGCCCCTGGAGAACCNNNNGTCCTNGGAGGCNTCCTGCAGANNTGGTACGCNGNTCACNTGCNTG

        9103                                                                    9184
Genbank ctgtggttgcagggtggactccgacgaccagtggggagagtactcctgcgtcttcctccccgagcccatgggcacggccaac
E2      NNNNGGTNNNNGGNNGGNTTCNNNNNNCCNNNGGGNNNNNNANTCNNNNNNNTTCTTCCCNNNNCCCNNGGNNNNGGCCANN
H3      CTGTGGTTGCAGGGTGGACTCCGACGACCAGTGGGGAGAGTACTCCTGCGTCTTCCTCCCCGAGCCCATGGGCACGGCCAAC
A2      CTGTGGTTGCAGGGTGGACTCCGANGACCAGTGGGGAGAGTACTCCTGCGTCTTCCTCCCCGAGCCCATGGGCACGGCCAAC
F3      CTGTGGTTGCAGGGTGGACTCCGACGACCAGTGGGGAGAGTACTCCTGCGTCT----------------------------
F4      CTGTGGTTGCAGGGTGGANTCCGACGACCAGTGGGGAGAGTACTCGTGCGTCTTCCTCCCCGAGCCCATGGGCACGTCCAAC
G1      CTGTGGTTGCAGGGTGGACTCCGACGACCAGTGGGGAGAGTACTCGTGCGTCTTCCTCCCCGAGCCCATGGGCACGGCCAAC
A3      CTGTGGTTGCAGGGTGGACTCCGACGACCAGTGGGGAGAGTACTCCTGCGTCTTCCTCCCCGAGCCCATGGGCACGGCCAAC
H5      CTGTGGTTGCAGGGTGGACTCCGACGACCAGTGGGGAGAGTACTCCTGCGTCTTCCTCCCCGAGCCCATGGGCACGGCCAAC
H6      CTGTGGTTGCAGNNTGGACTCNGANGACCAGTGGGGAGAGTANTCNNGCGTCTTCCTCCCCGAGCCCANGGGCACGGCCAAC

        9185                                                                    9266
Genbank atccagctccacggtgagtcctgcagccaggggtaccgggcaccaccgactgtcgggagaagttgttggcctgaggcacccg
E2      NNCNNNTTCCNNNGNNNNNCNNNNNNCCNGGGGNNCCGGNNNCCNCNNNNNGTCGGGAGAAGTTGTTGGCCTGAGGCACCCG
H3      ATCCAGCTCCACGGTGAGTCCTGCAGCCAGGGGTACCGGGCACCACCGAC----------------TGGCCTGAGGCACCCG
A2      ATCCAGCTCCACGGTGAGTCCTGCAGCCAGGGGTACCGGGCACCACCGACT--------------------------------
F3      --------------TGGGACCCCCAGANNTCNTNNGAGGTTCAGACTTGACTGGGACAGTTTTGCTTTTTCNNNGTGNCGNG
F4      ATCCAGCTCCACGGTGAGTCCTGCAGCCAGGGGTACCGGGCACCACCGACT--------------------------------
G1      ATCCAGCTCCACGGTGAGTCCTGCAGCCAGGGGTACCGGGCACCACCGACT--------------------------------
A3      ATCCAGCTCCACGGTGAGTCCTGCAGCCAGGGGTACCGGGCACCACCGACT--------------------------------
H5      ATCCAGCTCCACGGTGAGTCCTGCAGCCAGGGGTACCGGGCACCACCGACT--------------------------------
H6      ATCCAGCTNCANGGNGAGTCCTGCAGCCAGGGGTNCCGGNCACCNCCGANT--------------------------------

        9267                                                                    9348
Genbank gcacatcccagagccctggccccctgctccctggaggggaacagccctcctgcgggaggccggggatggggcgggcctgcg
E2      GCACATCCCAGAGCCCTGGCCCCCTGCTCCCTGGAGGGGAACAGCCCTCCTGCGGGAGGCCGGGGATGGGGGCGGGCCTGCG
H3      GCACATCCCAGAGCCCTGGCCCCCTGCTCCCTGGAGGGGAACAGCCCTCCTGCGGGAGGCCGGGGATGGGGGCGGGCCTGCG
A2      --------------------------------------------------------------------------------
F3      GNNNNNNCCNNNGAGNNNCNNGNNNNNCNTGGNNGCGTNNNNCAGAGCNNNTACNNNGNTCACNNNCCNGNNNTNGTTGCAGG
F4      --------------------------------------------------------------------------------
G1      --------------------------------------------------------------------------------
A3      --------------------------------------------------------------------------------
H5      --------------------------------------------------------------------------------
H6      --------------------------------------------------------------------------------

        9349                                                                    9430
Genbank gttccaggctcctctctctcaccctcctgtcagggcctcccagagtgaaggctgtgaagtcgtcagaacacatcaacgaggg
E2      GTTCCAGGCTCCTCTCTCTCACCCTCCTGTCAGGGCCTCCCAGAGTGAAGGCNGTGAAGTCGTCAGAACACATCAACGAGGG
H3      GTTCCAGGCTCCTCTCTCTCACCCTCCTGTCAGGGCCTCCCAGAGTGAAGGNCGTGAAGTCGTCAGAACACATCAACGAGGG
A2      ----------------------------------------------------------------------ACGAGGG
F3      GNNGANTCCGACGACCAGNNGGGAGAGTACTCNNGCGTCTTCCTCCCNNANNNCNNNNGNANNNCCAACATCCANCTNNACG
F4      ----------------------------------------------------------------------AACGAGGG
G1      ----------------------------------------------------------------------AACGAGGG
A3      ----------------------------------------------------------------------AACGAGGG
H5      ----------------------------------------------------------------------AACGAGGG
H6      ----------------------------------------------------------------------AACGAGGG

        9431                                                                    9512
Genbank ggagacggccatgctggtctgcaagtcagagtccgtgccacctgtcactgactgggcctggtacaagatcactgactctgag
E2      GGAGACGGCCATGCTGGTCTGCAAGTCAGAGTCCGTGCCACCNGTCACNGACNNNNNNNNNNNNN-----------------
H3      GGAGACGGCCATGCTGGTCTGCAAGTCAGAGTCCGTGCCACCTGTCACNGNNNNNNNNNNNNNNN-----------------
A2      GGAGACGGCCAT--NNGGNTGCAAGTCAGAGTCCGTGCCACCNGTCACNNACNNNNNNNNNNNN-----------------
F3      GNNANTNNTGCAGCCAGNGGTACCGNGCANCANCGACTAACGAGGGGGAGACGGCCATGCTGGTCTGCAAGTCAGAGTCCGT
F4      GGAGACGGCCATGCTGGT-TGCAAGTCAGAGTCCGTGCCACCNGTCACNGACNNNNNNNNNNNN-----------------
G1      GGAGACGGCCATGCNGG-NTGCAAGTCAGAGTCCGTGCCACCNGTCACNNACNNNNNNNNNNNN-----------------
A3      GGAGACGGCCATGCTGGTCTGCAAGTCAGAGTCCGTGCCACCNGTCACNGANNNNNNNNNNNNN-----------------
H5      GGAGACGGCCATGCTGGTCTGCAAGTCAGAGTCCGTGCCACCTGTCACTGACNNNNNNNNNNNNNN----------------
H6      GGAGACGGCCATGCTGGTCTGCAAGTCAGAGTCCGTGCCACCNGTCACNNACNNNNNNNNNN-------------------
```

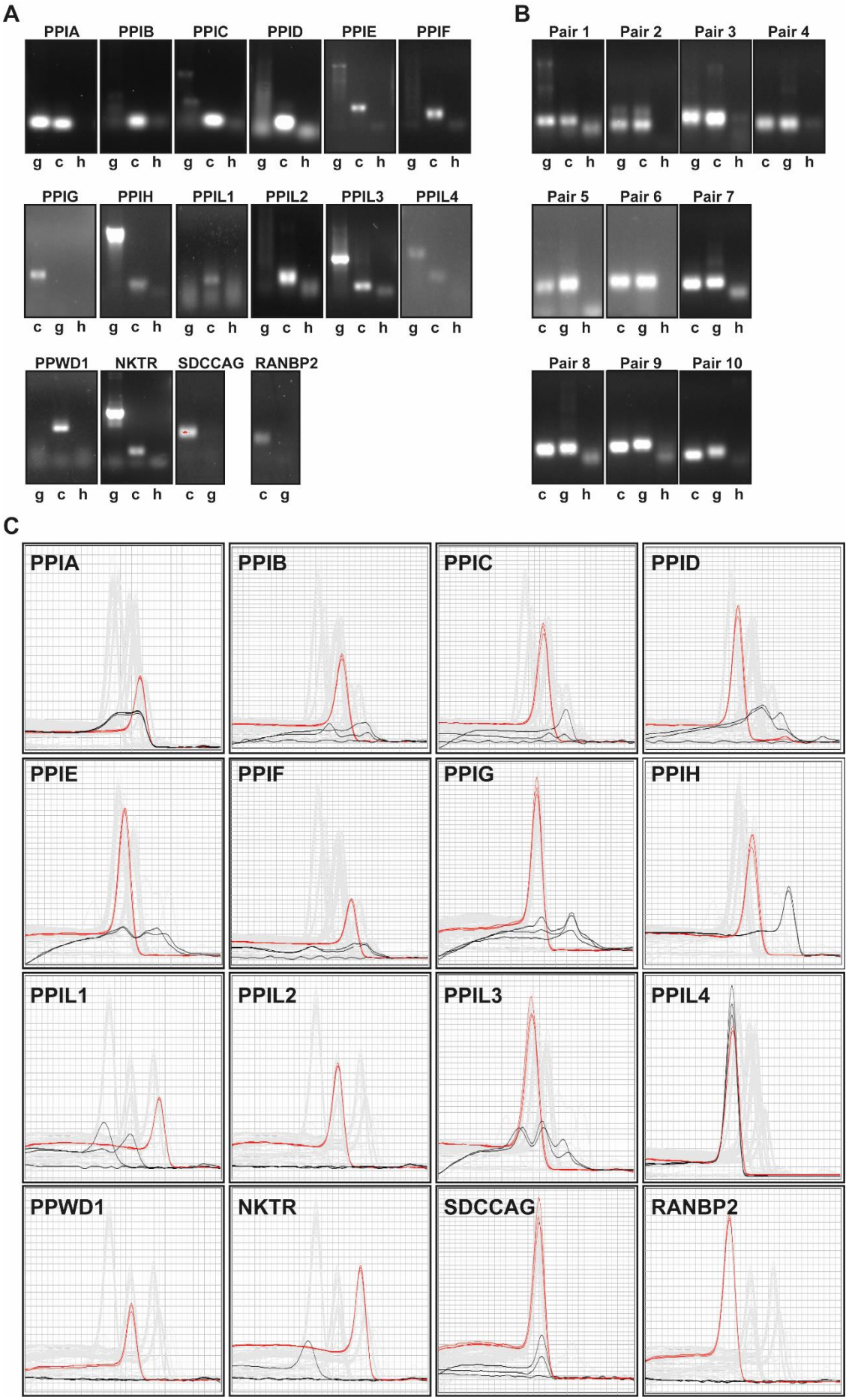

A
PPIA
PPIB
PPIC
PPID
PPIE
PPIF
g c h g c h g c h g c h g c h g c h
PPIG
PPIH
PPIL1
PPIL2
PPIL3
PPIL4
c g h g c h g c h g c h g c h g c h
PPWD1
NKTR
SDCCAG
RANBP2
g c h g c h c g c g
B
Pair 1
Pair 2
Pair 3
Pair 4
g c h g c h g c h c g h
Pair 5
Pair 6
Pair 7
c g h c g h c g h
Pair 8
Pair 9
Pair 10
c g h c g h c g h
C
PPIA
PPIB
PPIC
PPID
PPIE
PPIF
PPIG
PPIH
PPIL1
PPIL2
PPIL3
PPIL4
PPWD1
NKTR
SDCCAG
RANBP2

Figure S3: Optimisation of cyclophilin family qPCR. Related to Figure 9. *A) PCR products using the primer pairs and cycling conditions listed in table 2, amplified from genomic DNA (g), cDNA (c), or water (h). B) PCR products using 10 different primer pairs for amplification of PPIA mRNA amplified from genomic DNA, cDNA, and water. C) Melt curves for the qPCR products of each cyclophilin family member using conditions and primers in table 2. DNA was amplified from cDNA (red lines) and genomic DNA (black lines) in triplicate.*

Chapter 7:

General Discussion

7.1 Summary of Results

This thesis set out to achieve two main goals: first, to improve the model of iPSC-derived macrophages for the use in research. Specifically, by describing an open-sourced, defined, serum free medium, and investigating the importance of cell crowding in relation to macrophage phenotype and function. Second, to apply this model to investigate the function of specific proteins, during HIV-1 infection and the immune response. In particular, looking at the HIV-1 restriction protein TRIM5α, and a family of PPIases called cyclophilins.

7.1.1 Chapter 3: Defined, serum free, open-sourced medium for macrophage culture

In my first results chapter, I describe OXM, a defined, serum free, open-sourced medium in replacement of a commercial alternative of undisclosed composition that was originally designed for the expansion of lymphocytes *ex vivo*, X-VIVO™-15. While the protocol for macrophage differentiation from iPSC did not differ greatly from our previously described method (196), macrophages cultured in this new medium displayed improved signs of terminal differentiation. Cells were more adherent, less replicative, and showed closer metabolic gene signatures to primary tissue macrophages (microglia) compared to macrophages cultured in XVIVO. Furthermore, XVIVO cultured cells displayed higher expression of antiviral genes, which was reflected by a reduced susceptibility to single round HIV-1 infection. Therefore, OXM cultured cells provide a more useful model for investigating this virus. This would prove to be useful later in Chapter 5 when investigating TRIM5α and CyPA regulation of HIV-1 infection. Here, small differences between KO clone susceptibility and changes after pharmacological treatment may not have been detectible if cells had been cultured in XVIVO rather than OXM. In particular, the second role of CyPA in addition to protecting HIV against TRIM5α may not have been apparent. However, OXM should really be considered as a building block for improved differentiation protocols of iPSC-macrophages. Differences in yield highlight the potential for improvement, and the resting inflammatory state of macrophages in

OXM indicates either the need for co-culturing of these macrophages with other cells (372), or supplementation of OXM with cytokines, extracellular matrices, or metabolites derived from them.

7.1.2 Chapter 4: Density-dependent regulation of inflammation

In this chapter, I identified a major determinant of macrophage morphology, phenotype, and function, that appears to have been often overlooked in macrophage-based research. Having initially observed this feedback system by chance while investigating cyclophilin regulation of inflammation in Chapter 6, I went on to demonstrate how increasing cell number within a confined area results in a dramatic suppression of their cytokine response to a variety of pro-inflammatory stimuli. Further characterization of DDRI found a heterogeneity in cell morphology and phenotype. Some of this appeared to be linked, with differences in expression of surface markers like CD11b and CD45 depending on the cell morphology, while others were morphology independent. Transcriptomic analysis of macrophages plated at different densities revealed stark differences in profiles. Overall low and mid density cells were primed for an aggressive cytokine and chemokine response, cell death after stimulation, and possible increased proliferation. High density cells on the other hand were adjusted towards resolving the cause of inflammation, upregulating phagocytosis and lysosomal degradation, and transitioning the response towards the adaptive immune system via MHC class I signalling. Of greatest interest for future research, changes in plating density resulted in significant changes in expression of numerous genes related to Alzheimer's disease, indicating a clear potential role of DDRI in this disease. However, the precise mechanisms of DDRI remain unknown, with potential causes including, but not limited to, cell-cell or cell-extracellular matrix contacts (740, 741), metabolite concentrations (431, 445), and anti-inflammatory mediator quorum sensing (466).

7.1.3 Chapter 5: Cyclophilin A protects HIV-1 from TRIM5α

Chapter 5 was the first chapter to apply the iPSC-macrophage model towards investigation of specific protein functionality, and the first of two to describe the importance of CyPA within macrophages. Here, I studied TRIM5α, a viral restriction factor previously believed to be unable to recognize HIV-1, but capable of recognizing closely related SIV. Using KO iPSC-macrophages for TRIM5α, in combination with CyPA KO macrophages (generated in Chapter 6), I demonstrated that TRIM5α is capable of restricting HIV-1, but is actively prevented from doing so by CyPA. These findings support the conclusions of other manuscripts published within the duration of this thesis investigation (242, 329). Unlike these publications, I also investigated the potential mechanisms by which TRIM5α restricts HIV-1. Despite being important for the rescue of viral reverse transcription, inhibition of the proteasome was insufficient to rescue HIV-1 infectivity from TRIM5α restriction. Furthermore, neither was inhibition of innate immune activation, triggered either directly by TRIM5α or by detection of viral reverse transcripts by cGAS. Instead, I found that post-recognition by TRIM5α, HIV-1 is exposed to restriction by additional host factors SAMHD1 and TREX1. However, removing both of these proteins by CRISPR editing was insufficient to totally rescue viral infectivity, indicating the importance of another, as yet unidentified restriction factor. Finally, I also show evidence of a second role of CyPA during HIV-1 infection that is independent of TRIM5α and protects the virus prior to, or coinciding with, reverse transcription. This precise function remains undefined, but capsid mutant infectivity may indicate the involvement of capsid interactions both at the canonical HIV-CyPA interface, as well as a non-canonical interface independent of the CsA binding pocket on CyPA (586).

7.1.4 Chapter 6: Cyclophilin regulation of the innate immune response

In this final chapter, I explored further the function of CyPA, as well as its family members, into their potential regulation of the innate immune response. Initial broad inhibition of the cyclophilins using either the immunosuppressive drug CsA, or a non-immunosuppressive analogue NIM811, both demonstrated robust amplification of the innate

response to TLR activation. Another immunosuppressive drug FK506 which, like CsA, inhibits calcineurin as an off-target effect, had the converse effect, effectively suppressed the immune response. Transcriptional analysis demonstrated that cyclophilin inhibition upregulated inflammatory mediator mRNA levels within 4 hours of stimulation and this was maintained over a prolonged 24-hour period, while FK506 only appeared to influence gene transcription after approximately 24 hours. Using RNP-CRISPR-Cas9 KO cyclophilin cell lines I found that these pharmacological effects were largely independent of CyPA. At the same time, both CyPA and CyPB contribute to the suppression of the immune response to activation of different TLRs within macrophages. CyPA regulated the response to surface TLRs, particularly TLR1/2 and TLR4, while CyPB regulated TLR3. However, differences in inflammatory cytokine production by WT and KO cell lines were approximately only 2-fold and were independent of transcriptional changes in gene expression. Therefore, the specific mechanism of CyPA and CyPB regulation of macrophage inflammation, as well as the cyclophilin responsible for enhanced inflammation after pharmacological inhibition all remain unsolved. Finally, it should be noted that removing CyPA from macrophages did not result either in upregulation in other members of the cyclophilin family, nor affected iPSC-macrophage differentiation, contradicting previous publications stating otherwise (676, 718).

7.2 Current limitations

7.2.1 iPSC-derived macrophage differentiation

Differentiation of iPSC to macrophages in OXM reduced the total yield by approximately half when compared to culture in XVIVO. Therefore, XVIVO is promoting the proliferation of an unknown progenitor cell during differentiation when OXM is not. This highlights how, while the terminally differentiated macrophages generated from iPSC are now fairly well described through functional profiles, transcriptomics, and development ontogeny, the individual differentiation steps and progenitor cell types produced remain poorly defined. Other protocols offer more precise differentiation steps (194, 416, 417) or include isolation of specific

progenitor cells at different stages, like CD34+ positive cells (218, 404). However, with EB methodologies the number and location of these progenitors is not commonly described. Instead, it appears a stochastic approach is taken, where it is probable many EBs contain few if any of the required progenitor cell type. Instead we must rely on producing sufficient EB numbers to overcome this bottleneck.

In addition to undefined establishment of macrophage production, a major source of variability in iPSC-derived macrophage cultures is derived from the age of the cells within the cultures. In Chapter 3, transcriptomic comparisons revealed that this contributed to 15% of the variability, and in Chapter 6, I observed up to 100-fold differences in the cytokine response made by macrophages across sequential harvests from differentiation cultures. However, the true cause of variation over the age of a differentiation culture is unknown. Why do differentiation cultures eventually exhaust themselves? And what determines the relative “age” of different iPSC derived macrophages? In aging people, immunosenescence is typified by a depletion of HSCs and an impairment of cytokine production (742), which could explain culture exhaustion. However, given that I did not see an overall decline in cytokine production by my cultures over a 14-week period, the “age” variation observed here is more likely an accumulation of cellular stress. Considerable further characterisation is needed, then, to understand how our method evolves over time and whether a more consistent output can be generated. For example, closer regulation and uniformity in culturing and metabolite availability through the potential use of bioreactor-type cultures could create a more homogeneous population of macrophages (418).

7.2.2 Macrophage heterogeneity

When variation attributed to media type and cell age is subtracted from the total, there is a remaining 55% of variability left unaccounted for. While undoubtably some of this will be attributed to sample handling, it is reasonable to assume that macrophage heterogeneity will be a key contributor. Observation of macrophage morphology cultured in OXM or at different densities showed differences in shape, size, and adherence. Phenotyping in Chapter 4

demonstrated that this alone can result in changes in surface marker abundance and several papers have reported that macrophage shape can alter their inflammatory response (740, 741). As discussed in the Chapter 1 and 4, macrophages are highly plastic cells, and therefore this heterogeneity is both unsurprising and not necessarily undesirable. However, it emphasizes the need for single-cell resolution techniques if we are to uncover subtle changes in macrophages during homeostasis, immune stimulation, and infection. For example, in Chapter 5, macrophage infectivity by HIV-1 was frequently low (<10%) and never surpassed 30% unless SAMHD1 was knocked out. Why are these cells susceptible, but surrounding ones not? Is this relatively small percentage hiding potentially significant changes in antiviral response when individual genes are silenced? Likewise, the relatively small 2-fold difference in cytokine production observed in CyPA and CyPB KO macrophages post TLR stimulation may in-fact by substantially greater if we are to observe these macrophages at a single cell resolution.

7.2.3 CRISPR screening with iPSC-derived macrophages

Both Chapters 5 and 6 demonstrate the power of CRISPR-Cas9 editing in iPSC to make macrophages for precise interrogation of macrophage functionality beyond that previously reported using lentiviral polyclonal KO or RNA-mediated KD in primary macrophages. Without it, the second CyPA role in HIV-1 infection could only be dismissed as donor variability and deciphering which cyclophilin is responsible for CsA-enhanced inflammation would be near impossible. However, even with improved editing by transient methods like RNPs and clone screening approaches, CRISPR in iPSC is extremely slow, and success rate is low, as demonstrated by my failure to generate all cyclophilin KO cell lines originally planned. Additionally, investigations like mine may require additional editing of other genes, e.g., TREX1 and SAMHD1 in Chapter 5, within the same cell line as your original edit. With the probability of iPSC picking up chromosomal mutations and epigenetic changes increasing as passage numbers increase (743), there will inevitably be a limit on the number of sequential edits that can be made within iPSC before cells may lose pluripotency, spontaneously

differentiate, or fail to differentiate into macrophages. Therefore, there is a need to generate more rapid, higher efficiency, and potentially inducible methods of CRISPR editing in iPSC. For example, one can hypothesise that production of an inducible stable Cas9-expressing iPSC line could improve efficiency of editing and allow for faster editing of multiple genes of interest without the need for frequent stress inducing electroporation of iPSC (744).

iPSC and macrophages derived from them do not only lend themselves as a malleable system for targeted CRISPR editing, but also for large scale genome wide CRISPR screens. By using gRNAs as a genetic barcode, lentiviral CRISPR systems and high throughput reporter assays are being used to reproducibly identify individual genes that contribute to disease phenotypes and decipher cellular signalling pathways (745, 746). However, these screens require large quantities of cells in the range of $1x10^8$ cells (747). Even so, large scale screens will often utilise the minimal number of cells required to maximise the output, as demonstrated by a recent drug screen on macrophages seeking to drive M1 or M2 polarization (748). However, as I show in this thesis, this could mean we miss significant “hits” that may only become apparent when macrophages are plated at higher densities. In conclusion, this thesis emphasizes the ever-present need for greater definition of culturing conditions if we are to unlock the full potential of iPSC-derived macrophages as a model for investigating human disease.

7.3 Future directions

Chapters 3 and 4 have laid the groundwork for future exploration of macrophage differentiation and function. Building upon the description of OXM medium, next steps will need to improve macrophage yield and consistency. By comparing the efficacy of this media for differentiation of macrophages by alternative methods, such as monolayer methodologies (399), or by expanding culture size into large scale bioreactors (418), we can hopefully increase yield and better determine the required growth factors and their relative chronology, duration, and concentrations. This in turn could reduce the cost of this system, a current major

limitation in its accessibility to researchers. For DDRI, the primary goal going forward is to determine the mechanism of this feedback loop. I provide evidence this involves both soluble and insoluble signals, but in a “chicken or the egg” type scenario, it is unclear which comes first. Current literature in the field highlights the importance of NO (445), M-CSF concentrations (465, 468), and physical constraints (741) as known potential mechanisms. These will therefore need to be the first avenues explored, while simultaneously using high throughput informatic approaches such as LC-MS and single-cell RNA-Seq to identify alternative compounds of interest and better define the characteristics of these highly heterogeneous cells. In addition, I found evidence of DDRI playing a role in AD related gene regulation. This will be an exciting area for further exploration, requiring confirmation at the protein level, and evaluation of its functional importance such as changes in phagocytic capacity and response to dying neurons.

Chapters 5 and 6 have shed light on the function of cyclophilins in infection and the immune response. In Chapter 5, the mechanism for TRIM5α restriction of HIV-1 remains incomplete. Further KO cell lines for other HIV restriction factors, particularly those which share CA interactions with CyPA like Mx2 (513), need to be generated. Also, to determine the second function of CyPA, use of a broader panel of CA mutants may help determine essential CA residues. Site specific mutants of CyPA both within the CsA binding pocket and external to the CsA binding pocket at the reported non-canonical binding sites (586) will determine the relative importance of PPIase activity and the critical mode of CyPA-CA interaction. Finally, in Chapter 6, expansion of inflammatory response screening to include my other 2 KO lines, *PPIF* and *BSG*, will help determining whether mitochondrial stress or extracellular cyclophilins play a role in the CsA enhanced inflammatory response (648, 654). Additionally, expanding the KO pool to include other cyclophilins, both as single KO and as multiple KO, could identify the cyclophilin responsible. Description of the key intracellular signalling component for cyclophilin regulation of the inflammatory response is still needed, although expansion of the timescale of these experiments may be required to increase the differences in response observed and improve chances of detection.

Appendix

Licences

In order of appearance in this thesis:

"Development and Functional Differentiation of Tissue-Resident Versus Monocyte-Derived Macrophages in Inflammatory Reactions" Italiani and Boraschi *NSpring eBook* (2017). Figure 2.1: Origin of monocyte-derived macrophages (moMϕ) and tissue-resident macrophages (trMϕ). Licence number: 5042721051834. Licence date: 05/04/2021. License content publisher: Springer Nature.

"Tissue-Resident Macrophage Ontogeny and Homeostasis" Ginhoux and Guilliams *Immunity* (2016). Figure 3: Heterogeneity of Tissue-Resident Macrophage Ontogeny in Adult Tissues in the Steady State. Licence number: 5015880013192. Licence date: 25/02/2021. License content publisher: Elsevier.

"Macrophage Activation and Polarization: Nomenclature and Experimental Guidelines" Murray *et al. Immunity* (2014). Figure 1B: Framework for Describing Activated Macrophages. Licence number: 5015880111098. Licence date: 25/02/2021. License content publisher: Elsevier.

"Induced Pluripotent Stem Cells Meet Genome Editing" Hockemeyer and Jaenisch *Cell Stem Cell* (2016). Figure 1: Overview of the iPSC technology. Licence number: 5015871410788. Licence date: 25/02/2021. License content publisher: Elsevier.

"Capsid-Dependent Host Factors in HIV-1 Infection" Yamashita and Engelman *Trends in Microbiology* (2017). Figure 1A: HIV-1 Capsid Protein (CA) Structures and Common Host Factor Interaction Sites. Licence number: 5091551446441. Licence date: 17/06/2021. License content publisher: Elsevier.

"The Human Immunodeficiency Virus Capsid Is More Than Just a Genome Package" James and Jacques *Annual Review of Virology* (2018). Figure 1: Structural model of an HIV

capsid illustrating its distinctive cone shape. Licence number: 1126784-1. Licence date: 17/06/2021. License content publisher: Annual Reviews, Inc.

“Multiple cyclophilins involved in different cellular pathways mediate HCV replication” Gaither *et al. Virology* (2010). Figure 4: Several cyclophilin-mediated pathways play a role in maintaining HCV. Licence number: 5015880185808. Licence date: 25/02/2021. License content publisher: Elsevier.

“Capsid-Dependent Host Factors in HIV-1 Infection” Yamashita and Engelman *Trends in Microbiology* (2017). Figure 2: Capsid-Dependent Host Factors for Post-Entry Events of HIV-1 Infection. Licence number: 5015890426111. Licence date: 25/02/2021. License content publisher: Elsevier.

“Restriction of HIV-1 and other retroviruses by TRIM5” Ganser-Pornillos *et al. Nature Reviews Microbiology* (2019). Figure 2A-B: Structural and functional properties of TRIM5. Figure 3C: Mechanism of core recognition by TRIM5. Licence number: 5033280994026. Licence date: 20/03/2021. License content publisher: Springer Nature.

References

1. Tauber AI. 2003. Metchnikoff and the phagocytosis theory. Nat Rev Mol Cell Biol 4:897–901.

2. Edholm E-S, Kun H., Robert J. 2017. Evolutionary Aspects of Macrophages Polarization, p. 3–22. *In* Kloc, M (ed.), Macrophages Origin, Function and Biointervention, 62nd ed.

3. Gordon S, Plüddemann A. 2017. Tissue macrophages: Heterogeneity and functions. BMC Biol 15:1–18.

4. Mantovani A, Sica A, Sozzani S, Allavena P, Vecchi A, Locati M. 2004. The chemokine system in diverse forms of macrophage activation and polarization. Trends Immunol 25:677–686.

5. Chávez-Galán L, Olleros ML, Vesin D, Garcia I. 2015. Much more than M1 and M2 macrophages, there are also CD169+ and TCR+ macrophages. Front Immunol 6:1–15.

6. Roche PA, Furuta K. 2015. The ins and outs of MHC class II-mediated antigen processing and presentation. Nat Rev Immunol 15:203–216.

7. Mosser DM, Edwards JP. 2008. Exploring the full spectrum of macrophage activation. Nat Rev Immunol 8:958–969.

8. Gordon S, Martinez FO. 2010. Alternative activation of macrophages: Mechanism and functions. Immunity 32:593–604.

9. Gordon S, Plüddemann A. 2018. Macrophage clearance of apoptotic cells: A critical assessment. Front Immunol 9:1–9.

10. Guilliams M, Thierry GR, Bonnardel J, Bajenoff M. 2020. Establishment and Maintenance of the Macrophage Niche. Immunity 52:434–451.

11. Boyle W., Simonet W., Lacey D. 2003. Osteoclast differentiation and activation. Nature 423:337–342.

12. Hussell T, Bell TJ. 2014. Alveolar macrophages: Plasticity in a tissue-specific context. Nat Rev Immunol 14:81–93.

13. Li Q, Barres BA. 2018. Microglia and macrophages in brain homeostasis and disease. Nat Rev Immunol 18:225–242.

14. T'Jonck W, Guilliams M, Bonnardel J. 2018. Niche signals and transcription factors involved in tissue-resident macrophage development. Cell Immunol 330:43–53.

15. Yona S, Jung S. 2010. Monocytes: Subsets, origins, fates and functions. Curr Opin Hematol 17:53–59.

16. Wong KL, Yeap WH, Tai JJY, Ong SM, Dang TM, Wong SC. 2012. The three human monocyte subsets: Implications for health and disease. Immunol Res 53:41–57.

17. Boyette LB, MacEdo C, Hadi K, Elinoff BD, Walters JT, Ramaswami B, Chalasani G, Taboas JM, Lakkis FG, Metes DiM. 2017. Phenotype, function, and differentiation potential of human monocyte subsets. PLoS One 12:1–20.

18. Cros J, Cagnard N, Woollard K, Patey N, Zhang SY, Senechal B, Puel A, Biswas SK, Moshous D, Picard C, Jais JP, D'Cruz D, Casanova JL, Trouillet C, Geissmann F. 2010.

Human CD14dim Monocytes Patrol and Sense Nucleic Acids and Viruses via TLR7 and TLR8 Receptors. Immunity 33:375–386.

19. Lavin Y, Winter D, Blecher-Gonen R, David E, Keren-Shaul H, Merad M, Jung S, Amit I. 2014. Tissue-resident macrophage enhancer landscapes are shaped by the local microenvironment. Cell 159:1312–1326.

20. Beattie L, Sawtell A, Mann J, Frame TCM, Teal B, de Labastida Rivera F, Brown N, Walwyn-Brown K, Moore JWJ, MacDonald S, Lim EK, Dalton JE, Engwerda CR, MacDonald KP, Kaye PM. 2016. Bone marrow-derived and resident liver macrophages display unique transcriptomic signatures but similar biological functions. J Hepatol 65:758–768.

21. Gibbings SL, Goyal R, Desch AN, Leach SM, Prabagar M, Atif SM, Bratton DL, Janssen W, Jakubzick C V. 2015. Transcriptome analysis highlights the conserved difference between embryonic and postnatal-derived alveolar macrophages. Blood 126:1357–1366.

22. Italiani P, Boraschi D. 2017. Development and Functional Differentiation of Tissue-Resident Versus Monocyte-Derived Macrophages in Inflammatory Reactions, p. 23–43. *In* Kloc, M (ed.), Macrophages Origin, Function and Biointervention, 62nd ed. Springer International Publishing.

23. Ginhoux F, Schultze JL, Murray PJ, Ochando J, Biswas SK. 2016. New insights into the multidimensional concept of macrophage ontogeny, activation and function. Nat Immunol 17:34–40.

24. van Furth R, Cohn ZA, Hirsch JG, Humphrey JH, Spector WG, Langevoort HL. 1972. The mononuclear phagocyte system: a new classification of macrophages, monocytes, and their precursor cells. Bull World Health Organ 46:845–852.

25. Ginhoux F, Guilliams M. 2016. Tissue-Resident Macrophage Ontogeny and Homeostasis. Immunity 44:439–449.

26. Ginhoux F, Greter M, Leboeuf M, Nandi S, See P, Gokhan S, Mehler MF, Conway SJ, Ng LG, Stanley ER, Samokhvalov IM, Merad M. 2010. Fate mapping analysis reveals that adult microglia derive from primitive macrophages. Science (80-) 330:841–845.

27. Merad M, Manz MG, Karsunky H, Wagers A, Peters W, Charo I, Weissman IL, Cyster JG, Engleman EG. 2002. Langerhans cells renew in the skin throughout life under steady-state conditions. Nat Immunol 3:1135–1141.

28. Gomez Perdiguero E, Klapproth K, Schulz C, Busch K, Azzoni E, Crozet L, Garner H, Trouillet C, De Bruijn MF, Geissmann F, Rodewald HR. 2015. Tissue-resident macrophages originate from yolk-sac-derived erythro-myeloid progenitors. Nature 518:547–551.

29. Hashimoto D, Chow A, Noizat C, Teo P, Beasley MB, Leboeuf M, Becker CD, See P, Price J, Lucas D, Greter M, Mortha A, Boyer SW, Forsberg EC, Tanaka M, van Rooijen N, García-Sastre A, Stanley ER, Ginhoux F, Frenette PS, Merad M. 2013. Tissue-resident macrophages self-maintain locally throughout adult life with minimal contribution from circulating monocytes. Immunity 38:792–804.

30. Scott CL, Henri S, Guilliams M. 2014. Mononuclear phagocytes of the intestine, the skin, and the lung. Immunol Rev 262:9–24.

31. Bain CC, Bravo-Blas A, Scott CL, Gomez Perdiguero E, Geissmann F, Henri S, Malissen B, Osborne LC, Artis D, Mowat AMI. 2014. Constant replenishment from circulating monocytes maintains the macrophage pool in the intestine of adult mice. Nat

Immunol 15:929–937.

32. Molawi K, Wolf Y, Kandalla PK, Favret J, Hagemeyer N, Frenzel K, Pinto AR, Klapproth K, Henri S, Malissen B, Rodewald HR, Rosenthal NA, Bajenoff M, Prinz M, Jung S, Sieweke MH. 2014. Progressive replacement of embryo-derived cardiac macrophages with age. J Exp Med 211:2151–2158.

33. Clarke D, Vegiopoulos A, Crawford A, Mucenski M, Bonifer C, Frampton J. 2000. In vitro differentiation of c-myb(-/-) ES cells reveals that the colony forming capacity of unilineage macrophage precursors and myeloid progenitor commitment are c-Myb independent. Oncogene 19:3343–3351.

34. Vanhee S, De Mulder K, Van Caeneghem Y, Verstichel G, Van Roy N, Menten B, Velghe I, Philippé J, De Bleser D, Lambrecht BN, Taghon T, Leclercq G, Kerre T, Vandekerckhove B. 2015. In vitro human embryonic stem cell hematopoiesis mimics MYB-independent yolk sac hematopoiesis. Haematologica 100:157–166.

35. Buchrieser J, James W, Moore MD. 2017. Human Induced Pluripotent Stem Cell-Derived Macrophages Share Ontogeny with MYB-Independent Tissue-Resident Macrophages. Stem Cell Reports 8:334–345.

36. Bruttger J, Karram K, Wörtge S, Regen T, Marini F, Hoppmann N, Klein M, Blank T, Yona S, Wolf Y, Mack M, Pinteaux E, Müller W, Zipp F, Binder H, Bopp T, Prinz M, Jung S, Waisman A. 2015. Genetic Cell Ablation Reveals Clusters of Local Self-Renewing Microglia in the Mammalian Central Nervous System. Immunity 43:92–106.

37. Thornley TB, Fang Z, Balasubramanian S, Larocca RA, Gong W, Gupta S, Csizmadia E, Degauque N, Kim BS, Koulmanda M, Kuchroo VK, Strom TB. 2014. Fragile TIM-4-expressing tissue resident macrophages are migratory and immunoregulatory. J Clin Invest 124:3443–3454.

38. van de Laar L, Saelens W, De Prijck S, Martens L, Scott CL, Van Isterdael G, Hoffmann E, Beyaert R, Saeys Y, Lambrecht BN, Guilliams M. 2016. Yolk Sac Macrophages, Fetal Liver, and Adult Monocytes Can Colonize an Empty Niche and Develop into Functional Tissue-Resident Macrophages. Immunity 44:755–768.

39. Guilliams M, Svedberg FR. 2021. Does tissue imprinting restrict macrophage plasticity? Nat Immunol 22:118–127.

40. Horiuchi K. 2013. A brief history of tumor necrosis factor α - converting enzyme: An overview of ectodomain shedding. Keio J Med.

41. Lacy P, Stow JL. 2011. Cytokine release from innate immune cells: Association with diverse membrane trafficking pathways. Blood 118:9–18.

42. Schaub A, Glasmacher E. 2017. Splicing in immune cells-mechanistic insights and emerging topics. Int Immunol 29:173–181.

43. Perdiguero EG, Geissmann F. 2016. The development and maintenance of resident macrophages. Nat Immunol 17:2–8.

44. Varol C, Mildner A, Jung S. 2015. Macrophages: Development and tissue specializationAnnual Review of Immunology.

45. Gosselin D, Link VM, Romanoski CE, Fonseca GJ, Eichenfield DZ, Spann NJ, Stender JD, Chun HB, Garner H, Geissmann F, Glass CK. 2014. Environment drives selection and function of enhancers controlling tissue-specific macrophage identities. Cell 159:1327–1340.

46. Gautiar EL, Shay T, Miller J, Greter M, Jakubzick C, Ivanov S, Helft J, Chow A, Elpek

KG, Gordonov S, Mazloom AR, Ma'Ayan A, Chua WJ, Hansen TH, Turley SJ, Merad M, Randolph GJ, Best AJ, Knell J, Goldrath A, Brown B, Jojic V, Koller D, Cohen N, Brenner M, Regev A, Fletcher A, Bellemare-Pelletier A, Malhotra D, Jianu R, Laidlaw D, Collins J, Narayan K, Sylvia K, Kang J, Gazit R, Garrison BS, Rossi DJ, Kim F, Rao TN, Wagers A, Shinton SA, Hardy RR, Monach P, Bezman NA, Sun JC, Kim CC, Lanier LL, Heng T, Kreslavsky T, Painter M, Ericson J, Davis S, Mathis D, Benoist C. 2012. Gene-expression profiles and transcriptional regulatory pathways that underlie the identity and diversity of mouse tissue macrophages. Nat Immunol 13:1118–1128.

47. Okabe Y, Medzhitov R. 2016. Tissue biology perspective on macrophages. Nat Immunol 17:9–17.

48. Mills CD, Kincaid K, Alt JM, Heilman MJ, Hill AM. 2000. M-1/M-2 Macrophages and the Th1/Th2 Paradigm. J Immunol 164:6166–6173.

49. Mosser DM. 2003. The many faces of macrophage activation. J Leukoc Biol 73:209–212.

50. Murray PJ, Allen JE, Biswas SK, Fisher EA, Gilroy DW, Goerdt S, Gordon S, Hamilton JA, Ivashkiv LB, Lawrence T, Locati M, Mantovani A, Martinez FO, Mege JL, Mosser DM, Natoli G, Saeij JP, Schultze JL, Shirey KA, Sica A, Suttles J, Udalova I, vanGinderachter JA, Vogel SN, Wynn TA. 2014. Macrophage Activation and Polarization: Nomenclature and Experimental Guidelines. Immunity 41:14–20.

51. Takeuchi O, Akira S. 2010. Pattern Recognition Receptors and Inflammation. Cell 140:805–820.

52. Kawasaki T, Kawai T. 2014. Toll-like receptor signaling pathways. Front Immunol 5:1–8.

53. Sun L, Wu J, Du F, Chen X, Chen ZJ. 2013. Cyclic GMP-AMP synthase is a cytosolic DNA sensor that activates the type I interferon pathway. Science (80-) 339:786–791.

54. Hong C, Tijhuis AE, Foijer F. 2019. The cGAS Paradox: Contrasting Roles for cGAS-STING Pathway in Chromosomal Instability. Cells 8.

55. Martinez FO, Gordon S. 2014. The M1 and M2 paradigm of macrophage activation: Time for reassessment. F1000Prime Rep 6:1–13.

56. Barclay AN, Wright GJ, Brooke G, Brown MH. 2002. CD200 and membrane protein interactions in the control of myeloid cells. Trends Immunol 23:285–290.

57. A-Gonzalez N, Quintana JA, García-Silva S, Mazariegos M, de la Aleja AG, Nicolás-ávila JA, Walter W, Adrover JM, Crainiciuc G, Kuchroo VK, Rothlin C V., Peinado H, Castrillo A, Ricote M, Hidalgo A. 2017. Phagocytosis imprints heterogeneity in tissue-resident macrophages. J Exp Med 214:1281–1296.

58. Henson PM, Bratton DL. 2013. Antiinflammatory effects of apoptotic cells. J Clin Invest 123:2773–2774.

59. Zanoni I, Tan Y, Di Gioia M, Springstead JR, Kagan JC. 2017. By Capturing Inflammatory Lipids Released from Dying Cells, the Receptor CD14 Induces Inflammasome-Dependent Phagocyte Hyperactivation. Immunity 47:697-709.e3.

60. Stables MJ, Shah S, Camon EB, Lovering RC, Newson J, Bystrom J, Farrow S, Gilroy DW. 2011. Transcriptomic analyses of murine resolution-phase macrophages. Blood 118:192–208.

61. Nahrendorf M, Swirski FK. 2016. Abandoning M1/M2 for a network model of macrophage function. Circ Res 119:414–417.

62. Stout RD, Jiang C, Matta B, Tietzel I, Watkins SK, Suttles J. 2005. Macrophages Sequentially Change Their Functional Phenotype in Response to Changes in Microenvironmental Influences. J Immunol 175:342–349.

63. Xue J, Schmidt S V., Sander J, Draffehn A, Krebs W, Quester I, DeNardo D, Gohel TD, Emde M, Schmidleithner L, Ganesan H, Nino-Castro A, Mallmann MR, Labzin L, Theis H, Kraut M, Beyer M, Latz E, Freeman TC, Ulas T, Schultze JL. 2014. Transcriptome-Based Network Analysis Reveals a Spectrum Model of Human Macrophage Activation. Immunity 40:274–288.

64. Anders C., Lawton TM., Smith H., Garret J, Doucette M., Ammons MCB. 2020. Integrated Metabolomics, Transcriptomics, and Signal Protein Profile Define the Effector Function and Associated Metabotype of Five Polarized Macrophage Phenotypes. bioRxiv Prepr Serv Biol https://doi.org/https://doi.org/10.1101/2020.03.10.985788.

65. Bertani FR, Mozetic P, Fioramonti M, Iuliani M, Ribelli G, Pantano F, Santini D, Tonini G, Trombetta M, Businaro L, Selci S, Rainer A. 2017. Classification of M1/M2-polarized human macrophages by label-free hyperspectral reflectance confocal microscopy and multivariate analysis. Sci Rep 7:1–9.

66. Geijtenbeek TBH, Gringhuis SI. 2009. Signalling through C-type lectin receptors: Shaping immune responses. Nat Rev Immunol 9:465–479.

67. Lamkanfi M, Dixit VM. 2014. Mechanisms and functions of inflammasomes. Cell 157:1013–1022.

68. Rathinam VAK, Vanaja SK, Fitzgerald KA. 2012. Regulation of inflammasome signaling. Nat Immunol 13:333–342.

69. Nagata S, Hanayama R, Kawane K. 2010. Autoimmunity and the Clearance of Dead Cells. Cell 140:619–630.

70. Lemke G, Rothlin C V. 2008. Immunobiology of the TAM receptors. Nat Rev Immunol 8:327–336.

71. Desai BN, Leitinger N. 2014. Purinergic and calcium signaling in macrophage function and plasticity. Front Immunol 5:1–8.

72. Lewis CE, Pollard JW. 2006. Distinct role of macrophages in different tumor microenvironments. Cancer Res 66:605–612.

73. Lattin J, Zidar DA, Schroder K, Kellie S, Hume DA, Sweet MJ. 2007. G-protein-coupled receptor expression, function, and signaling in macrophages. J Leukoc Biol 82:16–32.

74. Link TM, Park U, Vonakis BM, Raben DM, Soloski MJ, Caterina MJ. 2010. TRPV2 has a pivotal role in macrophage particle binding and phagocytosis. Nat Immunol 11:232–239.

75. Kashio M, Sokabe T, Shintaku K, Uematsu T, Fukuta N, Kobayashi N, Mori Y, Tominaga M. 2012. Redox signal-mediated sensitization of transient receptor potential melastatin 2 (TRPM2) to temperature affects macrophage functions. Proc Natl Acad Sci U S A 109:6745–6750.

76. Compan V, Baroja-Mazo A, López-Castejón G, Gomez AI, Martínez CM, Angosto D, Montero MT, Herranz AS, Bazán E, Reimers D, Mulero V, Pelegrín P. 2012. Cell Volume Regulation Modulates NLRP3 Inflammasome Activation. Immunity 37:487–500.

77. Ip WKE, Medzhitov R. 2015. Macrophages monitor tissue osmolarity and induce

inflammatory response through NLRP3 and NLRC4 inflammasome activation. Nat Commun 6.

78. Haldar M, Kohyama M, So AYL, Kc W, Wu X, Briseño CG, Satpathy AT, Kretzer NM, Arase H, Rajasekaran NS, Wang L, Egawa T, Igarashi K, Baltimore D, Murphy TL, Murphy KM. 2014. Heme-mediated SPI-C induction promotes monocyte differentiation into iron-recycling macrophages. Cell 156:1223–1234.

79. Okabe Y, Medzhitov R. 2014. Tissue-specific signals control reversible program of localization and functional polarization of macrophages. Cell 157:832–844.

80. Liu PT, Stenger S, Li H, Wenzel L, Tan BH, Krutzik SR, Ochoa MT, Schauber J, Wu K, Meinken C, Kamen DL, Wagner M, Bals R, Steinmeyer A, Zügel U, Gallo RL, Eisanberg D, Hewison M, Hollis BW, Adams JS, Bloom BR, Modlin RL. 2006. Toll-like receptor triggering of a vitamin D-mediated human antimicrobial response. Science (80-) 311:1770–1773.

81. Ganeshan K, Chawla A. 2014. Metabolic regulation of immune responses. Annu Rev Immunol 32:609–634.

82. Hansson GK, Hermansson A. 2011. The immune system in atherosclerosis. Nat Immunol 12:204–212.

83. Moore KJ, Sheedy FJ, Fisher EA. 2013. Macrophages in atherosclerosis: A dynamic balance. Nat Rev Immunol 13:709–721.

84. Oh DY, Talukdar S, Bae EJ, Imamura T, Morinaga H, Fan WQ, Li P, Lu WJ, Watkins SM, Olefsky JM. 2010. GPR120 Is an Omega-3 Fatty Acid Receptor Mediating Potent Anti-inflammatory and Insulin-Sensitizing Effects. Cell 142:687–698.

85. Rahman M, Muhammad S, Khan MA, Chen H, Ridder DA, Müller-Fielitz H, Pokorná B, Vollbrandt T, Stölting I, Nadrowitz R, Okun JG, Offermanns S, Schwaninger M. 2014. The b-hydroxybutyrate receptor HCA 2 activates a neuroprotective subset of macrophages. Nat Commun 5:1–11.

86. Weigert A, Weis N, Brüne B. 2009. Regulation of macrophage function by sphingosine-1-phosphate. Immunobiology 214:748–760.

87. McCutcheon JC, Hart SP, Canning M, Ross K, Humphries MJ, Dransfield I. 1998. Regulation of macrophage phagocytosis of apoptotic neutrophils by adhesion to fibronectin. J Leukoc Biol 64:600–607.

88. Santiago-García J, Kodama T, Pitas RE. 2003. The class A scavenger receptor binds to proteoglycans and mediates adhesion of macrophages to the extracellular matrix. J Biol Chem 278:6942–6946.

89. Franco C, Britto K, Wong E, Hou G, Zhu SN, Chen M, Cybulsky MI, Bendeck MP. 2009. Discoidin domain receptor 1 on bone marrow-derived cells promotes macrophage accumulation during atherogenesis. Circ Res 105:1141–1148.

90. Leitinger B. 2011. Transmembrane collagen receptors. Annu Rev Cell Dev Biol 27:265–290.

91. Sturge J, Todd SK, Kogianni G, McCarthy A, Isacke CM. 2007. Mannose receptor regulation of macrophage cell migration. J Leukoc Biol 82:585–593.

92. Woo HJ, Shaw LM, Messier JM, Mercurio AM. 1990. The major non-integrin laminin binding protein of macrophages is identical to carbohydrate binding protein 35 (Mac-2). J Biol Chem 265:7097–7099.

93. McKee CM, Penno MB, Cowman M, Burdick MD, Strieter RM, Bao C, Noble PW. 1996.

Hyaluronan (HA) fragments induce chemokine gene expression in alveolar macrophages: The role of HA size and CD44. J Clin Invest 98:2403–2413.

94. Jang JY, Koh YJ, Lee SH, Lee J, Kim KH, Kim D, Koh GY, Yoo OJ. 2013. Conditional ablation of LYVE-1+ cells unveils defensive roles of lymphatic vessels in intestine and lymph nodes. Blood 122:2151–2161.

95. Termeer C, Benedix F, Sleeman J, Fieber C, Voith U, Ahrens T, Miyake K, Freudenberg M, Galanos C, Simon JC. 2002. Oligosaccharides of hyaluronan activate dendritic cells via Toll-like receptor 4. J Exp Med 195:99–111.

96. Foster SL, Medzhitov R. 2009. Gene-specific control of the TLR-induced inflammatory response. Clin Immunol 130:7–15.

97. Schroder K, Sweet MJ, Hume DA. 2006. Signal integration between IFNγ and TLR signalling pathways in macrophages. Immunobiology.

98. Kovarik P, Ebner F, Sedlyarov V. 2017. Posttranscriptional regulation of cytokine expression. Cytokine 89:21–26.

99. Sahoo A, Im SH. 2010. Interleukin and interleukin receptor diversity: Role of alternative splicing. Int Rev Immunol 29:77–109.

100. Murray RZ, Stow JL. 2014. Cytokine secretion in macrophages: SNAREs, Rabs, and membrane trafficking. Front Immunol 5:1–9.

101. Stanley AC, Lacy P. 2010. Pathways for cytokine secretion. Physiology 25:218–229.

102. Stow JL, Ching Low P, Offenhäuser C, Sangermani D. 2009. Cytokine secretion in macrophages and other cells: Pathways and mediators. Immunobiology 214:601–612.

103. Eder C. 2009. Mechanisms of interleukin-1β release. Immunobiology.

104. Evavold CL, Ruan J, Tan Y, Xia S, Wu H, Kagan JC. 2018. The Pore-Forming Protein Gasdermin D Regulates Interleukin-1 Secretion from Living Macrophages. Immunity 48:35-44.e6.

105. Martin-Sanchez F, Diamond C, Zeitler M, Gomez AI, Baroja-Mazo A, Bagnall J, Spiller D, White M, Daniels MJD, Mortellaro A, Penalver M, Paszek P, Steringer JP, Nickel W, Brough D, Pelegrin P. 2016. Inflammasome-dependent IL-1β release depends upon membrane permeabilisation. Cell Death Differ.

106. Van Gorp H, Van Opdenbosch N, Lamkanfi M. 2019. Inflammasome-dependent cytokines at the crossroads of health and autoinflammatory disease. Cold Spring Harb Perspect Biol 11.

107. He Y, Hara H, Núñez G. 2016. Mechanism and Regulation of NLRP3 Inflammasome Activation. Trends Biochem Sci 41:1012–1021.

108. Brooks AJ, Dehkhoda F, Kragelund BB. 2018. Cytokine Receptors, p. 157–186. *In* Belfiore, A, LeRoith, D (eds.), Principles of Endocrinology and Hormone Action. Springer, Cham.

109. Vanamee ÉS, Faustman DL. 2018. Structural principles of tumor necrosis factor superfamily signaling. Sci Signal 11:1–12.

110. Levine SJ. 2004. Mechanisms of Soluble Cytokine Receptor Generation. J Immunol 173:5343–5348.

111. Idriss HT, Naismith JH. 2000. TNFα and the TNF receptor superfamily: Structure-function relationship(s). Microsc Res Tech 50:184–195.

112. Duque GA, Descoteaux A. 2014. Macrophage cytokines: Involvement in immunity and infectious diseases. Front Immunol 5:1–12.

113. Cendrowski J, Mamińska A, Miaczynska M. 2016. Endocytic regulation of cytokine receptor signaling. Cytokine Growth Factor Rev 32:63–73.

114. Ceresa BP, Schmid SL. 2000. Regulation of signal transduction by endocytosis. Curr Opin Cell Biol 12:204–210.

115. Tada M, Takahama Y, Abe K, Nakatsuji N, Tada T. 2001. Nuclear reprogramming of somatic cells by in vitro hybridization with ES cells. Curr Biol 11:1553–1558.

116. Gurdon JB. 1962. The developmental capacity of nuclei taken from intestinal epithelium cells of feeding tadpoles. J Embryol Exp Morphol 10:622–640.

117. Kaufman MH, Evans MJ. 1981. Establishment in culture of pluripotential cells from mouse embryos. Nature 292:154–156.

118. Martin GR. 1981. Isolation of a pluripotent cell line from early mouse embryos cultured in medium conditioned by teratocarcinoma stem cells. Proc Natl Acad Sci U S A 78:7634–7638.

119. Thomson JA. 1998. Embryonic stem cell lines derived from human blastocysts. Science (80-) 282:1145–1147.

120. Takahashi K, Yamanaka S. 2006. Induction of Pluripotent Stem Cells from Mouse Embryonic and Adult Fibroblast Cultures by Defined Factors. Cell 126:663–676.

121. Takahashi K, Tanabe K, Ohnuki M, Narita M, Ichisaka T, Tomoda K, Yamanaka S. 2007. Induction of Pluripotent Stem Cells from Adult Human Fibroblasts by Defined Factors. Cell 131:861–872.

122. Velychko S, Adachi K, Kim KP, Hou Y, MacCarthy CM, Wu G, Schöler HR. 2019. Excluding Oct4 from Yamanaka Cocktail Unleashes the Developmental Potential of iPSCs. Cell Stem Cell 25:737-753.e4.

123. Jincho Y, Araki R, Hoki Y, Tamura C, Nakamura M, Ando S, Kasama Y, Abe M. 2010. Generation of genome integration-free induced pluripotent stem cells from fibroblasts of C57BL/6 mice without c-Myc transduction. J Biol Chem 285:26384–26389.

124. Nakagawa M, Koyanagi M, Tanabe K, Takahashi K, Ichisaka T, Aoi T, Okita K, Mochiduki Y, Takizawa N, Yamanaka S. 2008. Generation of induced pluripotent stem cells without Myc from mouse and human fibroblasts. Nat Biotechnol 26:101–106.

125. YU J, Vodyanik M., Smuga-Otto K, Antosiewicz-Bourget J, Frane J., Tian S, Nie J, Jonsdottir G., Ruotti V, Stewart I., Thomson J. 2008. Induced pluripotent stem cell lines derived from human somatic cells. Science (80-) 318:1917–1920.

126. Ban H, Nishishita N, Fusaki N, Tabata T, Saeki K, Shikamura M, Takada N, Inoue M, Hasegawa M, Kawamata S, Nishikawa SI. 2011. Efficient generation of transgene-free human induced pluripotent stem cells (iPSCs) by temperature-sensitive Sendai virus vectors. Proc Natl Acad Sci U S A 108:14234–14239.

127. Staerk J, Dawlaty MM, Gao Q, Maetzel D, Hanna J, Sommer CA, Mostoslavsky G, Jaenisch R. 2010. Reprogramming of human peripheral blood cells to induced pluripotent stem cells. Cell Stem Cell 7:20–24.

128. Rais Y, Zviran A, Geula S, Gafni O, Chomsky E, Viukov S, Mansour AA, Caspi I, Krupalnik V, Zerbib M, Maza I, Mor N, Baran D, Weinberger L, Jaitin DA, Lara-Astiaso D, Blecher-Gonen R, Shipony Z, Mukamel Z, Hagai T, Gilad S, Amann-Zalcenstein D, Tanay A, Amit I, Novershtern N, Hanna JH. 2013. Deterministic direct reprogramming

of somatic cells to pluripotency. Nature 502:65–70.

129. Woltjen K, Michael IP, Mohseni P, Desai R, Mileikovsky M, Hämäläinen R, Cowling R, Wang W, Liu P, Gertsenstein M, Kaji K, Sung HK, Nagy A. 2009. PiggyBac transposition reprograms fibroblasts to induced pluripotent stem cells. Nature 458:766–770.

130. Fusaki N, Ban H, Nishiyama A, Saeki K, Hasegawa M. 2009. Efficient induction of transgene-free human pluripotent stem cells using a vector based on Sendai virus, an RNA virus that does not integrate into the host genome. Proc Japan Acad Ser B Phys Biol Sci 85:348–362.

131. Eggenschwiler R, Cantz T. 2009. Induced pluripotent stem cells generated without viral integration. Hepatology 49:1048–1049.

132. Okita K, Nakagawa M, Hyenjong H, Ichisaka T, Yamanaka S. 2008. Generation of mouse induced pluripotent stem cells without viral vectors. Science (80-) 322:949–953.

133. Aasen T, Raya A, Barrero MJ, Garreta E, Consiglio A, Gonzalez F, Vassena R, Bilić J, Pekarik V, Tiscornia G, Edel M, Boué S, Belmonte JCI. 2008. Efficient and rapid generation of induced pluripotent stem cells from human keratinocytes. Nat Biotechnol 26:1276–1284.

134. Zhou T, Benda C, Dunzinger S, Huang Y, Ho JC, Yang J, Wang Y, Zhang Y, Zhuang Q, Li Y, Bao X, Tse HF, Grillari J, Grillari-Voglauer R, Pei D, Esteban MA. 2012. Generation of human induced pluripotent stem cells from urine samples. Nat Protoc 7:2080–2089.

135. Loh YH, Hartung O, Li H, Guo C, Sahalie JM, Manos PD, Urbach A, Heffner GC, Grskovic M, Vigneault F, William Lensch M, Park IH, Agarwal S, Church GM, Collins JJ, Irion S, Daley GQ. 2010. Reprogramming of T cells from human peripheral blood. Cell Stem Cell 7:15–19.

136. Liu G, David BT, Trawczynski M, Fessler RG. 2020. Advances in Pluripotent Stem Cells: History, Mechanisms, Technologies, and Applications. Stem Cell Rev Reports 16:3–32.

137. Si-Tayeb K, Noto FK, Nagaoka M, Li J, Battle MA, Duris C, North PE, Dalton S, Duncan SA. 2010. Highly efficient generation of human hepatocyte-like cells from induced pluripotent stem cells. Hepatology 51:297–305.

138. Zhang J, Wilson GF, Soerens AG, Koonce CH, Yu J, Palecek SP, Thomson JA, Kamp TJ. 2009. Functional cardiomyocytes derived from human induced pluripotent stem cells. Circ Res 104:30–41.

139. Karumbayaram S, Novitch BG, Patterson M, Umbach JA, Richter L, Lindgren A, Conway AE, Clark AT, Goldman SA, Plath K, Wiedau-Pazos M, Kornblum HI, Lowry WE. 2009. Directed differentiation of human-induced pluripotent stem cells generates active motor neurons. Stem Cells 27:806–811.

140. Zwi L, Caspi O, Arbel G, Huber I, Gepstein A, Park IH, Gepstein L. 2009. Cardiomyocyte differentiation of human induced pluripotent stem cells. Circulation 120:1513–1523.

141. Burridge PW, Matsa E, Shukla P, Lin ZC, Churko JM, Ebert AD, Lan F, Diecke S, Huber B, Mordwinkin NM, Plews JR, Abilez OJ, Cui B, Gold JD, Wu JC. 2014. Chemically defned generation of human cardiomyocytes. Nat Methods 11:855–860.

142. Krencik R, Weick JP, Liu Y, Zhang ZJ, Zhang SC. 2011. Specification of transplantable astroglial subtypes from human pluripotent stem cells. Nat Biotechnol 29:528–534.

143. Lapillonne H, Kobari L, Mazurier C, Tropel P, Giarratana MC, Zanella-Cleon I, Kiger L,

Wattenhofer-Donzé M, Puccio H, Hebert N, Francina A, Andreu G, Viville S, Douay L. 2010. Red blood cell generation from human induced pluripotent stem cells: Perspectives for transfusion medicine. Haematologica 95:1651–1659.

144. Chang CJ, Mitra K, Koya M, Velho M, Desprat R, Lenz J, Bouhassira EE. 2011. Production of embryonic and fetal-like red blood cells from human induced pluripotent stem cells. PLoS One 6.

145. Sato T, Stange DE, Ferrante M, Vries RGJ, Van Es JH, Van Den Brink S, Van Houdt WJ, Pronk A, Van Gorp J, Siersema PD, Clevers H. 2011. Long-term expansion of epithelial organoids from human colon, adenoma, adenocarcinoma, and Barrett's epithelium. Gastroenterology 141:1762–1772.

146. Dias J, Gumenyuk M, Kang H, Vodyanik M, Yu J, Thomson JA, Slukvin II. 2011. Generation of red blood cells from human induced pluripotent stem cells. Stem Cells Dev 20:1639–1647.

147. Wei H, Wang C, Guo R, Takahashi K, Naruse K. 2019. Development of a model of ischemic heart disease using cardiomyocytes differentiated from human induced pluripotent stem cells. Biochem Biophys Res Commun 520:600–605.

148. Lee H, Flynn R, Sharma I, Haberman E, Carling PJ, Nicholls FJ, Stegmann M, Vowles J, Haenseler W, Wade-Martins R, James WS, Cowley SA. 2020. LRRK2 Is Recruited to Phagosomes and Co-recruits RAB8 and RAB10 in Human Pluripotent Stem Cell-Derived Macrophages. Stem Cell Reports 14:940–955.

149. Hall-Roberts H, Agarwal D, Obst J, Smith TB, Monzón-Sandoval J, Di Daniel E, Webber C, James WS, Mead E, Davis JB, Cowley SA. 2020. TREM2 Alzheimer's variant R47H causes similar transcriptional dysregulation to knockout, yet only subtle functional phenotypes in human iPSC-derived macrophages. Alzheimer's Res Ther 12:1–27.

150. Miller JD, Ganat YM, Kishinevsky S, Bowman RL, Liu B, Tu EY, Mandal PK, Vera E, Shim JW, Kriks S, Taldone T, Fusaki N, Tomishima MJ, Krainc D, Milner TA, Rossi DJ, Studer L. 2013. Human iPSC-based modeling of late-onset disease via progerin-induced aging. Cell Stem Cell 13:691–705.

151. Piga D, Salani S, Magri F, Brusa R, Mauri E, Comi GP, Bresolin N, Corti S. 2019. Human induced pluripotent stem cell models for the study and treatment of Duchenne and Becker muscular dystrophies. Ther Adv Neurol Disord 12:1–28.

152. Okita K, Ichisaka T, Yamanaka S. 2007. Generation of germline-competent induced pluripotent stem cells. Nature 448:313–317.

153. Hockemeyer D, Jaenisch R. 2016. Induced pluripotent stem cells meet genome editing. Cell Stem Cell 18:573–586.

154. Wang Z, Troilo PJ, Wang X, Griffiths TG, Pacchione SJ, Barnum AB, Harper LB, Pauley CJ, Niu Z, Denisova L, Follmer TT, Rizzuto G, Ciliberto G, Fattori E, Monica NL, Manam S, Ledwith BJ. 2004. Detection of integration of plasmid DNA into host genomic DNA following intramuscular injection and electroporation. Gene Ther 11:711–721.

155. Nori S, Okada Y, Yasuda A, Tsuji O, Takahashi Y, Kobayashi Y, Fujiyoshi K, Koike M, Uchiyama Y, Ikeda E, Toyama Y, Yamanaka S, Nakamura M, Okano H. 2011. Grafted human-induced pluripotent stem-cell-derived neurospheres promote motor functional recovery after spinal cord injury in mice. Proc Natl Acad Sci U S A 108:16825–16830.

156. Nori S, Okada Y, Nishimura S, Sasaki T, Itakura G, Kobayashi Y, Renault-Mihara F, Shimizu A, Koya I, Yoshida R, Kudoh J, Koike M, Uchiyama Y, Ikeda E, Toyama Y, Nakamura M, Okano H. 2015. Long-term safety issues of iPSC-based cell therapy in a

spinal cord injury model: Oncogenic transformation with epithelial-mesenchymal transition. Stem Cell Reports 4:360–373.

157. Polo JM, Liu S, Figueroa ME, Kulalert W, Eminli S, Tan KY, Apostolou E, Stadtfeld M, Li Y, Shioda T, Natesan S, Wagers AJ, Melnick A, Evans T, Hochedlinger K. 2010. Cell type of origin influences the molecular and functional properties of mouse induced pluripotent stem cells. Nat Biotechnol 28:848–855.

158. Guenther MG, Frampton GM, Soldner F, Hockemeyer D, Mitalipova M, Jaenisch R, Young RA. 2010. Chromatin structure and gene expression programs of human embryonic and induced pluripotent stem cells. Cell Stem Cell 7:249–257.

159. Kim K, Doi A, Wen B, Ng K, Zhao R, Cahan P, Kim J, Aryee MJ, Ji H, Ehrlich LIR, Yabuuchi A, Takeuchi A, Cunniff KC, Hongguang H, McKinney-Freeman S, Naveiras O, Yoon TJ, Irizarry RA, Jung N, Seita J, Hanna J, Murakami P, Jaenisch R, Weissleder R, Orkin SH, Weissman IL, Feinberg AP, Daley GQ. 2010. Epigenetic memory in induced pluripotent stem cells. Nature 467:285–290.

160. Lister R, Pelizzola M, Kida YS, Hawkins RD, Nery JR, Hon G, Antosiewicz-Bourget J, Ogmalley R, Castanon R, Klugman S, Downes M, Yu R, Stewart R, Ren B, Thomson JA, Evans RM, Ecker JR. 2011. Hotspots of aberrant epigenomic reprogramming in human induced pluripotent stem cells. Nature 471:68–73.

161. Doi A, Park IH, Wen B, Murakami P, Aryee MJ, Irizarry R, Herb B, Ladd-Acosta C, Rho J, Loewer S, Miller J, Schlaeger T, Daley GQ, Feinberg AP. 2009. Differential methylation of tissue-and cancer-specific CpG island shores distinguishes human induced pluripotent stem cells, embryonic stem cells and fibroblasts. Nat Genet 41:1350–1353.

162. Hrvatin S, O'Donnell CW, Deng F, Millman JR, Pagliuca FW, DiIorio P, Rezania A, Gifford DK, Melton DA. 2014. Differentiated human stem cells resemble fetal, not adult, β cells. Proc Natl Acad Sci U S A 111:3038–3043.

163. Patel SJ, Yamauchi T, Ito F. 2019. Induced Pluripotent Stem Cell-Derived T Cells for Cancer Immunotherapy. Surg Oncol Clin N Am 28:489–504.

164. Nishimura T, Kaneko S, Kawana-Tachikawa A, Tajima Y, Goto H, Zhu D, Nakayama-Hosoya K, Iriguchi S, Uemura Y, Shimizu T, Takayama N, Yamada D, Nishimura K, Ohtaka M, Watanabe N, Takahashi S, Iwamoto A, Koseki H, Nakanishi M, Eto K, Nakauchi H. 2013. Generation of rejuvenated antigen-specific T cells by reprogramming to pluripotency and redifferentiation. Cell Stem Cell 12:114–126.

165. French A, Yang CT, Taylor S, Watt SM, Carpenter L. 2015. Human Induced Pluripotent Stem Cell-Derived B Lymphocytes Express sIgM and Can Be Generated via a Hemogenic Endothelium Intermediate. Stem Cells Dev 24:1082–1095.

166. Lee CZW, Kozaki T, Ginhoux F. 2018. Studying tissue macrophages in vitro: are iPSC-derived cells the answer? Nat Rev Immunol 18:716–725.

167. Senju S, Hirata S, Motomura Y, Fukuma D, Matsunaga Y, Fukushima S, Matsuyoshi H, Nishimura Y. 2010. Pluripotent stem cells as source of dendritic cells for immune therapy. Int J Hematol 91:392–400.

168. Sachamitr P, Leishman AJ, Davies TJ, Fairchild PJ. 2018. Directed differentiation of human induced pluripotent stem cells into dendritic cells displaying tolerogenic properties and resembling the CD141+ subset. Front Immunol 8.

169. Saeki K, Saeki K, Nakahara M, Matsuyama S, Nakamura N, Yogiashi Y, Yoneda A, Koyanagi M, Kondo Y, Yuo A. 2009. A Feeder-Free and Efficient Production of

Functional Neutrophils from Human Embryonic Stem Cells. Stem Cells 27:59–67.

170. Brok-Volchanskaya VS, Bennin DA, Suknuntha K, Klemm LC, Huttenlocher A, Slukvin I. 2019. Effective and Rapid Generation of Functional Neutrophils from Induced Pluripotent Stem Cells Using ETV2-Modified mRNA. Stem Cell Reports 13:1099–1110.

171. Sweeney CL, Teng R, Wang H, Merling RK, Lee J, Choi U, Koontz S, Wright DG, Malech HL. 2016. Molecular Analysis of Neutrophil Differentiation from Human Induced Pluripotent Stem Cells Delineates the Kinetics of Key Regulators of Hematopoiesis. Stem Cells 34:1513–1526.

172. Morishima T, Watanabe K ichiro, Niwa A, Fujino H, Matsubara H, Adachi S, Suemori H, Nakahata T, Heike T. 2011. Neutrophil differentiation from human-induced pluripotent stem cells. J Cell Physiol 226:1283–1291.

173. Focosi D, Amabile G. 2017. Induced Pluripotent Stem Cell-Derived Red Blood Cells and Platelet Concentrates: From Bench to Bedside. Cells 7:2.

174. Wiles M V., Keller G. 1991. Multiple hematopoietic lineages develop from embryonic stem (ES) cells in culture. Development 111:259–267.

175. Doetschman TC, Eistetter H, Katz M. 1985. The in vitro development of blastocyst-derived embryonic stem cell lines: Formation of visceral yolk sac, blood islands and myocardium. J Embryol Exp Morphol VOL. 87:27–45.

176. Anderson J., Bandi S, Kaufman D., Akkina R. 2006. Derivation of normal macrophages from human embryonic stem (hES) cells for applications in HIV gene therapy. Retrovirology 3.

177. Kaufman DS, Hanson ET, Lewis RL, Auerbach R, Thomson JA. 2001. Hematopoietic colony-forming cells derived from human embryonic stem cells. Proc Natl Acad Sci U S A 98:10716–10721.

178. Nakano T, Kodama H, Honjo T. 1994. Generation of lymphohematopoietic cells from embryonic stem cells in culture. Science (80-) 265:1098–1101.

179. Chen T, Wang F, Wu M, Wang ZZ. 2015. Development of hematopoietic stem and progenitor cells from human pluripotent stem cells. J Cell Biochem 116:1179–1189.

180. Garcia-Alegria E, Menegatti S, Batta K, Cuvertino S, Florkowska M, Kouskoff V. 2016. Emerging concepts for the in vitro derivation of murine haematopoietic stem and progenitor cells. FEBS Lett 590:4116–4125.

181. Rowe RG, Mandelbaum J, Zon LI, Daley GQ. 2016. Engineering Hematopoietic Stem Cells: Lessons from Development. Cell Stem Cell 18:707–720.

182. Seiler K, Tsuneto M, Melchers F. 2011. Experimental limitations using reprogrammed cells for hematopoietic differentiation. J Biomed Biotechnol 2011:3–8.

183. Sturgeon CM, Ditadi A, Awong G, Kennedy M, Keller G. 2014. Wnt Signaling Controls the Specification of Definitive and Primitive Hematopoiesis From Human Pluripotent Stem Cells. Nat Biotechnol 32:554–561.

184. Ditadi A, Sturgeon CM. 2016. Directed differentiation of definitive hemogenic endothelium and hematopoietic progenitors from human pluripotent stem cells. Methods 101:65–72.

185. Galat Y, Dambaeva S, Elcheva I, Khanolkar A, Beaman K, Iannaccone PM, Galat V. 2017. Cytokine-free directed differentiation of human pluripotent stem cells efficiently produces hemogenic endothelium with lymphoid potential. Stem Cell Res Ther 8:1–11.

186. Schmitt RM, Bruyns E, Snodgrass HR. 1991. Hematopoietic development of embryonic stem cells in vitro: Cytokine and receptor gene expression. Genes Dev 5:728–740.

187. Chadwick K, Wang L, Li L, Menendez P, Murdoch B, Rouleau A, Bhatia M. 2003. Cytokines and BMP-4 promote hematopoietic differentiation of human embryonic stem cells. Blood 102:906–915.

188. Tian X, Morris JK, Linehan JL, Kaufman DS. 2004. Cytokine requirements differ for stroma and embryoid body-mediated hematopoiesis from human embryonic stem cells. Exp Hematol 32:1000–1009.

189. Cerdan C, Rouleau A, Bhatia M. 2004. VEGF-A165 augments erythropoietic development from human embryonic stem cells. Blood 103:2504–2512.

190. Martin CH, Kaufman DS. 2005. Synergistic use of adult and embryonic stem cells to study human hematopoiesis. Curr Opin Biotechnol 16:510–515.

191. Pearson S, Sroczynska P, Lacaud G, Kouskoff V. 2008. The stepwise specification of embryonic stem cells to hematopoietic fate is driven by sequential exposure to Bmp4, activin A, bFGF and VEGF. Development 135:1525–1535.

192. Young DA, Lowe LD, Clark SC, Lowe LD, Clark SC. 2016. Comparison of the effects of IL-3 , factor in supporting monocyte differentiation in culture . Analysis of macrophage antibody-dependent cellular cytotoxicity . Information about subscribing to The Journal of Immunology is online at : Analysis of Macropha.

193. Grigoriadis AE, Kennedy M, Bozec A, Brunton F, Stenbeck G, Park IH, Wagner EF, Keller GM. 2010. Directed differentiation of hematopoietic precursors and functional osteoclasts from human ES and iPS cells. Blood 115:2769–2776.

194. Schwartz MP, Hou Z, Propson NE, Zhang J, Engstrom CJ, Costa VS, Jiang P, Nguyen BK, Bolin JM, Daly W, Wang Y, Stewart R, Page CD, Murphy WL, Thomson JA. 2015. Human pluripotent stem cell-derived neural constructs for predicting neural toxicity. Proc Natl Acad Sci U S A 112:12516–12521.

195. Lindmark H, Rosengren B, Hurt-Camejo E, Bruder CEG. 2004. Gene expression profiling shows that macrophages derived from mouse embryonic stem cells is an improved in vitro model for studies of vascular disease. Exp Cell Res 300:335–344.

196. van Wilgenburg B, Browne C, Vowles J, Cowley SA. 2013. Efficient, Long Term Production of Monocyte-Derived Macrophages from Human Pluripotent Stem Cells under Partly-Defined and Fully-Defined Conditions. PLoS One 8.

197. Jiang Y, Cowley SA, Siler U, Melguizo D, Tilgner K, Browne C, Dewilton A, Przyborski S, Saretzki G, James WS, Seger RA, Reichenbach J, Lako M, Armstrong L. 2012. Derivation and functional analysis of patient-specific induced pluripotent stem cells as an in vitro model of chronic granulomatous disease. Stem Cells 30:599–611.

198. Zhang H, Xue C, Shah R, Bermingham K, Hinkle CC, Li W, Rodrigues A, Tabita-Martinez J, Millar JS, Cuchel M, Pashos EE, Liu Y, Yan R, Yang W, Gosai SJ, Vandorn D, Chou ST, Gregory BD, Morrisey EE, Li M, Rader DJ, Reilly MP. 2015. Functional Analysis and Transcriptomic Profiling of iPSC-Derived Macrophages and Their Application in Modeling Mendelian Disease. Circ Res 117:17–28.

199. Kilfoil ML, Lasko P, Abouheif E. 2009. Stochastic variation: From single cells to superorganisms. HFSP J 3:379–385.

200. Lee SK. 2018. Sex as an important biological variable in biomedical research. BMB Rep 51:167–173.

201. Klein SL, Flanagan KL. 2016. Sex differences in immune responses. Nat Rev Immunol 16:626–638.

202. Hines WC, Su Y, Kuhn I, Polyak K, Bissell MJ. 2014. Sorting out the FACS: A devil in the details. Cell Rep 6:779–781.

203. Nielsen MC, Andersen MN, Møller HJ. 2020. Monocyte isolation techniques significantly impact the phenotype of both isolated monocytes and derived macrophages in vitro. Immunology 159:63–74.

204. Stewart-Phillips JL, Lough J, Phillips NC. 1991. The effect of a high-fat diet on murine macrophage activity. Int J Immunopharmacol 13:325–332.

205. Kostovcikova K, Coufal S, Galanova N, Fajstova A, Hudcovic T, Kostovcik M, Prochazkova P, Zakostelska ZJ, Cermakova M, Sediva B, Kuzma M, Tlaskalova-Hogenova H, Kverka M. 2019. Diet rich in animal protein promotes pro-inflammatory macrophage response and exacerbates colitis in mice. Front Immunol 10:1–14.

206. Chuong P, Wysoczynski M, Hellmann J. 2019. Do Changes in Innate Immunity Underlie the Cardiovascular Benefits of Exercise? Front Cardiovasc Med 6:1–7.

207. Boivin DB, James FO, Wu A, Cho-Park PF, Xiong H, Sun ZS. 2003. Circadian clock genes oscillate in human peripheral blood mononuclear cells. Blood 102:4143–4145.

208. Timmons GA, O'Siorain JR, Kennedy OD, Curtis AM, Early JO. 2020. Innate Rhythms: Clocks at the Center of Monocyte and Macrophage Function. Front Immunol 11:1743.

209. Helgason CD, Miller C. 2004. Basic Cell Culture ProtocolsBasic Cell Culture Protocols.

210. Day RM, Harbord M, Forbes A, Segal AW. 2001. Cantharidin blisters: A technique for investigating leukocyte trafficking and cytokine production at sites of inflammation in humans. J Immunol Methods 257:213–220.

211. Streck RJ, Jezewski HM, Rodriguez MI, Hurley EL, Rich GA, Braun KM, Pauly JL. 1994. A method for isolating human lung macrophages and observations of fluorescent phagocytes from the lungs of habitual cigarette smokers. J Immunol Methods 174:67–82.

212. Botting RA, Bertram KM, Baharlou H, Sandgren KJ, Fletcher J, Rhodes JW, Rana H, Plasto TM, Wang XM, Lim JJK, Barnouti L, Kohout MP, Papadopoulos T, Merten S, Olbourne N, Cunningham AL, Haniffa M, Harman AN. 2017. Phenotypic and functional consequences of different isolation protocols on skin mononuclear phagocytes. J Leukoc Biol 101:1393–1403.

213. Zhang X, Goncalves R, Mosser DM. 2008. The isolation and characterization of murine macrophages. Curr Protoc Immunol https://doi.org/10.1002/0471142735.im1401s83.

214. Tao L, Reese TA. 2017. Making Mouse Models That Reflect Human Immune Responses. Trends Immunol 38:181–193.

215. Alonso-Herranz L, Porcuna J, Ricote M. 2019. Isolation and Purification of Tissue Resident Macrophages for the Analysis of Nuclear Receptor Activity, p. 59–73. *In* Gage, M, Pineda-Torra, I (eds.), Lipid-Activated Nuclear Receptors. Humana Press, London.

216. Mak IWY, Evaniew N, Ghert M. 2014. Lost in translation: Animal models and clinical trials in cancer treatment. Am J Transl Res 6:114–118.

217. Siller R, Greenhough S, Park I-H, J. Sullivan G. 2013. Modelling Human Disease with Pluripotent Stem Cells. Curr Gene Ther 13:99–110.

218. Brault J, Goutagny E, Telugu N, Shao K, Baquié M, Satre V, Coutton C, Grunwald D,

Brion JP, Barlogis V, Stephan JL, Plantaz D, Hescheler J, Krause KH, Šarić T, Stasia MJ. 2014. Optimized generation of functional neutrophils and macrophages from patient-specific induced pluripotent stem cells: Ex vivo models of X0-Linked, AR220- and AR470-chronic granulomatous diseases. Biores Open Access 3:311–326.

219. Ishino Y, Shinagawa H, Makino K, Amemura M, Nakatura A. 1987. Nucleotide sequence of the iap gene, responsible for alkaline phosphatase isoenzyme conversion in Escherichia coli, and identification of the gene product. J Bacteriol 169:5429–5433.

220. Jinek M, Chylinski K, Fonfara I, Hauer M, Doudna JA, Charpentier E. 2012. A programmable dual-RNA-guided DNA endonuclease in adaptive bacterial immunity. Science (80-) 337:816–821.

221. Jansen R, Van Embden JDA, Gaastra W, Schouls LM. 2002. Identification of genes that are associated with DNA repeats in prokaryotes. Mol Microbiol 43:1565–1575.

222. Adli M. 2018. The CRISPR tool kit for genome editing and beyond. Nat Commun 9.

223. Ledford H, Callaway E. 2020. Pioneers of CRISPR gene editing win Chemistry Nobel. Nature 586:346–347.

224. Barrangou R, Fremaux C, Deveau H, Richards M, Boyaval P, Moineau S, Romero DA, Horvath P. 2007. CRISPR provides acquired resistance against viruses in prokaryotes. Science (80-) 315:1709–1712.

225. Sapranauskas R, Gasiunas G, Fremaux C, Barrangou R, Horvath P, Siksnys V. 2011. The Streptococcus thermophilus CRISPR/Cas system provides immunity in Escherichia coli. Nucleic Acids Res 39:9275–9282.

226. Brouns SJJ, Jore MM, Lundgren M, Westra ER, Slijkhuis RJH, Snijders APL, Dickman MJ, Makarova KS, Koonin E V., Van Der Oost J. 2008. Small CRISPR RNAs guide antiviral defense in prokaryotes. Science (80-) 321:960–964.

227. Gasiunas G, Barrangou R, Horvath P, Siksnys V. 2012. Cas9-crRNA ribonucleoprotein complex mediates specific DNA cleavage for adaptive immunity in bacteria. Proc Natl Acad Sci U S A 109:2579–2586.

228. Adli M. 2018. The CRISPR tool kit for genome editing and beyond. Nat Commun 9.

229. Cong L, Ran FA, Cox D, Lin S, Barretto R, Habib N, Hsu PD, Wu X, Jiang W, Marraffini LA, Zhang F. 2013. Multiplex genome engineering using CRISPR/Cas systems. Science (80-) 339:819–823.

230. Mali P, Yang L, Esvelt KM, Aach J, Guell M, DiCarlo JE, Norville JE, Church GM. 2013. RNA-guided human genome engineering via Cas9. Science (80-) 339:823–826.

231. Jinek M, East A, Cheng A, Lin S, Ma E, Doudna J. 2013. RNA-programmed genome editing in human cells. Elife 2013:1–9.

232. Carroll D. 2017. Genome editing: Past, present, and future. Yale J Biol Med 90:653–659.

233. Keller AA, Maeß MB, Schnoor M, Scheiding B, Lorkowski S. 2018. Transfecting macrophages, p. 187–195. *In* Rousselet, G (ed.), Methods in Molecular Biology. Humana Press.

234. Blagih J, Zani F, Chakravarty P, Hennequart M, Pilley S, Hobor S, Hock AK, Walton JB, Morton JP, Gronroos E, Mason S, Yang M, McNeish I, Swanton C, Blyth K, Vousden KH. 2020. Cancer-Specific Loss of p53 Leads to a Modulation of Myeloid and T Cell Responses. Cell Rep 30:481-496.e6.

235. Sokolowska O, Nowis D. 2018. STING Signaling in Cancer Cells: Important or Not? Arch Immunol Ther Exp (Warsz) 66:125–132.

236. Bosshart H, Heinzelmann M. 2016. THP-1 cells as a model for human monocytes. Ann Transl Med 4:4–7.

237. Sauer B, Henderson N. 1988. Site-specific DNA recombination in mammalian cells by the Cre recombinase of bacteriophage P1. Proc Natl Acad Sci U S A 85:5166–5170.

238. Abram CL, Roberge GL, Hu Y, Lowell CA. 2014. Comparative analysis of the efficiency and specificity of myeloid-Cre deleting strains using ROSA-EYFP reporter mice. J Immunol Methods 408:89–100.

239. Franke K, Kalucka J, Mamlouk S, Singh RP, Muschter A, Weidemann A, Iyengar V, Jahn S, Wieczorek K, Geiger K, Muders M, Sykes AM, Poitz DM, Ripich T, Otto T, Bergmann S, Breier G, Baretton G, Fong GH, Greaves DR, Bornstein S, Chavakis T, Joachim Fandrey MG, Wielockx B. 2013. HIF-1α is a protective factor in conditional PHD2-βdeficient mice suffering from severe HIF-2-induced excessive erythropoiesis. Blood.

240. Deng L, Zhou JF, Sellers RS, Li JF, Nguyen A V., Wang Y, Orlofsky A, Liu Q, Hume DA, Pollard JW, Augenlicht L, Lin EY. 2010. A novel mouse model of inflammatory bowel disease links mammalian target of rapamycin-dependent hyperproliferation of colonic epithelium to inflammation-associated tumorigenesis. Am J Pathol 176:952–967.

241. Bobadilla S, Sunseri N, Landau NR. 2013. Efficient transduction of myeloid cells by an HIV-1-derived lentiviral vector that packages the Vpx accessory protein. Gene Ther 20:514–520.

242. Kim K, Dauphin A, Komurlu S, McCauley SM, Yurkovetskiy L, Carbone C, Diehl WE, Strambio-De-Castillia C, Campbell EM, Luban J. 2019. Cyclophilin A protects HIV-1 from restriction by human TRIM5α. Nat Microbiol 4:2044–2051.

243. Leyva FJ, Anzinger JJ, McCoy JP, Kruth HS. 2011. Evaluation of transduction efficiency in macrophage colony-stimulating factor differentiated human macrophages using HIV-1 based lentiviral vectors. BMC Biotechnol 11.

244. Moyes KW, Lieberman NAP, Kreuser SA, Chinn H, Winter C, Deutsch G, Hoglund V, Watson R, Crane CA. 2017. Genetically Engineered Macrophages: A Potential Platform for Cancer Immunotherapy. Hum Gene Ther 28:200–215.

245. Lahouassa H, Daddacha W, Hofmann H, Ayinde D, Logue EC, Dragin L, Bloch N, Maudet C, Bertrand M, Gramberg T, Pancino G, Priet S, Canard B, Laguette N, Benkirane M, Transy C, Landau NR, Kim B, Margottin-Goguet F. 2012. SAMHD1 restricts the replication of human immunodeficiency virus type 1 by depleting the intracellular pool of deoxynucleoside triphosphates. Nat Immunol 13:223–228.

246. Freund EC, Lock JY, Oh J, Maculins T, Delamarre L, Bohlen CJ, Haley B, Murthy A. 2020. Efficient gene knockout in primary human and murine myeloid cells by non-viral delivery of crispr-cas9. J Exp Med 217.

247. Luo YL, Xu CF, Li HJ, Cao ZT, Liu J, Wang JL, Du XJ, Yang XZ, Gu Z, Wang J. 2018. Macrophage-Specific in Vivo Gene Editing Using Cationic Lipid-Assisted Polymeric Nanoparticles. ACS Nano 12:994–1005.

248. Hiatt J, Cavero D, McGregor M, Gordon D, Zheng W, Budzik J, Roth T, Haas K, Rathore U, Meyer-Franke A, Bouzidi M, Hultquist J, Wojcechowskyj J, Fontaine K, Pillai S, Cox J, Ernst J, Krogan N, Marson A. 2020. Efficient Generation of Isogenic Primary Human

Myeloid Cells using CRISPR-Cas9 Ribonucleoproteins. bioRxiv Prepr Serv Biol https://doi.org/10.1101/2020.03.13.991414.

249. Riggan L, Hildreth AD, Rolot M, Wong YY, Satyadi W, Sun R, Huerta C, O'Sullivan TE. 2020. CRISPR-Cas9 Ribonucleoprotein-Mediated Genomic Editing in Mature Primary Innate Immune Cells. Cell Rep 31:107651.

250. Lee Y, Mout R, Luther DC, Liu Y, Castellanos-García L, Burnside AS, Ray M, Tonga GY, Hardie J, Nagaraj H, Das R, Phillips EL, Tay T, Vachet RW, Rotello VM. 2019. In Vivo Editing of Macrophages through Systemic Delivery of CRISPR-Cas9-Ribonucleoprotein-Nanoparticle Nanoassemblies. Adv Ther.

251. Ray M, Lee YW, Hardie J, Mout R, Yeşilbag Tonga G, Farkas ME, Rotello VM. 2018. CRISPRed Macrophages for Cell-Based Cancer Immunotherapy. Bioconjug Chem 29:445–450.

252. Roberts AW, Popov LM, Mitchell G, Ching KL, Licht DJ, Golovkine G, Barton GM, Cox JS. 2019. Cas9+ conditionally-immortalized macrophages as a tool for bacterial pathogenesis and beyond. Elife 8:1–14.

253. Scharenberg SG, Poletto E, Lucot KL, Colella P, Sheikali A, Montine TJ, Porteus MH, Gomez-Ospina N. 2020. Engineering monocyte/macrophage−specific glucocerebrosidase expression in human hematopoietic stem cells using genome editing. Nat Commun.

254. Guttikonda SR, Sikkema L, Tchieu J, Saurat N, Walsh RM, Harschnitz O, Ciceri G, Sneeboer M, Mazutis L, Setty M, Zumbo P, Betel D, de Witte LD, Pe'er D, Studer L. 2021. Fully defined human pluripotent stem cell-derived microglia and tri-culture system model C3 production in Alzheimer's disease. Nat Neurosci https://doi.org/10.1038/s41593-020-00796-z.

255. Hsu DC, Sereti I. 2016. Serious Non-AIDS Events: Therapeutic Targets of Immune Activation and Chronic Inflammation in HIV Infection. Drugs 76:533–549.

256. Williams D, Veenstra M, Gaskill P, Morgello S, Calderon T, Berman J. 2014. Monocytes Mediate HIV Neuropathogenesis: Mechanisms that Contribute to HIV Associated Neurocognitive Disorders. Curr HIV Res 12:85–96.

257. Lamers SL, Rose R, Maidji E, Agsalda-Garcia M, Nolan DJ, Fogel GB, Salemi M, Garcia DL, Bracci P, Yong W, Commins D, Said J, Khanlou N, Hinkin CH, Sueiras MV, Mathisen G, Donovan S, Shiramizu B, Stoddart CA, McGrath MS, Singer EJ. 2016. HIV DNA Is Frequently Present within Pathologic Tissues Evaluated at Autopsy from Combined Antiretroviral Therapy-Treated Patients with Undetectable Viral Loads. J Virol 90:8968–8983.

258. Wong ME, Jaworowski A, Hearps AC. 2019. The HIV reservoir in monocytes and macrophages. Front Immunol 10.

259. Lang J, Cheng Y, Rolfe A, Hammack C, Vera D, Kyle K, Wang J, Meissner TB, Ren Y, Cowan C, Tang H. 2018. An hPSC-Derived Tissue-Resident Macrophage Model Reveals Differential Responses of Macrophages to ZIKV and DENV Infection. Stem Cell Reports 11:348–362.

260. German Advisory Committee Blood. 2016. Human Immunodeficiency Virus (HIV). Transfus Med Hemotherapy 43:203–222.

261. Sattentau QJ, Stevenson M. 2016. Macrophages and HIV-1: An Unhealthy Constellation. Cell Host Microbe 19:304–310.

262. Yukl SA, Sinclair E, Somsouk M, Hunt PW, Epling L, Killian M, Girling V, Li P, Havlir D

V., Deeks SG, Wong JK, Hatano H. 2014. A comparison of methods for measuring rectal HIV levels suggests that HIV DNA resides in cells other than CD4+ T cells, including myeloid cells. Aids 28:439–442.

263. Joseph SB, Swanstrom R, Kashuba ADM, Cohen MS. 2015. Bottlenecks in HIV-1 transmission: Insights from the study of founder viruses. Nat Rev Microbiol 13:414–425.

264. Groot F, Welsch S, Sattentau QJ. 2008. Efficient HIV-1 transmission from macrophages to T cells across transient virological synapses. Blood 111:4660–4663.

265. Bracq L, Xie M, Lambelé M, Vu L-T, Matz J, Schmitt A, Delon J, Zhou P, Randriamampita C, Bouchet J, Benichou S. 2017. T Cell-Macrophage Fusion Triggers Multinucleated Giant Cell Formation for HIV-1 Spreading. J Virol 91:1–19.

266. Williams DW, Eugenin EA, Calderon TM, Berman JW. 2012. Monocyte maturation, HIV susceptibility, and transmigration across the blood brain barrier are critical in HIV neuropathogenesis. J Leukoc Biol 91:401–415.

267. Le Douce V, Herbein G, Rohr O, Schwartz C. 2010. Molecular mechanisms of HIV-1 persistence in the monocyte-macrophage lineage. Retrovirology 7:1–16.

268. Igarashi T, Brown CR, Endo Y, Buckler-White A, Plishka R, Bischofberger N, Hirsch V, Martin MA. 2001. Macrophage are the principal reservoir and sustain high virus loads in rhesus macaques after the depletion of CD4+ T cells by a highly pathogenic simian immunodeficiency virus/HIV type 1 chimera (SHIV): Implications for HIV-1 infections of humans. Proc Natl Acad Sci U S A 98:658–663.

269. Honeycutt JB, Wahl A, Baker C, Spagnuolo RA, Foster J, Zakharova O, Wietgrefe S, Caro-Vegas C, Madden V, Sharpe G, Haase AT, Eron JJ, Garcia JV. 2016. Macrophages sustain HIV replication in vivo independently of T cells. J Clin Invest 126:1353–1366.

270. Peterson TA, MacLean AG. 2019. Current and Future Therapeutic Strategies for Lentiviral Eradication from Macrophage Reservoirs. J Neuroimmune Pharmacol 14:68–93.

271. Doitsh G, Galloway NLK, Geng X, Yang Z, Monroe KM, Zepeda O, Hunt PW, Hatano H, Sowinski S, Muñoz-Arias I, Greene WC. 2014. Cell death by pyroptosis drives CD4 T-cell depletion in HIV-1 infection. Nature 505:509–514.

272. Doitsh G, Cavrois M, Lassen KG, Zepeda O, Yang Z, Santiago ML, Hebbeler AM, Greene WC. 2010. Abortive HIV infection mediates CD4 T cell depletion and inflammation in human lymphoid tissue. Cell 143:789–801.

273. Clayton KL, Collins DR, Lengieza J, Ghebremichael M, Dotiwala F, Lieberman J, Walker BD. 2018. Resistance of HIV-infected macrophages to CD8+ T lymphocyte–mediated killing drives activation of the immune system. Nat Immunol 19:475–486.

274. Neil SJD, Zang T, Bieniasz PD. 2008. Tetherin inhibits retrovirus release and is antagonized by HIV-1 Vpu. Nature 451:425–430.

275. Cullen BR. 2006. Role and Mechanism of Action of the APOBEC3 Family of Antiretroviral Resistance Factors. J Virol 80:1067–1076.

276. Antonucci JM, Gelais CS, Wu L. 2017. The dynamic interplay between HIV-1, SAMHD1, and the innate antiviral response. Front Immunol 8:1–9.

277. Monroe KM, Yang Z, Johnson JR, Geng X, Doitsh G, Krogan NJ, Greene WC. 2014. IFI16 DNA sensor is required for death of lymphoid CD4 T cells abortively infected with HIV. Science (80-) 343:428–432.

278. Gao D, Wu J, Wu YT, Du F, Aroh C, Yan N, Sun L, Chen ZJ. 2013. Cyclic GMP-AMP synthase is an innate immune sensor of HIV and other retroviruses. Science (80-) 341:903–906.

279. Ganser-Pornillos BK, Pornillos O. 2019. Restriction of HIV-1 and other retroviruses by TRIM5. Nat Rev Microbiol 17:546–556.

280. Goujon C, Moncorgé O, Bauby H, Doyle T, Ward CC, Schaller T, Hué S, Barclay WS, Schulz R, Malim MH. 2013. Human MX2 is an interferon-induced post-entry inhibitor of HIV-1 infection. Nature 502:559–562.

281. Le Rouzic E, Belaïdouni N, Estrabaud E, Morel M, Rain JC, Transy C, Margottin-Goguet F. 2007. HIV1 Vpr arrests the cell cycle by recruiting DCAF1/VprBP, a receptor of the Cul4-DDB1 ubiquitin ligase. Cell Cycle 6:182–188.

282. Laguette N, Brégnard C, Hue P, Basbous J, Yatim A, Larroque M, Kirchhoff F, Constantinou A, Sobhian B, Benkirane M. 2014. Premature activation of the slx4 complex by vpr promotes g2/m arrest and escape from innate immune sensing. Cell 156:134–145.

283. Greenwood EJD, Williamson JC, Sienkiewicz A, Naamati A, Matheson NJ, Lehner PJ. 2019. Promiscuous Targeting of Cellular Proteins by Vpr Drives Systems-Level Proteomic Remodeling in HIV-1 Infection. Cell Rep 27:1579-1596.e7.

284. Vermeire J, Roesch F, Sauter D, Rua R, Hotter D, Van Nuffel A, Vanderstraeten H, Naessens E, Iannucci V, Landi A, Witkowski W, Baeyens A, Kirchhoff F, Verhasselt B. 2016. HIV Triggers a cGAS-Dependent, Vpu- and Vpr-Regulated Type I Interferon Response in CD4+ T Cells. Cell Rep 17:413–424.

285. Zahoor MA, Xue G, Sato H, Murakami T, Takeshima SN, Aida Y. 2014. HIV-1 Vpr induces interferon-stimulated genes in human monocyte-derived macrophages. PLoS One 9.

286. Amsler L, Verweij MC, Defilippis VR. 2013. The tiers and dimensions of evasion of the type i interferon response by human cytomegalovirus. J Mol Biol 425:4857–4871.

287. Bahar MW, Graham SC, Chen RAJ, Cooray S, Smith GL, Stuart DI, Grimes JM. 2011. How vaccinia virus has evolved to subvert the host immune response. J Struct Biol 175:127–134.

288. Bergantz L, Subra F, Deprez E, Delelis O, Richetta C. 2019. Interplay between Intrinsic and Innate Immunity during HIV Infection. Cells 8:922.

289. Towers GJ, Noursadeghi M. 2014. Interactions between HIV-1 and the cell-autonomous innate immune system. Cell Host Microbe 16:10–18.

290. Rasaiyaah J, Tan CP, Fletcher AJ, Price AJ, Blondeau C, Hilditch L, Jacques D a, Selwood DL, James LC, Noursadeghi M, Towers GJ. 2013. HIV-1 evades innate immune recognition through specific cofactor recruitment. Nature 503:402–405.

291. Schaller T, Ocwieja KE, Rasaiyaah J, Price AJ, Brady TL, Roth SL, Hué S, Fletcher AJ, Lee K, KewalRamani VN, Noursadeghi M, Jenner RG, James LC, Bushman FD, Towers GJ. 2011. HIV-1 Capsid-Cyclophilin Interactions Determine Nuclear Import Pathway, Integration Targeting and Replication Efficiency. PLoS Pathog 7:e1002439.

292. De Iaco A, Santoni F, Vannier A, Guipponi M, Antonarakis S, Luban J. 2013. TNPO3 protects HIV-1 replication from CPSF6-mediated capsid stabilization in the host cell cytoplasm. Retrovirology 10:20.

293. Achuthan V, Perreira JM, Sowd GA, Puray-Chavez M, McDougall WM, Paulucci-

Holthauzen A, Wu X, Fadel HJ, Poeschla EM, Multani AS, Hughes SH, Sarafianos SG, Brass AL, Engelman AN. 2018. Capsid-CPSF6 Interaction Licenses Nuclear HIV-1 Trafficking to Sites of Viral DNA Integration. Cell Host Microbe 24:392-404.e8.

294. Rossi E, Meuser ME, Cunanan CJ, Cocklin S. 2021. Structure, function, and interactions of the hiv-1 capsid protein. Life 11:1–25.

295. Campbell EM, Hope TJ. 2015. HIV-1 capsid: The multifaceted key player in HIV-1 infection. Nat Rev Microbiol 13:471–483.

296. Temple J, Tripler TN, Shen Q, Xiong Y. 2020. A snapshot of HIV-1 capsid–host interactions. Curr Res Struct Biol 2:222–228.

297. Yamashita M, Engelman AN. 2017. Capsid-Dependent Host Factors in HIV-1 Infection. Trends Microbiol 25:741–755.

298. James LC, Jacques DA. 2018. The human immunodeficiency virus capsid is more than just a genome package. Annu Rev Virol 5:209–225.

299. Burdick RC, Li C, Munshi MH, Rawson JMO, Nagashima K, Hu WS, Pathak VK. 2020. HIV-1 uncoats in the nucleus near sites of integration. Proc Natl Acad Sci U S A 117:5486–5493.

300. Burdick RC, Hu WS, Pathak VK. 2013. Nuclear import of APOBEC3F-labeled HIV-1 preintegration complexes. Proc Natl Acad Sci U S A 110.

301. Miller MD, Farnet CM, Bushman FD. 1997. Human immunodeficiency virus type 1 preintegration complexes: studies of organization and composition. J Virol 71:5382–5390.

302. Fassati A, Goff SP. 2001. Characterization of Intracellular Reverse Transcription Complexes of Human Immunodeficiency Virus Type 1. J Virol 75:3626–3635.

303. Yamashita M, Perez O, Hope TJ, Emerman M. 2007. Evidence for direct involvement of the capsid protein in HIV infection of nondividing cells. PLoS Pathog 3:1502–1510.

304. Yamashita M, Emerman M. 2004. Capsid Is a Dominant Determinant of Retrovirus Infectivity in Nondividing Cells. J Virol 78:5670–5678.

305. Francis AC, Melikyan GB. 2018. Single HIV-1 Imaging Reveals Progression of Infection through CA-Dependent Steps of Docking at the Nuclear Pore, Uncoating, and Nuclear Transport. Cell Host Microbe 23:536-548.e6.

306. Fernandez J, Machado AK, Lyonnais S, Chamontin C, Gärtner K, Léger T, Henriquet C, Garcia C, Portilho DM, Pugnière M, Chaloin L, Muriaux D, Yamauchi Y, Blaise M, Nisole S, Arhel NJ. 2019. Transportin-1 binds to the HIV-1 capsid via a nuclear localization signal and triggers uncoating. Nat Microbiol 4:1840–1850.

307. Francis AC, Marin M, Shi J, Aiken C, Melikyan GB. 2016. Time-Resolved Imaging of Single HIV-1 Uncoating In Vitro and in Living Cells. PLoS Pathog 12:1–28.

308. Burdick RC, Delviks-Frankenberry KA, Chen J, Janaka SK, Sastri J, Hu WS, Pathak VK. 2017. Dynamics and regulation of nuclear import and nuclear movements of HIV-1 complexesPLoS Pathogens.

309. Mallery DL, Márquez CL, McEwan WA, Dickson CF, Jacques DA, Anandapadamanaban M, Bichel K, Towers GJ, Saiardi A, Böcking T, James LC. 2018. IP6 is an HIV pocket factor that prevents capsid collapse and promotes DNA synthesis. Elife 7.

310. Jacques DA, McEwan WA, Hilditch L, Price AJ, Towers GJ, James LC. 2016. HIV-1

uses dynamic capsid pores to import nucleotides and fuel encapsidated DNA synthesis. Nature 536:349–353.

311. Ni T, Gerard S, Zhao G, Dent K, Ning J, Zhou J, Shi J, Anderson-Daniels J, Li W, Jang S, Engelman AN, Aiken C, Zhang P. 2020. Intrinsic curvature of the HIV-1 CA hexamer underlies capsid topology and interaction with cyclophilin A. Nat Struct Mol Biol 27:855–862.

312. Liu C, Perilla JR, Ning J, Lu M, Hou G, Ramalho R, Himes BA, Zhao G, Bedwell GJ, Byeon IJ, Ahn J, Gronenborn AM, Prevelige PE, Rousso I, Aiken C, Polenova T, Schulten K, Zhang P. 2016. Cyclophilin A stabilizes the HIV-1 capsid through a novel non-canonical binding site. Nat Commun 7.

313. Li Y, Kar AK, Sodroski J. 2009. Target Cell Type-Dependent Modulation of Human Immunodeficiency Virus Type 1 Capsid Disassembly by Cyclophilin A. J Virol 83:10951–10962.

314. De Iaco A, Luban J. 2014. Cyclophilin A promotes HIV-1 reverse transcription but its effect on transduction correlates best with its effect on nuclear entry of viral cDNA. Retrovirology 11:1–15.

315. Braaten D, Franke EK, Luban J. 1996. Cyclophilin A is required for an early step in the life cycle of human immunodeficiency virus type 1 before the initiation of reverse transcription. J Virol 70:3551–3560.

316. Burse M, Shi J, Aiken C. 2017. Cyclophilin A potentiates TRIM5α inhibition of HIV-1 nuclear import without promoting TRIM5α binding to the viral capsid. PLoS One 12:1–18.

317. Gamble TR, Vajdos FF, Yoo S, Worthylake DK, Houseweart M, Sundquist WI, Hill CP. 1996. Crystal structure of human cyclophilin A bound to the amino-terminal domain of HIV-1 capsid. Cell 87:1285–1294.

318. Bosco DA, Eisenmesser EZ, Pochapsky S, Sundquist WI, Kern D. 2002. Catalysis of cis/trans isomerization in native HIV-1 capsid by human cyclophilin A. Proc Natl Acad Sci U S A 99:5247–5252.

319. Ylinen LMJ, Schaller T, Price A, Fletcher AJ, Noursadeghi M, James LC, Towers GJ. 2009. Cyclophilin A Levels Dictate Infection Efficiency of Human Immunodeficiency Virus Type 1 Capsid Escape Mutants A92E and G94D. J Virol 83:2044–2047.

320. Di Nunzio F, Danckaert A, Fricke T, Perez P, Fernandez J, Perret E, Roux P, Shorte S, Charneau P, Diaz-Griffero F, Arhel NJ. 2012. Human Nucleoporins Promote HIV-1 Docking at the Nuclear Pore, Nuclear Import and Integration. PLoS One 7.

321. Bichel K, Price AJ, Schaller T, Towers GJ, Freund SM V, James LC. 2013. HIV-1 capsid undergoes coupled binding and isomerization by the nuclear pore protein NUP358. Retrovirology 10:1–12.

322. Zhang R, Mehla R, Chauhan A. 2010. Perturbation of host nuclear membrane component RanBP2 impairs the nuclear import of human immunodeficiency virus -1 preintegration complex (DNA). PLoS One 5.

323. Busnadiego I, Kane M, Rihn SJ, Preugschas HF, Hughes J, Blanco-Melo D, Strouvelle VP, Zang TM, Willett BJ, Boutell C, Bieniasz PD, Wilson SJ. 2014. Host and Viral Determinants of Mx2 Antiretroviral Activity. J Virol 88:7738–7752.

324. Liu Z, Pan Q, Liang Z, Qiao W, Cen S, Liang C. 2015. The highly polymorphic cyclophilin A-binding loop in HIV-1 capsid modulates viral resistance to MxB. Retrovirology 12:1–6.

325. Miles RJ, Kerridge C, Hilditch L, Monit C, Jacques DA, Towers GJ. 2020. MxB sensitivity of HIV-1 is determined by a highly variable and dynamic capsid surface 1–17.

326. Morger D, Zosel F, Bühlmann M, Züger S, Mittelviefhaus M, Schuler B, Luban J, Grütter MG. 2018. The Three-Fold Axis of the HIV-1 Capsid Lattice Is the Species-Specific Binding Interface for TRIM5α. J Virol 92:1–16.

327. Fricke T, White TE, Schulte B, Souza DA De, Vieira A, Dharan A, Campbell EM, Brandariz-nuñez A, Diaz-griffero F. 2014. MxB binds to the HIV-1 core and prevents the uncoating process of HIV-1 1–14.

328. Stremlau M, Perron M, Welikala S, Sodroski J. 2005. Species-Specific Variation in the B30.2(SPRY) Domain of TRIM5 Determines the Potency of Human Immunodeficiency Virus Restriction. J Virol https://doi.org/10.1128/JVI.79.5.3139-3145.2005.

329. Selyutina A, Persaud M, Simons LM, Bulnes-Ramos A, Buffone C, Martinez-Lopez A, Scoca V, Di Nunzio F, Hiatt J, Marson A, Krogan NJ, Hultquist JF, Diaz-Griffero F. 2020. Cyclophilin A Prevents HIV-1 Restriction in Lymphocytes by Blocking Human TRIM5α Binding to the Viral Core. Cell Rep 30:3766-3777.e6.

330. Hulme AE, Perez O, Hope TJ. 2011. Complementary assays reveal a relationship between HIV-1 uncoating and reverse transcription. Proc Natl Acad Sci U S A 108:9975–9980.

331. Black LR, Aiken C. 2010. TRIM5α Disrupts the Structure of Assembled HIV-1 Capsid Complexes In Vitro. J Virol 84:6564–6569.

332. Gao D, Wu J, Wu Y, Du F, Aroh C, Yan N, Sun L, Chen ZJ. 2013. Cyclic GMP-AMP Synthase Is an Innate Immune Sensor of HIV and Other Retroviruses. Science (80-) 1375:903–907.

333. Li Y, Altorelli NL, Bahna F, Honig B, Shapiro L, Palmer AG. 2013. IFI16 senses DNA forms of the lentiviral replication cycle and controls HIV-1 replication. Proc Natl Acad Sci U S A 110:19651.

334. Lahaye X, Satoh T, Gentili M, Cerboni S, Conrad C, Hurbain I, ElMarjou A, Lacabaratz C, Lelièvre JD, Manel N. 2013. The Capsids of HIV-1 and HIV-2 Determine Immune Detection of the Viral cDNA by the Innate Sensor cGAS in Dendritic Cells. Immunity 39:1132–1142.

335. Anderson JL, Campbell EM, Wu X, Vandegraaff N, Engelman A, Hope TJ. 2006. Proteasome Inhibition Reveals that a Functional Preintegration Complex Intermediate Can Be Generated during Restriction by Diverse TRIM5 Proteins. J Virol 80:9754–9760.

336. Fletcher AJ, Vaysburd M, Maslen S, Zeng J, Skehel JM, Towers GJ, James LC, Fletcher AJ, Vaysburd M, Maslen S, Zeng J, Skehel JM, Towers GJ. 2018. Trivalent RING Assembly on Retroviral Capsids Activates TRIM5 Ubiquitination and Innate Immune Article Trivalent RING Assembly on Retroviral Capsids Activates TRIM5 Ubiquitination and Innate Immune Signaling. Cell Host Microbe 24:761-775.e6.

337. Lienlaf M, Hayashi F, Di Nunzio F, Tochio N, Kigawa T, Yokoyama S, Diaz-Griffero F. 2011. Contribution of E3-Ubiquitin Ligase Activity to HIV-1 Restriction by TRIM5 rh: Structure of the RING Domain of TRIM5 . J Virol 85:8725–8737.

338. Jimenez-Guardeño JM, Apolonia L, Betancor G, Malim MH. 2019. Immunoproteasome activation enables human TRIM5α restriction of HIV-1. Nat Microbiol 4:933–940.

339. Rold CJ, Aiken C. 2008. Proteasomal Degradation of TRIM5 a during Retrovirus

Restriction 4.

340. Kutluay SB, Perez-caballero D, Bieniasz PD. 2013. Fates of Retroviral Core Components during Unrestricted and TRIM5-Restricted Infection. PLOS Pathog 9.

341. Wu X, Anderson JL, Campbell EM, Joseph AM, Hope TJ. 2006. Proteasome inhibitors uncouple rhesus TRIM5 ␣ restriction of HIV-1 reverse transcription and infection 5–10.

342. Tareen SU, Emerman M. 2011. Human Trim5 α has additional activities that are uncoupled from retroviral capsid recognition Mouse Trim5 α paralogs. Virology 409:113–120.

343. Lascano J, Uchil PD, Mothes W, Luban J. 2016. TRIM5 Retroviral Restriction Activity Correlates with the Ability To Induce Innate Immune Signaling. J Virol 90:308–316.

344. Pertel T, Hausmann S, Morger D, Züger S, Guerra J, Lascano J, Reinhard C, Santoni FA, Uchil PD, Chatel L, Bisiaux A, Albert ML, Strambio-De-Castillia C, Mothes W, Pizzato M, Grütter MG, Luban J. 2011. TRIM5 is an innate immune sensor for the retrovirus capsid lattice. Nature 472:361–365.

345. Jerebtsova M, Kumari N, Xu M, de Melo GBA, Niu X, Jeang KT, Nekhai S. 2012. HIV-1 resistant CDK2-knockdown macrophage-like cells generated from 293T cell-derived human induced pluripotent stem cells. Biology (Basel) 1:175–195.

346. Higaki K, Hirao M, Kawana-Tachikawa A, Iriguchi S, Kumagai A, Ueda N, Bo W, Kamibayashi S, Watanabe A, Nakauchi H, Suzuki K, Kaneko S. 2018. Generation of HIV-Resistant Macrophages from IPSCs by Using Transcriptional Gene Silencing and Promoter-Targeted RNA. Mol Ther - Nucleic Acids 12:793–804.

347. Kang HJ, Minder P, Park MA, Mesquitta WT, Torbett BE, Slukvin II. 2015. CCR5 disruption in induced pluripotent stem cells using CRISPR/Cas9 provides selective resistance of immune cells to CCR5-tropic HIV-1 virus. Mol Ther - Nucleic Acids 4:e268.

348. Taylor JP, Cash MN, Santostefano KE, Nakanishi M, Terada N, Wallet MA. 2018. CRISPR/Cas9 knockout of USP18 enhances type I IFN responsiveness and restricts HIV-1 infection in macrophages. J Leukoc Biol 103:1225–1240.

349. Rai MA, Hammonds J, Pujato M, Mayhew C, Roskin K, Spearman P. 2020. Comparative analysis of human microglial models for studies of HIV replication and pathogenesis. Retrovirology 17:1–21.

350. Alvarez-Carbonell D, Ye F, Ramanath N, Garcia-Mesa Y, Knapp PE, Hauser KF, Karn J. 2019. Cross-talk between microglia and neurons regulates HIV latency. PLOS Pathog 15:e1008249.

351. Selyutina A, Persaud M, Lee K, KewalRamani V, Diaz-Griffero F. 2020. Nuclear Import of the HIV-1 Core Precedes Reverse Transcription and Uncoating. Cell Rep 32:108201.

352. Yamashita M, Engelman AN. 2017. Capsid-Dependent Host Factors in HIV-1 Infection. Trends Microbiol 25:741–755.

353. Wang P, Heitman J. 2005. The cyclophilins. Genome Biol 6:226.

354. Rajiv C, Davis TL. 2018. Structural and functional insights into human nuclear cyclophilins. Biomolecules 8.

355. Manteca A, Pelaez AI, Zardoya R, Sanchez J. 2006. Actinobacteria cyclophilins: Phylogenetic relationships and description of new class- and order-specific paralogues. J Mol Evol 63:719–732.

356. Pandey S, Tripathi D, Khubaib M, Kumar A, Sheikh JA, Sumanlatha G, Ehtesham NZ,

Hasnain SE. 2017. Mycobacterium tuberculosis peptidyl-prolyl isomerases are immunogenic, alter cytokine profile and aid in intracellular survival. Front Cell Infect Microbiol 7:1–9.

357. Barik S. 2018. A Family of Novel Cyclophilins, Conserved in the Mimivirus Genus of the Giant DNA Viruses. Comput Struct Biotechnol J 16:231–236.

358. de Wilde AH, Pham U, Posthuma CC, Snijder EJ. 2018. Cyclophilins and cyclophilin inhibitors in nidovirus replication. Virology 522:46–55.

359. Hopkins S, Gallay PA. 2015. The role of immunophilins in viral infection. Biochim Biophys Acta - Gen Subj 1850:2103–2110.

360. Gaither LA, Borawski J, Anderson LJ, Balabanis KA, Devay P, Joberty G, Rau C, Schirle M, Bouwmeester T, Mickanin C, Zhao SC, Vickers C, Lee L, Deng G, Baryza J, Fujimoto RA, Lin K, Compton T, Wiedmann B. 2010. Multiple cyclophilins involved in different cellular pathways mediate HCV replication. Virology 397:43–55.

361. Dawar FU, Tu J. 2017. Cyclophilin A : A Key Factor in Virus Replication and Potential Target for Anti-viral Therapy 1–20.

362. Nigro P, Pompilio G, Capogrossi MC. 2013. Cyclophilin A: a key player for human disease. Cell Death Dis 4:e888.

363. Obata Y, Yamamoto K, Miyazaki M, Shimotohno K, Kohno S, Matsuyama T. 2005. Role of cyclophilin B in activation of interferon regulatory factor-3. J Biol Chem 280:18355–18360.

364. Liu W, Li J, Zheng W, Shang Y, Zhao Z, Wang S, Bi Y, Zhang S, Xu C, Duan Z, Zhang L, Wang YL, Jiang Z, Liu W, Sun L. 2017. Cyclophilin A-regulated ubiquitination is critical for RIG-I-mediated antiviral immune responses. Elife 6:1–21.

365. Sheng C, Yao C, Wang Z, Chen H, Zhao Y, Xu D, Huang H, Huang W, Chen S. 2018. Cyclophilin J limits inflammation through the blockage of ubiquitin chain sensing. Nat Commun 9.

366. Davis TL, Walker JR, Campagna-Slater V, Finerty PJ, Finerty PJ, Paramanathan R, Bernstein G, Mackenzie F, Tempel W, Ouyang H, Lee WH, Eisenmesser EZ, Dhe-Paganon S. 2010. Structural and biochemical characterization of the human cyclophilin family of peptidyl-prolyl isomerases. PLoS Biol 8.

367. Chighizola CB, Ong VH, Meroni PL. 2017. The Use of Cyclosporine A in Rheumatology: a 2016 Comprehensive Review. Clin Rev Allergy Immunol 52:401–423.

368. Bendickova K, Tidu F, Fric J. 2017. Calcineurin– NFAT signalling in myeloid leucocytes: new prospects and pitfalls in immunosuppressive therapy . EMBO Mol Med 9:990–999.

369. Naesens M, Kuypers DRJ, Sarwal M. 2009. Calcineurin inhibitor nephrotoxicity. Clin J Am Soc Nephrol 4:481–508.

370. Fernandes HJR, Hartfield EM, Christian HC, Emmanoulidou E, Zheng Y, Booth H, Bogetofte H, Lang C, Ryan BJ, Sardi SP, Badger J, Vowles J, Evetts S, Tofaris GK, Vekrellis K, Talbot K, Hu MT, James W, Cowley SA, Wade-Martins R. 2016. ER Stress and Autophagic Perturbations Lead to Elevated Extracellular α-Synuclein in GBA-N370S Parkinson's iPSC-Derived Dopamine Neurons. Stem Cell Reports 6.

371. Dafinca R, Scaber J, Ababneh N, Lalic T, Weir G, Christian H, Vowles J, Douglas AGL, Fletcher-Jones A, Browne C, Nakanishi M, Turner MR, Wade-Martins R, Cowley SA, Talbot K. 2016. C9orf72 Hexanucleotide Expansions Are Associated with Altered

Endoplasmic Reticulum Calcium Homeostasis and Stress Granule Formation in Induced Pluripotent Stem Cell-Derived Neurons from Patients with Amyotrophic Lateral Sclerosis and Frontotemporal Demen. Stem Cells 34:2063–2078.

372. Haenseler W, Sansom SN, Buchrieser J, Newey SE, Moore CS, Nicholls FJ, Chintawar S, Schnell C, Antel JP, Allen ND, Cader MZ, Wade-Martins R, James WS, Cowley SA. 2017. A Highly Efficient Human Pluripotent Stem Cell Microglia Model Displays a Neuronal-Co-culture-Specific Expression Profile and Inflammatory Response. Stem Cell Reports 8:1727–1742.

373. Morrison M, Klein C, Clemann N, Collier DA, Hardy J, Heiβerer B, Cader MZ, Graf M, Kaye J. 2015. StemBANCC: Governing Access to Material and Data in a Large Stem Cell Research Consortium. Stem Cell Rev Reports 11:681–687.

374. Beers J, Gulbranson DR, George N, Siniscalchi LI, Jones J, Thomson JA, Chen G. 2012. Passaging and colony expansion of human pluripotent stem cells by enzyme-free dissociation in chemically defined culture conditions. Nat Protoc 7:2029–2040.

375. Sanjana NE, Shalem O, Zhang F. 2014. Improved vectors and genome-wide libraries for CRISPR screening. Nat Methods 11:783–784.

376. Integrated DNA Technologies. 2019. Alt-R CRISPR-Cas9 System: Delivery of ribonucleoprotein complexes in HEK-293 cells using the Neon® Transfection System 1–11.

377. Katoh K, Standley DM. 2013. MAFFT multiple sequence alignment software version 7: Improvements in performance and usability. Mol Biol Evol 30:772–780.

378. Brinkman EK, Chen T, Amendola M, Van Steensel B. 2014. Easy quantitative assessment of genome editing by sequence trace decomposition. Nucleic Acids Res 42:1–8.

379. Carter GC, Bernstone L, Sangani D, Bee JW, Harder T, James W. 2009. HIV entry in macrophages is dependent on intact lipid rafts. Virology 386:192–202.

380. Chen S, Zhou Y, Chen Y, Gu J. 2018. Fastp: An ultra-fast all-in-one FASTQ preprocessor. Bioinformatics 34:i884–i890.

381. Srivastava A, Malik L, Sarkar H, Zakeri M, Almodaresi F, Soneson C, Love M, Kingsford C, Patro R. 2019. Alignment and mapping methodology influence transcript abundance estimation. bioRxiv 1–22.

382. Soneson C, Love MI, Robinson MD. 2016. Differential analyses for RNA-seq: Transcript-level estimates improve gene-level inferences [version 2; referees: 2 approved]. F1000Research 4:1–22.

383. Law CW, Chen Y, Shi W, Smyth GK. 2014. Voom: Precision weights unlock linear model analysis tools for RNA-seq read counts. Genome Biol 15:1–17.

384. Alhamdoosh M, Law CW, Tian L, Sheridan JM, Ng M, Ritchie ME. 2017. Easy and efficient ensemble gene set testing with EGSEA. F1000Research 6:1–38.

385. Abud EM, Ramirez RN, Martinez ES, Healy LM, Nguyen CHH, Newman SA, Yeromin A V., Scarfone VM, Marsh SE, Fimbres C, Caraway CA, Fote GM, Madany AM, Agrawal A, Kayed R, Gylys KH, Cahalan MD, Cummings BJ, Antel JP, Mortazavi A, Carson MJ, Poon WW, Blurton-Jones M. 2017. iPSC-Derived Human Microglia-like Cells to Study Neurological Diseases. Neuron 94:278-293.e9.

386. Spouge JL. 1992. Statistical analysis of sparse infection data and its implications for retroviral treatment trials in primates. Proc Natl Acad Sci U S A 89:7581–7585.

387. Edmonds TG, Ding H, Yuan X, Wei Q, Smith KS, Conway JA, Wieczorek L, Brown B, Polonis V, West JT, Montefiori DC, Kappes JC, Ochsenbauer C. 2010. Replication competent molecular clones of HIV-1 expressing Renilla luciferase facilitate the analysis of antibody inhibition in PBMC. Virology 408:1–13.

388. Ebrahimi KH, Howie D, Rowbotham JS, McCullagh J, Armstrong FA, James WS. 2020. Viperin, through its radical-SAM activity, depletes cellular nucleotide pools and interferes with mitochondrial metabolism to inhibit viral replication. FEBS Lett 594:1624–1630.

389. Alldritt I, Whitham-Agut B, Sipin M, Studholme J, Trentacoste A, Tripp JA, Cappai MG, Ditchfield P, Devièse T, Hedges REM, McCullagh JSO. 2019. Metabolomics reveals diet-derived plant polyphenols accumulate in physiological bone. Sci Rep 9:1–12.

390. Rajab N, Rutar M, Laslett AL, Wells CA. 2018. Designer macrophages: Pitfalls and opportunities for modelling macrophage phenotypes from pluripotent stem cells. Differentiation 104:42–49.

391. Härtlova A, Herbst S, Peltier J, Rodgers A, Bilkei-Gorzo O, Fearns A, Dill BD, Lee H, Flynn R, Cowley SA, Davies P, Lewis PA, Ganley IG, Martinez J, Alessi DR, Reith AD, Trost M, Gutierrez MG. 2018. LRRK2 is a negative regulator of Mycobacterium tuberculosis phagosome maturation in macrophages. EMBO J e98694.

392. Haenseler W, Zambon F, Lee H, Vowles J, Rinaldi F, Duggal G, Houlden H, Gwinn K, Wray S, Luk KC, Wade-Martins R, James WS, Cowley SA. 2017. Excess α-synuclein compromises phagocytosis in iPSC-derived macrophages. Sci Rep 7.

393. Garcia-Reitboeck P, Phillips A, Piers TM, Houlden H, Hardy J, Pocock JM. 2018. Human Induced Pluripotent Stem Cell-Derived Microglia-Like Cells Harboring TREM2 Missense Mutations Show Specific Deficits in Phagocytosis https://doi.org/10.1016/j.celrep.2018.07.094.

394. Brownjohn PW, Smith J, Solanki R, Lohmann E, Houlden H, Hardy J, Dietmann S, Livesey FJ. 2018. Functional Studies of Missense TREM2 Mutations in Human Stem Cell-Derived Microglia. Stem Cell Reports 10:1294–1307.

395. Karlsson KR, Cowley S, Martinez FO, Shaw M, Minger SL, James W. 2008. Homogeneous monocytes and macrophages from human embryonic stem cells following coculture-free differentiation in M-CSF and IL-3. Exp Hematol 36:1167–1175.

396. Cech TR, Eddy SR, Eisenberg D, Hersey K, Holtzman SH, Poste GH, Raikhel N V., Scheller RH, Singer DB, Waltham MC. 2003. Sharing publication-related data and materials: Responsibilities of authorship in the life sciences. Plant Physiol.

397. National Academy of Sciences, National Academy of Engineering (US) and Institute of Medicine (US) Committee on Science E and PP. 2009. On being a scientist: A guide to responsible conduct in research: Third editionOn Being a Scientist: A Guide to Responsible Conduct in Research: Third Edition. National Academies Press.

398. Morey RD, Chambers CD, Etchells PJ, Harris CR, Hoekstra R, Lakens D, Lewandowsky S, Morey CC, Newman DP, Schönbrodt FD, Vanpaemel W, Wagenmakers EJ, Zwaan RA. 2016. The Peer Reviewers' Openness Initiative: Incentivizing open research practices through peer review. R Soc Open Sci 3.

399. Cao X, Yakala GK, van den Hil FE, Cochrane A, Mummery CL, Orlova V V. 2019. Differentiation and Functional Comparison of Monocytes and Macrophages from hiPSCs with Peripheral Blood Derivatives. Stem Cell Reports 12:1282–1297.

400. Moore KJ, Fabunmi RP, Andersson LP, Freeman MW. 1998. In Vitro–Differentiated

Embryonic Stem Cell Macrophages. Arterioscler Thromb Vasc Biol 18:1647–1654.

401. Odegaard JI, Vats D, Zhang L, Ricardo-Gonzalez R, Smith KL, Sykes DB, Kamps MP, Chawla A. 2007. Quantitative expansion of ES cell-derived myeloid progenitors capable of differentiating into macrophages. J Leukoc Biol 81:711–719.

402. Senju S, Haruta M, Matsunaga Y, Fukushima S, Ikeda T, Takahashi K, Okita K, Yamanaka S, Nishimura Y. 2009. Characterization of dendritic cells and macrophages generated by directed differentiation from mouse induced pluripotent stem cells. Stem Cells 27:1021–1031.

403. Choi K, Vodyanik MA, Slukvin II. 2009. Generation of mature human myelomonocytic cells through expansion and differentiation of pluripotent stem cell–derived lin–CD34+CD43+CD45+ progenitors. J Clin Invest 119:2818.

404. Subramanian A, Guo B, Marsden MD, Galic Z, Kitchen S, Kacena A, Brown HJ, Cheng G, Zack JA. 2011. Macrophage differentiation from embryoid bodies derived from human embryonic stem cells. Hum Mesenchymal Embryonic Stem Cells 4:211–232.

405. Choi KD, Vodyanik M, Slukvin II. 2011. Hematopoietic differentiation and production of mature myeloid cells from human pluripotent stem cells. Nat Protoc 6:296–313.

406. Senju S, Haruta M, Matsumura K, Matsunaga Y, Fukushima S, Ikeda T, Takamatsu K, Irie A, Nishimura Y. 2011. Generation of dendritic cells and macrophages from human induced pluripotent stem cells aiming at cell therapy. Gene Ther 18:874–883.

407. Salvagiotto G, Burton S, Daigh CA, Rajesh D, Slukvin II, Seay NJ. 2011. A defined, feeder-free, serum-free system to generate In Vitro hematopoietic progenitors and differentiated blood cells from hESCs and hiPSCs. PLoS One 6.

408. Klimchenko O, Di Stefano A, Geoerger B, Hamidi S, Opolon P, Robert T, Routhier M, El-Benna J, Delezoide AL, Boukour S, Lescure B, Solary E, Vainchenker W, Norol F. 2011. Monocytic cells derived from human embryonic stem cells and fetal liver share common differentiation pathways and homeostatic functions. Blood 117:3065–3075.

409. Kambal A, Mitchell G, Cary W, Gruenloh W, Jung Y, Kalomoiris S, Nacey C, McGee J, Lindsey M, Fury B, Bauer G, Nolta JA, Anderson JS. 2011. Generation of HIV-1 resistant and functional macrophages from hematopoietic stem cell-derived induced pluripotent stem cells. Mol Ther 19:584–593.

410. Vodyanik MA, Bork JA, Thomson JA, Slukvin II. 2005. Human embryonic stem cell-derived CD34+ cells: Efficient production in the coculture with OP9 stromal cells and analysis of lymphohematopoietic potential. Blood 105:617–626.

411. Zhuang L, Pound JD, Willems JJLP, Taylor AH, Forrester LM, Gregory CD. 2012. Pure populations of murine macrophages from cultured embryonic stem cells. Application to studies of chemotaxis and apoptotic cell clearance. J Immunol Methods 385:1–14.

412. Yanagimachi MD, Niwa A, Tanaka T, Honda-Ozaki F, Nishimoto S, Murata Y, Yasumi T, Ito J, Tomida S, Oshima K, Asaka I, Goto H, Heike T, Nakahata T, Saito MK. 2013. Robust and Highly-Efficient Differentiation of Functional Monocytic Cells from Human Pluripotent Stem Cells under Serum- and Feeder Cell-Free Conditions. PLoS One 8:1–9.

413. Uenishi G, Theisen D, Lee JH, Kumar A, Raymond M, Vodyanik M, Swanson S, Stewart R, Thomson J, Slukvin I. 2014. Tenascin C promotes hematoendothelial development and T lymphoid commitment from human pluripotent stem cells in chemically defined conditions. Stem Cell Reports 3:1073–1084.

414. Lachmann N, Ackermann M, Frenzel E, Liebhaber S, Brennig S, Happle C, Hoffmann

D, Klimenkova O, Lüttge D, Buchegger T, Kühnel MP, Schambach A, Janciauskiene S, Figueiredo C, Hansen G, Skokowa J, Moritz T. 2015. Large-scale hematopoietic differentiation of human induced pluripotent stem cells provides granulocytes or macrophages for cell replacement therapies. Stem Cell Reports 4:282–296.

415. Mucci A, Kunkiel J, Suzuki T, Brennig S, Glage S, Kühnel MP, Ackermann M, Happle C, Kuhn A, Schambach A, Trapnell BC, Hansen G, Moritz T, Lachmann N. 2016. Murine iPSC-Derived Macrophages as a Tool for Disease Modeling of Hereditary Pulmonary Alveolar Proteinosis due to Csf2rb Deficiency. Stem Cell Reports 7:292–305.

416. Takata K, Kozaki T, Lee CZW, Thion MS, Otsuka M, Lim S, Utami KH, Fidan K, Park DS, Malleret B, Chakarov S, See P, Low D, Low G, Garcia-Miralles M, Zeng R, Zhang J, Goh CC, Gul A, Hubert S, Lee B, Chen J, Low I, Shadan NB, Lum J, Wei TS, Mok E, Kawanishi S, Kitamura Y, Larbi A, Poidinger M, Renia L, Ng LG, Wolf Y, Jung S, Önder T, Newell E, Huber T, Ashihara E, Garel S, Pouladi MA, Ginhoux F. 2017. Induced-Pluripotent-Stem-Cell-Derived Primitive Macrophages Provide a Platform for Modeling Tissue-Resident Macrophage Differentiation and Function. Immunity 47:183-198.e6.

417. Hansen M, Varga E, Aarts C, Wust T, Kuijpers T, von Lindern M, van den Akker E. 2018. Efficient production of erythroid, megakaryocytic and myeloid cells, using single cell-derived iPSC colony differentiation. Stem Cell Res 29:232–244.

418. Ackermann M, Kempf H, Hetzel M, Hesse C, Hashtchin AR, Brinkert K, Schott JW, Haake K, Kühnel MP, Glage S, Figueiredo C, Jonigk D, Sewald K, Schambach A, Wronski S, Moritz T, Martin U, Zweigerdt R, Munder A, Lachmann N. 2018. Bioreactor-based mass production of human iPSC-derived macrophages enables immunotherapies against bacterial airway infections. Nat Commun 9:1–13.

419. Mukherjee C, Hale C, Mukhopadhyay S. 2018. A Simple Multistep Protocol for Differentiating Human Induced Pluripotent Stem Cells into Functional Macrophages, p. 13–28. *In* Rousselet, G (ed.), Macrophages: Methods and Protocols. Springer New York, New York, NY.

420. Monkley S, Krishnaswamy JK, Goransson M, Clausen M, Mueller J, Thorn K, Hicks R, Delaney S, Stjernborg L. 2020. Optimised generation of iPSC-derived macrophages and dendritic cells that are functionally and transcriptionally similar to their primary counterparts. PLoS One 1–17.

421. Vaughan-Jackson A, Stodolak S, Ebrahimi KH, Browne C, Paul K. 2020. Differentiation of Human induced Pluripotent Stem Cells to Authentic Macrophages using Fully Defined, Serum Free, Open Source Media. bioRxiv https://doi.org/https://doi.org/10.1101/2020.10.27.357632.

422. Kennedy M, Keller G. 2007. Development of hemangioblast defines the onset of hematopoiesis in ES. Blood 12:3521–3528.

423. Nyamundanda G, Poudel P, Patil Y, Sadanandam A. 2017. A Novel Statistical Method to Diagnose, Quantify and Correct Batch Effects in Genomic Studies. Sci Rep 7:1–10.

424. Johnson WE, Li C, Rabinovic A. 2007. Adjusting batch effects in microarray expression data using empirical Bayes methods. Biostatistics 8:118–127.

425. Roszer T. 2015. Understanding the Mysterious M2 Macrophage through Activation Markers and Effector Mechanisms. Mediators Inflamm 2015:16–18.

426. Honeycutt JB, Thayer WO, Baker CE, Ribeiro RM, Lada SM, Cao Y, Cleary RA, Hudgens MG, Richman DD, Garcia JV. 2017. HIV persistence in tissue macrophages of humanized myeloid-only mice during antiretroviral therapy. Nat Med 23:638–643.

427. Honeycutt JB, Wahl A, Baker C, Spagnuolo RA, Foster J, Zakharova O, Wietgrefe S, Caro-vegas C, Madden V, Sharpe G, Haase AT, Eron JJ, Garcia JV. 2016. Macrophages sustain HIV replication in vivo independently of T cells. J Clin Invest 126:1353–1366.

428. Liu LT, Liang L, Wang W, Yan CQ, Zhang J, Xiao YC, Ye L, Zhao MX, Huang QS, Bian JJ, Shi ZF, Ke X, Zhang ZR. 2018. Isolariciresinol-9'-O-α-L-arabinofuranoside protects against hydrogen peroxide-induced apoptosis of human umbilical vein endothelial cells via a PI3K/Akt/Bad-dependent pathway. Mol Med Rep 17:488–494.

429. Vo Q V., Trenerry C, Rochfort S, Wadeson J, Leyton C, Hughes AB. 2014. Synthesis and anti-inflammatory activity of indole glucosinolates. Bioorganic Med Chem 22:856–864.

430. Berton G, Cassatella MA, Ross F. 1986. Molecular basis of macrophage activation . Expression of the low potential cytochrome b and its reduction upon cell stimulation in activated macrophages . Information about subscribing to The Journal of Immunology is online at : LOW POTENTIAL CYTOCHROME b. J Immunol 136:1393–1399.

431. Caputa G, Flachsmann LJ, Cameron AM. 2019. Macrophage metabolism: a wound-healing perspective. Immunol Cell Biol 97:268–278.

432. Weiskopf D, Weinberger B, Grubeck-Loebenstein B. 2009. The aging of the immune system. Transpl Int 22:1041–1050.

433. Simon AK, Hollander GA, McMichael A. 2015. Evolution of the immune system in humans from infancy to old age. Proc R Soc B Biol Sci 282.

434. Haspel JA, Anafi R, Brown MK, Cermakian N, Depner C, Desplats P, Gelman AE, Haack M, Jelic S, Kim BS, Laposky AD, Lee YC, Mongodin E, Prather AA, Prendergast B, Reardon C, Shaw AC, Sengupta S, Szentirmai É, Thakkar M, Walker WE, Solt LA. 2020. Perfect timing: Circadian rhythms, sleep, and immunity — An NIH workshop summary. JCI Insight 5:1–14.

435. Scott CL, Zheng F, De Baetselier P, Martens L, Saeys Y, De Prijck S, Lippens S, Abels C, Schoonooghe S, Raes G, Devoogdt N, Lambrecht BN, Beschin A, Guilliams M. 2016. Bone marrow-derived monocytes give rise to self-renewing and fully differentiated Kupffer cells. Nat Commun 7:1–10.

436. Shemer A, Grozovski J, Tay TL, Tao J, Volaski A, Süß P, Ardura-Fabregat A, Gross-Vered M, Kim J-S, David E, Chappell-Maor L, Thielecke L, Glass CK, Cornils K, Prinz M, Jung S. 2018. Engrafted parenchymal brain macrophages differ from microglia in transcriptome, chromatin landscape and response to challenge. Nat Commun 9:5206.

437. Ohgidani M, Kato TA, Setoyama D, Sagata N, Hashimoto R, Shigenobu K, Yoshida T, Hayakawa K, Shimokawa N, Miura D, Utsumi H, Kanba S. 2014. Direct induction of ramified microglia-like cells from human monocytes: Dynamic microglial dysfunction in Nasu-Hakola disease. Sci Rep 4:1–7.

438. Richard M. Ransohoff. 2016. Surprises from the sanitary engineers rock and rivers. NAtur 532.

439. Reyes L, Wolfe B, Golos T. 2017. Hofbauer Cells: Placental Macrophages of Fetal Origin. In: Kloc M. (eds) Macrophages. Results and Problems in Cell DifferentiationImmunology of the Skin: Basic and Clinical Sciences in Skin Immune Responsesversion 62. Springer International Publishing.

440. Abumaree MH, Al Jumah MA, Kalionis B, Jawdat D, Al Khaldi A, Abomaray FM, Fatani AS, Chamley LW, Knawy BA. 2013. Human Placental Mesenchymal Stem Cells

(pMSCs) Play a Role as Immune Suppressive Cells by Shifting Macrophage Differentiation from Inflammatory M1 to Anti-inflammatory M2 Macrophages. Stem Cell Rev Reports 9:620–641.

441. Kelly B, O'Neill LAJ. 2015. Metabolic reprogramming in macrophages and dendritic cells in innate immunity. Cell Res 25:771–784.

442. Freemerman AJ, Johnson AR, Sacks GN, Milner JJ, Kirk EL, Troester MA, Macintyre AN, Goraksha-Hicks P, Rathmell JC, Makowski L. 2014. Metabolic reprogramming of macrophages: Glucose transporter 1 (GLUT1)-mediated glucose metabolism drives a proinflammatory phenotype. J Biol Chem 289:7884–7896.

443. Mills EL, Kelly B, Logan A, Costa ASH, Varma M, Bryant CE, Tourlomousis P, Däbritz JHM, Gottlieb E, Latorre I, Corr SC, McManus G, Ryan D, Jacobs HT, Szibor M, Xavier RJ, Braun T, Frezza C, Murphy MP, O'Neill LA. 2016. Succinate Dehydrogenase Supports Metabolic Repurposing of Mitochondria to Drive Inflammatory Macrophages. Cell 167:457-470.e13.

444. Tannahill GM, Curtis AM, Adamik J, Palsson-Mcdermott EM, McGettrick AF, Goel G, Frezza C, Bernard NJ, Kelly B, Foley NH, Zheng L, Gardet A, Tong Z, Jany SS, Corr SC, Haneklaus M, Caffrey BE, Pierce K, Walmsley S, Beasley FC, Cummins E, Nizet V, Whyte M, Taylor CT, Lin H, Masters SL, Gottlieb E, Kelly VP, Clish C, Auron PE, Xavier RJ, O'Neill LAJ. 2013. Succinate is an inflammatory signal that induces IL-1β through HIF-1α. Nature 496:238–242.

445. Postat J, Olekhnovitch R, Lemaître F, Bousso P. 2018. A Metabolism-Based Quorum Sensing Mechanism Contributes to Termination of Inflammatory Responses. Immunity 49:654-665.e5.

446. Wei J, Guo H, Kuo PC. 2002. Endotoxin-Stimulated Nitric Oxide Production Inhibits Expression of Cytochrome c Oxidase in ANA-1 Murine Macrophages . J Immunol 168:4721–4727.

447. Romero-Garcia S, Moreno-Altamirano MMB, Prado-Garcia H, Sánchez-García FJ. 2016. Lactate contribution to the tumor microenvironment: Mechanisms, effects on immune cells and therapeutic relevance. Front Immunol 7.

448. Colegio OR, Chu NQ, Szabo AL, Chu T, Rhebergen AM, Jairam V, Cyrus N, Brokowski CE, Eisenbarth SC, Phillips GM, Cline GW, Phillips AJ, Medzhitov R. 2014. Functional polarization of tumour-associated macrophages by tumour-derived lactic acid. Nature 513:559–563.

449. Stoker MGP, Rubin H. 1967. Density dependent inhibition of cell growth in culture [25]. Nature 215:171–172.

450. McClatchey AI, Yap AS. 2012. Contact inhibition (of proliferation) redux. Curr Opin Cell Biol 24:685–694.

451. Mayor R, Carmona-Fontaine C. 2010. Keeping in touch with contact inhibition of locomotion. Trends Cell Biol 20:319–328.

452. Eagle H, Levine EM. 1967. Growth regulatory effects of cellular interaction. Nature 213:1102–1106.

453. Blunk T, Sieminski AL, Gooch KJ, Courter DL, Hollander AP, Nahir AM, Langer R, Vunjak-Novakovic G, Freed LE. 2002. Differential effects of growth factors on tissue-engineered cartilage. Tissue Eng 8:73–84.

454. Wu YK, Tu YK, Yu J, Cheng NC. 2020. The Influence of Cell Culture Density on the Cytotoxicity of Adipose-Derived Stem Cells Induced by L-Ascorbic Acid-2-Phosphate.

Sci Rep 10:1–11.

455. Sukho P, Kirpensteijn J, Hesselink JW, van Osch GJVM, Verseijden F, Bastiaansen-Jenniskens YM. 2017. Effect of Cell Seeding Density and Inflammatory Cytokines on Adipose Tissue-Derived Stem Cells: an in Vitro Study. Stem Cell Rev Reports 13:267–277.

456. Hamada K, Osaka M, Yoshida M. 2014. Cell density impacts epigenetic regulation of cytokine-induced E-selectin gene expression in vascular endothelium. PLoS One 9.

457. Rabinovsky ED, Le WD, McManaman JL. 1992. Differential effects of neurotrophic factors on neurotransmitter development in the IMR-32 human neuroblastoma cell line. J Neurosci 12:171–179.

458. Badoyannis HC, Sharma SC, Sabban EL. 1991. The differential effects of cell density and NGF on the expression of tyrosine hydroxylase and dopamine β-hydroxylase in PC12 cells. Mol Brain Res 11:79–87.

459. Jobin C, Gauthier J. 1997. Differential effects of cell density on 5-lipoxygenase (5-LO), five-lipoxygenase-activating protein (FLAP) and interleukin-1β (IL-1β) expression in human neutrophils. Inflammation 21:235–250.

460. Ahmad SA. 1998. High Density H U M a N Neutrophils Produce a Transferable Factor. Unpubl masters thesis. University of British Columbri.

461. Uhlin-Hansen L, Kolset SO. 1988. Cell density-dependent expression of chondroitin sulfate proteoglycan in cultured human monocytes. J Biol Chem 263:2526–2531.

462. Summers L, Kielty C, Pinteaux E. 2009. Adhesion to fibronectin regulates interleukin-1 beta expression in microglial cells. Mol Cell Neurosci 41:148–155.

463. Bagnall J, Boddington C, England H, Brignall R, Downton P, Alsoufi Z, Boyd J, Rowe W, Bennett A, Walker C, Adamson A, Patel NMX, O'Cualain R, Schmidt L, Spiller DG, Jackson DA, Müller W, Muldoon M, White MRH, Paszek P. 2018. Quantitative analysis of competitive cytokine signaling predicts tissue thresholds for the propagation of macrophage activation. Sci Signal 11:1–16.

464. Chen CC, Wang L, Plikus M V., Jiang TX, Murray PJ, Ramos R, Guerrero-Juarez CF, Hughes MW, Lee OK, Shi S, Widelitz RB, Lander AD, Chuong CM. 2015. Organ-level quorum sensing directs regeneration in hair stem cell populations. Cell 161:277–290.

465. Postat J, Bousso P. 2019. Quorum Sensing by Monocyte-Derived Populations. Front Immunol 10:1–7.

466. Antonioli L, Blandizzi C, Pacher P, Guilliams M, Haskó G. 2019. Rethinking Communication in the Immune System: The Quorum Sensing Concept. Trends Immunol 40:88–97.

467. Antonioli L, Blandizzi C, Pacher P, Guilliams M, Haskó G. 2018. Quorum sensing in the immune system. Nat Rev Immunol 18:537–538.

468. Zhou X, Franklin RA, Adler M, Jacox JB, Bailis W, Shyer JA, Flavell RA, Mayo A, Alon U, Medzhitov R. 2018. Circuit Design Features of a Stable Two-Cell System. Cell 172:744-757.e17.

469. Muldoon JJ, Chuang Y, Bagheri N, Leonard JN. 2020. Macrophages employ quorum licensing to regulate collective activation. Nat Commun 11:1–14.

470. Selkoe DJ, Hardy J. 2017. The amyloid hypothesis of Alzheimer's disease at 25 years. EMBO Mol Med 8:595–608.

471. Lane CA, Hardy J, Schott JM. 2018. Alzheimer's disease. Eur J Neurol 25:59–70.

472. Jones L, Holmans PA, Hamshere ML, Harold D, Moskvina V, Ivanov D, Pocklington A, Abraham R, Hollingworth P, Sims R, Gerrish A, Pahwa JS, Jones N, Stretton A, Morgan AR, Lovestone S, Powell J, Proitsi P, Lupton MK, Brayne C, Rubinsztein DC, Gill M, Lawlor B, Lynch A, Morgan K, Brown KS, Passmore PA, Craig D, Mcguinness B, Todd S, Holmes C, Mann D, Smith AD, Love S, Kehoe PG, Mead S, Fox N, Rossor M, Collinge J, Maier W, Jessen F, Schürmann B, van den Bussche H, Heuser I, Peters O, Kornhuber J, Wiltfang J, Dichgans M, Frölich L, Harald H, Hüll M, Rujescu D, Goate AM, Kauwe JSK, Cruchaga C, Nowotny P, Morris JC, Mayo K, Livingston G, Bass NJ, Gurling H, Mcquillin A, Gwilliam R, Deloukas P, Al-Chalabi A, Shaw CE, Singleton AB, Guerreiro R, Mühleisen TW, Nöthen MM, Moebus S, Jöckel KH, Klopp N, Wichmann HE, Rüther E, Carrasquillo MM, Pankratz VS, Younkin SG, Hardy J, O'Donovan MC, Owen MJ, Williams J. 2010. Genetic evidence implicates the immune system and cholesterol metabolism in the aetiology of Alzheimer's disease. PLoS One 5.

473. Jansen IE, Savage JE, Watanabe K, Bryois J, Williams DM, Steinberg S, Sealock J, Karlsson IK, Hägg S, Athanasiu L, Voyle N, Proitsi P, Witoelar A, Stringer S, Aarsland D, Almdahl IS, Andersen F, Bergh S, Bettella F, Bjornsson S, Brækhus A, Bråthen G, de Leeuw C, Desikan RS, Djurovic S, Dumitrescu L, Fladby T, Hohman TJ, Jonsson P V., Kiddle SJ, Rongve A, Saltvedt I, Sando SB, Selbæk G, Shoai M, Skene NG, Snaedal J, Stordal E, Ulstein ID, Wang Y, White LR, Hardy J, Hjerling-Leffler J, Sullivan PF, van der Flier WM, Dobson R, Davis LK, Stefansson H, Stefansson K, Pedersen NL, Ripke S, Andreassen OA, Posthuma D. 2019. Genome-wide meta-analysis identifies new loci and functional pathways influencing Alzheimer's disease risk. Nat Genet 51:404–413.

474. Salih DA, Bayram S, Guelfi S, Reynolds RH, Shoai M, Ryten M, Brenton JW, Zhang D, Matarin M, Botia JA, Shah R, Brookes KJ, Guetta-Baranes T, Morgan K, Bellou E, Cummings DM, Escott-Price V, Hardy J. 2019. Genetic variability in response to amyloid beta deposition influences Alzheimer's disease risk. Brain Commun 1:1–13.

475. Holbrook J, Lara-Reyna S, Jarosz-Griffiths H, McDermott MF. 2019. Tumour necrosis factor signalling in health and disease. F1000Research 8:111.

476. Balu A. 2016. Employees perception on job promotion strategies of town benefit fund (Kumbakonam) 2:41–46.

477. Jiang Z, Georgel P, Du X, Shamel L, Sovath S, Mudd S, Huber M, Kalis C, Keck S, Galanos C, Freudenberg M, Beutler B. 2005. CD14 is required for MyD88-independent LPS signaling. Nat Immunol 6:565–570.

478. Wiesner P, Choi SH, Almazan F, Benner C, Huang W, Diehl CJ, Gonen A, Butler S, Witztum JL, Glass CK, Miller YI. 2010. Low doses of lipopolysaccharide and minimally oxidized low-density lipoprotein cooperatively activate macrophages via nuclear factor κb and activator protein-1: Possible mechanism for acceleration of atherosclerosis by subclinical endotoxemia. Circ Res 107:56–65.

479. Borzęcka K, Płóciennikowska A, Björkelund H, Sobota A, Kwiatkowska K. 2013. CD14 mediates binding of high doses of LPS but is dispensable for TNF-α production. Mediators Inflamm 2013.

480. Yuan R, Geng S, Li L. 2016. Molecular mechanisms that underlie the dynamic adaptation of innate monocyte memory to varying stimulant strength of TLR ligands. Front Immunol 7:1–12.

481. Monguió-Tortajada M, Franquesa M, Sarrias MR, Borràs FE. 2018. Low doses of LPS exacerbate the inflammatory response and trigger death on TLR3-primed human monocytes article. Cell Death Dis 9.

482. Meng F, Lowell CA. 1997. Lipopolysaccharide (LPS)-induced macrophage activation and signal transduction in the absence of Src-family kinases Hck, Fgr, and Lyn. J Exp Med 185:1661–1670.

483. Swanson K V., Deng M, Ting JPY. 2019. The NLRP3 inflammasome: molecular activation and regulation to therapeutics. Nat Rev Immunol 19:477–489.

484. Chitu V, Stanley ER. 2006. Colony-stimulating factor-1 in immunity and inflammation. Curr Opin Immunol 18:39–48.

485. Lee PSW, Wang Y, Dominguez MG, Yeung YG, Murphy MA, Bowtell DDL, Stanley ER. 1999. The Cbl protooncoprotein stimulates CSF-1 receptor multiubiquitination and endocytosis, and attenuates macrophage proliferation. EMBO J 18:3616–3628.

486. Sayed FA, Telpoukhovskaia M, Kodama L, Li Y, Zhou Y, Le D, Hauduc A, Ludwig C, Gao F, Clelland C, Zhan L, Cooper YA, Davalos D, Akassoglou K, Coppola G, Gan L. 2018. Differential effects of partial and complete loss of TREM2 on microglial injury response and tauopathy. Proc Natl Acad Sci U S A 115:10172–10177.

487. Ji XH, Yao T, Qin JC, Wang SK, Wang HJ, Yao K. 2004. Interaction between M-CSF and IL-10 on productions of IL-12 and IL-18 and expressions of CD14, CD23, and CD64 by human monocytes. Acta Pharmacol Sin 25:1361–1365.

488. Sweet MJ, Campbell CC, Sester DP, Xu D, McDonald RC, Stacey KJ, Hume DA, Liew FY. 2002. Colony-Stimulating Factor-1 Suppresses Responses to CpG DNA and Expression of Toll-Like Receptor 9 but Enhances Responses to Lipopolysaccharide in Murine Macrophages. J Immunol 168:392–399.

489. Xue Q, Lu Y, Eisele MR, Sulistijo ES, Khan N, Fan R, Miller-Jensen K. 2015. Analysis of single-cell cytokine secretion reveals a role for paracrine signaling in coordinating macrophage responses to TLR4 stimulation. Sci Signal 8:ra59.

490. Casanova-Acebes M, Nicolás-Ávila JA, Yao Li JL, García-Silva S, Balachander A, Rubio-Ponce A, Weiss LA, Adrover JM, Burrows K, A-González N, Ballesteros I, Devi S, Quintana JA, Crainiciuc G, Leiva M, Gunzer M, Weber C, Nagasawa T, Soehnlein O, Merad M, Mortha A, Ng LG, Peinado H, Hidalgo A. 2018. Neutrophils instruct homeostatic and pathological states in naive tissues. J Exp Med 215:2778–2795.

491. Singh AK, Arya RK, Trivedi AK, Sanyal S, Baral R, Dormond O, Briscoe DM, Datta D. 2013. Chemokine receptor trio: CXCR3, CXCR4 and CXCR7 crosstalk via CXCL11 and CXCL12. Cytokine Growth Factor Rev 24:41–49.

492. Yang CH, Wei L, Pfeffer SR, Du Z, Murti A, Valentine WJ, Zheng Y, Pfeffer LM. 2007. Identification of CXCL11 as a STAT3-Dependent Gene Induced by IFN. J Immunol 178:986–992.

493. Groom JR, Luster AD. 2011. CXCR3 ligands: Redundant, collaborative and antagonistic functions. Immunol Cell Biol 89:207–215.

494. Torraca V, Cui C, Boland R, Bebelman JP, Van Der Sar AM, Smit MJ, Siderius M, Spaink HP, Meijer AH. 2015. The CXCR3-CXCL11 signaling axis mediates macrophage recruitment and dissemination of mycobacterial infection. DMM Dis Model Mech 8:253–269.

495. Petkovic V, Moghini C, Paoletti S, Uguccioni M, Gerber B. 2004. I-TAC / CXCL11 is a natural antagonist for CCR5 Abstract : The selective CXC chemokine receptor. J Leukoc Biol 76:701–708.

496. The Uniprot Consortium. 2019. UniProt: A worldwide hub of protein knowledge. Nucleic Acids Res 47:D506–D515.

497. Porcheray F, Viaud S, Rimaniol AC, Léone C, Samah B, Dereuddre-Bosquet N, Dormont D, Gras G. 2005. Macrophage activation switching: An asset for the resolution of inflammation. Clin Exp Immunol 142:481–489.

498. Mitroulis I, Alexaki VI, Kourtzelis I, Ziogas A, Hajishengallis G, Chavakis T. 2015. Leukocyte integrins: Role in leukocyte recruitment and as therapeutic targets in inflammatory disease. Pharmacol Ther 147:123–135.

499. Reilkoff RA, Bucala R, Herzog EL. 2011. Fibrocytes: Emerging effector cells in chronic inflammation. Nat Rev Immunol 11:427–435.

500. Pilling D, Fan T, Huang D, Kaul B, Gomer RH. 2009. Identification of markers that distinguish monocyte-derived fibrocytes from monocytes, macrophages, and fibroblasts. PLoS One 4:31–33.

501. Bucala R, Spiegel LA, Chesney J, Hogan M, Cerami A. 1994. Circulating fibrocytes define a new leukocyte subpopulation that mediates tissue repair. Mol Med 1:71–81.

502. Pavel M, Renna M, Park SJ, Menzies FM, Ricketts T, Füllgrabe J, Ashkenazi A, Frake RA, Lombarte AC, Bento CF, Franze K, Rubinsztein DC. 2018. Contact inhibition controls cell survival and proliferation via YAP/TAZ-autophagy axis. Nat Commun 9.

503. Zhao B, Wei X, Li W, Udan RS, Yang Q, Kim J, Xie J, Ikenoue T, Yu J, Li L, Zheng P, Ye K, Chinnaiyan A, Halder G, Lai ZC, Guan KL. 2007. Inactivation of YAP oncoprotein by the Hippo pathway is involved in cell contact inhibition and tissue growth control. Genes Dev 21:2747–2761.

504. Aragona M, Panciera T, Manfrin A, Giulitti S, Michielin F, Elvassore N, Dupont S, Piccolo S. 2013. A mechanical checkpoint controls multicellular growth through YAP/TAZ regulation by actin-processing factors. Cell 154:1047–1059.

505. Oren M, Aylon Y. 2014. The hippo signaling pathway and cancer. Hippo Signal Pathw Cancer 15:1–354.

506. Wada KI, Itoga K, Okano T, Yonemura S, Sasaki H. 2011. Hippo pathway regulation by cell morphology and stress fibers. Development 138:3907–3914.

507. Lee SJ, Drabik K, Van Wagoner NJ, Lee S, Choi C, Dong Y, Benveniste EN. 2000. ICAM-1-Induced Expression of Proinflammatory Cytokines in Astrocytes: Involvement of Extracellular Signal-Regulated Kinase and p38 Mitogen-Activated Protein Kinase Pathways. J Immunol 165:4658–4666.

508. Patel NR, Bole M, Chen C, Hardin CC, Kho AT, Mih J, Deng L, Butler J, Tschumperlin D, Fredberg JJ, Krishnan R, Koziel H. 2012. Cell Elasticity Determines Macrophage Function. PLoS One 7:1–10.

509. Rangamani P, Fardin MA, Xiong Y, Lipshtat A, Rossier O, Sheetz MP, Iyengar R. 2011. Signaling network triggers and membrane physical properties control the actin cytoskeleton-driven isotropic phase of cell spreading. Biophys J 100:845–857.

510. McWhorter FY, Wang T, Nguyen P, Chung T, Liu WF. 2013. Modulation of macrophage phenotype by cell shape. Proc Natl Acad Sci U S A 110:17253–17258.

511. Boechat N, Bouchonnet F, Bonay M, Grodet A, Pelicic V, Gicquel B, Hance AJ. 2001. Culture at High Density Improves the Ability of Human Macrophages to Control Mycobacterial Growth. J Immunol 166:6203–6211.

512. Nizami S, Hall-Roberts H, Warrier S, Cowley SA, Di Daniel E. 2019. Microglial inflammation and phagocytosis in Alzheimer's disease: Potential therapeutic targets. Br J Pharmacol 176:3515–3532.

513. Liu Z, Pan Q, Ding S, Qian J, Xu F, Zhou J, Cen S, Guo F, Liang C. 2013. The interferon-inducible MxB protein inhibits HIV-1 infection. Cell Host Microbe 14:398–410.

514. Kane M, Yadav SS, Bitzegeio J, Kutluay SB, Zang T, Wilson SJ, Schoggins JW, Rice CM, Yamashita M, Hatziioannou T, Bieniasz PD. 2013. MX2 is an interferon-induced inhibitor of HIV-1 infection. Nature 502:563–566.

515. Colomer-Lluch M, Ruiz A, Moris A, Prado JG. 2018. Restriction Factors: From Intrinsic Viral Restriction to Shaping Cellular Immunity Against HIV-1. Front Immunol 9:2876.

516. Towers GJ, Noursadeghi M. 2014. Interactions between HIV-1 and the cell-autonomous innate immune system. Cell Host Microbe 16:10–18.

517. Yan N, Regalado-magdos AD, Stiggelbout B, Lee-kirsch MA, Lieberman J. 2010. The cytosolic exonuclease TREX1 inhibits the innate immune response to human immunodeficiency virus type 1. Nat Publ Gr 11:1005–1013.

518. Meås HZ, Haug M, Beckwith MS, Louet C, Ryan L, Hu Z, Landskron J, Nordbø SA, Taskén K, Yin H, Damås JK, Flo TH. 2020. Sensing of HIV-1 by TLR8 activates human T cells and reverses latency. Nat Commun 11:1–16.

519. Altfeld M, Gale M. 2015. Innate immunity against HIV-1 infection. Nat Immunol 16:554–562.

520. Iwasaki A. 2012. Innate Immune Recognition of HIV-1. Immunity 37:389–398.

521. Zhu Y, Chen G, Lv F, Wang X, Ji X, Xu Y, Sun J, Wu L, Zheng YT, Gao G. 2011. Zinc-finger antiviral protein inhibits HIV-1 infection by selectively targeting multiply spliced viral mRNAs for degradation. Proc Natl Acad Sci U S A 108:15834–15839.

522. Mlcochova P, Sutherland KA, Watters SA, Bertoli C, Bruin RA, Rehwinkel J, Neil SJ, Lenzi GM, Kim B, Khwaja A, Gage MC, Georgiou C, Chittka A, Yona S, Noursadeghi M, Towers GJ, Gupta RK. 2017. A G1-like state allows HIV -1 to bypass SAMHD 1 restriction in macrophages . EMBO J 36:604–616.

523. Strebel K. 2013. HIV accessory proteins versus host restriction factors. Curr Opin Virol 3:692–699.

524. Stremlau M, Owens CM, Perron MJ, Kiessling M, Autissier P, Sodroski J. 2004. The cytoplasmic body component TRIM5α restricts HIV-1 infection in Old World monkeys. Nature 427:848–853.

525. Luban J, Bossolt KL, Franke EK, Kalpana G V., Goff SP. 1993. Human immunodeficiency virus type 1 Gag protein binds to cyclophilins A and B. Cell 73:1067–1078.

526. Yap MW, Nisole S, Lynch C, Stoye JP. 2004. Trim5α protein restricts both HIV-1 and murine leukemia virus. Proc Natl Acad Sci U S A 101:10786–10791.

527. Dufour C, Claudel A, Joubarne N, Merindol N, Maisonnet T, Masroori N, Plourde MB, Berthoux L. 2018. Editing of the human TRIM5 gene to introduce mutations with the potential to inhibit HIV-1. PLoS One 13:1–13.

528. Sokolskaja E, Sayah DM, Luban J. 2004. Target Cell Cyclophilin A Modulates Human Immunodeficiency Virus Type 1 Infectivity. J Virol 78:12800–12808.

529. Manel N, Hogstad B, Wang Y, Levy DE, Unutmaz D, Littman DR. 2010. A cryptic sensor for HIV-1 activates antiviral innate immunity in dendritic cells. Nature 467:214–217.

530. Thali M, Bukovsky A, Kondo E, Rosenwlrth B, Walsh CT, Sodroski J, Göttlinger HG. 1994. Functional association of cyclophilin a with HIV-1 virions. Nature 372:363–365.

531. Braaten D, Luban J. 2001. Cyclophilin A regulates HIV-1 infectivity, as demonstrated by gene targeting in human T cells. EMBO J 20:1300–1309.

532. Kootstra NA, Münk C, Tonnu N, Landau NR, Verma IM. 2003. Abrogation of postentry restriction of HIV-1-based lentiviral vector transduction in simian cells. Proc Natl Acad Sci U S A 100:1298–1303.

533. Besnier C, Takeuchi Y, Towers G. 2002. Restriction of lentivirus in monkeys. Proc Natl Acad Sci 99:11920–11925.

534. Qi M, Yang R, Aiken C. 2008. Cyclophilin A-Dependent Restriction of Human Immunodeficiency Virus Type 1 Capsid Mutants for Infection of Nondividing Cells. J Virol 82:12001–12008.

535. Yamashita M, Emerman M. 2009. Cellular Restriction Targeting Viral Capsids Perturbs Human Immunodeficiency Virus Type 1 Infection of Nondividing Cells. J Virol https://doi.org/10.1128/JVI.01084-09.

536. Mu D, Yang H, Zhu JW, Liu FL, Tian RR, Zheng HY, Han JB, Shi P, Zheng YT. 2014. Independent birth of a novel TRIMCyp in tupaia belangeri with a divergent function from its paralog TRIM5. Mol Biol Evol 31:2985–2997.

537. Malfavon-Borja R, Wu LI, Emerman M, Malik HS. 2013. Birth, decay, and reconstruction of an ancient TRIMCyp gene fusion in primate genomes. Proc Natl Acad Sci U S A 110.

538. Yap MW, Dodding MP, Stoye JP. 2006. Trim-Cyclophilin A Fusion Proteins Can Restrict Human Immunodeficiency Virus Type 1 Infection at Two Distinct Phases in the Viral Life Cycle. J Virol 80:4061–4067.

539. Sayah DM, Sokolskaja E, Berthoux L, Luban J. 2004. Cyclophilin A retrotransposition into TRIM5 explains owl monkey resistance to HIV-1. Nature 430:569–573.

540. Manel N, Hogstad B, Wang Y, Levy DE, Unutmaz D, Littman DR. 2010. A cryptic sensor for HIV-1 activates antiviral innate immunity in dendritic cells. Nature 467:214–217.

541. Berthoux L, Sebastian S, Sokolskaja E, Luban J. 2005. Cyclophilin A is required for TRIM5α-mediated resistance to HIV-1 in Old World monkey cells. Proc Natl Acad Sci U S A 102:14849–14853.

542. Wilen CB, Tilton JC, Doms RW. 2012. HIV: Cell binding and entry. Cold Spring Harb Perspect Med 2:1–5.

543. Munk C, Brandt SM, Lucero G, Landau NR. 2002. A dominant block to HIV-1 replication at reverse transcription in simian cells. Proc Natl Acad Sci 99:13843–13848.

544. Perez-Caballero D, Hatziioannou T, Yang A, Cowan S, Bieniasz PD. 2005. Human Tripartite Motif 5α Domains Responsible for Retrovirus Restriction Activity and Specificity. J Virol 79:8969–8978.

545. Gavegnano C, Kennedy EM, Kim B, Schinazi RF. 2012. The Impact of Macrophage Nucleotide Pools on HIV-1 Reverse Transcription, Viral Replication, and the Development of Novel Antiviral Agents. Mol Biol Int 2012:1–8.

546. Collin M, Gordon S. 1994. The kinetics of human immunodeficiency virus reverse transcription are slower in primary human macrophages than in a lymphoid cell line. Virology.

547. Gao D, Wu J, Wu Y, Du F, Aroh C, Yan N, Sun L, Chen ZJ. 2013. Cyclic GMP-AMP Synthase Is a Cytosolic DNA Sensor That Activates the Type I Interferon Pathway. Science (80-) 1375:903–907.

548. Ohainle M, Helms L, Vermeire J, Roesch F, Humes D, Basom R, Delrow JJ, Overbaugh J, Emerman M. 2018. A virus-packageable CRISPR screen identifies host factors mediating interferon inhibition of HIV. Elife 7:1–32.

549. Ohainle M, Kim K, Keceli SK, Felton A, Campbell E, Luban J, Emerman M. 2020. TRIM34 restricts HIV-1 and SIV capsids in a TRIM5α-dependent manner. PLoS Pathog 16:1–22.

550. Baldauf HM, Pan X, Erikson E, Schmidt S, Daddacha W, Burggraf M, Schenkova K, Ambiel I, Wabnitz G, Gramberg T, Panitz S, Flory E, Landau NR, Sertel S, Rutsch F, Lasitschka F, Kim B, König R, Fackler OT, Keppler OT. 2012. SAMHD1 restricts HIV-1 infection in resting CD4 + T cells. Nat Med 18:1682–1687.

551. Laguette N, Sobhian B, Casartelli N, Ringeard M, Chable-Bessia C, Ségéral E, Yatim A, Emiliani S, Schwartz O, Benkirane M. 2011. SAMHD1 is the dendritic- and myeloid-cell-specific HIV-1 restriction factor counteracted by Vpx. Nature 474:654–657.

552. Liu J, Farmer JD, Lane WS, Friedman J, Weissman I, Schreiber SL. 1991. Calcineurin is a common target of cyclophilin-cyclosporin A and FKBP-FK506 complexes. Cell 66:807–815.

553. Lee KE, Ambrose Z, Martin TD, Oztop I, Mulky A, Julias JG, Vandegraaff N, Baumann JG, Wang R, Yuen W, Takemura T, Shelton K, Taniuchi I, Li Y, Sodroski J, Littman DR, Coffin JM, Hughes SH, Unutmaz D, Engelman A, KewalRamani VN. 2010. Flexible Use of Nuclear Import Pathways by HIV-1. Cell Host Microbe 7:221–233.

554. Bejarano DA, Peng K, Laketa V, Börner K, Jost KL, Lucic B, Glass B, Lusic M, Müller B, Kräusslich HG. 2019. HIV-1 nuclear import in macrophages is regulated by CPSF6-capsid interactions at the nuclear pore complex. Elife 8:1–31.

555. Hollenbaugh JA, Tao S, Lenzi GM, Ryu S, Kim DH, Diaz-Griffero F, Schinazi RF, Kim B. 2014. dNTP pool modulation dynamics by SAMHD1 protein in monocyte-derived macrophages. Retrovirology 11:1–12.

556. Van Wilgenburg B, Moore MD, James WS, Cowley SA. 2014. The productive entry pathway of HIV-1 in macrophages is dependent on endocytosis through lipid rafts containing CD4. PLoS One 9:1–14.

557. Carter GC, Bernstone L, Baskaran D, James W. 2011. HIV-1 infects macrophages by exploiting an endocytic route dependent on dynamin, Rac1 and Pak1. Virology 409:234–250.

558. Ribeiro CMS, Sarrami-Forooshani R, Setiawan LC, Zijlstra-Willems EM, Van Hamme JL, Tigchelaar W, Van Der Wel NN, Kootstra NA, Gringhuis SI, Geijtenbeek TBH. 2016. Receptor usage dictates HIV-1 restriction by human TRIM5α in dendritic cell subsets. Nature 540:448–452.

559. Towers GJ, Hatziioannou T, Cowan S, Goff SP, Luban J, Bieniasz PD. 2003. Cyclophilin A modulates the sensitivity of HIV-1 to host restriction factors. Nat Med 9:1138–1143.

560. Sun L, Wu J, Du F, Chen X, Chen ZJ. 2013. Cyclic GMP-AMP Synthase Is an. Science (80-) 339:786–791.

561. Thompson JF, Reifenberger JG, Giladi E, Kerouac K, Gill J, Hansen E, Kahvejian A, Kapranov P, Knope T, Lipson D, Steinmann KE, Milos PM. 2012. Single-step capture and sequencing of natural DNA for detection of BRCA1 mutations. Genome Res 22:340–345.

562. Long JS, Giotis ES, Moncorgé O, Frise R, Mistry B, James J, Morisson M, Iqbal M,

Vignal A, Skinner MA, Barclay WS. 2016. Species difference in ANP32A underlies influenza A virus polymerase host restriction. Nature 529:101–104.

563. Hartkoorn RC, Uplekar S, Cole ST. 2014. Cross-resistance between clofazimine and bedaquiline through upregulation of mmpl5 in mycobacterium tuberculosis. Antimicrob Agents Chemother 58:2979–2981.

564. Ling CL, Oravcova K, Beattie TF, Creer DD, Dilworth P, Fulton NL, Hardie A, Munro M, Pond M, Templeton K, Webster D, Workman S, McHugh TD, Gillespie SH. 2014. Tools for detection of Mycoplasma amphoriforme: A primary respiratory pathogen? J Clin Microbiol 52:1177–1181.

565. Soll SJ, Wilson SJ, Kutluay SB, Hatziioannou T, Bieniasz PD. 2013. Assisted Evolution Enables HIV-1 to Overcome a High TRIM5α-Imposed Genetic Barrier to Rhesus Macaque Tropism. PLoS Pathog 9.

566. Javanbakht H, Diaz-Griffero F, Stremlau M, Si Z, Sodroski J. 2005. The contribution of RING and B-box 2 domains to retroviral restriction mediated by monkey TRIM5α. J Biol Chem 280:26933–26940.

567. Li X, Yeung DF, Fiegen AM, Sodroski J. 2011. Determinants of the higher order association of the restriction factor TRIM5α and other tripartite motif (TRIM) proteins. J Biol Chem 286:27959–27970.

568. Roulston A, Lin R, Beauparlant P, Wainberg MA, Hiscott J. 1995. Regulation of human immunodeficiency virus type 1 and cytokine gene expression in myeloid cells by NF-κB/Rel transcription factors. Microbiol Rev 59:481–505.

569. Rohr O, Marban C, Aunis D, Schaeffer E. 2003. Regulation of HIV-1 gene transcription: from lymphocytes to microglial cells. J Leukoc Biol.

570. Henderson AJ, Calame KL. 1997. CCAAT/enhancer binding protein (C/EBP) sites are required for HIV-1 replication in primary macrophages but not CD4+ T cells. Proc Natl Acad Sci U S A.

571. Okumura A, Alce T, Lubyova B, Ezelle H, Strebel K, Pitha PM. 2008. HIV-1 accessory proteins VPR and Vif modulate antiviral response by targeting IRF-3 for degradation. Virology 373:85–97.

572. Khan H, Sumner RP, Rasaiyaah J, Tan CP, Rodriguez-Plata MT, Van Tulleken C, Fink D, Zuliani-Alvarez L, Thorne L, Stirling D, Milne RS, Towers GJ. 2020. Hiv-1 vpr antagonizes innate immune activation by targeting karyopherin-mediated nf-κb/irf3 nuclear transport. Elife 9:1–29.

573. Langer S, Hammer C, Hopfensperger K, Klein L, Hotter D, Jesus PDD, Herbert KM, Pache L, Smith N, Merwe JAV Der, Chanda SK, Fellay J, Kirchhoff F, Sauter D. 2019. Hiv-1 vpu is a potent transcriptional suppressor of nf-kb-elicited antiviral immune responses. Elife 8:1–25.

574. Trotard M, Tsopoulidis N, Tibroni N, Willemsen J, Binder M, Ruggieri A, Fackler OT. 2016. Sensing of HIV-1 Infection in Tzm-bl Cells with Reconstituted Expression of STING. J Virol 90:2064–2076.

575. Liu R, Tan J, Lin Y, Jia R, Yang W, Liang C, Geng Y, Qiao W. 2013. HIV-1 Vpr activates both canonical and noncanonical NF-κB pathway by enhancing the phosphorylation of IKKα/B. Virology 439:47–56.

576. Liu R, Lin Y, Jia R, Geng Y, Liang C, Tan J, Qiao W. 2014. HIV-1 Vpr stimulates NF-κB and AP-1 signaling by activating TAK1. Retrovirology 11:1–14.

577. Kogan M, Deshmane S, Sawaya BE, Gracely EJ, Khalili K, Rappaport J. 2013. Inhibition of NF-κB activity by HIV-1 Vpr is dependent on Vpr binding protein. J Cell Physiol 228:781–790.

578. Mandell MA, Kimura T, Jain A, Johansen T, Deretic V. 2014. TRIM proteins regulate autophagy: TRIM5 is a selective autophagy receptor mediating HIV-1 restriction. Autophagy 10:2387–2388.

579. Kimura T, Mandell M, Deretic V. 2016. Precision autophagy directed by receptor regulators - emerging examples within the TRIM family. J Cell Sci 129:881–91.

580. Keown JR, Black MM, Ferron A, Yap M, Barnett MJ, Grant Pearce F, Stoye JP, Goldstone DC. 2018. A helical LC3-interacting region mediates the interaction between the retroviral restriction factor Trim5 and mammalian autophagy-related ATG8 proteins. J Biol Chem 293:18378–18386.

581. Saha B, Chisholm D, Kell AM, Mandell MA. 2020. A non-canonical role for the autophagy machinery in anti-retroviral signaling mediated by TRIM5α. PLoS Pathog.

582. Pereira-Lopes S, Celhar T, Sans-Fons G, Serra M, Fairhurst A-M, Lloberas J, Celada A. 2013. The Exonuclease Trex1 Restrains Macrophage Proinflammatory Activation. J Immunol 191:6128–6135.

583. Yuan F, Dutta T, Wang L, Song L, Gu L, Qian L, Benitez A, Ning S, Malhotra A, Deutscher MP, Zhang Y. 2015. Human DNA exonuclease TREX1 is also an exoribonuclease that acts on single-stranded RNA. J Biol Chem 290:13344–13353.

584. Antonucci JM, St Gelais C, De Silva S, Yount JS, Tang C, Ji X, Shepard C, Xiong Y, Kim B, Wu L. 2016. SAMHD1-mediated HIV-1 restriction in cells does not involve ribonuclease activity. Nat Med 22:1072–1074.

585. Ryoo J, Hwang SY, Choi J, Oh C, Ahn K. 2016. SAMHD1-mediated HIV-1 restriction in cells does not involve ribonuclease activity. Nat Med 22:1074–1075.

586. Liu C, Perilla JR, Ning J, Lu M, Hou G, Ramalho R, Himes BA, Zhao G, Bedwell GJ, Byeon I-J, Ahn J, Gronenborn AM, Prevelige P, Rousso I, Aiken C, Polenova T, Schulten K, Zhang P. 2016. Cyclophilin A stabilizes the HIV-1 capsid through a novel non-canonical binding site. Nat Commun 7:10714.

587. Matreyek KA, Yücel SS, Li X, Engelman A. 2013. Nucleoporin NUP153 Phenylalanine-Glycine Motifs Engage a Common Binding Pocket within the HIV-1 Capsid Protein to Mediate Lentiviral Infectivity. PLoS Pathog 9.

588. Dismuke DJ, Aiken C. 2006. Evidence for a Functional Link between Uncoating of the Human Immunodeficiency Virus Type 1 Core and Nuclear Import of the Viral Preintegration Complex. J Virol 80:3712–3720.

589. Dick RA, Mallery DL, Vogt VM, James LC. 2018. IP6 regulation of HIV capsid assembly, stability, and uncoating. Viruses 10:1–11.

590. Battivelli E, Migraine J, Lecossier D, Matsuoka S, Perez-Bercoff D, Saragosti S, Clavel F, Hance AJ. 2011. Modulation of TRIM5 Activity in Human Cells by Alternatively Spliced TRIM5 Isoforms. J Virol 85:7828–7835.

591. Handschumacher R., Harding M., Rice J, Drugge R. 1984. Specific Cytosolic Bidg Protein for Cyclosporin. Science (80-) 226:544–547.

592. Kallen J, Spitzfaden C, Zurini MGM, Wider G, Widmer H, Wuthrich K, Walkinshaw MD. 1991. Structure of human cyclophilin and its binding site for cyclosporine A determined by X-ray crystallography and NMR spectroscopy. Lett to Nat 3:276–279.

593. Ke H, Zydowsky LD, Liu J, Walsh CT. 1991. Crystal structure of recombinant human T-cell cyclophilin A at 2.5 Å resolution. Proc Natl Acad Sci U S A 88:9483–9487.

594. Ke H, Mayrose D, Belshaw PJ, Alberg DG, Schreiber SL, Chang ZY, Etzkorn FA, Ho S, Walsh CT. 1994. Crystal structures of cyclophilin A complexed with cyclosporin A and N-methyl-4-[(E)-2-butenyl]-4,4-dimethylthreonine cyclosporin A. Structure 2:33–44.

595. Sumethkul K, Kitumnuaypong T, Angthararak S, Pichaiwong W. 2019. Low-dose cyclosporine for active lupus nephritis: a dose titration approach. Clin Rheumatol 38:2151–2159.

596. Brandt C, Pavlovic V, Radbruch A, Worm M, Baumgrass R. 2009. Low-dose cyclosporine A therapy increases the regulatory T cell population in patients with atopic dermatitis. Allergy Eur J Allergy Clin Immunol 64:1588–1596.

597. Won Y -H, Sauder DN, Mckenzie RC. 1994. Cyclosporin A inhibits keratinocyte cytokine gene expression. Br J Dermatol 130:312–319.

598. Suzuki K, Saito K, Tsujimura S, Nakayamada S, Yamaoka K, Sawamukai N, Iwata S, Nawata M, Nakano K, Tanaka Y. 2010. Tacrolimus, a calcineurin inhibitor, overcomes treatment unresponsiveness mediated by P-glycoprotein on lymphocytes in refractory rheumatoid arthritis. J Rheumatol 37:512–520.

599. Liddicoat AM, Lavelle EC. 2019. Modulation of innate immunity by cyclosporine A. Biochem Pharmacol 163:472–480.

600. Du S, Hiramatsu N, Hayakawa K, Kasai A, Okamura M, Huang T, Yao J, Takeda M, Araki I, Sawada N, Paton AW, Paton JC, Masanori K, J. 2009. Suppression of NF-κ B by Cyclosporin A and Tacrolimus (FK506) via Induction of the C/EBP Family: Implication for Unfolded Protein Response. J Immunol 182:7201–7211.

601. Jennings C, Kusler B, Jones PP. 2009. Calcineurin inactivation leads to decreased responsiveness to LPS in macrophages and dendritic cells and protects against LPS-induced toxicity in vivo. Innate Immun 15:109–120.

602. Bendíčková K, Tidu F, De Zuani M, Kohoutková MH, Andrejčinová I, Pompeiano A, Bělášková S, Forte G, Zelante T, Frič J. 2019. Calcineurin inhibitors reduce NFAT-dependent expression of antifungal pentraxin-3 by human monocytes. J Leukoc Biol 107:497–508.

603. Howell J, Sawhney R, Testro A, Skinner N, Gow P, Angus P, Ratnam D, Visvanathan K. 2013. Cyclosporine and tacrolimus have inhibitory effects on toll-like receptor signaling after liver transplantation. Liver Transplant.

604. Herbst S, Shah A, Moya MM, Marzola V, Jensen1 B, Reed A, Birrell MA, Saijo S, Mostowy S, Shaunak S, Armstrong-James D. 2015. Phagocytosis-dependent activation of a TLR9–BTK– calcineurin–NFAT pathway co-ordinates innate immunity to Aspergillus fumigatus. EMBO Mol Med 7:240–258.

605. Tourneur E, Ben Mkaddem S, Chassin C, Bens M, Goujon JM, Charles N, Pellefigues C, Aloulou M, Hertig A, Monteiro RC, Girardin SE, Philpott DJ, Rondeau E, Elbim C, Werts C, Vandewalle A. 2013. Cyclosporine A Impairs Nucleotide Binding Oligomerization Domain (Nod1)-Mediated Innate Antibacterial Renal Defenses in Mice and Human Transplant Recipients. PLoS Pathog 9.

606. He B, Li QY, Wu YY, Ruan JL, Teng XM, Li DJ, Tang CL. 2020. Cyclosporin a protects JEG-3 cells against oxidative stress-induced apoptosis by inhibiting the p53 and JNK/p38 signaling pathways. Reprod Biol Endocrinol 18:1–9.

607. Kunz D, Walker G, Eberhardt W, Nitsch D, Pfeilschifter J. 1995. Interleukin 1 beta-

induced expression of nitric oxide synthase in rat renal mesangial cells is suppressed by cyclosporin A. Biochem Biophys Res Commun 216:438–446.

608. Rodrigues-Diez R, González-Guerrero C, Ocaña-Salceda C, Rodrigues-Diez RR, Egido J, Ortiz A, Ruiz-Ortega M, Ramos AM. 2016. Calcineurin inhibitors cyclosporine A and tacrolimus induce vascular inflammation and endothelial activation through TLR4 signaling. Sci Rep 6:1–16.

609. Andrés D, Alvarez AM, Díez-Fernández C, Zaragoza A, Cascales M. 2000. HSP70 induction by cyclosporine A in cultured rat hepatocytes: Effect of vitamin E succinate. J Hepatol 33:570–579.

610. El-Sheikh AAK, Morsy MA, Abdel-latif RG. 2019. Modulation of eNOS/iNOS by nebivolol protects against cyclosporine A-mediated nephrotoxicity through targeting inflammatory and apoptotic pathways. Environ Toxicol Pharmacol 69:26–35.

611. Lim BJ, Hong SW, Jeong HJ. 2009. Renal tubular expression of Toll-like receptor 4 in cyclosporine nephrotoxicity. Apmis.

612. Lamoureux F, Gastinel LN, Mestre E, Marquet P, Essig M. 2012. Mapping cyclosporine-induced changes in protein secretion by renal cells using stable isotope labeling with amino acids in cell culture (SILAC). J Proteomics 75:3674–3687.

613. Hendricks A, Elson-Riggins JG, Riddle AL, House AK, Varjonen K, Bond R. 2012. Ciclosporin modulates the responses of canine progenitor epidermal keratinocytes (CPEK) to toll-like receptor agonists. Vet Immunol Immunopathol 147:91–96.

614. Storogenko M, Pech-Amsellem MA, Kerdine S, Rousselet F, Pallardy M. 1997. Cyclosporin-A inhibits human endothelial cells proliferation through interleukin-6-dependent mechanisms. Life Sci 60:1487–1496.

615. González-Guerrero C, Ocaña-Salceda C, Berzal S, Carrasco S, Fernández-Fernández B, Cannata-Ortiz P, Egido J, Ortiz A, Ramos AM. 2013. Calcineurin inhibitors recruit protein kinases JAK2 and JNK, TLR signaling and the UPR to activate NF-κB-mediated inflammatory responses in kidney tubular cells. Toxicol Appl Pharmacol.

616. Kang YJ, Kusler B, Otsuka M, Hughes M, Suzuki N, Suzuki S, Yeh W-C, Akira S, Han J, Jones PP. 2007. Calcineurin Negatively Regulates TLR-Mediated Activation Pathways. J Immunol 179:4598–4607.

617. Göthel SF, Marahiel MA. 1999. Peptidyl-prolyl cis-trams isomerases, a superfamily of ubiquitous folding catalysts. Cell Mol Life Sci 55:423–436.

618. Lu KP, Finn G, Lee TH, Nicholson LK. 2007. Prolyl cis-trans isomerization as a molecular timer. Nat Chem Biol 3:619–629.

619. Colgan J, Asmal M, Neagu M, Yu B, Schneidkraut J, Lee Y, Sokolskaja E, Andreotti A, Luban J. 2004. Cyclophilin A regulates TCR signal strength in CD4+ T cells via a proline-directed conformational switch in Itk. Immunity 21:189–201.

620. Gustafson CL, Parsley NC, Asimgil H, Lee HW, Ahlbach C, Michael AK, Xu H, Williams OL, Davis TL, Liu AC, Partch CL. 2017. A Slow Conformational Switch in the BMAL1 Transactivation Domain Modulates Circadian Rhythms. Mol Cell 66:447-457.e7.

621. Sarkar P, Reichman C, Saleh T, Birge RB, Kalodimos CG. 2007. Proline cis-trans Isomerization Controls Autoinhibition of a Signaling Protein. Mol Cell 25:413–426.

622. Holliday MJ, Camilloni C, Armstrong GS, Vendruscolo M, Eisenmesser EZ. 2017. Networks of Dynamic Allostery Regulate Enzyme Function. Structure 25:276–286.

623. Adams BM, Coates MN, Jackson SR, Jurica MS, Davis TL. 2015. Nuclear cyclophilins

affect spliceosome assembly and function *in vitro*. Biochem J 469:223–233.

624. Galat A. 2004. Function-dependent clustering of orthologues and paralogues of cyclophilins. Proteins Struct Funct Genet 56:808–820.

625. Marks AR. 1996. Cellular functions of immunophilins. Physiol Rev 76:631–649.

626. Ferreira PA, Orry A. 2012. From Drosophila to humans: Reflections on the roles of the prolyl isomerases and chaperones, cyclophilins, in cell function and disease. J Neurogenet 26:132–143.

627. Brazin KN, Mallis RJ, Fulton DB, Andreotti AH. 2002. Regulation of the tyrosine kinase Itk by the peptidyl-prolyl isomerase cyclophilin A. Proc Natl Acad Sci 99:1899–1904.

628. Saleh T, Jankowski W, Sriram G, Rossi P, Shah S, Lee K-B, Cruz LA, Rodriguez AJ, Birge RB, Kalodimos CG. 2015. Cyclophilin A promotes cell migration via the Abl-Crk signaling pathway. Nat Chem Biol 12:117–123.

629. Bonfils C, Bec N, Larroque C, Del Rio M, Gongora C, Pugnière M, Martineau P. 2010. Cyclophilin A as negative regulator of apoptosis by sequestering cytochrome c. Biochem Biophys Res Commun 393:325–330.

630. Zhu C, Wang X, Deinum J, Huang Z, Gao J, Modjtahedi N, Neagu MR, Nilsson M, Eriksson PS, Hagberg H, Luban J, Kroemer G, Blomgren K. 2007. Cyclophilin A participates in the nuclear translocation of apoptosis-inducing factor in neurons after cerebral hypoxia-ischemia. J Exp Med 204:1741–1748.

631. Candé C, Vahsen N, Kouranti I, Schmitt E, Daugas E, Spahr C, Luban J, Kroemer RT, Giordanetto F, Garrido C, Penninger JM, Kroemer G. 2004. AIF and cyclophilin A cooperate in apoptosis-associated chromatinolysis. Oncogene 23:1514–1521.

632. Lin ZL, Wu HJ, Chen JA, Lin KC, Hsu JH. 2015. Cyclophilin A as a downstream effector of PI3K/Akt signalling pathway in multiple myeloma cells. Cell Biochem Funct 566–574.

633. Zheng J, Koblinski JE, Dutson L V., Feeney YB, Clevenger C V. 2008. Prolyl isomerase cyclophilin A regulation of Janus-activated kinase 2 and the progression of human breast cancer. Cancer Res 68:7769–7778.

634. Bauer K, Kretzschmar AK, Cvijic H, Blumert C, Löffler D, Brocke-Heidrich K, Schiene-Fischer C, Fischer G, Sinz A, Clevenger C V., Horn F. 2009. Cyclophilins contribute to Stat3 signaling and survival of multiple myeloma cells. Oncogene 28:2784–2795.

635. Kim H, Oh Y, Kim K, Jeong S, Chon S, Kim D, Jung MH, Pak YK, Ha J, Kang I, Choe W. 2015. Cyclophilin A regulates JNK/p38-MAPK signaling through its physical interaction with ASK1. Biochem Biophys Res Commun 464:112–117.

636. Sun S, Guo M, Zhang JB, Ha A, Yokoyama KK, Chiu RH. 2014. Cyclophilin a (CypA) interacts with NF-κB subunit, p65/RelA, and contributes to NF-κB activation signaling. PLoS One 9.

637. Duina AA, Kalton HM, Gaber RF. 1998. Requirement for Hsp90 and a CyP-40-type Cyclophilin in Negative Regulation of the Heat Shock Response Requirement for Hsp90 and a CyP-40-type Cyclophilin in Negative Regulation of the Heat Shock. J Biol Chem 273:18974–18978.

638. Park MS, Chu F, Xie J, Wang Y, Bhattacharya P, Chan WK. 2011. Identification of cyclophilin-40-interacting proteins reveals potential cellular function of cyclophilin-40. Anal Biochem 410:257–265.

639. Bernasconi R, Soldà T, Galli C, Pertel T, Luban J, Molinari M. 2010. Cyclosporine A-Sensitive, Cyclophilin B-Dependent endoplasmic reticulum-associated degradation.

PLoS One 5:1–7.

640. Chapman DC, Stocki P, Williams DB. 2015. Cyclophilin C Participates in the US2-Mediated Degradation of Major Histocompatibility Complex Class i Molecules. PLoS One 10:1–28.

641. Stocki P, Chapman DC, Beach LA, Williams DB. 2014. Depletion of cyclophilins B and C Leads to dysregulation of endoplasmic reticulum redox homeostasis. J Biol Chem 289:23086–23096.

642. Yamaguchi R, Hosaka M, Torii S, Hou N, Saito N, Yoshimoto Y, Imai H, Takeuchi T. 2011. Cyclophilin C-associated protein regulation of phagocytic functions via NFAT activation in macrophages. Brain Res 1397:55–65.

643. Kong W, Longaker MT, Lorenz HP. 2004. Cyclophilin C-associated protein is a mediator for fibronectin fragment-induced matrix metalloproteinase-13 expression. J Biol Chem 279:55334–55340.

644. Sasaki T, Brakebusch C, Engel J, Timpl R. 1998. Mac-2 binding protein is a cell-adhesive protein of the extracellular matrix which self-assembles into ring-like structures and binds β1 integrins, collagens and fibronectin. EMBO J 17:1606–1613.

645. Powell TJ, Schreck R, Mc MC, Hui T, Rice A, App H, Azam M, Ullrich A, Shawver LK. 1995. A tumor-derived protein which provides t-cell costimulation through accessory cell activation. J Immunother.

646. Ullrich A, Sures I, D'Egidio M, Jallal B, Powell TJ, Herbst R, Dreps A, Azam M, Rubinstein M, Natoli C, Shawver LK, Schlessinger J, Iacobelli S. 1994. The secreted tumor-associated antigen 90K is a potent immune stimulator. J Biol Chem 269:18401–18407.

647. Trahey M, Weissman IL. 1999. Cyclophilin C-associated protein: a normal secreted glycoprotein that down-modulates endotoxin and proinflammatory responses in vivo. Proc Natl Acad Sci U S A 96:3006–3011.

648. Porter GA, Beutner G. 2018. Cyclophilin D, somehow a master regulator of mitochondrial function. Biomolecules 8.

649. Meier JA, Hyun M, Cantwell M, Raza A, Mertens C, Raje V, Sisler J, Tracy E, Torres-Odio S, Gispert S, Shaw PE, Baumann H, Bandyopadhyay D, Takabe K, Larner AC. 2017. Stress-induced dynamic regulation of mitochondrial STAT3 and its association with cyclophilin D reduce mitochondrial ROS production. Sci Signal 10.

650. Nakahira K, Haspel JA, Rathinam VAK, Lee SJ, Dolinay T, Lam HC, Englert JA, Rabinovitch M, Cernadas M, Kim HP, Fitzgerald KA, Ryter SW, Choi AMK. 2011. Autophagy proteins regulate innate immune responses by inhibiting the release of mitochondrial DNA mediated by the NALP3 inflammasome. Nat Immunol 12:222–230.

651. Boengler K, Hilfiker-Kleiner D, Heusch G, Schulz R. 2010. Inhibition of permeability transition pore opening by mitochondrial STAT3 and its role in myocardial ischemia/reperfusion. Basic Res Cardiol 105:771–785.

652. Busetto V, Barbosa I, Basquin J, Marquenet É, Hocq R, Hennion M, Paternina JA, Namane A, Conti E, Bensaude O, Le Hir H. 2020. Structural and functional insights into CWC27/CWC22 heterodimer linking the exon junction complex to spliceosomes. Nucleic Acids Res 48:5670–5683.

653. Jia Z, Wang M, Li S, Li X, Bai XY, Xu Z, Yang Y, Li B, Li Y, Wu H. 2018. U-box ubiquitin ligase PPIL2 suppresses breast cancer invasion and metastasis by altering cell morphology and promoting SNAI1 ubiquitination and degradation article. Cell Death Dis

9.

654. Hoffmann H, Schiene-Fischer C. 2014. Functional aspects of extracellular cyclophilins. Biol Chem 395:721–735.

655. Caroni P, Rothenfluh A, McGlynn E, Schneider C. 1991. S-Cyclophilin: New member of the cyclophilin family associated with the secretory pathway. J Biol Chem 266:10739–10742.

656. Sherry B, Yarlett N, Strupp A, Cerami A. 1992. Identification of cyclophilin as a proinflammatory secretory product of lipopolysaccharide-activated macrophages. Proc Natl Acad Sci U S A 89:3511–5.

657. Seko Y, Fujimura T, Taka H, Mineki R, Murayama K, Nagai R. 2004. Hypoxia followed by reoxygenation induces secretion of cyclophilin A from cultured rat cardiac myocytes. Biochem Biophys Res Commun 317:162–168.

658. Suzuki J, Jin ZG, Meoli DF, Matoba T, Berk BC. 2006. Cyclophilin A is secreted by a vesicular pathway in vascular smooth muscle cells. Circ Res 98:811–817.

659. Yurchenko V, O'Connor M, Dai WW, Guo H, Toole B, Sherry B, Bukrinsky M. 2001. CD147 is a signaling receptor for cyclophilin B. Biochem Biophys Res Commun 288:786–788.

660. Schlegel J, Redzic JS, Porter CC, Yurchenko V, Bukrinsky M, Labeikovsky W, Armstrong GS, Zhang F, Isern NG, DeGregori J, Hodges R, Eisenmesser EZ. 2009. Solution Characterization of the Extracellular Region of CD147 and Its Interaction with Its Enzyme Ligand Cyclophilin A. J Mol Biol 391:518–535.

661. Yurchenko V, Zybarth G, O'Connor M, Dai WW, Franchin G, Hao T, Guo H, Hung HC, Toole B, Gallay P, Sherry B, Bukrinsky M. 2002. Active site residues of cyclophilin A are crucial for its signaling activity via CD147. J Biol Chem 277:22959–22965.

662. Jin ZG, Lungu AO, Xie L, Wang M, Wong C, Berk BC. 2004. Cyclophilin A is a proinflammatory cytokine that activates endothelial cells. Arterioscler Thromb Vasc Biol 24:1186–1191.

663. Arora K, Gwinn WM, Bower MA, Watson A, Okwumabua I, MacDonald HR, Bukrinsky MI, Constant SL. 2005. Extracellular Cyclophilins Contribute to the Regulation of Inflammatory Responses. J Immunol 175:517–522.

664. Denys A, Allain F, Carpentier M, Spik G. 1998. Involvement of two classes of binding sites in the interactions of cyclophilin B with peripheral blood T-lymphocytes. Biochem J 336:689–697.

665. Boulos S, Meloni BP, Arthur PG, Majda B, Bojarski C, Knuckey NW. 2007. Evidence that intracellular cyclophilin A and cyclophilin A/CD147 receptor-mediated ERK1/2 signalling can protect neurons against in vitro oxidative and ischemic injury. Neurobiol Dis 25:54–64.

666. Jin ZG, Melaragno MG, Liao DF, Yan C, Haendeler J, Suh YA, Lambeth JD, Berk BC. 2000. Cyclophilin A is a secreted growth factor induced by oxidative stress. Circ Res 87:789–796.

667. Kim H, Kim WJ, Jeon ST, Koh EM, Cha HS, Ahn KS, Lee WH. 2005. Cyclophilin A may contribute to the inflammatory processes in rheumatoid arthritis through induction of matrix degrading enzymes and inflammatory cytokines from macrophages. Clin Immunol 116:217–224.

668. Yang H, Chen J, Yang J, Qiao S, Zhao S, Yu L. 2007. Cyclophilin A is upregulated in

small cell lung cancer and activates ERK1/2 signal. Biochem Biophys Res Commun 361:763–767.

669. Yang Y, Lu N, Zhou J, Chen ZN, Zhu P. 2008. Cyclophilin A up-regulates MMP-9 expression and adhesion of monocytes/ macrophages via CD147 signalling pathway in rheumatoid arthritis. Rheumatology 47:1299–1310.

670. Wang L, Wang CH, Jia JF, Ma XK, Li Y, Zhu H Bin, Tang H, Chen ZN, Zhu P. 2010. Contribution of cyclophilin a to the regulation of inflammatory processes in rheumatoid arthritis. J Clin Immunol 30:24–33.

671. Yuan W, Ge H, He B. 2010. Pro-inflammatory activities induced by CyPA-EMMPRIN interaction in monocytes. Atherosclerosis 213:415–421.

672. Bahmed K, Henry C, Holliday M, Redzic J, Ciobanu M, Zhang F, Weekes C, Sclafani R, DeGregori J, Eisenmesser E. 2012. Extracellular cyclophilin-A stimulates ERK1/2 phosphorylation in a cell-dependent manner but broadly stimulates nuclear factor kappa B. Cancer Cell Int 12:1–13.

673. Kim K, Kim H, Jeong K, Jung MY, Hahn BS, Yoon KS, Kwan Jin B, Jahng GH, Kang I, Ha J, Choe W. 2012. Release of overexpressed CypB activates ERK signaling through CD147 binding for hepatoma cell resistance to oxidative stress. Apoptosis 17:784–796.

674. Marcant A, Denys A, Melchior A, Martinez P, Deligny A, Carpentier M, Allain F. 2012. Cyclophilin B Attenuates the Expression of TNF-α in Lipopolysaccharide-Stimulated Macrophages through the Induction of B Cell Lymphoma-3. J Immunol 189:2023–2032.

675. Shaw PE. 2002. Peptidyl-prolyl isomerases: A new twist to transcription. EMBO Rep 3:521–526.

676. Sànchez-Tilló E, Wojciechowska M, Comalada M, Farrera C, Lloberas J, Celada A. 2006. Cyclophilin A is required for M-CSF-dependent macrophage proliferation. Eur J Immunol 36:2515–2524.

677. Howard BA, Furumai R, Campa MJ, Rabbani ZN, Vujaskovic Z, Wang XF, Patz EF. 2005. Stable RNA interference-mediated suppression of cyclophilin A diminishes non-small-cell lung tumor growth in vivo. Cancer Res 65:8853–8860.

678. Lilie H, Buchner J, Lang K, Rudolph R. 1993. Prolyl isomerases catalyze antibody folding in vitro. Protein Sci 2:1490–1496.

679. Song J, Lu YC, Yokoyama K, Rossi J, Chiu R. 2004. Cyclophilin A is required for retinoic acid-induced neuronal differentiation in p19 cells. J Biol Chem 279:24414–24419.

680. Ansari H, Greco G, Luban J. 2002. Cyclophilin A Peptidyl-Prolyl Isomerase Activity Promotes Zpr1 Nuclear Export. Mol Cell Biol 22:6993–7003.

681. Galigniana MD, Morishima Y, Gallay PA, Pratt WB. 2004. Cyclophilin-A is bound through its peptidylprolyl isomerase domain to the cytoplasmic dynein motor protein complex. J Biol Chem 279:55754–55759.

682. Garcia-Moreno M, Noerenberg M, Ni S, Järvelin AI, González-Almela E, Lenz CE, Bach-Pages M, Cox V, Avolio R, Davis T, Hester S, Sohier TJM, Li B, Heikel G, Michlewski G, Sanz MA, Carrasco L, Ricci EP, Pelechano V, Davis I, Fischer B, Mohammed S, Castello A. 2019. System-wide Profiling of RNA-Binding Proteins Uncovers Key Regulators of Virus Infection. Mol Cell 74:196-211.e11.

683. Dawar FU, Wu J, Zhao L, Khattak MNK, Mei J, Lin L. 2017. Updates in understanding the role of cyclophilin A in leukocyte chemotaxis. J Leukoc Biol 101:823–826.

684. Meunier L, Usherwood, Young-Kwang Chung KT, Hendershot LM. 2002. A Subset of

Chaperones and Folding Enzymes Form Multiprotein Complexes in Endoplasmic Reticulum to Bind Nascent Proteins. Mol Biol Cell 13:4456–4469.

685. Rycyzyn MA, Clevenger C V. 2002. The intranuclear prolactin/cyclophilin B complex as a transcriptional inducer. Proc Natl Acad Sci U S A 99:6790–6795.

686. Price ER, Jin M, Lim D, Pati S, Walsh CT, Mckeon FD. 1994. Cyclophilin B trafficking through the secretory pathway is altered by binding of cyclosporin A. Proc Natl Acad Sci U S A 91:3931–3935.

687. Friedman J, Trahey M, Weissman I. 1993. Cloning and characterization of cyclophilin C-associated protein: a candidate natural cellular ligand for cyclophilin C. Proc Natl Acad Sci U S A 90:6815–9.

688. Baker JD, Shelton LB, Zheng D, Favretto F, Nordhues BA, Darling A, Sullivan LE, Sun Z, Solanki PK, Martin MD, Suntharalingam A, Sabbagh JJ, Becker S, Mandelkow E, Uversky VN, Zweckstetter M, Dickey CA, Koren J, Blair LJ. 2017. Human cyclophilin 40 unravels neurotoxic amyloids. PLoS Biol 15:1–22.

689. Galigniana MD, Harrell JM, O'Hagen HM, Ljungman M, Pratt WB. 2004. Hsp90-binding immunophilins link p53 to dynein during p53 transport to the nucleus. J Biol Chem 279:22483–22489.

690. Johnson JL, Toft DO. 1995. Binding of p23 and hsp90 during assembly with the progesterone receptor. Mol Endocrinol 9:670–8.

691. Mi H, Kops O, Zimmermann E, Jäschke A, Tropschug M. 1996. A nuclear RNA-binding cyclophilin in human T cells. FEBS Lett 398:201–205.

692. Jurica MS, Licklider LJ, Gygi SP, Grigorieff N, Moore MJ. 2002. Purification and characterization of native spliceosomes suitable for three-dimensional structural analysis. Rna 8:426–439.

693. Fair K, Anderson M, Bulanova E, Mi H, Tropschug M, Diaz MO. 2001. Protein Interactions of the MLL PHD Fingers Modulate MLL Target Gene Regulation in Human Cells. Mol Cell Biol 21:3589–3597.

694. Bourquin JP, Stagljar I, Meier P, Moosmann P, Silke J, Baechi T, Georgiev O, Schaffner W. 1997. A serine/arginine-rich nuclear matrix cyclophilin interacts with the C-terminal domain of RNA polymerase II. Nucleic Acids Res 25:2055–61.

695. Giardina SL, Coffman JD, Young H a, Potter SJ, Frey JL, Ortaldo JR, Anderson SK. 1996. Association of the expression of an SR-cyclophilin with myeloid cell differentiation. Blood 87:2269–74.

696. Ingelfinger D, Göthel SF, Marahiel MA, Reidt U, Ficner R, Lührmann R, Achsel T. 2003. Two protein-protein interaction sites on the spliceosome-associated human cyclophilin CypH. Nucleic Acids Res 31:4791–4796.

697. Misteli T. 2002. A cyclophilin functions in pre-mRNA splicing. EMBO J 21:470–480.

698. Obama K, Kato T, Hasegawa S, Satoh S, Nakamura Y, Furukawa Y. 2006. Overexpression of peptidyl-prolyl isomerase-like 1 is associated with the growth of colon cancer cells. Clin Cancer Res 12:70–76.

699. Xu C, Zhang J, Huang X, Sun J, Xu Y, Tang Y, Wu J, Shi Y, Huang Q, Zhang Q. 2006. Solution structure of human peptidyl prolyl isomerase-like protein 1 and insights into its interaction with SKIP. J Biol Chem 281:15900–15908.

700. Wang BB, Hayenga KJ, Payan DG, Fisher JM, Pharmaceuticals K, Avenue L, Francisco SS. 1996. Identification of a nuclear-specific cyclophilin which interacts with the

proteinase inhibitor eglin c. Biotechnology 319:313–319.

701. Espeseth AS, Huang Q, Gates A, Xu M, Yu Y, Simon AJ, Shi XP, Zhang X, Hodor P, Stone DJ, Burchard J, Cavet G, Bartz S, Linsley P, Ray WJ, Hazuda D. 2006. A genome wide analysis of ubiquitin ligases in APP processing identifies a novel regulator of BACE1 mRNA levels. Mol Cell Neurosci 33:227–235.

702. Pushkarsky T, Yurchenko V, Vanpouille C, Brichacek B, Vaisman I, Hatakeyama S, Nakayama KI, Sherry B, Bukrinsky MI. 2005. Cell surface expression of CD147/EMMPRIN is regulated by cyclophilin 60. J Biol Chem 280:27866–27871.

703. Chen J, Chen S, Wang J, Zhang M, Gon Z, Wei Y, Li L, Zhang Y, Zhao X, Jiang S, Yu L. 2015. Cyclophilin J is a novel peptidyl-prolyl isomerase and target for repressing the growth of hepatocellular carcinoma. PLoS One 10:1–21.

704. Huo DH, Yi LN, Yang J. 2008. Interaction with Ppil3 leads to the cytoplasmic localization of Apoptin in tumor cells. Biochem Biophys Res Commun 372:14–18.

705. Barak T, Sencicek AGE, Miyagishima DF, Henegariu O, Gorur KM, Bilguvar K, Gunel M. 2019. Identification of Peptidyl-Prolyl Cis-Trans Isomerase-Like 4 as a Disease Causing Gene in Intracranial Aneurysms and its Role in Vertebrate CNS Specific Angiogenesis. Neurosurgery 66:2019.

706. Jiang M, Ma Y, Ni X, Cao G, Ji C, Cheng H, Tang R, Xie Y, Mao Y. 2002. Molecular cloning and characterization of a novel human gene (ANP32E alias LANPL) from human fetal brain. Cytogenet Genome Res 97:68–71.

707. Han HF, Chen Q, Zhao WW. 2020. Long non-coding RNA RP11-284F21.9 functions as a ceRNA regulating PPWD1 by competitively binding to miR-769-3p in cervical carcinoma. Biosci Rep 40:1–12.

708. Davis TL, Walker JR, Ouyang H, MacKenzie F, Butler-Cole C, Newman EM, Eisenmesser EZ, Dhe-Paganon S. 2008. The crystal structure of human WD40 repeat-containing peptidylprolyl isomerase (PPWD1). FEBS J 275:2283–2295.

709. Rinfret A, Collins C, Ménard R, Anderson SK. 1994. The N-Terminal Cyclophilin-Homologous Domain of a 150-Kilodalton Tumor Recognition Molecule Exhibits Both Peptidylprolyl cis–trans-Isomerase and Chaperone Activities. Biochemistry 33:1668–1673.

710. Ulrich A, Wahl MC. 2014. Structure and evolution of the spliceosomal peptidyl-prolyl cis-trans isomerase Cwc27. Acta Crystallogr Sect D Biol Crystallogr 70:3110–3123.

711. Wu J, Matunis MJ, Kraemer D, Blobel G, Coutavas E. 1995. Nup358, a cytoplasmically exposed nucleoporin with peptide repeats, Ran- GTP binding sites, zinc fingers, a cyclophilin A homologous domain, and a leucine-rich region. J Biol Chem.

712. Ma S, Boerner JE, TiongYip CL, Weidmann B, Ryder NS, Cooreman MP, Lin K. 2006. NIM811, a cyclophilin inhibitor, exhibits potent in vitro activity against hepatitis C virus alone or in combination with alpha interferon. Antimicrob Agents Chemother 50:2976–2982.

713. Sun S, Guo M, Zhang JB, Ha A, Yokoyama KK, Chiu RH. 2014. Cyclophilin a (CypA) interacts with NF-κB subunit, p65/RelA, and contributes to NF-κB activation signaling. PLoS One 9.

714. Rasola A, Sciacovelli M, Chiara F, Pantic B, Brusilow WS, Bernardi P. 2010. Activation of mitochondrial ERK protects cancer cells from death through inhibition of the permeability transition. Proc Natl Acad Sci U S A 107:726–731.

715. British Society for Immunology. 2019. Pattern recognition receptors (PRRs): toll-like receptors 38–40.

716. Christian F, Smith E, Carmody R. 2016. The Regulation of NF-κB Subunits by Phosphorylation. Cells.

717. Ran FA, Hsu PD, Wright J, Agarwala V, Scott DA, Zhang F. 2013. Genome engineering using the CRISPR-Cas9 system. Nat Protoc 8:2281–2308.

718. Ramachandran S, Vinitha A, Kartha CC. 2016. Cyclophilin A enhances macrophage differentiation and lipid uptake in high glucose conditions: A cellular mechanism for accelerated macro vascular disease in diabetes mellitus. Cardiovasc Diabetol 15:1–19.

719. El-Brolosy MA, Stainier DYR. 2017. Genetic compensation: A phenomenon in search of mechanisms. PLoS Genet 13:1–17.

720. Vossaert L, O'Leary T, Van Neste C, Heindryckx B, Vandesompele J, De Sutter P, Deforce D. 2013. Reference loci for RT-qPCR analysis of differentiating human embryonic stem cells. BMC Mol Biol 14.

721. Kalagara R, Gao W, Glenn HL, Ziegler C, Belmont L, Meldrum DR. 2016. Identification of stable reference genes for lipopolysaccharide-stimulated macrophage gene expression studies. Biol Methods Protoc 1:1–8.

722. Obchoei S, Weakley SM, Wongkham S, Wongkham C, Sawanyawisuth K, Yao Q, Chen C. 2011. Cyclophilin A enhances cell proliferation and tumor growth of liver fluke-associated cholangiocarcinoma. Mol Cancer 10:1–15.

723. Shen Y, Li Y, Ye F, Wang F, Lu W, Xie X. 2010. Identification of suitable reference genes for measurement of gene expression in human cervical tissues. Anal Biochem 405:224–229.

724. Nazet U, Schröder A, Spanier G, Wolf M, Proff P, Kirschneck C. 2019. Simplified method for applying static isotropic tensile strain in cell culture experiments with identification of valid RT-qPCR reference genes for PDL fibroblasts. Eur J Orthod 42:359–370.

725. Gao YF, Zhu T, Mao CX, Liu ZX, Wang Z Bin, Mao XY, Li L, Yin JY, Zhou HH, Liu ZQ. 2016. PPIC, EMP3 and CHI3L1 Are Novel Prognostic Markers for High Grade Glioma. Int J Mol Sci 17.

726. Luu TC, Bhattacharya P, Chan WK. 2008. Cyclophilin-40 has a cellular role in the aryl hydrocarbon receptor signaling. FEBS Lett 582:3167–3173.

727. Wang X, Spandidos A, Wang H, Seed B. 2012. PrimerBank: A PCR primer database for quantitative gene expression analysis, 2012 update. Nucleic Acids Res 40:1144–1149.

728. Kato H, Takeuchi O, Mikamo-Satoh E, Hirai R, Kawai T, Matsushita K, Hiiragi A, Dermody TS, Fujita T, Akira S. 2008. Length-dependent recognition of double-stranded ribonucleic acids by retinoic acid-inducible gene-I and melanoma differentiation-associated gene 5. J Exp Med 205:1601–1610.

729. Annett S, Moore G, Robson T. 2020. FK506 binding proteins and inflammation related signalling pathways; basic biology, current status and future prospects for pharmacological intervention. Pharmacol Ther 215:107623.

730. Elloumi HZ, Maharshak N, Rao KN, Kobayashi T, Ryu HS, Mühlbauer M, Li F, Jobin C, Plevy SE. 2012. A cell permeable peptide inhibitor of NFAT inhibits macrophage cytokine expression and ameliorates experimental colitis. PLoS One 7:1–10.

731. Yazdi AS, Ghoreschi K. 2016. The Interleukin-1 Family, p. 21–29. *In* Ma, X (ed.), Regulation of Cytokine Gene Expression in Immunity and Diseases. Springer Netherlands, Dordrecht.

732. Kalliolias GD, Ivashkiv LB. 2016. TNF biology, pathogenic mechanisms and emerging therapeutic strategies. Nat Rev Rheumatol 12:49–62.

733. Mino T, Takeuchi O. 2013. Post-transcriptional regulation of cytokine mRNA controls the initiation and resolution of inflammation. Biotechnol Genet Eng Rev 29:49–60.

734. Brownell J, Bruckner J, Wagoner J, Thomas E, Loo Y-M, Gale M, Liang TJ, Polyak SJ. 2014. Direct, Interferon-Independent Activation of the CXCL10 Promoter by NF- B and Interferon Regulatory Factor 3 during Hepatitis C Virus Infection. J Virol.

735. Yeruva S, Ramadori G, Raddatz D. 2008. NF-κB-dependent synergistic regulation of CXCL10 gene expression by IL-1β and IFN-γ in human intestinal epithelial cell lines. Int J Colorectal Dis.

736. Guo M, James AW, Kwak JH, Shen J, Yokoyama KK, Ting K, Soo CB, Chiu RH. 2016. Cyclophilin A (CypA) Plays Dual Roles in Regulation of Bone Anabolism and Resorption. Sci Rep 6:22378.

737. Guo M, Shen J, Kwak JH, Choi B, Lee M, Hu S, Zhang X, Ting K, Soo CB, Chiu RH. 2015. Novel role for cyclophilin A in regulation of chondrogenic commitment and endochondral ossification. Mol Cell Biol 35:2119–30.

738. Xiao Y, Palomero J, Grabowska J, Wang L, De Rink I, Van Helvert L, Borst J. 2017. Macrophages and osteoclasts stem from a bipotent progenitor downstream of a macrophage/osteoclast/dendritic cell progenitor. Blood Adv 1:1993–2006.

739. Dawar FU, Tu J, Khattak MNK, Mei J, Lin L. 2017. Cyclophilin a: A key factor in virus replication and potential target for anti-viral therapy. Curr Issues Mol Biol 21:1–20.

740. Meli VS, Veerasubramanian PK, Atcha H, Reitz Z, Downing TL, Liu WF. 2019. Biophysical regulation of macrophages in health and disease. J Leukoc Biol 106:283–299.

741. Jain N, Moeller J, Vogel V. 2019. Mechanobiology of Macrophages: How Physical Factors Coregulate Macrophage Plasticity and Phagocytosis. Annu Rev Biomed Eng 21:267–297.

742. Aiello A, Farzaneh F, Candore G, Caruso C, Davinelli S, Gambino CM, Ligotti ME, Zareian N, Accardi G. 2019. Immunosenescence and its hallmarks: How to oppose aging strategically? A review of potential options for therapeutic intervention. Front Immunol 10:1–19.

743. Liang G, Zhang Y. 2013. Genetic and epigenetic variations in iPSCs: Potential causes and implications for application. Cell Stem Cell 13:149–159.

744. Castaño J, Bueno C, Jiménez-Delgado S, Roca-Ho H, Fraga MF, Fernandez AF, Nakanishi M, Torres-Ruiz R, Rodríguez-Perales S, Menéndez P. 2017. Generation and characterization of a human iPSC cell line expressing inducible Cas9 in the “safe harbor” AAVS1 locus. Stem Cell Res 21:137–140.

745. So RWL, Chung SW, Lau HHC, Watts JJ, Gaudette E, Al-Azzawi ZAM, Bishay J, Lin LTW, Joung J, Wang X, Schmitt-Ulms G. 2019. Application of CRISPR genetic screens to investigate neurological diseases. Mol Neurodegener 14:1–16.

746. Sharma S, Petsalaki E. 2018. Application of CRISPR-Cas9 based genome-wide screening approaches to study cellular signalling mechanisms. Int J Mol Sci 19.

747. Yau EH, Rana TM. 2018. Next-Generation Sequencing of Genome-Wide CRISPR Screens, p. 203–216. *In* Head, SR, Ordoukhanian, P, Salomon, DR (eds.), Next Generation Sequencing: Methods and Protocols. Springer New York, New York, NY.

748. Hu G, Su Y, Kang BH, Fan Z, Dong T, Brown DR, Cheah J, Wittrup KD, Chen J. 2021. High-throughput phenotypic screen and transcriptional analysis identify new compounds and targets for macrophage reprogramming. Nat Commun 12:1–14.